ISSN 1122-8628

TERRA ANTARTICA
AN ANTARCTIC EARTH SCIENCE JOURNAL

Volume 7, Number 1/2 - 2000

Studies from the Cape Roberts Project
Ross Sea, Antarctica

Initial Report on CRP-3

GUEST EDITORS

Peter J. Barrett, Massimo Sarti & Sherwood Wise

Cape Roberts Project
antarctica

Editorial Policy

Terra Antartica (ISSN 1122-8628) - established in 1994 - aims to favour the exchange of ideas and results in the field of Antarctic Earth Sciences. Contributions to the development of Antarctic Geology, Geophysics, Glacial Geology, and Glaciology from related areas, bordering Sciences, and technological advancement are expected. The Journal is open to the international community and is distributed worldwide. It publishes two issues per year. Additional thematic issues, devoted to specific topics and meetings, can also be published.

Publications should be in the form of articles, short notes, letters, and summary reports. Review papers on relevant topics may be accepted.

The Editorial Advisory Board will undertake the responsibility of refereeing procedure for the manuscripts. Guest-editors will undertake the responsibility of refereeing procedure for manuscripts for thematic issues.

The two issues will appear the first within the end of June and the second within the end of December. Instructions for contributors are reported on the inside back cover.

Subscription rates

2000

	UE countries	*Other countries*
Professionals	27 Euros	32 Euros
Students	15 Euros	20 Euros
Institutions	80 Euros	85 Euros

Overcharge for air mail despatch: 8 Euros/year.

Orders for subscriptions should be sent to *Terra Antartica Publication* (see addrress below). Back issues are still available (except Volume 1); prices are the same as 2000.

The price of one single issue is 40 Euros.

Terra Antartica
Publication

Museo Nazionale dell'Antartide '*Felice Ippolito*'
Sezione Scienze della Terra - Università degli Studi di Siena
Via del Laterino 8, 53100 Siena (Italia)
e-mail terranta@mna.unisi.it
fax ++39-0577-233 817

TERRA ANTARTICA
An International Journal on Antarctic Sciences
Volume 7, Number 1/2 - 2000

Studies from the Cape Roberts Project
Ross Sea, Antarctica

Initial Report on CRP-3

Contents

Foreword

This volume is the fifth of six issues of *Terra Antartica* to present the results of the Cape Roberts Project. In this project the Antarctic programmes of Australia, Britain, Germany, Italy, New Zealand, and the United States of America have collaborated to take a series of cores off the Antarctic coast. The coring is being carried out with a drilling rig set on the fast sea-ice to investigate climatic and tectonic history of the region (Barrett & Davey, 1992; International Steering Committee, 1994).

The first season's drilling in 1997, curtailed at a depth of 148 mbsf (metres below sea floor) after a storm-generated ice break-out, found a novel sea-ice-free carbonate facies in Quaternary strata and showed the younger part of the dipping strata off Cape Roberts to be around 17 Ma, some 10 m.y. younger than expected (Cape Roberts Science Team, 1998; Hambrey, Wise et al., 1998). In the second season, thicker sea ice provided time to overcome drilling problems with a difficult substrate, yielding 624 m of core with over 95% recovery. The occurrence of several volcanic-ash layers, a range of microfossil taxa, plus dating with Sr-isotopes and magnetostratigraphy, have provided a refined chronology for the numerous episodes of glacial advance and retreat recorded in the core (Cape Roberts Science Team, 1999; Barrett et al., in press).

Here we report on the successful drilling of CRP-3 to a depth of 939 mbsf with 97% recovery, completing the sampling of around 1 800 m of strata from the Cape Roberts sequence imaged along seismic line NBP9601-89. Sea-ice conditions were again good and the sea riser performed well in the deeper water. Drilling conditions were also good for most of the hole, though there were a number of drilling challenges at fault zones, loose sand intervals and at the altered margins of an intrusion encountered at 921 mbsf. Indeed, it was the second altered zone that led to the cessation of drilling. Nevertheless, CRP-3 must be seen as a technological triumph for the drill crew, exceeding the target depth by 239 m and becoming the deepest bedrock hole in Antarctica by a similar amount (CIROS-1 in 1986 was 702 m deep).

The Cape Roberts Science Team of some 60 scientific, technical and support staff also had its challenges in describing, sampling and reporting on over 900 m of core from one of the most complex depositional settings on earth, and to a tight publication deadline. We thank all of those who took part in the project for their commitment to producing and reporting on the core in a timely way. We also look forward in late 2000 to the final Cape Roberts special issue, the Scientific Report, with a more detailed analysis of results of the 1999 drilling, and to further publication in the open literature.

Peter Barrett

Carlo Alberto Ricci

November 1999

REFERENCES

Barrett P.J., Davey F.J., Ehrmann W.U., Hambrey M.J., Jarrard R., van der Meer J.J.M., Raine J., Roberts A.P., Talarico F. & Watkins D.H. (eds.), in press. Studies from the Cape Roberts Project, Ross Sea, Antarctica. Scientific Report on CRP-2/2A. *Terra Antartica.*

Barrett P.J. & Davey F.J., 1992. Cape Roberts Project Workshop Report. *Royal Society of New Zealand, Miscellaneous Series,* **23,** 38 p.

Cape Roberts Science Team, 1998. Initial Report on CRP-1, Cape Roberts Project, Antarctica. *Terra Antartica,* **5**(1), 1-187.

Cape Roberts Science Team, 1999. Studies from the Cape Roberts Project, Ross Sea, Antarctica. Initial Report on CRP-2/2A. *Terra Antartica,* **6**(1/2), 1-173, with Supplement, 245 p.

International Steering Committee, 1994. Cape Roberts Project - coring for Antarctic tectonic and climatic history. *EOS,* **75**(1), 2-3.

Hambrey M.J., Wise S.W., Barrett P.J., Davey F.J., Ehrmann W.U. Smellie J.L., Villa G. & Woolfe K.J. (eds.), 1998. Scientific Report on CRP-1, Cape Roberts Project, Antarctica. *Terra Antartica,* **5**(3), 713 p.

ACKNOWLEDGEMENTS

Scientific work for the Cape Roberts Project is supported through numerous grants from a range of government funding agencies in Australia, Britain, Germany, Italy, New Zealand and the United States of America. The Netherlands has also contributed through a grant from the Netherlands Science Foundation.

Support for the project from the US National Science Foundation, Crary Science and Engineering Center (CSEC) at McMurdo Station was exceptional, and for this we are grateful to Robbie Score and her staff. We are also most grateful to Steve Kottmeier, Jay Burnside and the science construction staff of Antarctic Support Associates (ASA) for help at McMurdo Station, and to Bill Haals, ASA Operations Manager McMurdo and Phil Parfett, ASA Fleet Operations Supervisor and their team for assistance in hauling fuel and resupply items across McMurdo Sound. The help of divers from CSEC (Rob Robbins and minder Robbie Score) for installing and recovering the air bags under the sea ice beneath the drill rig was also appreciated.

We also thank Pat Cooper and the drilling team for their skill, perseverance and ultimate success in this, the last hole of the series. Bain Webster and Johnny Hampton provided advice and consultation to the drilling operation. We are grateful to Jim Cowie and support staff for their work in the WINFLY period, maintenance of Cape Roberts camp and supplies. Alex Pyne once again chose a good sea ice site and ensured it was kept in good shape, along with his other science management tasks. ASA personnel in Denver processed DMSP satellite images, and Bob Onstott (ERIM) processed SAR images of the early season sea ice for Cape Roberts Project operations. Murray Knox carried out sea ice thickness and movement measurements in the drill site area. John Alexander, as Scott Base Liaison Officer, smoothed the path between McMurdo Station, Scott Base and Cape Roberts. Scott Base staff were also always ready to help, and especially for urgent engineering.

DMT, Essen, Germany, helped to support the project by providing access to the CoreScan® and software for scanning whole round core and core box images at reduced rates. We are grateful to Dr G. Rafat, DMT, for his time in setting up the CoreScan® at the Drill Site Laboratory.

Finally, a special thanks from the Cape Roberts Science Team to Jim Cowie, Project Manager, Alex Pyne, Science Support Manager and Pat Cooper, Drilling Manager for their collective leadership and commitment through the three seasons of drilling to get the most and the best core possible from the Cape Roberts sequence in a safe and timely way a well-judged path.

Ken Woolfe

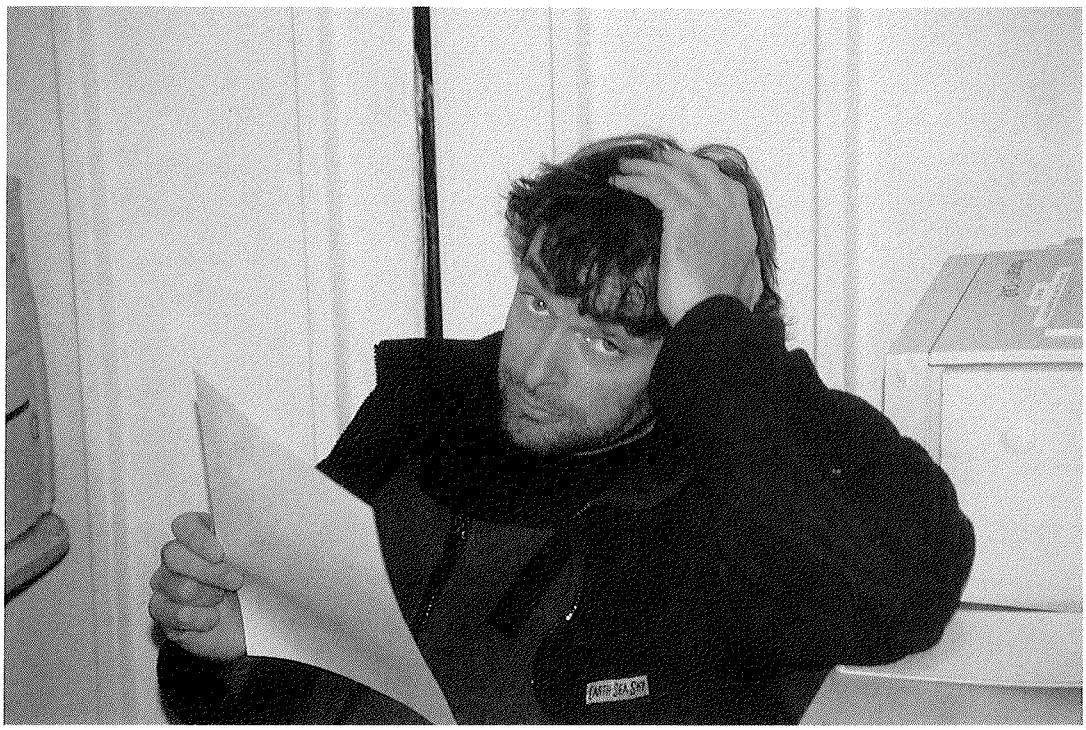

This issue with its supplement is dedicated to the memory of Ken Woolfe (1965-1999), man of many talents - scientist, outdoorsman, computer draughtsmaster, strategist, colleague and friend of the Cape Roberts Project. Ken died unexpectedly in Townsville, Australia, 2 days after returning from a successful 2 months with the Cape Roberts Project in Antarctica.

Ken's interest in the Antarctic began when, as a second year Geology student, he was selected to join a field party from Victoria University of Wellington. He went to the ice as assistant for a PhD student collecting samples from high peaks in the Beardmore Glacier area. Three years later he returned to the Antarctic after gaining support for a PhD project under Peter Barrett's supervision to survey the Beacon Supergroup strata over a 300 km length of the Transantarctic Mountains. The survey took 4 field seasons and involved over thousand kilometres of motor toboggan travel.

Ken graduated with his PhD in 1991, and soon after took a position as Lecturer in Environmental geology & Sedimentology at James Cook University of North Queensland in Townsville. There he developed a research interest in sedimentation in the Gulf of Papua and around the Great Barrier Reef.

Despite his new tropical base he still found a way in 1995 to return to the Antarctic. He did this by seeing the value of applying sequence stratigraphy to the study of glacial history from strata around the Antarctic margin, and then approaching the developing Cape Roberts Project for a place for Australia in the international consortium.

Ken was a tireless supporter of the Cape Roberts Project at every level, from the mind-numbing hours spent in draughting 1:20 scale logs (over 200 pages for CRP-3) to the scientific issues to the leadership he was showing in developing an international group to support drilling operations in a range of environments around the Antarctic margin. His written legacy is in over 50 papers in refereed journals and about 10 in review. Beyond that and over the last 20 years (or possibly longer) he has enthused, stimulated and challenged all of those around him. Such achievement, what a life, and what a loss.

Cape Roberts Project Personnel

INTERNATIONAL STEERING COMMITTEE

Professor Maria Bianca Cita
Dipartimento di Scienze della Terra
Università degli Studi di Milano
Via L. Mangiagalli 34, I 20133 Milano
ITALY
e-mail: cita@imiucca.csi.unimi.it

Dr Fred Davey
Institute of Geological & Nuclear Sciences Ltd
P O Box 30368, Lower Hutt
NEW ZEALAND
e-mail: f.davey@gns.cri.nz

Dr Franz Tessensohn
Bundesanstalt für Geowissenschaften und Rohstoffe
Stilleweg 2, D-30655 Hannover
GERMANY
e-mail: Franz.Tessensohn@bgr.de

Dr Mike Thomson
British Antarctic Survey
High Cross, Madingley Road, Cambridge CB3 0ET
UNITED KINGDOM
e-mail: m.thomson@bas.ac.uk

Professor Peter Webb
Department of Geological Sciences
Ohio State University
Columbus, Ohio 43210
UNITED STATES OF AMERICA
e-mail: webb.3@osu.edu

Dr Ken Woolfe
School of Earth Sciences
James Cook University
Townsville, Queensland 4811
AUSTRALIA
deceased

OPERATIONS/LOGISTICS MANAGEMENT GROUP

Ms Gillian Wratt (Convener)
Antarctica NZ
Private Bag 4745
Christchurch
NEW ZEALAND

Mr Erick Chiang
Office of Polar Programs
National Science Foundation
4201 Wilson Boulevard
Arlington, Virginia 22230
UNITED STATES OF AMERICA

Dr Ken Woolfe
School of Earth Sciences
James Cook University
Townsville, Queensland 4811
AUSTRALIA

Dr John Dudeney
British Antarctic Survey
High Cross Madingley Road
Cambridge CB3 OET
UNITED KINGDOM

Dr Mario Zucchelli
ENEA
Via Anguillarese, 3301 - Roma
00100 Roma AD
ITALY

Professor Dieter Fütterer
Alfred-Wegener-Institut
Postfach 12 01 81
D-27516 Bremerhaven
GERMANY

ADVISOR

Dr Scott Borg
National Science Foundation
4201 Wilson Boulevard
Arlington, Virginia 22230
UNITED STATES OF AMERICA

SCIENCE PARTICIPANTS

Professor Peter Barrett
Chief Scientist
School of Earth Sciences
Victoria University of Wellington
P O Box 600, Wellington
NEW ZEALAND
e-mail: Peter.Barrett@vuw.ac.nz

Professor Peter Webb
Crary Lab Science Leader
Department of Geological Sciences
Ohio State University
Columbus Ohio 43210
UNITED STATES OF AMERICA
e-mail: webb.3@osu.edu

Dr Fulvia Aghib
Sedimentologist
Dipartimento di Scienze della Terra
Università degli Studi di Milano
Via Mangiagalli 34, 20133 Milano
ITALY
e-mail: f.aghib@e35.gp.terra.unimi.it

Dr Mauro Alberti
Illustrator
Museo Nazionale dell'Antartide
Via del Laterino 8, 53100 Siena
ITALY
e-mail: alberti@mna.unisi.it

Ms Jo Anderson
Core Processing Technician
School of Earth Sciences
Victoria University of Wellington
P O Box 600, Wellington
NEW ZEALAND
e-mail: jo.anderson@vuw.ac.nz

Dr Rosemary Askin
Palynologist
Byrd Polar Research Center
Ohio State University
Columbus, Ohio 43210
UNITED STATES OF AMERICA
e-mail: askin.1@osu.edu

Mr Cliff Atkins
Technician/Sedimentologist
School of Earth Sciences
Victoria University of Wellington
P O Box 600, Wellington
NEW ZEALAND
e-mail: cliff.atkins@vuw.ac.nz

Mr Steven Bohaty
Palaeontologist (siliceous microfossils)
Department of Geosciences
University of Nebraska - Lincoln
Lincoln, Nebraska 68588-0340
UNITED STATES OF AMERICA
e-mail: sbohaty@unlserve.unl.edu

Ms Sonia Bryce
Assistant to Science Support Manager
Department of Geology
James Cook University
Townsville, Q 4811
AUSTRALIA
e-mail: sonya.bryce@jcu.edu.au

Dr Christian Bücker
Downhole Logger
Geowissenschaftliche Gemeinschaftsaufgaben
Stilleweg 2, D-30655 Hannover
GERMANY
e-mail: c.buecker@gga-hannover.de

Mr Stewart Bush
Thin Section Technician
School of Earth Sciences
Victoria University of Wellington
P O Box 600, Wellington
NEW ZEALAND
e-mail: stewart.Bush@vuw.ac.nz

Dr Michele Claps
Sedimentologist
Istituto di Scienze del Mare
Università degli Studi di Ancona
Via Brecce Bianche, 60131 Ancona
ITALY
e-mail: cli@dns.unife.it

Mr Matthew Curren
Assistant Core Curator
Antarctic Marine Geology Research Facility
108 Carraway Bldg., Florida State University
Tallahassee, Florida 32306-4100
UNITED STATES OF AMERICA
e-mail: curator@gly.fsu.edu

Dr Chris Fielding
Sedimentologist
Department of Earth Sciences
University of Queensland
Brisbane, QLD 4072
AUSTRALIA
e-mail: chrisf@earthsciences.uq.edu.au

Dr Fabio Florindo
Palaeomagnetist
Istituto Nazionale di Geofisica
Via di Vigna Murata 605, 00143 Roma
ITALY
e-mail:florindo@ing750.ingrm.it

Dr Simone Galeotti
Palaeontologist (foraminifera)
Istituto di Geologia
Università degli Studi di Urbino
Campus Scientifico, Loc. Crocicchia, 61029 Urbino
ITALY
e-mail: s.galeotti@uniurb.it

Dr Michael Hannah
Palynologist
School of Earth Sciences
Victoria University of Wellington
P O Box 600, Wellington
NEW ZEALAND
e-mail: michael.hannah@vuw.ac.nz

Mr Adam Harris
Palaeomagnetist Technician
Department of Geology
University of California
Davis, California 95616
UNITED STATES OF AMERICA
e-mail: harris@geology.ucdavis.edu

Professor David Harwood
Palaeontologist (siliceous microfossils)
Department of Geosciences
University of Nebraska - Lincoln
Lincoln, Nebraska 68588-0340
UNITED STATES OF AMERICA
e-mail: dharwood@unlserve.unl.edu

Dr Stuart Henrys
Marine Geophysicist
Institute of Geological & Nuclear Sciences
P O Box 30368, Lower Hutt
NEW ZEALAND
e-mail: s.henrys@gns.cri.nz

Mr Nick Jackson
Core Processing Technician
School of Earth Sciences
Victoria University of Wellington
P O Box 600, Wellington
NEW ZEALAND
e-mail: Nick.Jackson@vuw.ac.nz

Dr Thomas Janecek
Core Curator
Antarctic Marine Geology Research Facility
108 Carraway Bldg., Florida State University
Tallahassee, Florida 32306-4100
UNITED STATES OF AMERICA
e-mail: curator@gly.fsu.edu

Dr Richard Jarrard
Downhole Logging
Department of Geology and Geophysics
University of Utah
Salt Lake City, Utah 84112
UNITED STATES OF AMERICA
e-mail: jarrard@mines.utah.edu

Ms Shelley Judge
Core Scanning Technician
Department of Geological Sciences
Ohio State University
Columbus, Ohio 43210
UNITED STATES OF AMERICA
e-mail: judge.4@osu.edu

Dr Conrad Kopsch
Physical Properties Technician
Alfred-Wegener-Institut
Postfach 12 01 81, 27516 Bremerhaven
GERMANY

Professor Lawrence Krissek
Sedimentologist
Department of Geological Sciences
Ohio State University
Columbus, Ohio 43210
UNITED STATES OF AMERICA
e-mail: krissek@mps.ohio-state.edu

Dr Malcolm Laird
Sedimentologist
Department of Geological Sciences
University of Canterbury
Private Bag 4800, Christchurch
NEW ZEALAND
e-mail: m.laird@geol.canterbury.ac.nz

Dr Mark Lavelle
Sedimentologist
British Antarctic Survey
High Cross, Madingley Road, Cambridge CB3 0ET
UNITED KINGDOM
e-mail: m.lavelle@bas.ac.uk

Mr Wojciech Majewski
Micropalaeontology Technician
Department of Geological Sciences
Ohio State University
Columbus, Ohio 43210
UNITED STATES OF AMERICA
e-mail: majewski.9@osu.edu

Dr Tim Naish
Sedimentologist/Stratigrapher
Institute of Geological & Nuclear Sciences
P O Box 30 368, Lower Hutt
NEW ZEALAND
e-mail: t.naish@gns.cri.nz

Mr Marco Neumann
Sedimentologist
Institut für Geophysik und Geologie
Universität Leipzig
Talstrasse 35, D-04103 Leipzig
GERMANY
e-mail: ehrmann@rz.uni-leipzig.de

Dr Frank Niessen
Physical Properties Specialist
Alfred-Wegener-Institut
Postfach 12 01 81, 27516 Bremerhaven
GERMANY
e-mail: fniessen@awi-bremerhaven.de

Mr Matt Paterson
Core Processing Technician
School of Earth Sciences
Victoria University of Wellington
P O Box 600, Wellington
NEW ZEALAND
e-mail: Matt.Paterson@vuw.ac.nz

Dr Timothy Paulsen
Structural Geologist
Department of Geology
University of Wisconsin
Oshkosh, Wisconsin 54901
UNITED STATES OF AMERICA
e-mail: paulsen@uwosh.edu

Dr Massimo Pompilio
Petrologist
Istituto Internazionale di Vulcanologia
CNR
Piazza Roma 2, 95123 Catania
ITALY
e-mail: max@iiv.ct.cnr.it

Professor Ross Powell
Sedimentologist
Department of Geology and Environmental Geosciences
Northern Illinois University
DeKalb, Illinois 60115
UNITED STATES OF AMERICA
e-mail: ross@geol.niu.edu

Mr Alex Pyne
Sea Ice Specialist
School of Earth Sciences
Victoria University of Wellington
P O Box 600, Wellington
NEW ZEALAND
e-mail: alex.pyne@vuw.ac.nz

Dr Ghodrat Rafat
Core Scanning Technician
DMT - GeoTec
Franz-Fisher-Weg 61, D-45307 Essen
GERMANY
e-mail: rafat@geotec.dmt-fp.cubis.de

Dr Ian Raine
Palaeontologist (terrestrial palynomorphs)
Institute of Geological & Nuclear Sciences
P O Box 30 368, Lower Hutt
NEW ZEALAND
e-mail: i.raine@gns.cri.nz

Dr Andrew Roberts
Palaeomagnetist
School of Ocean & Earth Science, Univ. of Southampton
Southampton Oceanography Centre
European Way, Southampton SO14 3ZH
UNITED KINGDOM
e-mail: arob@mail.soc.soton.ac.uk

Dr Leonardo Sagnotti
Palaeomagnetist
Istituto Nazionale di Geofisica
Via di Vigna Murata 605, 00143 Roma
ITALY
e-mail: sagnotti@marte.ingrm.it

Ms Sonia Sandroni
Petrologist/Editorial Assistant
Dipartimento di Scienze della Terra
Università degli Studi di Siena
Via del Laterino 8, 53100 Siena
ITALY
e-mail: sandroni@unisi.it

Dr Massimo Sarti
Sedimentologist
Istituto di Scienze del Mare
Università degli Studi di Ancona
Via Brecce Bianche, 60131 Ancona
ITALY
e-mail: m.sarti@fastnet.it

Mr Peter Schulze
Downhole Logging Technician
Geowissenschaftliche Gemeinschaftsaufgaben
Stilleweg 2, D-30655 Hannover
GERMANY

Mr John Simes
Palynology Technician
Institute of Geological & Nuclear Sciences
P O Box 30 368, Lower Hutt
NEW ZEALAND
e-mail: j.simes@gns.cri.nz

Dr John Smellie
Petrologist
British Antarctic Survey
High Cross, Madingley Road
Cambridge CB3 0ET
UNITED KINGDOM
e-mail: j.smellie@bas.ac.uk

Mr Bruce Smith
Teacher Experiencing Antarctica
Appleton North High School
5000 N. Ballard Road
Appleton, Wisconsin 54915
UNITED KINGDOM
e-mail: j.smellie@bas.ac.uk

Mr Alfredo Sorice
Palaeomagnetist Technician
Istituto Nazionale di Geofisica
Via di Vigna Murata 605, 00143 Roma
ITALY
e-mail: sorice_a@ing750.ingrm.it

Dr Percy Strong
Palaeontologist (foraminifera)
Institute of Geological & Nuclear Sciences
P O Box 30 368, Lower Hutt
NEW ZEALAND
e-mail: p.strong@gns.cri.nz

Dr Franco Talarico
Petrologist
Dipartimento di Scienze della Terra
Università degli Studi di Siena
Via del Laterino 8, 53100 Siena
ITALY
e-mail: talaf@ dst.unisi.it

Dr Marco Taviani
Palaeontologist (macrofossils)
Istituto di Geologia Marina, CNR
Via Gobetti 101, I-40129 Bologna
ITALY
e-mail: taviani@igm.bo.cnr.it

Dr Vanessa Thorn
Photography Technician
School of Earth Sciences
Victoria University of Wellington
P O Box 600, Wellington
NEW ZEALAND
e-mail: drvan@paradise.net.nz

Professor Kenneth Verosub
Palaeomagnetist
Department of Geology
University of California
Davis, California 95616
UNITED STATES OF AMERICA
e-mail: verosub@geology.ucdavis.edu

Dr David Watkins
Palaeontologist (calcareous nannofossils)
Department of Geosciences
University of Nebraska
Lincoln, Nebraska 68588-0340
UNITED STATES OF AMERICA
e-mail: dwatkins1@unl.edu

Dr Gary Wilson
Palaeomagnetist
Department of Earth Sciences
University of Oxford
Parks Road, Oxford, OXI 3PR
UNITED KINGDOM
e-mail: gary.wilson@earth.ox.ac.uk

Dr Terry Wilson
Structural Geologist
Byrd Polar Research Center
Ohio State University
Columbus, Ohio 43210
UNITED STATES OF AMERICA
e-mail: twilson@mps.ohio-state.edu

Professor Sherwood Wise
Palaeontologist (calcareous nannofossils)
Department of Geology, 4100
Florida State University
Tallahassee, Florida 32306
UNITED STATES OF AMERICA
e-mail: wise@geomag.gly.fsu.edu

Dr Ken Woolfe
Sedimentologist
School of Earth Sciences
James Cook University
Townsville, Q 4811
AUSTRALIA
deceased

Dr John Wrenn
Palynologist
Department of Geology and Geophysics
Louisiana State University
Baton Rouge, Louisiana 70803
UNITED STATES OF AMERICA
e-mail: wrenn@gcol.lsu.edu

PROJECT STAFF

Mr Jim Cowie
Project Manager
Antarctica NZ
Private Bag 4745
Christchurch
NEW ZEALAND
e-mail: j.cowie@antarcticanz.govt.nz

Mr Alex Pyne
Science Support Manager
School of Earth Sciences
Victoria University of Wellington
P O Box 600, Wellington
NEW ZEALAND
e-mail: alex.pyne@vuw.ac.nz

Mr Pat Cooper
Drilling Manager
Rapid Creek, Waimangaroa
Westport
NEW ZEALAND

Mr John Alexander
Cape Roberts Liaison Officer
P O Box 314
Queenstown
NEW ZEALAND

WINFLY TEAM

Jim Cowie	Project Manager
Alex Pyne	Science Support Manager
Chris Hayes	Plant Operator/Mechanic
Murray Knox	Plant Operator
Colleen Clarke	Camp Manager/Paramedic
Brian Reid	Electrician
Jeremy Ridgen	Mechanic
Peter Sinclair	Carpenter
Richard Struthers	Carpenter/Field Assistant

CAMP SUPPORT

Alison Ward	Chef
Kath Varcoe	General Duties

DRILLERS

Pat Cooper	Drilling Manager
Malcolm Macdonald	Driller
Frank Tansey	Driller
Michael Avey	Assistant Driller
Chris Collie	Assistant Driller
David Eaton	Assistant Driller
Tony Kingan	Assistant Driller
Todd Symons	Assistant Driller
Sam Woodford	Assistant Driller
John Moore	Assistant Driller
Michael Archer	Assistant Driller

Terra Antartica
Initial Report on CRP-3
2000, 7(1/2), 1-209

Studies from Cape Roberts Project
Initial Report on CRP-3, Ross Sea, Antartica

Cape Roberts Science Team*

Abstract - The site for CRP-3, 12 km east of Cape Roberts (77.006° S; 163.719° E), was selected to overlap the lower Oligocene strata cored in nearby CRP-2/2A, and to sample the oldest strata in the Victoria Land Basin (VLB) for Paleogene climatic and tectonic history. As it transpired there was underlap of the order of 10s of metres. CRP-3 was cored from 3 to 939 mbsf (metres below the sea floor), with a core recovery of 97%. Coring took place from October 9 to November 19, 1999, on 2.0 to 2.2 m of sea ice and through 295 m of water. The Cenozoic strata cored were mostly glacially influenced marine sediments of early Oligocene age, though they may be earliest Eocene near the base, where at 823 mbsf Devonian Beacon sandstone was encountered. Following CRP-1 and CRP-2/2A, CRP-3 completes the coring of 1500 m of strata on the western margin of the VLB.

Core fractures and other physical properties, such as sonic velocity, density and magnetic susceptibility, were measured throughout the core. Down-hole logs for these and other properties were taken from 20 down to 900-919 mbsf. Also, vertical seismic profile data were gathered from shots offset both along strike and up dip from the hole. Sonic velocities in CRP-3 are close to 2.0 km/s in the upper 80 m, but become significantly faster below 95 mbsf, averaging 3.2+0.6 km/s to the bottom of the hole. An exception to this is an interval of dolerite conglomerate from 790 to *c.* 820 mbsf with a velocity of *c.* 4.5 km/s. Dip of the strata also increases down-hole from 10° in the upper 100 m to around 22° at the bottom. Over 3000 fractures were logged through the hole, and borehole televiewer imagery was obtained for most of the hole for orienting core and future stress field analysis. Two high-angle crush zones, interpreted as faults, were encountered at *c.* 260 and *c.* 540 mbsf, but no stratigraphic displacement could be recognised. A third fault zone is inferred from a low angle shear zone in the upper part of a coarse dolerite conglomerate from 790 to 805 mbsf. Temperature gradient was found to be $28.5°.km^{-1}$

Basement strata cored from 823 mbsf to the bottom of the hole are largely light-reddish brown medium-grained sandstone (quartz-cemented quartzarenite) with abundant well-defined parallel lamination. These features are comparable with the middle Devonian part of the Beacon Supergroup, possibly the Arena Sandstone. This interval also includes a body of intrusive rock from 901 to 920 mbsf. It has brecciated contacts and is highly altered but some tholeiitic affinity can be recognised in the trace element chemistry. Its age is unknown.

Post-Beacon sedimentation began on deeply eroded quartzarenite with the deposition of a thin sandstone breccia and conglomerate, probably as terrestrial talus, followed by dolerite conglomerate and minor sandstone of probable fluvial origin to 790 mbsf. Sedimentation continued in a marine setting, initially sandstone and conglomerate, but above *c.*330 mbsf the strata include mudstone and diamictite also. The older sandstone and conglomerate beds are seen as the products of rapid episodic sedimentation. They are interpreted by some as the product of glaciofluvial discharge into shallow coastal waters, and others as a result of sediment gravity flows, perhaps glacially sourced, into deeper water. The core above *c.* 330 mbsf has facies that allow the recognition of cyclic sequences similar to those in CRP-2A. Fourteen unconformity-bounded sequences have been recognised from 330 mbsf to the sea floor, and are interpreted in terms of glacial advance and retreat, and sea level fall and rise. Detailed lithological descriptions on a scale of 1:20 are presented for the full length of the core, along with core box images, as a 300 page supplement to this issue.

The strata cored by CRP-3 are for the most part poorly fossiliferous, perhaps as a consequence of high sedimentation rates. Nevertheless the upper 200 m includes several siliceous microfossil- and calcareous nannoplankton-bearing intervals. Siliceous microfossils, including diatoms, ebrideans, chrysophycean cysts and silicoflagellates are abundant and well-preserved in the upper 67 m – below this level samples are barren or poorly preserved, but contain residual floras that indicate assemblages were once rich. No siliceous microfossils were found below 193 mbsf.

*F. Aghib, M. Alberti, J. Anderson, R. Askin, C. Atkins, S. Bannister, P.J. Barrett, S. Bohaty, S. Bryce, C. Bücker, S. Bush, M. Claps, M. Curren, C. Fielding, F. Florindo, S. Galeotti, M. Hannah, A. Harris, D.H. Harwood, S. Henrys, N. Jackson, T. Janecek, R. Jarrard, S. Judge, C. Kopsch, L. Krissek, M. Laird, M. Lavelle, W. Majewski, T. Naish, M. Neumann, F. Niessen, M. Paterson, T. Paulsen, M. Pompilio, R. Powell, A. Pyne, G. Rafat, I. Raine, A. Roberts, L. Sagnotti, S. Sandroni, M. Sarti, J. Simes, J.L. Smellie, B. Smith, A. Sorice, P. Strong, F. Talarico, M. Taviani, V. Thorn, K. Verosub, D. Watkins, P.N. Webb, G. Wilson, T. Wilson, S. Wise, K. Woolfe, J. Wrenn

Calcareous nannofossils have a similar distribution but are generally well preserved. Foraminifera, marine and terrestrial palynomorphs, and marine macrofossils were found consistently down to *c.* 330 mbsf and sporadically to 525 mbsf. The taxa suggest marine deposition in water depths of *c.* 50 to 120 m. Below 525 mbsf no microfossils were found, apart from a mudstone with similar marine and terrestrial palynomorphs at 781 mbsf, and rare miospores in the conglomerate below 790 mbsf. The terrestrial miospore record, which includes several species of *Nothofagus* and podocarpaceous conifers, suggests low diversity woody vegetation, implying a cold temperate to periglacial climate for the hinterland throughout the period recorded by CRP-3. Important components of the warmer Eocene flora, known from erratics in southern McMurdo Sound, are missing, though the dominance of smectites in clays from strata below 650 mbsf suggests that the landscape prior to the time of deposition had experienced a more temperate weathering regime.

Biostratigraphy for the upper part of CRP-3 is provided by diatoms and calcareous nannofossils. The first appearance of *Cavitatus jouseanus* at 48 mbsf suggests an age of around 31 Ma for this horizon. The last appearance of *Transverspontis pulcheroides* at 114 mbsf in an interval of relatively high abundance indicates a reasonably sound age for this horizon at 32.5 $\pm$ 0.5 Ma. The absence of particular resistant diatoms that are older than 33 Ma supports an age that is younger than this for the upper 200 m of CRP-3. Marine palynomorphs, which occur sporadically down to 525 mbsf and in a single occurrence at 781 mbsf, have biostratigraphical potential once the many new species in this and other CRP cores are described, and FO and LO datums established. The mudstone at 781 mbsf has a new dinocyst species, rare *Lejeunecysta* cysts and a variety of acritarchs and prasinophytes, a varied marine assemblage that is quite different from and presumably younger than the well known Transantarctic Flora of mid to late Eocene age. On this basis and for the moment we conclude that the oldest strata in CRP-3 are earliest Oligocene (or possibly latest Eocene) in age – *c.* 34 Ma.

Over 1100 samples were taken for magnetic studies. Four magnetozones were recognised on the basis of NRM intensity and magnetic susceptibility, reflecting the change in sediment composition between quartz sand-dominated and dolerite-dominated. For this report there was time only to produce a magnetostratigraphy for the upper 350 m. This interval is largely of reversed polarity (5 normal intervals total 50 of the 350 m), in contrast to the dominantly normal polarities of CRP-2/2A, and is inferred to be Chron C12R. This extends from 30.9 to 33 Ma, consistent with the biostratigraphic datums from the upper part of CRP-3. The lower limit of reversed polarity has yet to be established. The short period normal events are of interest as they may represent cryptochrons or even polarity changes not recognised in the Geomagnetic Polarity Time Scale.

Erosion of the adjacent Transantarctic Mountains through the Kirkpatrick Basalt (Jurassic tholeiitic flows) and dolerite-intruded Beacon Supergroup (Devonian-Triassic sandstone) into granitic basement beneath is recorded by petrographical studies of clast and sand grain assemblages from CRP-3. The clasts in the lower 30 m of the Cenozoic section are almost entirely dolerite apart from a few blocks from the Beacon Supergroup beneath. Above this, however, both dolerite and granitoids are ubiquitous, the latter indicating that erosion had reached down to granitic basement even as the first sediment was accumulating in the VLB. No clasts or sand grains of the McMurdo Volcanic Group were found, but rare silt-size brown volcanic glass occurs in smear slides through most of CRP-3, and is interpreted as distal air fall from alkaline volcanism in northern Victoria Land. Jurassic basalt occurs as clasts sporadically throughout the sequence; in the sand fraction they decline upwards in abundance. The influence of the Devonian Beacon Supergroup is most striking for the interval from 600 to 200 mbsf, where quartz grains, from 10 to 50% of them rounded, dominate the sand fraction. Laminae of coal granules from the overlying Permian coal measures in all but the upper 150 m of the CRP-3 sequence show that these also were being eroded actively at this time.

CRP-3 core completed the stratigraphical sampling of the western margin of the VLB by not only coring the oldest strata (Seismic Unit V5) but also the basin floor beneath. This has several important tectonic implications:

- most of the Kirkpatrick Basalt and the Beacon Supergroup with the sills of Ferrar Dolerite have been eroded by the time down-faulting displaced the Beacon to form the basin floor.
- matching the Beacon strata at the bottom of CRP-3 with the equivalent strata in the adjacent mountains suggests *c.* 3 000 m of down-to-the-east displacement across the Transantarctic Mountain Front as a consequence of rifting and subsequent tectonic activity.
- the age of the oldest Cenozoic strata in CRP-3 (*c.* 34 Ma), which are also the oldest strata in this section of the VLB, most likely represents the initiation of the rift subsidence of this part of the West Antarctic Rift System.

This age for the oldest VLB fill is much younger than previously supposed by several tens of millions of years, but is consistent with newly documented sea floor spreading data immediately north of the northern Victoria Land continental margin. These new data sets will drive a re-evaluation of the relationship between initiation of uplift of the Transantarctic Mountains (currently *c.*55 Ma) and VLB subsidence.

1 - Introduction

BACKGROUND AND GEOLOGICAL SETTING

BACKGROUND

In this third and final season of drilling by the Cape Roberts Project, the aim was to complete a coring transect from the lower Miocene (17 Ma) strata cored by CRP-1 on Roberts ridge to the Eocene (*c.* 40 Ma) strata expected to lie at relatively shallow depths on the western margin of the Victoria Land Basin (VLB). The project is named after Cape Roberts, the staging point for the offshore drilling and a small promontory 125 km northwest of McMurdo Station and Scott Base (Fig 1.1). The project was designed for two tasks:

- to investigate the early history of the Antarctic ice sheet and the record of Antarctic climate prior to its inception, around 35 million years ago;
- to date the history of rifting of the Antarctic continent as recorded by the uplift of the Transantarctic Mountains and formation of the Victoria Land Basin.

This volume records work carried out from the final drill hole, CRP-3, which completed coring the lowest part of the Cape Roberts sequence at a depth of 939.42 mbsf on 19 November 1999 (Tab. 1.1). This first section outlines the geological setting of the drill site, and then describes the operating environment (climate and sea ice) and drilling activity. Core management and sampling from drill site to the Crary Science & Engineering Center (CSEC) at McMurdo Station are also described. The remainder of the report presents the first results and preliminary interpretations of the data from both the core and logging within the hole itself.

GEOLOGICAL SETTING

The geological setting of the Cape Roberts drill sites has been reviewed previously in Barrett et al. (1995) and

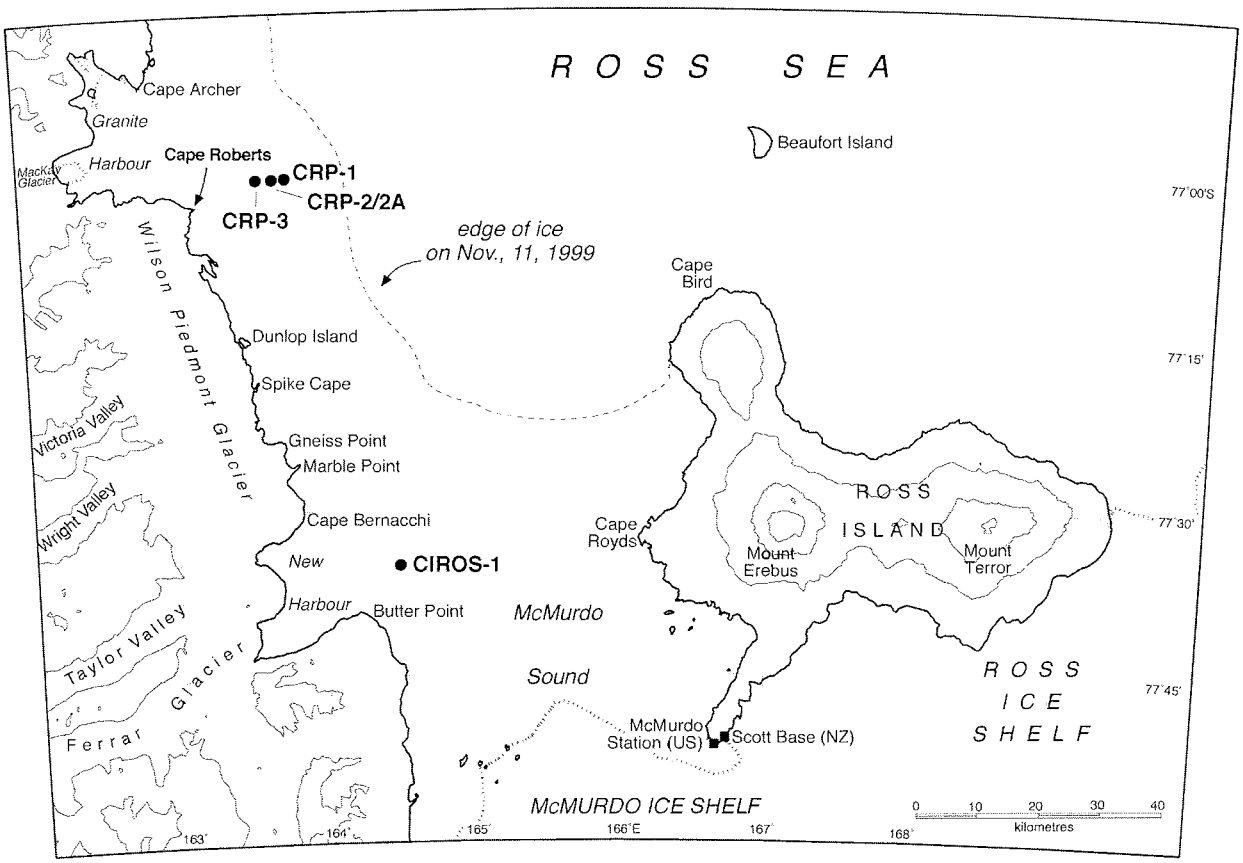

Fig. 1.1 - Map of the southwest corner of the Ross Sea, showing the locations of Cape Roberts, CRP-1, CRP-2/2A, CRP-3, and CIROS-1, and McMurdo Station/Scott Base, the main staging point for the project. The edge of the fast sea-ice, which provides the drilling platform, is also shown.

Tab. 1.1 - Site data for CRP-3.

Position:	11.76 km at 76° true from Cape Roberts	2.04 km at 255° true from CRP-2	
Latitude:	77.0106°S	Longitude:	163.6404°E
Water depth:	295 m	Fast ice thickness:	2.0-2.2 m
First core:	04.00 9 October 1999	Last core:	22.30 19 November 1999
Sea riser embedded to:	9.55 mbsf	Lateral ice movt from spudding:	5.0 m to 82° true
HQ core to:	345.85 mbsf	NQ core to:	939.42 mbsf
Recovery for hole:	97%	Phase 1 logging to:	345 mbsf
Phase 2 logging to:	773 mbsf	Phase 3 logging to:	918 mbsf
Deepest Cenozoic lithology & depth	Sandstone breccia from 822.87 to 823.11 mbsf	Age of oldest Cenozoic strata:	Earliest Oligocene or maybe latest Eocene
Deepest core lithology & depth	Light red-brown quartz-cemented quartz sandstone to 939.42 mbsf	Age of bedrock:	Devonian (probably mid Devonian)

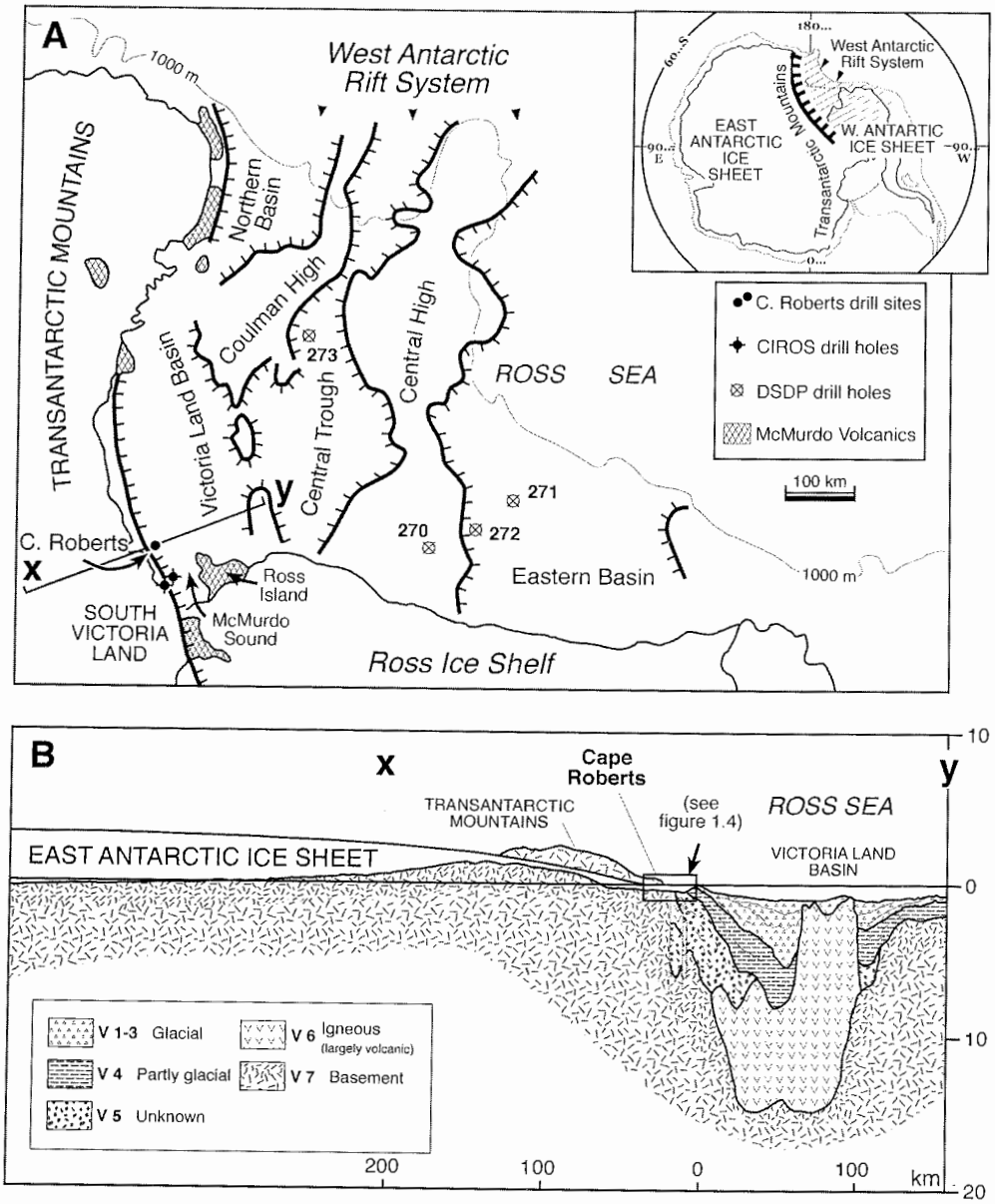

Fig. 1.2 - Map of the Ross continental shelf (A) and cross-section through the edge of the West Antarctic Rift System (B), showing the East Antarctic ice sheet, the Transantarctic Mountains and the Victoria Land Basin.

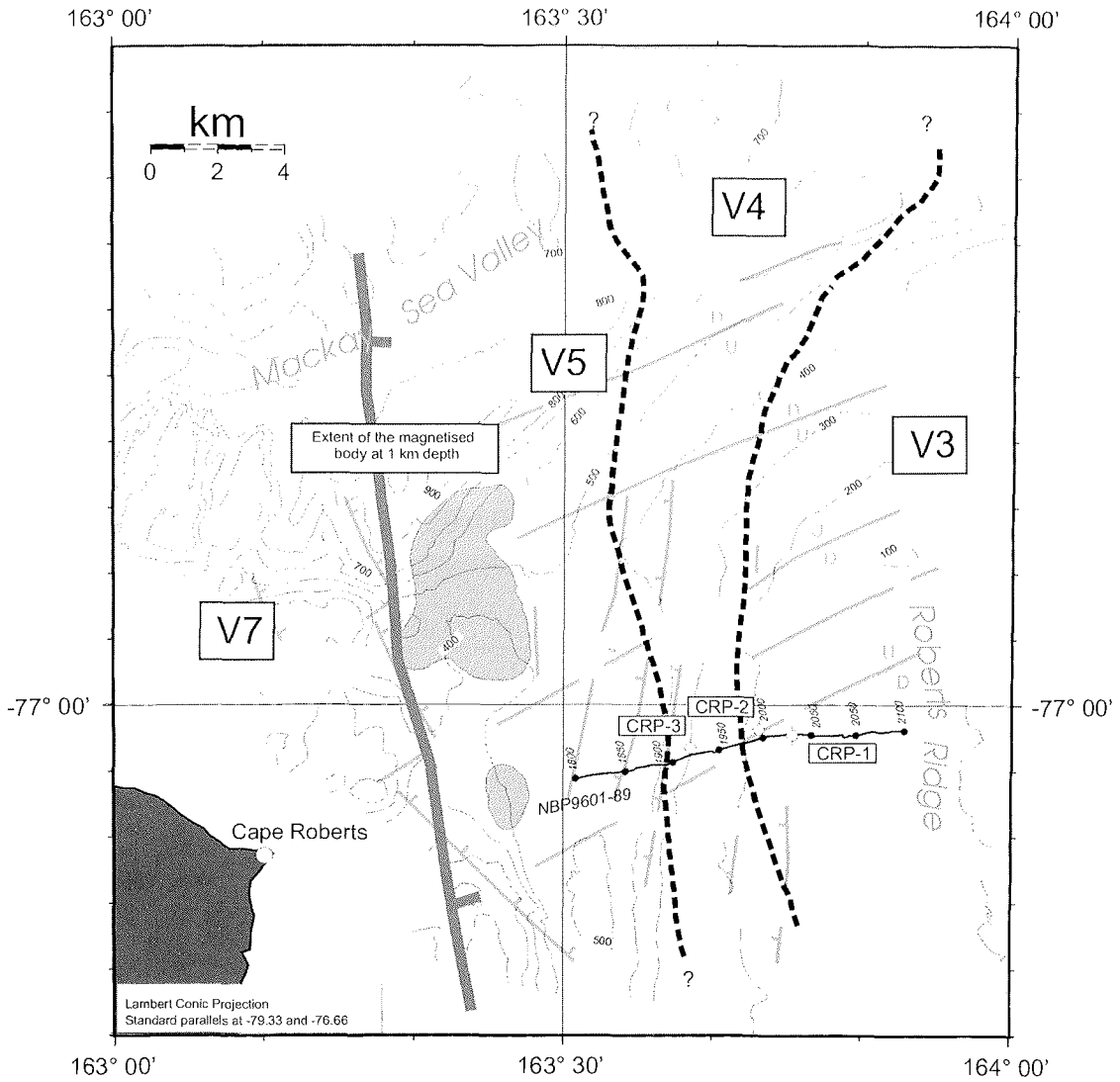

Fig. 1.3 - Map of the area off Cape Roberts (bathymetric contours in 50 metre intervals), showing the location of Roberts ridge, lines from key seismic surveys (dotted), the survey line on which the drill holes are based (solid, with drill sites) and the distribution of the older sedimentary sequences (V3, V4, V5) beneath the sea floor (dashed lines). The major fault inferred by Henrys et al. (1998) and the more complex fault systems interpreted by Hamilton et al. (1998) are also shown.

in last year's report on CRP-2/2A (Cape Roberts Science Team, 1999), and only a few brief comments are repeated here. Roberts ridge and CRP-3 (Fig. 1.2) lie on the western margin of the Victoria Land Basin, a trough at least 400 km long and *c.* 150 km wide filled with sediment of Cenozoic age, immediately seaward of the Transantarctic Mountains. Roberts ridge is separated from the early Palaeozoic basement rocks of the mountains by a major fault system, known as the Transantarctic Mountain Front, which parallels the present coast and represents the western edge of the VLB. Strata in the middle of the basin reach a thickness of 10-14 km, the oldest being interpreted as early rift-related volcanic rocks (Fig. 1.2, V6) (Cooper & Davey, 1987). Above these, lie the older sedimentary seismic sequences, V5 and V4. Through uplift and erosion along the basin margin, they now dip at between 10° and 15° eastward, and lie just beneath the sea floor on the western flank of Roberts ridge, a bathymetric high between 10 and 20 km off Cape Roberts. The younger sequences (V1-V3) are 5 km thick in the middle of the basin but thin to *c.* 300 m on Roberts ridge.

The main structural trend of the VLB is NNW, parallel to the axis of the Transantarctic Mountains. Northwest-trending, seismically defined faults demarcate presumed late Mesozoic half-grabens in the basin floor, and have been interpreted as terminating upward in the sedimentary section (Cooper & Davey, 1987). NNE- and ENE-trending faults have also been recognised in the mountains along the rift margin, and are interpreted to have formed, or have been reactivated, during transtension in more recent times (Wilson, 1995). Similar fault trends have been interpreted from seismic data from the basin margin off Cape Roberts (Hamilton et al., 1999) (Fig. 1.3).

Working backwards in time from the great east-

facing scarp of the present-day Transantarctic Mountains, we can deduce that the adjacent mountains were already deeply eroded and perhaps even approaching their present elevation by the earliest Miocene. This is evident from the dominance of basement lithologies as clasts in strata of this age in CRP-1 and the upper part of CRP-2A (Talarico et al., in press). Oligocene strata from the lower part of CRP-2A have also provided clast data, supported by sand provenance data (Smellie, in press), that suggest more extensive erosion of the cover beds (Beacon Supergroup and Ferrar Dolerite). Age constraints as well as sedimentary features hint at rapid contemporaneous basin subsidence. What did deeper drilling into the basin margin reveal?

OVERVIEW OF CRP-3

CRP-3 was drilled just 2 km west of CRP-2 and sited to overlap it stratigraphically by some 60 m (Fig. 1.4). Results from the hole are presented in the pages that follow, and a summary lithologic log is shown graphically in figure 1.5. The CRP-3 core down to 823 mbsf, where rift-margin bedrock was encountered, provides a continuation of the cold-climate story from CRP-2A back *c.* 34 Ma.Some glacio-eustatic cyclicity is evident, but becomes attenuated as the sediment record becomes increasingly coarser back in time. Despite the considerable thickness of sediment, the current judgement from a sparse microflora is that only 2 or 3 million years

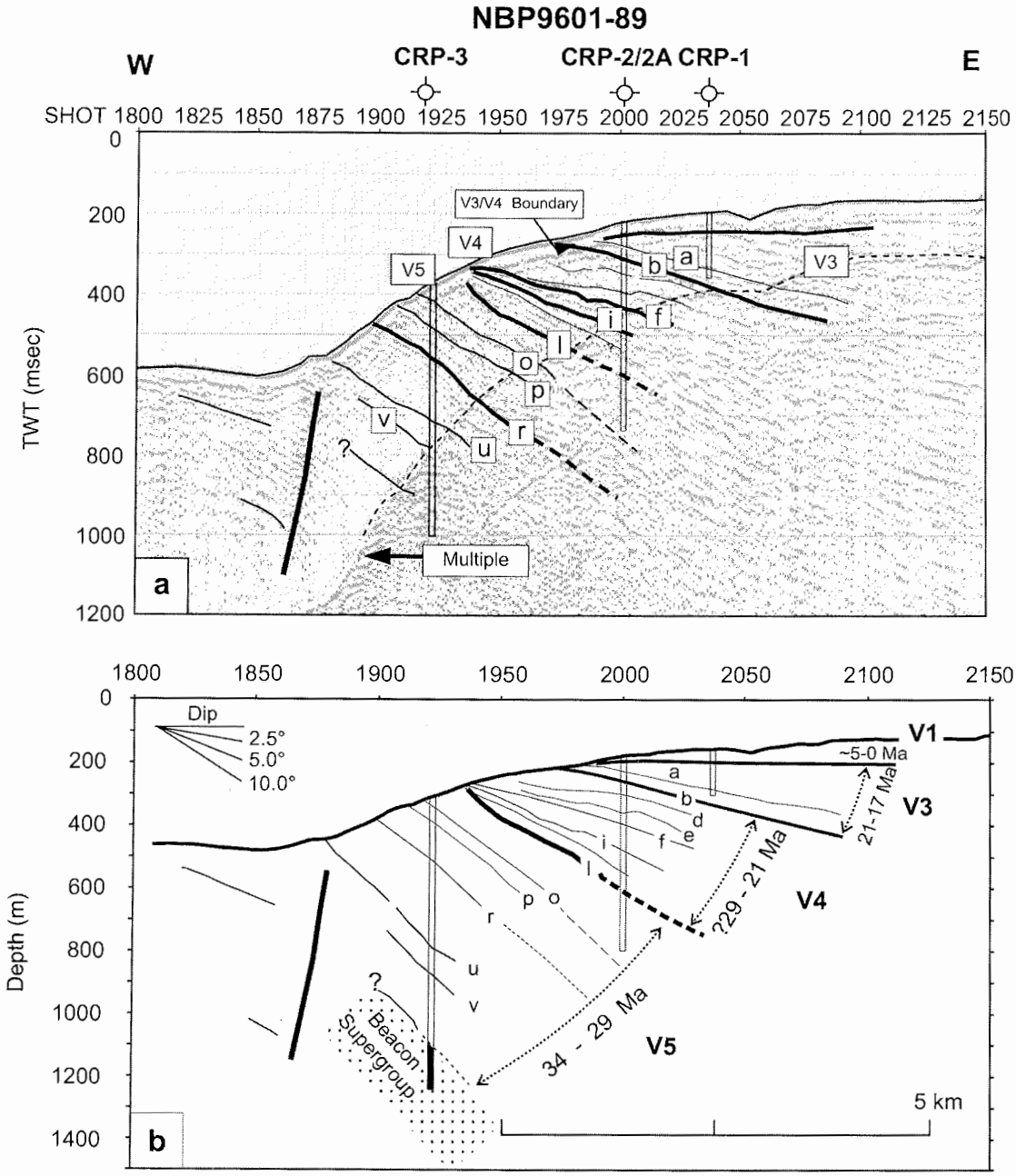

Fig. 1.4 - Geological section based on seismic data from NBP9601-89, showing CRP-1, CRP-2/2A and CRP-3, and ages obtained thus far by Wilson et al. (in press) and the Cape Roberts Science Team (this volume). The line is shown in bold on figure 1.3.

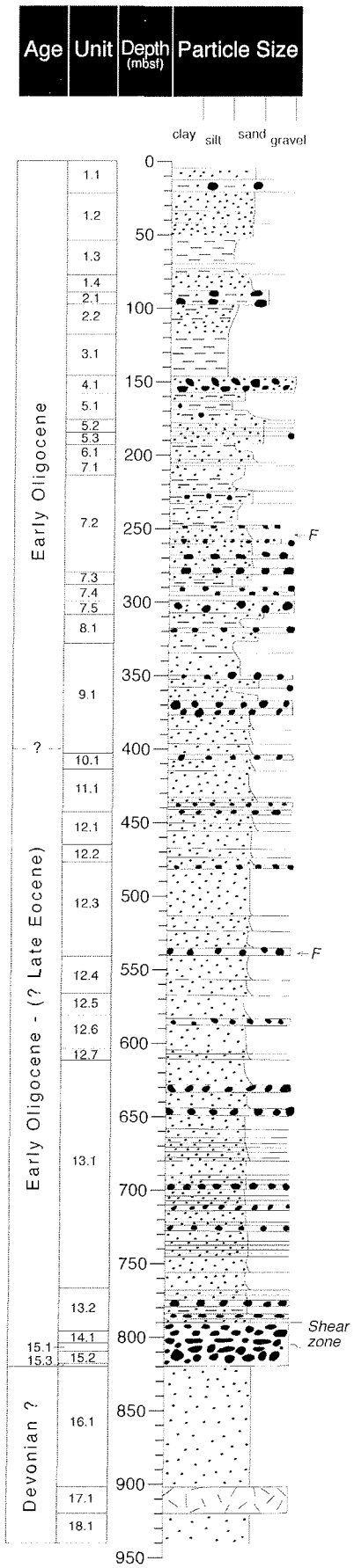

Fig. 1.5 - Stratigraphical column for CRP-3, showing the main lithological features and ages.

has been traversed. This is not enough to expect to reach back to warm middle Eocene times, nor is there any climatic indication of these times from the strata in CRP-3.

The rift margin bedrock described later in these pages is believed to be of mid Devonian sandstone of the Beacon Supergroup, around 3000 m below its stratigraphical position when projected eastward from the mountains to the west. Downhole logging has provided directional data on the attitudes of bedding and fault surfaces encountered in the drill hole so that a tectonic model for the behaviour of this rift margin can be attempted.

The piece-de-resistance for the drill hole is a body of rock 19 m thick that intruded the Beacon Supergroup near the base of the hole. Although it has a doleritic texture, it has other features, such as lack of graphic intergrowths and its pervasively altered state, that distinguish it from the widespread Ferrar Dolerite that intrudes the Beacon Supergroup throughout the length of the Transantarctic Mountains. Could it be a finger from the body causing the magnetic anomaly a few km west and northwest of the drill site (Fig. 1.3) that Bozzo et al. (1997) have modelled as a gently dipping broken slab? Or could it be a marginal facies of the volcanic rocks inferred to form Unit V6 (Cooper & Davey, 1987)? Or could the early stages of rifting be essentially free of magmatism, with all three features representing different phases of Jurassic Ferrar volcanism now preserved in the wall and floor of the West Antarctic Rift System? Do read on.

FAST ICE BEHAVIOUR, CURRENTS AND TIDES

INTRODUCTION

Knowledge of the history of the formation of fast ice in winter and its subsequent behaviour in the spring has been important for the safety and success of the Cape Roberts Project. The ice at any prospective drill site needs to be able to support around 55 tonnes of drilling and related equipment for a period of about 40 days. The pattern of ice growth for the previous two drilling seasons has been described in earlier reports (Cape Roberts Science Team, 1998, 1999). A similar but more complete set of observations follow, along with comments on techniques that have been adopted to ensure that the fast-ice platform is kept in the best possible condition throughout the drilling phase of the operation. Tides and currents also affect the drilling operation, the latter because of their influence on the sea riser, and are also discussed at the end of this section.

WINTER FAST ICE GROWTH

The growth, formation and breakout of fast ice in the south western Ross Sea was tracked from April through to

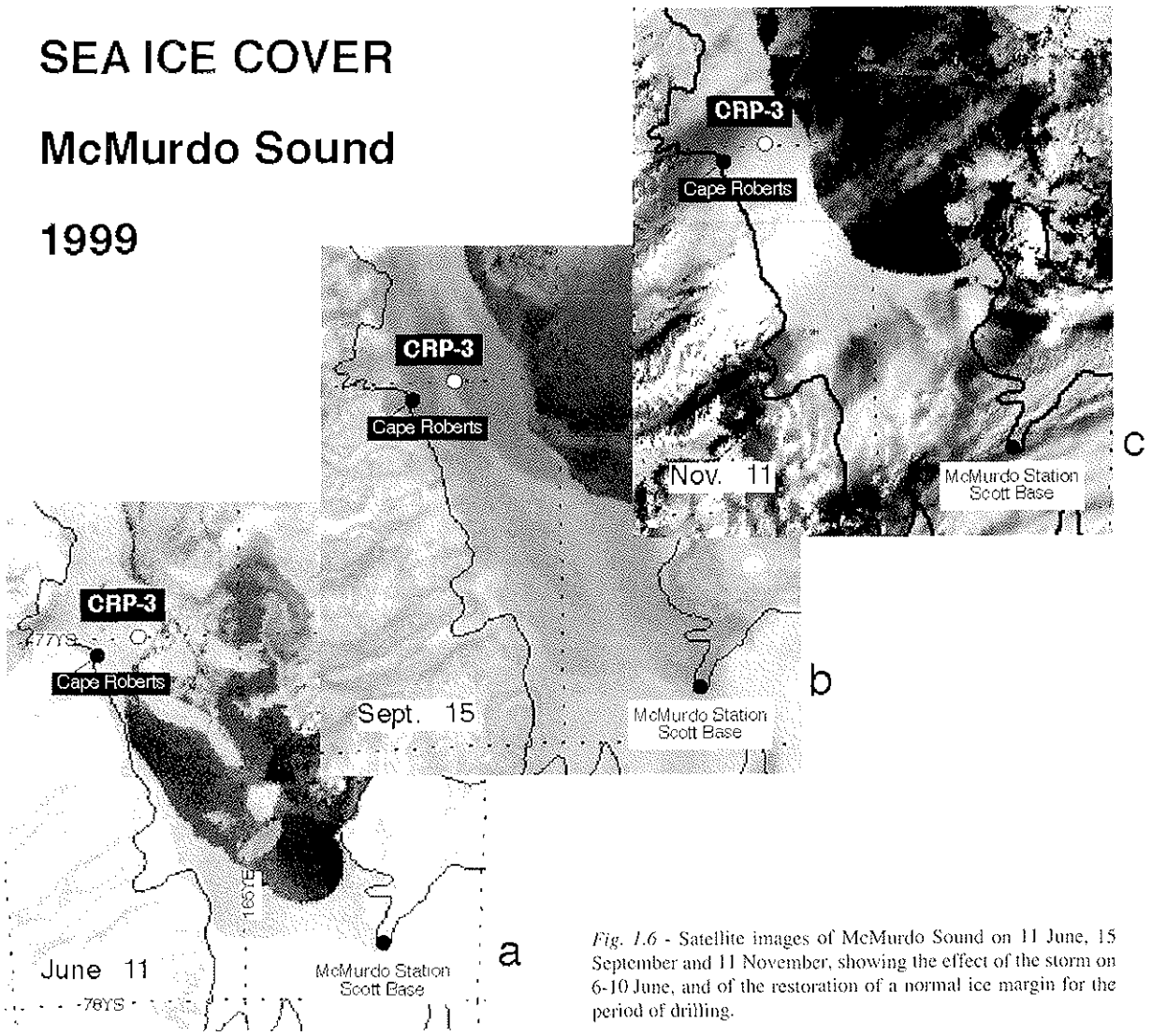

Fig. 1.6 - Satellite images of McMurdo Sound on 11 June, 15 September and 11 November, showing the effect of the storm on 6-10 June, and of the restoration of a normal ice margin for the period of drilling.

late September using weather satellite images (DMSP) downloaded at McMurdo Station and processed at ASA Headquarters in Denver. In the proposed area for drilling CRP-3 off Cape Roberts, fast ice had stabilised by mid April while in the southern part of McMurdo Sound, the fast ice continued to break out and did not stabilise until early July. Temperatures from mid April to mid May were 2°C cooler than the 18-year average (data source -Marble Point automatic weather station), promoting quick winter-ice growth in the drill site area. A compression event on 30 May caused northwest shearing of fast ice in the drill-site area and to the north in the offshore area of Granite Harbour. During 6-10 June, a storm event broke out fast ice along the Wilson Piedmont Glacier but did not appear to affect fast ice in the drill site area (Fig. 1.6).

The fast-ice history for 1999 was compared to winter fast-ice formation and break-out histories for the proceeding ten years (1988-1998) (Pyne, 1999) to determine whether the fast-ice sheet was again likely to provide a suitable platform for drilling as well as a surface resupply route through the southern and western part of McMurdo Sound. In the proposed drill site area, fast ice must stabilise in April-May to provide a guaranteed drilling platform in excess of 1.5 m thick by early October. In addition, post-June breakout events occurring in the fast ice either immediately north and/or south of the proposed drilling area are thought to reduce the protection for the fast ice, making it more susceptible to subsequent storms and possible break-out events. Resupply routes from McMurdo Station to Cape Roberts and out to the drill site must remain unaffected by break-out events from mid-June to ensure that sufficient ice thickness (1.2 m) is present for heavy vehicles.

In early July, the CRP International Steering Committee (ISC) met in Wellington to consider the fast-ice information and concluded that preparation for 1999 should proceed with a final confirmation to be made in early August, in line with the conclusions of the 10-year historical interpretation. The satellite image for August (Fig. 1.7) showed that the fast-ice margin and new ice that had formed after the 6-10 June storm event, remained stable. Growth rate predictions for the fast ice also

indicated that the mandatory 1.5-m thickness should be exceeded by 1 October in the proposed drilling area, allowing the rig to be set up and operated safely. After considering all of the relevant data, the ISC decided that CRP-3 should proceed unless the Winfly reconnaissance indicated otherwise.

WINFLY RECONNAISSANCE

During the Winfly reconnaissance period (21-25 August), measurements of fast-ice thickness were made on route from Scott Base to Cape Roberts and in the drill-site area offshore of Cape Roberts. These included a survey of the Cape Roberts crack (Pyne, 1986), which is several metres wide and runs through the fast ice in a north-south direction several km off Cape Roberts. The shortest practicable route this year between Cape Roberts camp and the CRP-3 site involved bridging the crack 10 km to the south of the cape, and was 23 km long, compared with a straight line distance of 12 km (Fig. 1.7).

Most of the fast ice between Cape Roberts and the drill site area that stabilised in mid April was in excess of 1.6 m thick on 23 August, but some smaller areas that formed after the 30 May shear event were only 1.2 m thick. Detailed mapping of the smooth ice plates (*i.e.* those that formed in mid-April) indicated that five areas were potentially suitable as a drilling platform (areas CRP99-1-5, Fig. 1.7). A drilling position on area 3, chosen in consultation with the ISC, was 270 m north of shot point 1920 on seismic line NBP9601-89. Interpretation of the geometry from the single channel seismic record suggested that this site should give

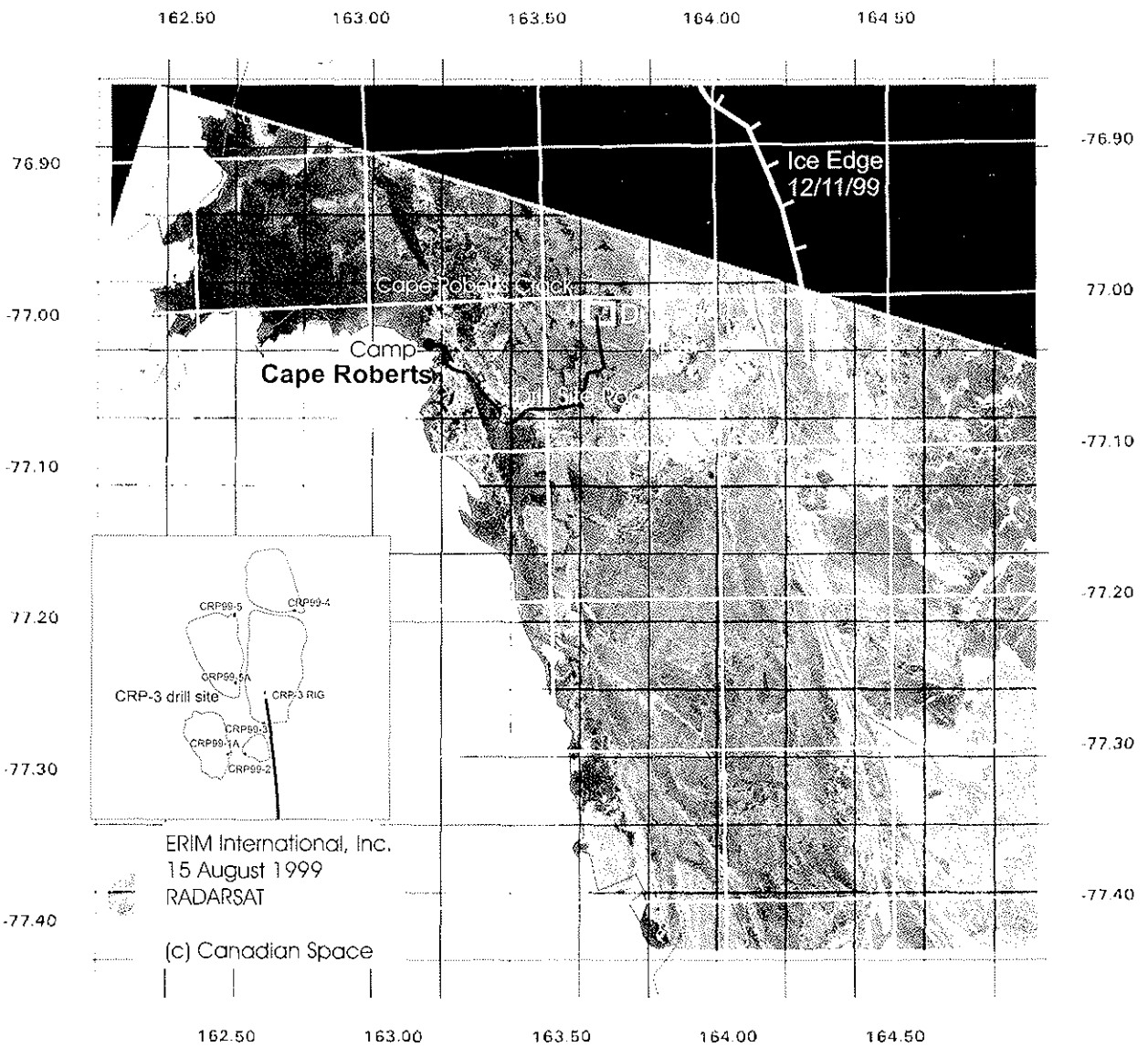

Fig. 1.7 - RADARSAT image for 15 August 1999, of the fast ice off Cape Roberts, showing the various plates and zones, with an inset showing the plates at and around the CRP-3 site. The Cape Roberts crack (dashed white line) and route from Cape Roberts to the drill site (solid black line) are also shown.

Tab. 1.2 - Summary of weather and fast-ice data collection.

Parameter	Position	Sampling frequency	Sampling period
Wind	Top of rig mast –12 m high	30-min avr.	16 Oct-22 Nov
Air temperature	3 m high	30-min avr.	16 Oct-22 Nov
Fast ice temp.	0.5 m below fast ice surface	30-min avr.	16 Oct-22 Nov
Fast ice lateral movt	4 sites close to drill site	6-10 days	10 Sept-14 Nov
Fast ice thickness	5 sites close to drill site	2 weeks	14 Oct-8 Nov
Freeboard	Under drill rig	Daily	3 Oct-15 Nov

approximately 60 m of overlap with the oldest strata cored in CRP-2.

FAST ICE MONITORING

During October, pack ice and refreeze ice obscured the position of the shear zone and fast-ice edge offshore of the drill site. Storm events in early November removed the pack, eroded some of the fast ice and established a 'normal' fast-ice edge 16 km NE and 14 km E of the drill site.

At the drill site, wind, air temperature, fast-ice temperature and fast-ice thickness have been measured throughout the drilling operation (Tab. 1.2) to monitor fast ice conditions. The rate of lateral movement (offset) of the fast ice was monitored as it affects the safe operation of the sea riser. Measurements were taken at three sites from 10 September, and also on the drill rig roof from 8 October, when the sea riser was spudded into the sea floor (Fig 1.7). Measurements were made by GPS and differentially post-processed against a base station at Cape Roberts 12 km away. The error ellipses of positions (95% precision) generally have axes less than 0.5 m.

At the drill site, relatively cool and settled weather was experienced during the month of October. However November was more unsettled with frequent storms with higher winds and warmer air temperatures (Fig. 1.8).

At the drill site, fast ice continued to grow through October and reached a thickness of 2.21 m by early November with 'anchor ice' forming on the sub-ice air bags to a depth of approximately 3 m below the base of the ice. Fast-ice temperature was measured by thermistor probe 0.5 m below the fast-ice surface in a shaded area behind the mud hut. It increased slowly from -12°C in early November to -8°C on 25 November when drilling activity ceased. Thus this year the ice did not become isothermal during the drilling phase of the operation in contrast to the fast ice in the latter stages of CRP-2A (Cape Roberts Science Team, 1999), when temperatures were warmer. Total lateral movement of the fast ice during the period of spud-in to cutting the sea riser at the sea floor was 6 m to the east (088°). Movement rates

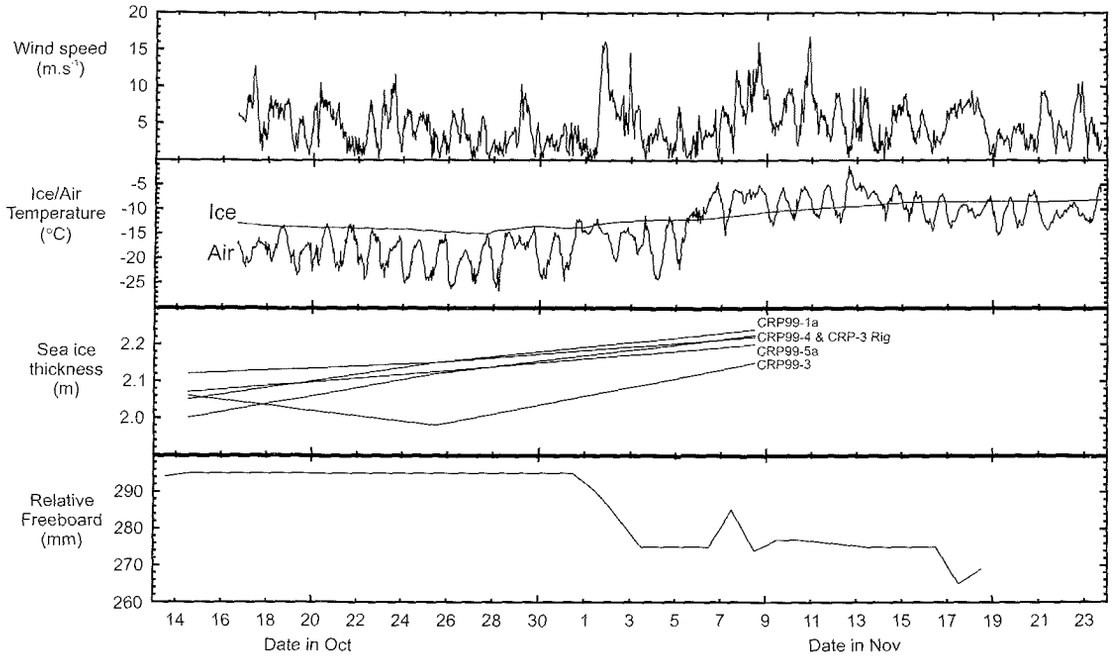

Fig. 1.8 - Weather and fast ice data plotted for the drilling period.

Fig. 1.9 - Tidal movement predicted for Cape Roberts for the periods of October and November.

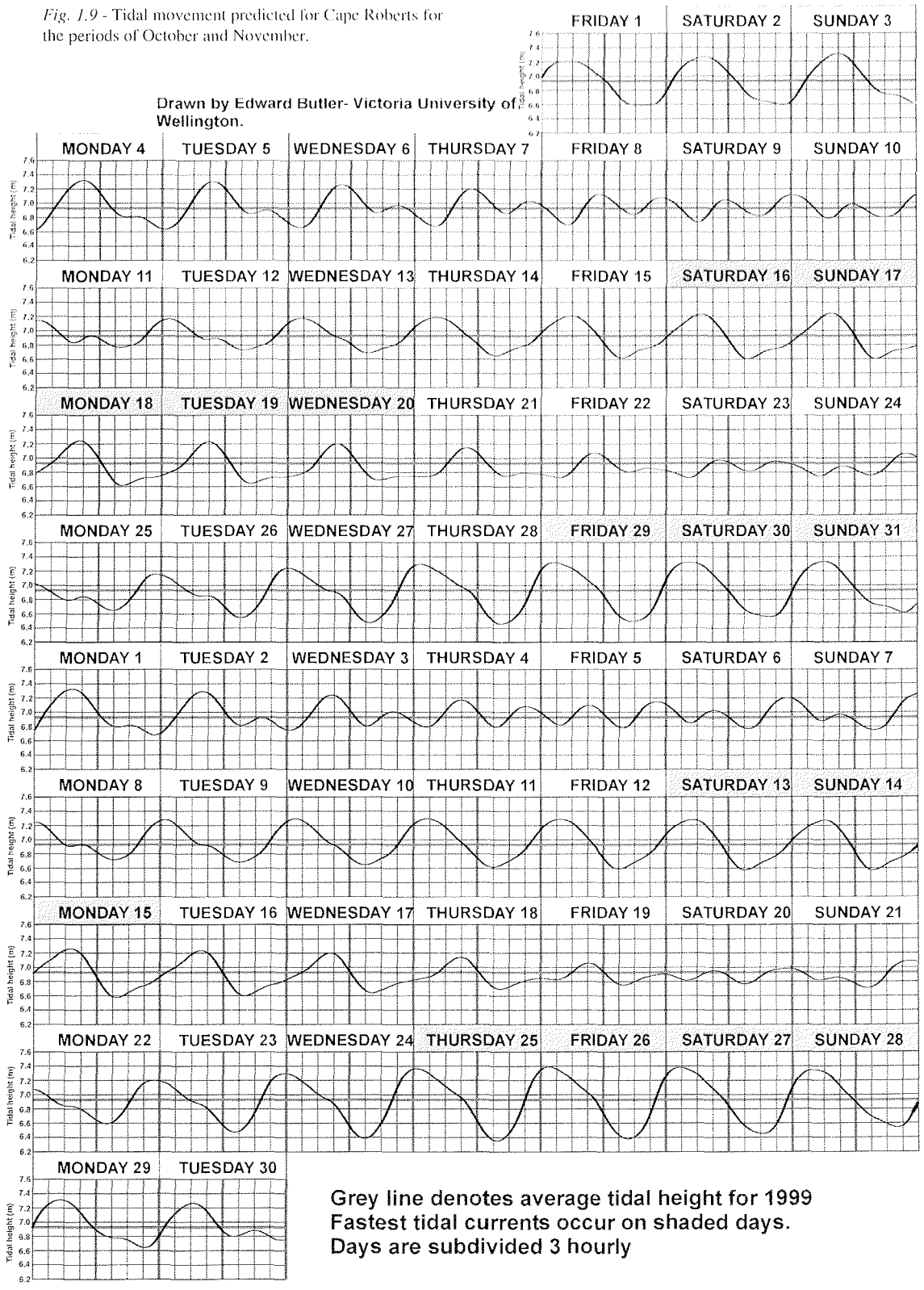

Tab. 1.3 - Summary of current meter deployments at proposed CRP-3 site.

File name	Deployment depth (m)	Deployment Period	Date	Period of spring-neap cycle
CRP3-98A.s4b	50	8 days	01-09/11/98	Neap-spring
CRP3-98B.s4b	55	3 weeks	10-27/11/98	Intermed. Neap-spring
CRP3VERT.s4b	Vertical	3-4 hours	28/11/98	Neap

during this period averaged 1.1 m/week, compared with 2.0 m/week during the drilling of CRP-2/2A in 1998.

Freeboard measurements were taken in the drilling and video hut fast-ice holes by measuring the distance from the water level to the top of a polythene ring, frozen into the fast ice and set 0.15 m above the fast-ice surface. Freeboard was largely maintained by deploying two air bags each with 5 tonnes of lift under the rig and mudroom. Losses in freeboard coincided with an increase in snow cover after storm events, but some recovery occurred after the snow was removed (Fig. 1.8). Freeboard under the drill rig was gradually lost as the ice warmed up. Freeboard at the mud huts was reduced to 95 mm by 15 November and remained stable.

On the fast-ice route to the drill site, the Cape Roberts crack was also monitored periodically (Fig. 1.6). The average weekly rate of spread was 0.3 m with the greatest spreading occurring during spring tides.

TIDE AND CURRENT MONITORING

The drilling operation is influenced not only by the lateral fast ice-movement but also by the vertical movement of the fast ice and the drag placed on the sea riser by tides and currents in the water column.

Tidal-height predictions for Cape Roberts were calculated on the basis of 12 months of records from the Cape Roberts tide gauge in 1998, using a tidal prediction program from the University of Hawaii Sea Level Centre. Tides are mixed (Fig. 1.9) with a maximum spring-tide and neap-tide range of *c.* 1.0 m and 0.3 m respectively. Spring tides are strongly diurnal (single cycle per day) while neap tides are characterised by two tidal cycles a day (semi-diurnal). Relative tidal heights measured on the rig floor this year show that tides are synchronous with the Cape Roberts tidal-height predictions (Fig. 1.9).

An investigation of currents was undertaken in November 1998, at the originally proposed CRP-3 site (located at 77.0151°S 163.6190°E and approximately 220 m west of the actual CRP-3 site) to establish a base-line for use in this year's drilling season. Water depth, current direction and current velocity were recorded using an S4 current meter. The instrument was deployed through a hole in the fast ice on three occasions during various stages of the spring-neap tidal cycle (Tab. 1.3). Vertical profiles were carried out to a water depth of 365 m, and longer-term static deployments were placed at elevations of 50 and 55 m water depth to measure mid-water current variations.

During spring tides, currents move in an anti-clockwise direction, through 360° over a 24-hr period with the larger flood tide of the day moving towards the northwest and continuing to swing around to the southeast for the subsequent low water (Fig. 1.10). At a water depth of 55 m during spring tides, current speeds reach a maximum of 0.3 ms^{-1} around low water and may remain above 0.2 ms^{-1} for up to 6 hrs on the largest of spring tides (Fig. 1.10). During neap tides, current speeds are mostly below 0.2 ms^{-1} throughout the water column, and at the sea floor, current speeds are <0.1 ms^{-1}. On only one occasion in October, during a

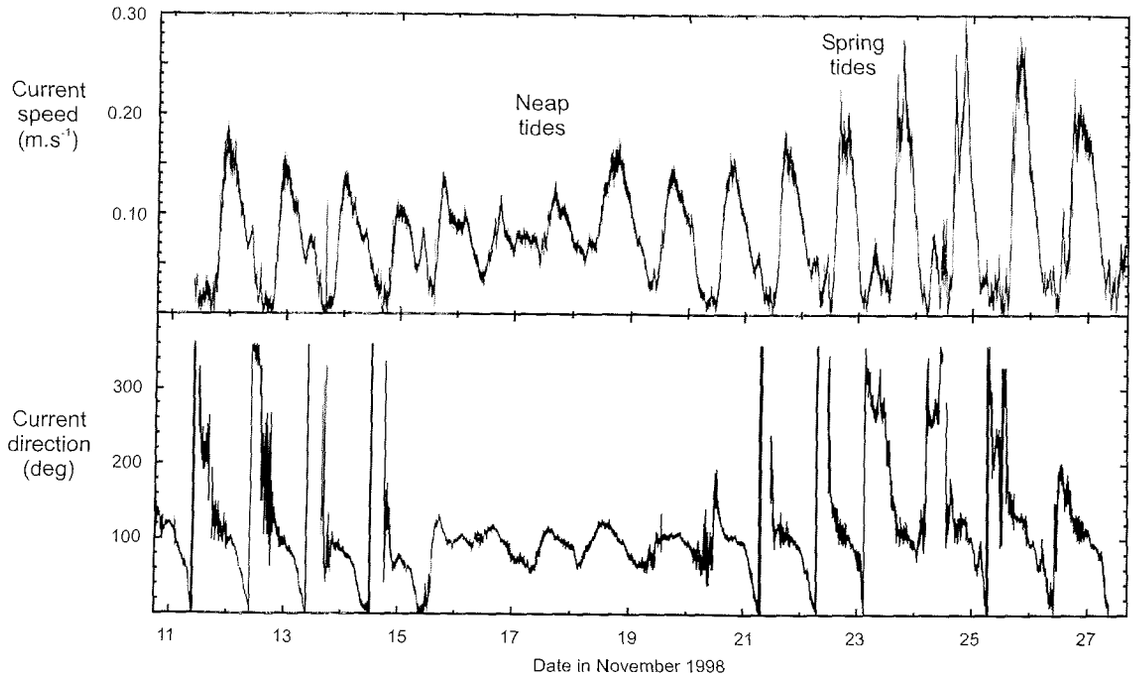

Fig. 1.10 - Current speed and direction at a site 220 m west of CRP-3 within the meter set at a depth of 50 m.

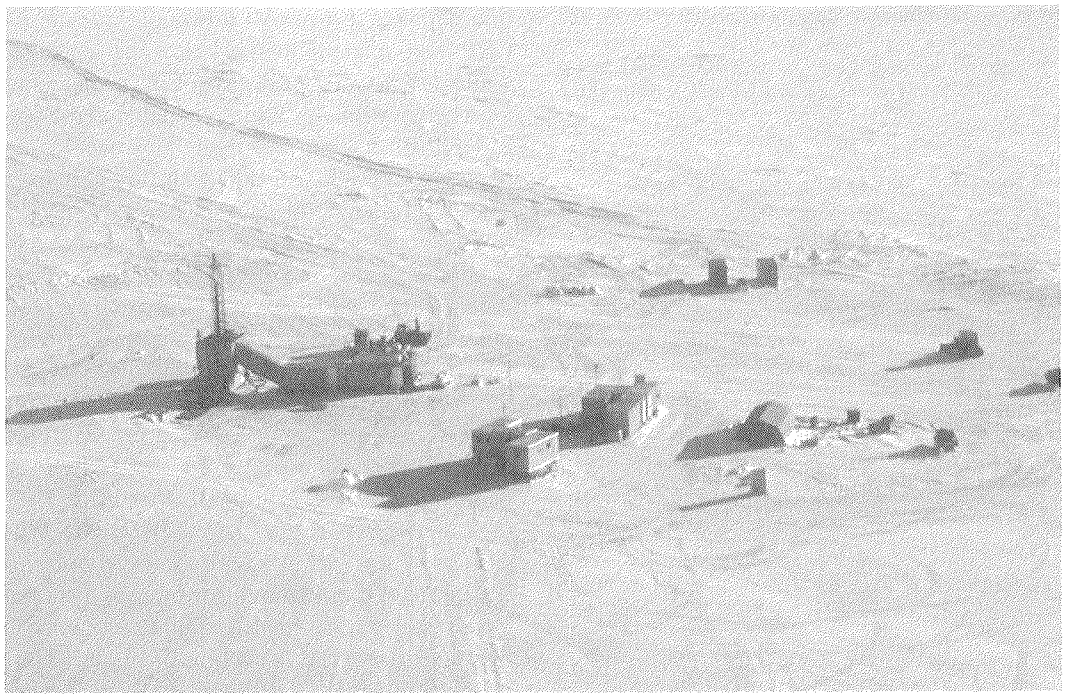

Fig. 1.11 - Aerial of view the CRP-3 drill site to show the layout of the rig, with sloping covered ramp down to the mudroom, and with core processing and physical properties laboratories in a cluster 30 m to the right.Photo: P.J. Barrett.

spring tide period, was there slight horizontal rotation of the sea riser (<1°) due to increased tidal speeds.

DRILLING OPERATIONS

INTRODUCTION

The drilling system was set up and operated as for CRP-2 and described in Cape Roberts Science Team (1999, p. 11). The layout of the rig and surrounding buildings is shown in figure 1.11, and the drilling system with sea riser installed and ready to continue drilling in figure 1.12. Core recovery began on 9 October and finished on 19 November at a depth of 939.42 mbsf. Downhole progress is shown in figure 1.13, with daily core summaries in table 1.4. Drilling activity is summarised in table 1.5.

SEA RISER DEPLOYMENT PHASE

The sea riser is a casing string of 5" OD flush-jointed high-strength drill pipe, comprised mostly of 5.5-m lengths with 3- and 1-m "shorts". It extends from just above the fast ice through the water column to a depth of several metres into the sea floor. Its functions are to support the rotating drill string in the water column, and to provide an annulus for returning drilling fluid to the rig. A casing shoe of hardened weld material (OD 5.5") was fitted to improve the cutting and flushing down

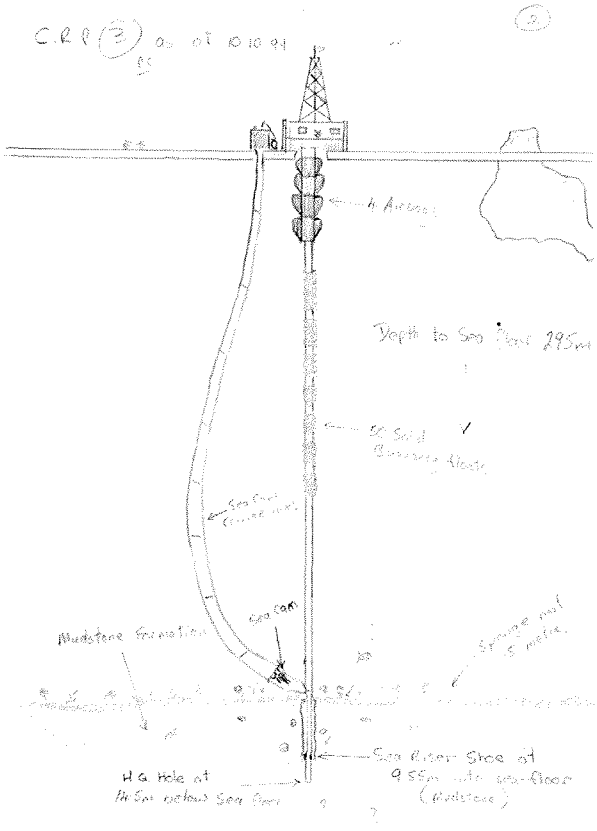

Fig. 1.12 - Drilling system set up at CRP-3 showing the sea riser set in mudstone. Sketch: Pat Cooper.

Tab. 1.4 - Summary data on downhole progress and core recovery. The 24-hour day extends from 08.00 to the same time the following day. Note that the bottom of the lowest core is at 939.42 mbsf on account of 0.13 m "stickdown" below the measured depth of the bottom of the coring run.

DATE	DEPTH	DRILLED	RECOVERED		
	(m)	(m)	(m)	(%)	(CUM%)
9 Oct	9.98	8.58	5.28	62%	62%
10 Oct	14.50	5.40	4.58	85%	75%
10 Oct	Sea riser cemented at 9.50 mbsf				
13 Oct	24.74	10.34	9.27	90%	82%
14 Oct	51.30	26.56	25.83	97%	90%
15 Oct	81.06	29.76	29.55	99%	94%
16 Oct	114.20	33.14	33.09	100%	95%
17 Oct	147.20	33.00	33.05	100%	96%
18 Oct	177.20	30.00	30.00	100%	97%
19 Oct	207.20	30.00	30.02	100%	98%
20 Oct	246.20	39.00	38.95	100%	98%
21 Oct	285.70	39.50	36.26	92%	97%
22 Oct	Change of HQ bit at 293 mbsf				
22 Oct	294.70	9.00	8.72	97%	97%
23 Oct	327.50	32.80	32.85	100%	97%
24 Oct	345.85	18.35	18.27	100%	97%
24 Oct	Beginning of down-hole logging to 345 mbsf				
29 Oct	Beginning of NQ coring – replaced surface set bit				
29 Oct	348.82	2.97	0.66	22%	97%
30 Oct	395.50	46.68	42.33	91%	96%
31 Oct	437.18	41.68	39.99	96%	96%
1 Nov	485.72	48.54	47.76	98%	96%
2 Nov	Change of NQ bit at 492 mbsf				
2 Nov	510.10	24.38	20.95	86%	96%
3 Nov	552.23	42.13	40.42	96%	96%
4 Nov	588.85	36.62	35.01	96%	96%
4 Nov	Change of NQ bit at 605 mbsf				
5 Nov	606.00	17.15	17.27	101%	96%
6 Nov6	640.30	34.30	32.70	95%	96%
7 Nov	668.90	28.60	28.44	99%	96%
8 Nov	704.91	36.01	35.89	100%	96%
9 Nov	738.00	33.09	33.12	100%	96%
10 Nov	774.00	36.00	35.94	100%	97%
11 Nov	Beginning of down-hole logging to 774 mbsf				
13 Nov	Continuing with NQ coring				
13 Nov	798.20	24.20	24.24	100%	97%
14 Nov	833.30	35.10	35.22	100%	97%
15 Nov	869.32	36.02	34.45	96%	97%
16 Nov	900.30	30.98	30.43	98%	97%
17 Nov	918.10	17.80	17.44	98%	97%
18 Nov	939.29	21.19	21.51	102%	97%

through the formation and to create an annulus between the formation and the riser.

The configuration of the floatation on the sea riser at the CRP-3 site was based on a water depth of 295 m, which was first measured on 4 October with a weight attached to the wire line. Twelve 4x1 m and one 2x1 m rigid flotation units were clamped on 5.5-m sea-riser lengths. This reduced the weight of the riser in sea water from 6580 kg to a residual weight of approximately 2000 kg once fully deployed to the sea floor. The residual weight is used to install the riser into the sea floor with washing and bumping (also termed jetting and jarring) techniques.

The sea floor consisted of a soft surficial muddy sponge mat about 0.5-m thick, underlain by soft sediments to a depth of 1.4 m. All downhole measurements for CRP-3 are made in metres below the sea floor (mbsf), which is taken to be the base of the sponge mat.

The sea riser was initially jetted into the sea floor to a depth of 1.4 m, and then hung from a hydraulic deployment frame beneath the drill floor in the "cellar". The HQ coring barrel was then run inside the riser to the bottom of the hole, and coring was progressively carried out in short runs of 1.5 to 2 m beyond the sea riser casing. After each run the riser was bumped into the newly cored hole. This method reveals the type of formation present, which allows us to assess its suitability as an anchor for the riser. It also recovers core virtually right from the sea floor for scientific study. This process was repeated to a depth of 9.55 mbsf, with HQ coring ahead to 14.50 mbsf confirming competent ground to that depth. The decision to cement the sea riser at 9.55 mbsf was made because a suitable interval of competent ground had been encountered, and continuing to bump the sea riser would have stressed it, perhaps leading to tool joint failure as resistance from the formation increased. The annulus was then cemented, with a visible return of cement to the sea floor on the submarine video system, indicating a gauge hole, with space for a good seal.

HQ DRILLING PHASE

We continued coring with the HQ drill string to a depth of 345.85 mbsf with a 3-m barrel and HQ3 impregnated-diamond series-2 bits, cutting core of 61 mm in diameter. Core was recovered by wire line with an inner tube containing stainless steel splits. Coring through this drilling phase averaged 28 m/24 hrs and ranged from 8 to 39 m/24 hrs (Fig. 1.13). The HQ drill rod was then cemented in from 345.55 up to 50 mbsf, using two HQ rubber cementing displacement bungs, in preparation for NQ coring.

NQ DRILLING PHASE

The cementing bungs were top drilled with an NQ surface-set stepped-faced diamond bit. An NQ3 series-2 impregnated-diamond bit was then substituted in place of the surface-set bit, and coring continued using a 6-m barrel cutting core 45 mm in diameter. Core was recovered with an inner tube containing steel splits, as 6-m stainless steel splits are unavailable. The NQ coring phase, which ran from 345.85 to 939.42 mbsf, averaged 31 m/24 hrs and ranged from 11-48 m/24 hrs (Fig. 1.13).

Core recovery for the entire hole averaged 97% with most of the loss coming from the initial HQ coring during deployment of the sea riser and in intervals of unconsolidated sands between 380 and 530 mbsf.

RECOVERY PHASE

On completion of the final logging run, we cemented the HQ-cased section of the hole to within 50 m of the sea floor, using HQ cementing plugs and the NQ drill string

Tab. 1.5 - Main drilling events during CRP-3.

Date	Drilling Activity
2/10/99	Drilled access hole for drill rig.
3/10/99	Diver installed air bags under sea ice beneath drill rig.
4/10/99	Prepared sea riser casing. Wire line measurement to sea floor =290 m.
5/10/99	Lowered 132 m of sea riser.
6/10/99	Lowered sea riser to about 280 m, including 12x4 m and 1x2 m rigid buoyancy modules.
7/10/99	Stripped over air bag tensioning system and prepared HQ drill string. 24 hour operation begins.
8/10/99	Lowered and bumped/washed in sea riser about 2.3 mbsf. Tagged sea floor at 295 mbsf (13.00 hrs). Ran HQ drill string and began slow coring from 2.8 to 5.4 mbsf
9/10/99	Cored to 6.9 mbsf, advanced riser to 4.3 mbsf, cored to 9.1 mbsf, advanced riser to 5.30 mbsf and cored to 13.17 mbsf.
10/9/99	Cored to 14.40 mbsf, ran in HQ drill string, advanced sea riser to 9.4 mbsf. Ran in HQ string with casing shoe, cemented sea riser and recovered HQ string.
11/10/99 – 12/10/99	Ran in HQ coring string.
13/10/99	Cored out cement and then cored formation from 14.40 to 24.74 mbsf.
14/10/99 – 24/10/99	Cored HQ from 24.74 to 345.85 mbsf.
24/10/99	Tripped out HQ string, changed core barrel to casing shoe for advancer. Set casing shoe at 18.3 mbsf and conditioned hole for downhole logging.
25/10/99-26/10/99	Downhole logging interval 18.30-255.00 mbsf.
26/10/99	Lowered HQ string with casing advancer to 345.80 mbsf, washed and drilled past shear zone. Cleared and conditioned hole and pulled back to 271.55 mbsf.
26/10/99-27/10/99	Downhole logging interval 271.50 to 345.50 mbsf.
27/10/99	Washed HQ casing to bottom of hole and cement with casing advancer.
27/10/99-28/10/99	Care and maintenance while cement set. Prepared NQ drill string and drilled out rubber bungs (used in cementing) with a stepped surface set diamond bit to 348.82 mbsf.
29/10/99-02/11/99	Changed to an impregnated-diamond series-2 bit and cored NQ from 348.82 to 492.10 mbsf.
02/11/99-05/11/99	Bit was replaced at 492.10 mbsf with another impregnated-diamond bit and NQ coring continued to 604.88 mbsf.
05/11/99-11/11/99	Bit was replaced at 604.88 mbsf with another impregnated-diamond bit and NQ coring continued to 774.00 mbsf.
11/11/99-13/11/99	Downhole logging interval 345.50 to 774.00 mbsf.
13/11/99-19/11/99	Continue coring in NQ with new impregnated-diamond bit from 774.00 to 939.42 mbsf.
19/11/99	Coring was terminated because of squeezing formation at 901.00-902.00 and 919.00-920.00 mbsf.
19/11/99-21/11/99	Downhole logging interval 774.00 to 918.00 mbsf.

for displacing cement. A hydraulically operated HQ casing cutter was run on the NQ drill string and the HQ casing was cut at 10 m below the sea floor. The sea riser was severed *c.* 3 m above the sea floor with a SwETech AB colliding drill collar charge type 2 (oil field-type explosive), which was wire-lined into position and exploded electrically. The sea riser and air-bag pipes were recovered in the following 24 hours.

The technical objectives planned for CRP-3 were to core continuously to a minimum depth of 700 mbsf, and to run a full set of geophysical logs for the hole. CRP-3 cored to 939 mbsf, and logging was carried out to a depth of 918 mbsf, over 30% beyond the target depth and a significant new benchmark for Antarctic bedrock drilling.

HYDROCARBON CONSIDERATIONS

We recognised that a deep hole in the sedimentary strata off Cape Roberts could potentially contain hydrocarbons, because small amounts of tar residue (dead oil) had been reported from around 632 mbsf in CIROS-1 (Barrett, 1989) and from below 500 mbsf in CRP-2A (Cape Roberts Science Team, 1999). Although the prospect of encountering hydrocarbons was considered very low, inflammable gas and hydrogen-sulphide Sieger series-2000 gas sensors were operated during the drilling for safety reasons. The air space above the mud-scavenge tank in the drill-rig cellar was continuously sampled through a heat-traced tube connected to a glycol trap (located on the rig floor). Gas

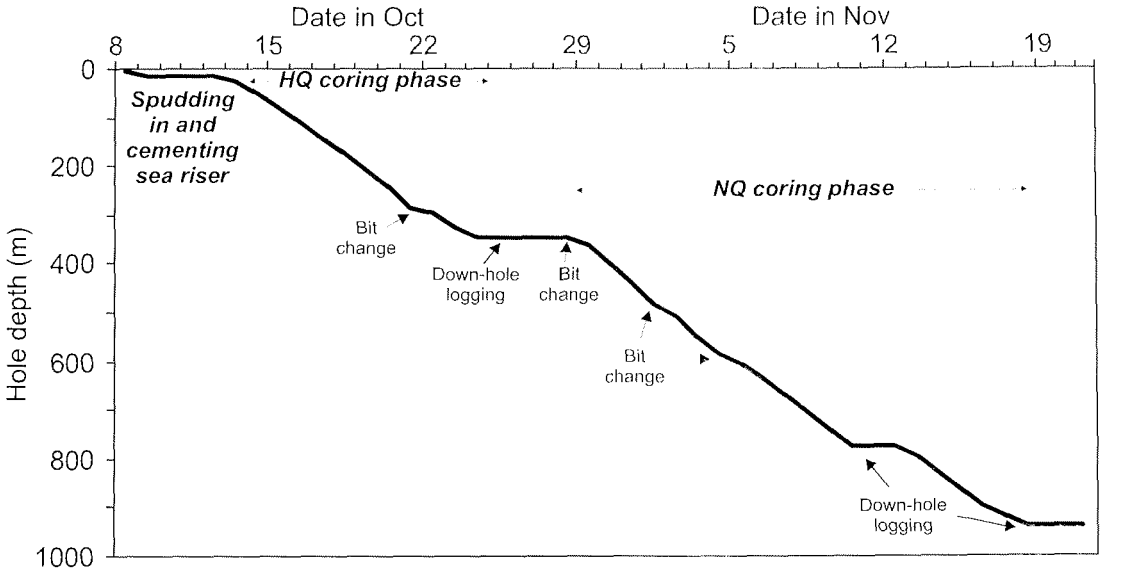

Fig. 1.13 - Downhole progress during the drilling of CRP-3.

extracted in this way was then pumped through tubing to the gas sensors in the generator hut workshop (passing through a warmed walkway and mud huts). The response time of the system was approximately 15 seconds. The inflammable gas sensor appeared to be affected by diurnal temperature changes and required periodic re-zeroing.

CORE MANAGEMENT AND SAMPLING

DRILL SITE AND CAPE ROBERTS CAMP

Initial core curation began at the drill site. Upon core recovery, downhole depths were measured on the core to the nearest centimetre and expressed as metres below the sea floor (mbsf).

The core was first cut into one-metre lengths and then longitudinally into an Archive Half and a Working Half using a rotary diamond saw. The Archive and Working halves were placed in separate core boxes (3 m *per* box for HQ size core and 4 m *per* box for NQ size core). Yellow plastic separators, with the mbsf depth written on them, were placed at one-metre intervals within the core box. Any voids in the core box were filled with foam blocking to minimize movement of the core during transport.

Sampling of the core also began at the drill site. A 10-cm section of the Working Half was taken at approximately 20 m intervals. This "fast-track" sample was sent the same day by helicopter to the palaeontologists at McMurdo Station for age determination. In addition to the "fast-track" sample, fourteen 10- to 20-cm long whole-core sections were removed from the core for clast-fabric and shape studies.

TRANSPORTATION

Core Boxes from Cape Roberts Drill Site to McMurdo Helicopter Pad. Insulated, vinyl-covered carrying cases, with a capacity of three or four core boxes each, were used to transport the core *via* helicopter between the Cape Roberts Drill Site and the Cape Roberts Camp, and then on to McMurdo Station. The carrying cases were placed inside the helicopter to protect the core from freezing. Two to four carrying cases (6-16 core boxes) were transported each day along with a "fast-track" sample. The Working and Archive halves of the core were sent on alternate days as a safety measure.

Core Boxes to Core Storage Facility (CSEC-CSF). The cases containing the core arrived at the McMurdo helicopter pad between 20.00 and 24.00 hrs each day and were transported, by truck, from the helicopter pad to the Crary Science and Engineering Center-Core Storage Facility (CSEC-CSF). The insulated cases were carried into the CSEC-CSF where the individual core boxes were removed from the carrying cases, logged in, and placed on shelving. The Archive and Working halves were placed in separate areas of the Facility. The CSEC-CSF was maintained at a temperature of 4°C and at a relative humidity of 60%.

SEQUENCE OF EVENTS IN THE CSEC CORE LABORATORY

Core Laboratory, McMurdo. A core laboratory was set up in room 201 of the CSEC. The walls, the floor, the benches, and all equipment in the room were thoroughly cleaned prior to the core arrival at the laboratory and at the end of each sampling session to minimize the potential

for contamination of the core. The temperature of the room was maintained at 18°C. The relative humidity of room 201 was low (40%), despite the addition of two humidifiers operating 24 hrs/day. The laboratory contained 10 m of bench space covered with an easily cleaned surface. Fluorescent lighting was augmented by high-intensity halogen lighting to enhance the viewing of the core.

The morning following the arrival of the core at McMurdo Station, the core boxes were repackaged into the insulated cases and then carried by hand to the Core Laboratory in the CSEC. The core boxes were removed from the carrying cases and placed on the laboratory benches in depth sequence.

Initial Core Appearance. In general, the core arrived from the Cape Roberts Camp in excellent condition. The core was moist, with a sheen of water on the cut surface of the sediment. Occasionally, minor longitudinal shifting had occurred within the individual metre-long sections. The cores were misted with filtered water on a regular basis to counteract the dehydration effects of the low humidity in the room.

Core Logs Rechecked, Photography, and Viewing of the Core. Each day 18 to 40 m of the Working Half of the core were logged and photographed by the sedimentologists, and the core logs received from the Cape Roberts Camp were checked for discrepancies against the core. Upon completion of core logging, the sedimentologists provided a short briefing and a tour of the displayed core to the Cape Roberts science group.

Selecting Sample Intervals. On average, 18 to 40 m of core were available for sampling each day. The investigators selected their sample intervals by placing disposable sample "flags" (a toothpick with an adhesive label wrapped around it) alongside the core. The palaeomagnetic investigators marked their samples by placing 4 x 7 mm slips of paper over their requested intervals.

Disputed Sample Intervals. Overlaps between investigators requesting the same interval were resolved through discussions with the on-ice parties involved, the curators, and the Cape Roberts Sample Committee (Harwood, Janecek, Powell, Talarico).

Data Entry. The curators entered the sample interval data into a relational database (4th Dimension). These data included: the investigator, hole number (CRP-3), box number (1-256), top interval of sample (mbsf), bottom interval of sample (mbsf), volume of the sample (cubic centimetres), date, and comments. The comments section recorded the type of sample taken (*e.g.* sediment, fossil, or clast) and the discipline and type of analysis to be performed on each sample (*e.g.* petrology-thin section or palaeontology-diatoms). This sample information and other coring information can be accessed through the WWW sites of the curatorial facilities at the Antarctic Marine Geology Research Facility, at the Florida State University in Tallahassee, Florida (www.arf.fsu.edu) and the Alfred-Wegener-Institute for Polar and Marine Research in Bremerhaven, Germany (www.pangaea.de).

SAMPLING

General Sampling. The core curators carried out the routine daily sampling, with over 5 900 samples taken for on-ice investigation. Common laboratory spatulas, small scoops, and forceps were used to remove samples from unlithified core. A diamond saw was used cut the more lithified material, as well as the large clasts. All of these tools were cleaned prior to the beginning of the sampling session and between the sampling of different intervals. At no time was any tool used more than once before it was cleaned. The sampling tools were washed with hot water and a laboratory detergent, rinsed with clean water, and then given a final rinse with filtered water. The tools were allowed to air dry to minimize the potential for contamination by paper or cloth fibre. The voids left in the core following extraction of the samples were filled with cut foam blocks to stabilize the core. Upon completion of sampling, the core was misted with filtered water and then returned to the CSEC-Core Storage Facility. The benches, the floor, and all sampling equipment were washed in preparation for the next shipment of core.

Palaeomagnetic Sampling. The palaeomagnetists conducted their own sampling. To avoid contamination of the core, orientated, coherent sections were removed from the core box, placed on a carrying tray, and taken to the palaeomagnetic sampling lab (a separate building located on the loading dock of CSEC room 201). A diamond drill was used to remove the sample and the remaining core section was replaced in the core box in the proper orientation.

CORE SHIPMENT

The core was re-examined in the CSEC-CSF prior to packaging for shipment to the core repositories in Florida and Germany. Additional foam blocking was added where needed, and the core was misted with filtered water again before the core-box lids were taped into place.

The core boxes were placed into specially constructed wooden boxes that contained nine separate compartments holding four boxes each. The containers were marked with arrows pointing to the upright position and with signs designating the correct temperature for transport (4°C/40°F). The wooden boxes were shipped in a refrigerated container via the cargo ship *Greenwave* to Lyttleton, New Zealand. The Working Halves of the core were off-loaded for ocean transport to Germany. The Archive Halves continued aboard the *Greenwave* to California, where they were off-loaded and transported overland *via* refrigerated truck to Florida.

Terra Antartica
Initial Report on CRP-3
2000, 7 (1/2)

2 - Core Properties and Downhole Geophysics

INTRODUCTION

We present here the results of a suite of structural and geophysical measurements on whole cores and in the borehole. The first section examines fracture patterns in the cores and discusses their distributions, styles, and tectonic significance. More than 3 000 fractures were logged in the whole cores, and most were also imaged with digital whole-core scans. These fractures include microfaults, veins, and drilling-induced fractures. Microfaults exhibit a fundamental change in style at about 790 mbsf, with dominantly normal faulting above this depth and oblique shearing below. Three large faults are identified, at *c.* 260, 539, and 790 mbsf.

The second section discusses physical property measurements, conducted on whole cores at a 2-cm spacing throughout the cored interval. The resulting core logs of P-wave velocity, density, and magnetic susceptibility are used to define physical-property-based units and to identify the influence of geological variables (*e.g.* clasts, cementation) on these physical properties.

The third section presents the results of downhole logging. Continuous geophysical measurements along the borehole wall were obtained by a suite of 10 logging tools, including porosity, lithology, imaging, and seismic-link tools. These logs, like the core logs of the previous section, define units with characteristic geophysical responses. The geophysical signatures of lithology, grain size, and diagenesis are identified.

One type of downhole measurement, the vertical seismic profile, is discussed in a separate section because measurement frequency and volume are quite different from the downhole logs. The vertical seismic profile, conducted at a 7.5-m spacing throughout CRP-3, provides a precise link between seismic reflection travel-times and drillhole depth. This time-to-depth conversion shows an excellent match to that determined independently from the whole-core velocity log of the second section. In addition to the near-vertical seismic profile, two offset seismic experiments were undertaken, to image seismic reflectors up to 300 m away from the drill site and thereby examine dips and lateral continuity of these seismic reflectors.

The final brief section draws together the results of the vertical seismic profile and whole-core velocity log to correlate between the CRP-3 depth record and a nearby seismic reflection line. Distinctive reflectors on the seismic section are converted to depth within CRP-3 using the velocity data of sections two and four. This correlation is tentatively refined based on identification of significant impedance changes within the whole-core velocity log.

FRACTURE ARRAYS

INTRODUCTION

The Cape Roberts Project drill holes are located along the rift margin between the Victoria Land Basin and the Transantarctic Mountains (Barrett et al., 1995). This major structural boundary, known as the Transantarctic Mountains Front, has been inferred to be a major normal-displacement fault zone that accommodated the relative motion associated with uplift of the mountains and subsidence of the adjacent rift basin. Fracture studies of the cores and borehole walls during CRP drilling were aimed at documenting the brittle deformation patterns associated with the evolution of the Transantarctic Mountains Front and the contemporary crustal stress directions across this boundary. The CRP cores provide the opportunity to document the timing of faulting based on crosscutting relations with Cenozoic strata encountered by the coring. The orientations of drilling-induced fractures record the modern crustal stress directions.

Fractures were abundant in strata cored by CRP-3, and over 3 000 fractures were logged in the *c.* 940 m of core obtained. In addition to small-scale faults and extension fractures, the drilling transected three larger-scale fault zones. Textural and kinematic data on these fault zones have been obtained by core-fracture logging, whereas information on the attitude and extent of these fault zones has been obtained by downhole logging. Ongoing work integrating core fracture logging and downhole data will allow us to orient the core fractures following methods established for CRP-2A (Paulsen et al., in press) and to provide an integrated analysis of fracturing in the vicinity of the CRP drillholes (Moos et al., in press; Wilson & Paulsen, in press).

FRACTURE STUDY PROCEDURES

Core-fracture logging was carried out on whole core at the Drill Site laboratory. Depths to the top and bottom of each fracture were recorded. Fracture dip and dip direction were measured with respect to a red line scribed the length of each core run. The surface of each open fracture was examined for fractographic features indicative of either shear or extensional mode of fracture origin. The textures of material filling fracture planes were examined macroscopically; detailed textural analysis will be the subject of future petrographic analysis.

As part of fracture logging, we identified intact core intervals, which are continuous lengths of core where no internal relative rotation has occurred. The intact core

intervals are bounded either by core-run breaks where the core ends could not be fitted together, or by fractures in the core where rotation occurred during the drilling. For both HQ and NQ core, *c.* 55% of core runs could be fitted together; the longest intact core intervals are *c.* 27 m long. This relatively high amount of intact core lengths will greatly facilitate core orientation, which will be achieved by feature matching between the core and oriented borehole televiewer (BHTV) imagery.

Both the whole core and slabbed core were scanned using the CoreScan® instrument leased from DMT, Germany. One-metre lengths of whole core were scanned by revolving the core on rollers as a digital line scanner traversed the length of the core. The uppermost portion of the core down to *c.* 73 mbsf and a few deeper sections of limited extent were too poorly indurated or too fractured to carry out whole-core scanning. It was possible to complete whole-core scanning of 77% of HQ core, 90% of NQ core, or 85% of the core overall. This provides an exceptional digital record of the core, which we will use for systematic comparisons with the BHTV and dipmeter logs to orient the core, to analyze fracture patterns, and to determine dip directions and angles for the strata. The entire working-half slabbed core was scanned in the core boxes; these scans are provided as an appendix to this report.

FRACTURE DISTRIBUTION AND DENSITY

A cumulative plot of the number of fractures *per* metre of core, smoothed by a 10-metre moving average filter, is provided in figure 2.1. All core fractures, including those of both natural origin and drilling- or coring-induced origin, are included on this plot. Fracture densities range between 1 and 9 fractures/metre. Some significant peaks represent increased abundance of natural fractures. The peak of 8 fractures/metre at *c.* 240 mbsf represents an increase in small-scale faults as the major fault zone at *c.* 260 mbsf is approached. The peak of *c.* 6 fractures/metre at 800 mbsf marks the major fault zone between *c.* 790-806 mbsf. There is also a striking increase in natural fracture abundance within the inferred Beacon strata at *c.* 823 mbsf down to the base of the core.

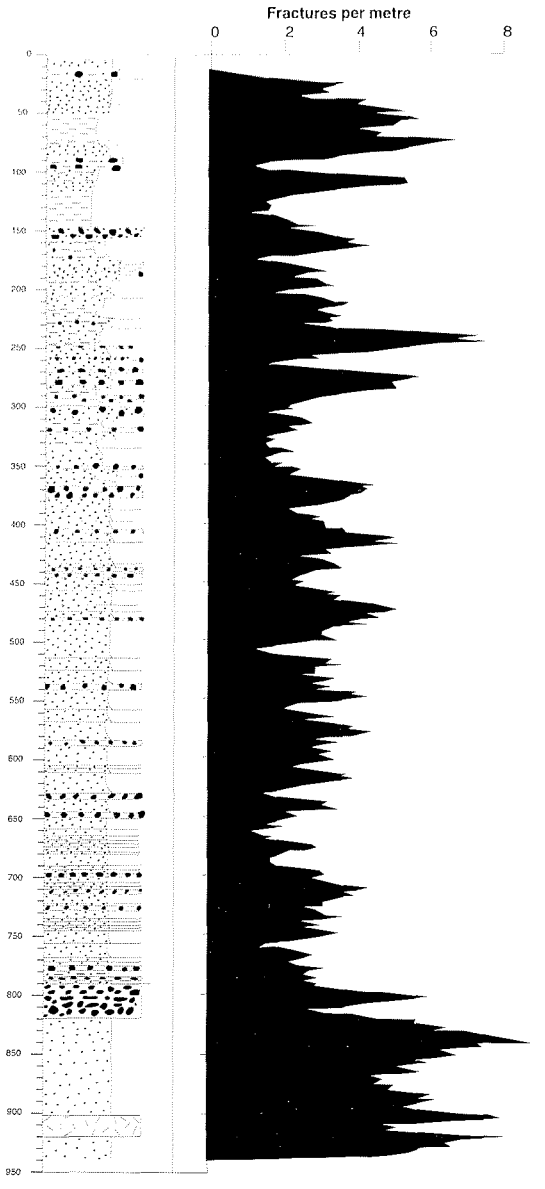

Fig. 2.1 - Fracture density *vs* depth and lithology in CRP-3 core. Number of fractures per metre of core smoothed by a 10-m moving average window. Major peaks at *c.* 240 and 790 mbsf are natural fractures related to large fault zones. Note the overall high fracture density associated with the inferred Beacon strata and intrusive porphyry below 823 mbsf.

INDUCED FRACTURES IN CRP-3 CORE

Petal, Petal-Centreline, and Core-Edge Fractures

Petal, petal-centreline and core-edge fractures are curviplanar, drilling-induced fractures that form in the host rock below the drill bit (Lorenz et al., 1990; Li & Schmitt, 1997, 1998). Petal-centreline and core-edge fractures both occur in CRP-3 core (Fig. 2.2), comprising a population of ~60 fractures. The majority of these drilling-induced fractures occur in the upper 225 m of the core where the material was less indurated. There are significantly fewer petal-centreline and core-edge fractures than in CRP-2A (Wilson & Paulsen, in press). Probable causes for the decreased abundance include a decrease in the drilling-mud density used in CRP-3 compared to CRP-2A because a decrease in drilling mud density would cause a decrease in the hydrostatic head exerted on the rock below. Alternatively, the decrease in abundance compared to CRP-2A could be related to the overall more indurated, stronger rock drilled at the base of CRP-2A and throughout CRP-3. Comparison with borehole televiewer imagery will allow us to determine the orientation of these drilling-induced fractures and, from that, the orientation of the maximum and minimum horizontal stresses, which are parallel and perpendicular respectively to the strike of these fracture planes.

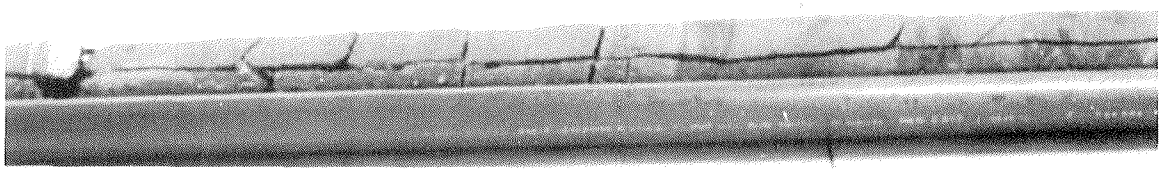

Fig. 2.2 - Petal-centreline fractures extending from *c.* 224.6 to 225 mbsf. Base of core to left; 61 mm diameter core.

Subhorizontal Tensile Fractures

A large population of subhorizontal fractures is present in CRP-3. In fine-grained mudstones and siltstones, well-developed surface fractographic features including hackle plume, arrest lines and twist hackle are present on these fracture surfaces, clearly documenting their formation as Mode 1 extension fractures. In the abundant sandstones cored in CRP-3, surface features were rare on the subhorizontal fractures, but they are also likely Mode 1 extension fractures. There are a variety of mechanisms for causing axial tension in the core. For example, Mode 1 extension fractures are typically induced at the end of a core run, when the driller retracts the drilling assembly off the bottom of the hole to break the cored rock from the uncored interval below. Other causes include raising the hydraulic chuck during drilling, handling-related flexure of the core, and disking, where tension arises when the core is released from the host rock upon entering the core barrel.

Other Drilling-, Coring-, and Handling-Induced Fractures

Fractures were also induced where advance of the core barrel was impeded by such factors as 'sticky' clay-rich material or abrupt changes from hard to soft material. In these areas, 'spin' fractures marked by circular grooves and/or torsion fractures were common. Some fractures developed during handling as the core was processed and transported.

NATURAL FRACTURES IN CRP-3 CORE

Microfaults

Discrete, planar microfaults of several types are abundant throughout CRP-3 core and provide a much more complete fault record than CRP-2A. Closed fractures that offset bedding planes with magnitudes of up to several cm are common. In the Oligocene strata these are almost always normal faults (Fig. 2.3). In the Beacon strata there are microfaults with both normal and reverse offset of bedding (Fig. 2.4). Many planar fracture surfaces sealed by carbonate cement or vein material have dips in the 60-80° range typical of normal faults. They show conjugate geometries and, where such surfaces opened during core handling, in some cases show striae on their surfaces, suggesting that most of these also mark fault planes. Planar fractures with well-developed slickensides, with or without evidence for bedding offset, are also common throughout the core (Fig. 2.5). Striae on the slickensided surfaces indicate that microfaults down to the fault zone encountered at *c.* 790 mbsf had very consistent dip-slip movement (Fig. 2.6a). Dip-slip microfaults commonly occur in a conjugate geometry, have dips that range from 55 to 70°, and display normal-sense displacement where bedding

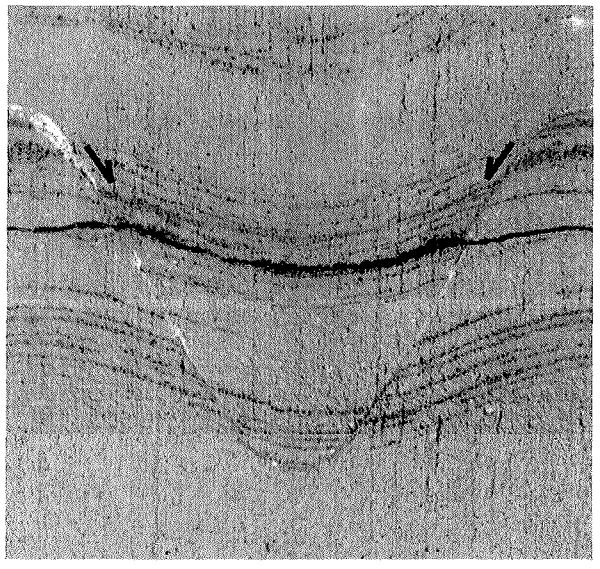

Fig. 2.3 - Normal fault offsetting coal laminae at 475.61-475.70 mbsf. Unrolled whole-core scan of 45-mm-diameter core.

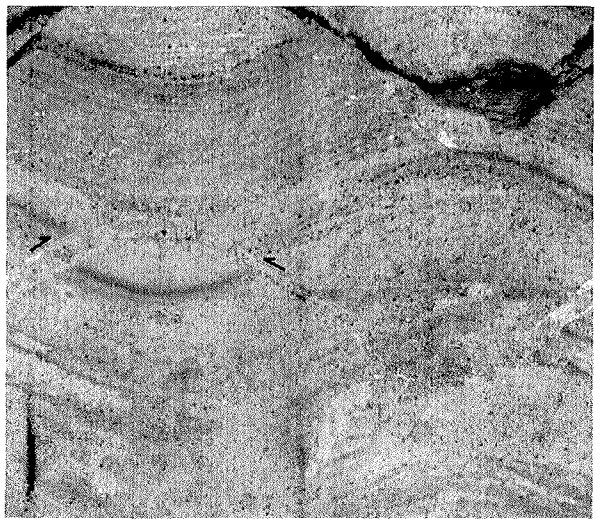

Fig. 2.4 - Calcite-cemented reverse fault in Beacon strata at 843.60-843.64 mbsf. Unrolled whole-core scan of 45-mm-diameter core.

Fig. 2.5 - Slickensided microfault surface showing dip-slip motion in Oligocene strata, 407.81-407.90 mbsf. Core is 45 mm in diameter.

was offset and/or surface shear-sense indicators are present. These attributes all indicate a normal-faulting regime with the greatest principal stress oriented vertically.

Beginning at the depth of the fault zone at 790 mbsf, striae on slickensided fault surfaces document a striking change from dip-slip motion to more complex, oblique shearing (Fig. 2.6b). Within the shear zone, approximately 44% of the microfaults with observable striae had striae with rakes of less than 45° (Fig. 2.7), indicating dominantly strike-slip movement, and the remainder show more steep striae rakes but still indicate oblique movement. The same kinematic pattern, with both strike-slip and oblique-slip faults, is characteristic of faulting below the 790 mbsf shear zone throughout the Beacon strata to the base of the core (Fig. 2.6c). Microfaults observed within the Beacon strata typically have lower dip angles (45-55°) than faults observed in Oligocene strata. Faults with an apparent reverse-sense offset of bedding, which were very rare in Oligocene strata, increase in abundance below the Oligocene/ Beacon contact. The limited kinematic data from slickenside surfaces suggest that the reverse-sense displacement may be due to oblique or strike-slip movement; however, we cannot rule out true dip-slip reverse displacement. Fault planes and fractures in the Beacon strata commonly are filled with either clay material or a coarse-grained fill with clastic appearance. At this stage it is not clear whether these fills represent cataclastic gouge and breccia or injected clastic material.

Veins

Fractures were classified as 'veins' where discrete, planar fractures were sealed by precipitated fill and showed no offset of bedding. Veins of a variety of types are common throughout CRP-3. Veins within the Oligocene section typically are filled with calcite and, less commonly, with pyrite. Fractures marked by planar bands of grey carbonate cement are also common in the Oligocene strata. Both of these vein types are very similar to those seen in the lower portion of CRP-2A core (Cape Roberts Science Team, 1999; Wilson & Paulsen, in press). Fault surfaces within the sheared dolerite between *c.* 790 and 810 mbsf and within the highly altered porphyritic intrusion between *c.* 900 and 920 mbsf have a fill of soft-green fibrous material, in some cases together with calcite, that grew during fault displacement. Within the Beacon strata, fracture planes are commonly outlined by bands or patches of yellow and gray noncalcareous material of unknown composition. The composition and textures of this widely varied vein material need to be examined in thin section.

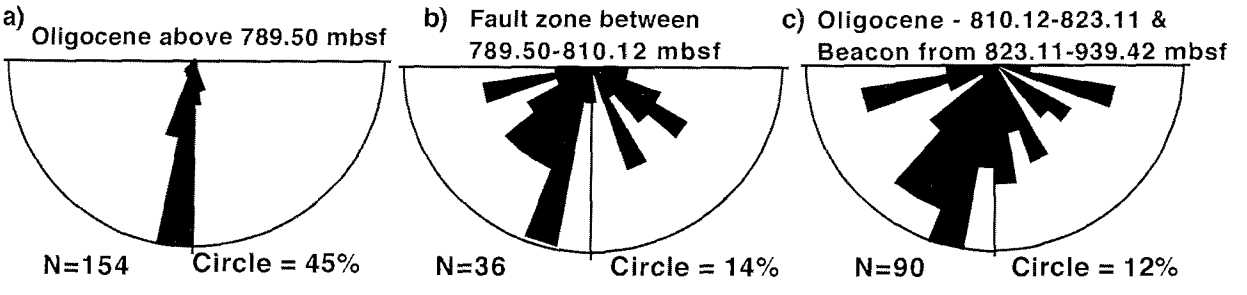

Fig. 2.6 - Rose diagrams of the rake of striae on fault surfaces for depth intervals as indicated. a) Note homogeneous, steep pitches in Oligocene strata indicating dip-slip motion; b) note change to more complex, oblique-slip shearing at fault zone beginning at 789.50 mbsf; c) note continuation of oblique-slip pattern through Oligocene and Beacon strata to base of core.

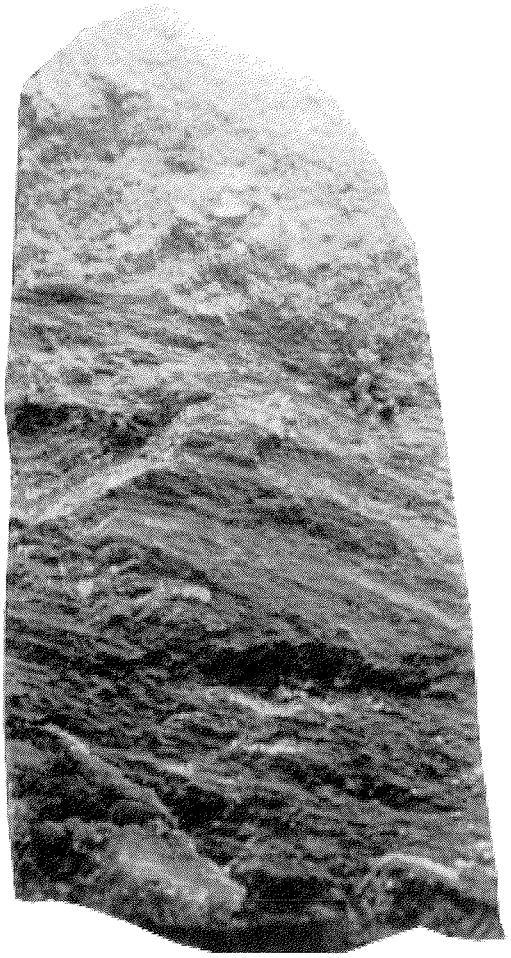

Fig. 2.7 - Low-angle oblique striae on microfault surface at 808.90-809.30 mbsf, indicating dominantly strike-slip movement.

Fig. 2.8 - Conjugate geometry of calcite veins at *c.* 407.28-407.39 mbsf, probably formed along fault planes.

Veins typically dip at moderate angles similar to microfaults, are 1-3 mm thick, and occur in spatial association with microfaults. Sparry calcite mineralization locally occurs in openings along faults that show offset of bedding, indicating mineralization in a dilatational fracture post-dating shearing. A few veins show a compound-branching or *en echelon* form typical of extensional Mode I fractures. The majority, however, are more likely to represent precipitation of vein material along fault planes because of their typical 50-70° dips and arrangement in conjugate geometries (Fig. 2.8).

Clastic Intrusions

Clastic intrusions (dykes) occur in the upper section of the core, filling fractures with typical dips between 40 and 75°. Dykes typically have sharp and planar boundaries, but less commonly irregular geometries. Dykes are commonly cemented with calcite and have thicknesses that typically range from 3 to 10 mm. In some cases the sedimentary injections appear to follow normal fault planes. Intrusions with an apparent clastic texture are common in Beacon strata, in association with breccias, described below.

LARGE FAULTS IN CRP-3

Three larger-scale fault zones were drilled at *c.* 260, 539, and 790 mbsf. The upper two fault zones are typical brittle faults. Only fallback material was obtained from the fault at 260 mbsf, consisting of intensely veined fragments and clay-size material. Dip-slip, normal-displacement, slickensided microfaults and calcite veins following microfaults increase in abundance downward through the core toward this fault zone, but are uncommon immediately below it. Most fault material at 539 mbsf was also not recovered; however, the lowermost surface is preserved in the core. A minimum displacement of 6 cm normal dip-slip separation is constrained by the extent of breccia fragments derived from a distinctive bed near the top of the core; however, total displacement is likely to be significantly larger. The fault surface is lined by up to 2 cm of calcite, including large, open vugs filled by sparry calcite. Both of these brittle fault zones were associated with extensive loss of drilling fluid into the borehole walls, indicating open fractures within the zone. They also are marked by negative temperature anomalies (see Downhole Logging section), documenting

high permeabilities along them. Although no direct indication of displacement sense or magnitude on these fault zones is available yet, the uniformity of the normal-sense dip-slip motion on microfaults throughout this portion of the Oligocene strata indicates these are likely normal faults. Preliminary examination of BHTV imagery did not reveal any clear record of the fault at 539 mbsf. Small faults above and below the fault at *c.* 260 mbsf dip moderately to the east; if these are synthetic to the large fault, it may also have an eastward dip.

A fault zone of markedly different character extends from *c.* 790 to 801.5 mbsf, with more localized faulting of similar character continuing down to *c.* 814 mbsf. The fault zone is dominated by coherent masses of dolerite crosscut by planar to irregular zones of fragmental material with a black, glassy matrix (Fig. 2.9). Clasts in the fragmented zones are dolerite, with rare sedimentary clasts. Clasts cross the spectrum of size from boulder to sand and of shape from angular to rounded (Fig. 2.10a). A smear slide of the glassy matrix material consisted of clay-size particles, and XRD analysis of a matrix sample at 798.03 mbsf showed quartz, plagioclase, illite, smectite and mixed-layer clay components (see section on X-Ray Mineralogy). Brittle fragmentation of the dolerite is indicated by the halos of clasts that surround the cobble- to boulder-size dolerite clasts. Gradations between these clast margins and ultrafine-grained, black matrix zones suggest that the clay-size matrix material was also formed by brittle cataclasis. When broken on any surface, the black matrix has an extreme, glassy polish and finely etched slickenlines indicating pervasive shear (Fig. 2.10b). In many cases, this black matrix material forms wispy injections into clast interiors, and these have helped to fragment the large clasts (Fig. 2.10a). Discrete microfault surfaces that cut the dolerite commonly show the same black, glassy surface material and/or have a fill of a soft, fibrous mineral with a greenish hue.

There is a wide range of attitudes of slickenlined surfaces within this fault zone; however, there appear to be two dominant fracture sets that may have a conjugate geometry. Slickenline orientations also show a range of rake angles on these fracture surfaces, ranging from high- to low-angle oblique slip (Fig. 2.6b). Because we do not yet have orientation for the core, we cannot analyze the fault zone kinematically. The few available shear-sense indicators derived from slickenfibre step directions on discrete microfault surfaces indicate both normal-left-lateral and normal-right-lateral oblique shear. BHTV imagery shows moderately to steeply west-dipping fractures and some fractures with shallow to moderate eastward dips within the fault zone, but it is unclear whether either of these fracture sets parallels the overall orientation of the fault zone.

Fig. 2.9 - Fragmental bands in fault zone from 790-801 mbsf interpreted to form by cataclasis. Unrolled whole-core scan of 45-mm-diameter core between *c.* 794.10 and 794.74 mbsf. Note planar zones of fragmental material with moderate to steep dips and dark bands of injected material connecting them (arrows).

BRECCIAS IN BEACON STRATA

Brecciation is very common within the inferred Beacon strata cored in the lower *c.* 100 m of the core,

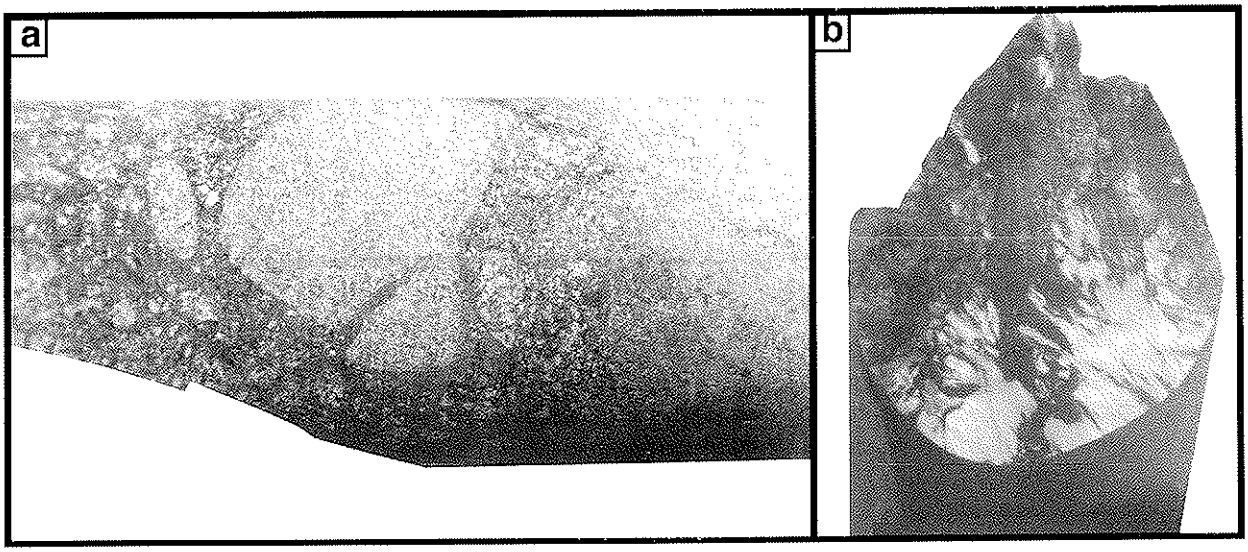

Fig. 2.10 - Textures in fragmental material interpreted as cataclasites in fault zone at 790-801 mbsf. a) Angular to subrounded clasts of wide range of grain sizes. Note matrix injected into clast, terminating inward and spalling off clast fragment. b) Glassy, polished and slickenlined surface in ultrafine-grained matrix interpreted to be ultracataclasite formed by pervasive shearing.

comprising up to 36% of the Beacon unit. Beacon fragments with angular to subrounded shapes float in a matrix of coarse sand-sized material. Rotation of bedding between clasts within the breccia documents post-lithification fragmentation. Whole-core observations showed that the most common form of the breccia bodies infills planar zones with steep dips (Fig. 2.11). In general the steep breccia zones transect bedding, but they locally branch into bedding planes, suggesting the brecciated material was injected. In association with the breccias are abundant planar injections with a clastic texture. These also mainly dip in the 60-80° range and crosscut bedding, but were locally injected along bedding planes. The material filling these injections includes coarse, rounded quartz grains clearly related to the host strata. It could be either cataclastically granulated host rock or remobilised sedimentary material of unknown source, although the latter is unlikely because of the compositional similarity to the lithified Beacon host rocks. Textural analysis of thin sections should resolve this question.

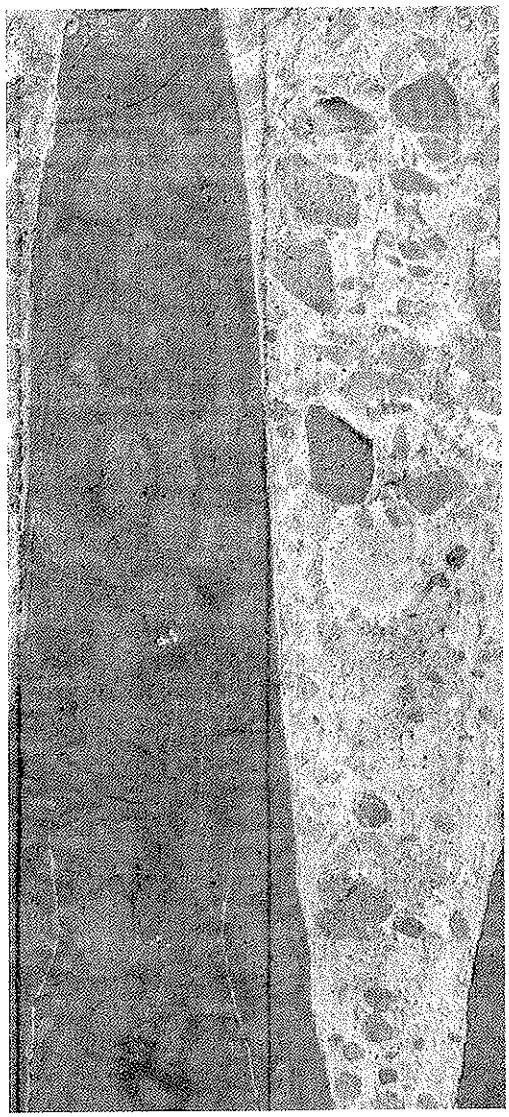

Fig. 2.11 - Breccia zone with planar margins in Beacon strata at *c.* 866.89 mbsf.

PHYSICAL PROPERTIES FROM ON-SITE CORE MEASUREMENTS

INTRODUCTION

We carried out core physical-property measurements (made on the core as opposed to in the bore hole) for CRP-3 in a similar manner to those for CRP-1 and CRP-2. For CRP-1 and CRP-2, physical properties were used to define and interpret stratigraphical patterns, including a comparison between lithology and sequences (Cape Roberts Science Team, 1998; Cape Roberts Science Team, 1999; Niessen & Jarrard, 1998; Niessen et al., 1998). For example, grain size has an effect on porosity

calculated from wet-bulk density (WBD) in the CRP-1 core. However, for CRP-2 we found that the effect of grain size on porosity and velocity is subtle because cementation is the primary control on velocity-porosity relationships in the deeper part of the hole. This is caused by particularly strong carbonate cementation (Niessen et al., in press).

In both CRP-1 and CRP-2, sequences are reflected by the cyclic pattern of magnetic susceptibility (MS). In the upper part of the CRP-1 core, this pattern is overprinted by volcanic debris derived from the McMurdo volcanic province. CRP-1 porosity decreases strongly down-core, which we interpreted as a secondary overprint on consolidation, such as overcompaction by ice and cementation (Niessen et al., 1998). However, it has to be considered that the core length of CRP-1 is only 147.7 m and that steep porosity gradients are also commonly observed over relatively short depth intervals in CRP-2. In the latter these are averaged out by an intercalation of strongly consolidated units with weakly or unconsolidated units of higher porosity, so that the overall porosity trend of CRP-2 was not oversteepened (Brink & Jarrard, in press).

The P-wave velocities of CRP-1 and CRP-2 were used to calculate acoustic travel times, which provided the link from seismic profiles to the cores. For CRP-3, a major goal is to use both density and velocity data to assess depth intervals for potential seismic reflectors in order to extend the calibration of regional seismic records of the Victoria Land Basin.

METHODS

Measurements at the drill-site laboratory included non-destructive, near-continuous determinations of wet bulk density (WBD), P-wave velocity (Vp), and magnetic susceptibility (MS) at 2-cm intervals. We used the Multi Sensor Core Logger (MSCL, GEOTEK Ltd., UK) to measure core temperature, core diameter, P-wave travel time, gamma-ray attenuation and MS. The technical specifications of the MSCL system are summarised in table 2.1. As with CRP-2, we logged the cores in plastic carriers to avoid destruction of non-consolidated rock material (Cape Roberts Science Team, 1999). Unlike CRP-2, the upper 38.13 m of CRP-3 HQ-size had to be logged on split-cores (archive halves). Data were logged in continuous intervals of 6 to 23 m. Prior to and after each of these logging intervals, calibration pieces of 0.4 m length were logged, including a blank carrier to measure non-attenuated gamma radiation. In addition, cylindrical standards (Tab. 2.2) for both HQ and NQ size were logged in order to monitor the accuracy of WBD and Vp values.

Settings and parameters of MS measurements are summarised in table 2.1. The sensor was tested using the Bartington sensor-specific core-calibration piece. No offset was observed. Data were corrected for loop-sensor and core diameter as follows:

$$MS\ (10^{-5}\ SI) = \text{measured value}\ (10^{-5}\ SI) / K\text{-rel} \quad (i)$$

This sensor correction is based on a modified algorithm provided by Bartington after the CRP-2 field season:

$$K\text{-rel} = -0.04018 + 5.5832 * (d/Dc)^{2.26973} \quad (ii)$$

where d = core diameter and Dc = coil diameter of the sensor. Resulting HQ and NQ K-rel is given in table 2.1.

Vp was measured using Acoustic Rolling Contact Transducers (ARC, GEOTEK Ltd., UK). The sensor settings and the calibration (quantification of P-wave travel time offset through the core carrier wall, transducer, and electronic delay) are described in detail in Cape Roberts Science Team (1999). P-wave velocities (Vp) were normalised to 20°C using the temperature logs:

$$Vp = Vpm + 3 * (20 - tm) \quad (iii)$$

where Vpm = P-wave velocity at measured temperature (Tab. 2.1); tm = measured temperature.

As during to the CRP-2 season, a laboratory-built P-wave registration apparatus was used in addition to the standard Vp-detection system of the GEOTEK Multi-Sensor-Core-Logger (MSCL) in order to digitise transmission seismograms. This system is described in detail in Cape Roberts Science Team (1999). The technical specifications are summarised in table 2.1.

WBD was determined as described in Cape Roberts Science Team (1999) and Weber et al. (1997). The settings of the CRP-3 gamma-detection system are summarized in table 2.1.

Porosity was calculated from the WBD as follows:

$$POR = (dg - WBD) / (dg - dw) \quad (iv)$$

where dg = grain density (2.7 g cm^{-3}); dw = pore-water density (1.03 g cm^{-3}).

The gamma-detector output was calibrated at the beginning of CRP-3 coring activity for the HQ whole settings and then recalibrated for HQ half-cores and NQ whole-cores. In addition, unattenuated measurements were made at the beginning of each run to monitor the stability of the gamma detector during the measuring process. The variation was minor (Tab. 2.2). The variation of the standards of all runs is plotted *versus* depth (Figs. 2.12 & 2.13) in order to ensure that there is no offset observed between the three different types of core logged (HQ half cores, HQ whole-cores and NQ whole cores). The statistics of the standards are summarised in table 2.2.

Down-core logs comprise nearly complete data sets for all lithological units. Only for those depth intervals where major disturbances were observed (cracks, fractured sections, gaps or heavily crumbled core) were data eliminated. Two different data sets are presented in this report. To report on general variability and to define core physical property (CPP) units, we smoothed the

Tab. 2.1 - Multi-Sensor-Core Logger (MSCL-25) specifications for CRP-3.

P-wave Velocity and Core Diameter	
Sensor orientation	vertical
Transducer	Acoustic Rolling Contact Transducer (GEOTEK Ltd.)
Transmitter pulse frequency	230 kHz
Transmitted pulse repetition rate:	100 Hz
Received pulse resolution	50 ns
P-wave travel-time offset	18.8 µs (HQ), 19.8 µs (NQ)
P-wave Transmission Seismograms	
ADC board	T3012 (National Instruments)
Sampling frequency and resolution	30 Mhz, 12 bit
Sampling interval	50 ns
Length of seismograms	200 ms
Wet Bulk Density	
Sensor orientation	vertical
Gamma ray source	Cs-137
Source activity	356 MBq
Source energy	0.662 MeV
Counting time	10 s
Collimator diameter	5 mm (whole cores HQ/NQ), 2.5 mm (half cores HQ)
Gamma detector	NaI-Scintillation Counter (John Count Scientific Ltd.)
Magnetic Susceptibility	
Loop sensor type	MS-2B (Bartington Ltd.)
Loop sensor diameter	80 mm
Loop sensor coil diameter	88 mm
Alternating field frequency	0.565 kHz
Sensitivity	1 s, 10s (HQ), 10 s (NQ)
Magnetic field intensity	approx. 80 A/m RMS
Loop sensor correction coefficient K-rel (HQ)	1.0884
Loop sensor correction coefficient K-rel (NQ)	0.5235
Temperature	
Sensor type	infrared

original data using a 20 data-point running window, then interpolated (32 000 data points per 600 m of core) and resampled using 0.05-m equal vertical spacing (Fig. 2.14). All data of good quality are presented without statistical treatment in two depth logs (0-500 mbsf and 500-940 mbsf, Figs. 2.15 & 2.16, respectively), and, in more detail, for some depth intervals where major boundaries were observed in the lithology (Figs. 2.17 to 2.19).

GENERAL OBSERVATIONS

Magnetic susceptibilities range on a large scale from near zero to up to 6259 (10^{-5} SI). Some sandstones even yielded negative susceptibilities (0 to -1), which are not shown in the graphs of this report because the data are plotted on a logarithmic scale. The highest susceptibilities are measured in dolerite clasts and intrusions. WBD ranges from 1.63 to 3.16 Mg m^{-3} with the lower values near the top of the core and maximum values in dolerite clasts. The corresponding porosities calculated after equation (iv) range from *c.* -0.27 to 0.64. Similar to results from CRP-1 and CRP-2, the assumption of constant grain density of 2.7 Mg m^{-3} (equation iv) results in negative porosities for clasts of higher grain density (Niessen & Jarrard, 1998; Niessen et al., in press). Vp ranges from *c.* 1 562 to 6 703 ms^{-1} and, in general, correlates remarkably well positively with density (Fig. 2.14). In the upper 820 mbsf, dispersion in the core physical property data is more common than in the lowermost part of CRP-3. Dominant gradients of physical properties are observed in the upper 140 m of the core and below *c.* 780 mbsf. However, systematic down-core trends in velocity, WBD, and porosity, which were clearly evident in data from CRP-1 and CRP-2, are not observed in CRP-3. This problem will be addressed in more detail in the CRP-3 Science Report.

Tab. 2.2 - Statistics on measured standards for CRP-3.

Standard material	Type of standard	Core diameter	Cross section	No. of measured standards	Min.	Max..	Mean	Std. Deviation
Alumin.	Density (Mg m^{-3})	HQ	1/2	4	2.69	2.72	2.7	--
Alumin	Velocity (m s^{-1})	HQ	1/2	4	6318	7061	6748	--
Plastic	Density (Mg m^{-3})	HQ	1/2	4	1.40	1.42	1.41	--
Plastic	Velocity (m s^{-1})	HQ	1/2	4	2326	2387	2350	--
Plastic	Diameter (mm)	HQ	1/2	4	4.49	4.50	4.495	--
Air (Io)	Radiation (CPS)	HQ	1/2	4	4966	4982	4974	--
Alumin.	Density (Mg m^{-3})	HQ	1/1	28	2.68	2.74	2.70	0.015
Alumin	Velocity (m s^{-1})	HQ	1/1	26	6571	7078	6824	153.41
Plastic	Density (Mg m^{-3})	HQ	1/1	52	1.40	1.44	1.42	0.009
Plastic	Velocity (m s^{-1})	HQ	1/1	48	2311	2447	2380	33.9
Water	Density (Mg m^{-3})	HQ	1/1	32	0.956	1.022	0.98	0.014
Water	Velocity (m s^{-1})	HQ	1/1	32	1476	1510	1492	9.11
Plastic	Diameter (mm)	HQ	1/1	50	5.96	6.49	6.13	0.10
Air (Io)	Radiation (CPI)	HQ	1/1	48	16225	16537	16378	91.9
Alumin.	Density (Mg m^{-3})	NQ	1/1	94	2.63	2.75	2.70	0.02
Alumin	Velocity (m s^{-1})	NQ	1/1	88	6535	7026	6824	103.8
Plastic	Density (Mg m^{-3})	NQ	1/1	96	1.37	1.46	1.42	0.017
Plastic	Velocity (m s^{-1})	NQ	1/1	96	2297	2433	2380	27.2
Plastic	Diameter (mm)	NQ	1/1	96	4.49	4.52	4.50	0.007
Air (Io)	Radiation (CPI)	NQ	1/1	96	15582	16017	15857	75.22

Note: Density of aluminum standard (1) = 2.7 Mg m^{-3}; velocity of aluminum standard = 6 800 ms^{-1}; density of plastic standard (2) = 1.42 Mg m^{-3}; velocity of plastic = 2 370 ms^{-1}; density of water (3) (including container at 20°C) = 1.0 Mg m^{-3}; velocity of water (including container at 20°C) = 1 493 ms^{-1}; CPS = counts *per* second.

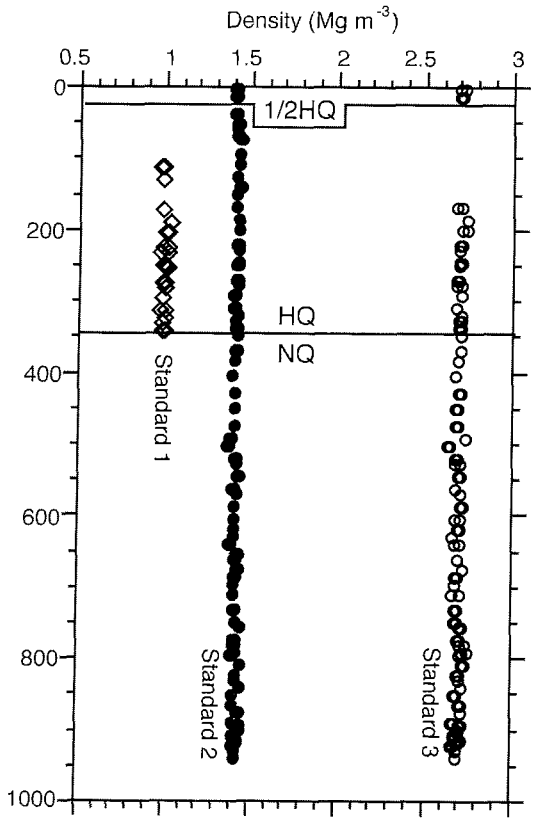

Fig. 2.12 - Measured densities of standards for different depth levels of CRP-3 core logging. Material and density of standards in table 2.2.

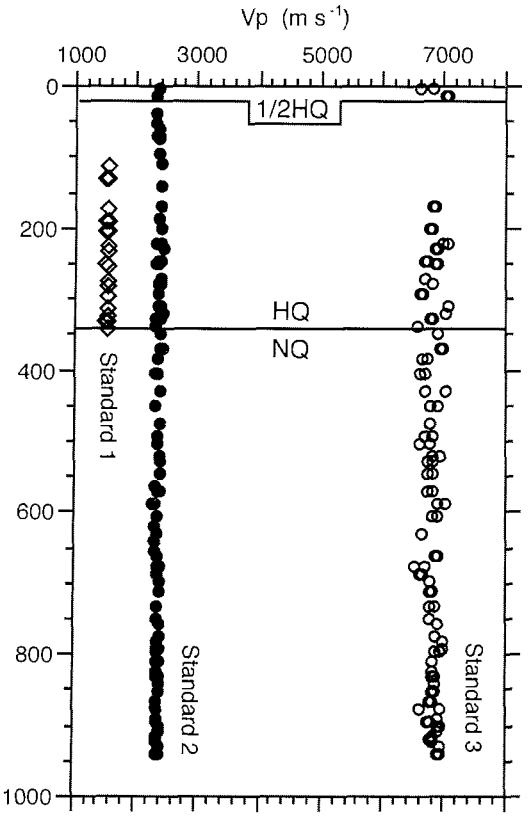

Fig. 2.13 - Measured velocities of standards for different depth levels of CRP-3 core logging. Material and velocity of standards in table 2.2.

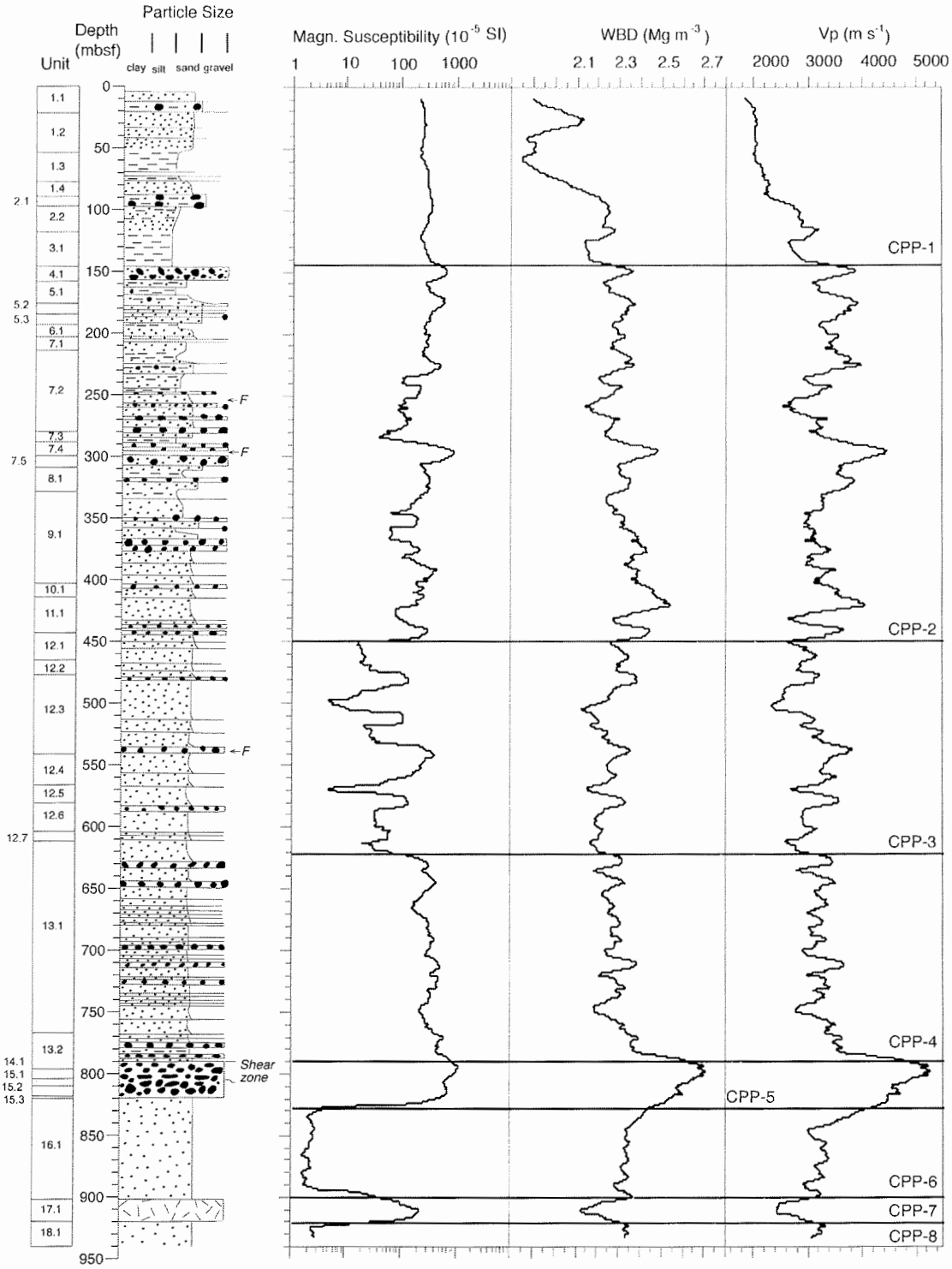

Fig. 2.14 - Core physical properties of CRP-3 and core-physical property units (CPP).

STRATIGRAPHY OF CORE PHYSICAL PROPERTIES

An overview of the down-core pattern of MS, WBD and Vp is presented in figure 2.14. By combining all three records together, eight major units (CPP-1 to CPP-8) can be distinguished (Fig. 2.14). At 144, 790, 823 and 901 mbsf, core physical property units match the units defined using CRP-3 bore-hole logs.

Unit CPP-1 extends from the top of the core to 144 mbsf. It is defined by relatively uniform MS and steep down-core gradients of WBD and velocity. Some fluctuations are superimposed on these gradients, in particular in the density data. The strong down-core gradient in velocity and density can probably be attributed to secondary diagenesis rather than primary compaction of the core. In this unit the core is also heavily fractured (coring

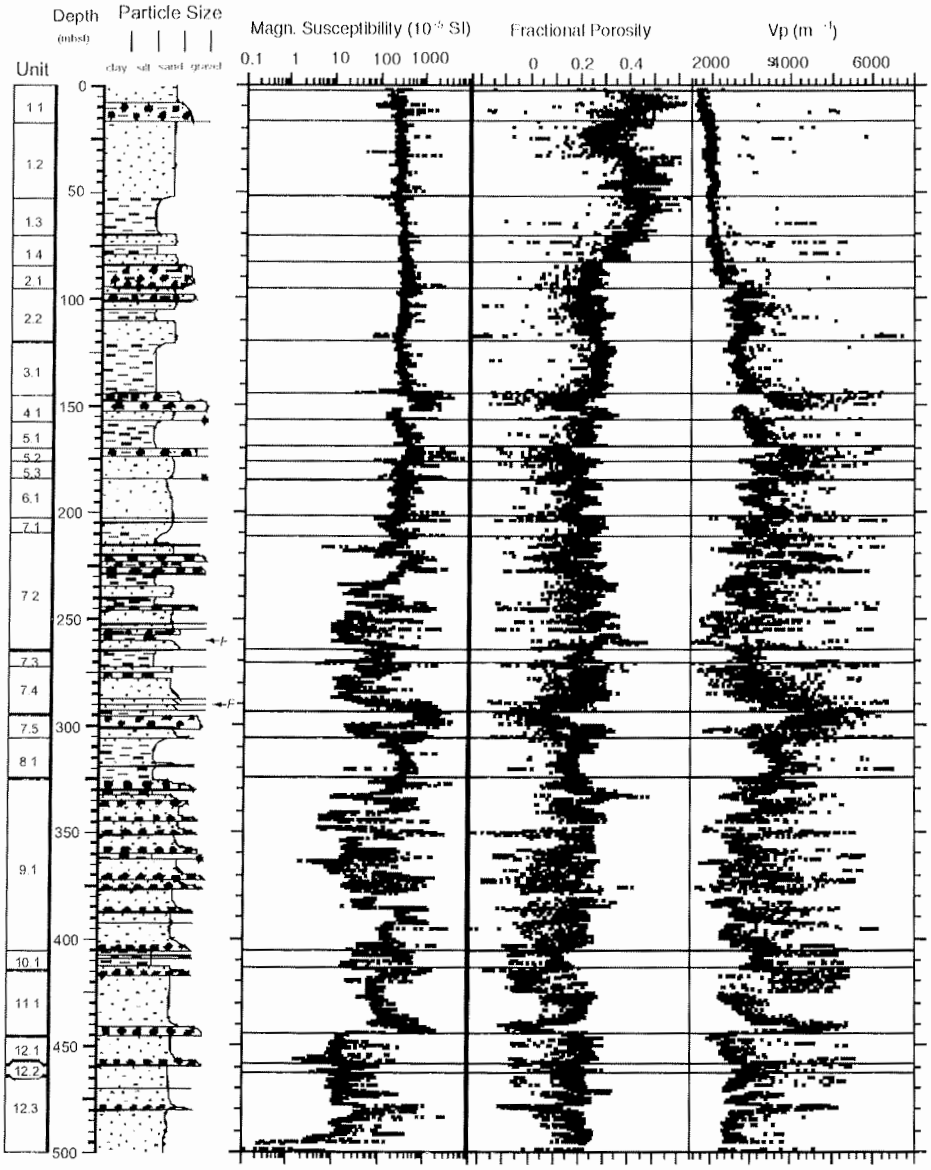

Fig. 2.15 - Log of all core physical-property data in the upper part of CRP-3. Horizontal lines represent boundaries of lithostratigraphical units.

induced, see preceding sections of this report), which indicates that most of its carbonate cement may have been dissolved towards the top of the core. The boundary to the next lower unit appears somewhat gradual.

Unit CPP-2 (144 to 450 mbsf) is characterised by relatively high values of MS, WBD and velocity, and it exhibits stronger fluctuations in all three parameters than above. Fluctuations correlate well between velocity and WBD logs, and to a lesser extent also with MS. It is notable that, on average, WBD increases slightly farther down-core, whereas no such gradient is evident in the velocity. The different trends in velocity and density may imply stronger cementation in the upper half of the unit because velocity is relatively high compared to WBD, indicating higher rigidity. The reason is that cementation can have a major effect on rigidity. Thus, increased rigidity towards the top of the unit can keep velocities high despite the decrease of WBD. The lower boundary of CPP-2 is sharp in MS but appears gradual in WBD and velocity.

Unit CPP-3 (450 to 620 mbsf) is defined by remarkably lower MS, in particular in two minima that correlate with light-coloured quartzose sandstone Units 12.3 and 12.5. The unit is also characterised by decreased WBD and velocities compared to underlying and overlying units. The pattern suggests that the unit is characterised by relatively mature sands that may have lost magnetic components during reworking and/or different type of erosion. The lower boundary is gradual in the WBD and velocity, but is more distinctive in the MS records.

Unit CPP-4 (620 to 790 mbsf) exhibits relatively small-scale oscillations in all three parameters. At the top of this unit, MS increases down-core by more than one order of magnitude and then stays relatively stable to the bottom of CPP-4. The character of core physical properties of this unit is quite similar to Unit CPP-2. The transition into the underlying Unit CPP-5 appears gradual.

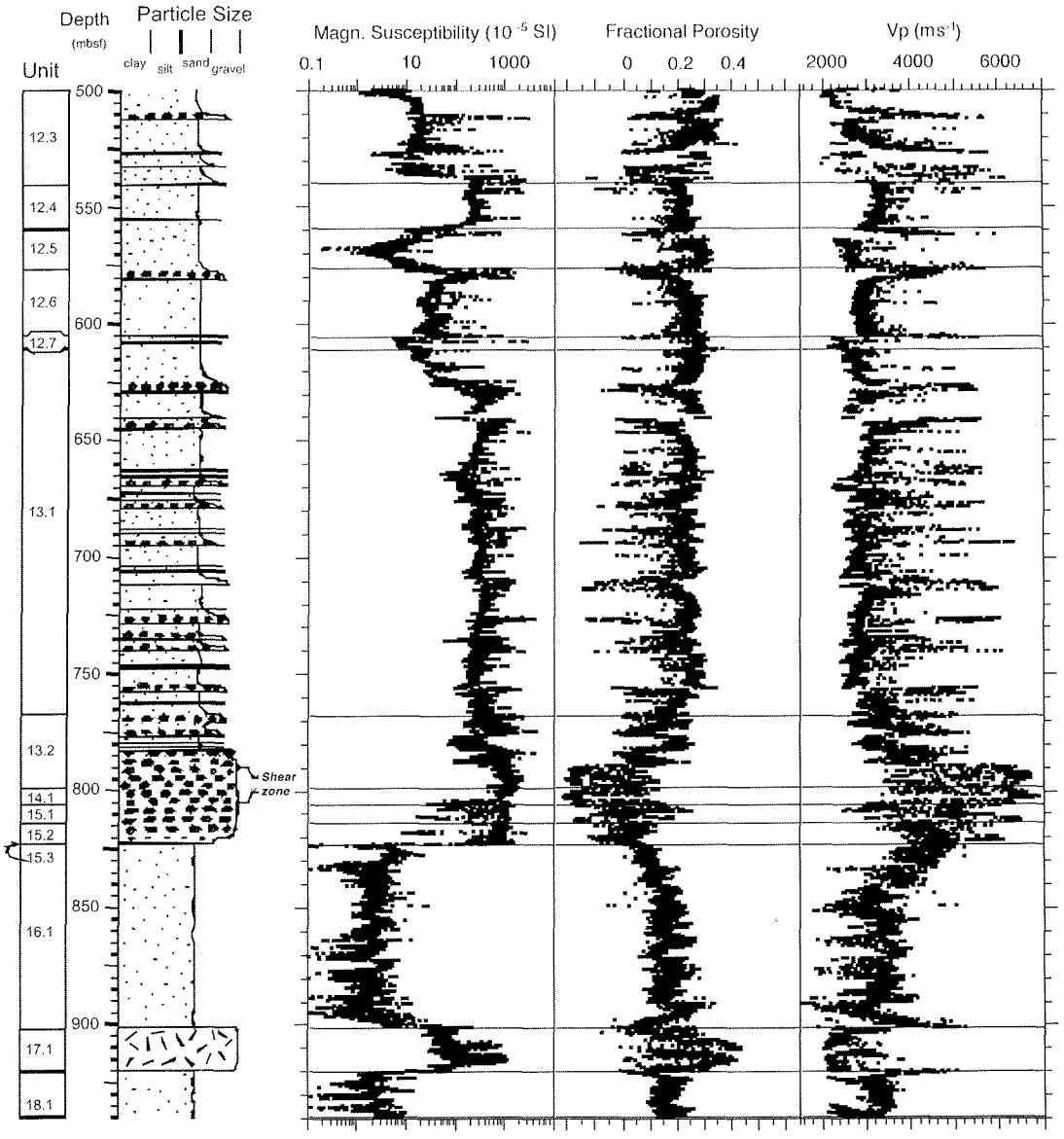

Fig. 2.16 - Log of all core physical-property data in the lower part of CRP-3. Horizontal lines represent boundaries of lithostratigraphical units.

This may be affected by smoothing the data because there is a rather sharp boundary in the fractional porosity and velocity at 790 mbsf on the unsmoothed data (Fig. 2.16)

Unit CPP-5 (790 to 823 mbsf) is characterised by a major maximum in MS, WBD and velocity. This CPP unit corresponds to LSU 14.1 to 15.3, which is dominated by dolerite breccia and conglomerate. Thus, the core physical properties of CPP-5 largely reflect the physical signature of Ferrar rocks. Because of the very steep increase of both WBD and velocity at the top, Unit CPP-5 may also form one of the strongest reflectors in seismic profiles across the drill site.

Unit CPP-6 (823 to 901 mbsf) is defined by a constantly very low MS and a gradual decrease in velocity. WBD is significantly lower than in the overlying Unit CPP-5 but slightly higher than in Units CPP-3 and CPP-4. Unit CPP-6 correlates with the Beacon sandstone (LSU 16.1).

Unit CPP-7 (901 to 920 mbsf) marks the altered dolerite intrusion of LSU 17.1. MS returns to values almost as high as in Unit CPP-5. But, in contrast to the dolerite-dominated Unit CPP-5, WBD and velocity are distinctly lower in CPP-7 as compared to the adjacent Beacon sandstone, probably because of extensive alteration of the intrusion. Both WBD and velocity are about as low as most minima observed in the units above.

Unit CPP-8 (920 to 939.42 mbsf) is very similar to Unit CPP-6 and correlates with the lower part of the Beacon sandstone in the core.

COMPARISON OF PHYSICAL PROPERTIES WITH LITHOLOGY AND SEQUENCES

Two logs of higher vertical resolution are presented (0-500 mbsf and 500-939.42 mbsf, Figs. 2.15 & 2.16, respectively) and compared with the lithological units. These detailed logs include porosity data calculated from WBD. It is evident that some major changes of core physical properties match lithological unit boundaries.

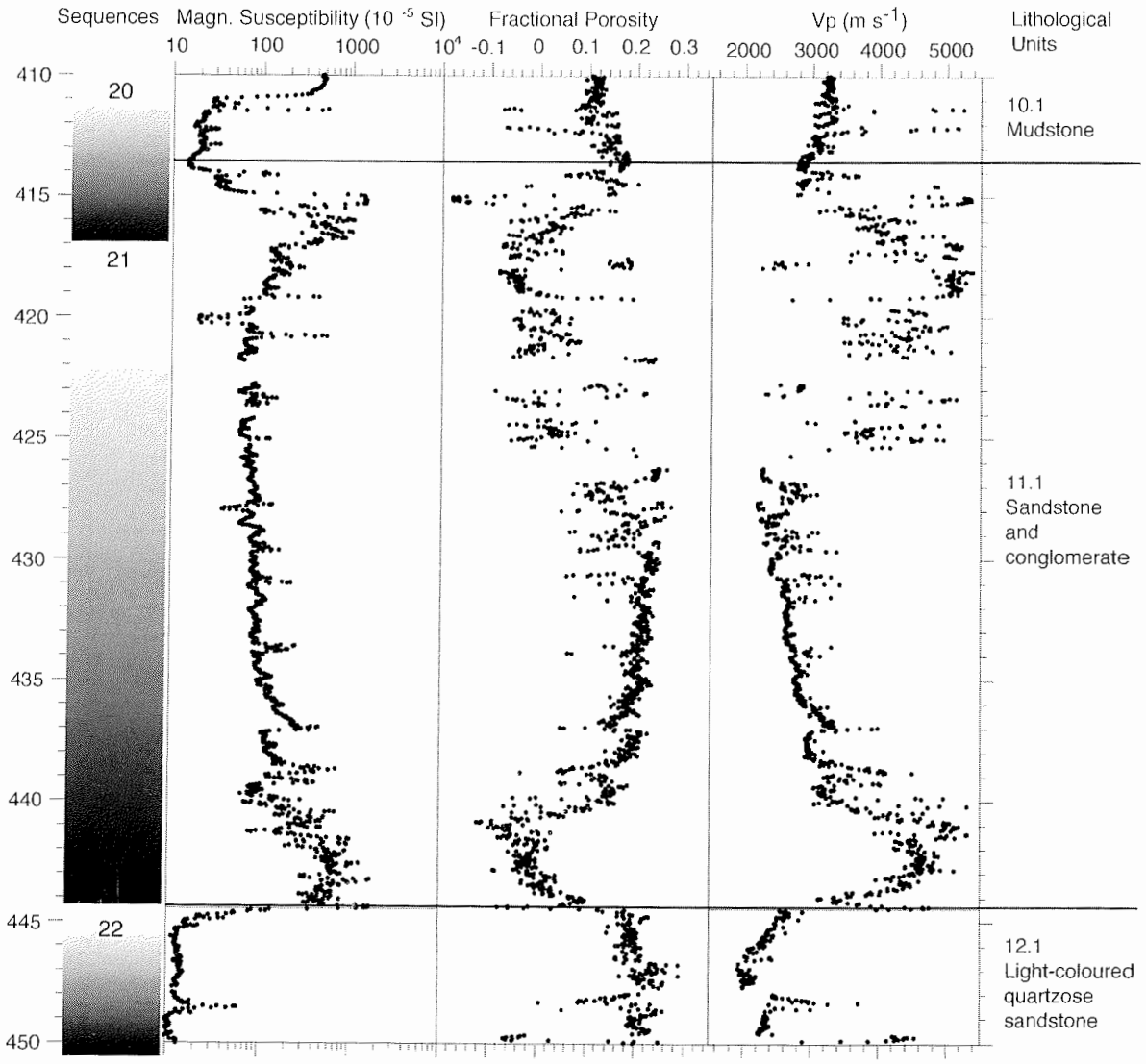

Fig. 2.17 - Comparison of core physical properties with lithological boundaries and sequence boundaries for a selected depth level of CRP-3.

However, many lithological boundaries are characterised by gradual rather than sharp changes in the physical property data.

Similar to CRP-1 and CRP-2, units containing large single clasts exhibit lower porosities, higher velocities, and large dispersion in all three parameters. For all units, where larger amounts of gravel were logged, a spike of higher velocity and lower porosity is notable in the physical property records. Usually these spikes reach velocities to about 6000 m s^{-1} and result in apparent negative porosities. The latter is indicative of basement rock clasts having densities well above the assumed grain density of 2.7 Mg m^{-3}. In most cases the occurrence of gravel and cobbles is also associated with increased MS. This kind of "bedrock signature" is best seen in the boulder-rich dolerite conglomerates and breccias of LSU 13.2, 15.1 and 15.2, where velocities exceed 6000 m s^{-1} and densities are as high as 3.06 Mg m^{-3}. The latter result in apparent negative velocities below -0.2. It is interesting to note that the relatively strong dispersion evident above 823 mbsf is not observed below this depth. The sandstones at the bottom of the core are older than the Ferrar, thus dolerite clasts do not occur in the core below 823 mbsf.

Low porosity and, in particular, high velocity values are not entirely restricted to lithologies rich in clasts. Despite lack of general depth trends in velocities and porosities, sandstones from different depth can have very different velocities and porosities. For example, at 40, 115, 445 and 900 mbsf velocities are *c.* 2 000, 3 000, 4 500 and up to 5 000 ms^{-1} respectively. The porosities in these intervals are 0.4, 0.2, 0.05, and 0. These differences are attributed to a combined effect of consolidation and cementation. The importance of cementation has already been pointed out for CRP-2 physical property data and was briefly discussed above. A detailed analysis of velocity/porosity relationships may help identify strongly cemented layers and will be presented in the CRP-3 Science Report.

The results from CRP-1 and CRP-2 demonstrated

that sedimentary sequences match the pattern of core physical boundaries better than lithological units. It is too early to compare the entire sequence stratigraphy of CRP-3 to the record of core physical properties. However, for Tertiary strata the depth interval from 410 to 450 mbsf was chosen as a key example to compare lithological boundaries and sequence boundaries with physical properties (Fig. 2.17). The lithology describes light-coloured quartzose sandstone (LSU 12.1) overlain by sandstones and conglomerate (LSU 11.1) grading into mudstones (LSU 10.1). Sequence boundaries are located at 416.99 and 444.44 mbsf (onset and top of Sequence 21). The lower lithological boundary at 444.44 mbsf matches the onset of Sequence 21. These boundaries are clearly reflected as steep gradients in MS, porosity and velocity (Fig. 2.17) at the base of the conglomerates at 416.99 and 444.44 mbsf. Within Sequence 21 fining upward is indicated by a gradual decrease in MS and velocity combined with increasing porosities.

This pattern is repeated by the MS data at the onset of Sequence 20. Susceptibility exhibits a rapid shift to values above 1 000 (10^{-5} SI), gradually decreasing back to the level of about 10 in the overlying mudstones. This suggests that MS may be a powerful tool to identify and interpret sequences in the CRP-3 record. In turn, it may suggest that the MS record may be largely controlled by environmental changes such as those induced by climate and sea level fluctuation.

Sequence boundary 20/21 (Fig. 2.17), however, is not clearly indicated in the porosity and velocity data because a distinct change is indicated within the sequence (at *c.* 425 mbsf) rather than at the sequence boundary (Fig. 2.17). Higher velocities and lower porosities above 425 mbsf may indicate differences in the cementation of the sandstone. This pattern may suggest that diagenetic effects on physical properties are superimposed on lithological changes. As in the example of Sequence 21, these effects may, in places, mask evidence of sequence boundaries in the velocity/porosity data. None of the physical properties marks a distinct shift at the lithological boundary between LSU 11.1 and 10.1.

The top of the Beacon sandstone (LSU 15.2) is characterised by a distinct lithological change from light red/brown quartzose sandstones into overlying dolerite-clast conglomerate intercalated with a relatively thin unit of sandstone-clast breccia. This boundary is important because it marks the penetration of CRP-3 drilling into Paleozoic bedrock. At this transition core physical properties are compared with lithologies between 817 and 827.5 mbsf (Fig. 2.18). The boundaries are marked distinctively by MS data. At the top of the Beacon, MS exhibits a significant minimum close to zero followed by a steep gradient through the sandstone-clast breccia into overlying dolerite conglomerates. MS increases over four orders of magnitude, which is the strongest gradient observed in the entire core. On the other hand, porosities fluctuate rather insignificantly at this boundary, and velocities even remain stable. The reason could be that the top of the Beacon is strongly cemented and thus exhibits velocities almost as high as in the lower part of the overlying dolerite-clast conglomerates.

Another major lithological change is the igneous intrusion into Beacon sandstone drilled between 901.48 and 919.95 mbsf. The upper and lower contacts of the intrusion are clearly evident in the record of core physical properties between 895 and 925 mbsf (Fig. 2.19). The igneous rock is characterised by MS of about 100 (10^{-5} SI), including several distinct spikes up to 1 000. Porosity of up to more than 0.4 is significantly higher than measured in the overlying and underlying sandstones. Velocities are about 1 000 m s^{-1} lower than those measured in the Beacon (LSU 16.1 and 18.1, Fig. 2.19). It is interesting to note that the intrusion has obviously altered the

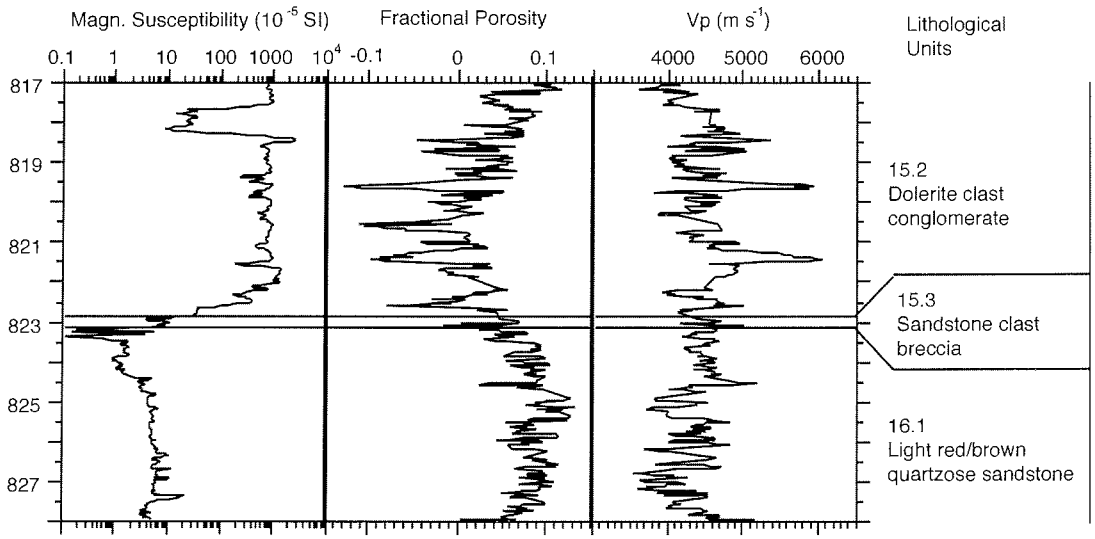

Fig. 2.18 - Comparison of core physical properties with lithological boundaries for a selected depth level of CRP-3 (transition into Beacon basement).

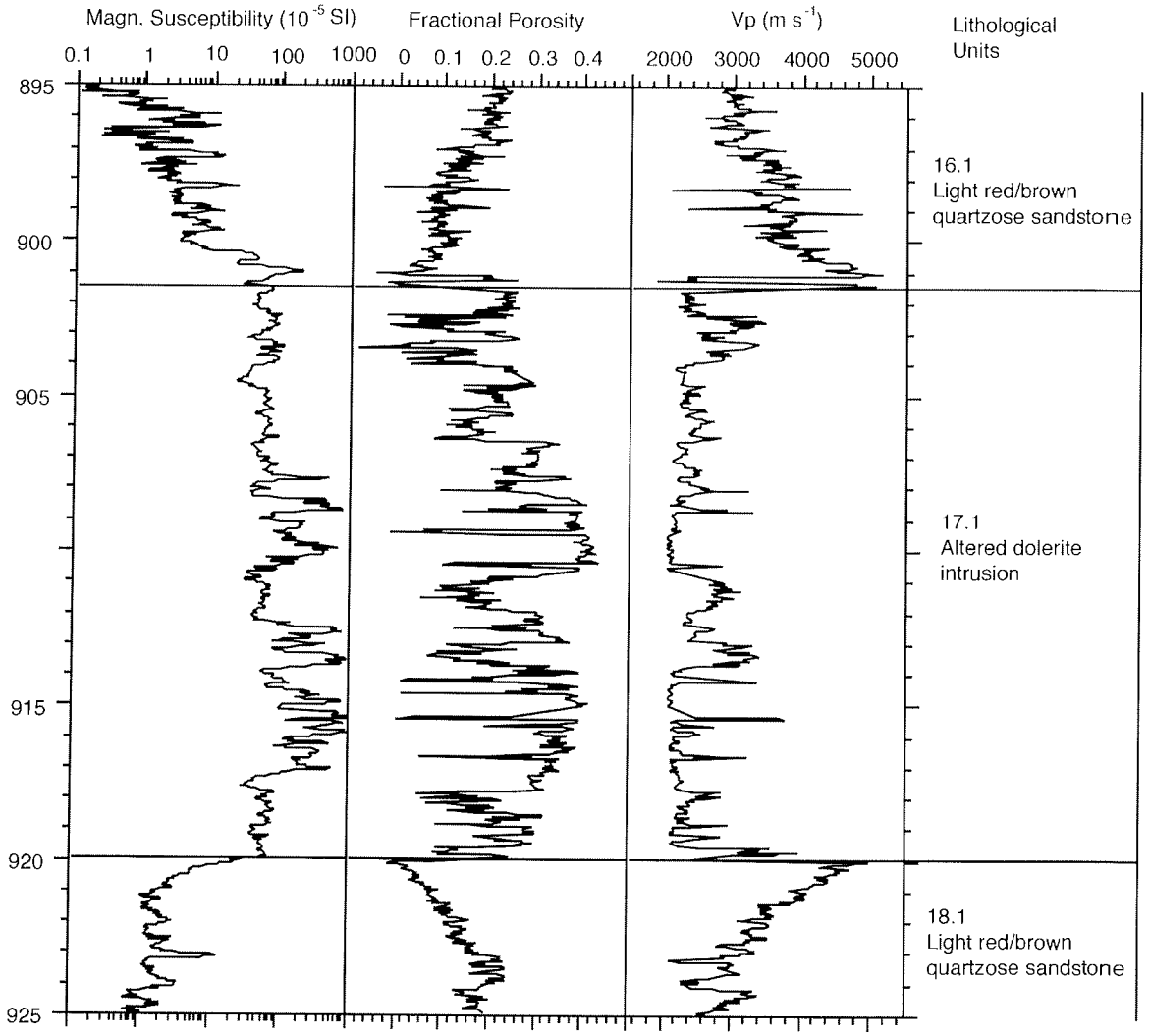

Fig. 2.19 - Comparison of core physical properties with lithological boundaries for a selected depth level of CRP-3 (contact of igneous intrusion with Beacon sandstone).

Beacon sandstones significantly near the contact zones. All core physical properties exhibit strong gradients towards the igneous rock over depth intervals of 5 to 6 m (Fig. 2.19). Sandstone velocities are as fast as 5 000 m s^{-1} directly above and below the contact, and porosity is decreased to zero. This indicates strongly cemented sands near the intrusion. Alteration is also indicated by magnetic susceptibility. Generally, the MS of the Beacon (LSU 16.1 and 18.1) is very low (mostly between 0 and 1, even negative in places), implying very low contents of ferromagnetic minerals such as magnetite. Towards the upper and lower contact of the intrusion, MS increases up to 100, which indicates a secondary overprint of the sandstones by precipitation of magnetic minerals. It is suggested that the entire pattern is indicative of hydrothermal activity associated with the intrusion.

TRANSMISSION SEISMOGRAMS

Seismograms recorded from the P-wave pulse through the core exhibit a broad range of shapes and frequency distributions, which have to be processed and analysed in detail. For marine sediment cores, Breitzke et al. (1998) demonstrate that the primary control on shape and frequency of full-waveform, ultrasonic-transmission seismograms is sediment grain size. Variation between coarse-grained sands and fine-grained clays can be visualised by plotting seismograms recorded at high vertical resolution *versus* depth. In addition, the authors present good correlations of spectral amplitudes in the range of -10 to -90 dB to grain size variations from 2 to 125 μm.

For CRP-3 full waveform transmission seismograms were recorded in 0.02-m depth intervals. In order to demonstrate that transmission seismograms change with grain size and rock type, seven continuous core sections between 1 and 2 m in length were selected from different lithologies and depths. Surfer software is used to bundle the seismograms and to plot them in three dimensions (amplitude, travel time and mbsf, Fig. 2.20) in order to visualise differences within a bundle of seismograms from a given lithology and also to compare different

lithologies. Preliminary results (Fig. 2.20) suggest a grain-size effect on seismogram wavelengths. From conglomerate to light-coloured quartzose sandstone and siltstone to claystones, a general decrease in seismogram wavelength is notable. This is less obvious for light red/brown quartzose sandstones from the Beacon, which are characterised by shorter wavelengths than expected from the grain size. Acoustic pulses through dolerite breccia create distinct oscillations on the entire 150 ms lenght of the recorded seismogram. This is very different from the sand to claystones but is somehow similar to conglomerate. This may be explained by the fact that the conglomerate seismograms are influenced by rock components and matrix. Seismograms of altered dolerite intrusions are different from those of dolerite breccia. The former have waveforms more similar to siltstones or claystones.

Within the individual depth intervals, seismograms also indicate the degree of down-core variability (Fig. 2.20). Siltstone and light red/brown quartzose sandstone exhibit little change whereas, for example, the claystone example presented is highly variable for both onset and waveform. This may suggest a secondary overprint by cementation in this unit. For conglomerate the strong variability observed is expected because the large differences between components and matrix predict this pattern. A systematic analysis of waveform spectra for the entire core in comparison with grain-size and/or cementation data may result in more quantitative correlations than described above.

DOWNHOLE LOGGING

CRP-3 is the second CRP hole with downhole logging. Sea-ice conditions terminated drilling at CRP-1 prior to downhole logging (Cape Roberts Science Team, 1998), whereas CRP-2 was logged (Cape Roberts Science Team, 1999) with a suite of tools similar to that employed at CRP-3. Analyses of the CRP-2 logs are presented in the CRP-2 Scientific Report (Brink & Jarrard, in press; Brink et al., in press; Bücker et al., in press a, in press b, Jarrard et al., in press; Moos et al., in press; Paulsen et al., in press).

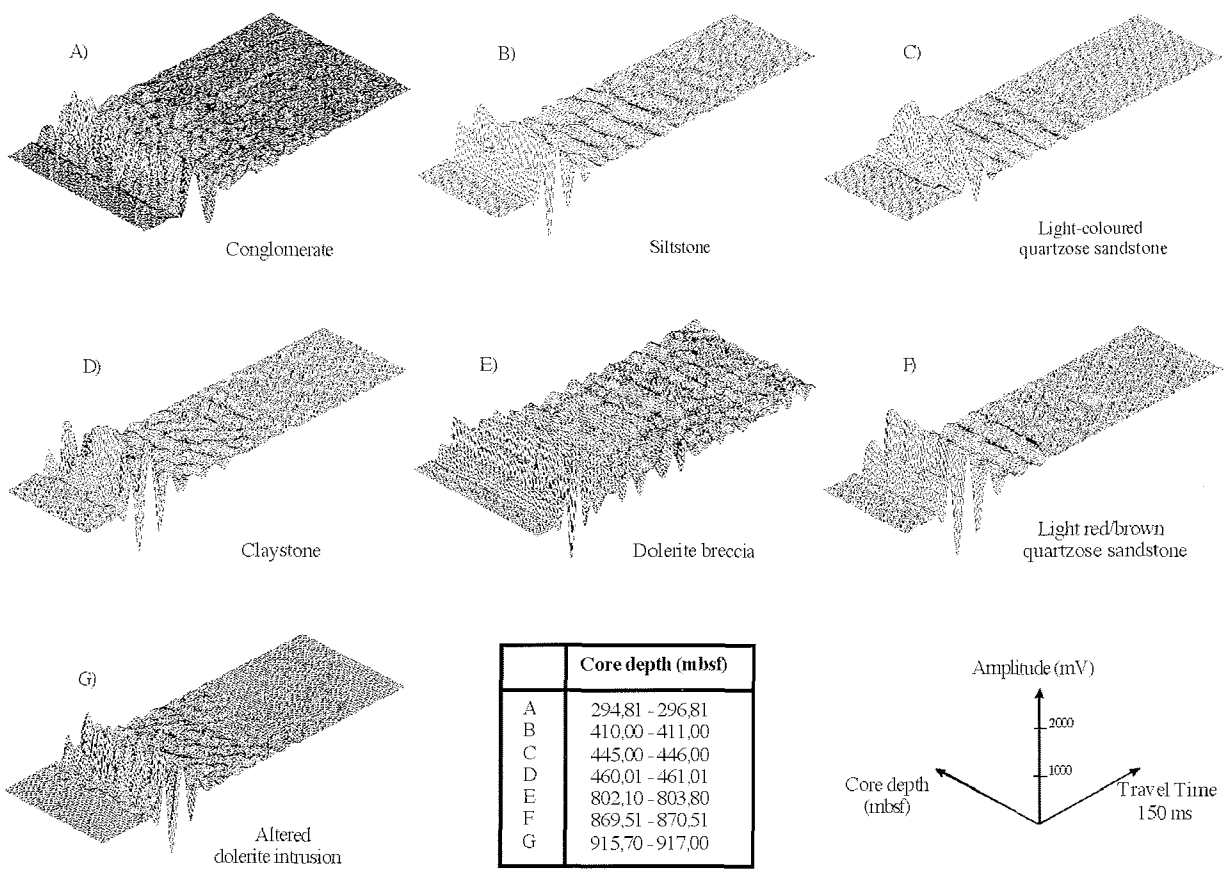

	Core depth (mbsf)
A	294,81 - 296,81
B	410,00 - 411,00
C	445,00 - 446,00
D	460,01 - 461,01
E	802,10 - 803,80
F	869,51 - 870,51
G	915,70 - 917,00

Fig. 2.20 - Full waveform transmission seismograms and their variation with depth (mbsf) from 7 different depth intervals and lithologies (A-G) of CRP-3.

LOGGING OPERATIONS

Downhole logging of CRP-3 was undertaken in four phases. The first two phases (25-27 October) occurred after completion of HQ (96-mm diameter) drilling, when total depth of the hole was 346 mbsf. Because the faulted interval 257-261 mbsf was deemed to be too unstable for open-hole logging, we first raised the HQ drillstring to 20 mbsf and logged the open-hole interval 20-256 mbsf. Next, the drillstring was lowered to 272 mbsf and the open-hole interval 272-346 mbsf was logged. This procedure used the drillstring as protection for the logging tools, but it prevented logging of the fault zone by tools unable to operate through pipe.

After this second phase of logging, the HQ drillstring was cemented in at 345 mbsf and used as casing for subsequent NQ (76-mm diameter) coring. The third phase of logging (11-12 November) occurred when NQ coring had reached 774 mbsf. The final phase of logging (19-22 November) was undertaken when NQ coring reached the final total depth for CRP-3, 939 mbsf.

Each logging phase included runs of the following logging tools: temperature, spectral gamma ray, dual laterolog, magnetic susceptibility, array induction, neutron porosity, borehole televiewer, sonic velocity, vertical seismic profile, and dipmeter. The sequence of these logging runs was generally as listed, with small variations, fulfilling a strategy of running tools without centralizers or pads first, thereby postponing possible hole degradation associated with drag on the borehole wall to maximize log quality and quantity. The first and last logs run were always temperature, as described later. In addition to this standard suite of CRP-3 downhole measurements, the fourth phase of logging included a density log and oblique seismic experiment.

Table 2.3 lists the logged interval for each tool and for each phase of logging.

A brief description of each logging tool, including both principles and applications, is given in the CRP-2 Initial Reports (Cape Roberts Science Team, 1999). Design of the vertical seismic profile and oblique seismic experiment are described in the Vertical Seismic Profiles section. Although the physics of operation of each tool is different, these tools can be grouped according to geological applications as follows: porosity tools (density, neutron porosity, array induction, dual laterolog, sonic velocity), lithology tools (gamma ray and magnetic susceptibility), structural imaging tools (dipmeter and borehole televiewer), and seismic-link tools (vertical seismic profile, oblique seismic experiment, sonic velocity, and density).

Almost all of the downhole tools run in CRP-3 are identical to those run in CRP-2. We modified the array induction tool run in CRP-2 prior to CRP-3 to improve performance. CRP-3 was logged with a different borehole televiewer than that used in CRP-2, but the overall principles and operations of both are similar. The new Antares tool is digital, uses a rotating mirror with stationary transducer, and picks traveltime and amplitude downhole. In contrast, the older tool is analog, uses a rotating transducer, and records the entire waveform for later analog-to-digital conversion and processing.

LOG RELIABILITY AND EDITING

Hole size had two effects on CRP-3 logging. First, a hole constriction or "bridge" prevented the tools from reaching the bottom 18-39 m of the hole. Sticky clays at the top and bottom of the volcanic intrusion had caused pipe to stick during drilling. The deeper boundary formed a bridge that stopped the first logging tool (temperature tool) at 921 mbsf. To prevent tool loss in these zones of tight hole, we initiated subsequent logging runs at shallower depths of 900-919 mbsf (Tab. 2.3).

Second, enlarged hole can degrade the accuracy of most log types. Fortunately, virtually all of CRP-3 had a hole diameter that was uniformly only slightly larger than bit size (Fig. 2.21), so hole conditions are not a significant source of error for the CRP-3 logs. We detected about one dozen washouts to enlarged hole size in the dipmeter caliper log. All are less than 0.3-m thick, and most occur at depths identified during the drilling as unstable hole associated with runny sands.

Measurements made by the density tool are unreliable in intervals with sudden changes in hole diameter, because this tool needs to maintain firm contact with the borehole wall. Loss of contact causes anomalously low bulk-density values. Only one spurious spike was observed in the density log: in the interval 346-348 mbsf, where drilling operations had deliberately fractured the borehole wall during a leak-off test of the cementing of the HQ drill rod. This spike has been deleted from the density log plot.

Rare spikes caused by artifacts are also observed on the following raw logs: the spectral gamma-ray concentration logs (K, Th, and U), the shallow-induction log, and the deep dual-laterolog. Spikes on the spectral gamma-ray concentration logs result from noise-induced incorrect partitioning of the spectrum of gamma-ray energies. This effect is evident as a sharp (<0.5 m thick) positive spike in one elemental concentration and corresponding negative spike in one of the other two elemental concentrations; these are deleted from the figures. A few spikes to impossible negative resistivities are evident on the shallow-induction log and deep dual-laterolog. For the latter, the spikes can be attributed to rock resistivities that are beyond the dynamic range of the instrument. These spikes were deleted from the figures.

Log quality and reliability are judged to be excellent for nearly all of the CRP-3 logging tools. We base this conclusion on the following criteria: internal consistency and calibration tests for some tools, replicability as observed in short intervals logged twice by the same tool, and similarity of log character among different logging tools that use different physics to detect the same geological variables.

Tab. 2.3 - Downhole logging tools run in CRP-3, along with tool abbreviations, tool names, tool specifications, and intervals logged in each of the four logging phases.

Tool Abbreviation	Tool Name	Units	Diameter (mm)	Speed (m/min)	Sample Interval (m)	Vertical Resolution (m)	Phase I depths (mbsf)	Phase II depths (mbsf)	Phase III depths (mbsf)	Phase IV depths (mbsf)	Total Metres Logged
SGR	Spectral Gamma Ray (GR, Potassium (K), Uranium (U), Thorium (Th))	API, %, ppm, ppm	52	1	0.1	0.3	0-256	272-346	330-774	750-920	944
DENS	Density	gcm^{-3}	48	4	0.1	0.25				0-902	902
NPHI	Neutron Porosity	%	eccen 42	3	0.1	0.5	0-256	272-346	0-774	750-902	1 274
SONIC	P-wave Velocity	kms^{-1}	42	4	0.1	0.4	20-256	272-346	320-774	750-902	906
VSP	Vertical Seismic Profiling		cen 48	na	7.5	na	20-256	272-346	320-774	750-902	906
BHTV	Borehole Televiewer		40	1	0.003	0.003	20-256	272-346	320-774	750-902	906
DLL	Dual Laterolog (Resistivities Rdeep, Rshallow)	Ohmm	cen 43	4	0.1	0.3	20-256	272-346	320-774	750-902	906
AIND	Array Induction (Resistivities at 4 frequencies)	Ohmm	52	4	0.1	0.6	20-256	272-346	320-774	750-902	906
DIP	Borehole Geometry (Inclination & Azimuth), 4-pad Conductivity, 4-arm Caliper, Magnetic Field (deltaZ)	degrees, degrees pad units, mm, nT	52	3	0.005	0.02	20-256	272-346	320-774	750-902	906
SUSC	Magnetic Susceptibility	10^{-4} SI	42	5	0.05	0.4	20-256	272-346	320-774	750-902	906
SALCT	Mud Temperature (Temp), Mud Conductivity (mud R)	°C, 1/Ohmm	40	10	0.1	0.2	0-256	0-346	0-774	0-902	2 278
										Sum:	11 740

Note: eccen - eccentralized tool; cen - centralized tool; na - not applicable.

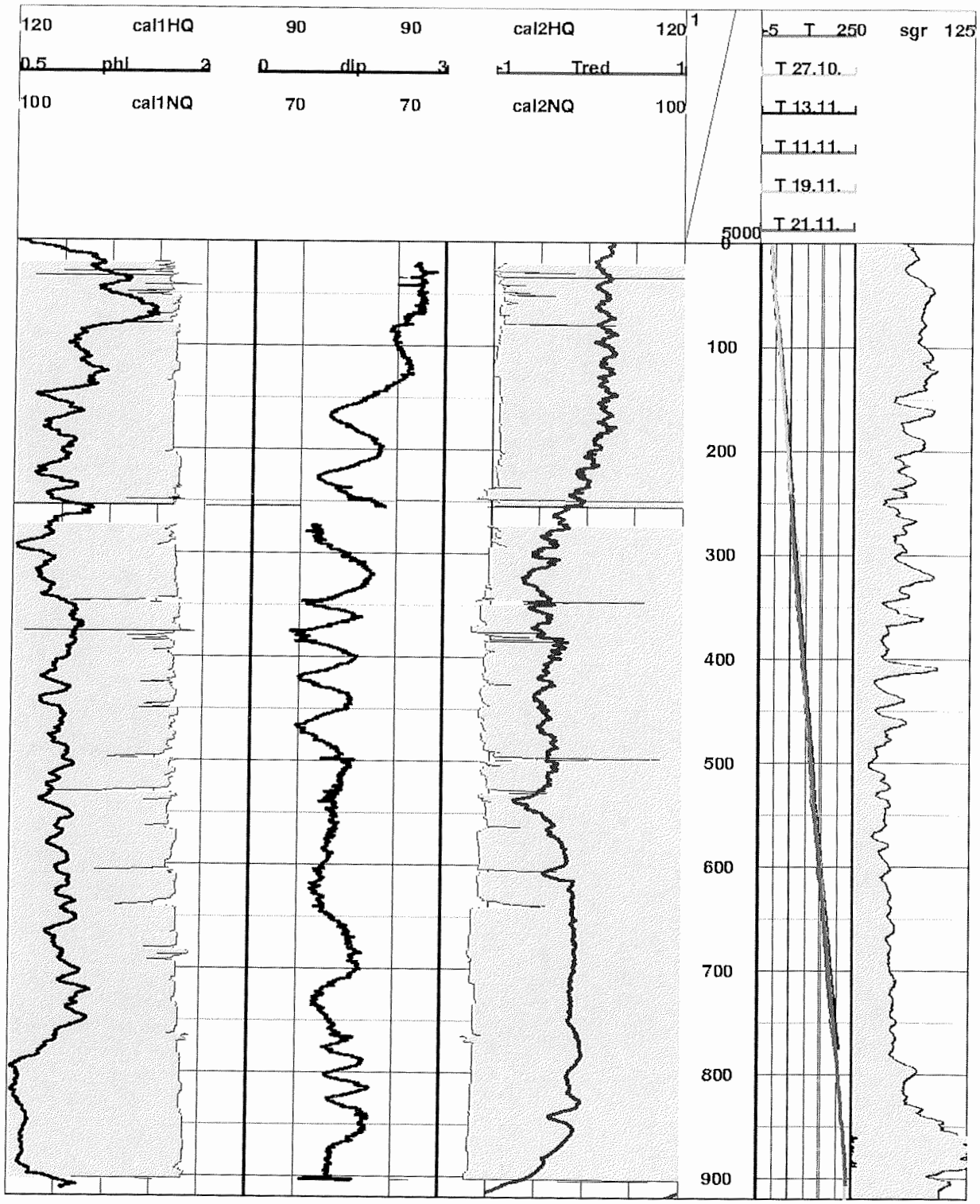

Fig. 2.21 - Hole size (caliper, in mm), hole deviation (deviation from vertical, in degrees), temperature (in °C), and gamma-ray (sgr) of the CRP-3 borehole. Note that the HQ and NQ caliper logs (grey shaded) are plotted with different ranges.

The one exception to this generalization concerning log quality is the sonic-velocity tool. This tool measures P-wave velocity based on picked traveltimes of refracted waves from a sound source to two receivers. Unfortunately, the strength of this refracted wave was generally too weak to be reliably detected by the far source-receiver combination. Consequently, most of this velocity log is unreliable, and the log is not shown in the summary figures of this volume. Sonic waveforms were recorded during logging, but repicking these waveforms is too time-consuming to be feasible in Antarctica.

Hole deviation must be corrected for any structural analysis of CRP-3 core or imaging log data. We measured

CRP-3 hole deviation with the dipmeter and televiewer tools, based on 3-axis magnetometer and 2- or 3-axis accelerometer recordings. Measured hole deviations in CRP-3 are remarkably small: 1.0°-2.5° to the southwest in the top 350 m, and about 1.5° to the southwest in the lower part of the hole.

The spectral gamma, neutron, density, and temperature tools are the only logging tools that can provide useful formation data through drillpipe. Pipe attenuation does affect the spectral gamma, neutron, and density logs, but these effects can be estimated and compensated for.

At CRP-3, we obtained through-pipe spectral gamma logs for the intervals 0-20 and 247-272 mbsf. We estimated the effect of pipe on K, Th, and U measurements by comparing open-hole and through-pipe data for the interval 247-272 mbsf; it was confirmed by observing the baseline shift across the pipe/open-hole transition at 20 mbsf. Uranium through-pipe logs are ~0.7 ppm higher than open-hole logs, whereas K and Th concentrations appear to be less affected by pipe. These logs have been corrected for pipe effects.

The raw neutron log is a ratio of counts measured at two detectors. The tool manufacturer, Antares, has calibrated this tool and determined the conversion from count ratio to porosity. The conversion, however, is dependent on detector window settings, and our logging used slightly different settings from those for the tool calibration. We used the whole-core porosity data of the Physical Properties from on-Site Core section to determine the appropriate conversion from neutron count ratio to porosity, and we observed that this conversion is systematically different from the Antares calibration. The HQ interval (above 345 mbsf) was initially logged open-hole with the neutron tool, but these data exhibit systematic discrepancies compared to whole-core porosities. Therefore, this interval was relogged through pipe during the third logging phase, and this latter log is the one presented in this volume. A subtle pipe effect appears to be present, as the through-pipe neutron porosities (0-345 mbsf) are generally slightly lower than whole-core porosities, and open-hole porosities (>345 mbsf) are slightly higher than whole-core porosities. This effect, however, is so small that no pipe correction was applied.

Open-hole density logs were obtained for the NQ portion of the hole, whereas through-pipe logs were run in the HQ portion (above 345 mbsf). Approximate correction for the through-pipe density values was undertaken by comparing average density values in the 100 m below and above the change from HQ to NQ drilling. The whole-core density logs of the Physical Properties from on-Site Core section demonstrate that average density for these two intervals is about the same. Comparison of log and core measurements provides a check of the quite different assumptions and techniques inherent in the two data types. Core and log measurements of bulk density are consistently very similar, indicating that both are reliable.

Depth shifts of as much as 1 m can occur among different logging runs, caused mostly by cable stretch. All such shifts have been removed by adjusting log depths to a standard log, the dual laterolog; usually, a single constant shift was needed for an entire log. A second depth shift was then applied: the full suite of downhole logs was shifted to a core-based standard, the whole-core porosity log. This shift increased with depth within each logging run, typically by about 1 m. The cause of this second, variable shift is cumulative stretch of the logging cable of about 0.1% associated with the increased cable weight *vs* depth.

LOGGING RESULTS

Figure 2.22 is a 2-page summary of the CRP-3 logs. For clarity, these logs are smoothed. Dipmeter and borehole-televiewer data are not shown, as these data require major processing; some preliminary televiewer observations are discussed in the Core Fracture section. Expanded log plots, at a scale of 100 m/page, are provided at the end of this chapter.

Temperature Logging

The temperature tool was run twice during each phase of logging; it was the first and last tool run. Circulation of drilling mud prior to logging lowered temperatures for the first run to less than equilibrium values, whereas temperatures during the second run are probably close to equilibrium values.

For nearly all of the logging tools used at CRP-3, logs were recorded only during the upcoming portion of the tool round trip to the bottom of the hole. Temperature logs, in contrast, were obtained during both downgoing and upcoming trips. Downgoing temperature logs are more reliable, because drillhole fluids are less disturbed by the tool movement.

Temperature logs can be run either open-hole or through-pipe; results are generally equivalent because the pipe conducts temperature from the formation to the drillhole fluid efficiently. Consequently, later phases of temperature logging encompassed nearly all of the hole, not just the newly drilled interval. The primary difference between open-hole and through-pipe temperature logs is that the former can respond to active fluid flow between the formation and drillhole, whereas such flow is retarded or stopped by pipe, particularly cemented pipe.

The CRP-3 temperature logs detected substantial fluid flow at five locations: 264, 537, 606, 748, and 840 mbsf (Fig. 2.21). In each case, a local temperature anomaly of −0.5 to −1.0° was observed in both open-hole logging runs. This anomaly could be caused either by active equilibrium fluid flow through an aquifer, or by drilling-induced fluid flow. We hypothesize that the latter is responsible for the CRP-3 anomalies, because the 264 mbsf anomaly had vanished by the time this interval was logged through pipe. Mud circulation during

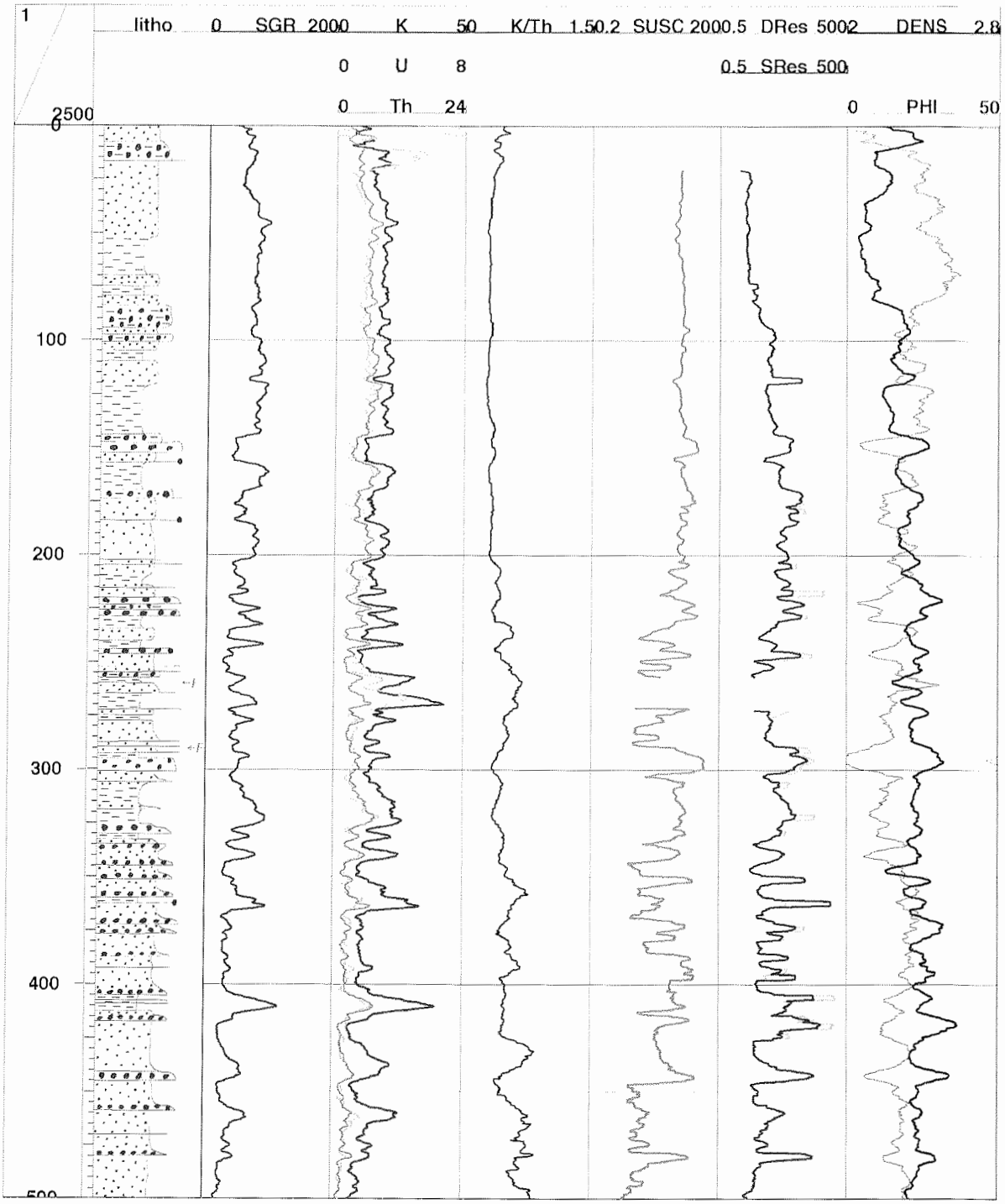

Fig. 2.22 - Summary of most CRP-3 downhole logs: spectral gamma ray (SGR) and its three components (K, Th, and U), dual laterolog (shallow SRes and deep DRes), neutron porosity (NPHIcor), bulk density (DENS), and magnetic susceptibility (SUSC). Note that the scales for SRes, DRes, and SUSC are logarithmic.

drilling generates slight overpressures that cause loss of mud into permeable formations, and this convective flux augments conductive cooling. Subsequently, formation temperatures rebound toward equilibrium, but these permeable zones take longer to achieve equilibrium and therefore cause negative temperature anomalies in the adjacent borehole fluids. Rebound is further retarded by the likelihood of subtle continued fluid flow into these zones during logging: a positive head was maintained during logging to prevent backflow, and this head induced a downward flow of 100/l *per* hour (~23 m/hr). Consequently, temperature anomalies mark the zones of highest permeability in CRP-3.

All except the 537 mbsf temperature anomaly exhibit high log-based porosities, and a high-porosity bed is present near the 537 mbsf anomaly, at 529-532 mbsf.

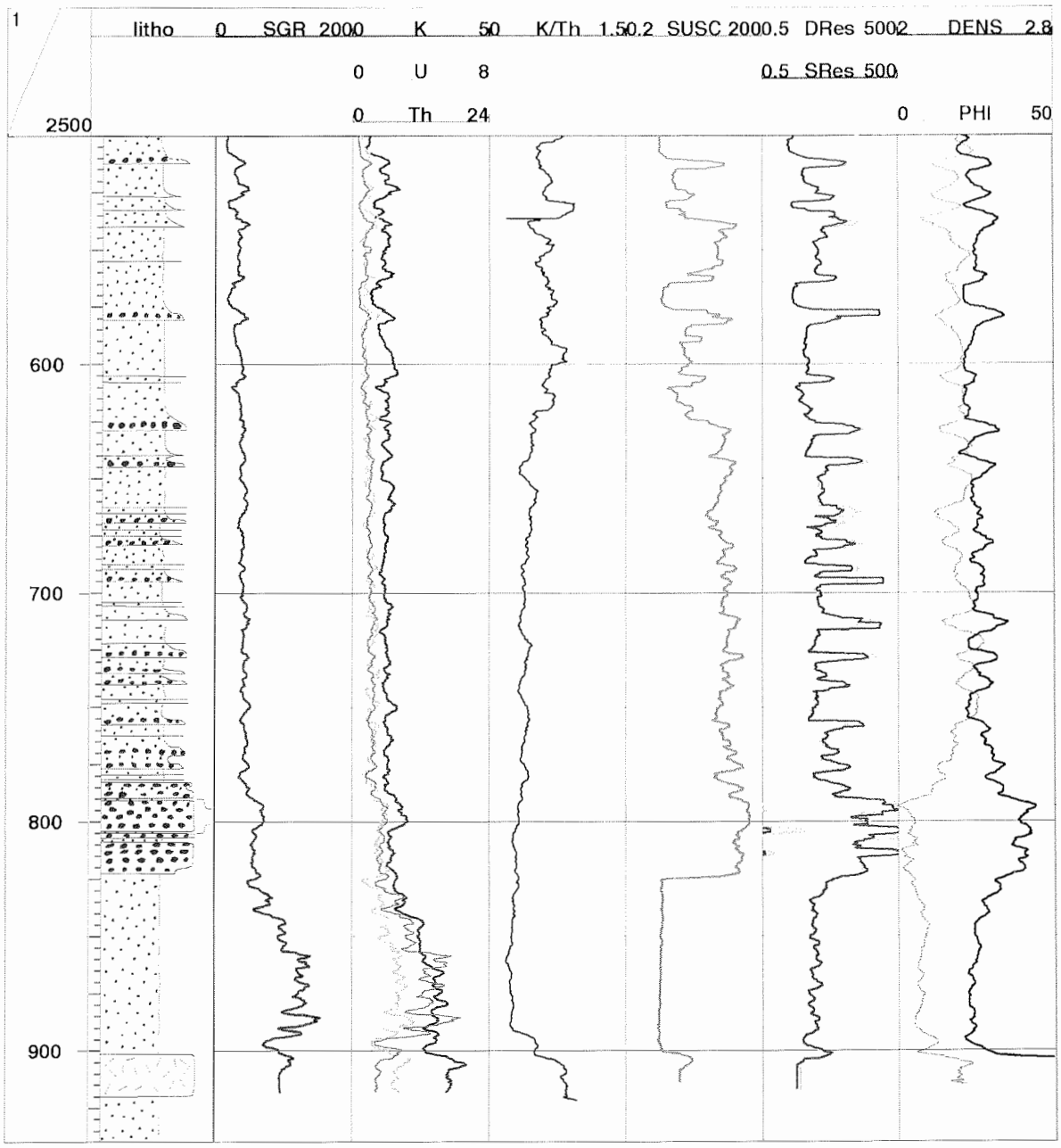

Fig. 2.22 - continued.

The two shallowest correspond to a fault and highly fractured interval, respectively, indicating that fracture permeability is probably responsible for the fluid flow. In contrast to these temperature responses, the fault zone at 789-806 mbsf has only a very small associated temperature anomaly. This fault zone, unlike the shallower ones, is clearly very low in porosity at present (Fig. 2.22) and is apparently low in permeability as well.

The equilibrium geothermal gradient at CRP-3 is apparently slightly nonlinear (Fig. 2.21), probably because downhole variations in porosity cause associated downhole fluctuations in thermal conductivity. Based on the seafloor temperature of -1.8°C and near-bottom temperature of 23.0°C at 870 mbsf, the average geothermal gradient is 28.5°C/km. This value is higher than the 24°C/km measured at CRP-2, because the CRP-2 temperature log was run only a few hours after completion of drilling, whereas the CRP-3 final temperature log was run 2.5 days after completion of drilling. This value is less than the geothermal gradients of 35°C/km measured at CIROS-1 (White, 1989), MSSTS-1 (Sissons, 1980), and DVDP-15 (Bucher & Decker, 1976). White (1989) calculated that the actual equilibrium thermal gradient at CIROS-1 is even higher, 40°C/km, based on extrapolation of time-temperature results with the method of Dowdle & Cobb (1975). That method, however, predicts an extremely nonlinear thermal gradient at CIROS-1.

Log-Based Units

Based on log responses, the interval 0-901 mbsf of CRP-3 can be divided into five logging units. Downhole changes, from top to bottom, are discussed in this section.

Log Unit I, 0-144 mbsf, is generally very homogeneous in log responses, particularly for the gamma-ray, magnetic susceptibility, and K/Th logs. Porosity varies smoothly and subtly, except for a rapid drop at 83-94 mbsf. This log unit is mostly finer grained and muddier than deeper units. The open-hole neutron log of this log unit, obtained during the first phase of logging, exhibited rapid fluctuations, but this pattern was not confirmed by the more reliable through-pipe logs of the third logging phase.

The transition from log Unit I to II is a sudden major increase in heterogeneity of all logs. It is placed at the top of the first bed with markedly lower porosity (low neutron porosity, high resistivity and density), lower susceptibility and gamma ray, and higher K/Th.

Log Unit II, 144-641 mbsf, is bimodal in all log responses, with one mode similar to log Unit I. Alternations on a scale of 10-30 m are probably lithological sequences. Most are marked by a basal conglomerate with high resistivity and density, low porosity, and high susceptibility. The gamma-ray responses of the conglomerates change downhole from low to high values, and the characteristic low K/Th signature becomes more distinctive downhole. The conglomerates are most evident as spikes on the resistivity logs, because of the combination of poor sorting and high cementation. Lithological changes from clean sand to muddy sand and silt also have visible log responses: decreasing porosity and increasing gamma ray and susceptibility.

The transition from log Unit II to III is somewhat arbitrary. It is identified as lying at 641 mbsf based primarily on the susceptibility log, which changes downhole from bimodal to more uniformly high at this depth. The K/Th baseline drops at ~617-641 mbsf. The bimodal character in porosity logs, however, continues below 641 mbsf with higher frequency variations; resistivity does show a step increase at about this depth. The bimodal response of gamma ray is lost earlier, across a transition zone at 412-463 mbsf.

Log Unit III, 641-790 mbsf, appears to be relatively homogeneous lithologically, with low gamma-ray and K/Th values and with high susceptibility. This log unit corresponds approximately to lithological Unit 13, although the top boundary is ill-defined in logs, as discussed above. Porosity is heterogeneous, with variations similar to those in log Unit II: low porosities in the conglomerates and cemented sandstones, with higher-porosity sandstones also present. Except for the conglomerates, grain-size changes are not as evident in gamma ray and susceptibility as in log Unit II; this observation is consistent with core descriptions of this unit as mostly greenish sandstone. However, fining- and coarsening-upward beds are apparently seen in the susceptibility log.

The transition from log Unit III to IV is a major, sudden decrease in porosity.

Log Unit IV, 790-823 mbsf, is characterized by very low porosity, high density, high susceptibility, and low gamma ray. This unit corresponds to lithological Units 14 and 15, consisting of a fault zone and underlying Tertiary sediments. The fault zone itself is characterized by enhanced gamma-ray values and by the highest susceptibility values of the entire borehole.

The transition from log Unit IV to V is a step upward in porosity, accompanied by a sudden step downward in susceptibility. This boundary, at 823 mbsf, is the sharpest boundary evident in the CRP-3 logs. It corresponds to the major unconformity between Tertiary and Devonian sedimentary rocks.

Log Unit V, 823-901 mbsf, is the upper portion of the Beacon Sandstone. It exhibits high and variable porosity, comparable to that of log Units II and III. Susceptibilities are the lowest of all CRP-3, generally below the noise level of the logging tool. The gamma-ray logs are surprisingly high and remarkably heterogeneous through this unit, including the highest K and Th concentrations of the entire hole. These high values are incompatible with expectations based on the mineralogical maturity of analogous Beacon outcrops, suggesting that diagenetic precipitation has enriched these sandstones in K and Th.

Clay Content

In many sedimentary environments, the gamma-ray log (SGR) can be used to identify sandstones and shales and to estimate shale content, because of the much higher concentrations of radioactive elements in clay minerals than in quartz. Similarly, the magnetic susceptibility log can also be used to distinguish finer-grained mudstones from coarser-grained sandstones, by detecting magnetic minerals that are generally found in the finer-grained sediments. Therefore, the combination of SGR and susceptibility logs usually provides a robust indicator of sandstone *vs* shale.

This expected gamma-ray pattern is obscured in formations with immature sands, containing substantial quantities of radioactive elements in minerals such as potassium feldspar. For example, Brink et al. (in press) found that both the gamma-ray and magnetic susceptibility logs for CRP-2 were generally more useful as provenance indicators than as sand/shale logs. They noted, however, that SGR did correlate with lithological changes in the lowest portion of CRP-2, the part most relevant to CRP-3 log responses.

The large-scale downhole pattern of gamma-ray variation within the Tertiary section consists of three zones: uniformly high SGR in the interval 0-144 mbsf, uniformly low SGR in the interval 462-823 mbsf, and an intervening transition zone of alternation between these two levels. Detailed comparison of gamma-ray responses

to provenance variations within CRP-3 is beyond the scope of this report. Our preliminary hypothesis, however, is that this broad pattern of downhole SGR variations reflects the combination of decreasing mud component and increasing Beacon source downhole. If so, the 144-462 mbsf transition zone is a particularly promising region for detailed provenance studies. The broad-scale changes in magnetic susceptibility, like those of gamma ray, appear to be more closely related to provenance changes than to variations in grain size.

Throughout most of the Tertiary CRP-3 sediments, small-scale variations in both SGR and magnetic susceptibility are positively correlated with variations in resistivity and density. This relationship is similar to that commonly seen for highly compacted sandstones and shales: silty and muddy beds are less porous and higher in both radioactive elements and magnetic minerals than are sandy beds. Comparison to core lithologies confirms that this predicted lithological association is present.

This association between high SGR and low porosities is not evident within the Beacon Sandstone, however. This interval exhibits extremely heterogeneous and often exceptionally high SGR, K, and Th. These values appear to be too high to be compatible with the mature mineralogy exhibited in Beacon outcrops; a later diagenetic enhancement of K and Th may be responsible. This hypothesized precipitation event is apparently independent of the leaching event that generated the high Beacon porosities, so the usual link between grain size and both porosity and clay content is not observed.

Porosity Variations

The neutron, density, sonic-velocity, and resistivity logs are often referred to as porosity logs, because porosity is the dominant variable affecting their log responses. Neutron porosity measures the total hydrogen content of the formation, including bound water in clays plus free water in pores. Thus, neutron porosities can be too high in formations that are rich in clay minerals. Resistivity can also be affected by clay minerals. Clay conducts electricity and therefore decreases resistivity in low-porosity rocks (Waxman & Smits, 1968), whereas clay increases pore tortuosity and therefore increases resistivity in high-porosity rocks (Erickson & Jarrard, 1998). At CRP-3, however, clay mineral concentration is so low that its influence on both neutron and resistivity is probably minor.

Porosities of most siliciclastic sediments depend on grain size and compaction history. Sea-floor porosities of well-sorted sands are about 30-40%, whereas clays have porosities of up to 80% (*e.g.* Shumway, 1960a, 1960b; Hamilton, 1971). Initial porosities are subsequently decreased by both mechanical compaction and chemical diagenesis. Pressure increase associated with burial accomplishes a modest degree of mechanical compaction for sands. The number and type of grain contacts change initially by more compact arrangement and later, with deeper burial, by plastic deformation of weaker minerals (Taylor, 1950; Hayes, 1979). Mechanical compaction is more intense in shaly sediments, as the initial "cardhouse" fabric of randomly oriented clay particles is forced into a generally parallel arrangement (*e.g.* Hedberg, 1936; Magara, 1980). With greater burial, chemical diagenesis - including pressure solution, recrystallization, and replacement - replaces physical compaction as the dominant mechanism of porosity reduction (*e.g.* Hayes, 1979; Foscolos, 1990; Hutcheon, 1990).

Figure 2.22 shows plots of the three porosity-sensitive logs. The broad trends in all three logs are very similar, except for a gradual decrease in resistivity that is expected to occur independently of porosity change. Rock resistivity depends on both porosity and pore-fluid resistivity. Pore-fluid resistivity decreases gradually downhole due to thermal gradient, causing an associated downhole decrease in observed formation resistivities that is superimposed on the pattern of porosity variations.

The changes in neutron porosity, resistivity, and density with depth do not follow a simple compaction profile, such as those usually found in siliciclastic sediments (Hamilton, 1976). No systematic depth-dependent porosity decrease is evident below 144 mbsf (Fig. 2.22). This CRP-3 pattern differs from the strong downhole porosity decreases observed at CRP-1 (Niessen et al., 1998) and CRP-2 (Brink et al., in press). Apparently, late-stage diagenesis and grain-size fluctuations affect present porosity much more than does the early history of mechanical compaction and cementation.

VERTICAL SEISMIC PROFILES

Three separate vertical seismic profiles (VSPs) were completed at CRP-3 (see Tab. 2.4 and Fig. 2.23). In addition, a number of tests of charge size and shot depth were also undertaken but excluded from further processing. A shot depth of 15 m below the surface was used for most of the survey (below 2 m of sea-ice and into 13 m of water). The clamping tool (developed by Antares, Germany) recorded oriented 3-component data. A reference 3-component geophone was also sited adjacent to the well. All 3-component geophone geometry parameters are recorded in the trace headers. Shots are recorded as 6-channel SEGY format; for reference, a description for each channel is shown in table 2.5.

Downhole recording was completed in three stages to coincide with changes in core barrel size (HQ to NQ) and at the completion of the well. For the HQ section (0 to 345 mbsf), VSP's were recorded open-hole prior to casing of this interval. Hole size was consistently very close to bit size so that clamping could be undertaken at a uniform depth interval. One shot was recorded at each geophone depth.

Analysis of VSP data provides:

- down-going travel-time data that can be used to

Tab. 2.4 - VSP experiments at CRP-3.

	Title	Depth Range	Geophone interval (m)	Position	Azim (degrees)	Offset (m)	Source	Objective
1	VSP	25 to 900 mbsf	7.5	77.1122°S 163.6413°E	162	74	Anzomex K 175 g	Near-vertical standard VSP for length of CRP-3
2	In-line Offset VSP	645 to 900 mbsf	7.5	77.0154°S 163.6463°E	162	553	Anzomex P 400 g	Improve seismic image of strike section beneath CRP-3
3	Ortho-gonal Offset VSP	645 to 900 mbsf	7.5	77.0116°S 163.6192°E	258	544	Anzomex P 400 g	Improve seismic image of dip section beneath CRP-3

Tab. 2.5 - Trace header nomenclature.

Channel	Orientation	Angle	Geophone	Sample Rate (micro sec)	Record Length (msec)
1	X	Variable	Well	500	2500
2	Y	Variable	Well	500	2500
3	Z	Vertical	Well	500	2500
4	X	South 162°	Reference	500	2500
5	Y	West 258°	Reference	500	2500
6	Z	Vertical	Reference	500	2500

determine velocities and to serve as a basis for comparison with downhole sonic and core measurements,
- up-going reflections that can be used to tie directly into marine seismic reflection data,
- information about strata below the bottom of the well.

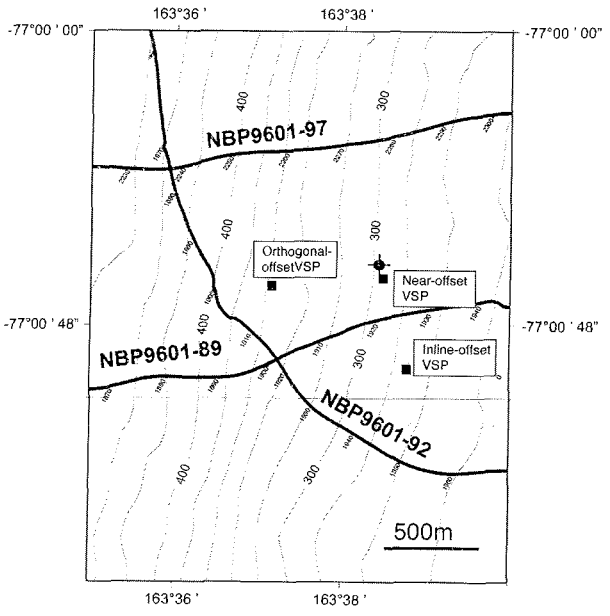

Fig. 2.23 - Detailed map of the drill site showing location of the VSP experiments, seismic-reflection lines (annotated with shot points), and bathymetry (contours in 20 metre intervals).

PROCESSING

The processing completed so far concentrated on near-vertical and offset Z-component data. Near-vertical X- and Y-component data have also been processed in an effort to recover shear-wave sections. Preliminary processing of the data includes trace display and editing. Down-going waves are marked by clear first arrivals and a low frequency (<10 Hz) complex coda that includes the source signature and shallow reverberations in the seaice and reflections from the seafloor. This wavetrain masks up-going reflection arrivals. Separation of down-going and up-going waves was carried out by median filtering and polygon mute in the frequency-wavenumber (f-k) domain. Figure 2.24 shows a series of plots representing progressive processing steps: a) raw data, b) processed up-going reflection data after f-k filtering, and c) aligned up-going wavefield. The aligned data have a static shift applied, equal to the first-arrival times. In this way the VSP can be compared to two-way traveltime, marine single-channel (SCS) reflection data. An 80 msec corridor after the first arrival is used to correlate well data to SCS reflection data (see Fig. 2.26). Further processing will involve deconvolution and wavelet extraction.

VELOCITY *VS* DEPTH

An important application of VSP data is to provide accurate velocity-depth data for the formations penetrated by the well. Downhole sonic logs (see section on Downhole Logging) and velocity measurements of the

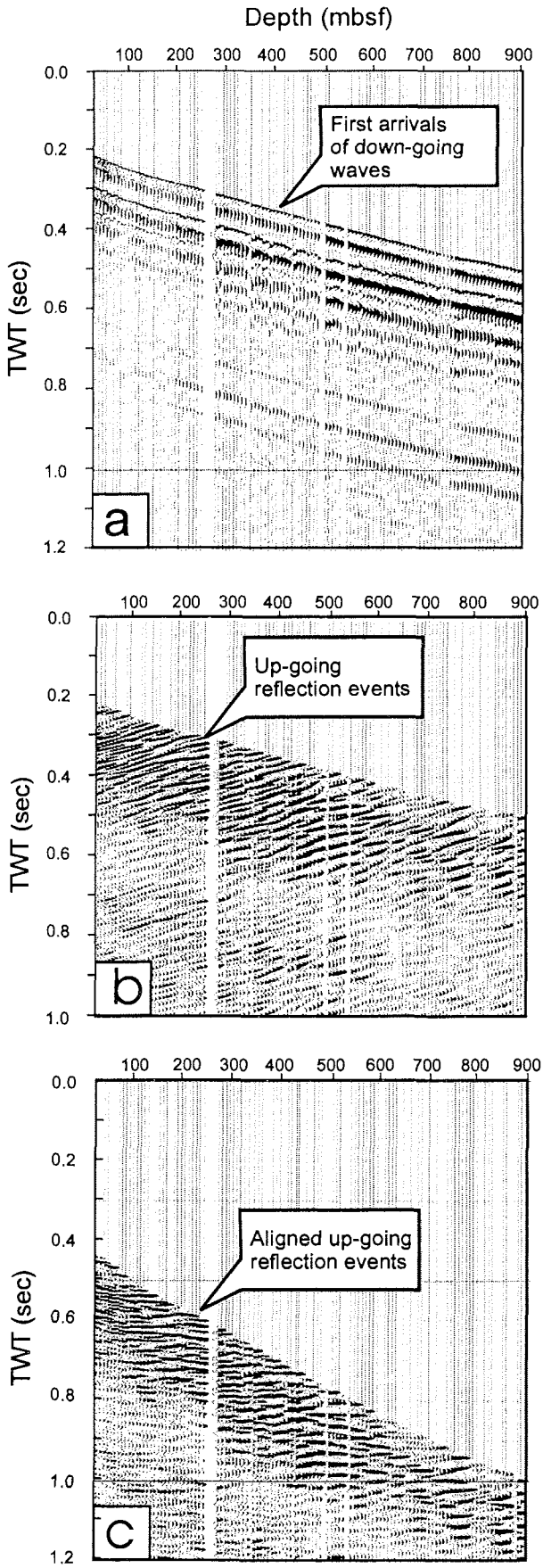

Fig. 2.24 - Progressive steps in the processing of the near-offset VSP vertical-component data. a) Raw data after editing of bad traces. b) Up-going wavefield after f-k filtering. c) Up-going wavefield aligned with first arrivals.

core (see section on Physical Properties) provide substantially greater depth resolution, but the VSP results are much less subject to borehole conditions. Indeed, they average over a much larger volume of the formation so that they provide velocities that are more representative of seismic reflection velocities than those obtained from core or downhole logs. Interval velocities are calculated from travel times picked off first-arrivals of near-offset VSP data (± 2 msec accuracy) and plotted as a function of depth together with core velocities in figure 2.25a. The core velocities are median-filtered over a sliding 10-m window of core. Our filter will also reject outliers if they are greater than 2.5 times the median value. A comparison of the velocity and time-depth curves (Fig. 2.25) show they are remarkably similar, with VSP velocities dominated by anomalies of wavelengths greater than 50 m. High-velocity peaks associated with thin (<20 m) conglomerate beds are not resolved in the VSP traveltime data. The dominance of high-velocity clasts within the core results in the two-way traveltime to depth conversions differing by about 20 to 30 m between 300 and 500 mbsf (see Fig. 2.25b). In general, velocities in CRP-3 are about 3.2 ± 0.6 km/s, apart from the first 80 m of core, where velocity is close to 2.0 km/s, and a 50-m dolerite shear and conglomerate zone from 790 to 823 mbsf, where velocity is greater than 4.5 km/s.

Traveltime data from the long-offset VSP data are also plotted in figure 2.25b. A small change in gradient is apparent in the in-line VSP data at the depth where the high velocity dolerite conglomerate is encountered in the well. This change in gradient is observed at a shallower depth in the orthogonal VSP data and indicates the upper contact on this interface has an apparent dip of about 10°

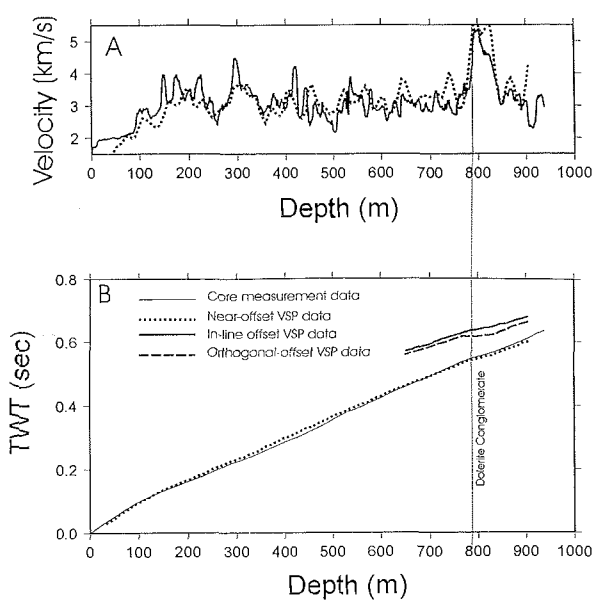

Fig. 2.25 – a) Velocity measurements on core samples smoothed with a 10-m median filter (shown in the solid line) and interval velocities derived from the near-offset VSP first arrival times (dashed). b) Traveltime depth curves from VSP experiments and core sample velocity measurements.

Tab. 2.6 - Correlation between seismic reflectors, reflectivity and velocity values from measurements on the core, and lithostratigraphical units in CRP-3.

Seismic Reflector		Lithostratigraphical correlation and depth	Comments and inferences
	twt bsl (ms)		
o*	420-430	Base of LSU 1.2 at 55 mbsf	Muddy Sandstone. Lowest significant velocity change in CRP-2A, within well-cemented sandstone; corresponds to a major reflector traced to a 100-m wide bench on the seafloor
p*	480-490	Base of LSU 2.1 at 95 mbsf	Sandy Diamictite.
q+	530-545	Boundary between LSU 3.1 and LSU 4.1 at 145 m bsf	Major impedance change between sandy mudstone and conglomerate.
r*	560-585	Within LSU 7.2 at *c* 225 mbsf	A series of thin bedded conglomerates gives a sharp increase in velocity c 225 mbsf
s+	610-640	Boundary between LSU 7.4 and LSU 7.5 at *c* 290 mbsf	Change in lithology from medium-grained sandstone to conglomerate. Corresponds to a significant velocity change.
t+	675-700	Within LSU 9.1 at *c* 360 mbsf	Minor velocity increase associated with thin (up to 1.5 m thick) conglomerate beds
u*	720-750	Near the base of LSU 11.1 at *c* 444 m	Corresponds to a strong reflector in VSP data and an increase in velocity.
Sea-floor multiple intersects CRP-3 at 770 ms bsl. Below this, interpretation of reflectors is more difficult.			
v*	770-800	Base of LSU 12.3 at c 540 mbsf	Conglomerates near the top of LSU 12.3 mark an increase in core and VSP velocity
w+	725-955	Top of conglomerate within LSU 13.2 at 783 mbsf	Top of dolerite breccia. Marked by >4.5 km/s velocity.

Note: LSU - Lithostratigraphical Sub-Unit; * - strongest and most persistent reflectors; + - not prominent on large scale near trace plot but observed in VSP data.

to the east. However, no corrections have been made for water depth changes or offset from the well.

CORRELATION OF SEISMIC REFLECTORS WITH CRP-3

An integrated plot is shown in figure 2.26. We have used the whole-core velocity and VSP data to derive time-depth conversion curves to map the seismic reflection section (left-hand side) to depth. These curves are overlaid on the time-aligned VSP. On the right-hand side, the stacked VSP data are compared to time-converted core-velocity measurements. In addition, we have used core-velocity and density data to derive a downhole reflection coefficient profile to associate the seismic data to the lithological logs.

CRP-3 reached a depth of 939.42 mbsf, equivalent to 1 030 msec two-way time below sea level (twt bsl). At least 9 seismic events can be identified at this depth or above in the SCS and VSP data (o to w). Table 2.6 summarizes the correlation between seismic reflectors from line NBP9601-89 and lithostratigraphical units in CRP-3.

Seismic events on SCS data (o, p, r, u, and v) were determined by correlating the highest positive amplitude wavelets that were laterally continuous away from the drill hole and can be related to the cored section. However, detailed linkages are uncertain because of 1) the low resolution of the seismic signal (wavelength ~ 30 m), 2) uncertainty in the traveltime depth curve (estimated to be ± 10-15 m), and 3) the surface seismic data is convolved with a complex source wavelet. The correlations we have proposed here will be further improved by the calculation of synthetic seismograms to be included in the Scientific Report.

We have used VSP seismograms, core measurement impedance data (Fig. 2.26), and changes in physical properties that extend over about 20 m to refine our correlations. For example, the highest reflection coefficients are encountered in dolerite dominated conglomerates, which have the highest velocities. Continuous layers of this lithology will yield bright and laterally continuous reflectors.

Appendix 2.1

1:500 SCALE DOWNHOLE LOGS

Summary of downhole logging results, plotted at 100 m/page. The columns show (from left to right): 1/500 - depth below sea floor in m, litho1 - simplified lithology from core observations, SGR - spectral gamma ray in API units, K - potassium in %, U - uranium in ppm, Th - thorium in ppm, K/Th - potassium/thorium ratio, SUSC - magnetic susceptibility in 10^{-5} SI, DRes - deep resistivity in Ohm•m, SRes - shallow resistivity in Ohm•m, DENS - bulk density in g/cc, PHI - neutron porosity in p.u.. SUSC, DRes, and SRes are plotted with a logarithmic scale.

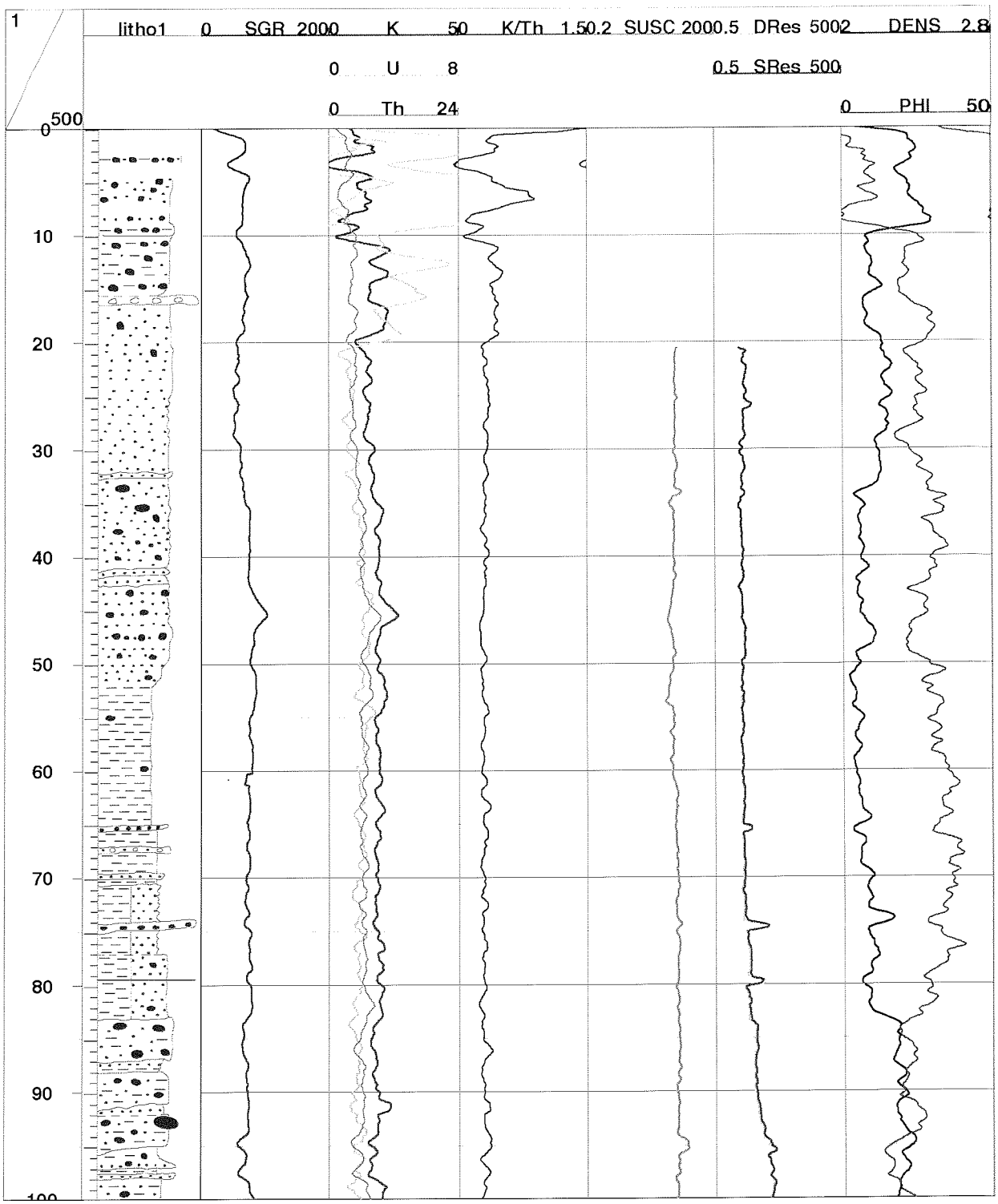

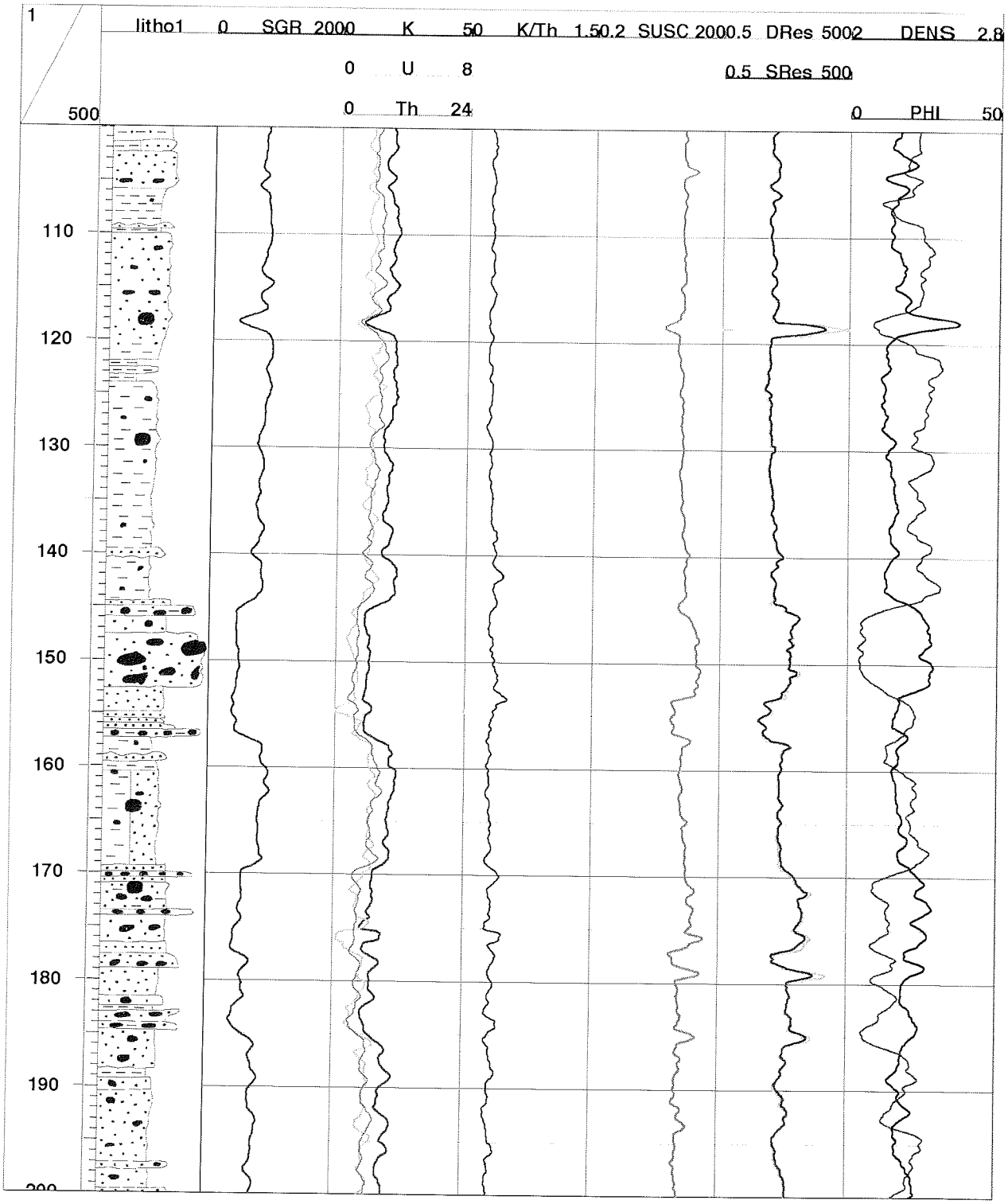
1
litho1
0 SGR 200
0 U 8
0 Th 24
K 50
K/Th 1.5
0.2 SUSC 200
0.5 SRes 500
0.5 DRes 500
2 DENS 2.8
0 PHI 50
500
110
120
130
140
150
160
170
180
190

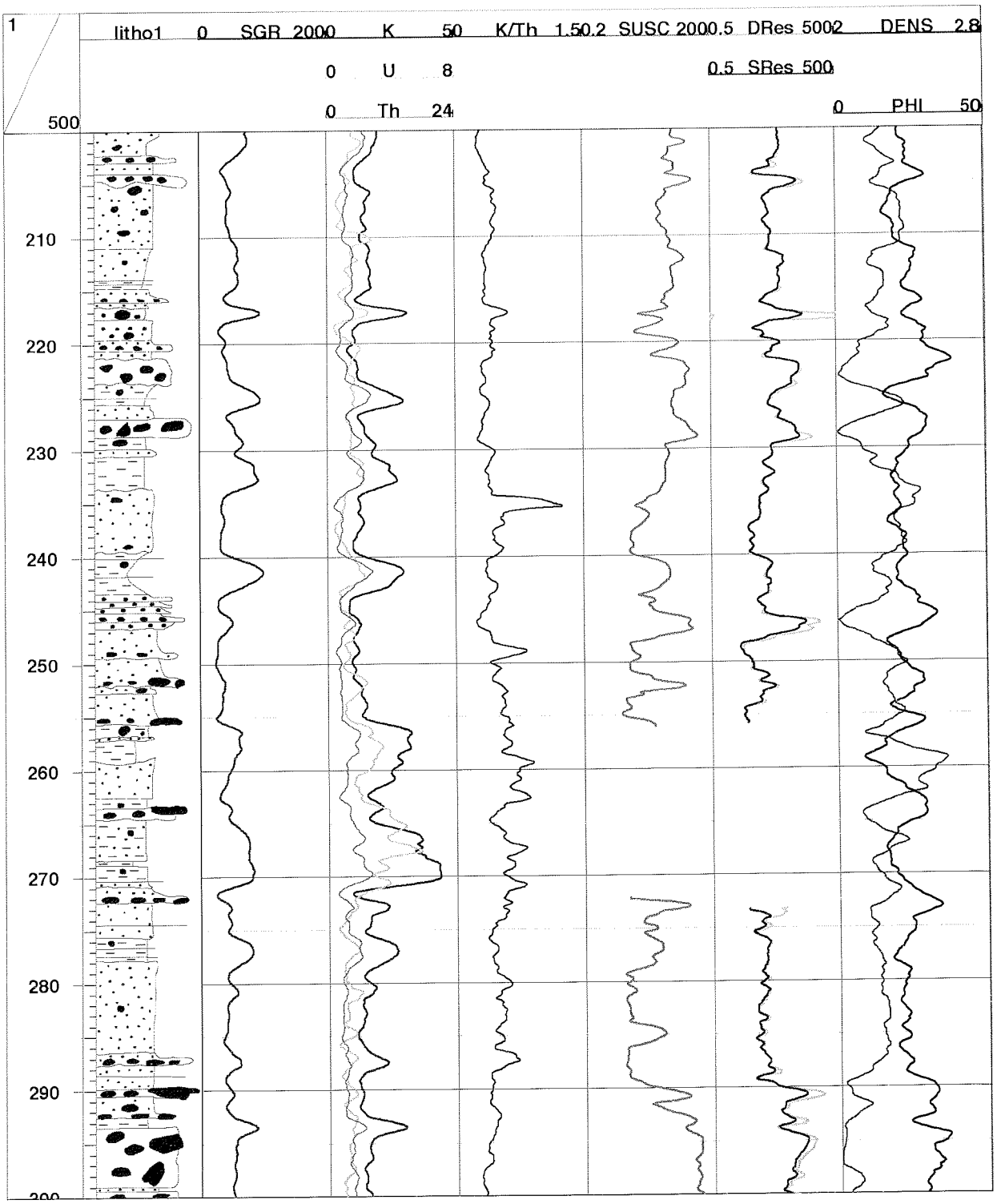
1
litho1
0 SGR 200
0 K 50
0 U 8
0 Th 24
K/Th 1.5
0.2 SUSC 200
0.5 DRes 500
2 DENS 2.8
0.5 SRes 500
0 PHI 50
500
210
220
230
240
250
260
270
280
290

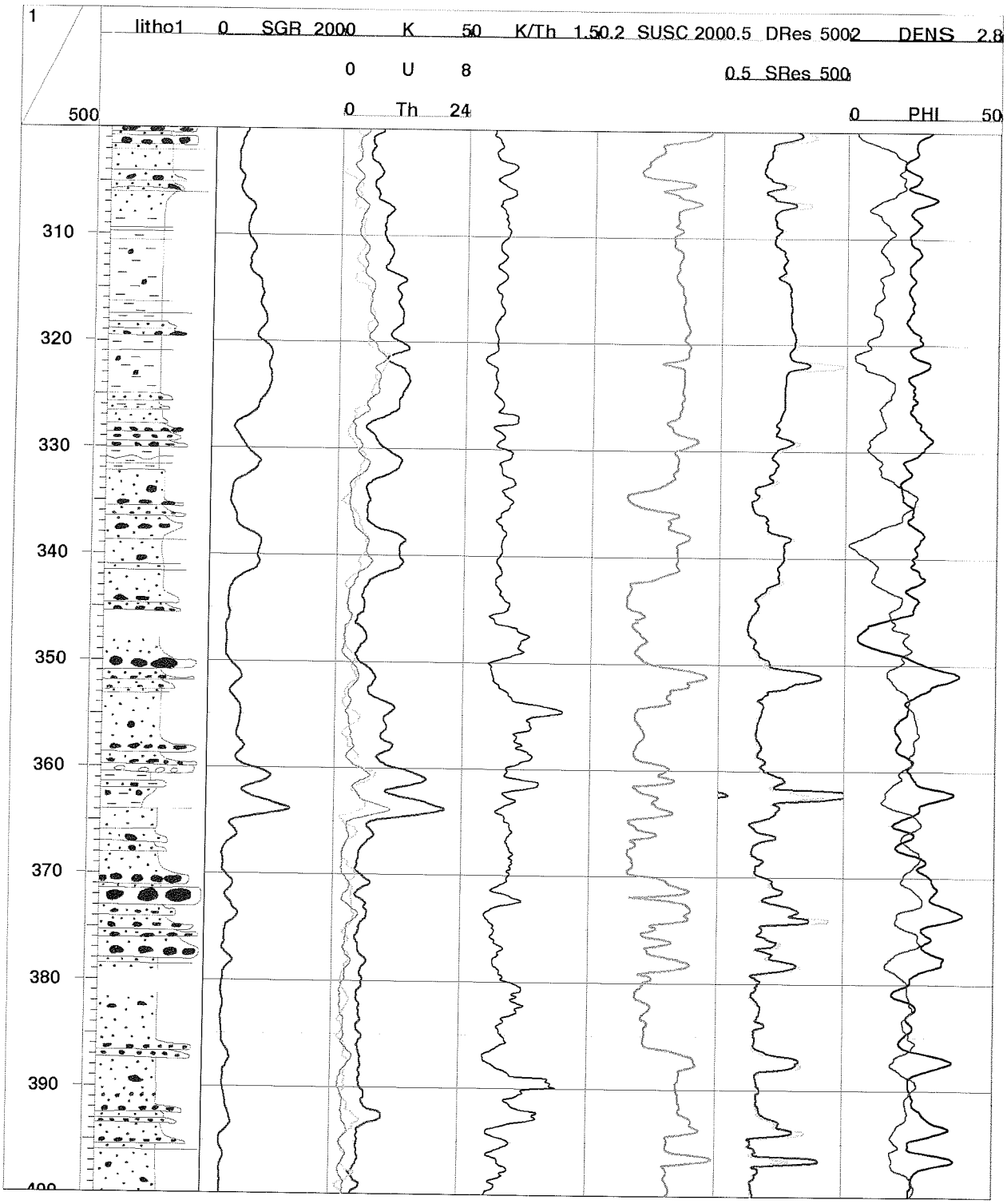
1
litho1
0 SGR 200
0
0
K 50
U 8
Th 24
K/Th 1.5
0.2 SUSC 200
0.5
DRes 500
2
SRes 500
DENS 2.8
0 PHI 50
500
310
320
330
340
350
360
370
380
390

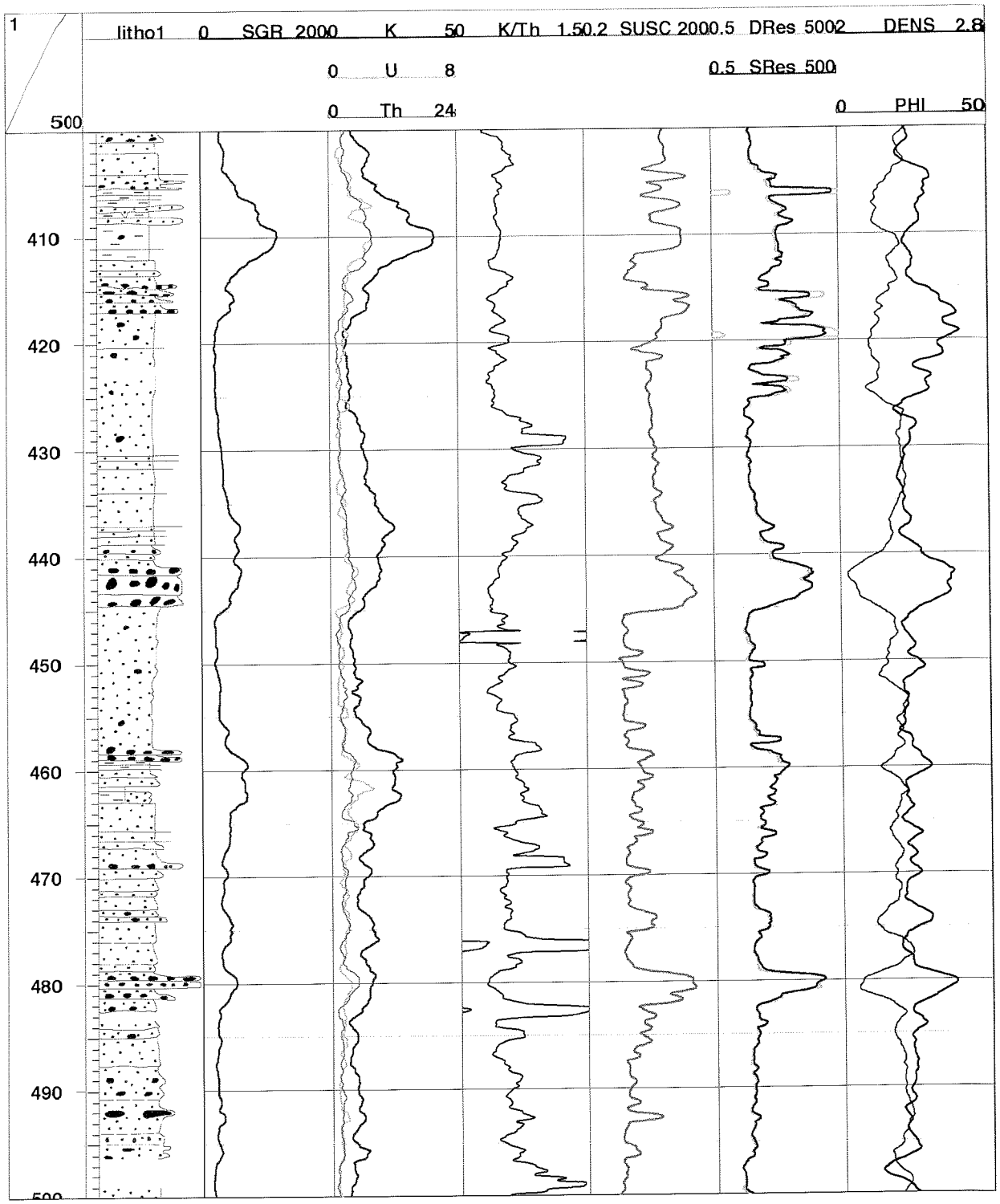
1
litho1
0 SGR 200
0 K 50
0 U 8
0 Th 24
K/Th 1.5
0.2 SUSC 200
0.5 DRes 500
0.5 SRes 500
2 DENS 2.8
0 PHI 50
500
410
420
430
440
450
460
470
480
490

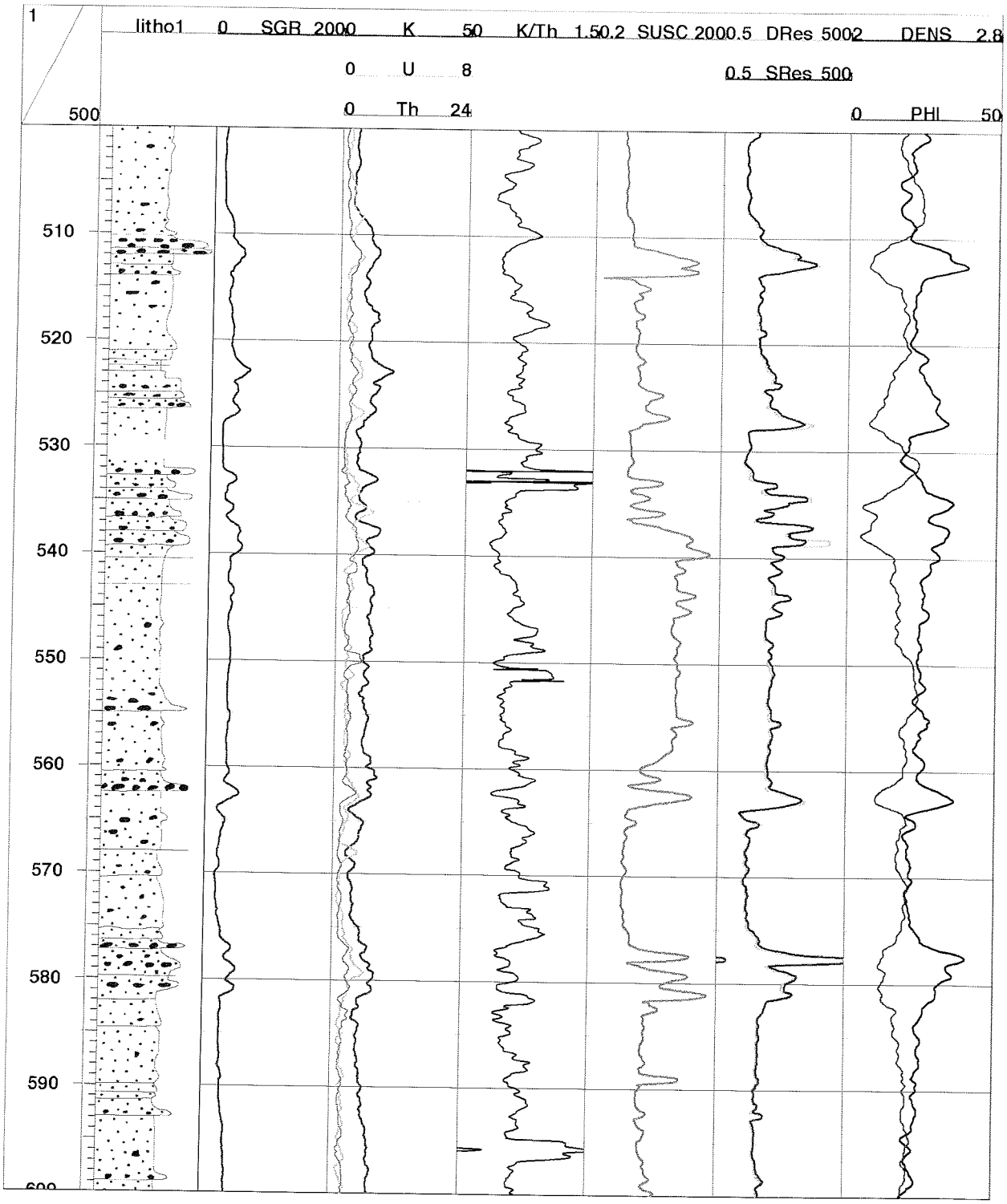
1
litho1
0 SGR 200
0 U 8
0 Th 24
K 50
K/Th 1.5
0.2 SUSC 200
0.5 DRes 500
2 DENS 2.8
0.5 SRes 500
0 PHI 50
500
510
520
530
540
550
560
570
580
590

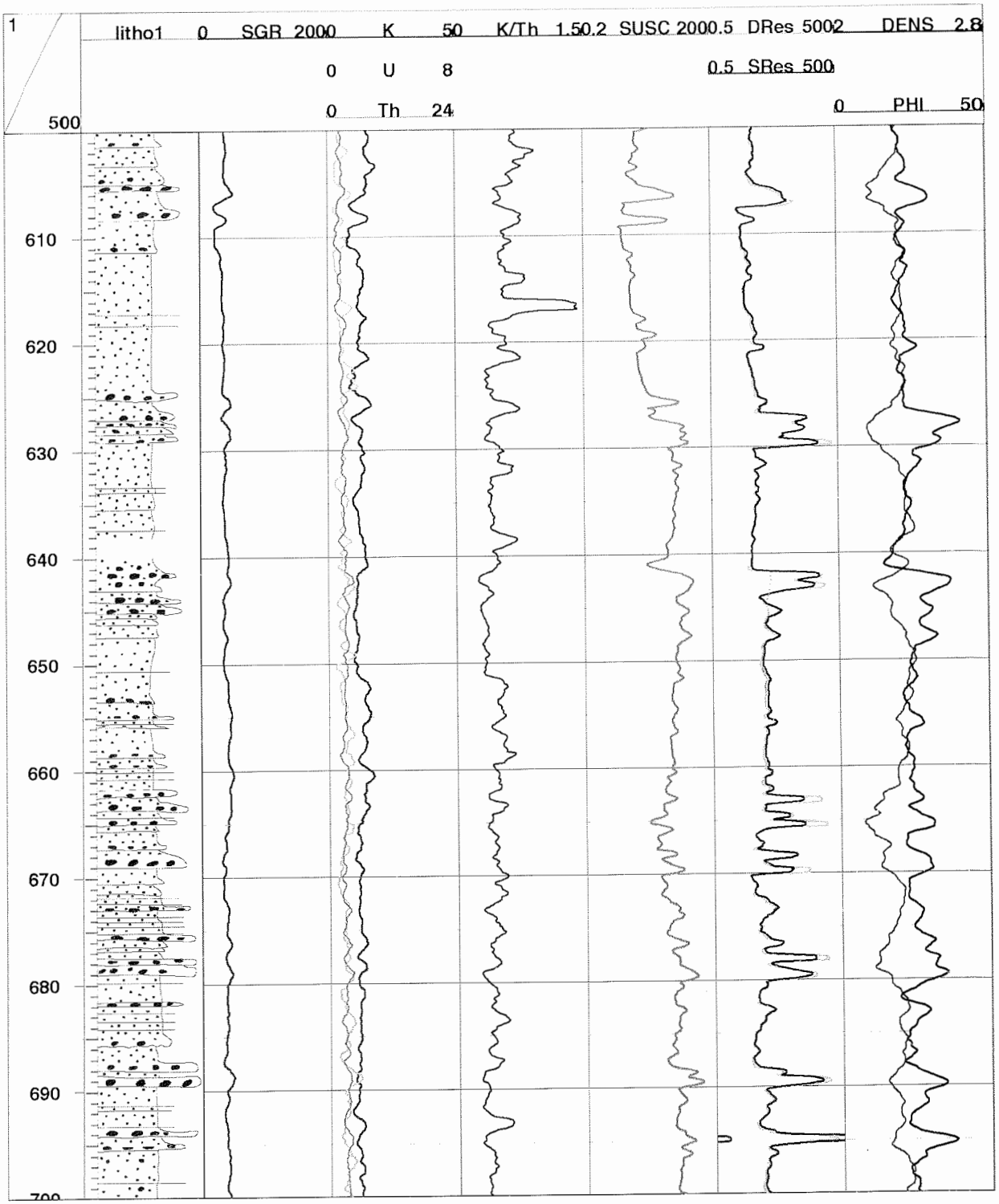
1
litho1
0 SGR 200
0
0
K 50
U 8
Th 24
K/Th 1.5
0.2 SUSC 200
0.5 DRes 500
2 DENS 2.8
0.5 SRes 500
0 PHI 50
500
610
620
630
640
650
660
670
680
690
700

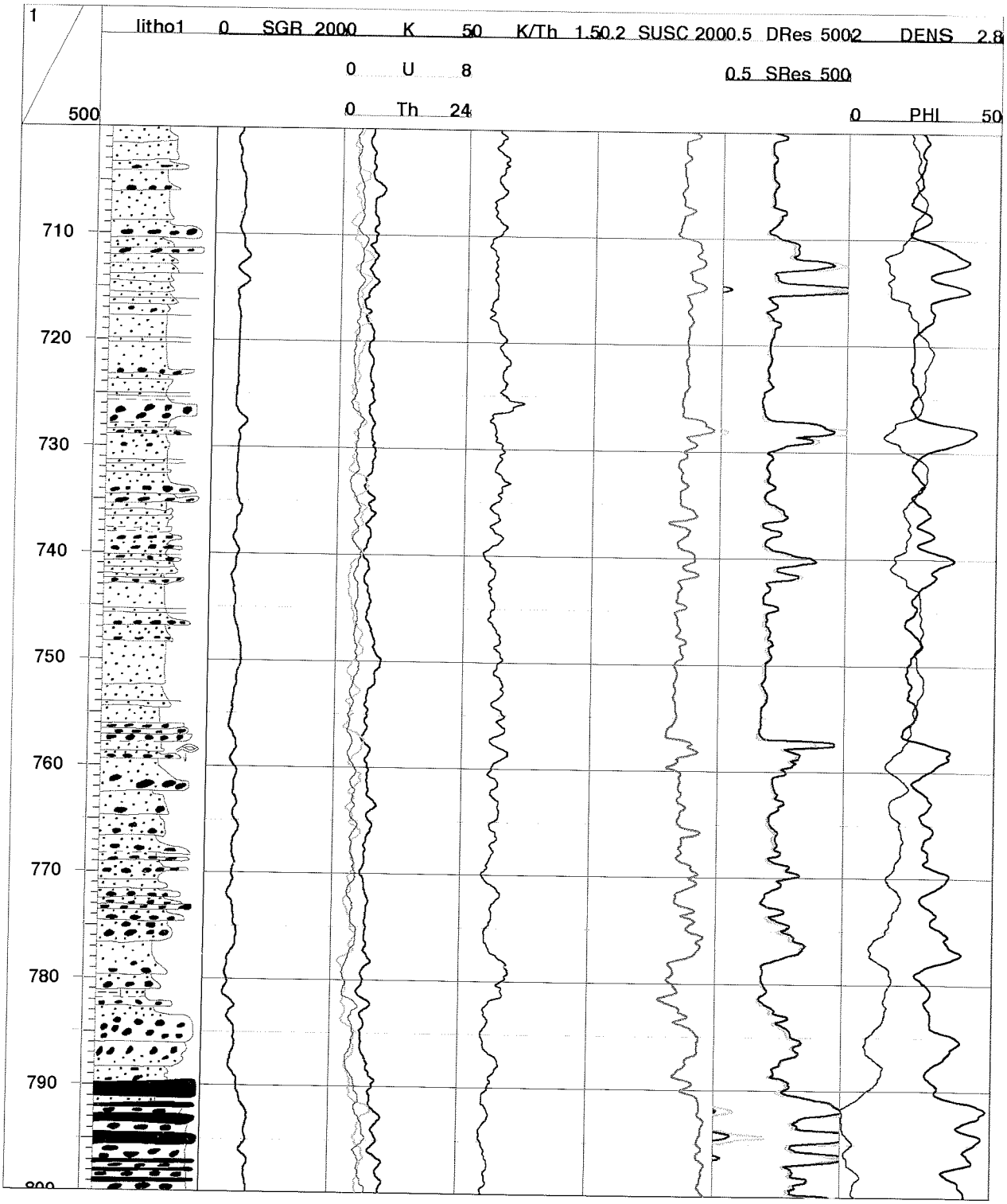
1
500
litho1
0 SGR 200
0 U 8
0 Th 24
K 50
K/Th 1.5
0.2 SUSC 200
0.5 DRes 500
2 DENS 2.8
0.5 SRes 500
0 PHI 50
710
720
730
740
750
760
770
780
790

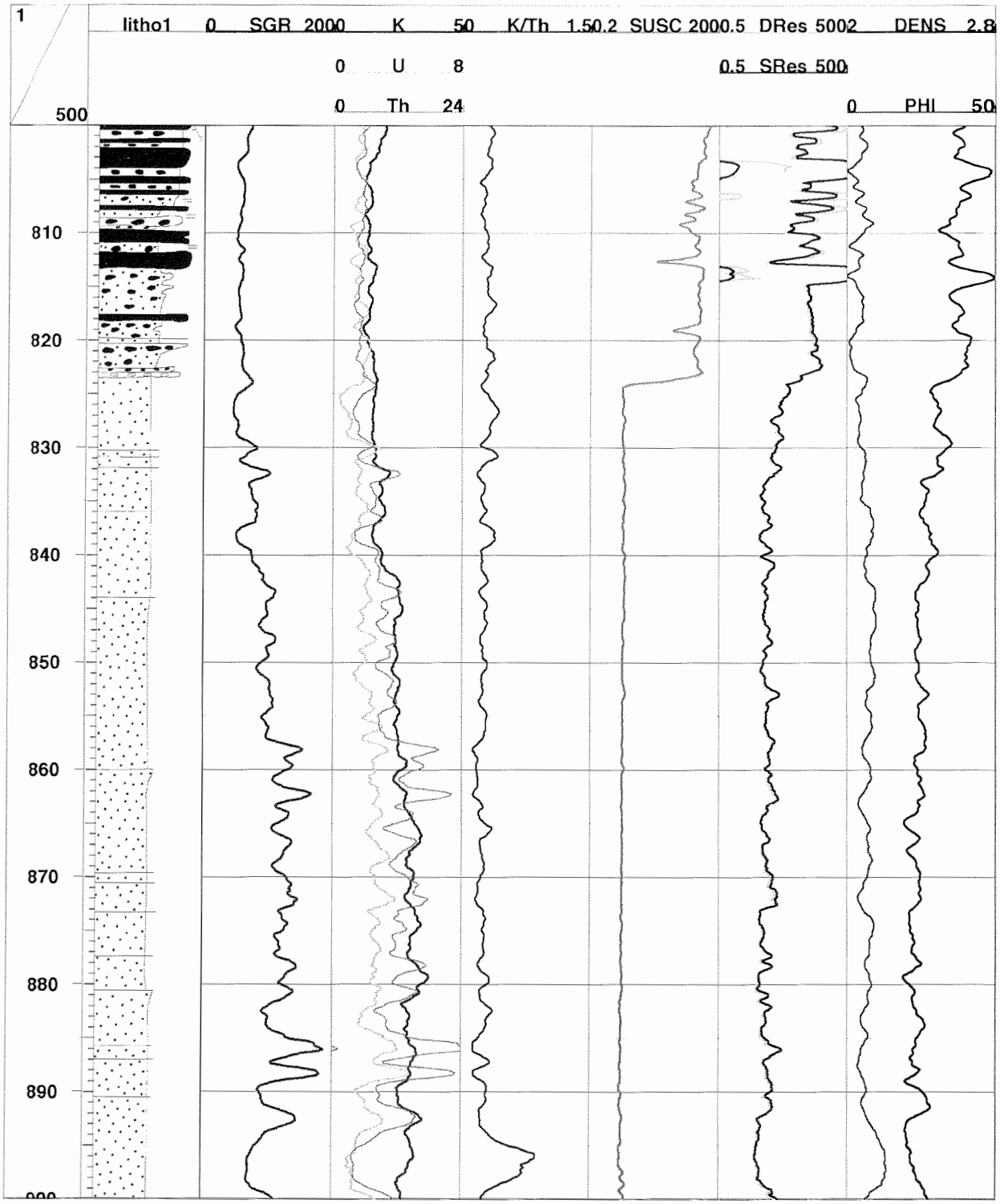
1
litho1
0 SGR 200
0 U 8
0 Th 24
K 50
K/Th 1.5
0.2 SUSC 200
0.5 DRes 500
0.5 SRes 500
2 DENS 2.8
0 PHI 50
500
810
820
830
840
850
860
870
880
890

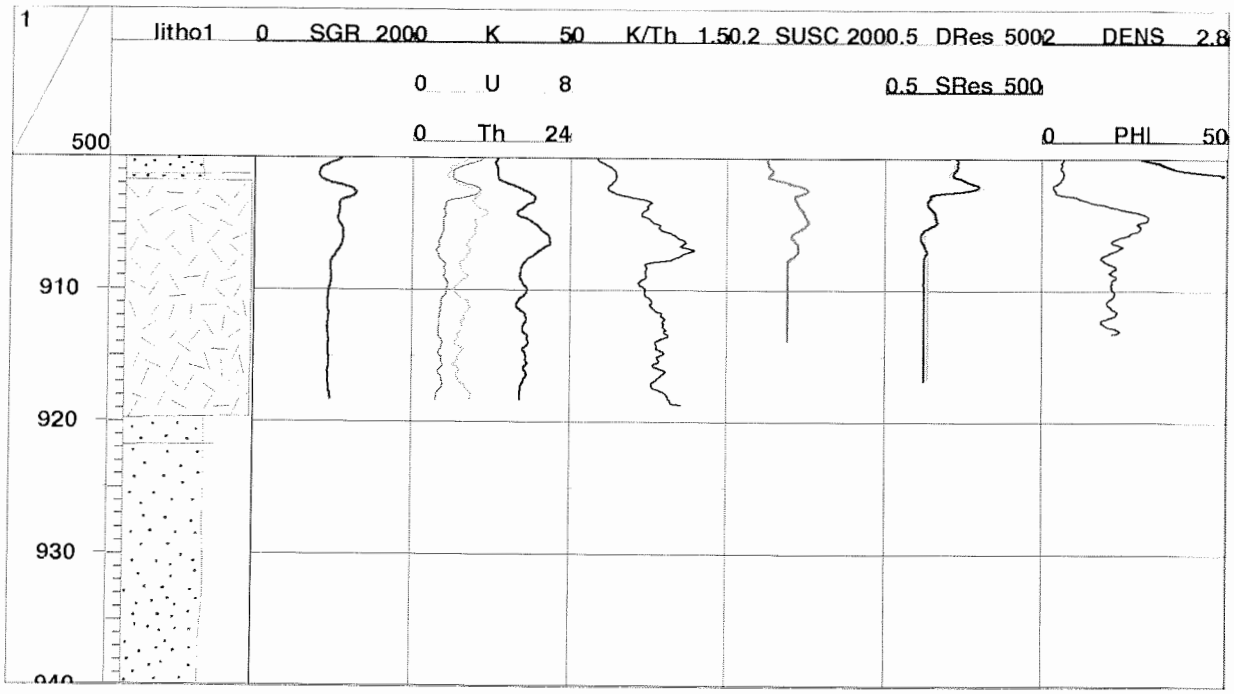
1
litho1
0 SGR 200
0 K 50
0 U 8
0 Th 24
K/Th 1.5
0.2 SUSC 200
0.5 DRes 500
2 DENS 2.8
0.5 SRes 500
0 PHI 50
500
910
920
930

Terra Antartica
Initial Report on CRP-3
2000, 7 (1/2)

3 - Lithostratigraphy and Sedimentology

INTRODUCTION

This chapter presents the results of a lithostratigraphical subdivision of the CRP-3 core, and of a variety of preliminary sedimentological investigations. In the first section, the core is divided into Lithostratigraphical Units and Sub-Units, and the lithologies in each are described. In the following section, a facies analysis provides a process and paleo-environmental interpretation of the core, from which preliminary depositional models are developed. This is in turn followed by: a sequence stratigraphical interpretation of the succession encountered in the drillhole; an initial exploration of potential, small-scale cyclicity in the core; a study of clast roundness trends; and a description and a preliminary interpretation of diagenetic and deformational features. Finally, a core description is shown at a scale of 1:500, including a summary of sequences, sedimentary environments, and glacial proximity.

The core has been divided into 18 lithostratigraphical units, based on major changes in lithology recognised by the scientific team at the Cape Roberts Camp during the drilling of CRP-3. The division draws attention to prominent lithologies such as major diamictite bodies and conglomerate-rich units. The major units are in turn divided into a total of 26 sub-units, based on smaller-scale lithological changes.

Ten recurrent lithofacies and one sub-lithofacies have been recognised in the CRP-3 core based on lithology or associations of lithologies, bedding contacts and bed thicknesses, texture, sedimentary structures, fabric and colour.

Facies 1 (mudstone) is interpreted as mainly suspension fallout deposits of relatively quiet, offshore-marine environments, while Facies 2 (interstratified sandstone and mudstone) is interpreted to reflect the increasing influence of current activity, and in some instances, waves. Facies 3 (poorly sorted, muddy very fine- to coarse-grained sandstones) is interpreted as the product of low-concentration sediment gravity flows across the sea floor. Facies 4 (moderately- to well-sorted, stratified fine-grained sandstones), which appears only rarely in CRP-3, is believed to record sediment deposition from dilute water currents and waves in a shallow-marine setting, which locally at least, was above storm wave base. Facies 5 (moderately-sorted stratified or massive fine- to coarse-grained sandstone) is interpreted, in the post-Beacon Supergroup portion of the core, to represent deposition from aqueous currents in shallow-marine environments subjected to a high rate of sediment supply. Facies 5* is designated to represent sandstones which are composed of dominantly medium-grained, well-sorted sandstone, with minor fine-and coarse-grained sandstone. These occur only in the Beacon Supergroup.

Facies 6 (stratified diamictite) and Facies 7 (massive diamictite) are interpreted to reflect a variety of depositional processes in ice-proximal, marine proglacial environments. Facies 8 (rhythmically interbedded sandstone and siltstone) is interpreted as resulting from suspension settling from turbid plumes originating from fluvial discharges into the sea and producing cyclopsam and cyclopel deposits in ice-proximal glacimarine environments.

Facies 9 (clast-supported conglomerate), is interpreted to have been deposited by, or redeposited by a mass-flow mechanism from fluvial discharges. Facies 10 (matrix-supported conglomerate) is inferred to have been deposited from high-density mass flows.

In a preliminary sequence stratigraphical analysis, we recognised 14 glacimarine depositional sequences from the top of the drillhole to a depth of 306.96 mbsf, together with a further 9 depositional sequences with a possible shallow-marine deltaic affinity but with less glacial influence down to a depth of 480.27 mbsf. The analysis is based on the recognition of repetitive vertical arrangements of the lithofacies summarised above. Most sequences are bounded by sharp erosion surfaces (Sequence Boundaries) that we infer mark abrupt, landward dislocations in facies and hence the interpreted environments of deposition.

The first 14 (glacimarine) sequences typically comprise a four-part architecture termed *Motif A* involving, in ascending order: A) a sharply-based, coarse-grained unit, and B) a fining-upward succession of sandstones into sandy mudstones, these two parts interpreted by the majority of the Science Team as a combined Lowstand and Transgressive Systems Tract deposit; C) a mudstone interval, commonly fossiliferous and in some cases coarsening upward into muddy sandstones, and D) a sharply-based, sandstone-dominated succession, these latter two parts interpreted as a combined Highstand and Regressive Systems Tract. Observations on the overall stratigraphical stacking pattern permit some preliminary speculations as to the geological factors responsible for the cyclical facies pattern.

The remaining 9 sequences with minor glacial influence typically comprise a two-part architecture termed *Motif B*, involving in ascending stratigraphic order: A) a sharp-based, poorly-sorted coarse-grained unit comprising clast or matrix-supported pebble/cobble conglomerate, pebbly sandstone and/or granular sandstone that are often arranged into superposed stacks of crudely graded beds, and interpreted as a combined Lowstand and Transgressive Systems Tract, and B) a

fining-upwards/gradational transition into an interval of well-sorted stratified (locally cross-stratified) sandstone, interpreted as a combined Highstand and Regressive Systems Tract.

Physical properties of two intervals (60.99 to 83.10 mbsf and 120.20 to 144.45 mbsf) were analysed to determine whether small-scale sedimentary cyclicity could be recognised. Spectral analysis has revealed a strong cyclic pattern in both the magnetic susceptibility and porosity records of these lithostratigraphical intervals. The result is highly suggestive of the existence of an external forcing mechanism controlling deposition in the intervals studied, and the periodicity ratios demonstrated from the magnetic susceptibility record may be consistent with ratios of orbital forcing functions.

The interval between 789.77 and 805.60 mbsf, described as a dolerite (cataclastic) breccia, displays evidence of intense shearing and fracturing. In an effort to determine whether or not the larger clasts were of sedimentary or tectonic origin, we examined their roundness characteristics. As the breccia zone was part of a larger interval of conglomerates dominated by dolerite clasts, we included within our examination clasts between 771.70 mbsf and 822.87 mbsf to determine roundness trends.

The data, presented as histograms displaying percent frequency of clasts in each of nine roundness categories, clearly show a transition from rounded to subangular in samples from beneath the breccia zone, through subangular in the breccia zone itself, and then with more rapid transition into rounded above. Within the breccia zone, a significant proportion of clasts (15%) is rounded, and many of the angular clasts appear to be derived from fractured rounded bodies. We interpret these results to indicate that the cataclastic breccia is primarily a sedimentary deposit that has been subsequently modified by shearing.

Outsize cobbles and boulders occur throughout the CRP-3 core in all lithologies. Although only the portion of the core below 350 mbsf was checked for the presence of faceted and striated clasts, they were found at multiple levels throughout this interval, and are inferred to be present in the dominantly glacially influenced upper part of the core as well. The presence of these faceted and striated clasts, and the occurrence of outsized boulders at all levels in the core indicates that ice-berg rafting of glacial debris with deposition by rainout was present throughout most of the period represented by the CRP-3 core.

Preliminary investigations into diagenesis of the CRP-3 core have revealed a variety of diagenetic features, many of which can be readily identified in hand specimen. These include carbonate concretions/nodules, carbonate cementation, pyrite, "black stains" within coarse lithologies, and mineral-fills in veins/fractures.

Carbonate cementation is the most common diagenetic feature throughout the core, and takes a variety of forms, including diffuse patches in many cases surrounding fossil shell material, small spherical nodules and larger ovoid nodules. It increases below about 280 mbsf, where it occurs as an extensive stratiform cementation. Many fractures and veins noted within the core are lined or filled by mineral material, notably carbonates and pyrite. Pyrite occurs as tiny grains dispersed within the matrix in all lithologies, and as infilling associated with calcite in sedimentary dykes. It is also present as a cementing phase, most commonly found filling burrows, and associated with detrital coal particles. The origin of black stains occurring within the matrix of conglomerates is uncertain, but is composed of organic matter of unknown composition.

The research reported in this section provides important documentation and useful first interpretations of depositional environments recorded in the CRP-3 core. Future work will undoubtedly reveal further details of the geological history of the Cape Roberts area.

DESCRIPTION OF SEQUENCE

The sedimentary sequence recovered in CRP-3 is shown graphically in figure 3.1. The Palaeogene portion of that sequence has been divided into 15 major lithostratigraphical units; many of those major units subsequently were divided into subunits, and all subdivisions have been numbered as lithostratigraphical subunits (LSU). Below a sharp erosional contact at 823.11 mbsf, the remainder of the cored sequence has been subdivided into three lithostratigraphical units. One of those units (LSU 17.1) is an igneous intrusion of intermediate composition, which is heavily altered and of unknown age; LSU 17.1 is overlain and underlain by lithostratigraphical units composed of Devonian sandstones (LSU 16.1 and LSU 18.1).

Lithostratigraphical subdivisions of the core were established in "real time" as the core was described at the Cape Roberts camp. As a result, the lithostratigraphical importance of a particular boundary (that is, whether the boundary separated subunits within a single lithostratigraphical unit or separate lithostratigraphical units) was assigned on the basis of lithological distributions seen within approximately the first 10 m underlying that boundary. For this reason, the hierarchy of lithostratigraphical units and subunits presented here provides an initial framework for describing the stratigraphical section in this report.

Each lithostratigraphical subdivision is described here. Preliminary interpretations of these rocks are given in the Facies Analysis section, where the lithostratigraphical subdivisions, the sedimentary facies, and their interpreted depositional environments are discussed in detail. Diagenetic features in the core are listed here in a general form; for example, the term "pyrite cement" is used to denote a variety of occurrences of diagenetic pyrite, including disseminated pyrite, pyrite micronodules, and true pyrite cement. The diagenetic features and their origin are discussed in more detail in the Diagenesis section.

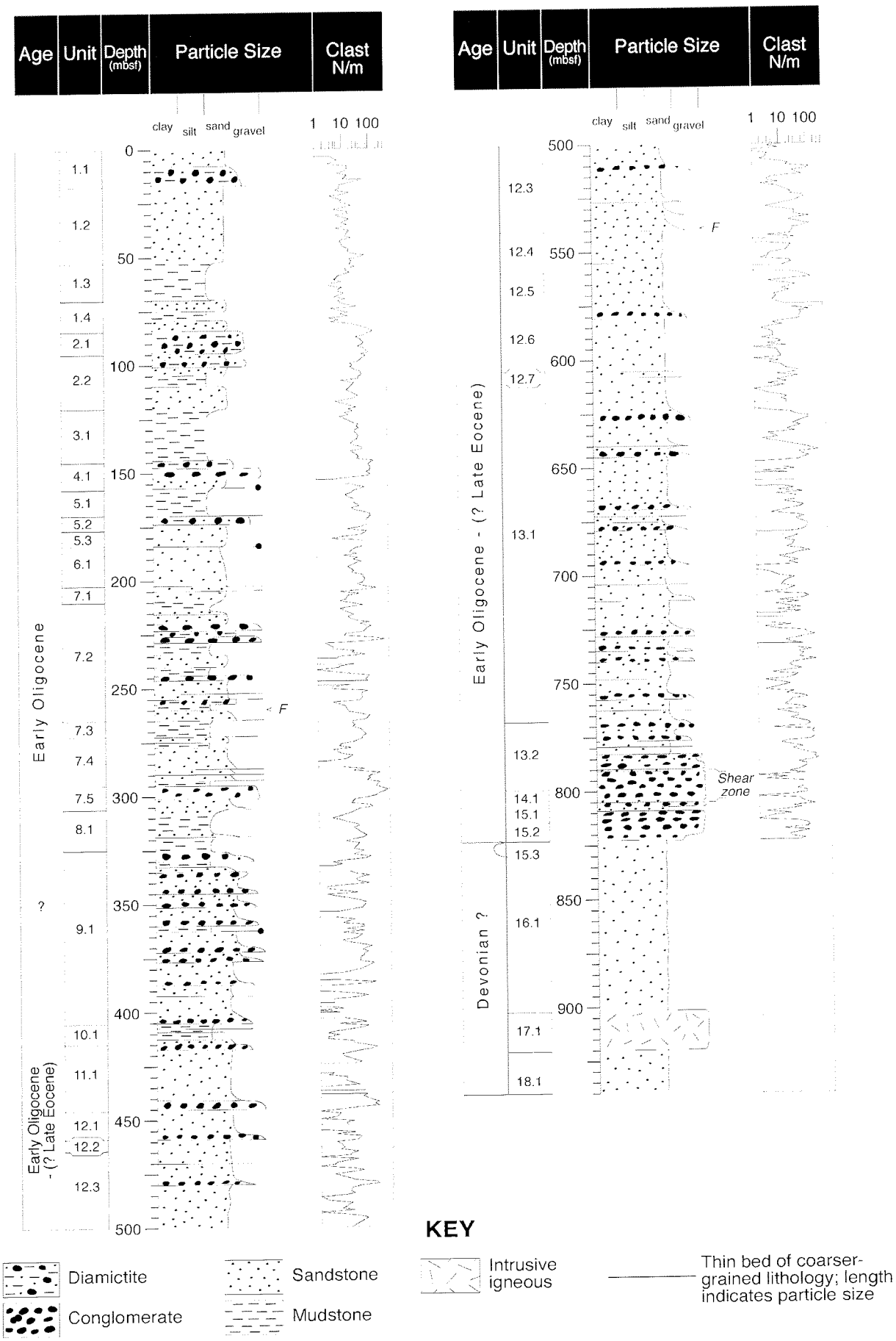

Fig. 3.1 - Graphical log of the sedimentary sequence recovered in CRP-3, showing lithostratigraphical subdivisions. Age for the Cenozoic strata are taken from the section on Chronology of CRP-3.

LITHOSTRATIGRAPHICAL SUB-UNIT 1.1 (2.80-16.72 mbsf), CLAST-POOR DIAMICTITE TO MUDDY SANDSTONE

LSU 1.1 is composed of massive, clast-poor sandy diamictite, which grades locally to clast-poor muddy diamictite and muddy sandstone with dispersed clasts. All lithologies are dark grey (5Y 4/1) in colour. Clasts in LSU 1.1 range from angular to subrounded in shape, and average granule to small pebble in size. The clasts are predominantly grey, fine- to medium-grained volcanic and intrusive lithologies, but a few are dark grey, fine-grained, pyrite-cemented sandstones and siltstones, up to 5 cm in diameter. LSU 1.1 is sparsely fossiliferous, with macrofossils occurring at two levels. Colour mottling, interpreted as resulting from bioturbation, is only present at 8.37 to 8.49 mbsf. A lens of sandstone at 12.12 to 12.22 mbsf records soft-sediment deformation, and a carbonate-cemented sedimentary dyke is present at 10.42 to 10.53 mbsf. The lower contact of LSU 1.1 is sharp.

LITHOSTRATIGRAPHICAL SUB-UNIT 1.2 (16.72 - 52.00 mbsf), MUDDY SANDSTONE

LSU 1.2 is composed of dark-grey (5Y 4/1) muddy sandstone and muddy fine-grained sandstone, both with dispersed clasts, and sparse laminations of siltstone and mudstone. The sandstones primarily are massive to weakly laminated at a cm-scale; at 27.70-30.80 mbsf, some of the laminae exhibit dips as steep as 30∞. Clasts generally are more abundant in the lower half of this unit than in the upper half, and include dolerites and granitoids. Below 26.03 mbsf, carbonate-cemented intraformational clasts are present in low abundance. Macrofossils are present throughout LSU 1.2, with relatively high concentrations at 38.40-39.40 mbsf, 41.00-44.00 mbsf, and 49.22-51.28 mbsf, and include serpulid tubes and molluscs. Simple tubular burrows occur at 50.18 and 50.46 mbsf. Fracturing is common, with intense fracturing and brecciation in zones up to 1 m thick. A calcite vein is present at 17.89-17.91 mbsf, and carbonate-cemented zones up to 25 cm thick occur sparsely throughout LSU 1.2. The lower contact of LSU 1.2 is gradational.

LITHOSTRATIGRAPHICAL SUB-UNIT 1.3 (52.00 - 70.40 mbsf), SANDY MUDSTONE

LSU 1.3 is composed of dark-grey (5Y 4/1) sandy mudstone, locally with dispersed clasts. The sandy mudstone is massive to weakly stratified (cm-scale), but becomes better-stratified downcore. Most of LSU 1.3 is bioturbated, and fossils are present above 65.22 mbsf. Macrofossils are concentrated at 61.08-61.35 mbsf (serpulid tubes and bivalves). Fractures are present throughout LSU 1.3, with some open and some filled with carbonate and/or pyrite. Scattered zones up to 30 cm thick are brecciated. A sedimentary dyke at 52.62-52.76 mbsf contains a complex carbonate fill, including dogtooth sparry calcite. Carbonate and pyrite are also present as sparse patches of cement. Thin beds/laminae of medium-grained sandstone occur at 64.39-64.41 mbsf (contains load casts and flame structures), 66.95-67.11 mbsf and 69.96-70.02 mbsf (both have a sharp base and contain rounded intraformational clasts). LSU 1.3 has a very gradational lower contact.

LITHOSTRATIGRAPHICAL SUB-UNIT 1.4 (70.40 - 83.10 mbsf), VERY FINE-GRAINED SANDSTONE AND MUDSTONE

LSU 1.4 comprises interlaminated-to-thinly bedded, very fine-grained sandstone and mudstone, with proportions of the two lithologies varying through this interval. Discrete sandstone beds up to 22 cm thick are present at 74.10-74.28, 76.20-76.24, 79.21-79.43, and 81.93-81.98 mbsf; some of these beds contain ripple cross-lamination and parallel lamination. Parallel-laminated intervals have dips less than 5∞. Other beds within LSU 1.4 lack primary structures, but contain a combination of sand, mud, and granules that apparently was mixed during deposition. Most beds show evidence of extensive soft-sediment deformation; bed bases are loaded, bed tops have flame structures, and beds commonly are deformed internally. No bioturbation is evident, but macrofossils are present at 75.53 and 76.03 mbsf. LSU 1.4 contains few fractures, but two microfaults are present below 79.50 mbsf. The lower contact of LSU 1.4 is sharp.

LITHOSTRATIGRAPHICAL SUB-UNIT 2.1 (83.10 - 95.48 mbsf), SANDY DIAMICTITE

LSU 2.1 is composed of clast-poor to locally clast-rich sandy diamictite, which grades locally to muddy medium-grained sandstone with dispersed clasts. These sediments are dark grey (5Y 4/1) in colour, and range from unstratified to locally vaguely stratified (defined by slight colour variations). Clasts appear randomly oriented in LSU 2.1. Clasts are up to 20 mm in size, and are predominantly subrounded to rounded dolerite and basalt. Minor clast lithologies include quartz, quartzose sandstone, and granitoid, and one clast at 88.16-88.21 mbsf is a transported, angular, serpulid-bearing, carbonate nodule. A small fragment of detrital coal is present at 93.61 mbsf. Accessory lithologies include a sharp-bounded, internally soft-sediment deformed, coarsening-upward bed at 87.16-87.75 mbsf (from sandy mudstone to fine-grained sandstone), and a sharp-bounded, unstratified sandy mudstone at 90.47-90.56 mbsf. Shell fragments, open fractures, and zones of carbonate cement are all present, but sparse, in LSU 2.1. The base of this unit is sharp, planar, and inclined.

LITHOSTRATIGRAPHICAL SUB-UNIT 2.2 (95.48 - 120.20 mbsf), MUDDY FINE-GRAINED SANDSTONE

LSU 2.2 is composed of fine-grained muddy sandstone with dispersed clasts, grading locally to clast-poor sandy diamictite. The dominant colour in this unit is dark grey (5Y 4/1), with crude cm- to dm-scale stratification outlined by slight colour variations in some intervals. Clasts are dominated by dolerites and diorites, with granule-sized coal fragments at 98.24-99.97 mbsf. Various forms of soft-sediment deformation are common to pervasive in LSU 2.2, including deformed bedding, load casts, and load balls. Deformation is particularly obvious at 100.73-102.02 mbsf, where mudstone and muddy fine-grained sandstone occur as distinct bodies separated by irregular, near-vertical boundaries. Sedimentary dykes are common above 98.20 mbsf and at 109.32-110.27 mbsf; dyke fills include claystone, sandstone, and pyrite-cemented sandstone. Shells and shell fragments are concentrated at 97.07-99.61 mbsf and below 119.00 mbsf. Carbonate-cemented patches and carbonate-filled veins are common, especially below 100.73 mbsf. The base of LSU 2.2 is gradational.

LITHOSTRATIGRAPHICAL SUB-UNIT 3.1 (120.20 - 144.67 mbsf), SANDY MUDSTONE

LSU 3.1 comprises sandy mudstone with dispersed clasts, which is vaguely stratified at a decimetre scale and becomes overprinted by colour mottling downcore. The colour mottling suggests that the sediment is slightly bioturbated. Minor lithologies include: 1) dark-grey claystone beds, less than 30 cm thick, at 122.58-124.50 mbsf; 2) medium-grained, well-sorted, quartzose sandstone, which is stratified but soft-sediment deformed, and contains abundant angular intraformational mudstone clasts, at 139.85-140.02 mbsf; and 3) interlaminated sandy mudstone and fine/medium-grained sandstone, with loading and water-escape structures, at 139.75-139.85 mbsf and 144.45-144.67 mbsf. Patchy carbonate cement is common, and shells/shell fragments are present to common. The base of LSU 3.1 is sharp.

LITHOSTRATIGRAPHICAL SUB-UNIT 4.1 (144.67 - 157.22 mbsf), PEBBLE TO COBBLE SANDY CONGLOMERATE AND SANDSTONE

LSU 4.1 contains pebble to cobble sandy conglomerate, greenish-black (5BG 2.5/1) sandstone with abundant clasts, and sandstone. Conglomerates and sandstones with abundant clasts are interbedded above 152.84 mbsf, whereas fine-grained to medium-grained sandstones are interbedded with minor amounts of dark grey mudstone and pebble to cobble conglomerate below 152.84 mbsf.

The conglomerates and sandstones with abundant clasts are moderately to poorly sorted, and contain both angular and rounded clasts. A few of the clasts are very well rounded. Clast abundance ranges from 10% to 80%, and clasts range in size up to 150 mm. Clasts are predominantly dolerite and other intrusives, with lesser proportions of quartz, granitoids, and other lithologies. The matrix is poorly sorted, medium-grained sandstone, with a black coating or cement around the framework grains. Dm-scale stratification is developed locally by grain-size changes; cross-stratification may be present in a sandier zone at 148.50-149.00 mbsf. The matrix is locally carbonate-cemented, and carbonate-filled hairline fractures are also present.

Below 152.14 mbsf, LSU 4.1 is dominated by well-sorted, well-stratified, fine-grained to medium-grained sandstones; parallel lamination, ripple cross-lamination, and cross-stratification are present. Some of these sandstones exhibit soft-sediment deformation and loading structures, as do dark-grey siltstones (less than 10 cm thick) interbedded with the sandstones at 155.16-156.36 mbsf. The interval below 152.84 mbsf is locally fractured and contains small faults, some of which are mineralised with carbonate. The sandstones (here with abundant clasts) and mudstones are interbedded with pebble to cobble conglomerates at 156.36-157.22 mbsf. The base of LSU 4.1 is sharp and planar.

LITHOSTRATIGRAPHICAL SUB-UNIT 5.1 (157.22 - 169.47 mbsf), SANDY MUDSTONE

LSU 5.1 comprises dark-grey (N4/) sandy mudstone with dispersed clasts, which is bioturbated throughout. Muddy medium-grained sandstone with dispersed clasts forms a sharp-based bed at 159.00-159.47 mbsf. Below 159.95 mbsf, the sandy mudstone with dispersed clasts is diffusely interbedded with muddy, very fine-grained sandstone with dispersed clasts, accompanied by soft-sediment deformation features. Shells and shell fragments are present throughout LSU 5.1, but are common to abundant below 165.60 mbsf. A pebble appears to puncture underlying laminae at 164.34 mbsf; angular clasts occur below this level, and a faceted clast is present at 167.42 mbsf. The entire unit contains carbonate-filled fractures and open fractures. The base of LSU 5.1 is sharp and planar.

LITHOSTRATIGRAPHICAL SUB-UNIT 5.2 (169.47 - 176.42 mbsf), MUDDY FINE-GRAINED SANDSTONE

LSU 5.2 consists predominantly of muddy fine-grained sandstone with dispersed clasts, but grades locally to sandy diamictite and conglomerate. The sandstone is dark grey and contains only rare vague lamination above 173.00 mbsf, but becomes well-stratified on a cm-scale below that level. Soft-sediment deformation, patchy carbonate cement, and possible sedimentary dykes also become more common below 173.00 mbsf. Shell fragments are present, but not common

in the sandstone. The diamictites range from clast-poor to clast-rich sandy diamictites; the conglomerates are muddy and sandy pebble conglomerates. Large clasts are dominated by dolerites, but smaller clasts include dolerites, granitoids (including the youngest occurrence of large pink/orange granitoids), and quartz. Clasts exhibit a range of shapes, including a relatively high abundance of angular and very angular clasts. The base of LSU 5.2 is sharp and inclined.

LITHOSTRATIGRAPHICAL SUB-UNIT 5.3 (176.42 - 184.45 mbsf), FINE-GRAINED TO COARSE-GRAINED SANDSTONE AND PEBBLE TO COBBLE CONGLOMERATE

Fine-grained to coarse-grained sandstones are the primary lithology of LSU 5.3, locally containing dispersed clasts. Clast concentration increases within some intervals of LSU 5.3, either within beds or because of mixing by soft-sediment deformation, to produce lesser amounts of pebbly sandstone and pebble to cobble conglomerate. Clasts are dominated by dolerite, with lesser amounts of other intrusives, granitoids, and orthoquartzites. The sandstones generally are moderately to well-sorted, mud-free, and show parallel lamination and cross-stratification. The bases of some sandstone beds exhibit load casts. Soft-sediment deformation is pervasive in the sandstones, and small faults are present above 179.50 mbsf. Shell fragments occur above 177.40 mbsf. Mudstones form recognizable bodies within intervals that have been extensively soft-sediment deformed (177.54-178.95 mbsf), and also form discrete interbeds within sandstone-dominated intervals (178.95-181.85 mbsf). Below 181.45 mbsf, well-sorted, well-stratified sandstone and pebbly sandstone grade downcore to vaguely stratified pebble conglomerate; a large pebble protrudes from the top of this bed. Patchy carbonate cement is common in LSU 5.3; the base of this unit is sharp and planar.

LITHOSTRATIGRAPHICAL SUB-UNIT 6.1 (184.45 - 202.18 mbsf), SANDY MUDSTONE AND MUDDY FINE-GRAINED SANDSTONE

LSU 6.1 is composed predominantly of sandy mudstone and muddy fine-grained sandstone, both with dispersed clasts. Less-abundant lithologies include fine- to medium-grained sandstone and mudstone, and intervals where fine-grained sandstone with dispersed clasts is interstratified, on a cm-scale, with muddy very fine sandstone with dispersed clasts and mudstone with dispersed clasts. Vague cm-scale stratification is present, especially below 193.50 mbsf. Clasts include angular to very angular dolerites, and rounded reworked nodules of carbonate-cemented mudstones (at 196.00-200.00 mbsf). Dark grey is the predominant colour in LSU 6.1. Soft-sediment deformation is pervasive, and sedimentary dykes are common at 189.50-194.50 mbsf. Shell fragments are relatively common throughout this unit, and 197.07-198.08 mbsf is weakly bioturbated. The base of LSU 6.1 is sharp and planar.

LITHOSTRATIGRAPHICAL SUB-UNIT 7.1 (202.18 - 211.40 mbsf), FINE-GRAINED SANDSTONE AND MEDIUM-GRAINED SANDSTONE

Fine-grained and medium-grained sandstones are the dominant lithologies in LSU 7.1, with lesser amounts of pebble to cobble conglomerate. Mud generally is lacking from all of these lithologies. Primary stratification is well-developed in much of this unit, and includes parallel lamination, ripple cross-lamination, and cross-bedding. Primary stratification is disrupted to varying degrees by soft-sediment deformation (including possible dish structures at 202.95-203.40 mbsf), by fracturing and small-scale faults, and possibly by low-angle shear zones at 204.57-205.47 mbsf (which may offset a large dolerite clast). Coal fragments are common in this unit, both in dispersed form and concentrated into discrete laminae. Two thin conglomerates (27 cm and 53 cm thick) are present in LSU 7.1; these range from granule through cobble conglomerate, but only the thinner bed is graded. The conglomerates are poorly sorted, range from clast-supported to matrix-supported, and have a matrix of medium-grained sandstone, whose grains bear a black surface stain or cement. Clasts are angular to well-rounded, up to 11 cm in diameter, and composed of dolerite (predominant), other intrusives and sedimentary rocks (including quartzarenites), and rare granitoids and quartz. Carbonate cement and carbonate-filled veins are present to abundant in some sections of this unit. The base of LSU 7.1 is gradational.

LITHOSTRATIGRAPHICAL SUB-UNIT 7.2 (211.40 - 264.33 mbsf), INTERBEDDED SANDY MUDSTONE, STRATIFIED SANDSTONES, AND CONGLOMERATE

LSU 7.2 comprises sandy mudstones with dispersed clasts, stratified sandstones, and conglomerates, interbedded at scales ranging from tens of cm to approximately 6 m. The sandy mudstone with dispersed clasts is dark grey, and exhibits vague stratification in some intervals. The sandstones range from very fine-grained to medium-grained, and are generally well-sorted and well-stratified, with parallel lamination, ripple cross-lamination, and cross-bedding. In some intervals, the stratification and primary structures are modified or entirely destroyed by soft-sediment deformation, which includes recumbent folds, load structures, and possible dish structures. Conglomerates range from granule- to cobble-conglomerates; pebble conglomerates are most common. The conglomerates are moderately to poorly sorted, contain angular to well-rounded clasts, have clast contents from 10% to 80%, and generally show weak to no stratification. The interval 243.78-252.00 mbsf contains three sharp-based beds, each less than 1 m thick, that fine upwards from conglomerate to sandstone or pebbly sandstone.

Clasts in LSU 7.2 are predominantly dolerite, with lesser abundances of other intrusives, quartz and granitoids, and sedimentary lithologies. Irregularly-shaped weathered clasts are present at 212.08-212.32 mbsf. Coal fragments are present to abundant in specific intervals within this unit, generally in the coarse-sand to granule-size fractions. Fossils are scarce, and only occur above 226.00 mbsf. Most of this unit has a dark-grey colour, due to the presence of a cement or a dark surface stain on the sand grains. Carbonate cement is distributed irregularly through this unit; pyrite cement, nodular carbonate cement, and secondary porosity are present locally. Sedimentary dykes, open and healed fractures, and small faults are also present to abundant in some intervals; one example is a single fracture at 217.47-220.47 mbsf, which changes from open to mineralised with carbonate along its length. The interval from 256.98 to 263.02 msbf is composed of heavily brecciated mudstone and sandstone, with extensive mineralised fractures; this may be a zone of faulting.

The base of LSU 7.2 is sharp and irregular.

LITHOSTRATIGRAPHICAL SUB-UNIT 7.3 (264.33 - 270.51 mbsf), SANDY MUDSTONE

LSU 7.3 comprises medium-grey to dark-grey sandy mudstone with dispersed clasts, which is locally carbonate-cemented and contains carbonate-filled fractures. At least two generations of fractures are present, as indicated where one fracture offsets another fracture. Disseminated pyrite is present. The dark colour of LSU 7.3 is caused by the presence of a black surface stain or cement on the sand grains. No primary structures can be seen, due to the extent of cementation and fracturing. Shells and shell fragments are present, most notably an articulated bivalve at 266.13 mbsf. LSU 7.3 has a gradational lower contact.

LITHOSTRATIGRAPHICAL SUB-UNIT 7.4 (270.51 - 293.43 mbsf), WELL-STRATIFIED MEDIUM-GRAINED SANDSTONE

The primary lithology in LSU 7.4 is well-stratified, medium-grained sandstone with dispersed clasts, which is interbedded with lesser amounts of sandy mudstone, sandstone with abundant clasts, and pebble to cobble conglomerate. The sandstones are predominantly medium-grained, but range from very fine- to medium-grained; they are generally well-sorted and well-stratified, with parallel lamination, ripple cross-lamination, and cross-bedding. Soft-sediment deformation features are present locally, but become more abundant below 288.00 mbsf. The sandy mudstone is medium grey and exhibits vague stratification in some intervals. The conglomerates range from granule- to cobble-conglomerates; pebble conglomerates are most common. The conglomerates are moderately to poorly sorted, contain angular to well-rounded clasts, have clast contents from 10% to 80%, and generally show weak to no stratification.

Clasts in LSU 7.4 are predominantly dolerite, with lesser abundances of other intrusives, quartz and granitoids, and sedimentary lithologies. A dolerite clast with a weathering rind is present at 284.20-284.24 mbsf, and pebbles with rims of pyrite cement occur at 287.13-287.85 mbsf. Coal fragments are present to abundant in specific intervals within this unit, generally in the coarse sand- to granule-size fractions. A deformed mass of fine- to medium-grained sandstone at 276.48-276.88 mbsf may be a sedimentary dyke. Patchy carbonate cement is widespread throughout LSU 7.4. One shell is present, at 278.02 mbsf. The interval 293.10-293.43 mbsf is an incoherent mix of basement clasts, sand, and carbonate cement, whose original lithology is unknown; this is interpreted as a strongly sheared and carbonate-cemented fault breccia. The base of LSU 7.4 is sharp.

LITHOSTRATIGRAPHICAL SUB-UNIT 7.5 (293.43 - 306.26 mbsf), PEBBLE TO COBBLE CONGLOMERATE

LSU 7.5 is dominated by pebble to cobble conglomerate above 300.22 mbsf, and conglomerate is interbedded with well-stratified, well-sorted, predominantly medium-grained sandstones below that level. In some intervals, the sandstones become pebbly sandstones. The conglomerates are moderately sorted, with a clast distribution that is apparently bimodal: one mode being 20 mm diameter or larger, the other granule-size. The conglomerates also are mostly clast-supported, with clast abundances averaging approximately 60%. Clasts are mostly dolerite, with lesser proportions of quartz sandstone and granitoid, and range in shape from very angular to well-rounded. A large proportion of the clasts are well-rounded. Stratification in the sandstones includes parallel laminations and cross-bedding. Carbonate cement is widespread in LSU 7.5; pyrite cement and secondary porosity are developed locally. The base of LSU 7.5 is gradational.

LITHOSTRATIGRAPHICAL SUB-UNIT 8.1 (306.26 - 324.88 mbsf), MUDDY FINE-GRAINED SANDSTONE AND SANDY MUDSTONE

The upper one-third of LSU 8.1 is predominantly muddy fine-grained sandstone with dispersed clasts, with a few thin interbeds (less than 10 cm thick) of medium-grained to pebbly medium-grained sandstone. The dominant lithology in the remainder of LSU 8.1 is sandy mudstone with dispersed clasts; one medium-grained sandstone and one muddy medium-grained sandstone are present (47 and 137 cm thick, respectively). The muddy medium-grained sandstone is an interbed that contains dispersed clasts and grades locally to both clast-poor and clast-rich sandy diamictite. The origin of the carbonate-cemented medium-grained sandstone is uncertain, as it may be either an *in situ* interbed or a large

sedimentary clast. Most of LSU 8.1 is bioturbated and weakly stratified; soft-sediment deformation is common in the sandstones. Large clasts occur only above 308.64 mbsf, and some have possible weathering rinds. Shells and shell fragments are present to common throughout LSU 8.1. Patchy carbonate cement is distributed throughout this unit, but is more abundant above 312.30 mbsf; pyrite cement is present, especially below 322.50 mbsf. The base of LSU 8.1 is gradational.

LITHOSTRATIGRAPHICAL SUB-UNIT 9.1 (324.88 - 406.00 mbsf), WELL-STRATIFIED SANDSTONE AND SANDY MUDSTONE

LSU 9.1 is composed of well-stratified sandstone, sandy mudstone, and muddy sandstone, all with dispersed clasts, interbedded at thicknesses ranging from less than 50 cm to greater than 4 m. Conglomerates also are present, but are approximately half as abundant as the well-stratified sandstones. The well-stratified sandstones range from fine-grained to medium-grained, and generally exhibit parallel lamination, ripple cross-lamination, and some cross-bedding; a few intervals, however, are only vaguely stratified. The well-stratified sandstones also form the thickest beds within LSU 9.1, which are generally sharp-based and are preferentially carbonate-cemented in the upper half of this unit. Conglomerates are the second most common lithology in LSU 9.1, being present as pebble to cobble conglomerate beds up to 1.5 m thick. These conglomerates range from matrix-supported to clast-supported, with angular to well-rounded clasts up to 80 mm in diameter. Dolerites are the most abundant clasts, with lesser amounts of other intrusives, granitoids, quartz, and sedimentary rocks. The conglomerates are poorly sorted, but have a bimodal distribution of clast sizes, together with a matrix of poorly sorted coarse to very coarse sandstone. The sandy mudstones are generally medium grey in colour, bioturbated, with some weak stratification, and soft-sediment deformed in some intervals. Shell fragments are present at 358.95-359.31 mbsf. Patchy carbonate cement, pyrite cement, and nodular carbonate cement occur irregularly above 387.30 mbsf; below that level, all three cement types are common. The base of LSU 9.1 is sharp and planar.

LITHOSTRATIGRAPHICAL SUB-UNIT 10.1 (406.00 - 413.56 mbsf), MUDSTONE

The dominant lithology in LSU 10.1 is medium-grey to dark-grey mudstone, which is internally unstratified but contains very low abundances of dispersed clasts. Above 408.42 mbsf and below 411.34 mbsf, the mudstone is interstratified with sharp-bounded sandstones of various grades (fine-grained sandstone and granule-to-pebbly medium- to coarse-grained sandstone). The sandstone beds range from less than 1 cm to 30 cm in thickness, are unstratified or parallel-stratified, and occasionally are overprinted by soft-sediment deformation. The sandstones are preferentially cemented with pyrite and carbonate. The base of LSU 10.1 is gradational.

LITHOSTRATIGRAPHICAL SUB-UNIT 11.1 (413.56 - 444.44 mbsf), SANDSTONE AND CONGLOMERATE

LSU 11.1 comprises sandstone and conglomerate, with sandstones approximately twice as abundant as conglomerates. Thicker conglomerates are concentrated in the upper 3 m and lower 4 m of this unit, whereas thin conglomeratic horizons are scattered through the interior of LSU 11.1. The sandstones are generally "clean" (*i.e.* they do not contain mud), moderately to well-sorted, fine- to coarse-grained, and stratified, with parallel stratification and some suggestions of possible cross-bedding. At 416.99-425.60 and 439.60-440.64 mbsf, gravel is common to abundant within the sandstone, both dispersed and concentrated in laminae. At 434.75-438.30 mbsf, unstratified fine-grained sandstone is interbedded with intervals of stratified fine-grained sandstone and rhythmic fine- to medium-grained sandstone laminae. The coarser-grained intervals range from pebbly medium- to coarse-grained sandstone to pebble conglomerate, with angular to well-rounded clasts, mainly of dolerite. Patchy carbonate cement and pyrite cement are distributed widely through LSU 11.1; nodular carbonate cement is present, but rare. A shell fragment is present at 422.75 mbsf. The base of LSU 11.1 is sharp.

LITHOSTRATIGRAPHICAL SUB-UNIT 12.1 (444.44 - 458.48 mbsf), LIGHT-COLOURED QUARTZOSE SANDSTONE

LSU 12.1 consists almost exclusively of "clean", well-sorted, grey (10Y 6/1) quartzose sandstone. The sandstone is medium- to fine-grained, generally with rare dispersed gravel, and shows local vague cross-bedding and parallel stratification above 450.67 mbsf and below 455.60 mbsf. Coal fragments are concentrated into numerous laminae within the sandstone at 456.14-456.41 mbsf. Two thin beds of small pebble conglomerate are present below 458 mbsf; these conglomerates are clast- to matrix-supported, moderately sorted, with angular to subrounded clasts less than 22 mm in diameter, mainly of dolerite, and with a matrix of fine- to coarse-grained sandstone. Patchy carbonate cement is common throughout LSU 12.1; nodular carbonate cement and pyrite cement are distributed sparsely in this unit. Steeply dipping carbonate-filled fractures are present below 452.70 mbsf. The base of LSU 12.1 is sharp.

LITHOSTRATIGRAPHICAL SUB-UNIT 12.2 (458.48 - 462.91 mbsf), SANDSTONE AND MUDSTONE

LSU 12.2 is composed of very fine- to fine-grained sandstone, sandy mudstone and mudstone, interstratified in beds that range from less than 1 cm to 1.2 m thick. The

sandstones contain some parallel stratification, and some are soft-sediment deformed. A few beds grade upward from fine-grained sandstone to sandy mudstone. Coal fragments are common, especially in the upper 2 m of LSU 12.2. Patchy carbonate cement is common. The base of LSU 12.2 is sharp and planar.

LITHOSTRATIGRAPHICAL SUB-UNIT 12.3 (462.91 - 539.31 mbsf), LIGHT-COLOURED QUARTZOSE SANDSTONE

LSU 12.3 is dominated by "clean", well-sorted, light-coloured, fine- to medium-grained, quartzose sandstones, most of which exhibit vague parallel stratification. Cross-bedding may be present in a few intervals, and low-angle divergent laminations at 517-519 mbsf may be suggestive of possible hummocky cross-stratification. Coal fragments are common in the sandstones, both dispersed and concentrated into laminae; coal laminae are abundant at 521.60-522.80 mbsf. Soft-sediment deformation is present, but rare. Pyrite and patchy carbonate cements are distributed widely in this unit. Shells and shell fragments are present at 466.79-466.82 mbsf. Conglomeratic intervals are relatively thin (ranging from less than 10 cm to greater than 120 cm thick), and consist of pebble to cobble conglomerate, matrix- to clast-supported, with angular to well-rounded clasts up to 180 mm in diameter. The clasts are mainly dolerite, and the matrix is fine- to coarse-grained sandstone. The base of LSU 12.3 is sharp, and is placed at the base of a 49-cm-thick dolerite boulder. A portion of the boulder may have been removed by a fault, and carbonate- and pyrite-filled fractures pass through the clast.

LITHOSTRATIGRAPHICAL SUB-UNIT 12.4 (539.31 - 558.87 mbsf), DARK-COLOURED SANDSTONE AND CONGLOMERATE

The dominant lithology in LSU 12.4 is dark greenish-grey (5GY 2.5/1) sandstone; pebbly sandstones and pebble conglomerates are minor lithologies. The dark greenish-grey sandstone is quartzose and mainly fine-grained, but a coating on the grains imparts the dark colour to this unit. The nature of this coating is unknown at present, but it may be due to the presence of chlorites. These sandstones locally are parallel stratified above 555.67 mbsf, but exhibit well-developed parallel laminations and cross-bedding below that level. Low-angle divergent laminations below 558 mbsf may be suggestive of possible hummocky cross-stratification. The sandstones contain dispersed clasts, with carbonate cement surrounding some clasts. Both open and carbonate-filled hairline fractures are present. Pebbly sandstone to pebble conglomerate occurs as several beds less than 50 cm thick. The conglomerates are poorly sorted, matrix- to clast-supported, with a matrix of fine-grained sandstone, and contain angular to well-rounded clasts that are mostly dolerite. The base of LSU 12.4 is gradational.

LITHOSTRATIGRAPHICAL SUB-UNIT 12.5 (558.87 - 576.28 mbsf), LIGHT-COLOURED QUARTZOSE SANDSTONE

The dominant lithology in LSU 12.5 is "clean", well-sorted, quartzose, light-coloured, medium-grained sandstone with rare scattered gravel. The sandstone is well-stratified only in the upper 2 m of LSU 12.5; it is uncemented to poorly cemented in some intervals (especially near intervals lost during coring), but becomes harder downcore due to more extensive carbonate cementation. Pebbly sandstones and a pebble to cobble conglomerate form minor lithologies. The conglomerate, at 561.37-562.54 mbsf, is poorly to moderately sorted, mostly clast-supported, with a matrix of poorly sorted medium-grained sandstone. Clasts are angular to well-rounded, less than 90 mm in diameter, and mainly composed of dolerite, with lesser amounts of granitoids, metamorphics, sedimentary lithologies, quartz, and basalt. The base of LSU 12.5 is gradational.

LITHOSTRATIGRAPHICAL SUB-UNIT 12.6 (576.28 - 605.90 mbsf), DARK-COLOURED SANDSTONE AND CONGLOMERATE

The dominant lithology in LSU 12.6 is poorly sorted, muddy, green-grey (10Y 3/1), medium- to fine-grained sandstone, with rare dispersed clasts. These sandstones show local parallel and inclined stratification, and have a mottled appearance that may be due to bioturbation. Nodular carbonate cement and narrow carbonate-filled fractures are abundant in this sandstone. Coal fragments are common at 588.00-592.00 mbsf, and are concentrated into laminae at 591.80-591.90 mbsf. Above 580.62 mbsf, LSU 12.6 comprises interbedded quartzose, well-sorted, fine- to medium-grained sandstone and pebble to cobble conglomerate. Pebbly sandstone and pebble conglomerate also form the basal 92 cm of this unit. The base of LSU 12.6 is sharp and planar.

LITHOSTRATIGRAPHICAL SUB-UNIT 12.7 (605.90 - 611.03 mbsf), LIGHT-COLOURED QUARTZOSE SANDSTONE

LSU 12.7 is dominated by "clean", grey (2.5Y 6/1), moderately sorted, quartzose, fine-grained sandstone, which is carbonate-cemented and contains low abundances of dispersed small coal particles. A pebble to cobble conglomerate, at 607.77-607.99 mbsf, is the only minor lithology in LSU 12.7. This conglomerate is poorly to moderately sorted, mainly clast-supported, and has a matrix of carbonate-cemented, poorly sorted fine- to coarse-grained sandstone. Clasts are angular to well-rounded, less than 87 mm in diameter, and composed mostly of dolerite. A wood fragment is present at 606.10 mbsf. The base of LSU 12.7 is gradational.

LITHOSTRATIGRAPHICAL SUB-UNIT 13.1 (611.03 - 767.70 mbsf), GREEN/GREY QUARTZOSE SANDSTONE AND MINOR CONGLOMERATE

The most abundant lithology in LSU 13.1 is dark greenish grey (5Y 2.5/1) quartzose, muddy fine-grained sandstone. This lithology forms more than 50% of this unit; the remainder is divided subequally between "clean" sandstones, matrix-supported conglomerates, and clast-supported conglomerates. The slightly muddy sandstones range from vaguely stratified to well-stratified, with parallel lamination and parallel rhythmic lamination; in some cases the laminae are defined by concentrations of gravel or coal fragments. Well-defined lamination is common in muddy sandstone beds at 635.00-644.38, 659.60-661.30, 663.70-664.40, and 695.30-700.28 mbsf. Local convex-up laminations at 743.72-752.43 mbsf (*e.g.* 748.62 mbsf) and low-angle divergent laminations at 704-705 and 764-765 mbsf may be suggestive of possible hummocky cross-stratification. Ripple cross-lamination, cross-bedding, and soft-sediment deformation are present locally within the muddy fine-grained sandstones.

The "clean" sandstones, which are most abundant above 635.52 mbsf, are greenish grey (5Y 5/2), quartzose, and fine-grained, with rare dispersed gravel and rare vague stratification. Nodular carbonate cement is common, and pyrite cement is rare in the "clean" sandstones. The conglomerates occur as beds that generally are less than 1 m thick, separated by 1-3 metres of sandstone. The conglomerates are pebble to cobble conglomerates, poorly sorted, matrix- to clast-supported, and with a matrix of poorly sorted fine- to coarse-grained sandstone. Clasts are angular to rounded, and dominated by dolerite, but with other lithologies present. Many of the conglomerates have gradational boundaries, although sharp-based conglomerates do occur occasionally.

An indurated mudstone clast with striations is present at 738.40-738.42 mbsf. The interval 752.43-753.40 mbsf has a mottled appearance, probably due to bioturbation. Patchy carbonate cementation is extensive in LSU 13.1, with lesser occurrences of pyrite and nodular carbonate cementation. The base of LSU 13.1 is gradational.

LITHOSTRATIGRAPHICAL SUB-UNIT 13.2 (767.70 - 789.77 mbsf), GREEN/GREY QUARTZOSE SANDSTONE AND PEBBLE CONGLOMERATE

LSU 13.2 is dominated by pebble to cobble conglomerates and pebbly sandstones, with lesser amounts of grey/green muddy sandstones. Many occurrences of the coarser-grained lithologies form fining-upward sequences, from a sharp-based conglomerate at the base to a pebbly sandstone at the top; a few are symmetrically graded or ungraded. Thicknesses of the fining-upward beds range from *c.* 40 cm to *c.* 1 m. The thickest conglomerate bed is almost 4.4 m thick, and appears to be symmetrically graded (782.80-787.15 mbsf). The conglomerates are pebble to cobble conglomerates, matrix- to clast-supported, and with a matrix of poorly sorted, muddy, medium-grained sandstone. Clasts are angular to well-rounded, and predominantly composed of dolerite. The muddy sandstones are fine- to medium-grained, and show vague to well-defined parallel stratification. Some of the sandstones are soft-sediment deformed, and concentrations of coal particles define both primary stratification and soft-sediment deformation features. Two indurated mudstone clasts, with striations, are present at 775.55 and 775.80 mbsf. A macrofossil is present at 781.34-781.36 mbsf. Patchy carbonate cement is common in LSU 13.2, and dispersed pyrite cement is common in its lower half. The base of LSU 13.2 is sharp.

LITHOSTRATIGRAPHICAL SUB-UNIT 14.1 (789.77 - 805.60 mbsf), DOLERITE BRECCIA

LSU 14.1 comprises a breccia, composed primarily (but not exclusively) of dolerite clasts. Intervals of carbonate-cemented, apparently stratified, fine- to medium-grained sandstone with dispersed small gravel, approximately 10-20 cm thick, are interbedded with the breccia. Above 803.92 mbsf, the breccia intervals are monomictic, with only dolerites present. The dolerite clasts, which range in size from pebbles to boulders, have been fractured, offset, and veined with carbonate. Within the breccia intervals, the fractured dolerite clasts are enveloped in a fine-grained matrix that is interpreted as a sheared, recrystallised foliated claystone. This matrix may be cataclastic in origin. Below 803.92 mbsf, LSU 14.1 is an oligomictic breccia; the largest clasts are dolerite, but angular to very angular pebbles to cobbles of quartzose sandstone are present to common. Rounded pebbles of dark-grey mudstone are also present, but are rare. Many of the sandstone clasts are fractured and/or veined, and the matrix is dark-grey, sheared, claystone and fine- to medium-grained sand or muddy sand. This matrix also may be cataclastic in origin. The base of LSU 14.1 is sharp and irregular.

LITHOSTRATIGRAPHICAL SUB-UNIT 15.1 (805.60 - 813.41 mbsf), LIGHT-COLOURED QUARTZOSE SANDSTONE WITH LARGE CLASTS

LSU 15.1 is composed of quartzose, light-brown (10Y 4/1), medium-grained sandstone and pebbly sandstone, up to 50 cm thick, alternating with dolerite clasts up to 1.6 m long. The sandstones are stratified, predominantly with parallel laminations, and the pebbly sandstones contain clasts of quartzose sandstone and rare dark-grey mudrock. The dolerite clasts contain some slicken-lined surfaces, fractures, and carbonate veins. The base of LSU 15.1 is sharp, and is placed at the bottom of a 1.6-m-thick dolerite boulder.

LITHOSTRATIGRAPHICAL SUB-UNIT 15.2 (813.41 - 822.87 mbsf), DOLERITE CLAST CONGLOMERATE

LSU 15.2 is a dark grey/blue (5GB 2.5/1) pebble to boulder conglomerate, very poorly sorted, mainly clast-supported, and with a matrix of well-rounded, moderately sorted, quartzose, black-stained, coarse-grained sandstone. Clasts in the conglomerate are subangular to well-rounded, and composed predominantly of dolerite; however, quartzose sandstone clasts are also present in low abundances, most notably a quartzose sandstone boulder at 817.64-818.30 mbsf. Most of the dolerite clasts are less than 150 mm in diameter, although the largest dolerite clast is 660 mm in diameter. Clast abundances decrease in some intervals of LSU 15.2, producing small-pebble conglomerates with angular clasts. Rims of carbonate cement on some clasts, carbonate-filled fractures, and carbonate-filled veins occur throughout LSU 15.2. Sand-filled sedimentary dykes show consistent steep dips, and cut dolerite clasts throughout this unit. The base of LSU 15.2 is sharp and irregular.

LITHOSTRATIGRAPHICAL SUB-UNIT 15.3 (822.87 - 823.11 mbsf), SANDSTONE CLAST BRECCIA

LSU 15.3 is a sedimentary breccia, comprising poorly sorted clasts of light red/brown quartzose sandstone contained within a matrix of quartzose, clay-rich, medium-grained sandstone. The breccia is clast-supported and crudely stratified, with clasts less than 65 mm in diameter. A distinct irregular surface is present at 822.95 mbsf; above this level, the sandstone clasts are rounded to well-rounded, whereas angular sandstone clasts dominate the interval below 822.95 mbsf. The base of LSU 15.3 is sharp and irregular.

LITHOSTRATIGRAPHICAL SUB-UNIT 16.1 (823.11 - 901.48 mbsf), LIGHT RED/BROWN QUARTZOSE SANDSTONE

LSU 16.1 is dominated by light red/brown (5YR 6/6) medium-grained, quartzarenite sandstone, with some coarse- to very coarse-grained sand present, both dispersed and concentrated in discrete laminae. In general, the sandstone is well-stratified, mostly with parallel lamination defined by colour and grain-size variations; however, cross-stratification is present locally, and some intervals between 855 and 890 mbsf show no stratification, perhaps because of a bioturbation overprint. Average dip of the stratification is approximately 15°. Open and carbonate-filled fractures are common, sometimes showing offsets across the fractures. LSU 16.1 contains local zones of brecciation throughout its length. At 866.70-867.52 mbsf, the core exposes the wall of a broad vertical fracture, which juxtaposes unstratified but coherent medium-grained sandstone against the brecciated sandstone that fills the fracture. Below 895.50 mbsf, blue/grey zones and laminae become more common, fracture fills of grey/purple clay are present, and the sandstone becomes more compact and harder. The abundance of carbonate-filled fractures increases below 898.90 mbsf, and the sandstone becomes purple-coloured (5P 2/2) and strongly carbonate-veined below 900.40 mbsf. A brecciated zone is present at 901.09-901.30 mbsf, with light brown (7.5YR 4/4), angular to very angular bodies of altered intrusive rock in a fine-grained matrix of the same colour. The base of LSU 16.1 is sharp and irregular.

An alternative interpretation of the contact between LSU 16.1 and LSU 17.1, which has been proposed by petrologists working at CSEC but has not been followed in this report, places the base of the sandstone (LSU 16.1) at 901.09 mbsf. In this interpretation, the brecciated zone at 901.09-901.30 mbsf is the top of the intrusion, and the sandstone at 901.30-901.48 mbsf is a fragment that was entrained, but not completely assimilated, within the intrusion.

LITHOSTRATIGRAPHICAL SUB-UNIT 17.1 (901.48 - 919.95 mbsf), ALTERED DOLERITE(?) INTRUSION

LSU 17.1 is heavily-altered intrusive or subvolcanic rock, which was classified as a dolerite during initial description of the core. Subsequent thin-section examination has highlighted the heavily-altered nature of this interval; however, the absence of quartz in altered glassy intervals suggests that the original glass was at least intermediate in composition (see Igneous Intrusion section). A light brown (7.5YR 4/4) breccia of the altered igneous rock extends from 901.48 to 902.10 mbsf; the same rock is more coherent below 902.10 mbsf, although restricted zones of brecciation extend to approximately 906 mbsf. Where less brecciated and/or altered, the intrusion is light blue-grey (5BG 5/1), becoming purple (5P 2/2) downcore. Zones and veins of cream- to brown-coloured alteration persist throughout LSU 17.1. Brecciated zones and the light brown colour become more common below approximately 918 mbsf. LSU 17.1 has a strongly brecciated, sharp and irregular base.

LITHOSTRATIGRAPHICAL SUB-UNIT 18.1 (919.95 - 939.42 mbsf), LIGHT RED/BROWN QUARTZOSE SANDSTONE

LSU 18.1 is dominated by light red/brown (5YR 6/6) medium-grained, quartzarenite sandstone, with some coarse- to very coarse-grained sand present, both dispersed and concentrated in discrete laminae. In general, the sandstone is well-stratified, mostly with parallel lamination defined by colour and grain-size variations. Cross-stratification is present locally, and some intervals show no stratification, perhaps because of bioturbation or soft-sediment deformation overprints. Average dip of the stratification is approximately 15°. Open and

carbonate-filled fractures are common, sometimes showing offsets across the fractures. Notable examples include a 4-cm-wide, near-vertical fracture, filled with a breccia of sandstone clasts and clay, at 927.90-928.54 mbsf, and a 3-cm-wide fracture, filled with sandstone breccia and clay, at 934.76-935.10 mbsf. LSU 18.1 is brecciated locally. The sandstone is tough, hard, purple-stained and carbonate-veined above 920.25 mbsf, and similar characteristics become more common below 935.10 mbsf.

FACIES ANALYSIS

The lithofacies scheme used for CRP-3 follows that for CRP2/2A (Cape Roberts Science Team, 1999) with the exception of two facies (intraformational clast breccia and volaniclastics) that occur in CRP-2 but not in CRP-3. Although the same scheme is followed, modifications to the descriptions have been made to include characteristics peculiar to CRP-3.

FACIES 1 - MUDSTONE

Facies 1 consists of massive, very fine sandy mudstone and mudstone. The mudstone facies varies from silty claystone and clayey siltstone that locally grades vertically to sandstone over tens of centimetres. The mudstone includes intervals that are laminated to thinly bedded, as shown both by colour changes and by inclusion of siltstone and very fine sandstone laminae (Fig. 3.2 a, b & c). Beds above about 350 mbsf are up to 10 to 15 m thick whereas below that depth, mudstone is rare and thin, generally being less than 1 m thick. Generally, bioturbation is weak but locally some intervals lack evidence of primary original stratification without necessarily being bioturbated. Where stratified, this facies shows soft-sediment deformation structures

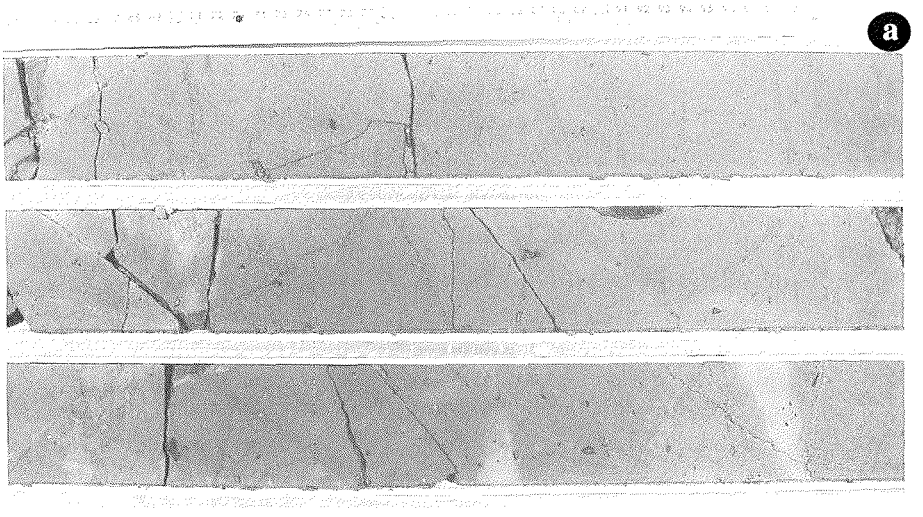

Fig. 3.2 - a) Mudstone of Facies 1 at 55.61-58.04 mbsf, shown here with laminae at inconsistent dips, dispersed clasts and patches of carbonate cement.

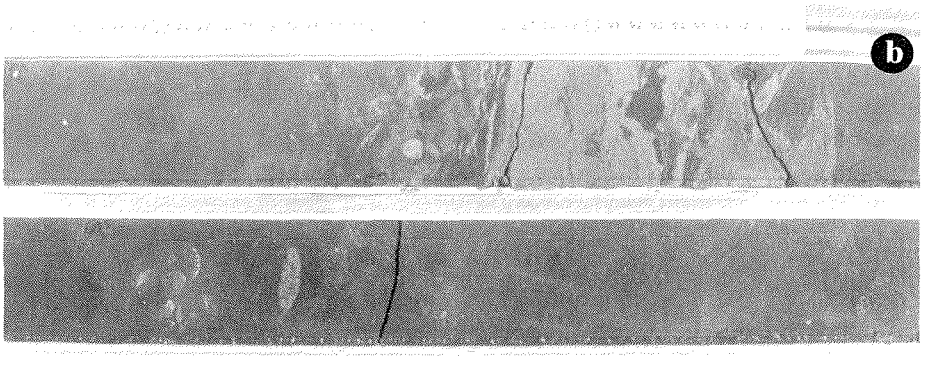

Fig. 3.2 - b) Massive mudstone of Facies 1 at 139.62-141.05 mbsf with soft-sediment deformed sandstone and bioturbation in the upper core section and a concentration of macro-fossils (solitary scleractinian corals, serpulid tubes and a carditid bivalve) in the lower core section.

Fig. 3.2 - c) Massive mudstone of Facies 1 at 407.01-407.43 mbsf overlain by matrix-supported conglomerate of Facies 10 which loaded into the mudstone below while it was still soft.

Fig. 3.2 - d) Interbedded sandstone and mudstone of Facies 2 at 458.68-462.11 mbsf exhibiting local soft-sediment loading and micro-faulting. The sandstone is cross-bedded, has local coal fragments and is carbonate cemented.

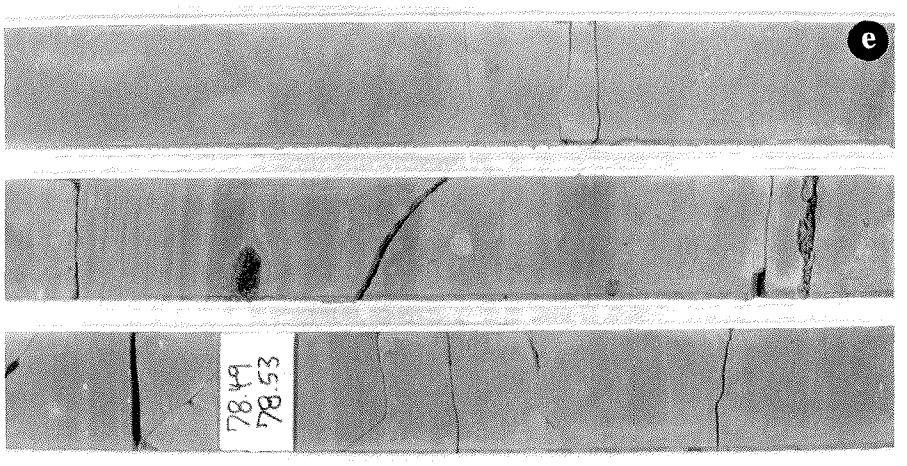

Fig. 3.2 - e) Interlaminated and thinly interbedded mudstones and very fine- to fine-grained sandstones of Facies 2 at 76.42-78.88 mbsf. The image shows rhythmic inter-bedding, sharp-bounded and some normally graded sandstone beds, diffuse patches of carbonate cementation and dispersed clasts, one of which shows an impact structure from being dropped onto the sea floor. The muddy intervals are vaguely laminated in the style of cyclopels of Facies 8.

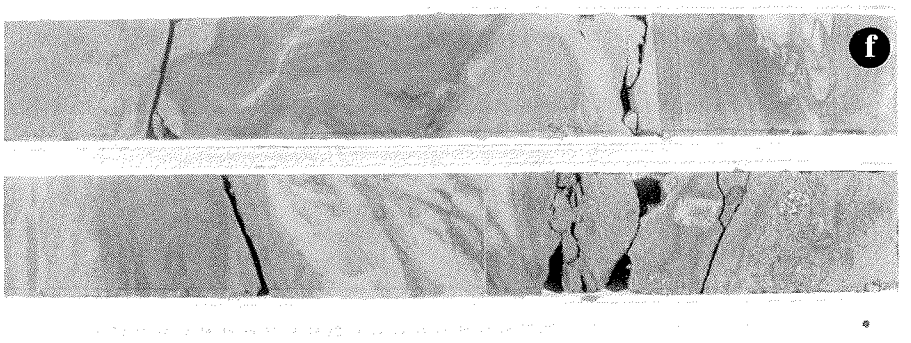

Fig. 3.2 - f) Interlaminated and thinly interbedded very fine- to fine-grained sandstone and mudstone of Facies 2 at 155.04-156.47 mbsf showing soft-sediment deformation in the form of injection, flame and microfault structures, and local bioturbation.

through discrete intervals, and locally that deformation is intense. Dispersed clasts occur within many intervals of this facies, and they vary from less than 1% to increasing quantities such that the mudstone locally grades into muddy diamictite. Mudstones are commonly interbedded with massive to normally graded, moderately sorted and ripple cross-laminated very fine- to medium-grained sandstone and massive, poorly sorted, muddy very fine-grained sandstone. Marine macrofossils and their fragments are commonly scattered through mudstone facies.

Facies 1 mudstones represent the quietest water conditions within the CRP-3 sequence. These are thought to be hemipelagic sediment which, due to their high silt content, probably had their main contributions from fluvially-derived turbid plumes discharging into coastal waters. These sediments also had contributions from distal or dilute sediment gravity flows in the form of very fine sand and silt laminae and from icebergs contributing lonestones as well as contributing sand and more silt particles.

Fig. 3.2 - g) Poorly sorted, muddy, vaguely stratified fine- to medium-grained sandstone of Facies 3 at 681.62-685.05 mbsf. This lithofacies is locally characterised by gravel horizons, commonly with diffuse contacts, as are shown here.

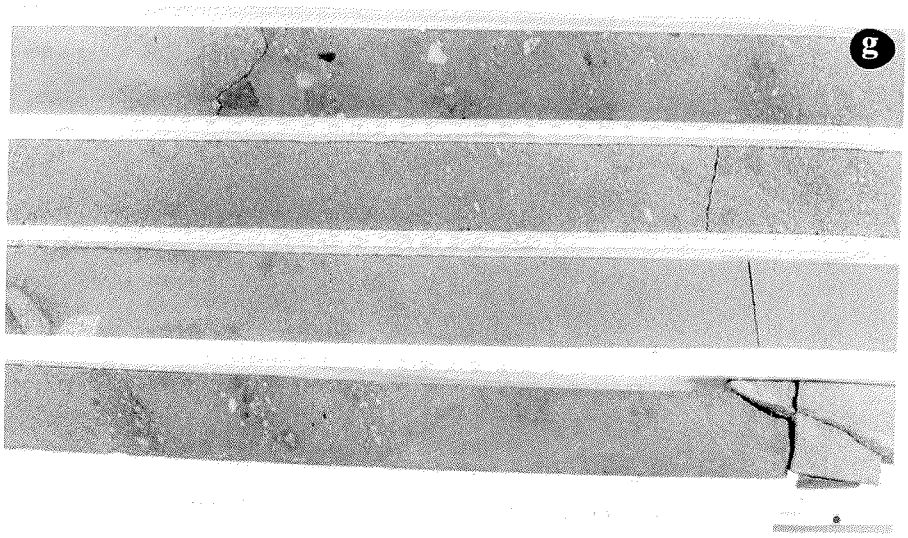

Fig. 3.2 - h) A variation of poorly-sorted, muddy sandstone of Facies 3 at 169.49-170.91 mbsf with dispersed gravel and a local concentration of clasts making a matrix-supported conglomerate with indistinct contacts.

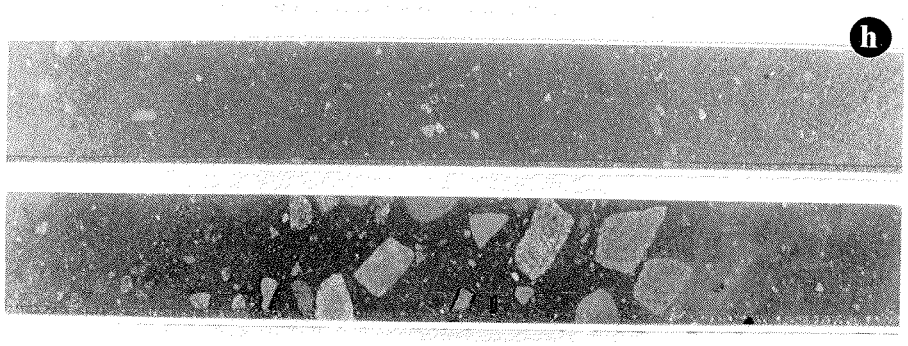

Fig. 3.2 - i) Poorly sorted muddy sandstone of Facies 3 at 116.88-117.30 mbsf with better sorted very-fine grained sandstone to siltstone laminae that show loading and soft sediment deformation. Clasts are rare.

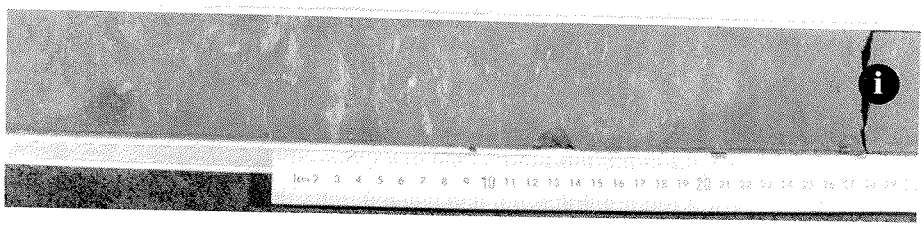

Fig. 3.2 - j) Well-sorted, fine-grained, finely laminated sandstones of Facies 4 at 745.95-749.38 mbsf. Note the horizontally laminated and low-angle cross-bedded nature of the sandstones, especially in the first and fourth core section. The stratification includes curved, convex-upward lamination reminiscent of small-scale hummocky cross-stratification. Small black particles are detrital coal, probably reworked from the Beacon Supergroup. Facies 4 sandstones in the two middle core sections appear structureless, and one interval of poorly sorted, pebbly, muddy sandstone occurs in the third core section.

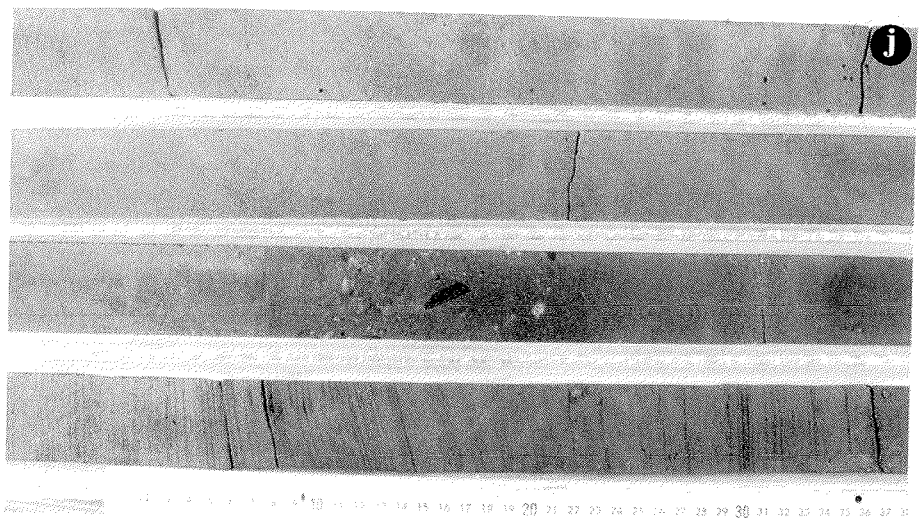

FACIES 2 - INTERSTRATIFIED SANDSTONE AND MUDSTONE

Facies 2 comprises very fine- and fine- to locally medium-grained sandstone, interstratified with very fine-grained sandy mudstone, the sandstone having sharp lower contacts and sharp or gradational upper contacts (Fig. 3.2 d, e, f, & r). The sandstone is either massive or normally graded and locally includes ripple cross-lamination, some of which appears to have been wave-influenced, and planar lamination in the upper, finer-grained intervals of the sandstone beds. Interstratification is on a scale that ranges from lamination to beds a few metres thick, and when laminated, units may include siltstone laminae. Where bioturbation occurs it is commonly within the finer-grained intervals, especially the mudstones. Dispersed lonestones locally deform laminae beneath them and are interpreted as dropstones. Intervals may fine upward through an increasing proportion of mudstone strata, with a corresponding increase in bioturbation upward, or they may coarsen upward through an increasing number of sandstone beds. Soft-sediment deformation is common within depositional intervals or may occur on a slightly larger scale to include several intervals; clastic dykes occur locally. Marine macrofossils are common.

Bioturbation and marine macrofossils indicate a submarine environment of deposition for this facies. That being the case, the trend of normal grading, including parallel-laminated and ripple cross-laminated sandstones passing up to massive and laminated mudstones, is characteristic of a range of current types from low to moderate density sediment gravity flows to that of combined wave and current action. Common soft-sediment deformation and clastic dykes imply that the succession's pore-water pressure was at times high and that sediments were rapidly deposited.

FACIES 3 - POORLY SORTED (MUDDY) VERY FINE TO COARSE-GRAINED SANDSTONE

Varieties of poorly sorted sandstones characterize Facies 3 (Fig. 3.2 g, h & i). The facies varies from fine- to coarse-grained sandstones that are massive to parallel laminated or bedded; some beds are normally graded, but very locally they show reverse grading. The muddy, very fine and fine sandstone may be locally ripple cross-laminated and include mudstone laminae, which may show soft-sediment folding. Coarse to very coarse sand and clasts are dispersed throughout. Locally, where clasts are abundant in the medium to coarse sandstones, they may be sufficiently concentrated to form matrix-supported conglomerate or may exhibit coarse tail fining-upward trends. In some intervals dispersed clasts increase up-core, defining coarsening upward trends into matrix-supported conglomerate. In addition, conglomerates occur locally at the base of beds, generally above sharp contacts. Commonly, when the sandstones are massive, clasts may be concentrated at one horizon and then progressively become dispersed upward while the matrix remains the same sand size throughout. This indicates either that two beds had been amalgamated or that there was variation within one depositional event. In contrast, stratified sandstone intervals may be produced by either alternating sand grain-size changes or variation in proportions of mud, causing colour variations. Shapes of dispersed clasts and those in the conglomerates range from angular to rounded. These muddy sandstones locally may be interbedded with Facies 5 sandstones; they grade vertically into mudstone or locally exhibit fining trends in the sands from fine to very fine-grained, with a concomitant increase in mudstone. Soft-sediment deformation is apparent only locally as are fragmental coal partings. Facies 3 is locally weakly bioturbated, has local lonestones as outsized clasts and has rare marine macrofossils.

Those units exhibiting grading trends in both sand and gravel sizes may be indicative of medium- to high-density sediment gravity flow deposits which, at least when they contain fossils or are interbedded with other units with fossils, are of marine origin. Alternatively, these may represent waning stages of traction flows. Some of the thicker massive beds of very fine to fine sandstone may include very rapidly sedimented deposits from fluvial discharges on deltas or grounding-line fans, where they form highly sediment-charged plumes of suspended sediment as they enter sea. Icebergs are most likely the source of most lonestones.

FACIES 4 - MODERATELY- TO WELL-SORTED STRATIFIED FINE-GRAINED SANDSTONE

Moderately- to well-sorted fine sandstones, which exhibit low-angle cross-bedding and cross-lamination or are planar thin-bedded to laminated, characterize Facies 4 (Fig. 3.2 i, j & k). This facies is relatively rare, but where it occurs it includes possible hummocky cross-stratification (HCS) where laminae have a similar convex upward shape. However, it is difficult to assign unequivocally in the narrow core. Compositionally, these sandstones are rich in quartz and locally contain coal grains dispersed along laminae or constituting distinct laminae. Very fine, medium and coarse sand occurs locally. These units are most commonly associated and interbedded with sandstones of Facies 5. Some intervals exhibit penecontemporaneous soft-sediment folding and microfaulting. Facies 4 sandstone is also locally weakly bioturbated.

The delicate laminations preserved in this facies are indicative of dilute tractional currents with quiescent periods represented by mudstone. Their association with other marine facies, the low-angle discordances, and the presence of possible HCS infers a marine setting within or about storm wave base.

Fig. 3.2 - k) Well-sorted, fine-grained, finely laminated, sandstones of Facies 4 at 663.40-664.82 mbsf interbedded with moderately sorted medium- to coarse-grained sandstones of Facies 5. Facies 4 occurs between 663.60 and 664.64 mbsf exhibiting cross-stratification and angular clasts lying flat on bedding planes. Facies 5 sandstones have dispersed clasts and intervals where clasts are concentrated into matrix-supported conglomerate.

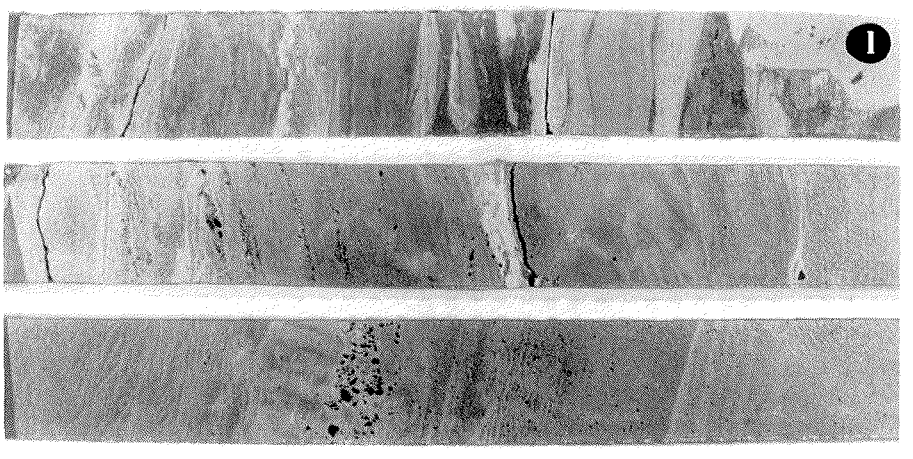

Fig. 3.2 - l) Moderately to well sorted, fine- to medium-grained sandstones of Facies 5 at 205.48-207.90 mbsf, showing horizontal lamination (first and third runs), ripple cross-lamination (first and third core sections) and cross-bedding (second core section). Ripple forms in the first core section appear symmetrical possibly indicating formation by waves or combined-current flows. Soft-sediment deformation structures such as microfaulting, loading and folding are common, but most striking are the fluid escape, dish and pillar structures in the third run where a thin bed of coal fragments has been disrupted during the fluid escape process.

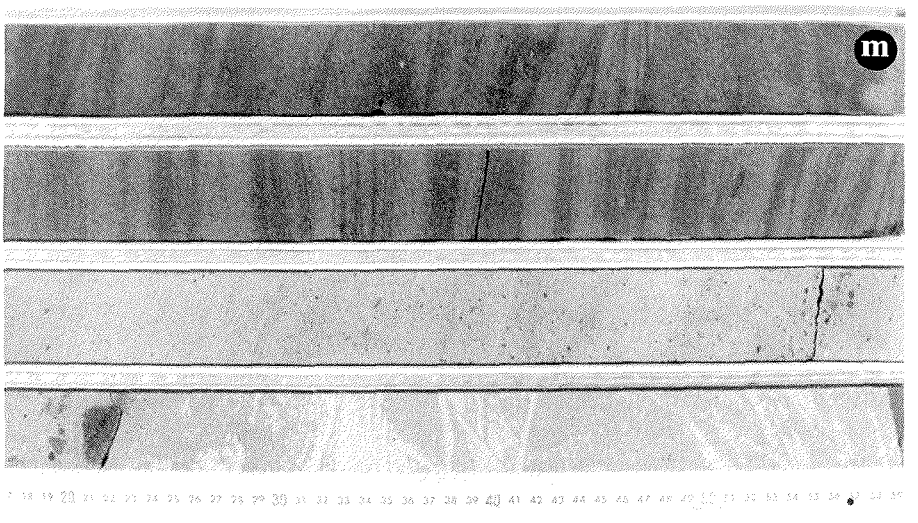

Fig. 3.2 - m) Moderately to well sorted, fine- to medium-grained sandstones of Facies 5 at 557.18-556.59 mbsf end showing strong to weak horizontal lamination and cross-bedding. Some laminae in the top two core sections have vague upward curvature and low angle-discordances that may be indicative of hummocky cross-stratification.

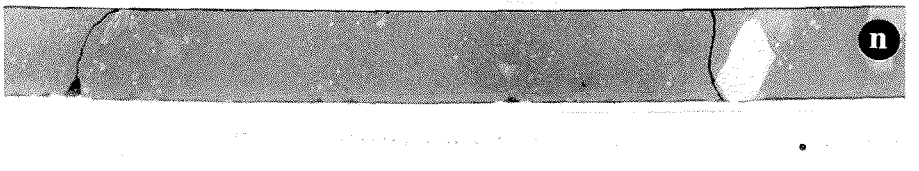

Fig. 3.2 -n) This is an example of the sandstone of Facies 5 where it is more massive at 433.51-434.94 mbsf, and where stratification is shown by gravel concentrations with very diffuse contacts.

FACIES 5 - MODERATELY SORTED STRATIFIED OR MASSIVE FINE- TO COARSE-GRAINED SANDSTONE

Facies 5 represents moderately sorted medium-grained sandstone (Fig. 3.2 l, m, n, o & p) that is locally fine- or coarse-grained. Beds are commonly planar- or cross-stratified, but they may contain apparent HCS or can appear massive. They have abundant to dispersed very coarse sand and clasts, some of them angular. Locally, fragmental coal laminae and beds are common. Some massive beds appear amalgamated where they are defined by clast layers that are concentrated at one horizon, but then become progressively dispersed upward while the matrix remains the same sand size over the apparent contact. They could also be caused through variations in one flow. Facies 5 sandstone is also locally weakly to moderately bioturbated and contains marine macrofossils. These sandstones contain isolated intervals of soft-sediment deformation and local lonestones that show evidence of either being dropped, or are outsized.

Marine currents are the most likely depositional mechanism for this facies, perhaps on a shoreface to about storm-wave base, with local hiatuses marked by gravelly layers. Coarse-tail graded units may also originate from sediment gravity flows or may represent waning flow stages of traction currents. The facies may appear massive because of uniformity of grain size. The environment was under the influence of icebergs due to the presence of lonestones; some of the massive beds perhaps may be from iceberg turbation.

Facies 5* is designated to represent the sandstones of LSU 16.1 and 18.1, which are part of the bedrock sandstone of the Beacon Supergroup. This subfacies is composed of dominantly medium-grained, well sorted sandstone, with minor fine- and coarse-grained sandstone (Fig. 3.2q). This facies lacks both gravel and mud. This designation has been assigned on the basis that it closely resembles Facies 5 of the younger succession both in sedimentary textures and structures. However, there are some differences in detail, such as:

1. the laminated medium-grained sandstones have dominantly horizontal or parallel lamination in which individual laminae are very well sorted and some are cross-bedded at both small-scale (0.1-0.2 m sets) and larger (<0.5+ m). These are interpreted as having been deposited under unidirectional water flow;
2. very delicately laminated, medium- or fine-grained sandstones with laminae defined by grain-size variation. Each lamina is almost exclusively one grain-size fraction (mainly medium sand) and most laminae are horizontal/parallel, but some are inclined, and a few clearly form parts of cross-sets. Some intervals show low-angle bedding discordances or low-angle ripple cross-lamination. These intervals are thought to have been deposited by wind, representing probable wind-ripple lamination;
3. massive medium-grained sandstone occurs over short intervals (<0.15 m, typically), being internally unstratified with uniform grain-size distribution. Such intervals are interpreted as possible aeolian grainflow deposits, or as products of liquefaction;
4. some intervals of medium-grained sandstone, commonly less than 1 m thick, are described as being "destratified", locally showing colour-mottling and possible dish structures. This sand may have experienced soft-sediment deformation by liquefaction, or bioturbation (which is less likely) or tectonic deformation associated with fracturing and brecciation (which is thought to be even less likely).

Overall, Facies 5* is thought to represent a sub-humid to semi-arid continental setting with some fluvial activity (?ephemeral) and periods of sand reworking by the wind.

FACIES 6 - STRATIFIED DIAMICTITE

Stratified diamictite comprising Facies 6 is clast-rich to clast-poor and sandy or muddy. This facies most commonly exhibits no apparent clast orientation, although clast a-axes are locally aligned with stratification (Fig. 3.2 r & s). It occurs only in the upper 370 m of the core. The stratification style is most commonly laminated and thin bedded, which varies from weakly- to well-defined. Stratification is formed by mudstone, siltstone and very fine to very coarse sandstone strata which vary in their mud content. Strata are also produced by increasing mean sand size from fine-grained in the diamictite matrix to medium-grained in the laminae, or by varying proportions of mud. Clasts are angular to rounded and locally are mainly of dolerite. Facies 6 commonly grades into or out of massive diamictite, and thinner beds of the facies are locally interstratified with conglomerates, sandstones, massive diamictites and mudstones. Soft-sediment deformation is locally strong. Stratified diamictites are not bioturbated, but some include marine macrofossils.

The poorly sorted character and presence of outsized clasts in some areas allow alternative interpretations of this facies. The diamictic character may originate from debris flow deposition combined with ice-rafting that also introduces clasts. Some units, especially those that grade into and out of massive diamictites, may result from direct rain-out of ice-rafted debris that is acted on by currents to produce lamination of the matrix. Alternatively, subglacial tills can exhibit these types of structures.

FACIES 7 - MASSIVE DIAMICTITE

Massive diamictite of Facies 7 is less common than stratified diamictite, but it also occurs in the upper parts of the core. It varies from clast-rich to clast-poor and may be sandy or muddy (Fig. 3.2r). When the matrix is sandy, the diamictite locally grades into sandstone by decreasing clast proportions, whereas, when the matrix

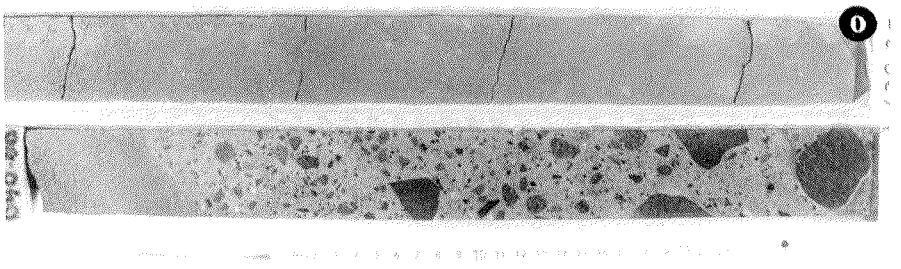

Fig. 3.2 - o) Massive to weakly stratified fine-grained sandstone of Facies 5 at 637.89-641.29 mbsf which is locally interstratified with matrix-supported conglomerate (Facies 9), which in this example here, is carbonate cemented.

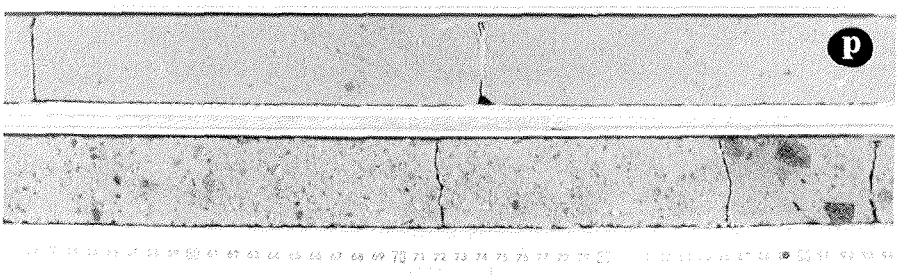

Fig. 3.2 - p) A variety of Facies 5 at 493.51-494.92 mbsf which is clean, well-sorted quartzose sandstone fining-upward from medium- to very coarse-grained sandstone to fine-grained sandstone over one metre or more. The coarser-grained interval has dispersed gravel, which is commonly angular.

Fig. 3.2 - q) This is an example of the special type of Facies 5 denoted as Facies 5* at 886.48-889.89 mbsf, which is interpreted as part of the bedrock sandstone of the Beacon Supergroup. This interval shows very well sorted, horizontal or parallel laminated, medium-grained sandstone (core section 4) deposited under unidirectional water flow; finely laminated, medium- to fine-grained sandstones with intervals showing low-angle bedding discordances or low-angle ripple cross-lamination (core section 3), perhaps deposited by wind; "destratified" sandstone (core section 2), locally showing colour-mottling due to either liquefaction or bioturbation; and brecciation (core section 1 and part of core section 2).

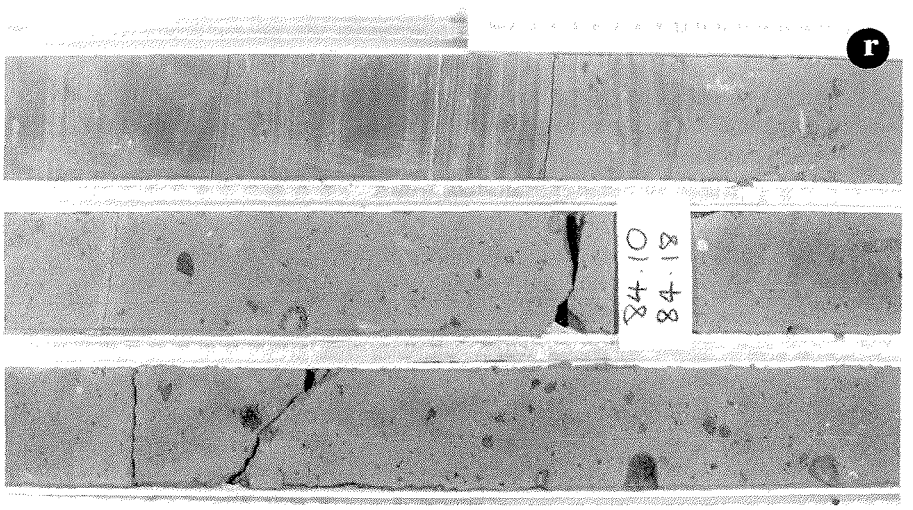

Fig. 3.2 - r) Stratified (Facies 6) and massive (Facies 7), sandy diamictite at 82.78-85.29 mbsf in which clasts range from angular to subrounded and they show no preferred orientation. In core section 1, the diamictite passes gradationally upward into stratified sandstone and mudstone of Facies 2 and 8. A bivalve fragment occurs in the diamictite at 83.96 mbsf.

is muddy, the diamictite locally grades through pebbly mudstone into mudstone by decreasing clast proportions. Locally, the mud content of sandy diamictite increases with the decrease in clast proportions. At the other extreme, clasts rarely increase in proportion, and the diamictite locally grades into conglomerate that is commonly matrix-supported. Where the diamictite facies does not grade from underlying units, the lower contact is sharp and commonly loaded or soft-sediment deformed. Most commonly, clasts have no apparent orientation, but rarely a-axes have an apparent preferred sub-horizontal orientation. Clast shape ranges from angular to rounded. Thinner beds of this facies commonly are interstratified with mudstones, sandstones and stratified diamictites. Marine macrofossils and one leaf are included in sediments of this facies.

Of all of the facies, this one is the most likely to be of subglacial origin, but at least at this initial stage of interpretation, none are interpreted to be of that origin. Beds that show gradations into other types of facies are more attributable to rain-out processes from floating ice or amalgamated debris-flow deposits. Some of the intervals do contain marine macrofossils, and this facies is commonly bounded by sequences that also contain evidence of submarine deposition.

FACIES 8 - RHYTHMICALLY INTERSTRATIFIED SANDSTONE AND SILTSTONE

Very fine and fine sandstone occurs rhythmically interstratified with mudstone, where the sandstones are most commonly massive and have sharp upper and lower contacts. As Facies 8, these sediments may grade into mudstone which may include discrete siltstone laminae that range from one-grain thick up to 1 mm thick with sharp contacts (Fig. 3.2 e & r). Lonestones are present and locally deform laminae beneath, but outsized clasts may also occur locally as one-grain-thick granule laminae. Commonly, Facies 8 is either included within intervals of Facies 2 or occurs above or below them; diamictites are also locally thinly interbedded with Facies 2. Soft-sediment deformation occurs within many intervals.

This facies is intimately associated with marine sequences. Its rhythmicity in sandstone-mudstone and mudstone-siltstone couplets is indicative of very highly turbid overflow plumes originating from fluvial discharges into the sea that produce cyclopsam and cyclopel deposits. They have a close association with diamictites, commonly in intervals overlying them.

FACIES 9 - CLAST-SUPPORTED CONGLOMERATE

The clast-supported conglomerate of Facies 9 is massive and poorly sorted, with a matrix of poorly sorted, very fine- to coarse-grained sand (Fig. 3.2 t, u, v & w). Generally, there appears to be no preferred clast orientation, and some units include angular clasts among the more common subangular to subrounded types. Units of this facies most commonly have sharp lower contacts but locally grade up from sandstones through matrix-supported conglomerate into the clast-supported conglomerate. However, this facies commonly grades upward into matrix supported conglomerate by decreasing clast proportions. Internally, Facies 9 may grade normally from cobble to small-pebble conglomerate.

The coarse nature and presence of subangular to subrounded clasts indicate that these deposits were deposited by or were redeposited from fluvial discharges. This facies may be submarine by association with marine sequences. The sediment may have been transported in suspension in turbulent subglacial conduit discharges. Alternatively, it could represent high density, gravity-driven, mass flows or redeposited conglomerates, especially where it grades into matrix-supported types. Iceberg rafting could contribute the angular clasts.

FACIES 10 - MATRIX-SUPPORTED CONGLOMERATE

Facies 10 is matrix-supported conglomerate that is commonly massive and very poorly sorted (Fig. 3.2 c, t & u). Its characteristics are similar to those of Facies 9, but clasts are fewer and are dispersed within matrix sand. The conglomerates appear to have higher proportions of angular clasts than do clast-supported varieties. As described under Facies 9, this facies may grade to clast-supported conglomerates and arise transitionally from sandstone by an increase in clast proportions. They most commonly show coarse-tail, fining-upward grading but also, the reverse occurs with the coarse-tail coarsening upward.

The dispersed nature of clasts in a sandy matrix and trends in grading indicate this facies was deposited from high-density mass flows. It may have been redeposited from a mixing of fluvial or shallow-marine facies close to source. Alternatively, it may represent the waning flow stage of traction currents or locally, higher in the core, they may have been deposited from suspension after transport in turbulent subglacial conduit discharges.

SEQUENCE STRATIGRAPHY

Preliminary results of a sequence stratigraphical analysis of CRP-3 drill core, identify 23 depositional sequences. While the term "sequence" has a specific usage and is applied to genetically-related unconformity bounded packages of strata that are inferred to have accumulated during a cycle of relative sea-level change (Vail, 1987), we apply the term here to repetitive assemblages of facies that are bounded by sharp erosion surfaces. In previous studies of CRP drill core, we have adapted the use of sequences within glacimarine settings to include those sediments that accumulate during cycles of glacier advance and retreat that may also occur in

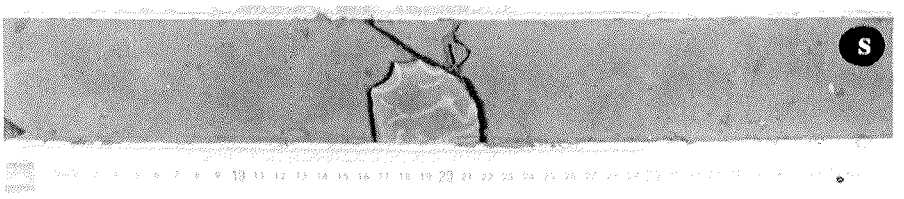

Fig. 3.2 - s) Crudely stratified sandy diamictite of Facies 6 at 87.98-88.43 mbsf, which includes an older sedimentary clast containing bryozoans.

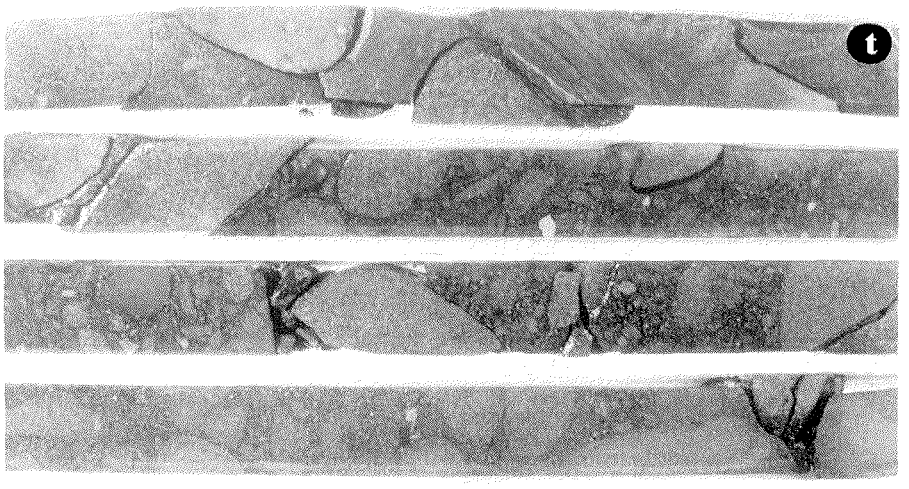

Fig. 3.2 - t) Well rounded clasts occur in matrix- to clast-supported dolerite conglomerate (Facies 9 and 10) at 813.98-817.40 mbsf. Clasts range up to boulder size, they have no apparent preferred orientation, and they include some quartz pebbles and one angular sandstone cobble (core section 1), which indicate admixtures from different sources.

Fig. 3.2 - u) Clast- and matrix-supported conglomerates of Facies 9 and 10 at 147.05-147.47 mbsf. Clasts are up to cobble size, they are angular to rounded, and they show no preferred orientation. The matrix is muddy, poorly-sorted, medium-grained sandstone. Stratification is locally developed by particle size changes; a vein is filled with white carbonate that includes clasts and matrix from the conglomerate.

Fig. 3.2 - v) Crudely stratified, matrix-supported conglomerate of Facies 9 at 150.55-150.98 mbsf with clasts ranging from angular to rounded and showing no preferred orientation. The conglomerate is interbedded with thin, fine- to medium-grained sandstone showing soft- sediment deformation.

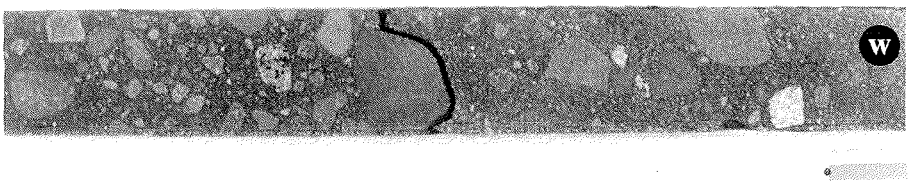

Fig. 3.2 - w) Massive, matrix-supported, medium- to small-pebble conglomerate of Facies 9 at 228.61-229.04 mbsf with randomly oriented clasts that are angular to rounded. The matrix is poorly-sorted medium-grained sandstone.

concert with relative sea-level changes. Twenty-three sequences of probable early Oligocene age were identified in CRP-3 above 480.27 mbsf (Fig. 3.3).

We have not identified sequences in the stratigraphical interval between 480.27 and 823.11 mbsf. We observe that the lower part of the cored interval undoubtedly contains repetitive packages of conglomerate and sandstone. However, due to the complex nature of the repetitions, we did not consider it possible to established a sequence framework at the time of writing the *Initial Report*. We anticipate that integration of the sedimentological and physical properties data will eventually enable a sequence framework to be established for the lower part of CRP-3 for publication in the *Science Report*.

Our sequence analysis follows the approach applied by Fielding et al. (1998; in press). The lithostratigraphical description and facies analysis of the core sediments presented in this volume is used here as the basis for the interpretation of depositional cyclicity. Thus, the described lithofacies are used to construct the sequence architecture and enable environmental changes within a sequence to be evaluated.

STRATIGRAPHICAL ARCHITECTURE OF DEPOSITIONAL SEQUENCES

Sequence Bounding Surfaces

Surfaces bounding CRP-3 sequences are sharp, unweathered, sub-planar surfaces that cut across mudstone or sandstone facies of the underlying sequences, and mark abrupt facies dislocations between these underlying strata and superjacent diamictites and conglomerates (Fig. 3.4a). The surfaces locally exhibit minor cm-scale erosional relief, load casting and sedimentary injection. Where major facies dislocations occur across sequence boundaries, significant erosion and time missing is inferred for the underlying sequences.

Vertical Organisation of Intrasequence Facies

The recognition of vertically-stacked, cyclical facies successions bounded by sharp erosion surfaces that mark prominent lithological dislocations, allows the upper 480.27 mbsf of the cored interval to be subdivided readily into sequences. Two styles of sequence architecture are recognised on the basis of these facies stacking patterns.

Sequences 1-14 typically comprise a four-fold lithological architecture termed *Sequence Motif A*, which includes the following *Facies Assemblages* in ascending stratigraphical order (Figs. 3.5 & 3.6):

(A1) A sharp-based, poorly-sorted coarse-grained basal unit (2-20 m thick) typically overlies the sequence boundary, comprising either massive diamictite (Facies 7), pebbly-sandstone (Facies 3) and/or matrix-supported conglomerate (Facies 10). The matrix-supported conglomerates are dominated by subangular to subrounded, poorly-sorted pebbles and cobbles, and in many cases comprise crude coarse-tail, fining-upwards beds of up to 3 m thick. Massive diamictites are clast-poor and vary from sandy- to muddy diamictite units up to 6 m in thickness. Both diamictite and conglomerate beds may grade in and out of poorly-sorted pebbly sandstones and muddy sandstones containing dispersed clasts (Facies 3). Typically these facies show soft-sediment deformation and contain a sparse macro- and microfauna.

(A2) The boundary between Facies Assemblage A1 and A2 is typically gradational, but in some cases may be abruptly gradational. This unit comprises broadly fining-upwards interval (up to 25 m thick) of poorly-sorted muddy sandstone (Facies 3), interstratified sandstone and mudstone (Facies 2), rhythmically-interstratified sandstone and mudstone (Facies 8) and fine sandy mudstone and mudstone (Facies 1, 2). Poorly sorted sandstones may display normal grading, coarse-tail fining-upwards grading and become better sorted at their tops. Interstratified sandstone and mudstones may be massive but in many cases display local normal and reversed grading, planar stratification or ripple lamination. The rhythmically-interstratified sandstones and mudstones are often associated with lonestones, dropstones and outsized clasts. Typically this overall fining-upwards unit also displays an up-section increase in fossil material and bioturbation passing up to massive and locally laminated sandy mudstone and mudstone (Fig. 3.4b). Outsized material decreases in abundance upwards.

(A3) The transition from Facies Assemblage A2 to Facies Assemblage A3 is abruptly gradational. This interval comprises a mudstone (up to 20 m thick) (Facies 1) that passes gradationally upwards into a regressive muddy sandstone, poorly sorted sandstone (Facies 3) and into a well-sorted sandstone (Facies 4) (up to 20 m thick).

(A4) In some cases an upper interval of interstratified, well-sorted, massive, to cross-stratified sandstone occurs (Facies 4, 5) (2-10 m thick). This facies assemblage comprises numerous tractional sedimentary structures such as low-angle planar cross-stratification, ripple lamination, high-angle planar cross-stratification, parallel-planar lamination and possible swaly and hummocky cross-stratification (Fig. 3.4c). The transition between Facies Assemblage A4 and underlying Facies Assemblage A3 may be abruptly gradational, or exhibit minor erosional relief.

Sequences 15-23 typically comprise a two-fold lithological architecture, termed *Sequence Motif B*, which includes the following *Facies Assemblages* in ascending stratigraphical order (Fig. 3.5 & 3.6):

(B1) A sharp-based, poorly-sorted, coarse-grained unit (2-20 m thick) comprising clast, or matrix-supported pebble/cobble conglomerate (Facies 9,

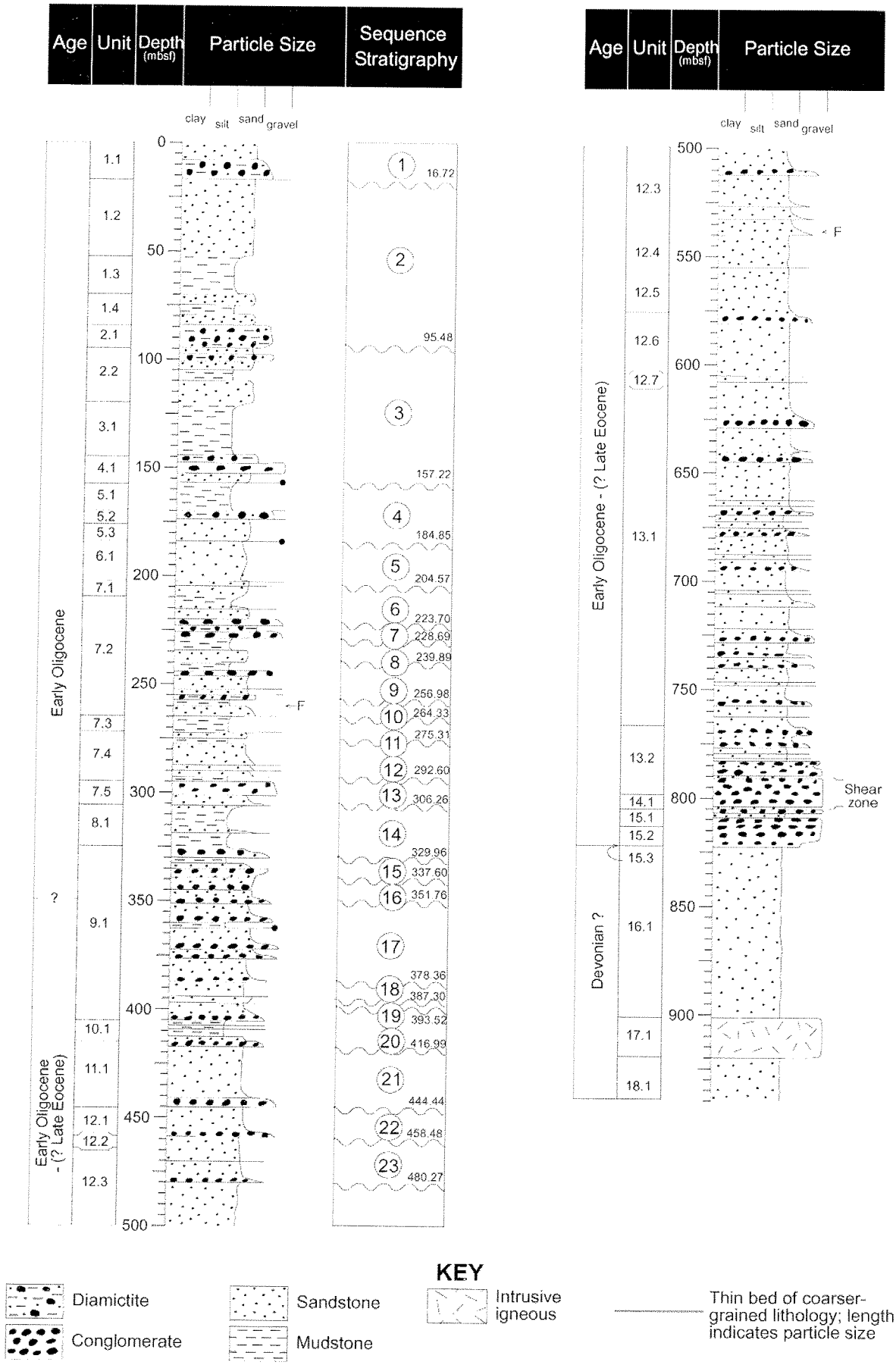

Fig. 3.3 - Sequence stratigraphical intepretation of CRP-3 above 480.27 mbsf.

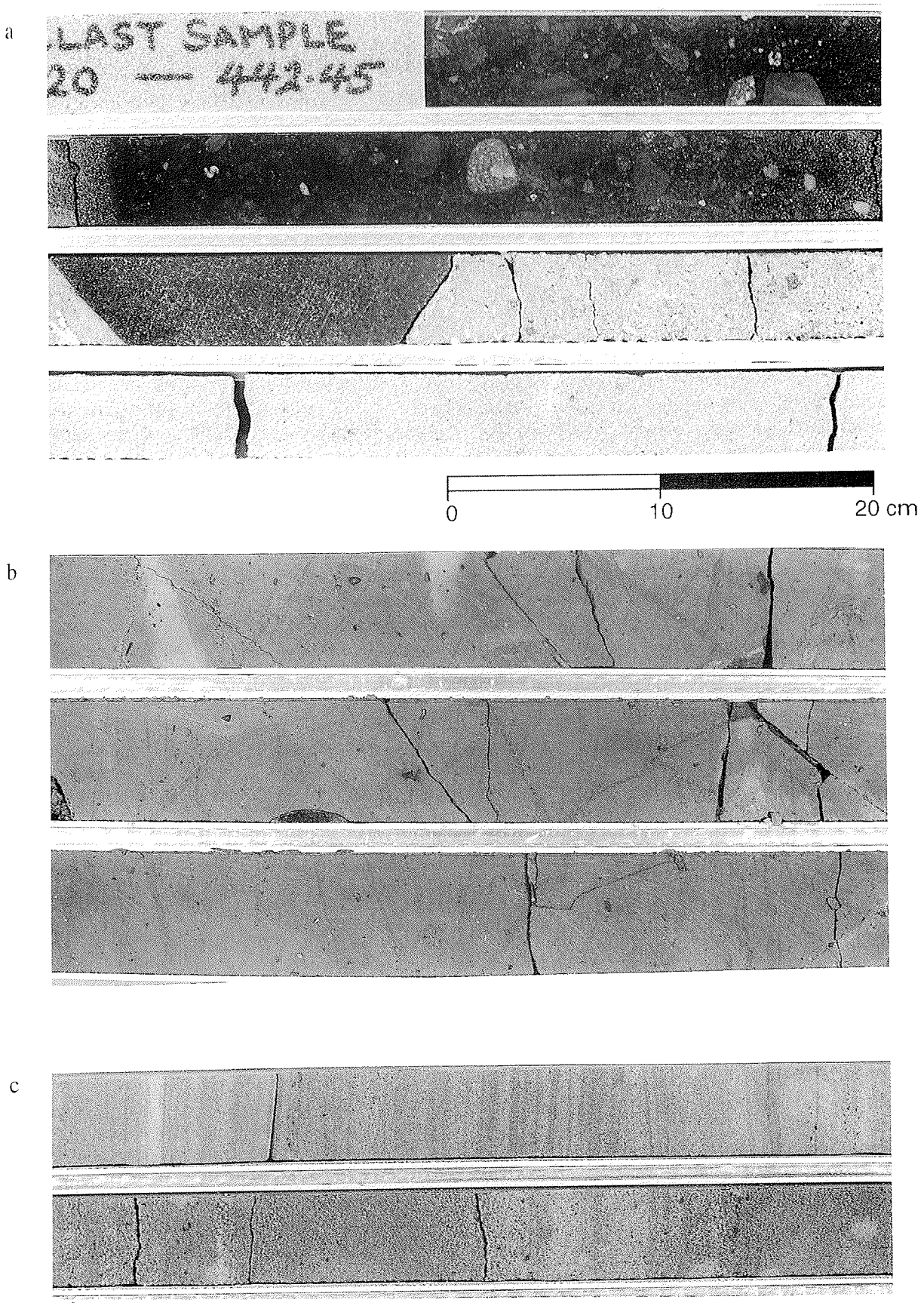

Fig. 3.4 - a) Photo of sequence boundary at 444.44 mbsf, base of Sequence 21. Erosion surface truncates well-sorted, stratified sandstone (Facies 5; white), and is overlain by a matrix-supported pebble/cobble conglomerate (Facies 10; black). Note large dolerite bounder above contact. *b)* Bioturbated, fractured, massive to weakly laminated mudstone with dispersed clasts (Facies 1) is assigned to the HST of Sequence 2. Note burrows in top right corner. *c)* Well-sorted, low-angle cross-stratified, planar cross-stratified and possibly hummocky cross-stratified sandstone (Facies 5) typical of the RST.

10), pebbly-sandstone and/or granular sandstone (Facies 3) that are often arranged into superposed stacks of graded beds. The conglomerates are dominated by subangular to subrounded, poorly-sorted pebbles and cobbles, and in many cases comprise crude coarse-tail, fining-upwards beds of up to 3 m thickness. Conglomerate beds may grade in and out of poorly-sorted pebbly sandstone and muddy sandstone containing dispersed clasts assigned to Facies 3.

(B2) A fining-upwards/gradational transition into an interval (up to 25 m thick) of well-sorted stratified (sometimes cross-stratified) sandstone (Facies 4 and 5). This facies assemblage comprises numerous tractional sedimentary structures such as low-angle, planar cross-stratification, ripple lamination, high-angle planar cross-stratification, parallel-planar lamination and possible swaly and hummocky cross-stratification.

Although Sequences 15-18 have been classified as *Motif B*, they are somewhat transitional between the two motifs and may contain poorly-sorted muddy sandstone/ sandy mudstone (Facies 3) and mudstone (Facies 1) in their upper parts. It is important to note that the two sequence motifs outlined above are idealised motifs that encapsulate the two main styles of sequence architecture observed in Sequences 1-23. While type examples for each motif are shown in figure 3.5 (Sequence 2 for *Motif A* and Sequence 21 *Motif B*), we acknowledge that minor variations in architecture occur within every sequence. These variations can be seen from the vertical facies successions for the individual sequences shown in the depositional history section (Fig. 7.4) and on the 100m/page logs in appendix 3.1.

SEQUENCE STRATIGRAPHICAL INTERPRETATION

The paleoenvironmental interpretation of the lithofacies, and hence the environmental changes recorded in the sequences, are based largely on multiple criteria such as grain size, depth palaeoecology of constituent faunal assemblages, ichnofabrics, sedimentary structures, and intra-sedimentary deformation features. However, given the paucity of depth-diagnostic fauna/flora and sedimentary structures in both CRP-1, CRP-2/2A, and CRP-3, it has been necessary to assume that grain-size changes reflect changes in depositional energy, and therefore, broadly correspond to changes in palaeobathymetry and glacial proximity. Such a contention appears to be valid for proximal and distal glacial facies that have been identified on multiple criteria other than grain size (Powell et al., 1998; in press), yet show a strong correspondence with variations in sediment calibre. Definitive faunal and sedimentological evidence for water-depth changes over much of CRP-3 are absent. However, many parts CRP-2/2A contained features supporting a nearshore interpretation for coarse-grained sediments and a more distal offshore marine setting for fine-grained sediments. We use the same grain size/depth relationship here, because the top 350 m of CRP-3 exhibits a very similar sequence architecture to that of CRP-2/2A. It should be noted that the following sequence stratigraphical interpretation, while supported by many of the Cape Roberts Science Team, does not reflect the views of all sedimentologists on the project.

Sequence Boundary Formation

The authors of the CRP-2/2A sequence stratigraphy reports suggested that sequence boundaries coincided with *glacial surfaces of erosion* (GSE) that record periods of local glacier advance across the sea floor during glacio-eustatic sea-level fall (*e.g.* Fielding et al. 1998; in press). It is suggested here for CRP-3 that sequence boundaries may represent the distal equivalents of GSEs, in cases where the grounding line was proximal but landward of the drillsite (*Motif A*). Alternatively, they may have formed under paraglacial conditions and represent the distal effects of glacial advance and/or a relative fall in base level in a shallow-marine deltaic setting (*Motif B*). In contrast to the traditional Exxon definition of the sequence boundary, which was developed from studies of non-glaciated continental margins (*e.g.* Vail, 1987), GSEs and their more distal correlative conformities do not necessarily mark a basinward migration and downward shift of the shoreline during falling relative sea level. Rather, they may be the product of erosion caused by either debris flows spilling off the front of proglacial grounding line fans and deltas and/or the direct grounding of advancing glacier ice onto the sea-floor. The latter process has probably not occurred in CRP-3 as there is no evidence so far to support ice contact and sub-glacial processes. It is important to note that GSE formation can also occur independently of glacio-eustatic sea-level oscillations and produce an unconformity of only local areal extent.

Notwithstanding these added complications inherent at glacimarine basin margins, we view the *Motif A* sequence boundaries recorded in the cored interval above 306.26 mbsf (Fig. 3.3) as primarily reflecting glacier advance in concert with a eustatic drawdown of base-level. Such a contention is supported by the recognition of sedimentological evidence for palaeobathymetric deepening and shallowing cycles within sequences. That grounded ice periodically approached the site of CRP-3 is consistent with the location of the drillsite near the palaeo-Mackay Valley, close to the western margin of the West Antarctic Rift System.

The basal portions of *Motif B* Sequences 14-23 represent positions significantly basinward of the glacial-maximum grounding line, which may have been subaerial. These sequences display sharp lower boundaries, with superjacent shallow-water conglomerate facies that are interbedded with, or form graded bases to, overlying sandstones. The absence of

diamictite and the occurrence of sharp-based graded conglomerate/sandstone beds in association with well sorted stratified sandstones leads us to interpret these sequence boundaries as current-scoured in a shallow submarine environment, perhaps delta front. The graded conglomerates themselves are the products of waning flow and may have been deposited as debris flows or by tractional currents during phases of increased glacial meltwater discharge and sediment supply to the coastline. Thus, we view the graded coarse-grained deposits overlying the sequence boundary as transgressive and probably deposited during climatic amelioration and relative base-level rise. In this case the sequence boundaries mark transgressive surfaces (*e.g.* ravinement surfaces) superimposed on the subaerial unconformity, or its submarine conformity.

Lowstand and Transgressive Systems Tracts (Facies Assemblage A1, A2 & B1)

The coarse-grained basal units of the sequences comprise massive diamictite, clast- and matrix-supported conglomerate and/or interstratified poorly-sorted sandstone (Facies Assemblages A1 and B1). Conformably overlying this facies assemblage, in Sequences 1-13 (*Motif A*), is a lower interval (up to 30 m) of massive to weakly laminated/bedded, poorly-sorted sandstone and muddy-sandstone, and occasionally with rhythmically-stratified mudstone and sandstone that typically passes upwards into a weakly bioturbated, sparsely fossiliferous muddy sandstone to mudstone facies (Facies Assemblage A2).

The diamictic facies are consistent with a combination of glacimarine processes, including melt-out and rainout during ice withdrawal, and proglacial debris-flow deposition with ice rafting. Conglomerate facies are also consistent with ice proximal and/or ice distal glacimarine sedimentation and paraglacial marine delta front deposition (*Motif B*). Conglomerate facies probably represent short-flow fluvial deposition, deposition associated coastal delta outflow, and redeposited fluvial conglomerates on a delta front. Distinguishing proglacial sediments deposited during ice advance from proglacial sediments deposited during retreat is inherently difficult, as the sedimentological characteristics of these deposits are identical in modern glacial environments. Therefore, the coarse-grained basal facies (Fig. 3.4a) are considered to have a polyphase origin representing ice-proximal (*Motif A*) and ice-distal proglacial deposition (*Motif B*) during advance and withdrawal of glacier ice from a shallow marine setting. In the case of *Motif B* sequences, CRP-3 was in an ice-distal setting and fluctuations in ice front were probably subaerial. The generally fining-upwards texture of basal coarse-grained units suggests that they are more likely to be the product of a retreating ice margin rather than an advancing one.

Consequently, we assign basal diamictite and conglomerate facies (Facies Assemblages A1, and B1) to both the *lowstand systems tract* (LST) and the *transgressive systems tract* (TST) (Figs. 3.5 & 3.6). It is generally not possible to identify the LST/TST boundary. However, given the paucity of facies that could be readily interpreted as subglacial origin, it is suggested that the basal diamictites comprise a predominantly transgressive record of glacial retreat. Typically, diamictite clast fabrics are weakly oriented or random, suggesting a large component of rainout debris which, in many cases, may have been remobilized in subsequent gravity flows as evidenced by syndepositional soft-sediment deformation structures, intraclasts, and clastic intrusion features. Rhythmically stratified facies that occur immediately above coarse-grained Facies Assemblage A1 within the base of Facies Assemblage A2 are considered ice proximal, yet more distal than Facies Assemblage A1. They are the product of suspension from turbid sediment-charged plumes that are associated with subglacial streams discharging near grounding line fans (Powell et al., 1998). Upper portions of TSTs (Facies Assemblage A2) display clear fining-upwards trends and are sometimes capped by a sparsely fossiliferous and bioturbated sandy mudstone (Fig. 3.6B; *e.g.* Sequences 2 and 3) corresponding to a zone of maximum water depth, the glacial minimum, and lowest sedimentation rate in a cycle.

Highstand Systems Tracts (Facies Assemblage A3, B2)

Facies Assemblage A3 comprises weakly bioturbated and sparsely fossilifereous sandy mudstone and mudstone that passes up-section into poorly-sorted sandy facies. We suggest that this regressive mudstone to sandstone interval results from sediment infilling during the highstand and/or early fall of sea-level. Accordingly, this facies succession is assigned to the *highstand systems tract* (HST). For Sequences 15-23 (*Motif B*), which lack mud, such shoaling trends are more difficult to identify, but may be evidenced by an increase of well-sorted, sometimes cross-stratified, and possibly hummocky cross-stratified quartz sandstones (Facies Assemblage B2).

Highstand systems tract deposits are interpreted as forming during the late rise, stillstand and early fall of a relative sea-level cycle (*e.g.* Vail, 1987; Posamentier et al., 1988). In offshore locations the *downlap surface* (DLS) marks the base of a HST, which is broadly coincident with the level of maximum palaeo-water depth termed the *maximum flooding surface* (MFS). At seismic scale the MFS represents a change from retrogradational to progradational cross-sectional stratal geometries (*e.g.* van Wagoner et al., 1988, 1990). In CRP-3 drill-core sequences, it is not possible to evaluate downlap. Nevertheless, the TST/HST boundary is placed at an abruptly gradational transition between fining-upwards sandstone facies and mudstone facies (*Motif A*) or well-sorted sandstones (*Motif B*) in most sequences.

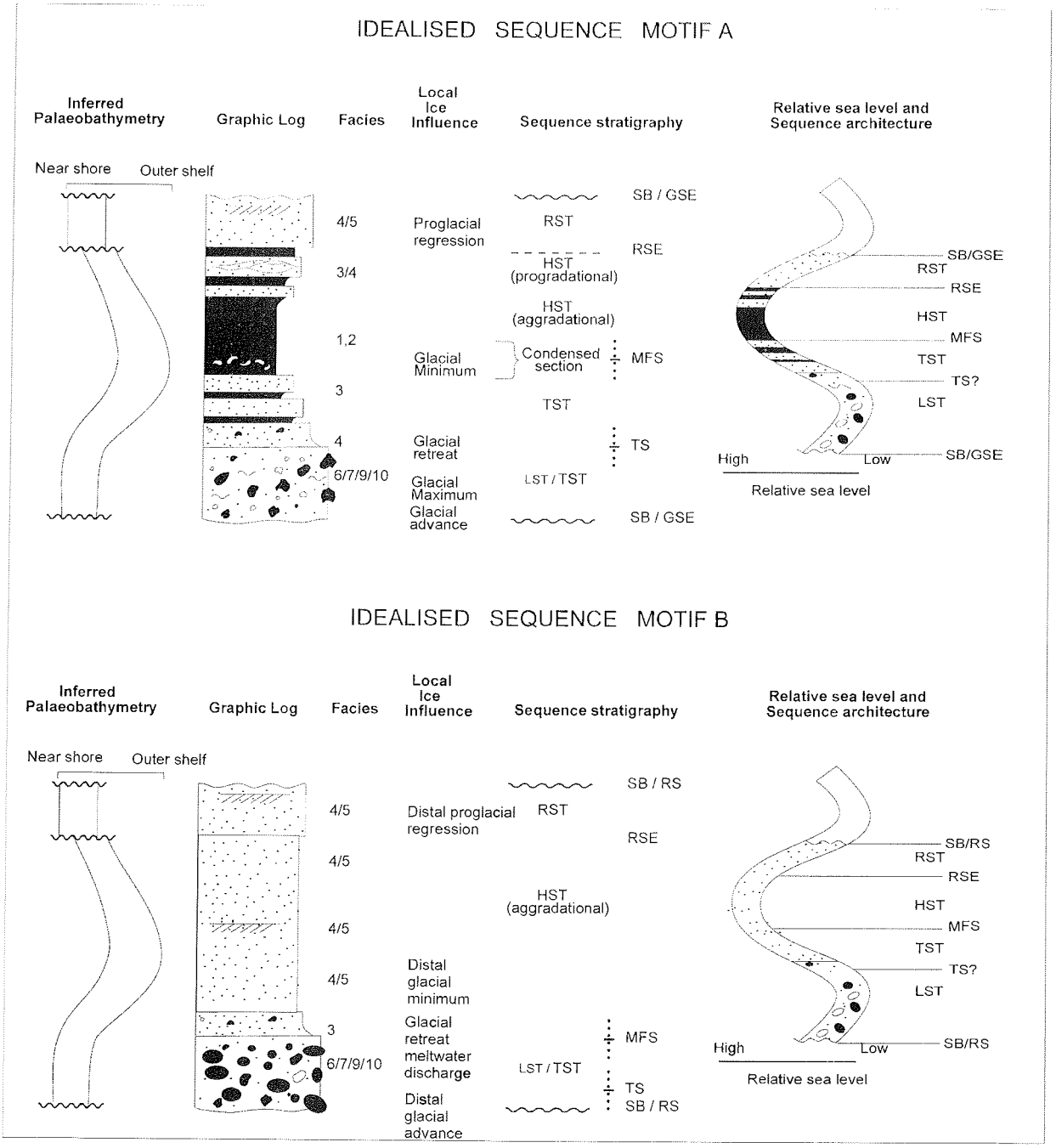

Fig. 3.5 - Idealised sequence motifs observed in CRP-3 and interpreted controls on depositional architecture.

Regressive Systems Tracts (Facies Assemblage A4, B2)

Motif A Sequences 2, 3, 5, 8 and 14, and *Motif B* Sequences 15-23 include in their upper parts a shallow-marine facies succession of probable innermost shelf to shoreface origin, which is often sharp-based. These facies include moderately- to well-sorted, stratified fine sandstone, and moderately sorted, stratified or massive medium to coarse sandstone. They display a variety of tractional sedimentary structures (Fig. 3.4c), including planar bedding and lamination, ripple cross-lamination, high-angle cross-stratification, low-angle cross-stratification, and probable hummocky cross-stratification collectively indicative of shallow-marine environments above wave base. The occurrence of sharp-based, shallow-marine sands at the top of sequences, the strongly progradational character of the succession, and the subsequent truncation by overlying sequence boundaries, are all consistent with sediments deposited during a period of falling relative sea-level, or forced regression (Fig. 3.5). We tentatively interpret these regressive sandstones as forming in a proglacial deltaic and/or shallow-marine deltaic environments during ice advance and/or a drawdown of base-level.

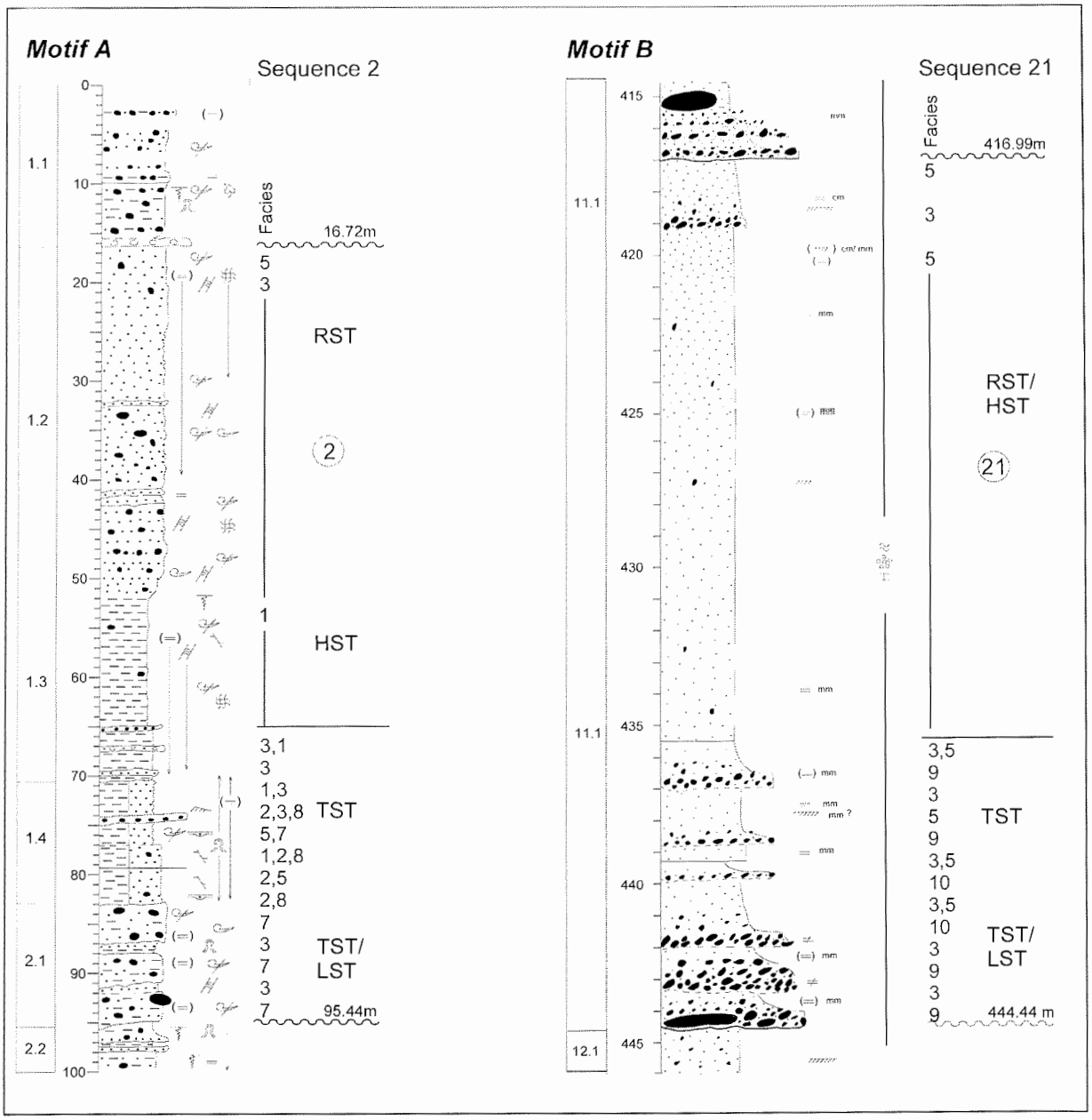

Fig. 3.6 - Type examples of Sequence Motif A and Sequence Motif B.

Strata deposited during gradual or stepwise forced regression accumulate as a basinward-descending and offlapping series of wedges, bounded below by an abruptly gradational (*e.g.* Naish & Kamp, 1997; Naish et al., in press a) or erosional downlap surface (*e.g.* Plint, 1988) and above by a subaerial unconformity (often removed by marine ravinement), which corresponds to the sequence boundary. Naish & Kamp (1997) have referred to this distinctive stratal package as the *regressive systems tract* (RST), and view it as the logical counterpart to the transgressive systems tract. In many cases, it is not possible to locate the lower boundary of the RST precisely, where the contact with the underlying highstand systems tract is gradational, but typically it corresponds to an abruptly gradational transition from mudstone to sandstone. The upper bounding surface of the RST, the subaerial unconformity which is often marked by fluvial channel incision or delta abandonment, passes into a correlative submarine unconformity landward of the lowstand shoreline, where it marks the base of the lowstand systems tract (LST). In CRP-1 and CRP-2/2A the upper bounding unconformity of the RST is marked by the GSE. However, in CRP-3 this boundary may be the product of current erosion and may appear conformable in many cases.

DISCUSSION AND IMPLICATIONS FOR ANTARCTIC GLACIAL HISTORY

Twenty-three cycles of local advance and retreat, and/or meltwater discharge of the Mackay Glacier in concert with relative sea-level fluctuations during the early Oligocene can be identified on basis of the preliminary facies and sequence stratigraphical analysis of the CRP-3 drill core. Although punctuated by significant unconformities, the cored interval may be relatively more complete than CRP-1 and CRP-2/2A owing to the lack of evidence of ice grounding. Nevertheless some sequences may be the amalgamated product of several severely truncated sequences. Broad constraints on the amplitudes of palaeobathymetric fluctuations reveal cyclical changes in water depth from shoreface to shelf water depths, perhaps of 50 m magnitude.

Preliminary magnetostratigraphical results (this volume) imply a thick interval of reversed polarity in the upper part of the core that may span up to 20 sequences, implying that individual depositional sequences in certain parts of the core may correspond to Milankovitch orbital frequencies (eccentricity). Such an interpretation is consistent with the Milankovitch frequency of sequence cyclicity established for Sequences 9, 10 and 11 in CRP-2/2A (Naish et al., in press b), and has several important implications, notably (A) that the cored interval contains an incomplete record for the early Oligocene of western Ross Sea with large periods of time represented at sequence-bounding unconformities, and (B) where sequences are preserved, they may represent an important ice-proximal record of orbital control on the early dynamics of the Antarctic ice sheet, which has significant implications for understanding the origin of inferred Oligocene global eustatic sea-level change (*cf.* Zachos et al., 1996).

The upcore transition from shallow-marine deltaic *Motif B* sequences to ice-proximal glacimarine *Motif A* sequences implies a progressive increase in ice influence in the region of the drillsite and may record a progressive climatic deterioration during the early development of the East Antarctic ice sheet. Further chronostratigraphical analyses must be undertaken for the CRP-3 *Science Results* volume in order to evaluate the stratigraphical architecture for sediments below 480.27 mbsf and the depositional frequencies inherent in this important ice-proximal Antarctic record.

HIGH-FREQUENCY ANALYSIS OF PHYSICAL PROPERTIES PERIODICITIES IN FINE-GRAINED SEDIMENTS

INTRODUCTION

The following is a pilot study to search for periodicities in fine-grained sediments of CRP-3, which might have been controlled by deterministic (*i.e.* non random) forcing processes. Cyclicities recorded at various scales in sedimentary successions are instrumental in understanding periodic changes in the depositional environments, as a possible response to external forcing. Periodic orbital perturbations of the Earth, ranging from 10 k.y. to 100 k.y. (Milankovitch cycles: eccentricity, obliquity and precession, Berger & Loutre, 1994) have a direct and important effect on the climatic changes at a global scale; the resulting variations in climatic conditions are very likely a possible cause of changes in sedimentary environments and sedimentation patterns (Fischer, 1986; Fischer et al., 1990; Fischer & Bottjer, 1991; de Boer & Smith, 1994; House, 1995). This suggested link between perturbing astronomical factors and cyclicity in the sedimentary successions can therefore be used to refine and ultimately to calibrate existing timescales. In cases where biostratigraphical and magnetostratigraphical frameworks do not provide chronological constrains or are poorly defined, the recognition of non-random orbital-climatic periodicities in the sedimentary record may be used to give estimates of the duration of these stratigraphical intervals and ultimately to suggest a complementary orbital forcing timescale (House, 1995).

Physical properties of selected intervals of the CRP-1 and CRP-2/2A cored successions were previously analysed to see if their fluctuations could represent a sensitive record of high-frequency periodicities (Niessen et al., 1998; Cape Roberts Science Team, 1999; Claps et al., in press). The results were sufficiently promising to encourage us to test the CRP-3 core using a similar approach to search for cyclic patterns.

At the time of this writing, biostratigraphical and magnetostratigraphical analyses on CRP-3 are not yet complete, therefore the absence of an age-model will limit the final interpretation in terms of the time duration of the periodicity window investigated. Moreover, we emphasise that the results presented here represent a preliminary study to explore the feasibility of a systematic search for cyclicity through the entire cored succession, with the possible integration of other data sets when these become available.

METHODOLOGY

Data Acquisition

We applied spectral analysis techniques to short arrays of data extracted from the low-field magnetic susceptibility and porosity analysis of the core (see Chapter 2). Physical properties were measured continuously along the core at the drill site laboratory, with a constant sampling interval of 2 cm (Niessen et al., 1998). The magnetic susceptibility was measured using a Bartington MS-2 magnetic susceptibility metre connected to a loop sensor of 80 mm internal diameter. The acquired values were later corrected for loop-sensor and core diameter to obtain a normalized data series.

Wet bulk density was measured from attenuation of a gamma-ray beam transmitted from a radioactive source through the core-centre and the underlying carrier. The results were calibrated for the different core diameters to equalize the final values, which were then converted into porosity values.

Intervals Analysed

Two depth series were analysed in this study, which cover the intervals between 60.99 and 83.10 mbsf (part of LSU 1.3 and LSU 1.4) and between 120.20 and 144.45 mbsf (LSU 3.1). The first interval (between *c.* 60.99 and 83.10 mbsf) consists of sandy mudstone and very fine sandstone, with gradational contacts and variable proportions between the two lithologies. Locally sandy beds with parallel and ripple-cross laminations, from cm to dm-scale, are present. Clasts (mainly dolerite) are present, but they are commonly concentrated in beds. The second interval (between *c.* 120.20 and 144.45 mbsf) consists of sandy mudstone, vaguely stratified in places, with dispersed clasts (primarily of dolerite). Weak carbonate cementation zones occur in a few places. Bioturbation affects the succession only locally and at a small scale.

The character of the sedimentation appears to be quite uniform throughout the two intervals tested. Sedimentological evidence, such as absence of major re-deposited units or breaks in the succession, suggests that no important hiatuses are likely to be present in these intervals. For these reasons we assumed that sedimentation was continuous and that the sedimentation rate had remained relatively constant for an appreciable time span.

In the cases where the analysed intervals showed discontinuities due to fractures, unconsolidation or poor recovery of the core, the physical properties might have been yielded anomalous values. Similarly, igneous clasts or zones of carbonate cementation scattered through the core might have altered the original signal, introducing anomalously high peaks. In these cases the values were not taken into consideration and were substituted by interpolation. After "cleaning" and "filtering" the original logs, the data were resampled with the same 2-cm constant rate.

The logs of the low-field magnetic susceptibility and porosity exhibit a very strong cyclic signal, and provide an unique opportunity for testing the existence of high-frequency cycles in the sedimentary record. This is clearly shown in figure 3.7 by the existence of various orders of long and short wavelength cyclicity bundled together in a complex hierarchy.

Spectral Analysis

To perform high-frequency analysis on a stratigraphical data set, we apply a combination of two different spectral algorithms, each one performing a specific task with particular advantages (Pestiaux & Berger, 1984; Hinnov & Goldhammer, 1991; Reijmer et al., 1994). Using this approach, problems concerning the treatment of stratigraphical data can be tested, and a better control against possible mathematical artifacts and the presence of variable amplitude noise levels can be obtained. To prevent possible alteration of the signal amplitude in parts of the function, and to obtain the highest level of precision during processing, some conditions must be checked before running the appropriate algorithms. First, the effect of long-term trends, which can cause a shift of the real amplitude in parts of the series, should be compensated for and eventually subtracted (linear trend and mean correction, Diggle, 1990). Then, it must be verified that the statistical properties of the time series remain unaltered by shifts in the sampled interval origin (stationary condition).

We processed the data series using two spectral estimators (Paillard et al., 1996). Because each processing routine is sensitive to a specific character of the time series, this approach permits a better resolution of the major properties of the original signal. The Maximum Entropy algorithms (ME, Press et al., 1989) is a very powerful algorithm designed to fit the sharp spectral peaks in the signal, giving a high-frequency resolution within the range of autoregressive models selected in the analysis, together with a good control on the regularity of the *quasi*-periodic frequency. These advantages may sometimes be diminished by the lack of a statistical confidence estimate and some non-linearity in the evaluation of spectral lines, and can therefore produce undesirable spurious results. To test the statistical significance of the spectral values, we used the ME method in conjunction with the Blackman-Tukey routine (BT), a very stable procedure for processing time series (Blackman & Tukey, 1958). This algorithm estimates the autocorrelation function from the data series, weighted by a Tukey or Welch window (Harris, 1978) to discard possible bias, and computes the Fourier transform to obtain the power spectrum. Its design enables an estimation of some *a priori* random-noise models, like those originating by low-order autoregressions (Hinnov & Goldhammer, 1991), which are likely to be incorporated into the depth series when dealing with stratigraphical data. The spectral peaks are tested against two orders of autoregression and only the values passing the two noise levels are taken into consideration and labelled with the appropriate value. The combination of these techniques permits a better reconstruction of the most important spectral features and therefore ensures a high degree of significance when interpreting the results.

The spectra presented in this study display the power values, expressed in arbitrary units, on the y-axis while the x-axis refers to frequencies in cycles/metre, from low-frequency (long periodicities, on the left side) to high-frequency (short periodicities, on the right side). Peaks that are statistically significant (passing the 95% confidence level) and which exceed the noise levels

(given by the two first orders of autoregression, but not shown here) are converted in length of periodicity in cm, while the others remained statistically meaningless and are disregarded. If the analysis obtained by the ME and BT routines show similar values, then the number used for labelling the spectral peak is normally detected by the ME algorithm, since it provides a higher level of resolution.

INTERPRETATION OF THE SPECTRAL PEAKS

The data series investigated in detail for the lithological intervals are displayed in figure 3.7. The results of the frequency analysis for each lithostratigraphical interval are briefly described, with the highest power peaks expressed in cm.

Interval 60.99-83.10 mbsf

We processed the magnetic susceptibility data series using the ME algorithm (with length of the autocovariance series equals to 20%): the most prominent peaks correspond to periodicities of 580, 160 and 80 cm (Fig. 3.8). All these spectral lines are well above the noise levels tested by the BT routine (with length of the autocovariance series equals to 30%, Fig. 3.8), which confirms the obtained values, with a shift of the lowest frequency from 580 to 590 cm.

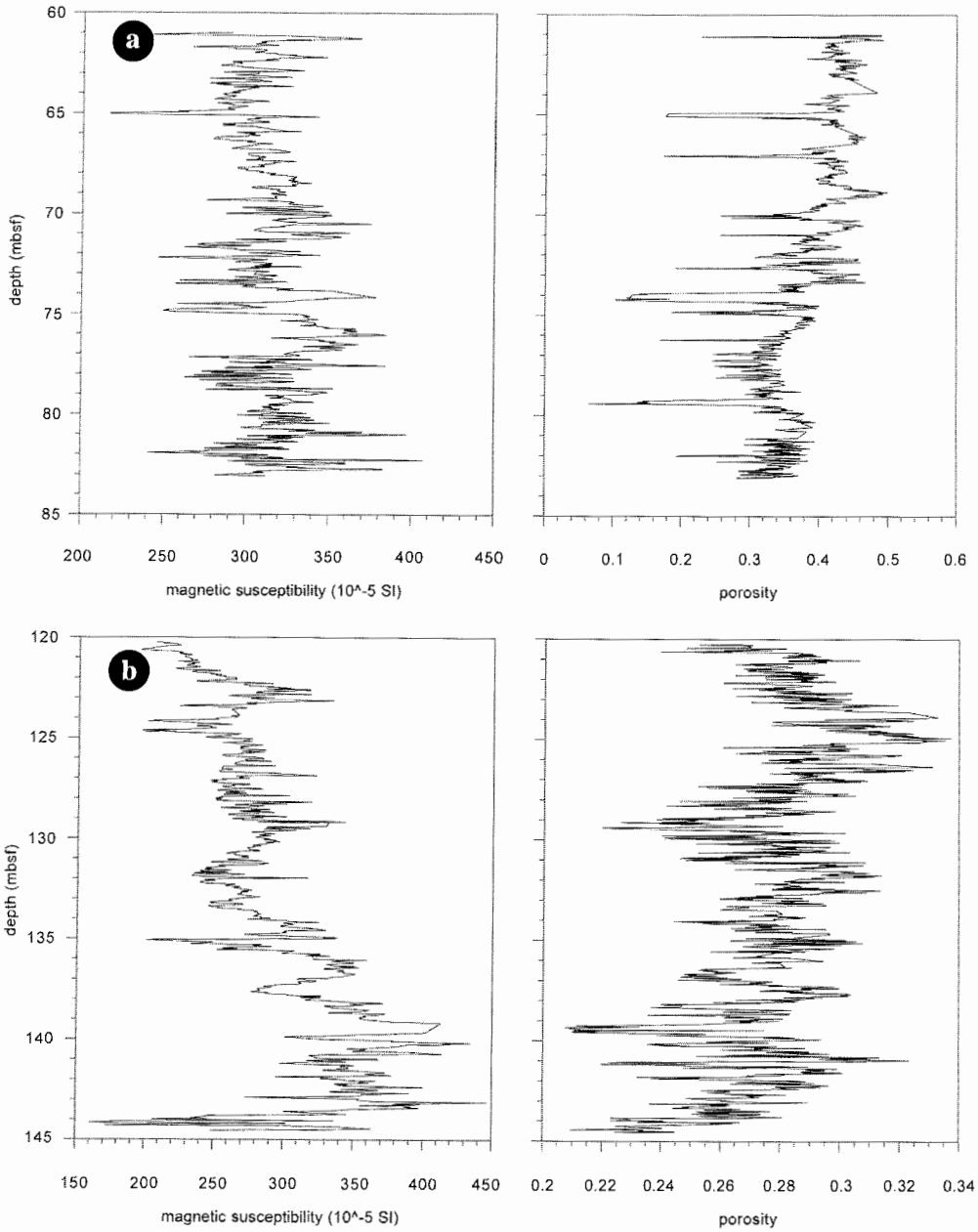

Fig. 3.7 - a) The low-field magnetic susceptibility and porosity data series of the interval between 60.99 and 83.10 mbsf (part of LSU 1.3 and LSU 1.4), plotted *versus* depth. *b)* The low-field magnetic susceptibility and porosity data series of the interval between 120.20 and 144.45 mbsf (LSU 3.1), plotted *versus* depth.

Two out of three of these peaks agree well with those computed for the porosity data series in the same intervals, with dominant spectral power concentrated at 252, 155 and 73 cm. We obtained these values by calculating the ME spectra (with length of the autocovariance series set to 15%, Fig. 3.9) and then checking the stability against noise levels by applying the BT algorithm (with length of the autocovariance series equals to 40%, Fig. 3.9), which shows a dispersion of energy around 155 cm (171-141 cm). The only difference between the two spectra resides in the abrupt shift of the dominant low-frequency line from 580 cm in the magnetic susceptibility series to 252 cm in the porosity one.

Interval 120.20-144.45 mbsf

The most likely spectral features of the magnetic susceptibility data series are displayed in figure 3.10, which shows the results of the ME processing. The spectral components were resolved by setting to 17% the length of the autocovariance series, and reveal peaks at 970 and 330 cm. Two low-power peaks are also present around 130-100 cm. The stability of these peaks is confirmed after testing the same series by BT analysis, with peaks at 1 000, 330 and two close peaks at 135-105 cm (with the length of the autocovariance series set to 30%, Fig. 3.10).

We processed the porosity data series for the same intervals, using both spectral estimators: two major peaks in the ME analysis (by setting the length of the autocovariance series to 15%) occur at 750 cm in the low-frequency side of the spectrum and at 135 cm in the high-frequency one (Fig. 3.11). In the BT analysis (with lenght of the autocovariance series equals to 30%) the same 750 and 130 cm spectral lines are present, while a broad side-lobe shifted towards the leftmost side of the spectra occurs at 99 cm (Fig. 3.11). The comparison between the two analysed data series highlights a major shift of the lowermost frequency from 970 to 750 cm, a peak at 330 cm that characterises only the magnetic susceptibility series, and the presence of common peaks between 130 and 100 cm.

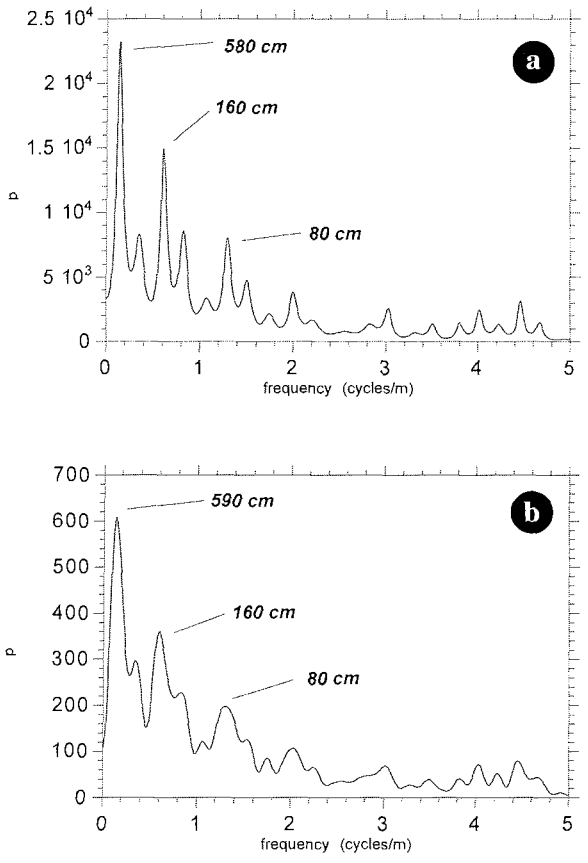

Fig. 3.8 - a) Maximum Entropy spectral analysis of the magnetic susceptibility data series of the interval 60.99 - 83.10 mbsf (length of the autocovariance series is 20%). The highest peaks are labelled and point to the most powerful single frequency lines, at 580, 160 and 80 cm. *b)* Blackman-Tukey spectral analysis of the magnetic susceptibility data series of the interval 60.99 - 83.10 mbsf (length of the autocovariance series is 30%). This algorithm indicates the statistically significant broad groups of periodicities above the noise levels.

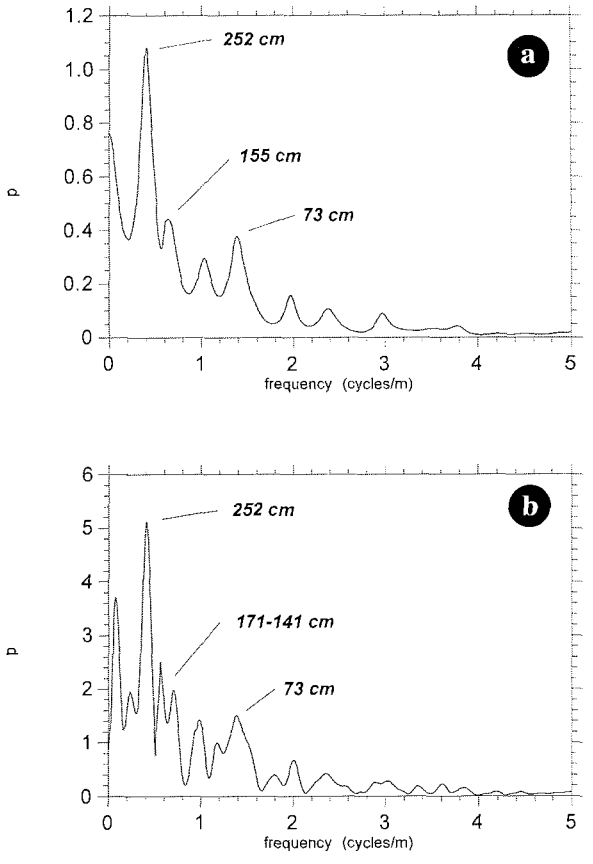

Fig. 3.9 - a) Maximum Entropy spectral analysis of the porosity data series of the interval 60.99-83.10 mbsf (length of the autocovariance series is 15%). The dominant peaks are displayed and refer to the periodicities at 252, 155 and 73 cm. *b)* Blackman-Tukey spectral analysis of the porosity data series of the interval 60.99-83.10 mbsf (length of the autocovariance series is 40%). This algorithm indicates the statistically significant broad groups of periodicities above the noise levels.

It should be pointed out that the processed data series appear to be almost noise-free, and only a few spectral lines fall below noise levels. These latter are, therefore, regarded as not real periodicity, but as the product of highly-periodic *quasi*-random noise.

DISCUSSION

The high power and the quite narrow frequency band of the detected periodicities point to a clear cyclic forcing process, which should have controlled both the magnetic susceptibility and porosity fluctuations in the stratigraphical records. Since in the spectra many of the peaks occurred at quite similar frequencies, it is possible to summarize the most likely spectral features of the analysed physical properties (magnetic susceptibility and porosity) in the two intervals, as they are computed from the ME algorithm. Cyclic oscillations in the interval 60.99-83.10 mbsf occur with the following periodicities: from 580 to 252 cm, at 160-155 cm, and at 80-73 cm, while in the interval 120.20-144.45 mbsf they span the following periodicities: from 970 to 750 cm, at 330 cm and between 130 and 100 cm.

The spectral analysis proves clearly the existence of a regular cyclic pattern in both the magnetic susceptibility and porosity records of these lithostratigraphical intervals and allows us to discard a stochastic mechanism as controlling their fluctuations. Therefore, questions arise on the nature of the periodic forcing mechanism.

If we compare the periodicities expressed in cm each against the other and compute the relative ratios, by normalizing the values to the highest frequency in the spectra, the obtained ratios refer to hierarchies of decreasing wavelength from low to high frequency. The application of this method is of considerable significance because then the frequency lines in the spectra point directly to the ratios between the hierarchic levels of the cycles (Fischer et al., 1991; Hinnov & Goldhammer, 1991; Claps & Masetti, 1994; Claps et al., in press). The same reasoning can be applied to the time duration of the

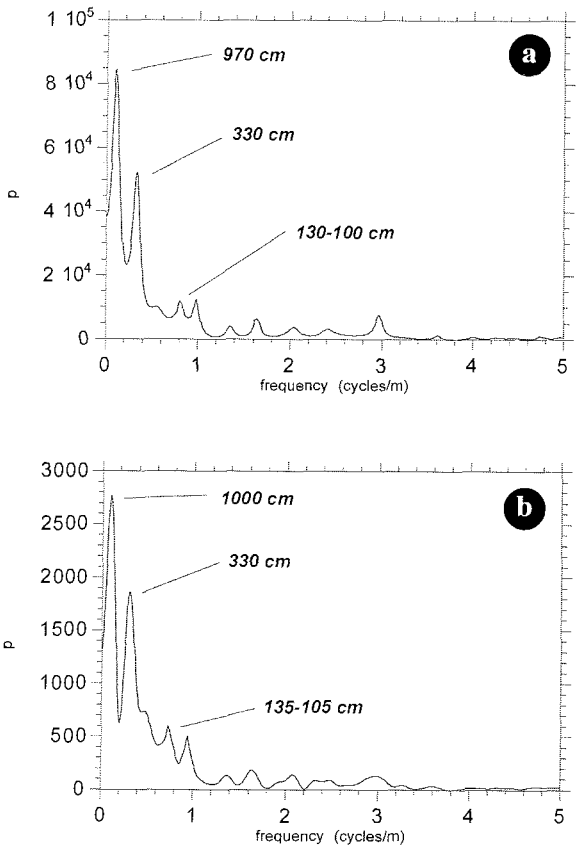

Fig. 3.10 - a) Maximum Entropy spectral analysis of the magnetic susceptibility data series of the interval 120.20-144.45 mbsf (length of the autocovariance series is 17%). Two high-power spectral peaks are present in the left-side of the spectra at 970 and 330 cm, while two dispersed low-energy peaks span from 130 to 100 cm. *b)* Blackman-Tukey spectral analysis of the magnetic susceptibility data series of the interval 120.20-144.45 mbsf (length of the autocovariance series is 30%). This algorithm indicates the statistically significant broad groups of periodicities above the noise levels.

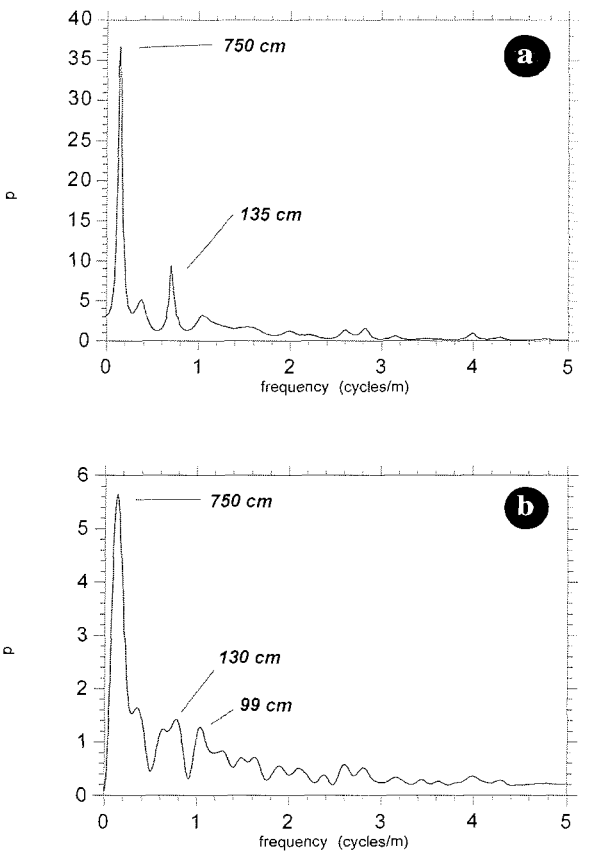

Fig. 3.11 - a) Maximum Entropy spectral analysis of the porosity data series of the interval 120.20-144.45 mbsf (length of the autocovariance series is 15%). Two periodicities appear dominant in the processed spectra and refer to the values of 750 and 135 cm. *b)* Blackman-Tukey spectral analysis of the porosity data series of the interval 120.20-144.45 mbsf (length of the autocovariance series is 30%). This algorithm indicates the statistically significant broad groups of periodicities above the noise levels.

orbital perturbations. The values predicted for the Milankovitch orbital cycles during the Cenozoic are as follows: 19-23 k.y. for the precession, 41-54 k.y. for the obliquity and 95-123 k.y. for the short-term eccentricity cycles (Berger, 1984; Berger & Loutre, 1994). When these time durations are normalized to the shortest periodicities of the orbital perturbations (the precession cycles), the relative ratios are:

eccentricity	obliquity	precession
6.5-4.2	2.8-1.8	1

When the peaks detected in the magnetic susceptibility series are normalized to the highest frequency, the ratios for each interval appear as follows:

interval 60.99-83.10 mbsf

wavelengths	580 cm	160 cm	80 cm
ratios	7.2	2	1

interval 120.20-144.45 mbsf

wavelengths	970 cm	330 cm	130 cm
ratios	7.5	2.5	1

The matches between these observed ratios and those obtained from the Milankovitch orbital forcing periodicities (short term eccentricity, obliquity and precession cycles) are good when considering that the values 2 and 2.5 fall within the range of the obliquity/precession ratio. Some difference occurs when the values 7.2-7.5 are related to the eccentricity/precession ratio, giving a slightly higher value.

As far as porosity is concerned, the ratios for each interval appear as follows:

interval 60.99-83.10 mbsf

wavelengths	252 cm	155 cm	73 cm
ratios	3.4	2.1	1

interval 120.20-144.45 mbsf

wavelengths	750 cm	135 cm
ratios	5.5	1

Although a cyclic pattern is recognizable for porosity, the ratios computed for both the two intervals do not always show a clear correspondence with the orbital ratios. Nevertheless the ratio 2.1 in the interval 60.99-83.10 mbsf and the ratio 5.5 in the interval 120.20-144.45 mbsf might be related respectively to the obliquity and eccentricity orbital perturbations. Moreover some of the peaks (*e.g.* at 155 and 73 cm in the interval 60.99-83.10 mbsf) have approximately the same values with respect to the magnetic susceptibility series.

CONCLUSION

The analysis carried out in this preliminary study allow tentative conclusions on the nature of cyclic patterns recognized in CRP-3:

- the magnetic susceptibility and porosity records studied in two selected intervals of the CRP-3 succession display a clear cyclic signal;
- the spectral analysis of the data series demonstrate a deterministic control of the physical property records, and this suggests an external forcing mechanism driving the deposition of the lithostratigraphical intervals tested;
- the magnetic susceptibility record in particular demonstrates that controlling periodicities are in tune with the Milankovitch orbital perturbations, and some of these periodicities are echoed by the porosity record.

This quantitative approach suggests that fluctuations of the physical properties provide a sensitive tool for recording high-frequency periodicities. This pilot study should, therefore, encourage further analysis to be carried on other intervals of the CRP-3, and cross-correlated with other sets of parameters. Moreover, it will offer a broader and better understanding of the effect of deterministic external forcing mechanisms on the sedimentation in the marine and glaciomarine environments at the margin of the Antarctic Ice Sheet during the Cenozoic.

DIAGENESIS

INTRODUCTION

In this preliminary study we evaluate macroscopic diagenetic features recorded throughout CRP-3. The main purpose is to provide a comprehensive description of these features to be compared to those recorded in CRP-2/2A. CRP-3 consists of 823 m of Cenozoic sedimentary strata, representing Victoria Land Basin fill deposited on Devonian Beacon sandstone associated with a shallow mafic intrusive body and clastic or cataclastic injection material.

DIAGENETIC FEATURES WITHIN THE CENOZOIC SEDIMENTARY SEQUENCE (0-823 MBSF)

The main macroscopic diagenetic features recorded throughout the Cenozoic sedimentary sequence include: carbonate concretions and nodules associated with skeletal material, carbonate cementation, pyrite, "black stains" within the matrix of coarse lithologies, mineral-fills in veins and fractures.

Carbonate Cementation Associated with Skeletal Material

Carbonate cement, the most common precipitant throughout the core, displays different main diagenetic fabrics. Calcium carbonate occurs as fringing and patchy cements associated with shell debris, as pervasive cement in all lithologies, as microcrystalline and/or sparry calcite-fills in fractures and veins, and as carbonate-cemented

"nodules" within sandstone lithologies.

Carbonate cementation is rare in the upper 120 mbsf of the core, where it usually occurs as light-coloured patches, one to several cm across. Sparse carbonate patches appear to be associated with the skeletal material at depths of 54.23, 56.05, 59.60, 64.42, 86, 98.20 mbsf. Shells (especially bivalves, and, to a lesser extent, brachipods, gastropods, serpulid tubes; see section on Macrofossils) mainly occur as fragments and show all degrees of preservation, from well preserved, partially dissolved, to totally dissolved (solution-moulds) (Fig. 3.12a).

Carbonate cementation increases below 120 mbsf, and becomes extensive below 239 mbsf in all lithologies (Fig. 3.12 b & c). In such cases, the precipitation of calcium carbonate is related to fossil shell material. Below 120 mbsf carbonate cementation occurs as a diagenetic process associated with shell debris that produces fossiliferous concretions and nodules. Incipient diagenesis is indicated by corrosion and partial dissolution of the calcareous biogenic tests (macrofossils) at different depths (120-122.40, 124.50-127.80, 128.60, 130.55, 130.66, 137.21-137.25, 140.70, 144.50, 157.73, 165.30-169.50, 184.85-188.62, 190.50-190.74, 192.62-194.39, 200.20-201.50, 215.75 and 216 mbsf). As mentioned above, mainly bivalves show a wide variety of preservational stages ranging from well preserved, partially dissolved, to solution moulds cemented by calcitic cements (Fig 3.12b). Heavily corroded tests may be internally cemented by sparry calcite; in some cases, the moulds are filled by fine drusy calcitic cement (solution-cavity fill), as previously recorded for carbonate fossiliferous concretions and nodules throughout CRP-1 and CRP-2/2A (Claps & Aghib, 1998; Baker & Fielding, 1998; Taviani & Claps, 1998; Cape Roberts Science Team, 1999; Aghib et al., in press).

Below 330 mbsf, the sedimentary sequence is virtually barren of foraminifers and macrofossils. A single gastropod mould was recorded at 359.11 mbsf within muddy, well stratified sandstones (LSU 9.1). Below this depth, no carbonate concretions and nodules containing shell debris were recorded.

Carbonate-Cemented Sandstones

Extensive carbonate cementation occurs in sandstone lithologies as nodules in greenish muddy sandstones and in light-coloured clean sandstones. Carbonate-cemented nodules, 1 to 40 mm across, were first observed within coarse both uncemented sand and fine-medium muddy sandstone, at a depth around 234.83 mbsf. These were previously recorded for CRP-2/2A below a depth of 500 mbsf (see Cape Roberts Science Team, 1999; Aghib et al., in press).

From 239 to 280 mbsf, the carbonate-cemented nodules are dispersed within the sandstones. Below 280 mbsf, where carbonate cementation increases, the nodules range in size up to 4 cm, often coalesced to form well-cemented horizons (Fig. 3.12g). They were recovered at various depths, usually in muddy greenish sandstones that ranged from well- to poorly-sorted and from fine- to coarse-grained (see section Description of the sequence). From a depth of 540 to 789.77 mbsf, the sandstones show an unusual "greenish" colour, probably due to the presence of clay minerals (smectite?).

Light-coloured sandstones are well-sorted, clean and the original stratification is defined and enhanced by the carbonate cementation (Fig. 3.12f). These were recovered particularly in two intervals (380-570 mbsf and 605-610 mbsf).

No evidence of shell material was recorded throughout the carbonate-cemented sandstones, which might be considered barren of calcareous macro/microfossils. Detrital coal grains are common however, and occur in millimetric layers and/or dispersed throughout the carbonate-cemented sandstones. Macroscopic evidences of coal/carbonate replacement were recorded at different depths in the core at 658.54, 661.10, 719.70, 735.48, 737-737.48, 741.48-743.40, 748.36, 754.54-756.15, 757.90, 761.70, 770.32 mbsf (Fig.3.12 h & i).

Although the source of the carbonate for cementation has yet to be ascertained, we saw no evidence of dissolution affecting biogenic tests in terms of incipient/late stage of diagenesis, however, a biogenic origin of the carbonate can be still considered one possibility. Macroscopically, similar cements from lithologies in CRP-2/2A display a fabric composed of a first-stage calcite rim around grains and a late-stage pervasive calcite precipitate (Aghib et al., in press). In the same example, calcitic cementation occurs within detrital grains of coal particles that seem to be partly consumed, suggesting organic carbon-carbonate diagenesis where coal might act as the nucleus for their formation (Lamothe et al., 1983; Aghib et al., in press). A second possible source of carbonate for cementation and nodule formation might be Cambrian/Precambrian marble that occur below the Beacon Supergroup in this section of the Transantarctic Mountains. The possible role of carbonate-rich (hydrothermal?) waters moving from these rocks along the rift-fault system and into the Oligocene basin-fill sediments is the subject of future research for the CRP-3 *Science Results* volume.

Black Stains within Coarse Lithologies

Blackish stains within the clayey matrix of pebbly/cobble dark conglomerates were observed from a depth of 182.00 mbsf. In smear slides, the black stain seems to be composed of a fine-grained matrix with abundant dispersed organic matter, often associated with fine-grained pyrite framboids (Fig.3.12d).

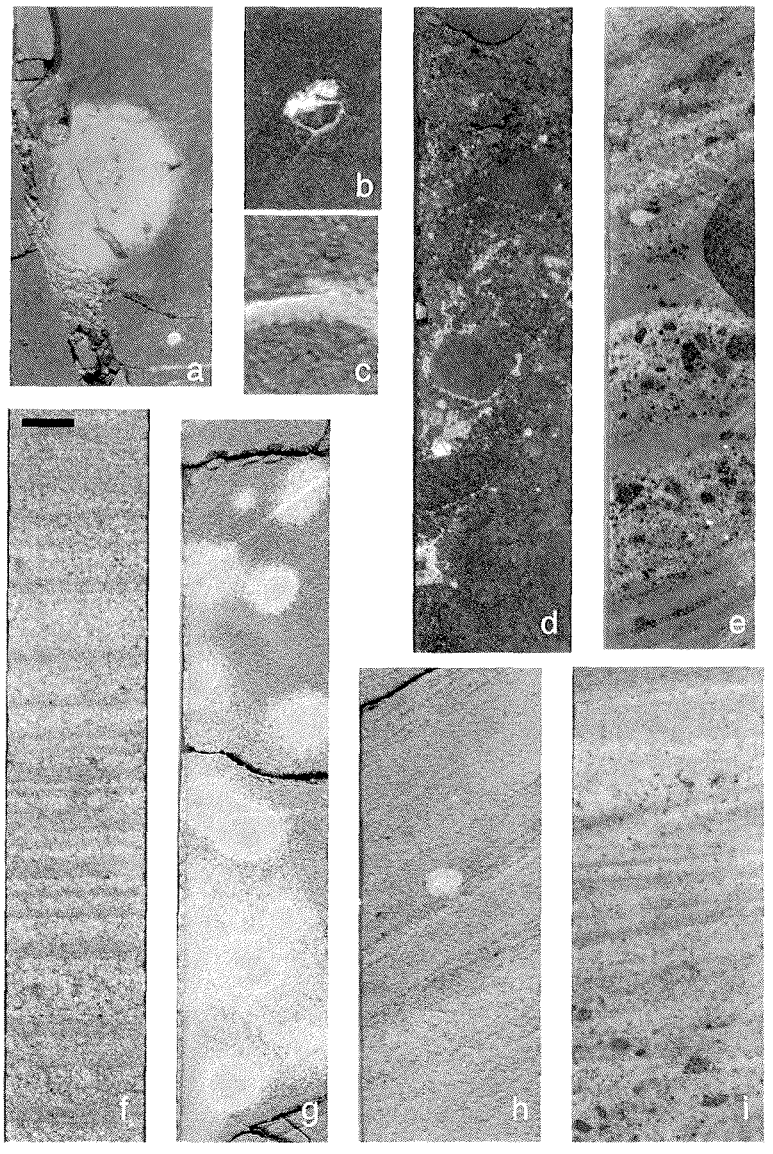

Fig. 3.12 – Close-ups from CRP-3 core showing some macroscopic diagenetic features associated with carbonate cementation (scale bar 1 cm). *a)* Large carbonate concretions containing partially dissolved serpulid tubes (61.20 mbsf); *b)* diffuse patchy carbonate cementation containing a fragment of bivalve (120.27 mbsf); *c)* gastropod mould partially cemented by sparry and drusy carbonate (359.11 mbsf); *d)* pebbly conglomerate showing "blackish stains" and evidence of carbonate cementation around grains (377.42 mbsf); *e)* strongly carbonate cemented pebbly conglomerate (663.70 mbsf); *f)* light well-sorted clean sandstones where the original stratification is enhanced by the carbonate cementation (519.50 mbsf); *g)* "nodular" carbonate-cemented sandstones, passing from sparse 1 cm in size carbonate-cemented nodules dispersed in the sandstones to coalesced nodules (238.12 mbsf); *h)* nodular carbonate cementation around detrital coal grains (770.30 mbsf); *i)* diffuse carbonate cementation within layers containg abundant detrital coal fragments (757.90 mbsf).

Mineral-Fills in Veins and Fractures

In the upper 120 mbsf, there are fractures and veins (hairline) filled by calcite. Their first occurrence is at 18 mbsf, and they recur downcore; their orientation varies from horizontal to vertical with respect to bedding, ranging in size from less than 1 mm to 10 mm wide. Hairline fractures were observed, especially in fine-grained lithologies, and are filled by finely microcrystalline calcite cement. Below 120 mbsf, calcite mineral-fills begin to be intensely developed along fractures and microfaults/faults, especially in the intervals at the depth of 229.50-233.50, 232-233.50, 260.60-261.40, 263.20-270.50, 538.80-539.30 (within a dolerite boulder), 788.97-789.77 mbsf. Calcite-filled veins and fractures often display a halo of diffused cementation, several centimeters wide within the host lithologies (Fig. 3.13a). The fill fabric consists of different generations of fringing calcitic cements and subsequent sparry/drusy-calcite crystal growth (Fig. 3.13 b, c & d).

Pyrite

Distinct authigenic pyrite phases are recognized within the CRP-3 sedimentary sequence. Finely divided pyrite is present in a range of morphologies. It occurs as

submicroscopic crystals and framboids dispersed within the matrix in all lithologies, from a depth of 18 mbsf, becoming more abundant below 100 mbsf. In addition to that, pyrite occurs as infillings associated with a thin light-coloured calcite or possibly siderite rim in 1-cm-wide sedimentary dykes, in silt/sand lithologies at different depths below 84.90 mbsf. A third occurrence is pyrite as a cement phase, rimming grains and around later-formed carbonates (calcite), suggesting a tentative paragenesis with subsequent generations of cements (Fig. 3.13 e & f).

Pyrite might form during an early stage of diagenesis, followed by a later phase of extensive carbonate cementation. Below a depth of 280.00 mbsf, in fine and very fine sandstones, detrital coal fragments are abundant and are partially replaced by microcrystalline pyrite, suggesting bacterially-mediated redox reactions in organic-rich detrital grains (Berner, 1984). An early stage of diagenesis related to pyrite formation was also recorded for CRP-2/2A (see Cape Roberts Science Team, 1999).

Zeolites

Zeolites occur replacing possible volcanic clasts as much as 10 mm long below 743.64 mbsf.

DIAGENETIC FEATURES BELOW 823 MBSF

These diagenetic features and mineralogical components are related to the Devonian Beacon sandstone basement and are associated with breccias and clastic/cataclastic injections.

Calcite mineral-fills of fractures/faults are present within the Beacon sandstones and within the intrusion, associated with clastic/cataclastic injections. The fractures within the highly brecciated upper contact between Beacon sandstones and the igneous intrusion(from 898.90-901.30 mbsf; see sections on Facies Analysis and Core Fractures) are likely a product of hydrothermal fracturing and are thus discussed in the related chapter. Below the igneous intrusion, at the lower contact with the altered Beacon sandstones, calcitic-fills are also present and mineralizations occur only as millimetric patches of sulphide minerals (Zn? sphalerite?) dispersed within the Beacon sandstones below the depth of 922.60 mbsf (Fig. 3.13g). The occurrence of sulphide mineralizations might indicate hydrothermal fluid circulation (see section on Igneous Intrusion in the Petrology chapter).

SUMMARY OF RESULTS AND FUTURE RESEARCH

Previous studies described the diagenetic features of CRP-1 (Baker & Fielding, 1999) and CRP-2/2A, located along a transect east of CRP-3, and from CIROS-1 on the western edge of the Victoria Land Basin (Bridle & Robinson, 1990). Carbonate cementation associated with shell material occurring virtually in all lithologies suggests a clear relationship between selective dissolution of calcareous biogenic tests and precipitation of authigenic carbonate as previously described by Claps & Aghib (1998) and by Aghib et al. (in press) in CRP-1 and CRP-2/2A. The carbonate-cemented sandstones form a 400-m-thick sedimentary sequence and might represent all stages of cementation within sandy lithologies, ranging from sparse centimetric carbonate-cemented nodules, to abundant millimetric/centimetric carbonate-cemented nodules, to well-cemented sandstones. The carbonate cementation might be related

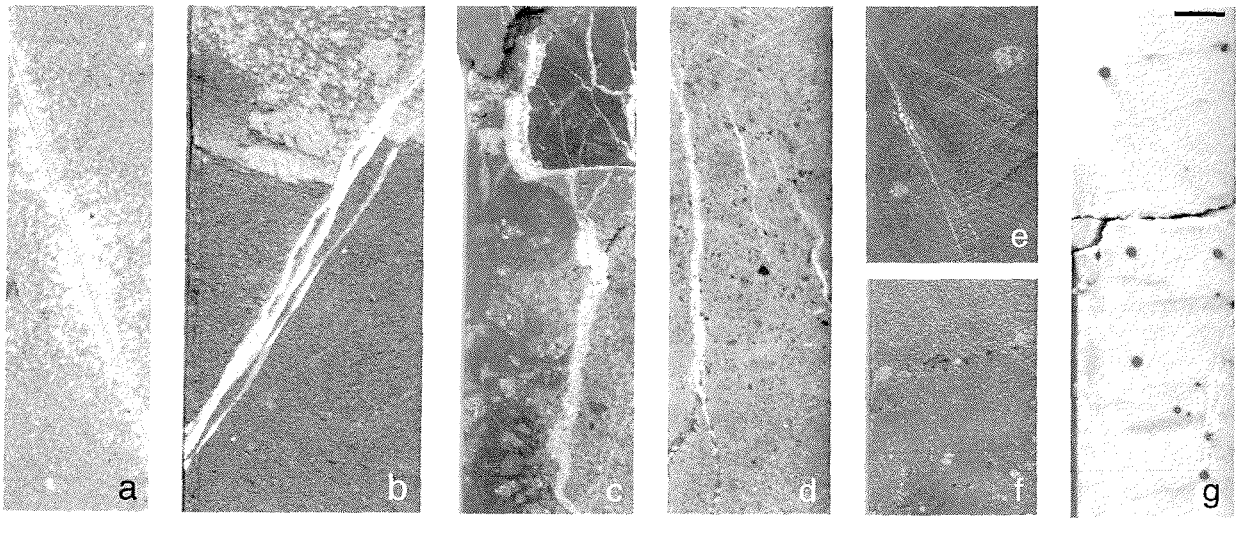

Fig. 3.13 – Photos from CRP-3 core showing some macroscopic diagenetic features (scale bar 1 cm). *a)* Calcite mineral-fills showing carbonate diffusion from the vein to the host lithology (454.10 mbsf); *b* and *c)* calcite-fills develop along fractures/microfaults showing two phases of cementation (b at 250.37 mbsf; c at 407.13 mbsf); *d)* calcite-fills developed around coal grains (761.30 mbsf); *e)* pyrite framboids within a hairline calcite fracture (410.13 mbsf); *f)* pyrite cement within coal grains (718.68 mbsf); *g)* millimetric "spots" of sulphide mineralizations dispersed within sandy lithologies and in fractures (922.70 mbsf).

to an organic carbon-carbonate diagenesis, as suggested by carbonate cementation within the detrital coal fragments, as reported in Aghib et al. (in press) for carbonate-cemented sandstones from CRP2/2A. A hydrothermal origin might also be possible considering the tectonic setting of the site and the possible presence of marble below the section penetrated by CRP-3.

Another area of future research will be the correlation of diagenetic features *versus* depth with high-resolution core physical properties (see Section on Physical Properties from on-site core measurements). The diagenesis appears therefore unrelated to a simple increasing overburden, the diagenetic process affecting the sediments are therefore related to the fluid flow migration and their evolution within the sediments. The variations throughout the sequences are confirmed by the complex trend of the high-resolution core physical properties. Therefore, a systematic study of the diagenetic fronts may provide insight on the significance of the reflectors and may thus help their reinterpretation.

CLAST FEATURES: STRIAE, SIZE AND ROUNDNESS

INTRODUCTION AND DESCRIPTION

The CRP-3 core has clasts present throughout its entire length, ranging in size from millimetres (mm) to 1.2 metres (m) in diameter. Although we removed thirteen whole-round core samples of clast-rich intervals for three-dimensional fabric analysis and clast-shape analysis, we will present the results from this work in the CRP-3 *Science Report* volume. Characteristics such as size, composition and roundness have been included routinely as part of the core log descriptions, but other features such as striae on clasts have been less frequently noted.

We document here striated clasts (*e.g.* Fig. 3.14) found in the interval from 350 mbsf to the base of the Cenozoic section (Fig. 3.15). This interval is interpreted to represent largely shallow-marine sedimentation with markedly less glacial influence than in the upper 300 m (see Sequence Stratigraphy section). The distribution of striated clasts is sparse, sporadic and is not restricted to any particular depositional facies. The presence of striae is largely determined by the lithology of the clast. Those most commonly striated are fine-grained, indurated mudstone, but these are rare. A few other sedimentary clasts and occasional dolerite clasts also carry striae.

Out-sized clasts are also plotted (Fig. 3.15). We define these as clasts 0.1 m or more in diameter and 100 times larger than the mean diameter of the enclosing sediment; they range up to 0.77 m in cored length. We have chosen to plot only clasts in non-conglomeratic sediment, as it is difficult to see how these can have been transported to their present site by non-rafting processes, *e.g.* traction currents or sediment-gravity flows. Out-sized clasts also occur in conglomerate beds, but these might have been transported by non-rafting processes. Possible mechanisms for the emplacement of the out-sized clasts in the sandstone beds include rafting in tree roots, kelp or sea- or glacier-ice.

Fig. 3.14 - Striated mudstone clast from 738.40-738.42 mbsf. Core is 45 mm in diameter.

INTERPRETATION

We interpret the striated clasts, which are also facetted and sub-rounded, to be the result of abrasion in the basal ice of a glacier, and introduced into the marine environment by glaciers calving at the coast. This supports ice-berg rafting as the mechanism for transporting the outsized clasts. Although the number of striated clasts is small, only a small proportion of the clasts have exposed surfaces and are of lithologies in which striae form and survive. We suggest therefore that the small number of stones reported here represents the "tip of an ice-berg", and document a substantial glacial influence in the transport of sediments into the marine environment. These observations suggest to us that glaciers were present and actively calving debris-laden ice at sea level during a considerable proportion of time and perhaps even most of the time represented by the core to a depth of *c.* 780 mbsf.

ROUNDNESS CHARACTERISTICS OF CLASTS IN THE INTERVAL FROM 770 TO 823 MBSF

The interval from 789.77 to 805.60 mbsf in the CRP-3 core is described as a dolerite (cataclastic) breccia (LSU 14.1). This unusual interval is dominated by brecciated boulders and clasts of which *c.* 95% are of dolerite. The rock shows evidence of intense shearing and is described as having fractured, off-set and veined clasts separated by a fine-grained cataclastic matrix (sheared, recrystallised, foliated claystone) with abundant slicken-lined surfaces, with a green fibrous mineral on

some surfaces.

To investigate the origin of the texture of the sheared dolerite breccia further, we described clast roundness to show the trends above, within and below the breccia. This was achieved by visually estimating clast roundness in the cut face of the core using the visual roundness chart of Krumbein (1941). Whole clasts larger than approximately 10 mm in diameter and less than the diameter of the core (45 mm) were recorded. Four intervals were selected from Facies 9 (clast-supported conglomerate) and Facies 10 (matrix-supported conglomerate) within LSU 13.2 (Fig. 3.15). Clasts from within the dolerite breccia interval were grouped into a single sample, as were all clasts from Facies 9 and 10 in

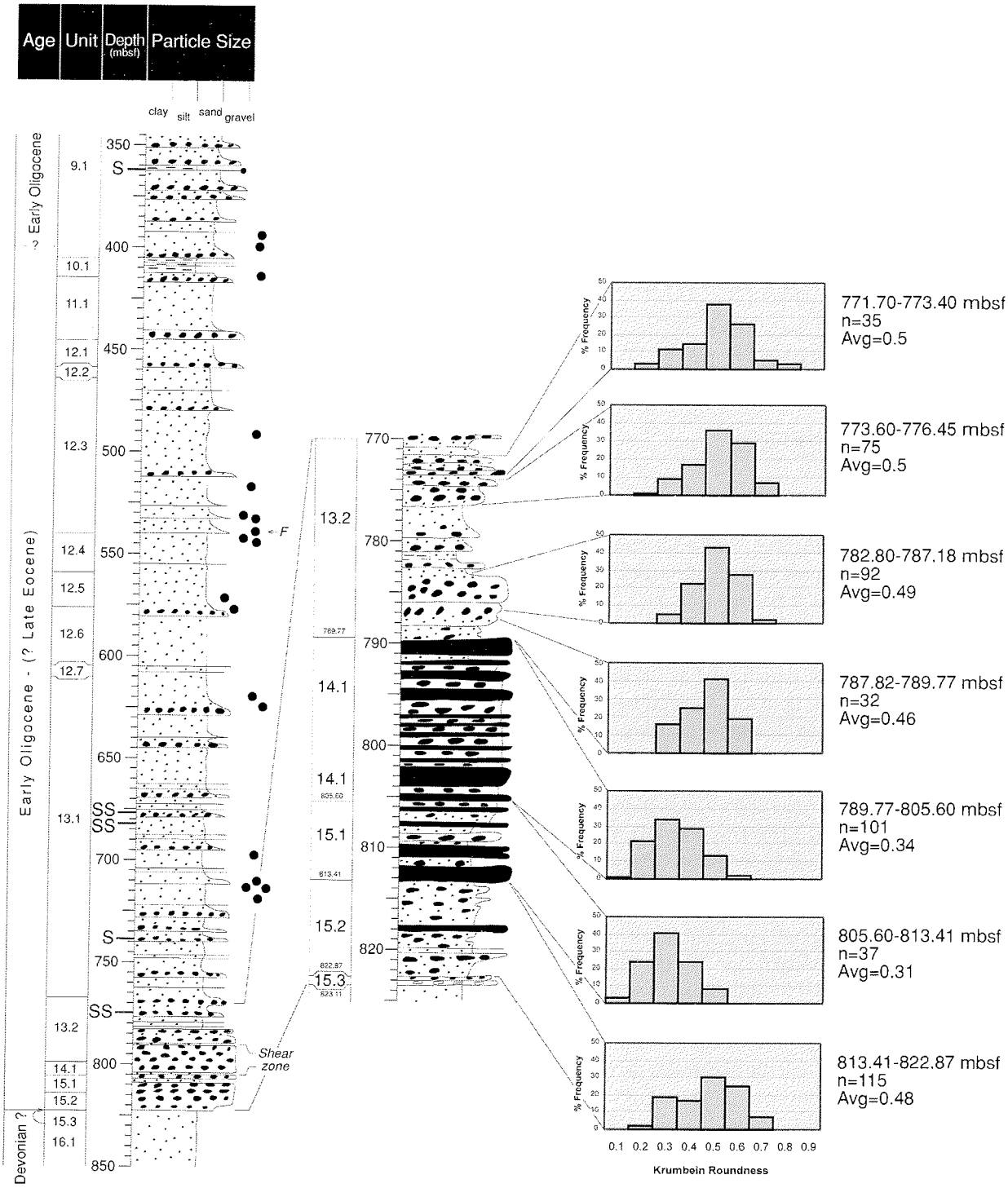

Fig. 3.15 - Partial graphical log of CRP-3 core showing locations of striated clasts (S), and out-sized clasts (●). Enlargement shows the interval 770.00-825.00 mbsf and clast roundness histograms. Krumbein roundness values correspond to Powers roundness classes (Powers, 1953) as follows: very angular (0.0–0.17); angular (0.17–0.25); subangular (0.25–0.35); subrounded (0.35–0.49); rounded (0.49–0.70); well rounded (0.70–1.00).

the underlying LSU 15.1, (805.60-813.41mbsf) and LSU 15.2, (813.41-822.87 mbsf). These data are presented as histograms displaying percent frequency of clasts in each of nine roundness categories (Fig. 3.15).

DESCRIPTION

The histograms for the upper two intervals (771.70-773.40 and 773.60-776.45 mbsf) display broad roundness distributions with average roundness values of 0.5 (rounded). Interestingly, both contain angular and well-rounded tails, indicating a mix of fluvially rounded and glacially influenced sediment (two striated clasts are reported at 775.55 and 775.80 mbsf).

The next two intervals (782.80-787.18 mbsf and 787.82-789.77 mbsf) both show a slight shift to a sub-rounded average, but still retain a modal roundness peak of 0.5. The roundness distribution also has a slightly narrower spread, with few clasts in the angular and well-rounded categories.

The most significant change occurs with the transition to the sheared dolerite breccia (789.77-805.60 mbsf) and a marked shift of both the modal peak and the average roundness to subangular (0.34). Almost 23% of clasts (both dolerite and less common quartzose sandstone) fall into the very angular and angular categories. This appears to be the result of pervasive deformation from shearing having fractured and offset clasts. Nevertheless, a significant proportion (15%) falls into the rounded category. Several dolerite clasts display a rough surface texture, despite an overall rounded appearance. Some have striae that could be interpreted as glacial, but the rough texture and common slicken-lined and tectonically polished surfaces make a tectonic origin more likely. Interestingly, the larger dolerite clasts appear to be better rounded than smaller clasts. Further work is needed to verify this.

LSU 15.1 (805.60-813.41 mbsf) below the dolerite breccia also has a modal peak and average roundness (0.31) in the subangular category, with 27% very angular and angular clasts. This appears to be related to the high proportion of quartzose sandstone in the unit, which is typically more angular. This unit does not display the pervasive deformation of the sheared dolerite breccia but slicken-lined clasts are still common.

The lowest interval, LSU 15.2 (813.41-822.87 mbsf), is described as a poorly-sorted dolerite-dominated conglomerate. It shows a return to the broad roundness distribution seen in the intervals above the sheared dolerite breccia, with a modal peak in the rounded category and average roundness of 0.48 (sub-rounded). The presence of angular and well-rounded clasts suggests a mix of fluvial and perhaps talus-derived sediment.

INTERPRETATION

The intense tectonic deformation evident in the dolerite breccia (LSU 14.1) is also indicated by the fractured and offset clasts clearly visible in the core face. However, the interval also contains a significant number of rounded and even well-rounded clasts. It is possible that some crude rounding could occur due to tectonic deformation processes. However, the combination of well-rounded clasts, the mix of lithologies, and apparent faint stratification suggest that the interval is a sedimentary deposit that has been subsequently modified by tectonic events, masking some of its original characteristics.

Appendix 3.1

1:500 SCALE CORE LOGS

Core logs on a scale of 1:500 summarising lithology, showing clast variation and diagenetic features. Inferred depositional environment is also shown, along with changes in sea level and ice margin. The basis for these interpretations is presented and discussed in the Lithology and Sedimentology chapter.

KEY

LITHOLOGY

- Diamictite
- Conglomerate
- Sandstone
- Mudstone
- Intrusive igneous

A combination of these lithologies also occurs:

- Lonestones (extraformational)
- Intraformational clasts
- Thin bed of coarser-grained lithology; length indicates particle size

STRUCTURES

Fossils

- Macrofossils (whole/broken)
- Trace fossils and bioturbation
- Plant fossil
- Coal fragments
- Wood fragment

Sedimentary

- Laminated/ bedded
- (—) If in parentheses bedding/ lamination is vague
- Ripple lamination
- Cross-stratification
- Hummocky cross-stratification
- Lonestones (*e.g.* dropstones)
- Sedimentary intrusion
- Load structures
- Soft-sediment deformation
- Brecciation
- Microfaults
- Shear zone

DIAGENESIS

- Mineral-filled fractures
- Pyrite
- Calcareous concretions/nodules
- Carbonate cement

SEQUENCE STRATIGRAPHY

- Sequence boundary
- (1) Sequence number

GLACIAL PROXIMITY

- i Ice marginal
- p Proximal
- d Distal
- n Non-glacial

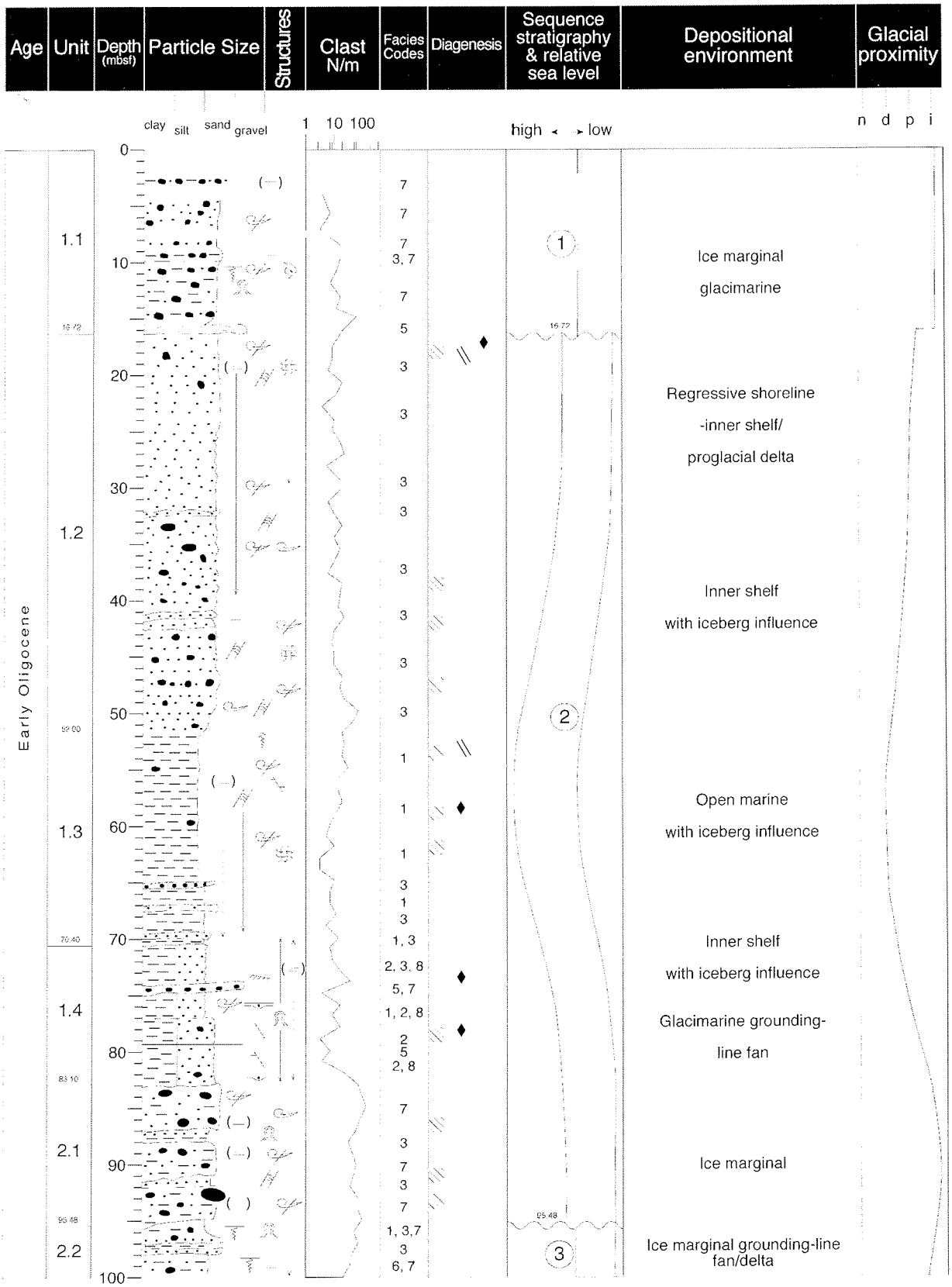
Age
Unit
Depth (mbsf)
Particle Size
Structures
Clast N/m
Facies Codes
Diagenesis
Sequence stratigraphy & relative sea level
Depositional environment
Glacial proximity
clay silt sand gravel
1 10 100
high low
n d p i
Early Oligocene
1.1
1.2
1.3
1.4
2.1
2.2
Ice marginal glacimarine
Regressive shoreline -inner shelf/ proglacial delta
Inner shelf with iceberg influence
Open marine with iceberg influence
Inner shelf with iceberg influence
Glacimarine grounding-line fan
Ice marginal
Ice marginal grounding-line fan/delta

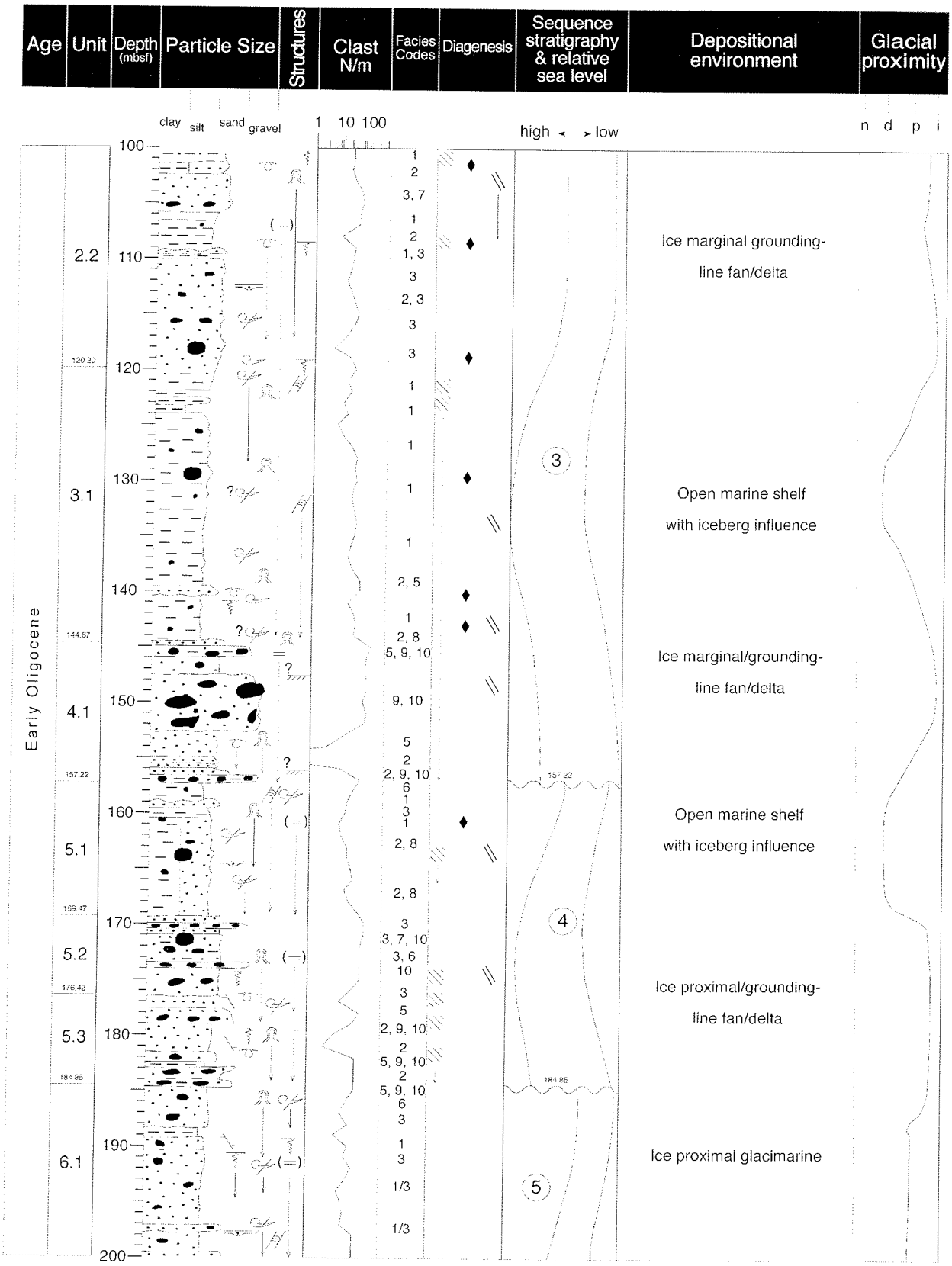
Age
Unit
Depth (mbsf)
Particle Size
Structures
Clast N/m
Facies Codes
Diagenesis
Sequence stratigraphy & relative sea level
Depositional environment
Glacial proximity
clay silt sand gravel
1 10 100
high low
n d p i
Early Oligocene
2.2
3.1
4.1
5.1
5.2
5.3
6.1
100
110
120
130
140
150
160
170
180
190
200
Ice marginal grounding-line fan/delta
Open marine shelf with iceberg influence
Ice marginal/grounding-line fan/delta
Open marine shelf with iceberg influence
Ice proximal/grounding-line fan/delta
Ice proximal glacimarine

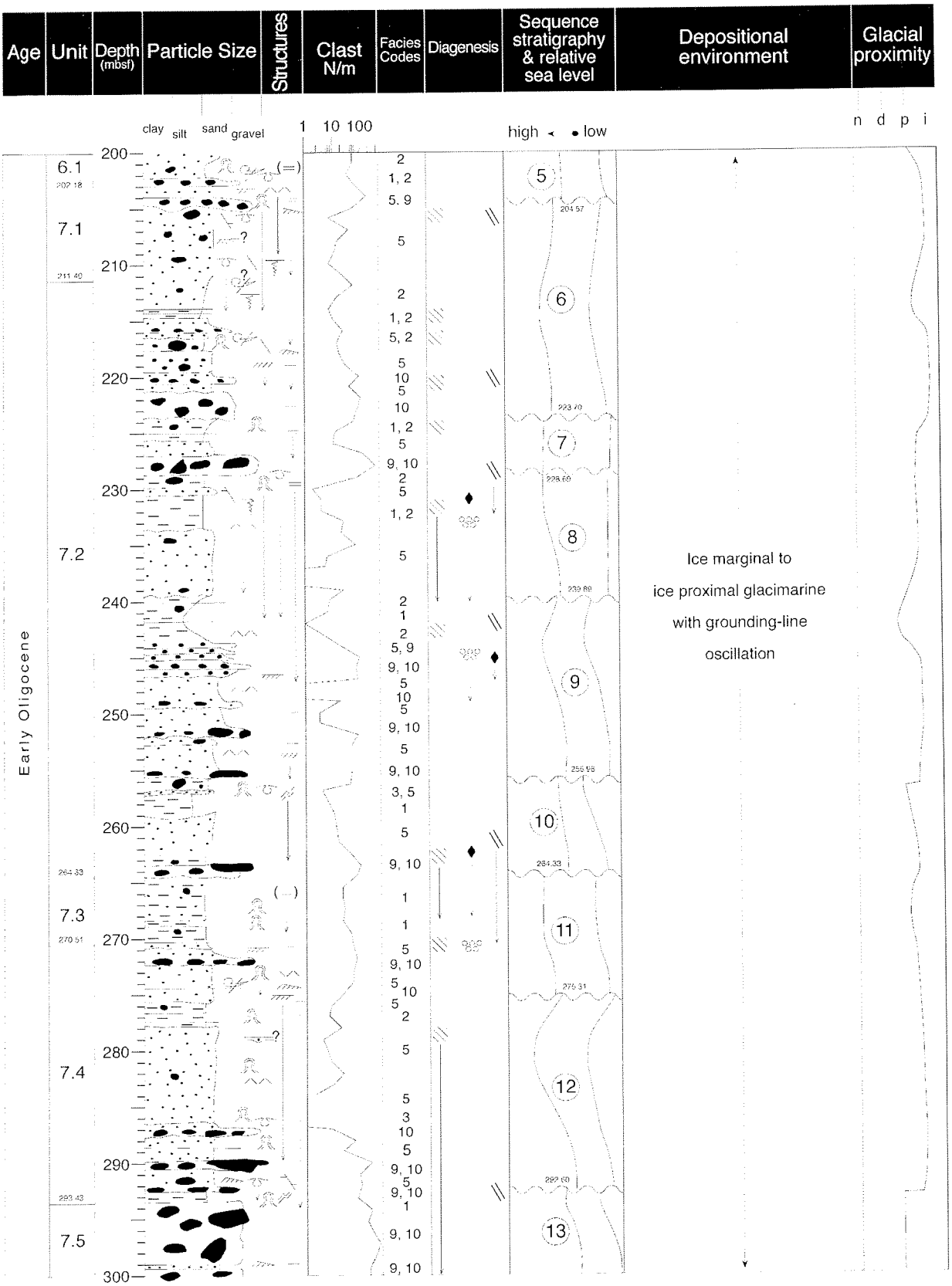
Age
Unit
Depth (mbsf)
Particle Size
Structures
Clast N/m
Facies Codes
Diagenesis
Sequence stratigraphy & relative sea level
Depositional environment
Glacial proximity
clay silt sand gravel
1 10 100
high low
n d p i
Early Oligocene
6.1
7.1
7.2
7.3
7.4
7.5
200
210
220
230
240
250
260
270
280
290
300
Ice marginal to ice proximal glacimarine with grounding-line oscillation

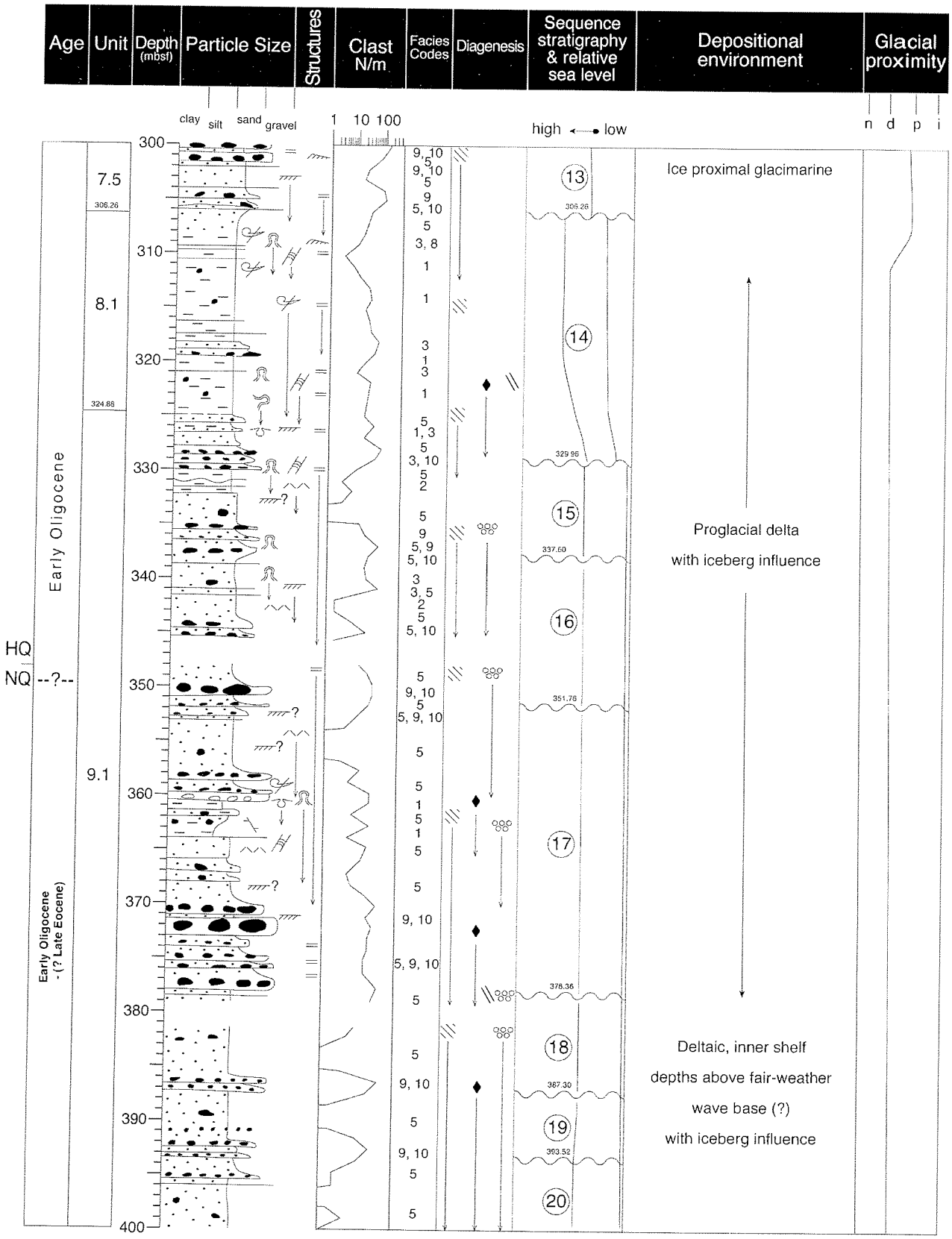
Age
Unit
Depth (mbsf)
Particle Size
Structures
Clast N/m
Facies Codes
Diagenesis
Sequence stratigraphy & relative sea level
Depositional environment
Glacial proximity
clay silt sand gravel
1 10 100
high low
n d p i
Early Oligocene
Early Oligocene - (? Late Eocene)
HQ
NQ --?--
7.5
8.1
9.1
306.26
324.88
329.96
337.60
351.76
376.36
387.30
393.52
Ice proximal glacimarine
Proglacial delta with iceberg influence
Deltaic, inner shelf depths above fair-weather wave base (?) with iceberg influence

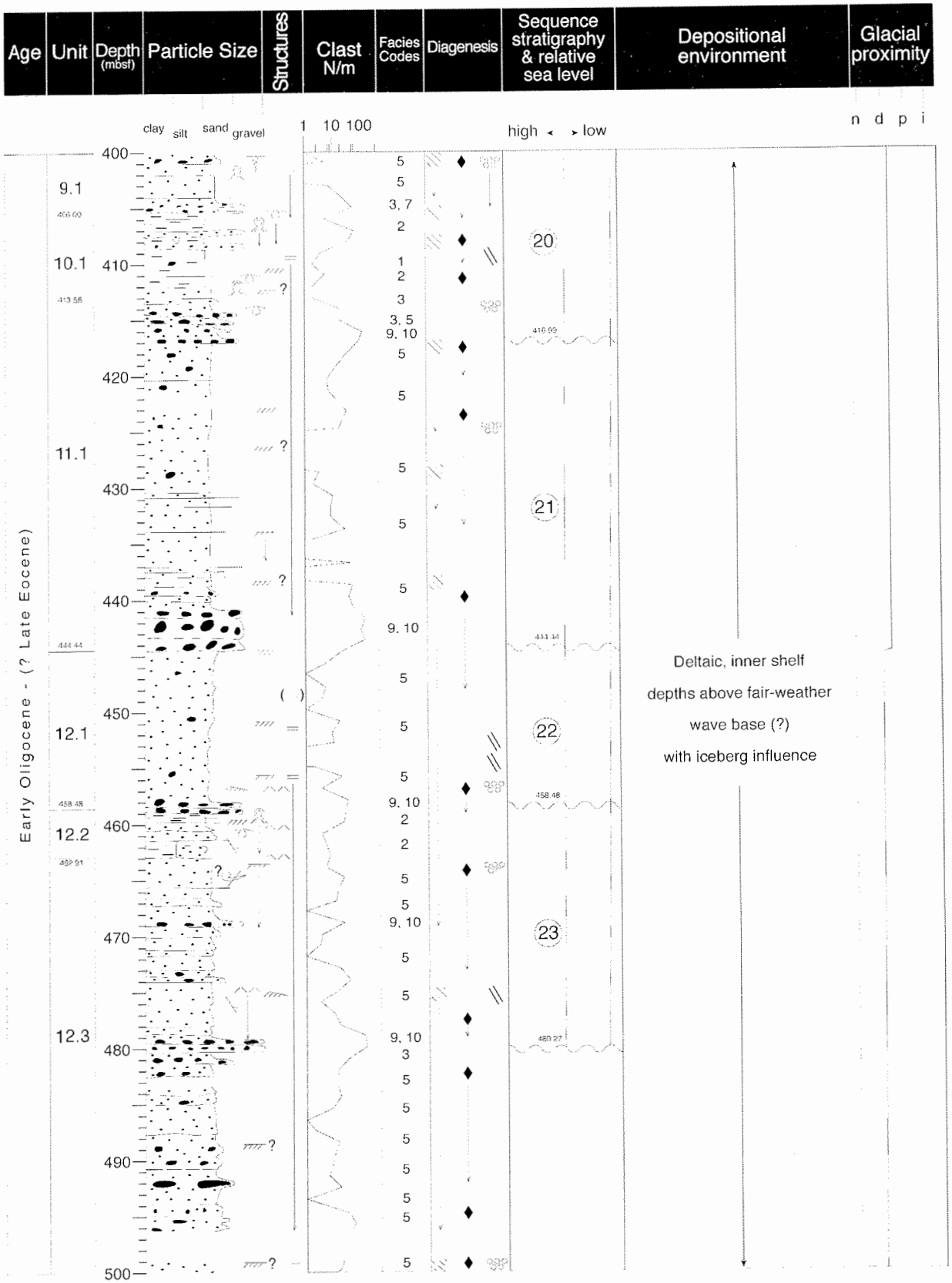
Age
Unit
Depth (mbsf)
Particle Size
Structures
Clast N/m
Facies Codes
Diagenesis
Sequence stratigraphy & relative sea level
Depositional environment
Glacial proximity
clay silt sand gravel
1 10 100
high low
n d p i
Early Oligocene - (? Late Eocene)
9.1
10.1
11.1
12.1
12.2
12.3
400
410
420
430
440
450
460
470
480
490
500
20
21
22
23
Deltaic, inner shelf
depths above fair-weather
wave base (?)
with iceberg influence

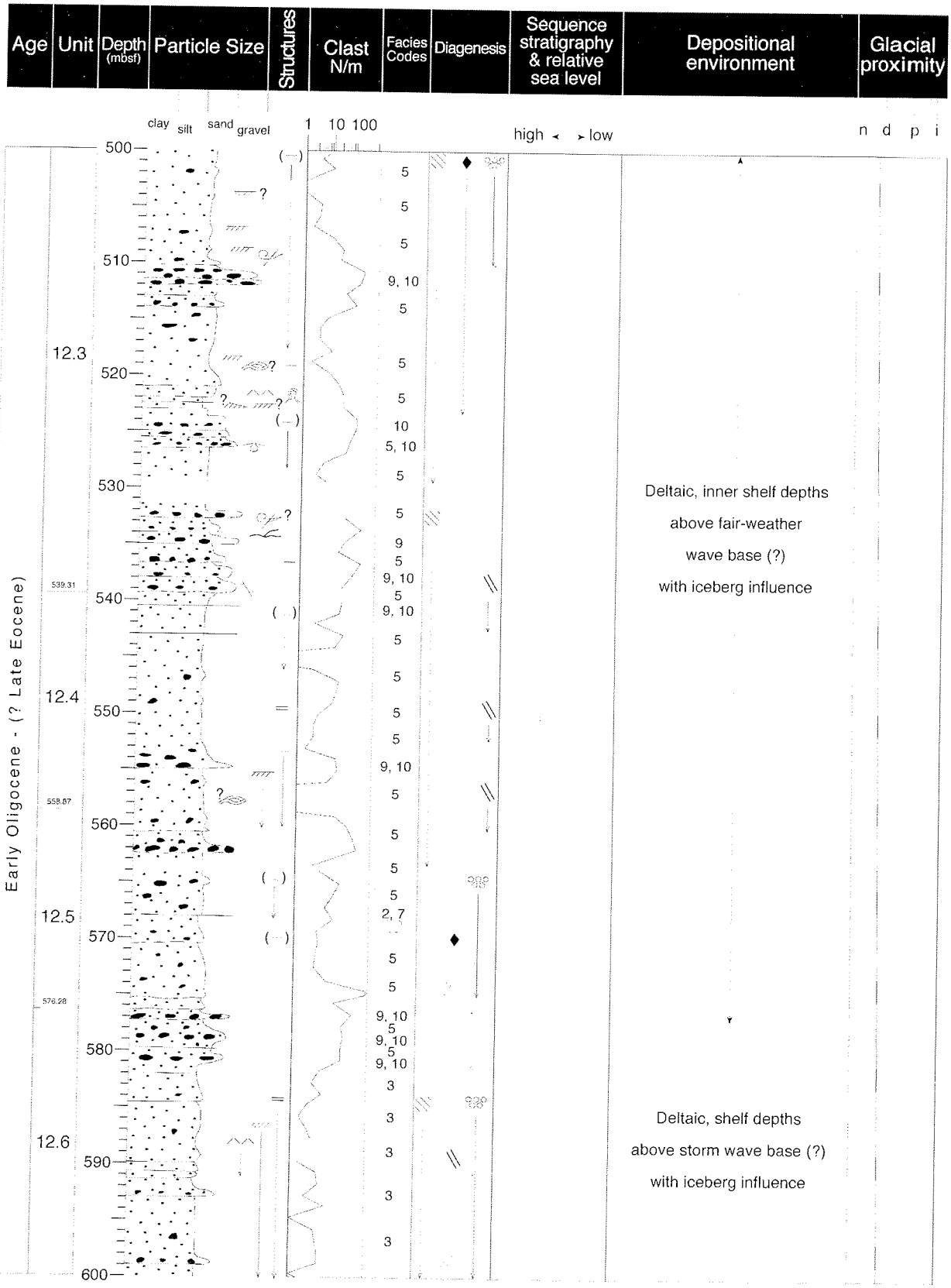
Age
Unit
Depth (mbsf)
Particle Size
Structures
Clast N/m
Facies Codes
Diagenesis
Sequence stratigraphy & relative sea level
Depositional environment
Glacial proximity
clay silt sand gravel
1 10 100
high low
n d p i
Early Oligocene - (? Late Eocene)
12.3
12.4
12.5
12.6
539.31
558.87
576.28
Deltaic, inner shelf depths above fair-weather wave base (?) with iceberg influence
Deltaic, shelf depths above storm wave base (?) with iceberg influence

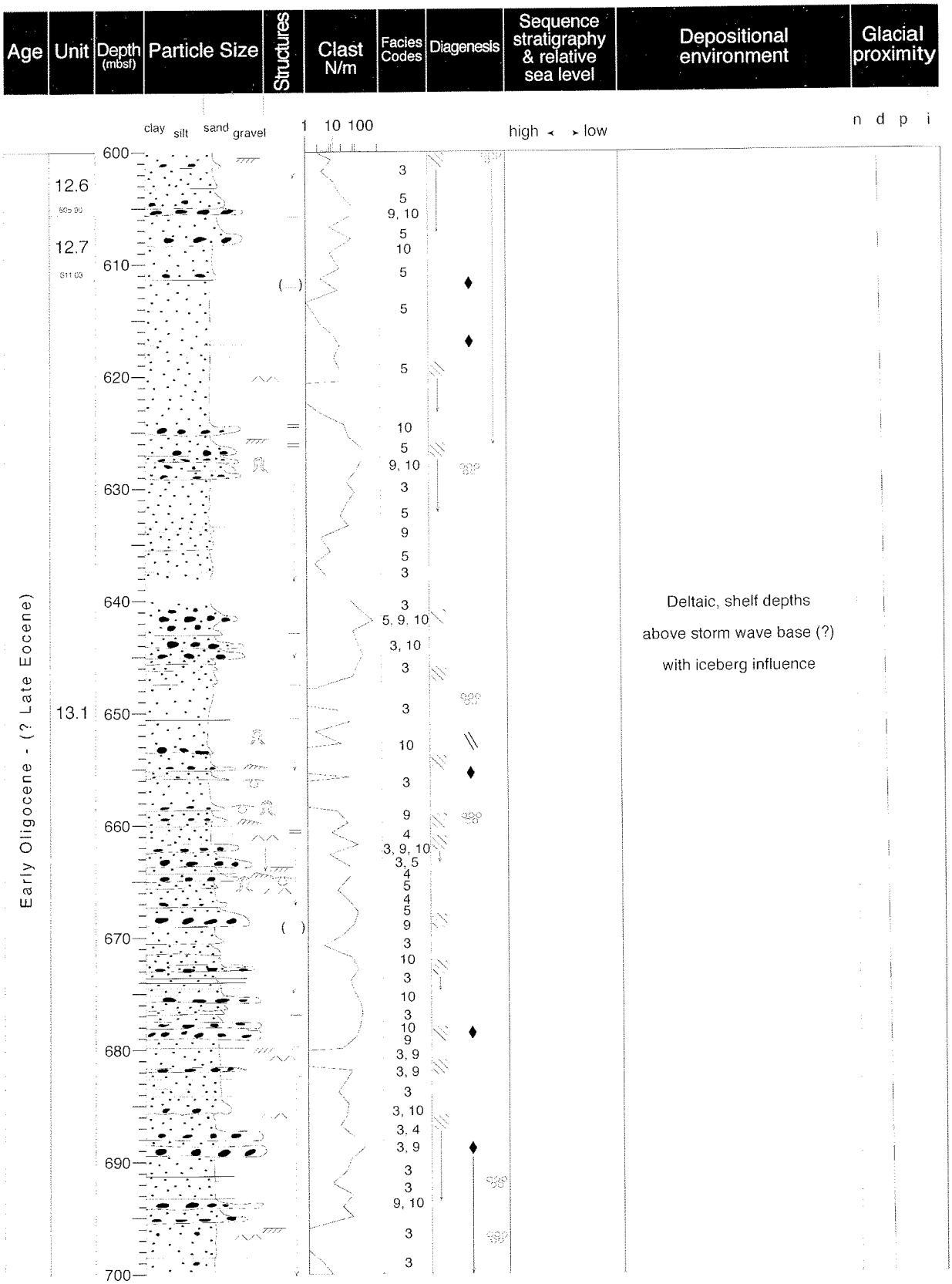
Age
Unit
Depth (mbsf)
Particle Size
Structures
Clast N/m
Facies Codes
Diagenesis
Sequence stratigraphy & relative sea level
Depositional environment
Glacial proximity
clay silt sand gravel
1 10 100
high low
n d p i
Early Oligocene - (? Late Eocene)
12.6
12.7
13.1
600
610
620
630
640
650
660
670
680
690
700
Deltaic, shelf depths
above storm wave base (?)
with iceberg influence

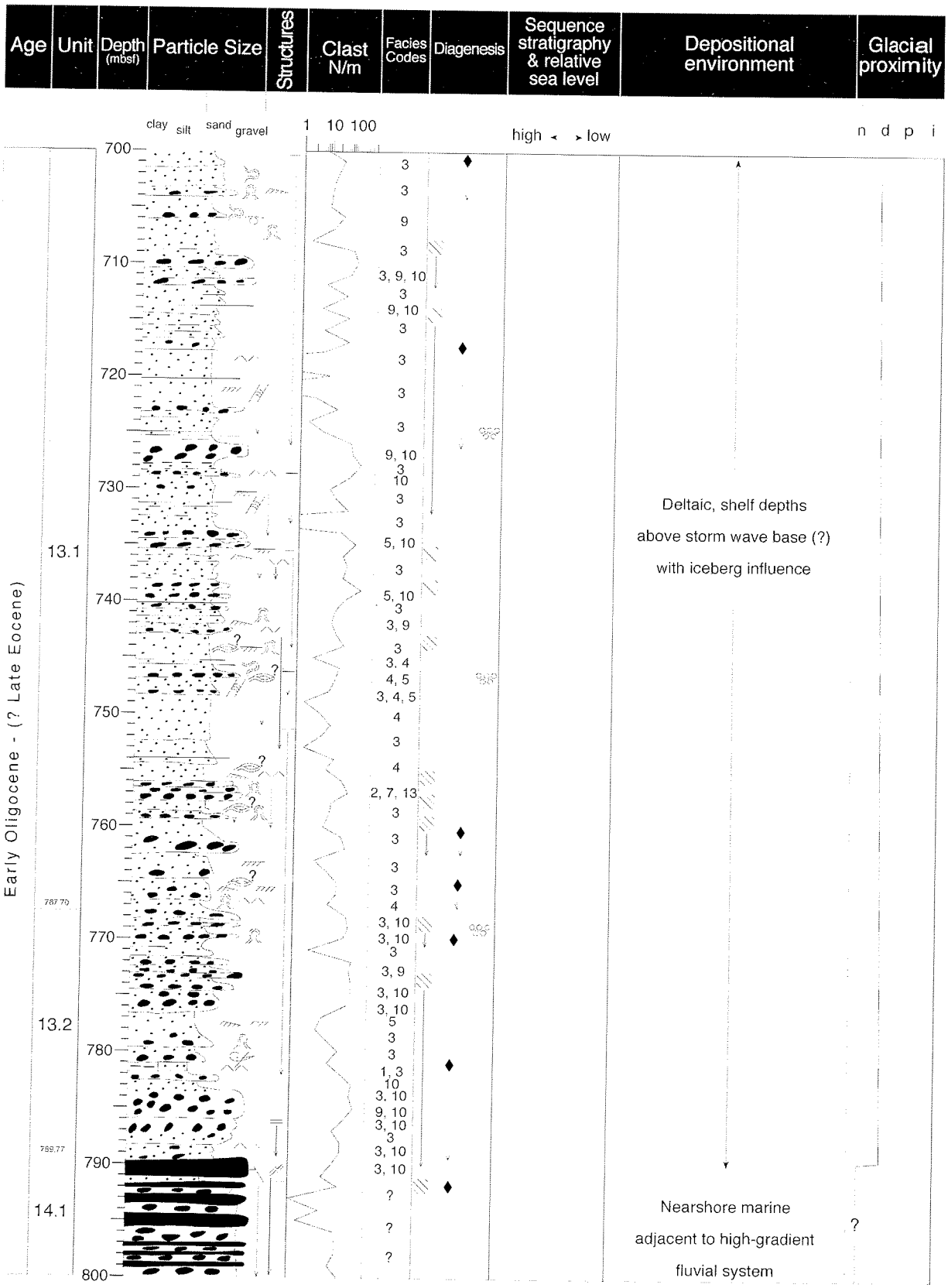
Age
Unit
Depth (mbsf)
Particle Size
Structures
Clast N/m
Facies Codes
Diagenesis
Sequence stratigraphy & relative sea level
Depositional environment
Glacial proximity
clay silt sand gravel
1 10 100
high low
n d p i
Early Oligocene - (? Late Eocene)
13.1
13.2
14.1
787.70
789.77
Deltaic, shelf depths
above storm wave base (?)
with iceberg influence
Nearshore marine
adjacent to high-gradient
fluvial system

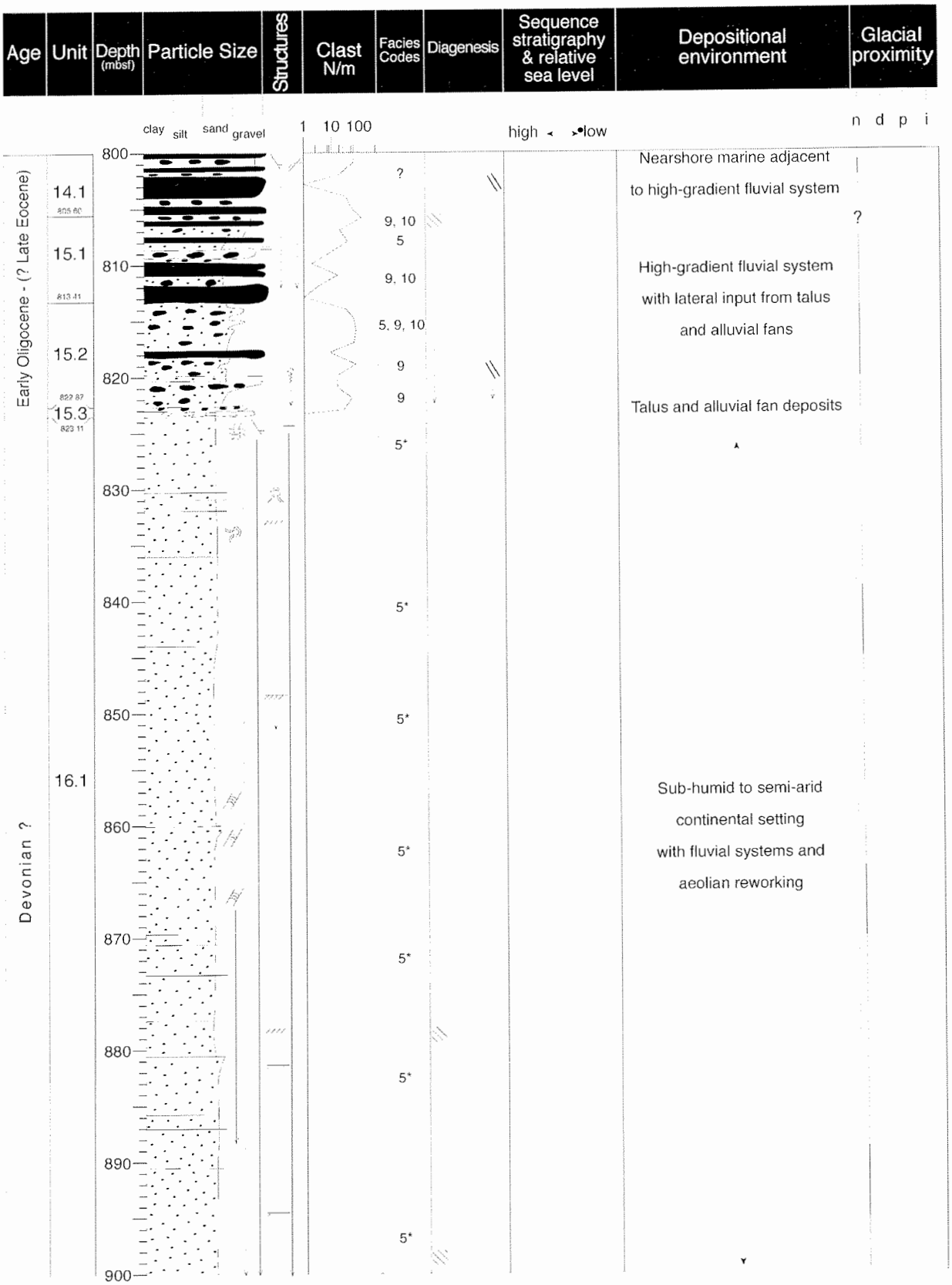
Age
Unit
Depth (mbsf)
Particle Size
Structures
Clast N/m
Facies Codes
Diagenesis
Sequence stratigraphy & relative sea level
Depositional environment
Glacial proximity
clay silt sand gravel
1 10 100
high low
n d p i
Early Oligocene - (? Late Eocene)
Devonian ?
14.1
805.80
15.1
813.41
15.2
822.87
15.3
823.11
16.1
800
810
820
830
840
850
860
870
880
890
900
?
9, 10
5
9, 10
5, 9, 10
9
9
5*
5*
5*
5*
5*
5*
5*
Nearshore marine adjacent to high-gradient fluvial system
High-gradient fluvial system with lateral input from talus and alluvial fans
Talus and alluvial fan deposits
Sub-humid to semi-arid continental setting with fluvial systems and aeolian reworking
?

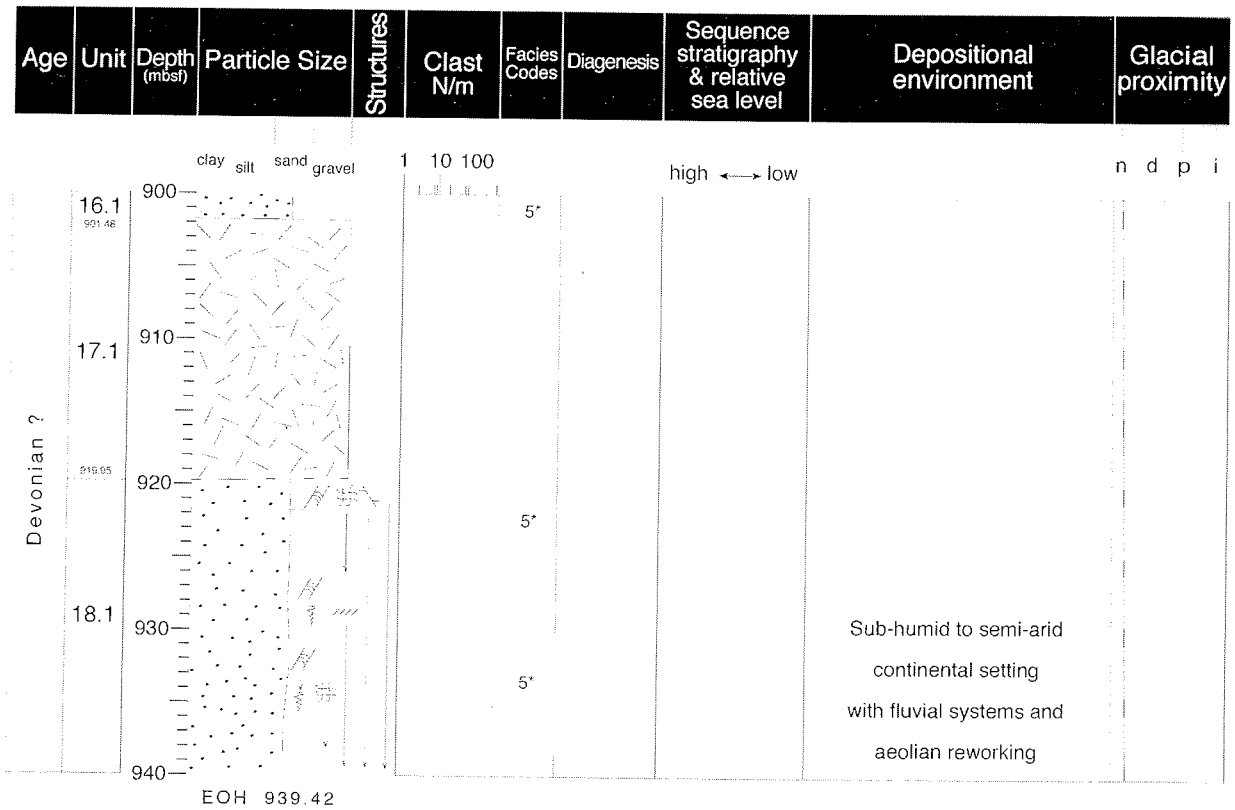
Age
Unit
Depth (mbsf)
Particle Size
Structures
Clast N/m
Facies Codes
Diagenesis
Sequence stratigraphy & relative sea level
Depositional environment
Glacial proximity
clay silt sand gravel
1 10 100
high ←→ low
n d p i
Devonian ?
16.1
991.46
17.1
916.95
18.1
900
910
920
930
940
5*
5*
5*
Sub-humid to semi-arid continental setting with fluvial systems and aeolian reworking
EOH 939.42

Terra Antartica
Initial Report on CRP-3
2000, **7** (1/2)

4 - Petrology

INTRODUCTION

For the initial petrological characterisation of samples from CRP-3, we followed the practices adopted in previous CRP investigations (Cape Roberts Science Team, 1998, 1999). The primary division for investigations was based on grain size, corresponding to clasts (larger than 2 mm in diameter), sand grains and mudrocks. In addition to the down-core distribution of clasts, which were logged for clast type, number and dimensions, separate studies were also carried out on the different lithological clast types, which were subdivided into pre-Devonian basement clasts, sedimentary clasts (probably representing the Beacon Supergroup) and volcanic clasts (Ferrar Supergroup). As well as visual examination, each of the clast groups was described petrographically to better characterise the groups and to confirm macroscopic identifications. Unlike previous studies for the *Initial Reports*, uncovered, unstained thin sections were used to characterise the sand-grain fraction in sandstones. The modal counts, while still qualitative, are believed to be more accurate than those obtained previously using smear slides. Finally, XRD measurements, using an automated diffractometer system, were used to identify the types and distribution of clay minerals in sieved mudrock-fraction splits of fine-sediment samples; these were also separately analysed by XRD for their bulk mineralogy. Together, these methods were used mainly to document the provenance and downhole provenance variations in CRP-3.

DISTRIBUTION OF CLASTS

Petrological and distribution data collected on clasts from CRP-2/2A (Talarico et al., in press) indicated that their downcore modal and compositional variations provide a potential tool for unravelling the complex interplay between tectonic, volcanic and glaciomarine-sedimentary processes during the formation of the Victoria Land Basin and the uplift of the Transantarctic Mountains (TAM) in Cenozoic time. For instance, a pilot frequency analysis (in preparation) on clast population from CRP-2/2A (Sequences 9, 10, and 11) outlined periodicities possibly driven by Milankovitch orbital variations (100 Ka and 21 Ka). These preliminary results pointed to a previously undocumented but significant climatic influence on clast distribution. The CRP-3 clast dataset may potentially enlarge the application of this pilot study to a larger distribution-data population, thus providing further constraints on environmental interpretations.

An investigation of the distribution of clasts in CRP-3 was performed following the same procedure adopted in CRP-2/2A. We logged and counted 27 778 clasts on the basis of both lithology and grain size in the *c.* 823-m-thick Cenozoic section of CRP-3. This study also included sampling and thin-section examination of all lithologies to improve their characterisation (see sections below on Basement, Volcanic and Sedimentary Clasts for further detailed petrographical information).

The total number of clasts per unit length shows major variations from 0-10 counts *per* metre for mud- or sand-rich intervals (*e.g.* LSU 1.3) to >150 counts *per* metre for diamictite units (*e.g.* LSU 2.1) and conglomerate units (*e.g.* LSU 12.3). Sharp variations across lithological boundaries are commonly present, as well as within-unit fluctuations.

We distinguished five main lithological groups. Their main petrographical features and clast dimensions can be summarised as follows:

1) Dolerites s.l.. Generally medium-grained and fresh and common in all units. However, a few scattered occurrences of deeply altered granules and small pebbles were noted in LSU 3.1, 5.1, 6.1, 11.1, 12.4, 13.1 and at the bottom of LSU 15.2. Dolerite clasts show the widest range in size, ranging from granule to boulders as much as 2 m across;
2) Sedimentary rocks. These include at least 4 lithological types (see section on Sedimentary Clasts): quartz-arenites, poorly- to moderately-sorted sandstone, grey to black siltstones, and coal; these clasts mainly belong to the small-pebble class, apart from coal fragments, which mainly occur as granules;
3) Granitoids. These consist mainly of biotite±hornblende monzogranites, with minor occurrence of leucotonalite, mostly represented within the granule class (fragments of quartz and/or pink feldspar crystals, and lithic fragments);
4) Volcanic rocks and sub-volcanic rocks. This group includes very fine-grained dolerite, non-vesicular basalt and amygdale-bearing altered basalt. All of these varieties mainly form granules to small pebbles;
5) Metamorphic rocks. A variety of metamorphic rocks, ranging from basement rocks such as orthogneiss, paragneiss and marble, to low-grade metasedimentary rocks of various origins are represented in this class (see section on Basement Clasts). All of these rock types only occur as small pebbles.

The distribution of these different lithological types is schematically shown in figure 4.1. Both granitoids and dolerites are ubiquitous, with dolerite persistently forming the dominant lithology throughout the core. In contrast, all other lithologies show a more restricted distribution.

Volcanic and very fine-grained dolerite clasts are abundant and persistent in the upper 0-150 mbsf interval, but they form a sparse clast population below 150 mbsf, with dominant amygdale-bearing altered basalts. Further information on the distribution of different volcanic varieties is given in the section on Volcanic Clasts.

Sedimentary clasts show a wider distribution and are significantly more abundant below 150 mbsf. Coal fragments are very rare in the upper 150 m of the cored succession; only one occurrence was detected at 43 mbsf (LSU 1.2). In contrast, coal is persistently present from 159 mbsf downcore, and very abundant, particularly in LSU 7.1 and in the lower

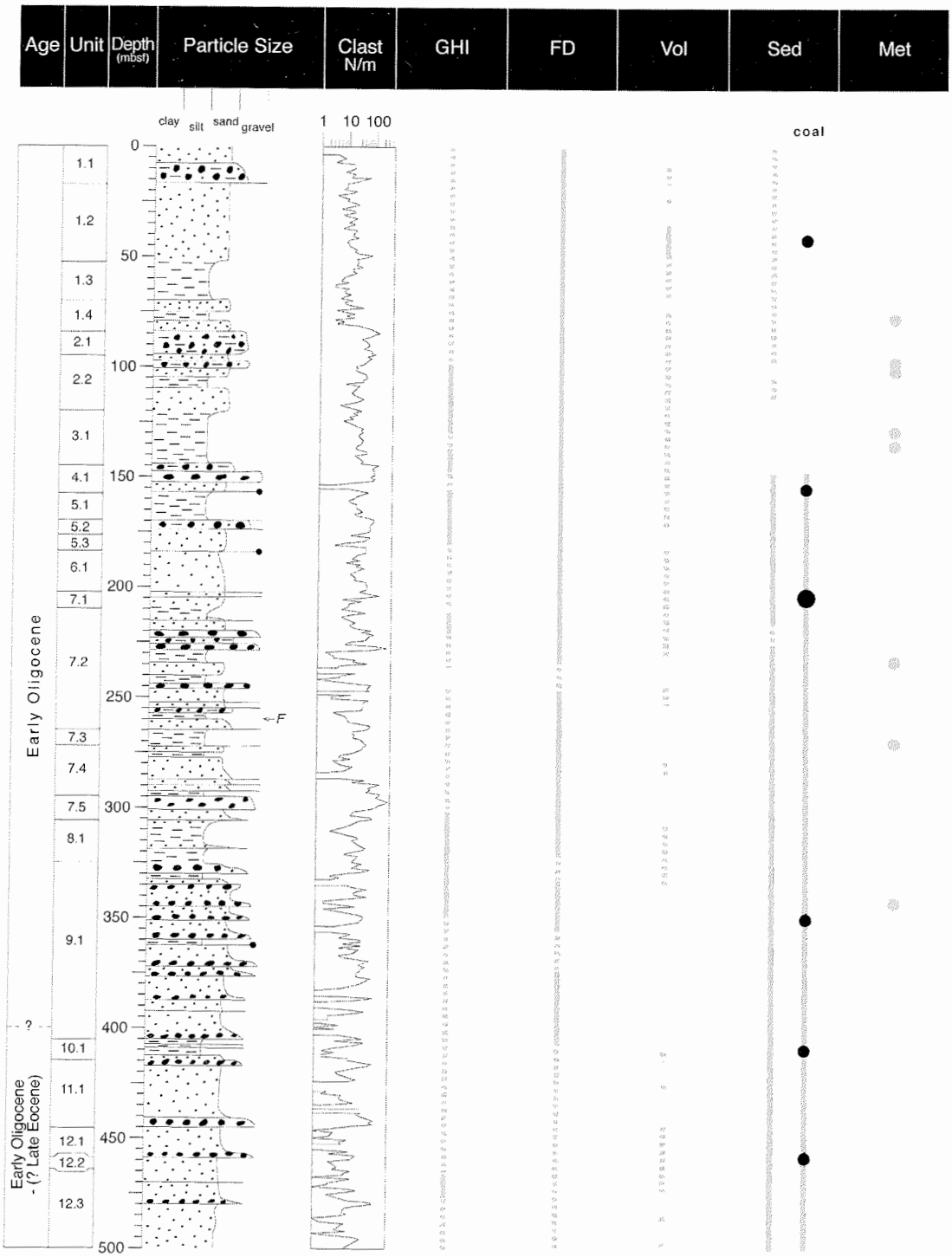

Fig. 4.1 - Distribution of main lithologies occurring as granule to boulder-grade clasts throughout CRP-3 core. Continuous lines indicate abundant (>15-20% total number of clasts) contents and persistent occurrence; dotted lines show intervals characterised by impersistent and/or very low occurrences. Small dots indicate the occurrence of few clasts (1-5); large dots, the occurrence of several clasts (>20).
GHI: granitoids; FD: fine- to medium-grained dolerite; Vol: very fine-grained dolerite and non-vesicular basalts; Sed: sedimentary rocks; Met: metamorphic rocks. See text for further comments and discussion.

part of LSU 12.5.

Metamorphic rocks are definitely the least abundant of all represented lithologies and form scattered occurrences throughout the core (section on Basement Clasts and Fig. 4.2).

The analysis of distribution patterns of clasts allows preliminary provenance inferences and some constraints on the uplift and erosional history of the Transantarctic Mountains. In agreement with conclusions drawn on provenance of clasts from drillcores CRP-1 (Talarico & Sandroni, 1998) and CRP-2/2A (Talarico et al., in press), preliminary petrographical data from CRP-3 confirm a local source, with the Cambro-Ordovician crystalline

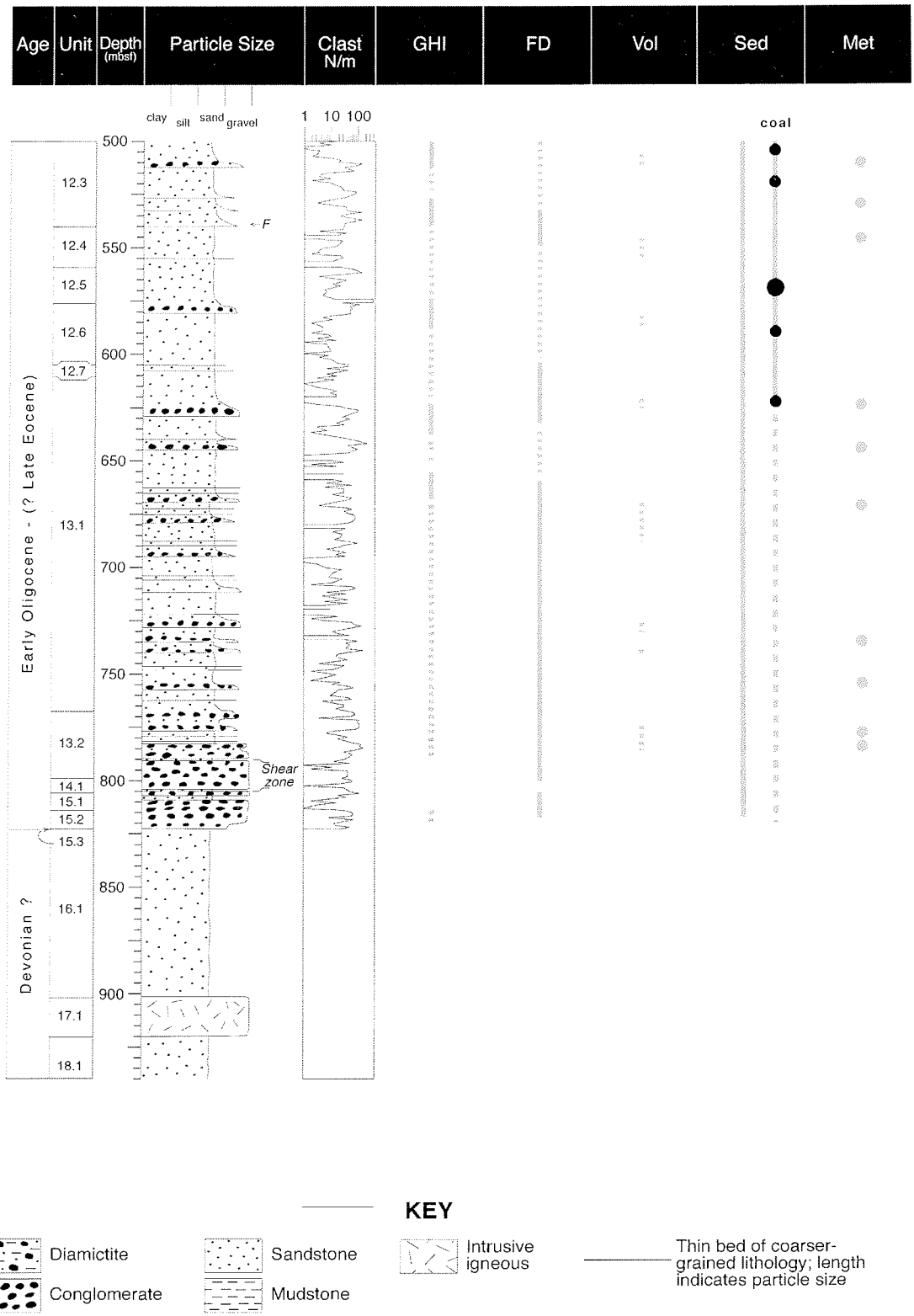

Fig. 4.1 - continued

basement, the Jurassic Ferrar Supergroup intrusive and volcanic suites, and the Devonian to Triassic Beacon Supergroup (Taylor and Victoria groups) acting as the major parent rock-units.

As demonstrated for CRP-2/2A (Talarico et al., in press), the compositional variability of clasts provides clear evidence of an evolving source area that documents stages of the erosional-tectonic evolution of the sector of the Transantarctic Mountains facing the CRP drilling sites. Unroofing of the deeper basement rocks should have occurred after an initial phase of erosion that primarily affected the uppermost part of the basement (near-Kukri peneplain zone) and the overlying cover rocks (the Taylor Group, the Ferrar Dolerite and, subordinately, the Kirkpatrick Basalt).

CRP-3 modal and compositional data indeed echo the same trends detected in the lowermost part of CRP-2/2A, providing another critical tie-boundary at *c.* 150 mbsf (which corresponds to seismic reflector *p*, see section on Correlation of Seismic Reflectors). Similarly to the boundary located at 307 mbsf in CRP-2/2A, the *c.* 150 boundary in CRP-3 points to a relatively rapid provenance change from a lower clast assemblage sourced mainly from the Beacon Supergroup (including the Weller Coal Measures) and the Ferrar Supergroup (including the stratigraphically upper Kirkpatrick Basalt), to an upper clast assemblage mainly derived by Ferrar Supergroup rock units. It is noteworthy that the influx of detritus derived from granitic basement rock units, although impersistent and with variable, generally low proportions, was continuous throughout most of the depositional record, suggesting that the sub-Kukri basement was exposed even in the earliest part of the sedimentary history of western Victoria Land Basin at CRP-3.

BASEMENT CLASTS

As in previous drillholes (MSSTS-1, CIROS-1, CRP-1, CRP-2/2A) on the western edge of the Victoria Land Basin (Hambrey et al., 1989; Cape Roberts Science Team, 1998a, 1998d; Talarico & Sandroni, 1998; Talarico et al., in press), the CRP-3 borehole provides clear evidence of a multi-component source for the supply of granule- to boulder-sized clasts to the Cenozoic sedimentary sequences in the McMurdo Sound. This varied provenance closely mirrors the present-day on-shore geological units of the Transantarctic Mountains in southern Victoria Land, and among these units, those comprising granitoid and amphibolite-facies metasediments of the early Paleozoic Ross Orogen are a major component.

We focus on the preliminary petrographical examination of pre-Devonian basement clasts and clasts of metamorphosed sedimentary rocks within the lower Oligocene-?Late Eocene strata of the CRP-3 drillhole. It includes the description of all clasts belonging to the granule, pebble and cobble grain-size classes, and some inferences concerning the most likely source-rock units. Sampling, macroscopic observations, and preliminary petrographical analyses (polarized-light microscopy) were performed following the same procedures and sample management adopted for CRP-1 and CRP-2/2A (Cape Roberts Science Team, 1998b, 1998c, 1999).

RESULTS

Clast counts in CRP-3 (see section on Distribution of Clasts) indicate that basement clasts are highly variable throughout the cored interval, but basement clasts are systematically less abundant than other lithologies (particularly dolerite and sedimentary rocks). In terms of dimension, finer pebbles (diameters <1 cm) and granules generally prevail over larger-sized clasts, which are very few and unevenly scattered (Fig. 4.2).

Granule-sized debris mainly consist of quartz and lesser feldspar, but pebble-sized clasts offer a significantly wider range of lithological types. The main lithological types can be grouped into two major groups: granitoids and less common metamorphic rocks.

Figure 4.2 shows the lithological range, distribution and position of the different rock types within the lithostratigraphical units identified in the CRP-3 core. Forty samples representative of all lithological types were collected and are listed in table 4.1. The table includes information on the lithology, the most relevant petrographical features (namely, textural, microstructural and alteration data), the most likely source-rock units in the crystalline basement of South Victoria Land, and stratigraphical position.

Granitoid pebbles consist of dominant grey, biotite-bearing monzogranite, pink biotite-hornblende monzogranite and biotite-bearing leucomonzogranite (Fig. 4.3). Minor lithologies include: actinolite-bearing leucotonalite, biotite-muscovite leucogranite, biotite porphryry, foliated biotite leucomonzogranite, and biotite-hornblende microdiorite. Preliminary microscopic examination revealed that all granitoid types show a variably developed low- to very-low-grade metamorphic alteration; allanite, zircon/monazite, apatite and rare tourmaline were found to be the most common accessory minerals in all granitoids.

The group of metamorphic clasts includes both rocks of igneous (namely granitic) derivation (mylonitic biotite with or without garnet orthogneiss, hornblende-bearing biotite orthogneiss) and metasedimentary rocks, including muscovite-tourmaline quartzite, biotite-bearing meta-quartz arenite, biotite±calcite meta-siltstone, biotite-clinoamphibole meta-marl, calcite-clinoamphibole-biotite-metafeldsarenite, graphite-bearing marble, sillimanite-biotite paragneiss, and calcite-biotite schist.

Microscopic examination of selected metamorphic clasts suggests that these rocks reflect a rather wide

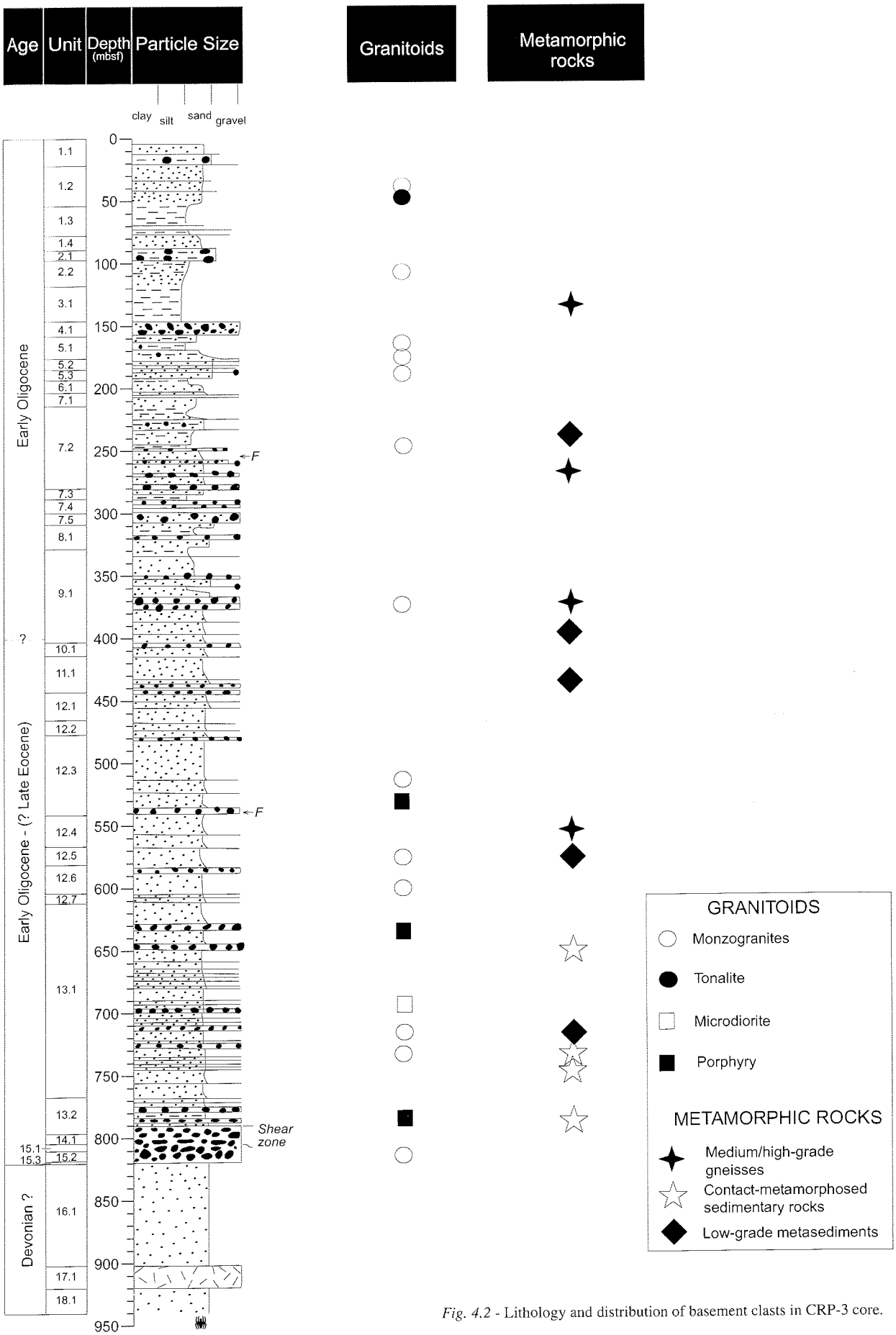

Fig. 4.2 - Lithology and distribution of basement clasts in CRP-3 core.

Tab. 4.1 - Basement clasts in Cenozoic sedimentary strata recovered by CRP-3 drillhole: list of sampled clasts and preliminary petrographical data. Note: lithostratigraphical unit designation follows figure 3B-1 of section on Description of Sequence. Mineral abbreviations according to Kretz (1983). G.H.I.C.: Granite Harbour Igneous Complex; K.G.: Koettlitz Group; B.S.: Beacon Supergroup; S.G.: Skelton Group.

Sample code	Box	Top (mbsf)	Bottom (mbsf)	Lithology	Main petrographical features	Inferred provenance	LU
TAL2	8	30,61	30,63	grey Bt-bearing monzogranite	equigranular (fine-grained), hypidiomorphic	G.H.I.C.	1,2
TAL4	13	43,57	43,58	pink Bt-Hbl bearing monzogranite	equigranular (medium-grained), hypidiomorphic	G.H.I.C.	1,2
TAL5	15	50,25	50,27	Act-bearing leucotonalite	heterogranular (fine- to medium-grained), hypidiomorphic, altered	G.H.I.C.	1,2
TAL11	34	107,32	107,36	Bt-bearing leucomonzogranite	heterogranular (fine- to medium-grained), hypidiomorphic, slightly foliated fabric, strongly altered	G.H.I.C.	2,2
TAL16	42	132,19	132,21	Ms-Tur bearing quartzite	equigranular (fine-grained), subpoligonal granoblastic texture, slightly foliated	K.G.	3,1
TAL22	53	166,18	166,20	mylonitic Grt-Bt leuco-orthogneiss	heterogranular (fine- to medium-grained), gneissic texture (mm-scale compositional layering) with mm-sized feldspar porphyroclasts	K.G.	5,1
TAL23	54	168,73	168,79	Bt-bearing monzogranite	inequigranular (fine- to coarse-grained), hypidiomorphic, slightly altered	G.H.I.C.	5,1
TAL26	57	176,03	176,09	pink Bt-Hbl monzogranite	inequigranular (fine- to coarse-grained), porphyritic, mm-sized feldspar phenocrysts and fine-grained allotriomorphic groundmass	G.H.I.C.	5,2
TAL27	57	178,41	178,44	pink Bt-Hbl monzogranite	equigranular (medium-grained), hypidiomorphic, altered	G.H.I.C.	5,3
TAL36	70	216,98	217,24	grey Bt-bearing leucomonzogranite	inequigranular (fine- to medium-grained), hypidiomorphic, sub-solidus deformational microstructures, altered	G.H.I.C.	7,2
TAL41	74	227,98	228,01	Bt-bearing meta-quartz arenite	equigranular (fine-grained), interlobate granoblastic	B.S.? (contact metamorphosed?)	7,2
TAL42	75	231,78	238,80	mylonitic Bt leuco-orthogneiss	heterogranular (fine- to medium-grained), gneissic texture (mm-scale compositional layering) with mm-sized feldspar porphyroclasts	K.G.	7,2
TAL43	83	256,38	256,40	pink Bt-Hbl monzogranite	inequigranular (fine- to medium-grained), hypidiomorphic, altered	G.H.I.C.	7,2
TAL57	109	335,31	335,35	pink Bt-Hbl monzogranite	inequigranular (fine- to medium-grained), hypidiomorphic, altered	G.H.I.C.	9,1
TAL58	109	337,19	337,23	a) Hbl-bearing Bt orthogneiss; b) Bt-bearing metasiltstone	a) heterogranular (fine- to medium-grained), gneissic texture (mm-scale compositional layering) with ribbon-like quartz aggregates; b) very fine-grained to fine-grained, grain size and compositional layering, Bt and Opm spots	a) K.G. b) B.S.? (contact metamorphosed?)	9,1
TAL59	110	337,57	337,61	Gph-bearing marble	inequigranular (fine- to medium-grained), grain size layering, interlobate granoblastic	K.G.	9,1
TAL62	118	370,24	370,27	grey Bt-bearing granite	equigranular (medium-grained), hypidiomorphic	G.H.I.C.	9,1
TAL75	135	442,79	442,83	Bt-bearing meta-quartz arenite	fine-grained, Bt spots	B.S.? (contact metamorphosed?)	11,1
TAL78	145	482,52	482,54	grey Bt granite	equigranular (medium-grained), hypidiomorphic	G.H.I.C.	12,3
TAL79	146	488,61	488,63	grey Bt granite	equigranular (medium-grained), hypidiomorphic	G.H.I.C.	12,3
TAL82	157	536,60	536,62	red porphyry	mafic and feldspar phenocrysts set within a very fine-grained altered groundmass	G.H.I.C.?	12,3
TAL83	161	554,70	554,76	Sil-Bt paragneiss	fine-grained, compositional layering, granolepidoblastic	K.G.	12,4
TAL84	163	561,54	561,58	black Czo/Ep-Cal-Bt metasiltstone	very fine-grained, compositional layering, interlobate granoblastic	B.S.? (contact metamorphosed?)	12,5
TAL85	163	561,91	561,97	pink Bt monzogranite	equigranular (fine-grained), hypidiomorphic	G.H.I.C.	12,5
TAL92	173	605,77	605,80	Bt-Ms leucogranite	equigranular (fine-grained), hypidiomorphic	G.H.I.C.	12,6
TAL96	179	627,17	627,20	dark grey porphyry	feldspar phenocrysts set within a very fine-grained altered groundmass	G.H.I.C.?	13,1
TAL97	179	628,06	628,08	foliated Bt leucomonzogranite	beterogranular (fine- to medium-grained), gneissic texture with mm-sized feldspar porphyroclasts and quartz ribbons	G.H.I.C.	13,1
TAL98	179	628,69	628,71	Cal-Bt schist	very fine-grained, compositional layering, lepidogranoblastic	S.G.? /B.S.? (contact metamorphosed?)	13,1
TAL99	182	641,50	641,52	Bt-Hbl microdiorite	equigranular (fine-grained), hypidiomorphic/sub-ophitic	G.H.I.C.	13,1
TAL100	182	644,50	644,52	Bt orthogneiss	heterogranular (fine- to medium-grained), interlobate granoblastic and quartz ribbons	G.H.I.C.?/K.G.?	13,1
TAL103	190	675,63	675,65	grey Bt-bearing monzogranite	inequigranular (fine- to medium-grained), hypidiomorphic, sub-solidus deformational microstructures	G.H.I.C.	13,1
TAL109	199	713,29	713,31	Bt-Hbl monzogranite	equigranular (medium-grained), hypidiomorphic, altered	G.H.I.C.	13,1
TAL110	205	734,67	734,71	Leyerd Bt-Cam-Qtz metamarl	very fine- to fine grained, compositional and grain size layering, granoblastic Cal-rich layers, lepidogranoblastic Bt-rich layers	S.G.? /B.S.? (contact metamorphosed?)	13,1
TAL112	206	738,45	738,48	pink Bt-Hbl granite	equigranular (coarse-grained), hypidiomorphic, altered	G.H.I.C.	13,1
TAL113	210	756,16	756,19	Cal-Cam-Bt meta-feldsarenite	very fine-grained, compositional layering, interlobate lepidogranoblastic	S.G.? /B.S.? (contact metamorphosed?)	13,1
TAL118	215	774,96	774,99	Bt meta-sandstone	very fine-grained, compositional layering, interlobate lepidogranoblastic	S.G.? /B.S.? (contact metamorphosed?)	13,2
TAL119	217	781,93	781,97	Bt meta-sandstone	very fine-grained, compositional layering, interlobate lepidogranoblastic	S.G.? /B.S.? (contact metamorphosed?)	13,2
TAL121	218	785,56	785,63	light grey porphyry	feldspar phenocrysts set within a very fine-grained altered groundmass	G.H.I.C.?	13,2
TAL125	225	815,23	815,25	grey Bt granite	equigranular (medium-grained), hypidiomorphic	G.H.I.C.	15,2

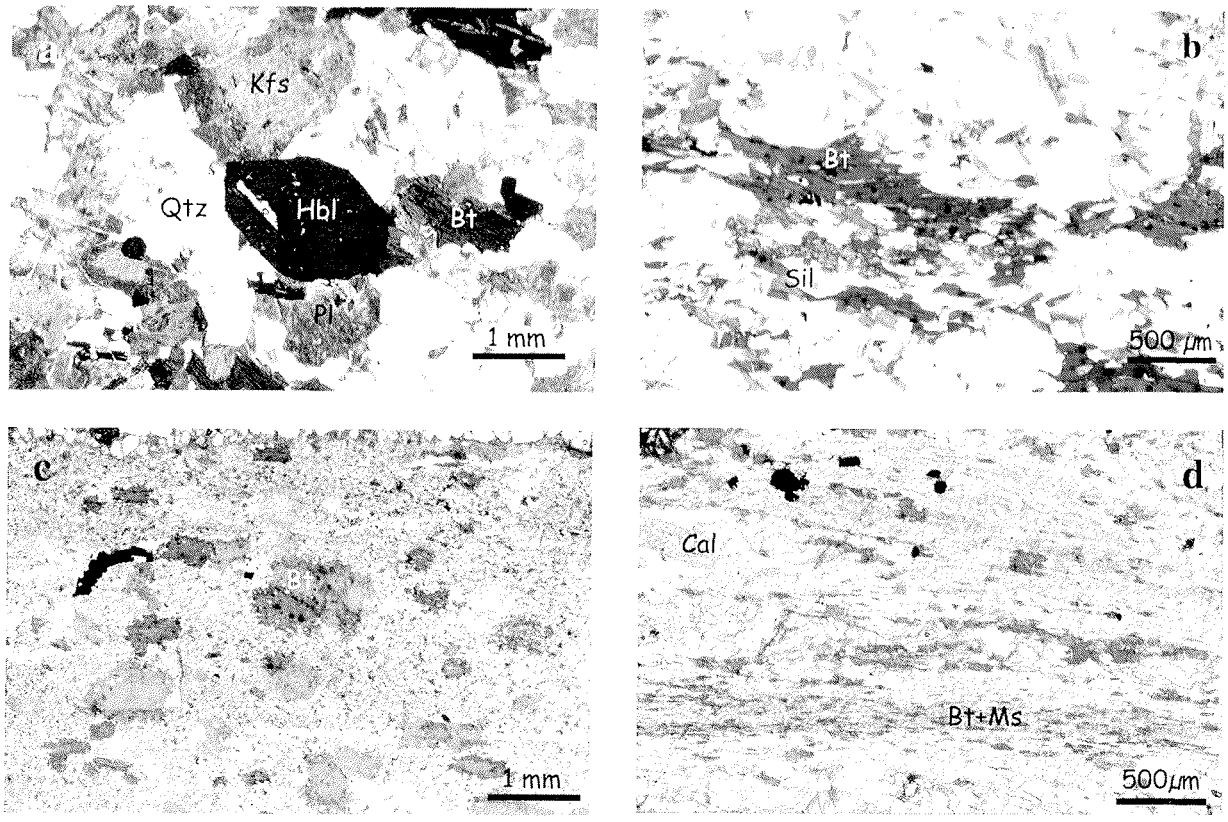

Fig. 4.3 - Photomicrographs of the principal basement rock types in CRP-3 core. a) Pink biotite-hornblende granite (738.45 mbsf), hypidiomorphic texture with altered alkali feldspar (Kfs) phenocrysts, saussuritized plagioclase (Pl), chloritized biotite flakes (Bt) and interstitial quartz (Qtz);b) sillimanite-biotite paragneiss (554.70 mbsf): the foliation is defined by the preferential dimensional orientation of biotite and sillimanite, matrix minerals include K-feldspar, plagioclase and quartz; c) contact-metamorphosed metasiltstone (561.54 mbsf): randomly oriented flakes of biotite indicate a static recrystallization typical of low-grade contact metasedimentary rocks; d) calcite-bearing biotite schist (628.69 mbsf): the foliation is defined by biotite and muscovite fine-grained lepidoblasts.

spectrum of metamorphic conditions. Orthogneisses, sillimanite-biotite paragneiss (Fig. 4.3) and marble show mineral assemblages and microstructures consistent with upper amphibolite-facies regional metamorphic conditions. In contrast, meta-quartz arenite and metasiltstone are characterised by mineral assemblages indicative of biotite-zone (low-grade) conditions, with either decussate, spotted microstructures diagnostic of contact metamorphism, or oriented fabrics indicative of syn-tectonic recrystallizations, most likely related to regional metamorphism (Fig. 4.3).

PROVENANCE

Preliminary petrographical investigations indicate that several basement lithologies were involved as sources of basement clasts in the Cenozoic sedimentary strata recovered in the CRP-3 drillhole. As in CRP-1 and CRP-2/2A (Talarico & Sandroni, 1998; Talarico et al., in press), most of the basement pebbles were supplied by source-rock units belonging to the Cambro-Ordovician Granite Harbour Igneous Complex, which is the dominant component in the local basement (Gunn & Warren, 1962; Allibone et al., 1993a, 1993b). Like CRP-1 and CRP-2/2A, the ubiquitous occurrence of undeformed biotite±hornblende monzogranite pebbles throughout the cored interval apparently reflects the dominance of these lithologies in the onshore basement. Preliminary data concerning the other, less common and impersistent, granitoid varieties are also consistent with a local provenance.

Metamorphic rocks such as biotite-sillimanite paragneiss and biotite-garnet orthogneiss are also known to be a common metasedimentary lithologic type in the amphibolite-facies Koettlitz Group south of Mackay Glacier (Grindley & Warren, 1964; Williams et al., 1971; Findlay et al., 1984; Allibone, 1992; Turnbull et al., 1994). Petrographically similar orthogneiss types were also found in CRP-1 and in CRP-2/2A. CRP-3 is apparently devoid of Ca-silicate rocks, which were found to be relatively common in the two previous CRP drillholes. In contrast, clasts of contact-metamorphosed terrigeneous-sedimentary rocks and of foliated low-grade metasediments are rather abundant, even if scattered throughout the core below *c.* 228 mbsf.

The occurrence of low-grade metasandstone showing

foliated fabrics is notheworthy as the onshore exposures of these rocks are very limited and restricted to areas between the Skelton and Koettlitz Glaciers, about 200 km south of the CRP-3 drillsite (Skelton Group; Grindley & Warren, 1964).

The provenance and primary geological setting of contact-metamorphosed sedimentary rocks remain uncertain. Apart from the thermal-metamorphic overprint, these rocks show a broad lithological and petrographical similarity with comparable rock types occurring in the Beacon Supergroup. In such case, the contact-metamophic overprint could be related to thermal and hydrothermal processes which accompanied the emplacement and cooling of Ferrar Supergroup intrusive and sub-volcanic suites. However, a provenance from presently unknown post-Jurassic (?Paleogene) sedimentary sequences deposited on down-faulted blocks within the Victoria Land Basin cannot be excluded.

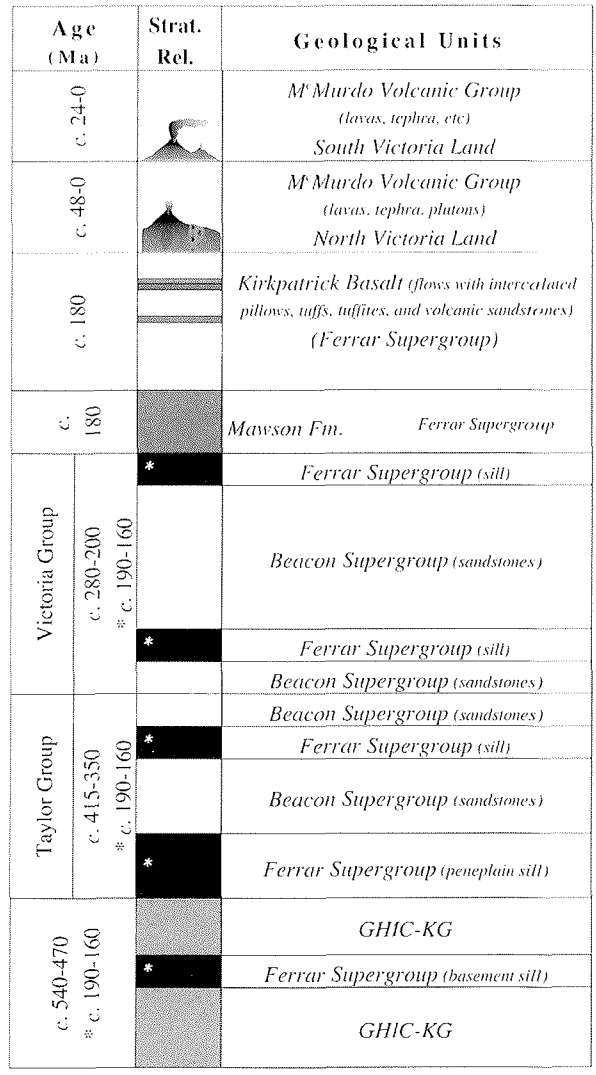

Fig. 4.4 - Schematic stratigraphical relationships for rocks cropping out in southern Victoria Land. Ages from Elliot et al. (1986), Roland & Worner (1996), McIntosh (in press), Turnbull et al. (1994). GHIC: Granite Harbour Igneous Complex, KG: Koettlitz Group.

VOLCANIC CLASTS

METHODS

We studied volcanic material in CRP-3 at two different scales. Volcanic clasts, with sizes ranging from granule to boulder, were investigated by classical petrographical methods, including thin-section examination. Sand to silt fractions were also collected regularly and analysed by means of smear slides for the presence of glass shards, in order to record the volcanic activity coeval with the deposition.

Both coarse- and fine-grained materials were sampled for further geochemical and mineralogical analyses.

VOLCANIC CLASTS

Volcanic clasts are medium- to fine-grained black to grey mafic rocks. Their shape varies from subangular to subrounded. They are generally massive, although vesicular fragments with vesicles filled with secondary minerals are also common. The abundance of vesicular clasts seems to increase downcore.

All the sampled clasts share the same mineral assemblage: major minerals are plagioclase and clinopyroxene, whereas pigeonite, K-feldspar, orthopyroxene and quartz are also found in most of the specimens. Ilmenite and magnetite are ubiquitous accessory minerals. Alteration is significant and affects mainly pyroxenes and the groundmass. Clasts in which the original mineral assemblage is totally replaced by secondary minerals are uncommon.

The above mineral assemblage is known to be typical of the Ferrar Supergroup rocks that display a subalkaline affinity and have a Jurassic age (Elliot et al., 1995; Kyle, 1999). These rocks crop out as sills (Ferrar dolerite), lava flows (Kirkpatrick flows), and pyroclastic deposits (Mawson Formation, Kirkpatrick Basalt pyroclasts) (Fig. 4.4) throughout the Transantarctic Mountains. Consequently, rocks of the Ferrar Supergroup could be the main source of volcanic detritus in CRP-3. Fragments showing a mineral assemblage (olivine, alkali pyroxene or amphibole) typical of the McMurdo volcanic group (McMVG) (Cape Roberts Science Team, 1998b) are not represented in any of the CRP-3 specimens.

Textural and grain-size features observed in thin sections enabled us to divide all the sampled clasts into three groups. Table 4.2 gives a list of the sampled clasts, core depth and group attribution. The number of clasts in each different group does not reflect the relative abundance of these clasts in the core.

Group I consists of medium to fine-grained holocrystalline rocks, with subophitic texture (Fig. 4.5a). Plagioclase is the most abundant phase, forming

subhedral crystals (maximum length = 2 mm); Composition, estimated by optical methods, varies from oligoclase to labradorite. In some crystals, sericite extensively replaces crystals. Augitic clinopyoxene is subordinate and forms subhedral and anhedral crystals (maximum length = 4 mm); in most samples it is largely alterated to smectites. Pigeonite is minor as well and appears associated with clinopyroxene as subhedral crystals. Both rhombohedral and cubic Fe-Ti oxide are present in most samples. Less frequently, only acicular ilmenite crystals with a leucoxene coating are found. In most samples, fine-grained quartzo-feldspathic intergrowths are visible in interstices between plagioclase and pyroxene crystals.

In fine-grained clasts plagioclase is euhedral, pyroxenes tend to be acicular and a very fine-grained cryptocrystalline matrix is quite often deeply altered to sericite and clay minerals.

Group II is made-up of medium- to fine-grained hypocrystalline rocks with textures varying from intergranular to intersertal (Fig. 4.5b). We can consider these rocks aphyric, since crystals sizes are almost constant. Plagioclase is the most abundant phase and forms a complex network of acicular crystals with pyroxene. The composition of plagioclase ranges from oligoclase to labradorite. Clinopyroxene crystals are rarely preserved, being frequently transformed to smectite. Sometimes relics of the original clinopyroxene are preserved only at the core of the large prismatic crystals. Pigeonite is rare, while orthopyroxene occurs as single-prismatic, euhedral crystals. Anhedral quartz is present as discontinuous segregations. The interstitial material ranges from very fine-grained cryptocrystalline matrix, in which Fe-Ti oxides and pyroxene microlites replaced by smectites are barely recognisable, to a very rare, palagonitised brown glass that embodies tiny plagioclase and pyroxene aggregates. Group II clasts are generally non-vesicular, even though we detected some irregularly shaped vesicles filled by secondary minerals (carbonate, chalcedony, cristobalite, zeolites).

Group III includes aphyric and weakly porphyritic clasts, generally hypocrystalline with rare holohyaline terms. These rocks show a low vesicularity, even though in some specimens amygdales filled with secondary minerals form as much as 30% of the rocks (Fig. 4.5c). In these clasts we observed few hypidiomorphic andesine to labradoritic plagioclase and augitic clinopyroxene phenocrysts. Sometimes anhedral quartz forms discontinuous segregations (*c.* 1 mm across), but more than 90% of the rock comprises a quenched matrix (Fig.4.5d) consisting of acicular crystals of plagioclase and feathery microlites of clinopyroxene. These are arranged as a felt-like network, whose interstices are occupied by blocky Fe-Ti oxides, cryptocrystalline clay-altered material, and more rarely, brown palagonitic glass. In the more vesiculated, scoriaceous clasts, portions with clear brown glass without microlites become predominant.

Tab. 4.2 - Main textural characters, sizes and group attribution of volcanic clasts in CRP-3.

Depth (mbsf)	Clast size (cm)	Crystallinity - Texture	Grain size	Group
5,93	nd	holocrystalline, subophitic	medium	I
6,66	nd	holocrystalline, subophitic	medium-fine	I
9,44	nd	holocrystalline, subophitic	medium-fine	I
33,60	8	holocrystalline, subophitic	medium-fine	I
42,70	nd	holocrystalline, subophitic	medium-fine	I
47,46	nd	holocrystalline, subophitic	medium-fine	I
70,09	2	holocrystalline, subophitic	medium	I
73,86	1	hypocrystalline, variolitic	very fine	III
73,90	1	hypocrystalline, intersertal	fine	II
91,18	>4	holocrystalline, subophitic	fine	I
105,39	1,5	hypocrystalline, variolitic	very fine	III
149,70	3,5	hypocrystalline, intersertal	fine	II
150,08	0,5	hypocrystalline, intergranular	medium	II
151,43	3	hypocrystalline, variolitic	very fine	III
163,26	>2	glassy, amygdaloid, palagonitic		III
165,91	1,5	holocrystalline, subophitic	medium	I
178,77	2,5	hypocrystalline, intersertal	fine	II
178,79	1,5	hypocrystalline, intergranular	fine	II
182,26	<1	hypocrystalline, intergranular	fine	II
183,91	4	hypocrystalline, intergranular	fine	II
184,34	4	hypocrystalline, intersertal	fine	II
208,88	<.5	hypocrystalline, intergranular	medium	II
235,97	2	hypocrystalline, intergranular	medium	II
248,70	1,5	holocrystalline, subophitic	fine	I
251,52	1,5	holocrystalline, subophitic, altered	fine	I
263,11	15	holocrystalline, subophitic	fine	I
264,34	1,5	holocrystalline, subophitic	medium-fine	I
292,04	>3	holocrystalline, subophitic	medium-fine	I
306,59	1	glassy, amygdaloid, palagonitic		III
307,91	>3	hypocrystalline, intergranular	medium	II
313,96	>4	hypocrystalline, intergranular	medium	II
328,40	nd	holocrystalline, subophitic, altered	fine	I
337,34	nd	holocrystalline, subophitic	fine	I
344,61	4	holocrystalline, subophitic, altered	medium-fine	I
369,91	<1	holocrystalline, subophitic	medium	I
370,18	2	hypocristalline, hyalopilitic	very fine	III
372,50	>4	hypocrystalline, intergranular	fine	II
375,76	>4	holocrystalline, subophitic	medium	I
377,46	<1	holocrystalline, subophitic	medium-fine	I
377,70	>5	holocrystalline, subophitic	medium-fine	I
386,83	<1	hypocrystalline, intergranular	medium	II
387,05	4	hypocrystalline, intergranular	medium	II
414,15	1,5	hypocrystalline, variolitic, amygdaloid	very fine	III
415,43	1,5	holocrystalline, subophitic	medium-fine	I
423,32	1	holocrystalline, subophitic	fine	I
439,23	<1	holocrystalline, subophitic	medium	I
441,85	1,5	hypocrystalline, variolitic	very fine	III
450,49	4,5	hypocrystalline, intergranular	fine	II
462,76	0,6	holocrystalline, subophitic	fine	I
464,71	2,5	hypocrystalline, intergranular, vesicular	medium	II
469,24	4	hypocrystalline, variolitic, amygdaloid	very fine	III
479,03	<1.5	hypocrystalline, intergranular	fine	II
480,55	1	glassy, palagonitic		III
495,46	3	holocrystalline, subophitic	medium	I
516,71	4	hypocrystalline, intergranular	fine	II
544,37	4	hypocristalline, hyalopilitic	very fine	III
548,30	1	holocrystalline, subophitic	medium-fine	I
562,13	2	hypocrystalline, variolitic, amygdaloid	very fine	III
568,26	1,5	hypocrystalline, variolitic, amygdaloid	very fine	III
570,54	2,5	glassy, palagonitic		III
578,16	2	holocrystalline, subophitic	fine	I
580,34	<1	hypocrystalline, variolitic, amygdaloid	very fine	III
593,28	2	holocrystalline, subophitic	medium	I
605,33	1	holocrystalline, subophitic	fine	I
625,08	2	hypocrystalline, intergranular, vesicular	fine	II
627,11	>4	hypocrystalline, variolitic	very fine	III
635,89	2	hypocrystalline, intergranular	fine	II
653,66	1,5	glassy, amygdaloid		III
665,09	1,5	holocrystalline, subophitic	medium	I
671,44	2	holocrystalline, subophitic	fine	I
683,64	1,5	holocrystalline, subophitic	medium	I
690,40	3,5	glassy, amygdaloid, palagonitic		III
727,61	3	hypocrystalline,intersertal, vesicular	fine	II
735,01	1,5	hypocrystalline,intersertal, vesicular	fine	II
738,71	1	holocrystalline, subophitic	fine	I
769,30	3	holocrystalline, subophitic	fine	I
788,20	>4	holocrystalline, subophitic	fine	I
789,59	2,5	hypocrystalline, intersertal	fine	II

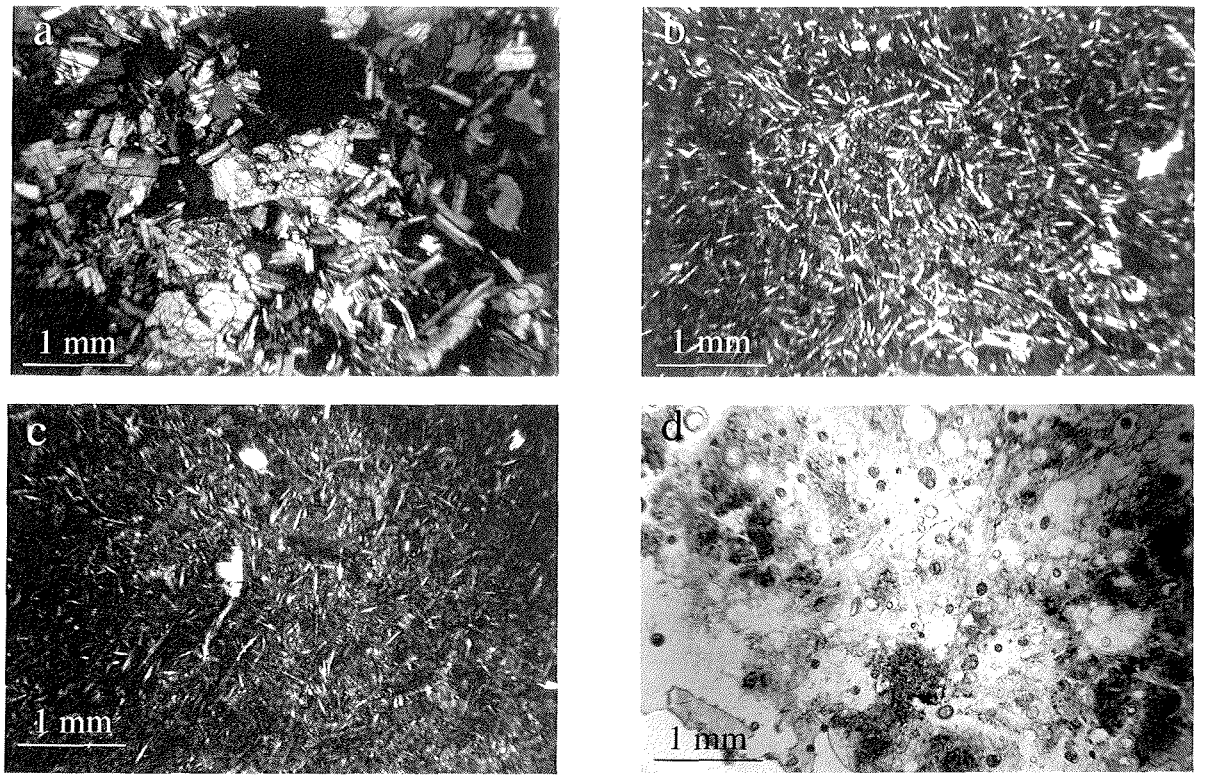

Fig. 4.5 - Photomicrograph of CRP-3 selected clasts; *a)* medium-grained group I clast with subophitic texture; *b)* medium-grained group II clast showing acicular plagioclase and clinopyroxene and intergranular texture; *c)* amygdaloid texture in a vesicular glassy clast of group III; *d)* plagioclase phenocryst and quenched crystals in a clast from group III.

PRELIMINARY CONCLUSIONS ON VOLCANIC-CLAST PROVENANCE

The above textural differences are related to cooling rate and perhaps to different emplacement mechanisms. Subophitic textures are typical of intrusive magmatic bodies as sills, but may be found as well in the inner portions of thick lava flows that undergo a very slow cooling. Intersertal to intergranular textures, with a variable abundance of interstitial glass, are quite common in lava flows or can be found in the external portions of dykes and sills. Glass-rich volcanics and quenched crystals indicate a high cooling rate, such as for those associated with magma chilled by contact with water or country rocks.

Hence, we can use textural characteristics of the clasts to infer their possible relationship with Ferrar Supergroup outcrops on land. As a matter of fact, clasts of group I showing subophitic textures should have been derived by the erosion of Ferrar sills that intrude the basement and Beacon sedimentary cover at different levels (Fig. 4.4).

Clasts of group II could represent the external part of these sills, but more probably they are eroded fragments of the Kirkpatrick lava flows. It is worth noting the close correspondence among some CRP-3 clasts, that show distinctive single orthopyroxene crystals, and the Mount Fazio Chemical Type (MFCT) lavas described in Mesa Range by Elliot et al. (1995), that display this similar but unusual character. The MFCT lavas are thought to occur in the lower part of the Kirkpatrick volcanic succession.

Clasts of group III possibly derive from the external portions of the Kirkpatrick lava flows. Features observed in the least vesicular clasts belonging to this group seem to match those of Scarab Peak chemical type rocks (SPCT) that, following Elliot et al. (1995), cap the Kirkpatrick succession in the Mesa Range area. Alternatively, glassy portions could be pillow-lavas fragments derived from the middle part of the Kirkpatrick group (discrete horizons between lava flows; Roland & Worner, 1996). Finally, the glassy scoriaceous clasts may be derived from pyroclastic or volcanoclastic deposits that form the lower part of the Kirkpatrick succession (Fig. 4.4, Kirkpatrick Basalt pyroclasts, Mawson and Exposure Hill Formations) (Elliot et al., 1986).

GLASS SHARDS

A very small number of volcanic glass shards was detected in smear slides of most of the sand-silt fractions of CRP-3 (Tab. 4.3). They are very scant (maximum of 10 shard per smear slide), display angular to subangular shapes and have sizes ranging from 30 to 200 μm. Small grain size, flake-like shapes and very low abundance impede easy recognition and an accurate evaluation of

modal abundance in thin sections (see section on Sand Mineralogy).

The more abundant type is brown to light brown glass (sideromelane); colourless and light-green (evolved?) varieties are less common. Most of them appear to be fresh; palagonite and clay-mineral alteration are uncommon. Some glass shards embody small opaque grains (Fe-Ti oxides?) or feldspar fragments, whereas vesicles are rare.

On the whole, glass fragments found in CRP-3 show petrographical features similar to those found in CRP 2-2/A, where lapilli and glass shards, with alkaline compositions typical of M^{c}MVG rocks, were found above 320 mbsf. However, size and abundance of glass fragments at CRP-3 are significantly different from those of the upper portion of CRP2/2A: these instead match the pattern found in the lower section of the same site (below 320 mbsf), where glass shards are almost absent and magmatic affinities are still undefined. Nevertheless, since the compositional data, which remain the critical discriminating factor to indirectly infer the age of the volcanism, are not available for CRP-3 glass shards, hypotheses on their origin could still be formulated on the basis of textures, size, and abundance. The small size of the glass shards and their scarcity indicate a distant source, whatever their origin. If the shards are a distal air-fall deposit, the alkaline volcanism, active in northern Victoria Land since 48 Ma (Tonarini et al., 1997), can be postulated as a possible source. Conversely, since shards show low or no vesiculation and their outlines seem mainly controlled by fracture surfaces rather than by broken bubble walls, an origin by fragmentation processes driven by a violent water/ice-magma interaction can alternatively be inferred. In this case glass shards may indicate volcanic activity coeval with deposition in which external water is involved (subglacial eruptions?) or may represent erosion and reworking of older phreatomagmatic deposits interlayered with the Kirkpatrick succession (Elliot et al., 1986).

SEDIMENTARY CLASTS

We present here a preliminary petrographical investigation on selected sedimentary-clast samples from CRP-3. In terms of grain size, all specimens studied belong to the pebble group. They can vary from rounded to subangular. We recognised six principal lithological categories: quartzarenite, feldspathic arenite, feldspathic wacke, siltstone, claystone and coal clasts. The majority of the clasts belong to the quartzo-feldispatic group. The main petrographical features are summarized as follows:

1) Quartzarenites. These consist of moderately sorted sandstone. Quartz grains vary from coarse to medium in size and from rounded to well rounded in shape. Grains are compositionally represented mainly by quartz, some of which have small inclusions; minor components are fine-grained fragments of altered plagioclase, potassium feldspar, and metamorphic-rock fragments. The cement around the detrital quartz grains consists of a well developed phase of authigenic quartz overgrowth, with the grain surface often marked by a thin layer of inclusions (probably iron oxides). Locally, some interstitial clay/silt matrix is present, mainly mica derived from plagioclase alteration.
2) Feldspathic arenites. These consist of very poorly sorted sandstone. Grains vary in size from fine to medium and from angular to subrounded in shape. The clay component is dispersed throughout the matrix, together with silt particles. Grains are dominantly represented by quartz; other components are potassium feldspar and plagioclase (altered in carbonate and micas). Lithic fragments of dolerite and basement rocks are common. Both biotite and muscovite flakes are present and show deformation and kink structures. Intergrowths of chlorite and muscovite in the form of rosette-shaped clusters of plate-like crystals (possibly from the alteration of plagioclase) are present in some specimens, either attached to detrital quartz grains or as growths in the pore voids.
3) Felspathic wackes. These consist of very poorly sorted sandstone. Grains vary in size from fine to very fine and from angular to very angular in shape. Grains are dominantly represented by quartz; other components are potassium feldspar and plagioclase (often altered to carbonate and micas). Lithic fragments of dolerite and basement rocks are also present. The matrix is represented by abundant clay components, which in cases can become dominant in percentage. Silt particles are also common.
4) Siltstones. These are represented by dominant silt-sized grains, mainly subangular to angular in shape and within a clay matrix. Quartz and plagioclase grains are also present, ranging in size from fine- to very fine-grained. Plagioclase grains show a variable degree of alteration to mica. Metamorphic rock fragments may also be present.
5) Claystones. These are represented by an unresolvable clay matrix. The sand- and silt-sized detrital component is characterized by quartz grains (from very fine to medium size) and rare plagioclase grains, many of which show a diffuse alteration to micas and carbonate. In some, cases a thin isopachous carbonate rim surrounds the quartz grains.
6) Coal fragments. These can vary in size from granules to pebbles and, in shape, from subrounded to angular. The majority of the specimens have a detrital origin, but a few have a flakey appearance. At the macroscopic level they appear to still be unlithified, suggesting an *in-situ* coalification process at a shallow burial depth. The detrital coal clasts commonly show an amorphous microstructure; in some cases, microfractures and cracks (possibly induced by dessication or compression) filled by clay components are present. Detrital components

Tab. 4.3 - Occurrence and estimated abundance of glass shards in CRP-3.

Depth (mbsf)	LSU	Grain size	Abundance	Type	Dim. (mm)
3,00	1,1	diamictite	x	brown	0,10
6,00	1,1	diamictite	xx	brown	0,20
9,40	1,1	diamictite	x	brown	0,05
9,86	1,1	diamictite	x	brown	0,06
16,10	1,1	diamictite	xx	brown	0,20
16,75	1,2	muddy sandstone	x	brown	0,05
32,55	1,2	muddy sandstone	x	brown	0,05
33,14	1,2	muddy sandstone	x	brown	0,15
49,40	1,2	muddy sandstone	x	brown	0,05
155,45	4,1	fine sandstone	x	brown	0,15
155,55	4,1	fine sandstone	x	brown	0,05
155,91	4,1	fine sandstone	r-?	brown	
155,93	4,1	fine sandstone	x	brown	0,05
157,79	5,1	sandy siltstone	a		
172,96	5,2	muddy sandy pebble conglomerate	r-?	brown	
177,17	5,3	medium sandstone	r-?	brown	
179,39	5,3	sandy siltstone and very fine and fine sandstone	x	brown	0,05
181,28	5,3	sandy siltstone and very fine and fine sandstone	x	brown	0,05
185,13	6,1	muddy fine grained sandstone	x	brown, green	0,07
187,05	6,1	muddy fine grained sandstone	a		
187,07	6,1	muddy fine grained sandstone	a		
189,21	6,1	siltstone	a		
189,21	6,1	siltstone	a		
190,17	6,1	muddy very fine sandstone	xx	colourless, brown	0,10
190,33	6,1	muddy very fine sandstone	x	brown	0,07
192,84	6,1	muddy very fine sandstone	xx	colourless, brown	0,10
193,97	6,1	muddy very fine sandstone	r-?	brown	
195,84	6,1	muddy very fine sandstone	x	colourless	0,10
196,04	6,1	muddy very fine sandstone	a		
200,71	6,1	muddy very fine sandstone	a		
201,13	6,1	muddy very fine sandstone	a		
201,97	6,1	muddy very fine sandstone	a		
230,00	7,2	fine sandstone	x	brown	0,05
234,67	7,2	medium sandstone	x	brown	0,05
239,19	7,2	medium sandstone	x	brown	0,05
242,30	7,2	siltstone	x	brown	0,05
289,99	7,4	pebble boulder conglomerate	x	brown	0,05
310,50	8,1	muddy fine sandstone	x	brown	0,05
311,00	8,1	muddy fine sandstone	x	brown	0,05
320,60	8,1	sandy siltstone	r-?	brown, colourless	
321,50	8,1	sandy siltstone	xx	brown, colourless	0,05
333,22	9,1	sandstone fine	x	brown	0,05
364,10	9,1	medium to fine sandstone	a		
373,84	9,1	medium to fine sandstone	xx	brown, colourless	0,30
384,70	9,1	medium to fine sandstone	x	brown	0,10
385,30	9,1	medium to fine sandstone	a	brown	
391,00	9,1	medium to fine sandstone	r-?	brown	
398,50	9,1	medium to fine sandstone	a		
401,84	9,1	medium to fine sandstone	r-?	colourless	
405,80	9,1	medium to fine sandstone	r-?	colourless, green	
406,23	10,1	sandy siltstone	x	colourless, brown	0,05
408,65	10,1	sandy siltstone	x	colourless, brown	0,05
413,07	10,1	siltstone	xx	brown, green	0,10
419,90	11,1	medium to fine sandstone	n		
423,21	11,1	medium to fine sandstone	n		
423,26	11,1	medium to fine sandstone	r-?	green	
428,80	11,1	coarse to fine sandstone	r-?	brown, colourless	
436,06	11,1	coarse to fine sandstone	x	brown	0,10
439,90	11,1	medium sandstone	r-?	brown, green	
440,26	11,1	medium sandstone	x	brown	0,10
443,03	11,1	pebble to cobble conglomerate	x	brown, ligth, green	0,05
475,77	12,3	fine sandstone	a		
480,51	12,3	muddy sandstone fine to coarse	a		
480,67	12,3	muddy sandstone fine to coarse	x	brown	0,05
480,72	12,3	muddy sandstone fine to coarse	a		
481,13	12,3	muddy sandstone fine to coarse	r-?	brown	
481,70	12,3	fine to coarse sandstone	a		
483,78	12,3	fine to coarse sandstone	a		
486,03	12,3	fine to coarse sandstone	x	brown	0,10
489,75	12,3	fine to coarse sandstone	a		

a: absent, r-?: very rare or dubious, x: <5 per smear slide, xx:>5 per smear slide

Grain size as reported in core log

Tab. 4.3 - Continued

Depth (mbsf)	LSU	Grain size	Abundance	Type	Dim. (mm)
490.50	12.3	fine to coarse sandstone	a		
500.80	12.3	sandstone	r-?	brown	
501.00	12.3	sandstone	r-?	colourless, vesicular	
510.10	12.3	fine to medium sandstone	a		
518.20	12.3	fine to medium sandstone	a		
522.99	12.3	muddy sandstone very fine	x	brown, colurless	0.05
527.09	12.3	very fine sandstone	r-?	brown	
539.70	12.4	pebbly medium grained sandstone	r-?	brown	
543.00	12.4	fine sandstone	xx	brown	0.10
543.01	12.4	fine sandstone	a		
544.05	12.4	fine sandstone	a		
544.71	12.4	fine sandstone	a		
546.98	12.4	fine sandstone	a		
550.95	12.4	fine sandstone	x	light brown	0.05
554.60	12.4	fine sandstone	a		
560.22	12.5	sandstone	a		
560.60	12.5	sandstone	a	brown, vesicular	
561.60	12.5	sandstone	a		
569.42	12.5	sandstone	a		
581.82	12.6	sandstone	x	brown	0.05
581.98	12.6	sandstone	x	brown	0.05
585.75	12.6	sandstone	a		
590.00	12.6	sandstone	a		
596.74	12.6	sandstone	x	brown	0.04
601.53	12.6	sandstone	x	brown	0.05
606.10	12.7	sandstone	a		
609.52	12.7	sandstone	a		
612.40	13.1	sandstone	r-?	brown	
617.60	13.1	sandstone	a		
619.93	13.1	sandstone	r-?	brown	
620.43	13.1	sandstone	r-?	dark brown	
625.14	13.1	sandstone	r-?	dark brown	
629.24	13.1	sandstone	a		
631.81	13.1	sandstone	a		
634.72	13.1	sandstone	r-?	brown	
638.23	13.1	sandstone	a		
638.30	13.1	sandstone	a		
642.08	13.1	sandstone	a		
644.03	13.1	sandstone	r-?	colourless	
647.77	13.1	sandstone	a		
654.80	13.1	sandstone	x	light-brown	0.05
655.30	13.1	sandstone	r-?	brown	
658.47	13.1	sandstone	a		
658.90	13.1	sandstone	r-?	brown, palagonitic	
666.03	13.1	sandstone	xx	brown	0.05
666.50	13.1	sandstone	x	brown, green	0.05
677.67	13.1	sandstone	a		
683.86	13.1	sandstone	a		
691.11	13.1	sandstone	x	brown, colourless	0.05
692.73	13.1	sandstone	a		
696.38	13.1	sandstone	x	light brown	0.05
701.12	13.1	sandstone	a		
702.48	13.1	sandstone	a		
704.83	13.1	sandstone	r-?	brown	
706.98	13.1	sandstone	x	brown	0.05
710.65	13.1	sandstone	x	brown, green	0.03
715.03	13.1	sandstone	a		
717.41	13.1	sandstone	r-?	brown, ligth brown	
720.97	13.1	sandstone	a		
725.46	13.1	sandstone	a		
731.28	13.1	sandstone	a		
733.67	13.1	sandstone	a		
735.32	13.1	sandstone	xx	brown, palagonitic	0.10
735.61	13.1	sandstone	xx	brown	0.05
737.05	13.1	sandstone	a		
743.03	13.1	sandstone	r-?	brown	
744.06	13.1	sandstone	a		
752.29	13.1	sandstone	r-?	brown	
752.44	13.1	sandstone	x	colourless, vesicular	0.05
756.00	13.1	sandstone	x	brown	0.10

(mainly quartz) in the silt and very fine sand-size range are scattered through the compacted organic matter.

At the time of this writing and on the basis of the lithological characterization of the sedimentary clasts from CRP-3, we can conclude that quartzarenite, siltstone and coal clasts are likely derived from various formations of the Beacon Supergroup that crop out in the Transantarctic Montains, where all these described lithologies are well represented. The feldspathic arenites and wackes are presumed, on account of the dolerite fragments that they contain to have been eroded from older Cenozoic strata on the maring of the Victoria Land Basin.

X-RAY MINERALOGY

SEDIMENT BULK MINERALOGY

In order to generally characterize the bulk mineralogy of the sediments overlying "basement" in CRP-3, we analyzed 30 "fast-track" samples using a Rigaku Miniflex+ x-ray diffraction (XRD) system at the Crary Science and Engineering Center (CSEC). Two samples from the intrusion within "basement" also were analyzed, but those results are discussed separately below. The materials were analyzed, and the diffraction patterns were processed with JADE 3+ software, using procedures described in the CRP-1 *Initial Report* (Cape Roberts Science Team, 1998, p. 84-85).

Sample locations and the minerals identified in each sample are listed in table 4.4. Quartz is the dominant phase in each sediment sample, with feldspars (plagioclases and lesser amounts of K-feldspars) present in most samples. Illite is present in most samples above *c.* 143 mbsf, and a variety of clay minerals (including mixed-layer clays and smectite) is present below *c.* 620 mbsf. Other minerals show low-intensity peaks on the XRD patterns, suggesting low abundances, and occur in only one or a few samples; these include augite, which is a detrital phase, pyrite, which is a diagenetic product, and analcime, which is identified with less confidence and may be a product of *in situ* alteration.

The data generated by these analyses cannot be used quantitatively to determine the abundances of the various minerals present. However, comparing the intensities of two XRD peaks (one chosen for each mineral of interest) can provide a useful qualitative indicator of variations in the relative abundances of those two phases through a stratigraphical section. The same peak area ratios have been calculated for CRP-3 samples as were used to determine total feldspar/quartz and K-feldspar/quartz ratios for the CRP-1 and CRP-2/2A *Initial Reports* (Cape Roberts Science Team, 1998, p. 84-85). The resulting stratigraphical profiles of feldspar/quartz and K-feldspar/quartz peak-intensity ratios are shown in figures 4.6 and 4.7, respectively.

The feldspar/quartz ratio profile (Fig. 4.6) shows relatively high values in the upper portion of the section (above *c.* 140 mbsf), generally low but variable values from *c.* 140 to *c.* 600 mbsf (with a single-point peak at *c.* 400 mbsf), and an increase to more consistent values below 600 mbsf. The K-feldspar/quartz ratio profile (Fig. 4.7) has a very different structure, with low values through most of CRP-3, and higher values only present at *c.* 257-408 mbsf and below *c.* 750 mbsf. One potential reason for these compositional variations is changes in sediment grain size, since feldspar/quartz ratios tend to decrease as grain size decreases (Blatt, 1992). Such a grain-size control does not appear to have been a major influence on these curves, however, because most "fast-

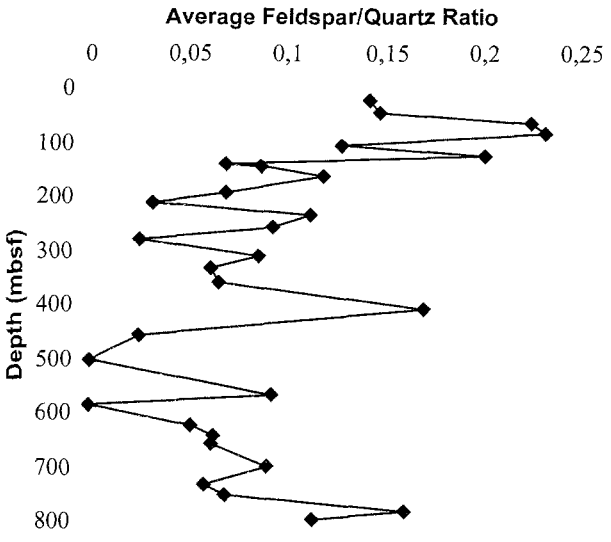

Fig. 4.6 - Stratigraphical profile of feldspar/quartz XRD peak intensity ratios for bulk sediments from CRP-3. Each ratio plotted is the average of three separate peak intensity ratios. The feldspar considered in these ratios is predominantly plagioclase.

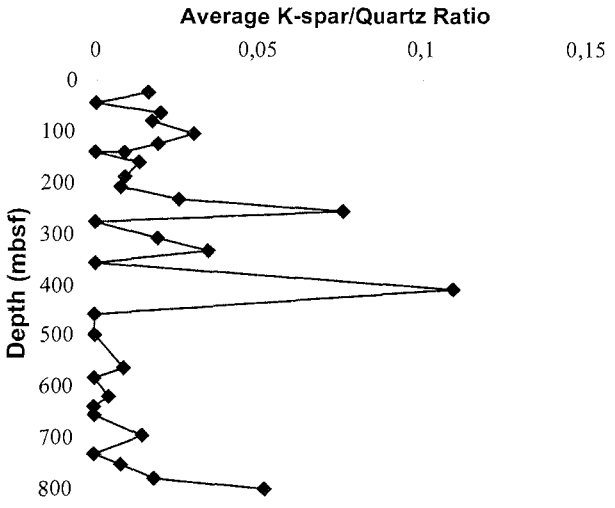

Fig. 4.7 - Stratigraphical profile of K-feldspar/quartz XRD peak intensity ratios for bulk samples from

Tab. 4.4 - Minerals identified by x-ray diffraction analysis in bulk samples from CRP-3.

Depth (mbsf)	Minerals Present
22.25	Quartz, plagioclase (albite and anorthite)
44.18	Quartz, plagioclase (albite and anorthite), K-feldspar (?sanidine)
63.00	Quartz, plagioclase (albite and anorthite), K-feldspar (orthoclase, sanidine, microcline), illite, ?augite
82.35	Quartz, plagioclase (albite and anorthite), K-feldspar (orthoclase), illite
106.40	Quartz, plagioclase (albite and anorthite), K-feldspar (orthoclase and sanidine), illite
123.65	Quartz, plagioclase (albite and anorthite), K-feldspar (orthoclase, sanidine, and microcline), illite
141.23	Quartz, plagioclase (anorthite), illite, minor pyrite, ?minor calcite
142.40	Quartz, plagioclase (albite)
162.14	Quartz, plagioclase (albite and anorthite)
190.79	Quartz
210.00	Quartz, plagioclase (anorthite), ?anorthoclase, ?mixed-layer chlorite/illite, analcime-C
232.47	Quartz, plagioclase (albite), K-feldspar (orthoclase and sanidine), illite
257.10	Quartz, plagioclase (albite), anorthoclase
278.53	Quartz, minor calcite
311.16	Quartz, ?plagioclase, mixed-layer clays (?chlorite/illite)
332.04	Quartz, anorthoclase, ?mixed-layer clays
359.29	Quartz, plagioclase (albite), ?mixed-layer clays
408.61	Quartz, plagioclase (albite and anorthite), K-feldspar (orthoclase and sanidine), chlorite to chlorite/illite mixed layer clays
457.40	Quartz, ?plagioclase
500.26	Quartz
564.43	Quartz, plagioclase (albite and anorthite)
584.47	Quartz
621.75	Quartz, mixed-layer clays (chlorite/illite or smectite/illite)
640.72	Quartz, mixed-layer clays (chlorite/illite or smectite/illite), minor plagioclase
656.54	Quartz, plagioclase (albite and anorthite), mixed-layer clays (chlorite/illite or smectite/illite)
697.40	Quartz, plagioclase (albite and anorthite), K-feldspar, mixed-layer clays (chlorite/illite or smectite/illite)
731.38	Quartz, plagioclase, mixed-layer clays (chlorite/illite or smectite/illite)
751.43	Quartz, plagioclase (albite and anorthite), mixed-layer clays (chlorite/illite or smectite/illite), ?K-feldspar
781.42	Quartz, plagioclase (albite and anorthite), K-feldspar (sanidine), smectite, illite/smectite mixed-layer clays
798.03	Quartz, plagioclase (albite and anorthite), illite, smectite, ?illite/smectite mixed-layer clays

track" samples were taken from zones with a significant sandstone component. As a result, the grain size of the bulk sediment analyzed does not appear to vary significantly between samples, thereby minimizing the possibility that the patterns observed in figures 4.6 and 4.7 are primarily a result of grain-size changes downcore.

A second possible explanation for the patterns seen in figures 4.6 and 4.7 is a change in sediment provenance during the period of deposition. The possible role of changes in sediment source can be evaluated by comparing the variations in bulk mineralogy, sand-fraction composition (see Sand Mineralogy section) and coarse-clast composition (see Basement Clasts section) downcore. This comparison indicates relatively consistent patterns of variation in all three compositional parameters, which aids in interpreting the bulk mineralogical data. Above *c.* 200 mbsf, the feldspar/quartz ratio of the bulk sediment is relatively high, the feldspar/quartz ratio in the sand fraction is relatively high, and the clast population contains significant abundances of Ferrar Dolerite detritus relative to Granite Harbor Intrusives and sedimentary clasts. All of these lines of evidence suggest that Ferrar Dolerite exposures were a significant sediment source during deposition of the upper 200 m of CRP-3, and contributed feldspar-rich detritus that raised the feldspar/quartz ratio of the bulk sediment. The abundance of rounded quartz grains in the sand fraction has been interpreted to indicate that the lower Beacon Supergroup (the Taylor Group) was also a significant sediment source; the combination of abundant recycled quartz and little K-feldspar from the Ferrar Dolerite, therefore, produced the low K-feldspar/quartz ratios found in the bulk sediment above 200 mbsf.

From *c.* 200 to *c.* 600 mbsf, the feldspar/quartz ratio

Tab. 4.5 -Minerals identified by x-ray diffraction analysis of clay-sized fractions of samples from CRP-3.

Depth (mbsf)	Minerals Present
44.18	Chlorite, illite, ?illite/smectite mixed-layer clays, ?minor kaolinite, quartz, plagioclase, calcite
190.79	Chlorite, illite, quartz
257.10	Chlorite, ?illite, mixed-layer clays (?chlorite/illite and ?illite/smectite), quartz, plagioclase
408.65	?Chlorite, illite, illite/smectite mixed-layer clays, ?kaolinite, quartz, plagioclase
697.40	Smectite, smectite/chlorite mixed-layer clays, illite, quartz, ?calcite, ?chlorite
781.42	Smectite, mixed-layer clays (smectite/chlorite and smectite/illite), ?chlorite, ?illite, quartz
798.03	Smectite, illite/smectite mixed-layer clays, quartz, plagioclase, ?chlorite

of the bulk sediment is relatively low but variable (with a single-point maximum at *c.* 410 mbsf), the K-feldspar/quartz ratio of the bulk sediment is low (except for a single-point maximum at *c.* 410 mbsf), feldspar and volcanic lithic-fragment abundances are relatively low and quartz abundances are relatively high in the sand-grain counts, whereas clast populations are variable. However, clasts of Granite Harbor Intrusives and sedimentary lithologies generally are more abundant than clasts of Ferrar Dolerite. These compositions suggest that the Ferrar Dolerite was a relatively less important sediment source during deposition of this interval than it was during deposition of the upper 200 m of CRP-3. Although the bulk mineralogy, sand-grain compositions, and clast abundances have not been compared in detail, it is interesting to note that the maxima in bulk feldspar/quartz and K-feldspar/quartz at *c.* 410 mbsf correspond to an increase in the feldspar/quartz ratio of the sand fraction, and to a brief increase in the abundances of Granite Harbor Intrusive and Ferrar Dolerite clasts relative to sedimentary clasts (which are predominantly quartz sandstones). Thus, these three compositional data sets provide a consistent picture of a relatively short-term change in sediment provenance that spans the complete spectrum of grain size; the causes of this short-term change, however, are unknown at this time.

Below *c.* 600 mbsf, the feldspar/quartz ratio of the bulk sediment increases to consistently intermediate values, the abundances of feldspar and volcanic-lithic fragments increase while the abundance of quartz decreases in the sand fraction, and clast compositions are variable. The K-feldspar/quartz ratio also increases, but only below *c.* 750 mbsf. We interpret the changes in sand-fraction composition as recording a shift in sediment source, from the quartzose Taylor Group to the more feldspathic Victoria Group of the Beacon Supergroup. Changes in the bulk mineralogy are consistent with this proposed shift.

CLAY MINERALOGY

The clay-sized fractions separated from seven CRP-3 "fast-track" samples were analyzed by x-ray diffractometry at CSEC, with the goal of determining the clay-mineral assemblages present through the stratigraphical section. After sieving at 63 mm, the clay-sized fraction was separated by settling, with settling times calculated from Stokes' Law. The decanted clay-sized fraction was then concentrated by incomplete evaporation, an aliquot of the clay/water suspension (< 5 ml) was placed on an aluminum disk, and the water was evaporated, producing a texturally oriented mount. Each sample was placed in an ethylene glycol-saturated atmosphere for 12 hours prior to analysis. Samples were scanned over the range 2-35° 2θ in steps of 0.01° 2θ, with a scan time of 2 sec/step. The x-ray diffractograms were processed using JADE 3+ software, and also by comparison with standard references (Chen, 1977).

The minerals identified in each clay-sized sample are listed in table 4.5; no attempt is made here to determine either relative or absolute abundances of the various phases present. Chlorites, illites, quartz, plagioclase and a variety of mixed-layer clays occur consistently in the assemblages above *c.* 410 mbsf, whereas smectites, smectite-bearing mixed-layer clays, and quartz occur consistently in the assemblages below 650 mbsf. Chlorites and illites are typical detrital clay minerals, generally produced by physical weathering with little or no chemical alteration (Chamley, 1989). As a result, these clay minerals generally dominate modern high-latitude sediments, where the clays have experienced little chemical weathering (Griffin et al., 1968). Both minerals could be provided by erosion of Beacon Supergroup and basement rocks exposed in the Transantarctic Mountains. In contrast, smectites generally are produced by chemical weathering, and form by hydrolysis in environments with slow movement of soil-water (Chamley, 1989). As a result, smectites generally are not abundant in modern high-latitude sediments and soils (Griffin et al., 1968; Chamley, 1989), except in areas where volcanic rocks are important sediment sources. In such areas, the volcanic rocks can yield considerable smectite, even under polar conditions (Ehrmann et al., 1992; Ehrmann, 1998b).

The clay-mineral assemblage present above *c.* 410 mbsf suggests a predominance of physical weathering in the sediment-source regions, consistent with the evidence for glacially influenced deposition in the upper part of CRP-3. The shift to smectite-bearing assemblages below *c.* 650 mbsf may be explained in one of three ways: 1) that weathering conditions in the sediment source areas were wetter (and perhaps somewhat warmer) during deposition of the interval below *c.* 650 mbsf, 2) that the older sediment sources included volcanic rocks that were not present during deposition of the younger part of CRP-3, or 3) that diagenetic processes preferentially produced smectite in the deeper part of CRP-3. As discussed previously, the bulk-sediment mineralogy and the sand-fraction composition both suggest that Victoria Group rocks supplied detritus to the older section at CRP-3, based on increased abundances of feldspar and felsic-volcanic grains. Although cold-climate weathering of such grains might produce some smectite, it is also possible (and perhaps more likely) that the appearance of smectites records a shift to climates more favourable for chemical weathering. If the change in clay mineral assemblages does record a climatic shift, then this change may correlate with a similar compositional change that has been recognized in Southern Ocean cores and CIROS-1 (Ehrmann & Mackensen, 1992; Ehrmann et al., 1992; Ehrmann, 1997; Ehrmann, 1998a), and that lies just above the Eocene/Oligocene boundary (dated at 33.7 Ma on the timescale of Berggren et al., 1995). The palaeoclimatical and chronostratigraphical significance of this compositional change will be examined more closely in future studies. Finally, the appearance of these smectite-rich clays during microscope examination is reminiscent of the appearance of diagenetic clays found in other settings (see Calcareous Nannofossil section). This possible mechanism of formation will be evaluated by future studies of the clays using scanning electron microscopy.

BULK MINERALOGY OF THE INTRUSION AT 901.48-919.95 MBSF

Two samples from the intrusion within the "basement" at CRP-3 were analyzed for bulk mineralogy by XRD, using the same techniques as those employed to determine bulk-sediment composition. The samples analyzed are from 903.34 and 915.42 mbsf. The upper sample, taken from the altered and brecciated edge of the intrusion, contains quartz, feldspar (?especially K-feldspar), illite, chlorite, mixed-layer clays (probably smectite/illite and illite/chlorite forms), siderite, and ?Mg-calcite. The lower sample, taken within the body of the intrusion, contains quartz, magnesite, smectite, mixed-layer clays (probably smectite/illite forms), ?kaolinite, ?Mg-calcite, and ?serpentine group minerals.

SAND GRAINS

The modal composition of the sand fraction in CRP-3 samples was examined to determine the range of sand-sized mineral and lithic grains present, to estimate their relative proportions, and to provide initial information on provenance and temporal variations. Previous studies in the area described sand grains and provenance of samples from the MSSTS-1 and CIROS-1 drill holes, both situated *c.* 80 km to the south, and in CRP-1 and CRP-2/2A, situated <1.5 km east of CRP-3 (Barrett et al., 1986; George, 1989; Smellie, 1998, in press). Like those authors, we report a varied provenance that resembles the local geology of the Transantarctic Mountains (TAM) in southern Victoria Land, including granitoid and metamorphic rocks of an Upper Precambrian–lower Palaeozoic 'basement', quartzose sedimentary rocks of the Devonian–Triassic Beacon Supergroup, and sills, dykes and lavas of the Jurassic Ferrar Supergroup (dolerite and basalt). A major difference with the previous studies, however, is a complete absence in CRP-3 of grains derived from alkaline volcanic rocks of the Cenozoic McMurdo Volcanic Group.

METHODS

For CRP-3, we selected *c.* 110 sandstone samples, which were impregnated with epoxy resin prior to making uncovered, unstained thin sections. Sampling intervals generally varied from *c.* 5-10 m, but only a few samples were suitable for counting at depths above 180 mbsf owing to substantial muddy matrices in those sandstones. We selected 71 samples for modal analysis for this report. One hundred grains were counted in each sample, exclusive of matrix (<30 μm), using the Gazzi-Dickinson point counting method. The modal data are summarised in table 4.6. Because of the low count total and lack of staining, the point counting results reported here should be regarded as qualitative. In particular, it was not practical to discriminate between plagioclase and alkali feldspar during counting and only total feldspar was recorded. However, because of the greater certainty of grain identifications compared to working with smear slides (*cf.* Cape Roberts Science Team, 1998, 1999), the CRP-3 modes are probably more reliable estimates of the sandstone modal compositions than those reported in previous *Initial Reports* of the project.

RESULTS

The CRP-3 sandstone samples range in grain size from very fine to medium/coarse but they are predominantly fine- to very fine-grained (*c.* 70% of samples). However, the proportion of these finer samples is lower than in previous CRP drill holes (*e.g.* 85% of counted samples in CRP-2/2A were fine- or very fine-grained; Cape Roberts Science Team, 1999). There is no

Tab. 4.6 - Qualitative detrital modes of sandstones in CRP-3, based on counts of 100 sand grains per sample and using unstained thin sections.

mbsf	Qr	Qa	Qtot	Ftot	P	Lv	Ls	Lm	Qp	Other
24,32	6	67	73	8	17	0	0	0	0	2
67,06	9	54	63	21	12	2	1	0	0	1
89,5	5	60	65	21	11	1	1	0	0	1
177,22	9	69	78	16	1	3	0	0	0	2
183,69	5	83	88	7	2	3	0	0	0	0
202,59	9	80	89	7	0	2	0	0	1	1
207,71	0	84	84	6	1	4	0	0	0	5
226,42	25	44	69	23	6	1	0	0	0	1
235,5	10	65	75	15	7	2	0	0	0	1
249,67	26	56	82	9	4	5	0	0	0	0
256,66	17	70	87	7	1	2	0	0	0	3
259,28	11	75	86	8	3	2	0	0	0	1
270,97	25	63	88	5	0	7	0	0	0	0
279,68	4	74	78	12	6	2	0	0	0	2
286,17	3	68	71	22	2	2	0	0	0	3
289,22	17	66	83	8	5	2	0	0	1	1
315,77	15	66	81	16	1	2	0	0	0	0
326,67	10	80	90	6	0	2	0	0	0	2
335,96	13	69	82	9	5	2	0	0	0	2
345,76	34	57	91	6	2	1	0	0	0	0
348,7	28	65	93	2	0	1	4	0	0	0
351,88	13	52	65	14	15	4	0	0	0	2
358,95	9	61	70	12	9	4	2	0	0	3
369,64	9	68	77	13	4	4	0	0	0	2
375,32	30	61	91	4	3	2	0	0	0	9
383,76	21	63	84	6	1	9	0	0	0	0
387,46	9	78	87	5	2	3	0	0	0	3
390,78	9	62	71	15	7	7	0	0	0	0
396,58	30	52	82	8	5	5	0	0	0	0
405,75	6	65	71	17	3	5	0	0	0	4
413,09	16	56	72	18	8	2	0	0	0	0
415,94	8	69	77	11	0	4	0	0	0	8
422,81	23	68	91	5	1	3	0	0	0	0
426,77	7	76	83	10	1	6	0	0	0	0
437,12	6	78	84	12	3	1	0	0	0	0
445,23	23	64	87	7	1	4	0	0	1	0
449,73	17	77	94	3	0	2	0	0	1	0
455,81	8	80	88	5	2	4	0	0	0	1
460,13	2	75	77	13	7	3	0	0	0	0
473,61	13	71	84	9	5	2	0	0	0	0
475,34	6	73	79	9	4	7	0	0	1	0
480,68	18	60	78	9	10	2	0	0	0	1
481,22	23	67	90	6	1	3	0	0	0	0
486,03	34	61	95	2	0	2	0	0	1	0
495,15	25	73	98	1	0	1	0	0	0	0
500,21	45	55	100	0	0	0	0	0	0	0
509,36	19	67	86	7	0	6	0	0	0	1
513,17	22	69	91	6	0	1	0	0	0	2
525,36	36	61	97	0	1	2	0	0	0	0
533,26	19	73	92	1	5	2	0	0	0	0
543,87	9	70	79	9	5	7	0	0	0	0
550,03	3	79	82	7	7	3	0	1	0	0
571,8	14	83	97	1	0	2	0	0	0	0
615,37	6	73	79	7	4	10	0	0	0	0
626,18	11	71	82	10	4	4	0	0	0	0
630,38	11	70	81	15	1	3	0	0	0	0
643,11	4	66	70	10	7	13	0	0	0	0
655,86	4	57	61	25	6	7	0	0	0	1
664,03	2	75	77	12	1	3	1	0	0	6
673,28	3	76	79	11	5	5	0	0	0	0
681,02	2	61	63	16	8	12	0	0	0	1
686,52	6	79	85	8	3	4	0	0	0	0
696,77	1	71	72	19	1	8	0	0	0	0
715,48	2	67	69	8	12	11	0	0	0	0
724,08	1	57	58	20	9	13	0	0	0	0
730,87	4	71	75	14	3	6	0	0	0	2
735,39	2	65	67	21	1	10	0	0	0	1
737,35	1	67	68	14	6	11	0	0	0	1
750,02	0	72	72	17	4	5	0	0	0	2
770,26	0	67	67	17	8	7	0	1	0	0
787,66	2	78	80	7	5	6	0	0	0	2

Abbreviations: mbsf - metres below sea floor; Qr - rounded quartz; Qa - angular quartz; Qtot - total quartz; Ftot - plagioclase and alkali feldspar;
P - pyroxene; Lv - volcanic lithic grains; Ls - sedimentary lithic grains; Lm - metamorphic tectonite grains; Qp - polycrystalline quartz; other - accessory minerals (see text).

obvious systematic down-core variation in grain size, but samples coarser than fine sandstone are almost absent below 550 mbsf (only one sample). By comparison with previous studies (Smellie, 1998, in press), the most important effect of grain-size variations on the modal data set is likely to be increased data scatter, but the effect is unlikely to mask major provenance-related variations.

Mineral types encountered in CRP-3 are essentially identical to those described in previous CRP reports (see Cape Roberts Science Team, 1998, 1999). However, no alkaline pyroxenes or amphiboles, volcanic glass or fresh alkaline-volcanic lithic grains were encountered in CRP-3. The modal data are dominated by quartz (Q) and feldspar (F), which together usually comprise 86-97% of the mode (mean value *c.* 92%; Fig 4.8). Quartz occurs as rounded- to well-rounded (Qr) and angular- to sub-rounded grains (Qa), but the latter (Qa) are dominant and normally form >60% of the quartz-grain population (Fig. 4.8). Pyroxene (P) grains are also an important detrital component. The pyroxene is fresh and abundant in samples obtained above 180 mbsf, but it is invariably partially replaced by smectite (or rare carbonate) in lower samples. In the deepest samples, it is sometimes hard to distinguish smectite-altered pyroxene from abundant phyllosilicate cement, but fresh pyroxene relicts are usually present.

A variety of lithic grains is also present, forming up to 13% by volume. They include: dolerite; fine basalt; felsic lava; fine quartz-muscovite and ribbon-quartz tectonites; granitoids; polycrystalline quartz (Qp); graphic-textured grains; and a few grains of mudrock or rare muddy, very-fine sandstone (Ls). Several basalt types were distinguished, with variably lathy feldspar (corresponding to Group II volcanic clasts?; see section on Volcanic Clasts) or curved acicular to feathery feldspar or pyroxene crystallites (Group III volcanic clasts?; section on Volcanic Clasts), rod-shaped or rarely dendritic opaque oxide, and/or snowflake-textured devitrified groundmasses. The felsic lavas are formed of fine feldspathic or quartzo-feldspathic crystalline mosaics (chert-like) with scarce feldspar microphenocrysts. Granitoids are represented by grains of coarse polycrystalline quartz, and muscovite–quartz and quartz–alkali feldspar crystalline aggregates. Graphic-textured grains (*i.e.* composed of geometrically intergrown quartz and feldspar) are ubiquitous and may have had a source either in tholeiitic dolerite or granitoids. Fresh brown and very rare green and colourless glass grains were observed in smear slides, but were not encountered in any of the thin sections examined in the modal study (see section on Volcanic Clasts). All of the lithic-sedimentary (Ls) grains are conspicuously muscovite-bearing. A few may be syn-sedimentary, but Ls grains are generally very rare.

All other grain types are present in trace amounts (*i.e.* <<1% of the total mode). They include unaltered pale-green and pale-brown amphibole (hornblende), brown biotite, muscovite, opaque grains (typically well rounded and probably mainly coal), zircon, sphene and garnet. Other, much less common accessories include bioclastic carbonate and silica, and epidote.

Most of the samples are cemented by a combination of phyllosilicate (rimming grains and as a pore filling) and/or carbonate, or else have a phyllosilicate-rich muddy matrix.

MODAL VARIATIONS

Quartz contents commence relatively low (60-75%) in samples below 180 mbsf but rise in samples below that depth (Fig. 4.8). A few samples are composed almost entirely of quartz, and most of the CRP-3 sandstones are more quartz-rich than any of the samples obtained in CRP-1 and CRP-2/2A. The proportion of quartz rises to a peak around 550 mbsf, and falls to lower values in the samples below that depth. Rounded–well rounded quartz grains are a conspicuous and characteristic feature of samples above 550 mbsf, but they rapidly diminish and become scarce below that depth. Feldspar contents vary antithetically to quartz, as also found in both CRP-1 and CRP-2/2A, but Q/F ratios show a slight gradual increase to 550 mbsf, falling at a steeper gradient thereafter.

Modal data for pyroxene are very variable, probably as a result of the low total counts for 100 grains (Cape Roberts Science Team, 1999). They generally form 2-10% of the mode, but pyroxene may be absent in a few samples. Conversely, pyroxene is more common (11-17%), and strikingly fresh, in samples above 180 mbsf, in part of the core dominated by dolerite clasts (see section on Distribution of Clasts). Other mineral grains (hornblende, opaque oxide, zircon, sphene, garnet) occur as 1-4 grains each *per* thin section. However, whereas opaque grains and zircon occur throughout the sequence, sphene and garnet are virtually absent below *c.* 475 mbsf (Tab. 4.7). Biotite occurs as free grains above 375 mbsf. Below that depth it is found only within quartz crystals.

No modal counts were made for the individual lithic-grain types, but petrographical observations indicate that dolerite and basaltic grains are ubiquitous (Tab. 4.8). They are particularly common above 180 mbsf, and there is a second zone with conspicuous dolerite grains between 480 and 530 mbsf. Granitoids and metamorphic tectonites are sparsely present down to 390 and 486 mbsf, respectively, and essentially vanish below. Finally, fine-grained felsic lavas also occur throughout the section. They are sparse above 280 mbsf but show a notable steady increase below *c.* 550 mbsf; they may be responsible for the observed increase in counts for total lithic grains to the base of the CRP-3 sequence.

PROVENANCE

All the grain types observed in CRP-3 have been described previously from cores recovered at other sites in the McMurdo Sound region, and they indicate a

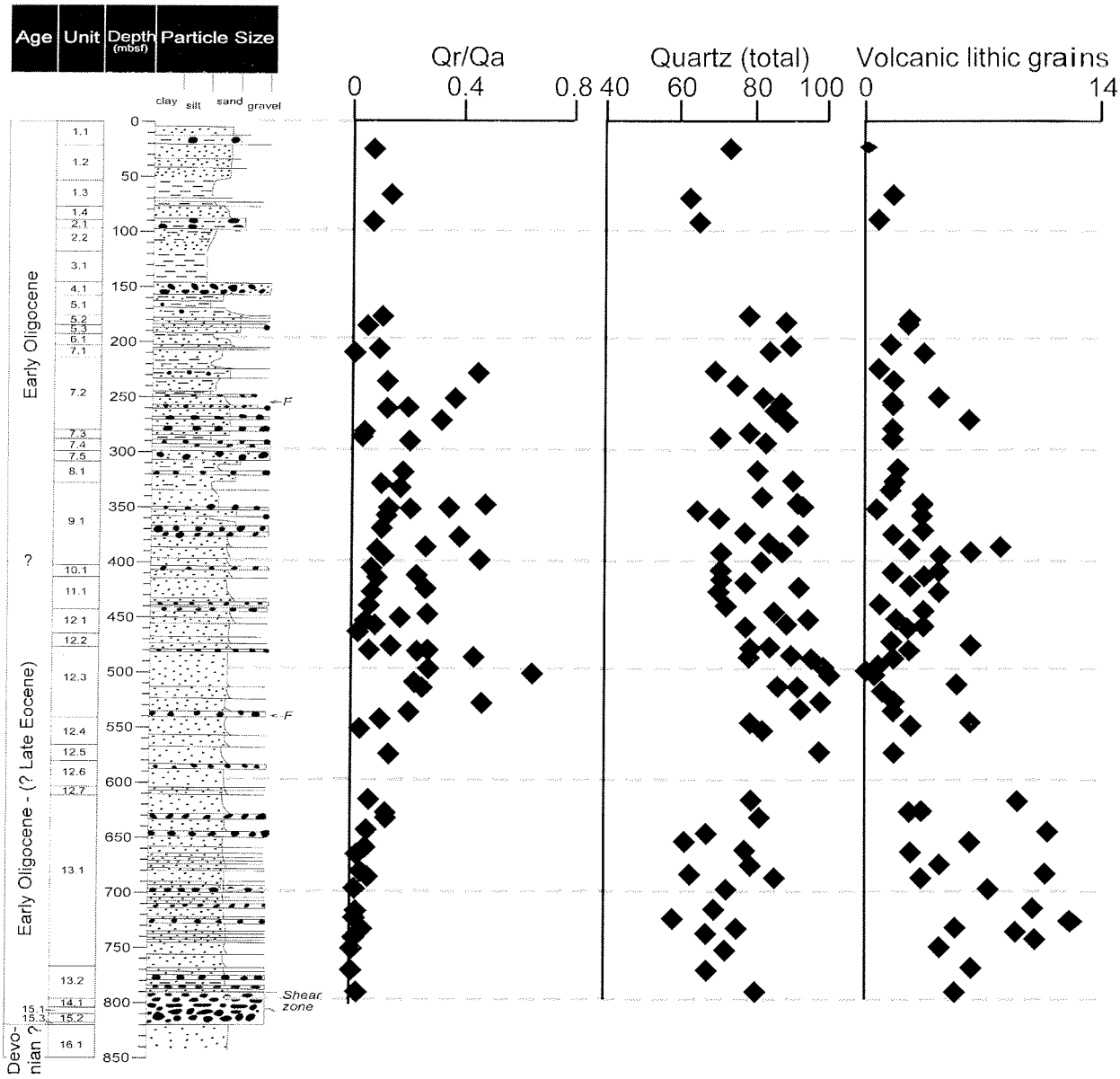

Fig. 4.8 - Summary diagram showing selected qualitative detrital modes for sand-grade samples from CRP-3, illustrating variations of compositional features with depth in the sequence. Note the several changes, present in all three modal parameters, which occur at *c.* 550 mbsf. Abbreviation: Qr/Qa – ratio of rounded to angular quartz grains.

similar, presumably local (TAM), provenance affecting all sediments. There is no evidence for a more distant source. However, whereas CRP-1 sandstones (mainly Miocene) were derived from a mixture of granitoid and volumetrically minor metamorphic 'basement' rocks (Beacon Supergroup sediments and Ferrar Supergroup dolerite), an important petrological transition was recorded in CRP-2/2A at 307 mbsf (upper Oligocene). That transition was interpreted by some to record an important downward change from granitoid- and Ferrar-dominated sediments above to mainly Beacon- and Ferrar-dominated sediments below, although both 'types' alternated in the lower half of the CRP-2/2A sequence probably due to climatic influences (Smellie, in press; see also section on Tectonic History). The sandstones in CRP-3 apparently extend the trends observed in CRP-2/2A, with a clear continuing influence from Ferrar Supergroup detritus (dolerites and Kirkpatrick basalts). Ferrar-derived detritus is particularly important in the upper 180 mbsf. In addition, the high Qr/Qa ratios of most samples could indicate a provenance derived at least partly in the lower Beacon Supergroup (Taylor Group), in which rounded quartz grains are abundant (*cf.* Smellie, 1998, in press). By contrast, Qr/Qa ratios diminish progressively in samples below 550 mbsf. There are also significant changes in other modal values

Tab. 4.7 - Schematic summary showing the down-hole distribution of accessory minerals in CRP-3 sandstones.

mbsf	hornblende	biotite	muscovite	opaques	zircon	sphene	garnet	other
24.32	x	x?		x				
67.06		x		x		x		
89.5	x	x	x	x		x	x	epidote?, bioclastic carb
177.22	x	x		x				epidote
183.69	x			x	x			
202.59	x	x	x	x		x	x	
207.71	x		x	x	x		x	detrital carbonate?
226.42		x?	x (in qtz)	x				
235.5	x	x		x				
249.67								
256.66	x	x	x	x	x	x	x	bioclastic carbonate
259.28								
270.97								
279.68		x?	x	x				epidote
286.17	x		?	x	x	?		clinozoisite?
289.22	x			x	x	x	x	
315.77		x?	x	x	x			bioclastic carbonate
326.67	x	x	x		x	x		
335.96	x	x	?	x	x	x	x	
345.76	?		x (in qtz)	x	x			
348.7	x		x	x			x	
351.88				x				
358.95	x	x?		x	x		x	epidote
369.64	x			x				epidote
375.32		x (in qtz)		x	x		x	
383.76				x				
387.46	x			x	x	x	x	
390.78				x	x			
396.58	x							
405.75	x	x?	x	x	x		x	epidote
413.09					x			
415.94	x		x	x	x	x?	x	
422.81	x			x?	x		x	
426.77	x	x (in qtz)		x	x			
437.12	x			x	x	x	x	
445.23	x	x (in qtz)			x			
449.73	x		x	x		x?	x	
455.81	x	x	x		x	x	x	
460.13	x	x (in qtz)	x		x	x	x	
473.61	x			x		x		
475.34	x	x (in qtz)	x	x	x	x	x	epidote?
480.68	?				x			
481.22	x	x (in qtz)						
486.03	x		x (in qtz)					
495.15	x (in qtz)	x (in qtz)	x (in qtz)	x				
500.21		x (in qtz)			x			
509.36	x			x				
513.17	x			x				
525.36								
533.26	x	x (in qtz)	x (in qtz)	x	x (in qtz)			
543.87	x			x	x			
550.03	x	x (in qtz)		x	x			
571.8			x	x			x	
615.37	x			x		x		epidote
626.18	x	x (in qtz)	x	x	x			
630.38	x	x (in qtz)			x			
643.11	x	x (in qtz)		x	?			
655.86	x?		x	x	x			
681.02		x (in qtz)	x (in fsp)	x	x	x?		
730.87	x			x	x	x?		epidote?
737.35	x		x	x	x	x		
750.02	x	x	x	x	x	x		

Abbreviations: mbsf - metres below sea floor; qtz -quartz; fsp - feldspar

Tab. 4.8 - Schematic summary showing the down-hole distribution of lithic sand grains in CRP-3 sandstones.

mbsf	Lm	felsic Lv	Basaltic Lv (1)	Basaltic Lv (2)	dolerite	graphic	granite	Qp	Ls
24,32				x	**X**	x			
67,06			x		x	x		x	
89,5					x	x	x		
177,22		x?	**X**	x	**X**			x	x
183,69			**X**		x		x		
202,59	x	x	x		**X**	x			
207,71									x
226,42			**X**	x	x	x		x	
235,5	x				x	x		x	x
249,67									
256,66		x?			x				
259,28					x		x?		x
270,97									
279,68		x			x	x			
286,17		x				x			
289,22	x	x	x		x	x	x		
315,77		x	x		**X**		x	x	
326,67		x	x	x	x	x			
335,96	x		x						
345,76	x?	x		x	x		x	x	
348,7		x			x				x
351,88		x		x	x	x	x		
358,95	x	x			x				x
369,64		x			**X**	x	x		x
375,32				x	x	x		x	x
383,76		x	x	x	x	x	x	x	
387,46		x		x	x	x			
390,78		x			x			x	x
396,58			x		**X**		x	x	x
405,75	x	x		x	x			x	
413,09					x			x	
415,94	x?	x				x			
422,81		x			x	x		x	
426,77		**X**		x	x	x			
437,12	x	x							
445,23	x		**X**	**X**	x			x	x
449,73				x	x				
455,81		**X**				x			
460,13	x	x			x				
473,61	x	x			x			x	
475,34	x	x				x			
480,68		x		x	**X**	x		x	x
481,22		x		x	x	x			
486,03	x	x	**X**		**X**	x		x	
495,15		x		x	x			x	
500,21		x		x	x	x		x	
509,36		x		x					
513,17		x		x	**X**			x	
525,36									
533,26		x			**X**		x	x	
543,87		x	x		x	x		x	
550,03		**X**			x				
571,8		**X**			x	x		x	
615,37		x				x			
626,18		x	x		x	x			x
630,38	x?	**X**	x	x	x				
643,11		x	x	x	x	x			
655,86	x	**X**		x		x	x?		
681,02	x	**X**	x		x	x			
730,87		**X**	x	x		x			
737,35	x	**X**		x		x		x?	
750,02	x?	x		x					

x - present; **X** - dominant

Abbreviations: Lm - quartz-mica tectonite, ribbon quartz; Lv - volcanic lithic grains; Basaltic Lv (1) - fine basalts with feathery texture or rod-like opaque oxide; Basaltic Lv (2) - fine basalt with lathy plagioclase; graphic - graphic-textured quartz-feldspar; Qp - polycrystalline quartz, chalcedony; Ls - mudstone, sandstone (micaceous).

coincident with the change to lower Qr/Qa ratios: Q and Q/F ratios decrease, whereas F and volcanic lithic grains (Lv) increase (Fig. 4.8).

Some of the modal values of samples from below 550 mbsf in CRP-3 are similar to those in CRP-1 and CRP-2/2A sandstones derived from granitoids. Granitoids form a persistent 25% of the clast population right to the base of CRP-3, and a granitoid source is thus possible for the sand-grain population (see sections on Distribution of Clasts and Tectonic History). Conversely, the upper Beacon Supergroup (Victoria Group) is composed of sandstones that are more feldspathic, less quartzose, with few rounded quartz grains, and containing a significant proportion of felsic volcanic grains. It is also possible, therefore, that the CRP-3 sandstones below 550 mbsf were sourced in the Victoria Group. The trends observed and the virtual absence of rounded quartz grains could be interpreted to suggest that large outcrops of Taylor Group sandstones were not exposed in the period below *c.* 550 mbsf.

Finally, apart from rare grains of brown and colourless glass of uncertain composition (Kirkpatrick Basalt Group?), the absence of alkaline minerals, tephra layers and fresh volcanic lithic grains in CRP-3 strongly suggests that volcanism of the McMurdo Volcanic Group commenced at *c.* 25 Ma in the McMurdo Sound region (*cf.* Bellanca et al., in press; Krissek & Kyle, in press; Smellie, in press) and did not extend back to Eocene times, as was formerly inferred (George, 1989).

IGNEOUS INTRUSION

PETROGRAPHY AND RELATIONSHIP WITH HOST ROCKS

LSU 17.1 comprises a magmatic body, intruded in the Beacon sandstones, that is deeply altered and brecciated at its margins.

We carried out detailed lithological observations on the core and sampling followed by a preliminary petrographical study of the thin sections and smear slides related to the intrusion and the host rocks. The data we obtained allowed us to recognize the following intervals:

a) interval between 900.40 and 901.09 mbsf, thickness 0.69 m: this interval includes the hardened portion of the Beacon sandstone (LSU 16.1) closely superjacent to the intrusion. In this interval the Beacon sandstone changes progressively downcore in colour, from pale red/brown (5YR6/6) to pale purple (5P2/2), and shows carbonate (Mg or Fe ?) or silica veins and incipient brecciation. However, there are no significant changes in the petrography and mineral assemblage of the rocks;

b) interval between 901.09 and 902.10 mbsf, thickness 1.01 m: breccia with angular and subangular fragments of the Beacon sandstones (maximum apparent size 15 cm) and the underlying intrusive rocks, immersed in a fine-grained brown (7.5YR4/4) matrix. Petrographically, the brown matrix appears to be composed of very abundant reddish hematite grains, smectite flakes, plagioclase microlites and very minor (and dubious) brown-glass shards. Igneous clasts (901.80 mbsf) are strongly weathered, although the rock texture is generally preserved: this is a hypocrystalline, aphyric rock, with a few (<5%) large (2-mm) phenocrysts of which only the outlines are still recognizable. The clasts consist of tabular sericitised plagioclase and prismatic (augite ?) to equant (ortho ?) pyroxenes totally replaced by hematite, clay minerals and carbonate. The groundmass has a texture varying from intersertal to intergranular and is composed of altered subhedral plagioclases (now sericite). Between them, reddish hematite grains are abundant and probably have replaced mafic minerals. Interstitial areas with anhedral feldspars (albite or K-feldspar), smectites, serpentine and ilmenite needles are also found and have probably replaced original glass. The absence of quartz suggests that the glass was not more evolved than intermediate in composition.The largest sandstone fragment (901.30-901.45 mbsf) is angular, shows several carbonate-filled fractures and is bounded for most of its visible outline by a thin rim (0.5-1 cm) of chilled magma, pale green in colour. This indicates that it was formerly in close contact with the magma; it could be perhaps a portion of host rocks overhanging the intrusion or more probably a clast dislodged by the intruding magma. Petrographical analysis of the rim surrounding this country rock fragment was carried out through microscopic examination across the interface at 901.42 mbsf. The chilled margin here shows scattered mm-sized relic domains retaining a subophitic texture and partially altered plagioclase laths. These domains are set within a deeply altered brown groundmass (smectite?) that also includes lighter-coloured patches of chlorite ± serpentine (?), altered glass (?) and scattered grains of quartz (xenocrysts).Veins, 1 mm-thick and consisting of (Mg?) carbonate (±Fe hydroxide inclusions), intersect both matrix and relict domains. Carbonate also forms a continuous rim parallel to the contact between the intrusive rock and the sandstone. There is also a network of thin veins aligned parallel to the contact within the sandstone itself. The sandstone is a quartz-arenite consisting of rounded to subangular grains of quartz grains, polycrystalline quartz lithic fragments, K-feldspar and plagioclase, zircon and scattered deformed biotite. The contact zone consist of a 1- to 3-mm-thick layer

Terra Antartica
Initial Report on CRP-3
2000, 7 (1/2)

5 - Palaeontology

INTRODUCTION

We examined six groups of fossils during the initial core-characterisation phase of CRP-3 drilling: siliceous microfossils, calcareous nannofossils, foraminifers, marine palynomorphs, terrestrial palynomorphs (miospores), and invertebrate macrofossils. Each of these groups provides the means for biostratigraphical dating or palaeoenvironmental reconstruction, or both.

Siliceous microfossils, including diatoms, ebridians, chrysophycean cysts, and silicoflagellates, are the primary means of biostratigraphical age determination in the Cenozoic of the Antarctic margin. In addition, they provide information on the nature of mesotrophic or neritic surface waters (planktonic), nearshore bottom conditions (benthic), and offshore transport (allochthonous benthic) of fine-grained material.

Calcareous nannoplankton inhabit surface waters in abundance only under oligotrophic nutrient levels, and thus are an important indicator of the invasion of oceanic surface-water masses into the Ross Sea. Benthic foraminifers and invertebrate macrofossils indicate past seafloor conditions including temperature and substrate character. In addition, their shells (if well preserved) contain carbonate that may be used for geochemical age determination (Sr), palaeothermometry ($\delta^{18}O$) and seawater carbon chemistry ($\delta^{13}C$).

Marine palynomorphs offer the potential for biostratigraphical age determination and palaeo-environmental characterisation in the Oligocene and Neogene. Miospores offer a way to monitor the evolution of adjacent terrestrial ecosystems in marine sedimentary rocks. Because of the significant changes in climatic regime during the Cenozoic, miospore stratigraphy also can provide age determination. Finally, all of the microfossils can provide monitors on the intensity and provenance of sedimentary rock erosion. This is especially true of the highly resistant palynomorphs.

PATTERNS OF FOSSIL OCCURRENCE

Siliceous microfossils occur within the upper 200 m of CRP-3 (Fig. 5.1), although high abundance and well-preserved assemblages are restricted to the upper 67 m. Within this upper 67 m, two distinct intervals of good abundance and preservation (3.05 to 16.00 and 33.95 to 66.70 mbsf) are separated by an interval with low abundance and generally poor preservation. Sparse assemblages of highly fragmented, etched or replaced (silicified casts) specimens of siliceous microfossils are present sporadically in the interval from 67 to 193.16 mbsf. Below this level, no siliceous microfossils were observed.

Calcareous nannofossils are restricted largely to the upper 194 m of the core, where they occur as sparse assemblages of low species richness. Four intervals of nannofossil occurrence are separated by barren intervals from 7 to 16, 48 to 77, and 162 to 178 mbsf. Preliminary count data indicate a significant increase in nannofossil abundance as a sedimentary component between 100 and 124 mbsf, with a maximum at 114 mbsf and secondary peaks at 100, 106, and 121 mbsf. Preservation is generally very good to excellent, although some of the sparser samples have significantly degraded preservation. Nannofossils largely disappear from the section at 193.14 mbsf, although a single occurrence at 266.27 mbsf suggests more samples below 200 mbsf may yield fossils upon closer examination.

Foraminiferal occurrence is largely restricted to the cored interval above 340 mbsf, where slightly more than half of the samples examined bear these fossils. Calcareous benthic foraminifers are the dominant form, with rare agglutinated taxa present only in a few samples. No specimens of planktonic foraminifers were seen above 340 mbsf, although a single specimen of *Globigerina* sp. was observed from 705.97 mbsf. Four intervals of benthic foraminiferal occurrence are separated by barren intervals from 65 to 85 mbsf, 210 to 250 mbsf, and 268 to 310 mbsf. A major peak in abundance of foraminifers as a sedimentary component occurs from 106 to 115 mbsf, with secondary peaks at 10.65, 44.12, 45.72, and 162.16 mbsf. Preservation is generally fair to good, suggesting little diagenetic alteration.

Macrofossils occur within the finer grain sedimentary rocks (mudstones and muddy sandstones) throughout the upper 330 m of the cored interval (Fig. 5.1). Macrofossil density in the core varies through this interval, with an average of about 7 macrofossils or macrofossil fragments per 10 metres of core. The abundance maximum occurs from 120 to 130 mbsf, with secondary peaks at 190 to 200 and 310 to 320 mbsf. Macrofossils become rare below 330 mbsf, with only five specimens between 330 to 540 mbsf. The rest of the cored interval, below 540 mbsf, is barren of macrofossils with the exception of a plant stem impression at 730.48 to 730.56 mbsf and a single modiolid mussel at 781.35 mbsf. Bivalves are the most common macrofossil in the core, comprising about 80% of the identifiable invertebrate macrofossil material. Important secondary components include brachiopods, serpulids, echinoids, and gastropods. Preservation of the macrofossils is variable, although almost all of them show evidence of dissolution. The high frequency of broken shells in some lithostratigraphical units is attributed to significant corrosion of the shell material.

of carbonate-cemented sandstone with subrounded, coarser-grained quartz, minor K-feldspars (microclinic) and zircon grains. No microscopic evidence of high-T contact metamorphism was detected. Very fine-grained greenish-phyllosilicate aggregates (sericite±chlorite intergrowth) occurring as interstitial phases, could represent a very low-T recrystallisation of an original clay matrix;

c) interval between 902.10 and *c.* 918.00 mbsf, thickness 15.90 m: this zone includes most of the magmatic body. It is mainly massive and ranges in colour from blue-grey (5BG5/1), in the upper part, to purple (5P2/2), in the lower portions. On the whole, the rock forming the intrusion is highly alterated even if some differences between different portions related to the depth seem to exist. The samples from the upper part (902.13, 903.30 mbsf) tend to preserve the original texture better although no original mineralogy can be detected. Petrographical features are similar to those of the clasts in zone b (see above), but the plagioclase in the groundmass tends to be more euhedral, hematite is less abundant, chlorite and smectite replacing mafic phases are more abundant than in the upper zone. In samples from the lower portion of the intrusion (912.22, 913.21, 915.00, 916.48 mbsf), the texture, as well as the original mineralogy, is totally destroyed: an anastomising web of carbonates, smectites, probably serpentine, and hematite completely replaces most of the rock. The intrusion is crossed by several alteration veins or brecciated horizons filled by brown fine-grained material similar to that forming the zone b. A preliminary comparison (by means of smear slides) of matrix found in veins at different depths, suggested some variability: at 904.05 and 908.08 mbsf matrix is mainly chlorite and sericite, whereas at 905.20 mbsf smectite and sericite are the most abundant minerals and hematite and plagioclase grains are minor;

d) interval between *c.* 918–918.95 mbsf, thickness 0.95 m: breccia with angular and subangular fragments, frequently deeply altered. Clasts belong both to the underlying Beacon sandstones and to the intrusion. They are immersed in a fine-grained brown (7.5YR4/4) matrix mineralogically similar to that observed in zone b;

e) interval below 919 mbsf: the Beacon sandstone underlying the intrusion, shows a progressive change in colour, from purple (5P2/2) to light red/brown (5YR6/6), and a decrease of hardness with distance from the interface with the upper breccia.

CHEMISTRY

Four samples representing different horizons of the igneous intrusion (at 903.35, 909, 915.33, and 906.96 mbsf) were analysed for major and trace elements by XRF at Victoria University, Wellington. Results are reported in table 4.9.

The chemical compositions of these rocks confirm the occurrence of extensive weathering, as previously observed in thin sections. In all samples, major element concentrations appear to be strongly modified by alteration processes as large loss of ignition values (LOI) and normative corundum in the CIPW norm (Tab. 4.9) are detected. Thus, measured concentrations do not represent the original compositions of the igneous body and cannot be used to infer magmatic affinity.

However, significant differences exist among specimens: these are consistent with petrographical observations that indicate a primary effect of the weathering processes in the lower portion of the igneous body at a depth below 909.00 mbsf, although an original compositional zoning cannot be excluded. Specimens from the lower portion of the intrusion show highest LOI values, anomalously large iron contents and low silica concentrations. Highest iron content, associated with the largest LOI, can be mainly ascribed to the diffuse occurrence of Fe-carbonate (see also Clay Mineralogy section) and subordinately to the presence of haematite. In this case LOI would represent mainly the CO_2 loss.

Minor and trace elements show an analogous variability that can be ascribed to re-mobilisation due to alteration. However, some elements (Ti, P, Zr, Nb, Y) that are known to be less affected by alteration processes can still be used for comparisons with exposed igneous rocks and to infer the magmatic affinity. In figure 4.9 the samples of the CRP-3 intrusions are plotted in the classification-discrimination diagram of Floyd & Whinchester (1978), based on ratios of immobile elements. Even though a significant scatter exists, they fall inside the subalkaline field, astride the divide between basaltic and andesitic compositions. These results rule out the parentage of these rocks with the alkaline Cenozoic magmatism and suggest rather a close correspondence with Jurassic Subalkaline rocks (Ferrar Supergroup). Also samples of the CRP-3 intrusion show Zr-Nb ratios quite close to those observed in Ferrar tholeites (Fig. 4.10).

EMPLACEMENT STYLE AND HYPOTHESIS ON ORIGIN AND AGE

The geometrical relationships outlined above between the intrusion and the country rock and the petrographical characterization of the former can be used make inferences on the emplacement and cooling styles of the intrusion. The inferred presence of glass in the magmatic rock points to relatively fast cooling of the margin of the magmatic body, whereas the occurrence of breccia in a clay-rich zone indicates an important episode of brittle deformation and hydrothermal alteration at a lower temperature that must have accompanied or followed the emplacement. The hydrothermal processes were sufficiently intense that the outer part of the intrusion (zone b and d) was mechanically and chemically modified. The lack of significant thermal metamorphic effects suggests that intrusion occurred in a short time

Tab. 4.9 - Chemicalcomposition and CIPW norm of CRP-3 igneous intrusion.

sample	903.35 mbsf	906.94 mbsf	909 mbsf	915.33 mbsf
SiO2	56,53	54,00	34,24	38,52
TiO2	1,01	0,97	0,62	0,64
Al2O3	24,57	20,97	15,91	15,29
Fe2O3	4,87	8,55	20,64	18,46
MnO	0,01	0,06	0,16	0,18
MgO	0,92	1,23	2,19	2,74
CaO	0,57	0,80	2,40	3,78
Na2O	0,56	0,63	0,19	0,12
K2O	2,40	1,88	2,87	3,60
P2O5	0,03	0,13	0,10	0,11
LOI	9,36	10,71	20,91	17,46
sum	100,83	99,93	100,23	100,90
		CIPW Norm (Fe2O3/FeO=0.15)		
Q	39,32	39,96	1,60	1,09
C	20,09	18,94	8,37	4,59
or	14,18	12,56	16,96	21,27
ab	4,74	6,03	1,61	1,02
an	2,63	3,53	11,25	18,03
hy	7,25	14,90	32,75	31,16
mt	0,84	1,67	3,56	3,18
il	1,92	2,08	1,18	1,22
ap	0,07	0,34	0,23	0,25
		Trace Element (ppm)		
As	1	12	2	0
Ba	179	198	577	521
Ce	38	65	29	30
Cr	75	73	150	135
Cu	77	90	110	93
Ga	22	19	21	21
La	15	18	21	10
Nb	7	8	5	4
Ni	36	57	51	98
Pb	9	16	9	8
Rb	70	75	64	181
Sc	47	73	52	53
Sr	84	150	61	56
Th	5	5	2	2
U	2	3	1	2
V	149	155	194	185
Y	13	27	34	50
Zn	42	66	584	131
Zr	163	144	95	98

Analysts :R. Grapes, J.E. Patterson
(Victoria Univ. Analytical Facility - Wellington, NZ)

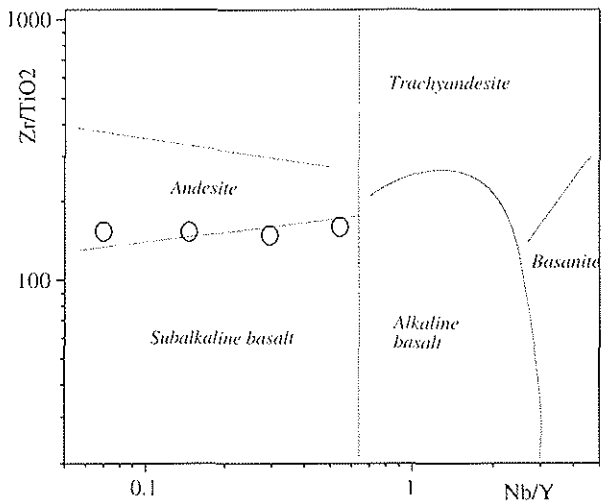

Fig. 4.9 - Discrimination and classification diagram according to Floyd & Whinchester (1978). Open circles: CRP-3 igneous intrusion specimens.

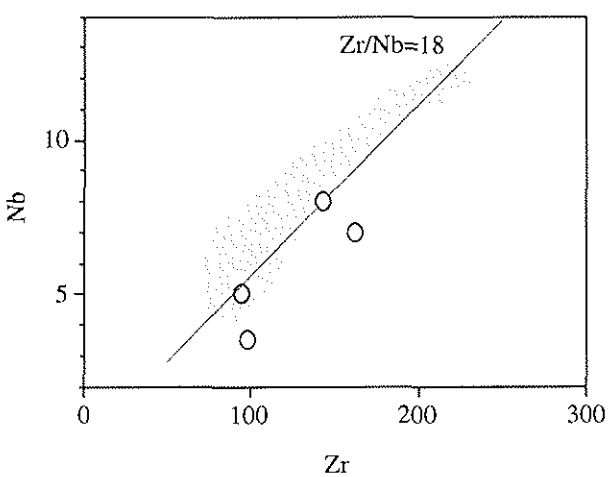

Fig. 4.10 - Correlation plot of Zr *vs* Nb. Open circles: CRP-3 igneous intrusion specimens; stippled area and best fitting curve are relative to Ferrar tholeiites of Hornig (1993).

span. The lack of vesiculation appears to exclude emplacement at shallow depths (*e.g.* neck or plug). The process responsible for the peripheral alteration could have been secondary boiling of the magma.

Even if chemical composition of the igneous intrusion points unequivocally to a parentage in Jurassic tholeiitic magmatism, its emplacement style shown in the CRP-3 intrusion is rather unusual for Ferrar dolerites. These normally show only a sharp contact with the host rocks (Roland & Worner, 1996). In addition, in Ferrar sills an extended crystallization due to a low-cooling rate produces very evolved residual liquids and quartz precipitation. These are lacking in the CRP-3 intrusion. However, fine-grained rocks with intergranular to intersertal textures were also found as clasts in CRP-3 (see Volcanic Clast section) and are known to form margins of some Ferrar sills (Elliot et al., 1995). On the other hand, some alkaline intrusions show important hydrothermal aureoles (*e.g.* Volcan Hills, Armienti et al., 1994) although chemical composition and mineral assemblages are very different from those of the CRP-3 intrusion.

Terra Antartica
Initial Report on CRP-3
2000, **7** (1/2)

5 - Palaeontology

INTRODUCTION

We examined six groups of fossils during the initial core-characterisation phase of CRP-3 drilling: siliceous microfossils, calcareous nannofossils, foraminifers, marine palynomorphs, terrestrial palynomorphs (miospores), and invertebrate macrofossils. Each of these groups provides the means for biostratigraphical dating or palaeoenvironmental reconstruction, or both.

Siliceous microfossils, including diatoms, ebridians, chrysophycean cysts, and silicoflagellates, are the primary means of biostratigraphical age determination in the Cenozoic of the Antarctic margin. In addition, they provide information on the nature of mesotrophic or neritic surface waters (planktonic), nearshore bottom conditions (benthic), and offshore transport (allochthonous benthic) of fine-grained material.

Calcareous nannoplankton inhabit surface waters in abundance only under oligotrophic nutrient levels, and thus are an important indicator of the invasion of oceanic surface-water masses into the Ross Sea. Benthic foraminifers and invertebrate macrofossils indicate past seafloor conditions including temperature and substrate character. In addition, their shells (if well preserved) contain carbonate that may be used for geochemical age determination (Sr), palaeothermometry ($\delta^{18}O$) and seawater carbon chemistry ($\delta^{13}C$).

Marine palynomorphs offer the potential for biostratigraphical age determination and palaeo-environmental characterisation in the Oligocene and Neogene. Miospores offer a way to monitor the evolution of adjacent terrestrial ecosystems in marine sedimentary rocks. Because of the significant changes in climatic regime during the Cenozoic, miospore stratigraphy also can provide age determination. Finally, all of the microfossils can provide monitors on the intensity and provenance of sedimentary rock erosion. This is especially true of the highly resistant palynomorphs.

PATTERNS OF FOSSIL OCCURRENCE

Siliceous microfossils occur within the upper 200 m of CRP-3 (Fig. 5.1), although high abundance and well-preserved assemblages are restricted to the upper 67 m. Within this upper 67 m, two distinct intervals of good abundance and preservation (3.05 to 16.00 and 33.95 to 66.70 mbsf) are separated by an interval with low abundance and generally poor preservation. Sparse assemblages of highly fragmented, etched or replaced (silicified casts) specimens of siliceous microfossils are present sporadically in the interval from 67 to 193.16 mbsf. Below this level, no siliceous microfossils were observed.

Calcareous nannofossils are restricted largely to the upper 194 m of the core, where they occur as sparse assemblages of low species richness. Four intervals of nannofossil occurrence are separated by barren intervals from 7 to 16, 48 to 77, and 162 to 178 mbsf. Preliminary count data indicate a significant increase in nannofossil abundance as a sedimentary component between 100 and 124 mbsf, with a maximum at 114 mbsf and secondary peaks at 100, 106, and 121 mbsf. Preservation is generally very good to excellent, although some of the sparser samples have significantly degraded preservation. Nannofossils largely disappear from the section at 193.14 mbsf, although a single occurrence at 266.27 mbsf suggests more samples below 200 mbsf may yield fossils upon closer examination.

Foraminiferal occurrence is largely restricted to the cored interval above 340 mbsf, where slightly more than half of the samples examined bear these fossils. Calcareous benthic foraminifers are the dominant form, with rare agglutinated taxa present only in a few samples. No specimens of planktonic foraminifers were seen above 340 mbsf, although a single specimen of *Globigerina* sp. was observed from 705.97 mbsf. Four intervals of benthic foraminiferal occurrence are separated by barren intervals from 65 to 85 mbsf, 210 to 250 mbsf, and 268 to 310 mbsf. A major peak in abundance of foraminifers as a sedimentary component occurs from 106 to 115 mbsf, with secondary peaks at 10.65, 44.12, 45.72, and 162.16 mbsf. Preservation is generally fair to good, suggesting little diagenetic alteration.

Macrofossils occur within the finer grain sedimentary rocks (mudstones and muddy sandstones) throughout the upper 330 m of the cored interval (Fig. 5.1). Macrofossil density in the core varies through this interval, with an average of about 7 macrofossils or macrofossil fragments per 10 metres of core. The abundance maximum occurs from 120 to 130 mbsf, with secondary peaks at 190 to 200 and 310 to 320 mbsf. Macrofossils become rare below 330 mbsf, with only five specimens between 330 to 540 mbsf. The rest of the cored interval, below 540 mbsf, is barren of macrofossils with the exception of a plant stem impression at 730.48 to 730.56 mbsf and a single modiolid mussel at 781.35 mbsf. Bivalves are the most common macrofossil in the core, comprising about 80% of the identifiable invertebrate macrofossil material. Important secondary components include brachiopods, serpulids, echinoids, and gastropods. Preservation of the macrofossils is variable, although almost all of them show evidence of dissolution. The high frequency of broken shells in some lithostratigraphical units is attributed to significant corrosion of the shell material.

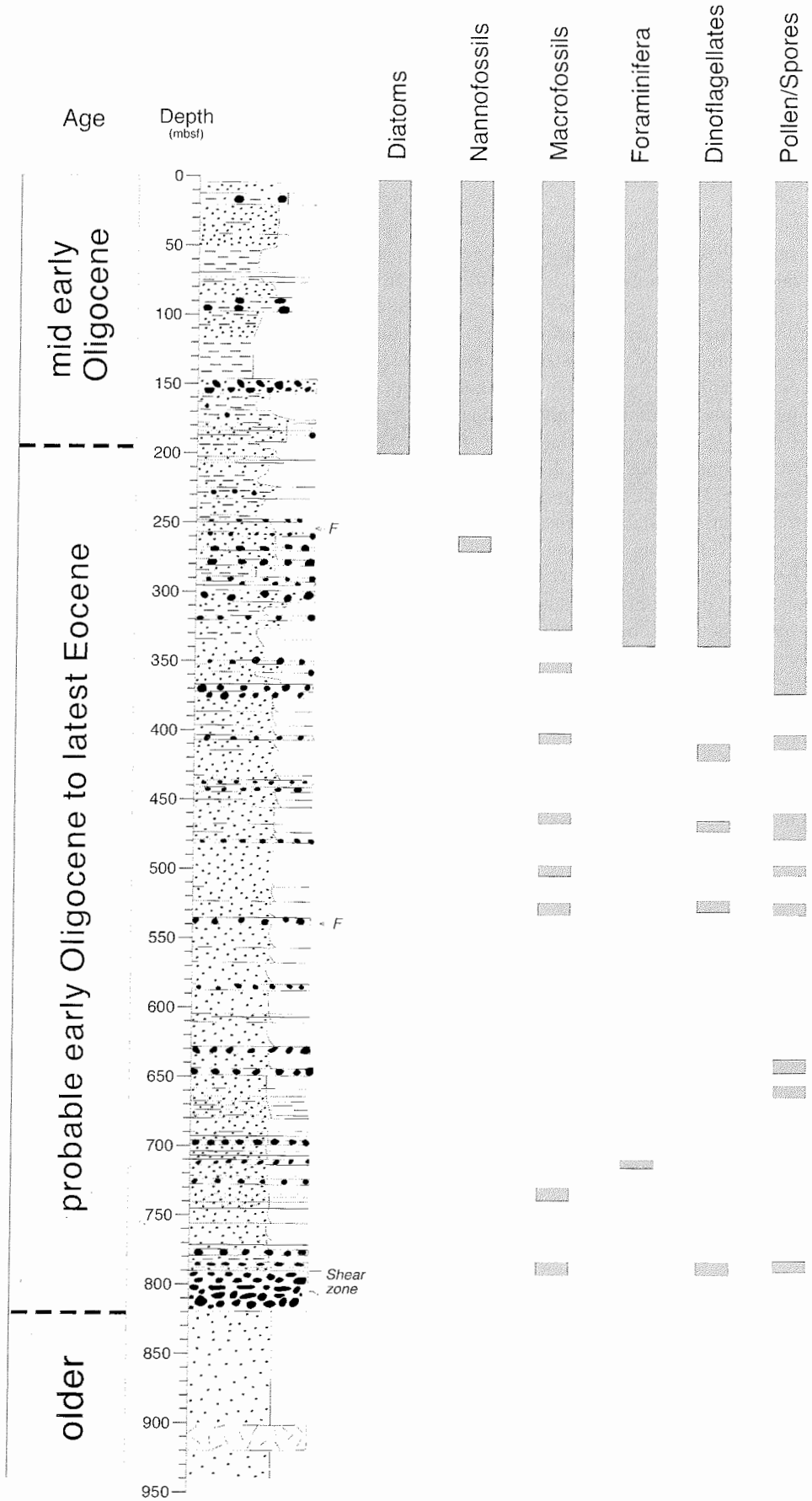

Fig. 5.1 - Generalised distribution of fossil groups in CRP-3 based on initial core characterisation. Grey bars indicate known occurrences of fossil group.

Marine palynomorphs are a consistent microfossil component in the fine-grained sedimentary rocks through the upper 257 m of CRP-3. They occur in moderate to low levels of abundance and diversity throughout this upper interval. Their occurrence becomes more sporadic from about 260 to 332 mbsf. Below this horizon, marine palynomorphs occur only in isolated samples. There are two distinct abundance peaks, at 521.76 and from 781.36 to 788.69 mbsf, within a thick sequence of dominantly coarse-grained clastic sedimentary rocks that appear to be otherwise barren or nearly barren of marine palynomorphs on initial examination.

Terrestrial palynomorphs have their greatest abundance and species richness in the upper 230 m of CRP-3. Three distinct intervals of relatively high miospore abundance occur at about 114, 190, and 225 mbsf. Miospore abundance drops to very low levels between 230 and 300 mbsf, and rises slightly from 300 to 340 mbsf. Below this level, miospores occur at only trace levels down to 781 to 789 mbsf, where there is a slight increase. A few specimens have been isolated from the fine-grain matrix within the dolerite breccias of the interval designated as the "shear zone". A few samples were examined from the upper part of the Beacon Supergroup sandstones, but proved to be barren.

BIOSTRATIGRAPHY

Initial core characterisation yielded biostratigraphical information largely for the upper 200 m of the core. Two biostratigraphical datums in this interval allow correlation with the better-documented sections of deep-sea Southern Ocean drillcores. The first appearance datum (FAD) of the diatom *Cavitatus jouseanus* occurs at 48 mbsf in CRP-3. This datum is known to occur in the uppermost part of C12R in the Southern Ocean proper, placing it at approximately 31 Ma. The nannofossil *Transversopontis pulcheroides* has its last appearance datum (LAD) at 114 mbsf in CRP-3. This LAD occurs in the middle of the *Blackites spinosus* Zone (mid to lower C12R) in the Southern Ocean, indicating an age of approximately to 32.4 ± 0.5 Ma. The position of both these datums in the interval from 48 to 114 mbsf in CRP-3 indicates a mid early Oligocene age for this part of the core. In addition, the absence of *Hemiaulus caracteristicus* throughout the section that contains diatoms (0-193.6 mbsf) indicates that this entire interval is less than *c.* 33 Ma, as is shown conservatively in figure 5.1 (the dashed line at 193.60 mbsf in this figure may be depicted deeper in the section elsewhere in these *Initial Reports*).

Two specimens of the pollen *Myricipites harrisii* occur at 781.36 mbsf. If these specimens are in place, it suggests that the base of the Cenozoic sedimentary section in CRP-3 may be late Eocene in age. This age determination is based on analogy with the New Zealand palynological record that records a change upsection in the dominant flora from a *Myricipites harrisii*-dominated one to a *Nothofagus brassii*-dominated one near the top of the Kaiatan Stage. Additional work is necessary to establish whether this palynoflora is in place and can be used as a reliable age indicator. The same sample contains an oligotaxic dinoflagellate cyst assemblage dominated by an unknown dinocyst. Asssociated with this new species is a specimen of *Lejeunacysta* similar to those occurring higher in CRP-3. Since these are new taxa, their biostratigraphical significance is unknown.

The limited time available at the Crary Science and Engineering Center (CSEC) for initial core characterisation precluded a more extensive examination of fossil assemblages for biostratigraphy. Additional examination of samples, as well as collection of new samples, should provide further age constraints.

PALAEOENVIRONMENT

No palaeontological data are presently available from the basal ("Beacon") portion of the corehole, and it is not discussed further. There are sporadic occurrences of marine palynomorphs, macrofossils, and foraminifers from the lower portion of the Cenozoic section (*c.* 340 to 780 mbsf). These occurrences suggest that the sedimentary rocks at the base of the section (*c.* 705 to 790 mbsf) and from 350 to 525 mbsf are marine in origin. The interval from *c.* 525 to 700 mbsf is barren of any fossils other than isolated occurrences of miospores, yielding no useful information on palaeoenvironment.

The presence of dinoflagellate cysts, invertebrate macrofossils, and benthic foraminifers from 200 to 350 mbsf indicates marine conditions were consistent over the depositional site. Both macrofossils and benthic foraminifers indicate shelfal palaeowater depths. Benthic foraminifersl assemblages suggest a range of 50 to 200 m water depth, while macrofossils generally suggest a range of 30 to 120 m. Combining these ranges yields an estimated water depth of 50 to 120 m for most of this interval.

The presence of siliceous microfossils and calcareous nannofossils in the upper 200 m of the section indicates the presence of oceanic waters within the photic zone during the middle of the early Oligocene. The most abundant phytoplankton fossils in this stratigraphic interval, the diatoms, contain a relatively high proportion of resting spores (*e.g.*, *Chaetoceros* and *Stephanopyxis*). The high relative abundance of ebridians and chrysophycean cysts in these assemblages indicates a shelfal depositional environment. The paucity of benthic diatoms (0-5%) indicates that the photic zone did not reach the sediment-water interface during deposition, suggesting that the few benthic diatoms in these assemblages were washed in from shallower environments. Alternatively, the sediment-water interface may have been in the photic zone only episodically, resulting in small standing crops of benthic diatoms. Calcareous nannofossil assemblages in the upper 200 m of CRP-3 indicate episodic invasion of more oligotrophic oceanic surface waters into the area during the middle of the early Oligocene. These

assemblages consisted almost exclusively of species of *Dictyococcites*, suggesting significant ecological exclusion of other taxa known from coeval deposits in the Southern Ocean.

Estimates of palaeowater depth based on benthic foraminifers and macrofossils suggest a continuation of mid to outer shelfal conditions. Combined estimates yield the same 50-120 m palaeowater depth for the upper 200 mbsf. Dinoflagellate cyst assemblages suggest similar water-depth ranges. Modioloid assemblages in the upper part of this interval (*c.* 5-12 mbsf) suggest the deeper part of this water-depth range for Lithostratigraphic Unit 1.

The terrestrial miospore record suggests a fairly constant vegetational cover for the adjacent landscape during the deposition of the upper *c.* 360 m of the section. The recovered assemblages suggest a low-diversity *Nothofagus*-podocarp scrubland. Low absolute abundance of miospores suggests that this vegetation was patchy; more stunted vegetation and bare ground is likely to have prevailed in upland and exposed areas.

SILICEOUS MICROFOSSILS

INTRODUCTION

Siliceous microfossils (marine diatoms, ebridians, silicoflagellates, chrysophycean cysts, and endoskeletal dinoflagellates) are the primary biostratigraphical tool in post-Eocene, southern high-latitude sedimentary successions. Biosiliceous sediments are particularly well-known from Southern Ocean deep-sea sections, and are the main source of taxonomical and biostratigraphical reference material for siliceous microfossil assemblages recovered in Cape Roberts Project (CRP) cores. Most reports on siliceous microfossils from these deep-sea sections focus on the stratigraphical distribution of marine diatoms. Important Southern Ocean diatom records are derived from sections recovered on DSDP Leg 29 (Hajós, 1976), DSDP Leg 35 (Schrader, 1976), DSDP Leg 36 (Gombos, 1977), DSDP Leg 71 (Gombos & Ciesielski, 1983), ODP Leg 119 (Baldauf & Barron, 1991), and ODP Leg 120 (Harwood & Maruyama, 1992). Eocene and Oligocene diatom occurrences for DSDP sites 274, 278, and 511 (from legs 28, 29, and 71) are summarized in Fenner (1984). Several reports from stratigraphical sections outside of the Antarctic region also contribute useful information for interpreting diatom stratigraphy of CRP cores (Gladenkov & Barron, 1995; Scherer & Koç, 1996; Schrader & Fenner, 1976; Gladenkov, 1998).

Stratigraphical drilling and piston coring on the Antarctic shelf to date has provided only a limited number of reference sections. These sections indicate significant differences between diatom assemblages from the Antarctic shelf and those from the pelagic realm of the Southern Ocean (hereafter referred to as "Southern Ocean" taxa, etc.). Documentation of siliceous-microfossil floras in Antarctic shelf sections provided a basic framework for the development of an Oligocene-Miocene biostratigraphy for this region. Diatom biostratigraphy is now sufficiently advanced to allow application of many datums, but refined zonal schemes and chronostratigraphical constraints for these biostratigraphical datums are still under development. Reference sections for Miocene and Oligocene diatom biostratigraphical data from the Antarctic shelf include DSDP Leg 28 cores (McCollum, 1975; Savage & Ciesielski, 1983; Steinhauff et al., 1987); the MSSTS-1drillcore (Harwood, 1986); the CIROS-1 drillcore (Harwood, 1989); RISP Site J-9 (Harwood et al., 1989b), ODP Leg 119 cores (Baldauf & Barron, 1991; Barron & Mahood, 1993; and Mahood et al., 1993); and the CRP-1 and CRP-2/2A drillcores (Harwood et al., 1998; Scherer et al., in press). Additionally, parts of the Eocene are known from glacial erratic boulders collected from southern McMurdo Sound (Harwood & Bohaty, in press).

In Antarctic shelf sections, pelagic marker taxa from the Southern Ocean proper are generally rare and occurrences are discontinuous. Despite the rare occurrence of marker taxa, a paucity of chronostratigraphical calibration for these shelf sections has forced a reliance on age control from deep-sea Southern Ocean diatom stratigraphy (*e.g.* Barron & Baldauf, 1991; Harwood & Maruyama, 1992; Ramsay & Baldauf, 1999). Current knowledge provides for the development of a general biostratigraphical framework, but hiatuses in these shelf sections lead to the coincidence of truncated ranges of numerous taxa. Drilling on the Antarctic shelf, however, as at CRP-1 to -3, holds great promise for the acquisition of a diatom-based stratigraphy that could reach an age resolution of less than one million years for most of the Oligocene and lower Miocene. This developing zonation includes a mixture of range zones, partial-range zones, concurrent-range zones, and interval zones based on first and last appearance datums. We prefer to use first occurrence datums, as these limit problems associated with microfossil recycling that is common in glacially influenced environments.

METHODS

We prepared samples for siliceous microfossil analysis at a sample spacing of 1-2 m in the upper 200 m of CRP-3 (Tab. 5.1, Fig. 5.2). Sampling and slide preparation focused on the upper 70 m, where diatoms are abundant and well-preserved; approximately 100 samples were analyzed within this interval. Below 200 mbsf, "fast-track" samples were prepared at an average sample spacing of *c.* 20 m.

All CRP-3 samples collected for siliceous microfossil examination were initially prepared as strewn-slides of raw sediment. Approximately 1 cc of each sample was 'gently' crushed, placed in a 50 ml plastic vial, disaggregated in water, stirred, and settled for 30 seconds

Tab. 5.1 - CRP-3 relative diatom abundance data, 0-100 mbsf.

Top	Bottom	Abundance	Top	Bottom	Abundance
2,85	2,86	R	46,84	46,85	R
3,05	3,06	F*	47,60	47,61	F
5,01	5,02	C	47,87	47,88	A
6,87	6,88	C	48,43	48,44	F
7,85	7,86	A	48,44	48,45	F
8,15	8,16	C	49,67	49,68	A
8,88	8,89	C	50,47	50,48	C
9,69	9,70	C	50,89	50,90	A
10,48	10,49	R	51,56	51,57	C
10,78	10,79	C	52,54	52,55	F
11,12	11,13	C	52,91	52,92	R
11,63	11,64	C	54,19	54,20	A
12,19	12,20	A	54,54	54,55	A
12,64	12,65	A	54,77	54,78	A
13,72	13,73	A	55,66	55,67	A
14,28	14,29	F	56,16	56,17	C
14,46	14,47	C	56,84	56,85	A
15,68	15,69	T	57,71	57,72	A
15,99	16,00	F	57,80	57,81	A
17,82	17,83	T	58,95	58,96	C
18,02	18,03	R	59,21	59,22	A
18,19	18,20	T	59,66	59,67	C
19,10	19,11	T	60,13	60,14	F
19,62	19,63	T	61,10	61,11	C
20,46	20,47	T	61,70	61,71	C
21,36	21,37	T	62,12	62,13	A
22,12	22,13	T	62,46	62,47	A
22,26	22,27	F	62,98	62,99	A
22,75	22,76	T	63,64	63,65	C
24,20	24,21	R	64,04	64,05	F
25,08	25,09	B	64,44	64,45	C
25,94	25,95	T	64,57	64,58	F
26,72	26,73	T	64,93	64,94	T
28,44	28,45	R	65,90	65,91	F
28,70	28,71	R	66,16	66,17	F
30,50	30,51	T	66,56	66,57	R
32,20	32,21	F	66,70	66,71	F
32,51	32,52	T	68,59	68,60	T
33,21	33,22	T	70,60	70,61	R
33,95	33,96	F	71,27	71,28	T
34,57	34,58	R	71,54	71,55	T
35,70	35,71	C	72,89	72,91	T
36,61	36,63	C	73,61	73,62	T
37,29	37,30	A	74,93	74,94	T
37,71	37,73	A	76,08	76,09	T
38,78	38,79	C	77,11	77,12	T
39,34	39,35	C	77,80	77,81	T
39,35	39,36	A	80,33	80,34	T
40,63	40,64	R	80,91	80,92	T
41,00	41,01	C	81,98	81,99	T
41,75	41,76	C	82,34	82,35	T
41,76	41,77	T	83,04	83,05	T
43,09	43,10	A	85,46	85,47	T
43,10	43,13	C	87,14	87,15	T
43,70	43,72	F	88,18	88,19	R*
43,72	43,73	C	89,25	89,26	T
44,18	44,27	F	90,86	90,87	T
44,50	44,52	C	91,91	91,92	B
44,93	44,94	F	92,94	92,95	T
45,63	45,64	F	93,52	93,53	T
46,04	46,05	R	96,06	96,07	T
46,42	46,43	C	98,13	9,14	T

*sedimentary clast sample

(to remove sand). A small aliquot of the supernatant was pipetted onto a cover slip, allowed to dry, and then mounted onto a glass slide with Norland Optical Adhesive #61. As necessary, selected samples and sedimentary clasts were reacted in H_2O_2 and/or HCl to remove organic material and carbonate cement, respectively. In many samples, diatoms were concentrated by sieving at 6 or 10 mm (using nylon screens) or at 25 mm (using stainless-steel mesh sieves) in an attempt to remove clay-size particles and to concentrate microfossils. A few samples were further prepared with density-separation, using a heavy-liquid solution of sodium polytungstate (mixed at 2.2 specific gravity).

We determined relative diatom abundance per sample (Fig. 5.2) from strewn slides of unsieved material, according to the criteria outlined below. Total abundance of diatoms was estimated at 750x magnification. The amount of fine-grained biosiliceous fragments was also considered in these estimates, in order to help assess and interpret intervals of both significant biosiliceous sedimentation and absence of diatom production.

B = Barren: no diatom valves or fragments were observed.
T = Trace/Reworked: rare fragments were observed.
R = Rare: 1 complete valve observed in 5-30 fields-of-view.
F = Frequent: 1 complete valve observed in 1-5 fields-of-view.
C = Common: 2-5 complete valves observed per field-of-view (or "frequent" occurrence with a large component of the silt- and clay-sized fraction of biosiliceous fragments).
A = Abundant: >5 complete valves observed per field-of-view (or "common" occurrence with most of the silt- and clay-sized fraction of biosiliceous material).

The abundance of individual taxa (Tab. 5.2) was also estimated at 750x magnification following the divisions outlined below:

r = Reworked or redeposited.
fr = Fragments: rare fragment(s) of the taxon noted.
X = Present: complete specimens rare (<1 per traverse).
R = Rare: 1 specimen in 5-30 fields of view.
F = Frequent: 1 specimen in 1-5 fields of view.
C = Common: 1 specimen in every field of view.
A = Abundant: 2 specimens per field of view.

Siliceous microfossil data collected from CRP-3 include many informal taxonomic designations. These designations follow those presented for CRP-2/2A (Scherer et al., in press) and will be formally named and described in separate publications. Reference to taxa listed in table 5.2 can be found in the literature cited above.

RESULTS

Siliceous microfossils are present in the upper 200 m of the CRP-3 drillcore in variable abundance (Fig. 5.2) and preservation. Excellent diatom preservation and high abundance characterize siliceous microfossil assemblages in the upper 67 m, except for the interval between *c.* 17 and 33 mbsf, which contains only a trace of diatoms. Below this level, the sediments are either barren or contain poorly-preserved siliceous microfossils that are highly fragmented, etched (through dissolution), or are replaced as silicified casts. Several intervals in this lower zone represent "residual" assemblages that were once rich in siliceous microfossils (*e.g.*, *c.* 120-130 mbsf and *c.* 190-195 mbsf). These assemblages are interpreted to have undergone significant diagenetic alteration, including dissolution and replacement.

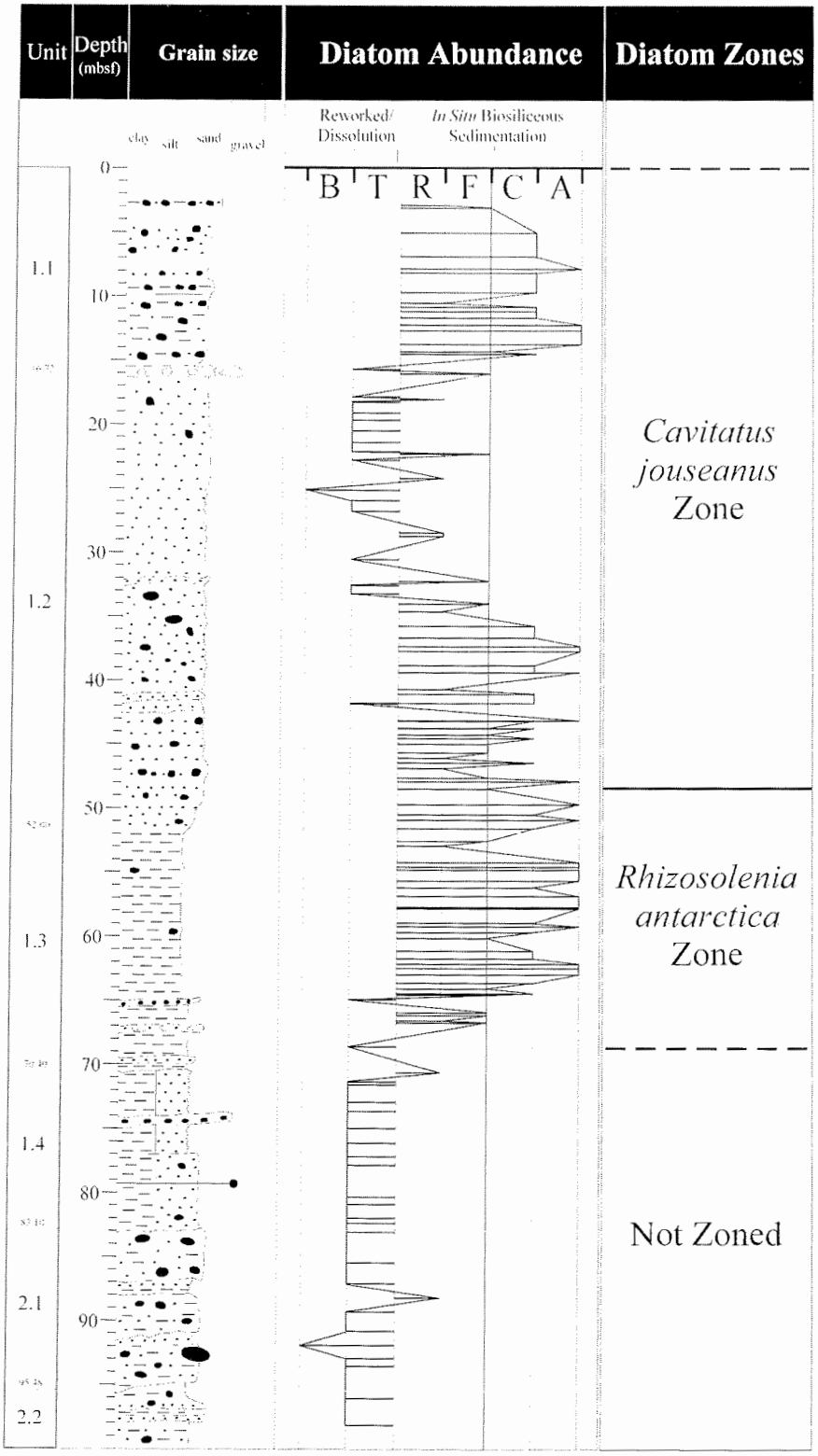

Fig. 5.2 - Total diatom abundance for the upper 100 metres of CRP-3, plotted against the lithological summary log. Abundance categories are defined as follows: B = barren; T = trace; R = rare; F = frequent; C = common; A = abundant.

The CRP-3 drillcore recovered a fossil record of more than 120 marine diatom taxa, 6 silicoflagellate taxa, 8 ebridian and other siliceous flagellate taxa, and 3 chrysophyte cyst taxa. Diatom assemblages from LSU 1.1, 1.2, and 1.3 (2.85 to 66.71 mbsf) are the most diverse, well-preserved and abundant in CRP-3. The only poorly-preserved interval within this section is the upper *c.* 13 metres of LSU 1.2, between 15.68 and 28.44 mbsf (Fig. 5.2).

Diatom assemblages recovered from CRP-3 are relatively uniform in composition and are dominated by marine planktic taxa of the genera *Chaetoceros,*

Stephanopyxis, Skeletonemopsis, Kisseleviella, Ikebea, Kannoa, Pseudotriceratium, and *Pyxilla*. Benthic diatom taxa occur throughout this interval, but represent <5% of the total assemblage. This low abundance and their sporadic stratigraphical occurrence suggest displacement from an adjacent coastal zone into a depositional setting inferred to be below the euphotic zone. Based on these inferences, we interpret paleo-water depths to be greater than 50-70 mbsf. No significant changes in water depth were identified from the diatom assemblage data. Diatom genera associated with freshwater environments were not encountered in CRP-3.

AGE AND STRATIGRAPHICAL CORRELATION

Several of the diatom taxa in CRP-3 assemblages are well-documented in Southern Ocean drillcores (Harwood & Maruyama, 1992). As indicated previously, however, most Southern Ocean taxa are rare in CRP-3 and occur sporadically. Until a biozonation is developed for Antarctic shelf sediments, correlation and age control for CRP-3 must be derived through linkage to the Southern Ocean diatom biostratigraphy.

In CRP-3, the first occurrence (FO) of *Cavitatus jouseanus* occurs between 48.44 and 49.68 mbsf (Tab. 5.2, Fig. 5.3) and marks the base of the *Cavitatus jouseanus* Zone of Scherer et al. (in press). The top of this zone is identified by the last occurrence (LO) of *Rhizosolenia antarctica,* which is noted in the CRP-2A drillcore up to a depth of 441.85 mbsf (Scherer et al., in press).

The age of the FO of *Cavitatus jouseanus* has been determined at several Southern Ocean sites, but is applied in the present study with some caution. In ODP Hole 748B (Kerguelen Plateau), this datum occurs within the lower part of the calcareous nannofossil *Chiasmolithus altus* Zone, within Chron C12n (Harwood & Maruyama, 1992; Harwood et al., 1992; Wei & Wise, 1992). The age of this datum is inferred from a position near the base of C12n at *c.* 30.9 Ma (using the time scale of Berggren et al., 1995). The FO of *C. jouseanus* in ODP Hole 744A (Kerguelen Plateau) also occurs within the lower part of the calcareous nannofossil *Chiasmolithus altus* Zone, near the boundary between chrons C12n and C12r in ODP Hole 744A (Baldauf & Barron, 1991; Barron et al., 1991, Figure 10). Fenner (1984) questioned the utility of the FO of *Cavitatus jouseanus* due to its rare and sporadic occurrence within the *Rhizosolenia oligocaenica* Zone in DSDP Site 274. The record in ODP Hole 748B also reflects this rare and sporadic occurrence in the lower range of *C. jouseanus*, suggesting the age of this datum could be slightly older than reported above. A conservative approach would place the FO of *Cavitatus jouseanus* within the upper part of Chron C12r.

The FO of *Rhizosolenia antarctica* between 68.60 and 70.61 mbsf in CRP-3 marks the base of the *Rhizosolenia antarctica* Zone of Fenner (1984). The top of this zone, as presented here in a provisional zonation, is coincident with the base of the overlying *C. jouseanus* Zone. Fenner (1984) notes that the FO of *Rhizosolenia antarctica* occurs in DSDP Hole 511 within the uppermost part of the calcareous nannofossil *Blackites spinosus* Zone. In ODP Hole 744A, the FO of *Rhizosolenia antarctica* is recorded within Chron C13n, in the lower *Blackites spinosus* calcareous nannofossil Zone (Baldauf & Barron, 1991; Barron et al., 1991). Based on this occurrence, the lower range of *Rhizosolenia antarctica* is interpreted as incomplete in the CRP-3 drillcore, as it is truncated at an underlying interval of poor preservation (*c.* 70 mbsf) (Figs. 5.2 & 5.3). Given the high sediment accumulation rates in lower Oligocene sediments at the mouth of Mackay Valley (CRP-3), the lowest occurrence of *R. antarctica* at 68.60 mbsf most likely represents a stratigraphic position well above the FO of this taxon. From these data, an age of *c.* 33.1 to 30.9 Ma is inferred for the 48.44 to 68.60 mbsf interval of CRP-3.

The section of CRP-3 below *c.* 70 mbsf is unzoned at the present time due to poor preservation. Diverse, but poorly-preserved assemblages of siliceous microfossils, however, are noted sporadically in down to *c.* 195 mbsf (Tab. 5.2). These assemblages and the well-preserved, overlying assemblages in CRP-3 are different from the lowermost Oligocene to upper Eocene assemblages reported from CIROS-1 (Harwood, 1989; Bohaty & Harwood, in press). Several taxa present in the *Rhizosolenia oligocaenica* Zone below the unconformity at *c.* 366 mbsf in CIROS-1 (Harwood et al., 1989a, Fig. 1) are absent from the diatom-bearing intervals of CRP-3. These taxa include the diatoms *Hemiaulus caracteristicus, Stephanopyxis splendidus,* and *Porotheca danica* (formally *Pterotheca danica*), and the ebridians *Ebriopsis crenulata* (loricate and non-loricate), *Parebriopsis fallax,* and *Pseudammodochium dictyoides* (Fig. 5.3). This indicates that the upper 200 m of the CRP-3 drillcore is equivalent to part of the interval missing within the unconformity at 366 mbsf in CIROS-1.

The LO of the resistant and distinctive diatom *Hemiaulus caracteristicus* occurs within Chron C13n in ODP Hole 744A (Baldauf & Barron, 1991). The LO of *H. caracteristicus* is also known from DSDP Hole 511 within the lower part of the *Blackites spinosus* calcareous nannofossil Zone (see Fenner, 1984), but it occurs several 10s of meters below the FO of *Rhizosolenia antarctica* in DSDP Hole 511 (discussed above). From these data, the absence of *H. caracteristicus* in CRP-3 suggests an age younger than *c.* 33 Ma (Chron C13n) for sediments above 200 mbsf.

Comparison of the diatom assemblages present near the bottom of CRP-2A with those in the upper intervals of CRP-3 provides a means to estimate the overlap of these two drillcores. Poor preservation and absence of siliceous microfossils, however, in the lower 60 m of CRP-2A limits the resolution of this approach. Figure 5.3 presents the ranges of key siliceous microfossil taxa between these two drillcores. Six taxa are present at the top of the CRP-3 drillcore that are not present in the lowest diatom-bearing intervals of CRP-2A at *c.* 564 mbsf. Taxa

Tab. 5.2 - Relative abundance and occurrence data for selected siliceous microfossil taxa in the upper 100 metres of CRP-3. For abundance categories see p. 137.

Depth (mbsf)	Diatoms																																	Zonation
	Asteroiampra punctifera	*Asteromphalus oligocaenicus*	*Cavitatus jouseanus*	*Cavitatus* sp. A cf. *miocenicus*	*Eurossia irregularis*	*Eurossia irregularis* (swollen valve)	*Hemiaulus dissimilis*	*Hemiaulus incisus*	*Hemiaulus rectus* var *twista*	*Kisseleviella* sp. F	*Kisseleviella* sp. G	*Pyxilla reticulata*	*Pyxilla johnsoniana*	*Rhizosolenia antarctica*	*Rhizosolenia oligocaenica*	*Rouxia granda*	*Sceptroneis lingulatus*	*Sceptroneis talwani*	*Skeletonema? penicillus*	*Skeletonema? utriculosa*	*Skeletonemopsis mahoodii*	*Sphyncolethus pacificus*	*Stellarima primalabiata*	*Stephanopyxis oamaruensis*	*Stictodiscus kittonianus*	*Thalassiosira mediaconvexa*	*Vulcanella hannae*	**Ebridians and chrysophyte cysts** *Calicipedinium* sp. A	*Ebrinula paradoxa*	*Archaeosphaerridium australensis*	*Archaeosphaerridium tasmaniae*	
2,85					fr	R	R				X	R									R											R	
3,05			F				R			R	R	R		R	X				X													R	
6,87					R	R	R				R	R									F											R	
7,85	?				R	R	R		?	R	R	F	R				R		R	R	R	R		X	R		fr		?	R		F	
8,15			R		R		F				X	C	R				X	X	X		F		X		X							R	
9,69			X		R	R	R			R	R	R	R	X		X		R	R		R						X					X	
10,78			?		R	R	R		X	R	R	R	R	X					R	R	F		fr	R	R		R			R		R	
12,64					R	X	R			R	X	F	R	X		R		R	X		F												
13,72					R	R	R			R	R	R	R	R			R	fr	R	R	R											R	
14,46			X		R		F			X	X	R	F	X			X		X	R	R											R	
22,26					R		R				R	R					R		R	R	F											R	*Cavitatus jouseanus* Zone
24,20												X																				X	
25,94												X																					
28,44					X		R		X		X	R	X					R		X	X			X	X							R	
28,70					R	R	R		R	R	R	R	R				R		R	R	R	fr			R	X						R	
32,20							X				R	R	R	X	X			X			R											X	
33,95					R	R	R		R	R	R	R					R		R	R	F				R							R	
34,57					X		X													X	R											X	
36,61			X		X	R	R				F	F	R			X			X		C				R	F						R	
37,29	X		?		X		R				R	R	X					R	R	R	F					R						X	
38,78					R	X	R	X		R	F	F	R			R	X	R			F					R							
39,34			fr		R		R			X	R	R	X			X	R	R	R		F				X	R							
41,00			X				R				F	R	X		X			R	X	X	F				X	R							
43,70					R	R	X				R	X	R		X			R	X		R					R				X		X	
44,18	X	R				X	R				R	R			X			X			R	X	R		X	X				R		F	
44,93			R		X		X					R					X	X			R				X	X						X	
46,84				R			R					R	X					X	X	X	R											R	
48,43			X		R		R					R	X					R			R	R			R	X						R	
49,67		R			R	R	R		X		R	R	X	X					X	R	F	R			R	R				R		R	
50,47					R	R	R		R	X	R	R			R					R	R	R		X	R		R					F	*Rhizosolenia antarctica* Zone
51,56				X	R	R	F				R	F	R	X	R		X		X		C						X					R	
54,19					F		F				F	F	R	R					R	R	C								X			R	
54,77	X				F	F	R				R	F	F		X			X	R		A	?										X	
56,16				X	F	R	R				F	F	R	R				?	R		A											X	
57,71					R	R	R				F	R	R		X						A	X	X									R	
59,66					R		X				R	R	R	R					R		A											X	
61,70					F	R	R				F	F	R					?	X		A					R							
62,46				R	F	R	R				R	F	R						X		A					R						X	
62,98					R	R	R				R	R		X			?		X		F			X								R	
63,64					R		R				X	F		X	X				X	X	F					X						X	
64,44				X	X		R				X	R	X	X				X		X	F											R	
65,90					R		X				X	R							X		C					X						X	
66,70				fr	X		X					R	X					?		X	F											X	
68,59							X					X		X					R		F											X	
70,60					X		R					X								X	R											X	unzoned
71,27					X							R																					
72,89							X					X																					
73,61												X	X								R											X	
77,80												X									X												
81,98							L					fr									L											L	
82,34												X																				X	
101,03												X																					
117,07					L	L	L				L	L	L							L	X										L	L	
123,65							R				X	R									X											R	
127,11							L				R	L								L	L											L	
157,75											X	L									L											L	
190,81												fr									?												
193,16											fr	fr									X								X	L	X		

present in CRP-3, but not present in CRP-2A, include: *Hemiaulus rectus* v. *twista*, *Skeletonema*? *utriculosa*, *Sphyncolethus pacificus*, *Stictodiscus kittonianus*, *Skeletonema*? *penicillus*, and *Ebrinula paradoxa*. *Kisseleviella* sp. G is common in CRP-3 samples, but occurs only rarely in 2 samples from CRP-2A. Additionally, *Pseudammodochium lingii* occurs down to 465.00 mbsf in CRP-2A, but does not occur at all in CRP-3. From these data, siliceous microfossil assemblages in the upper portion of CRP-3 are sufficiently different from those in the lower portion of CRP-2A to argue for only minimal or no overlap of these drillcores

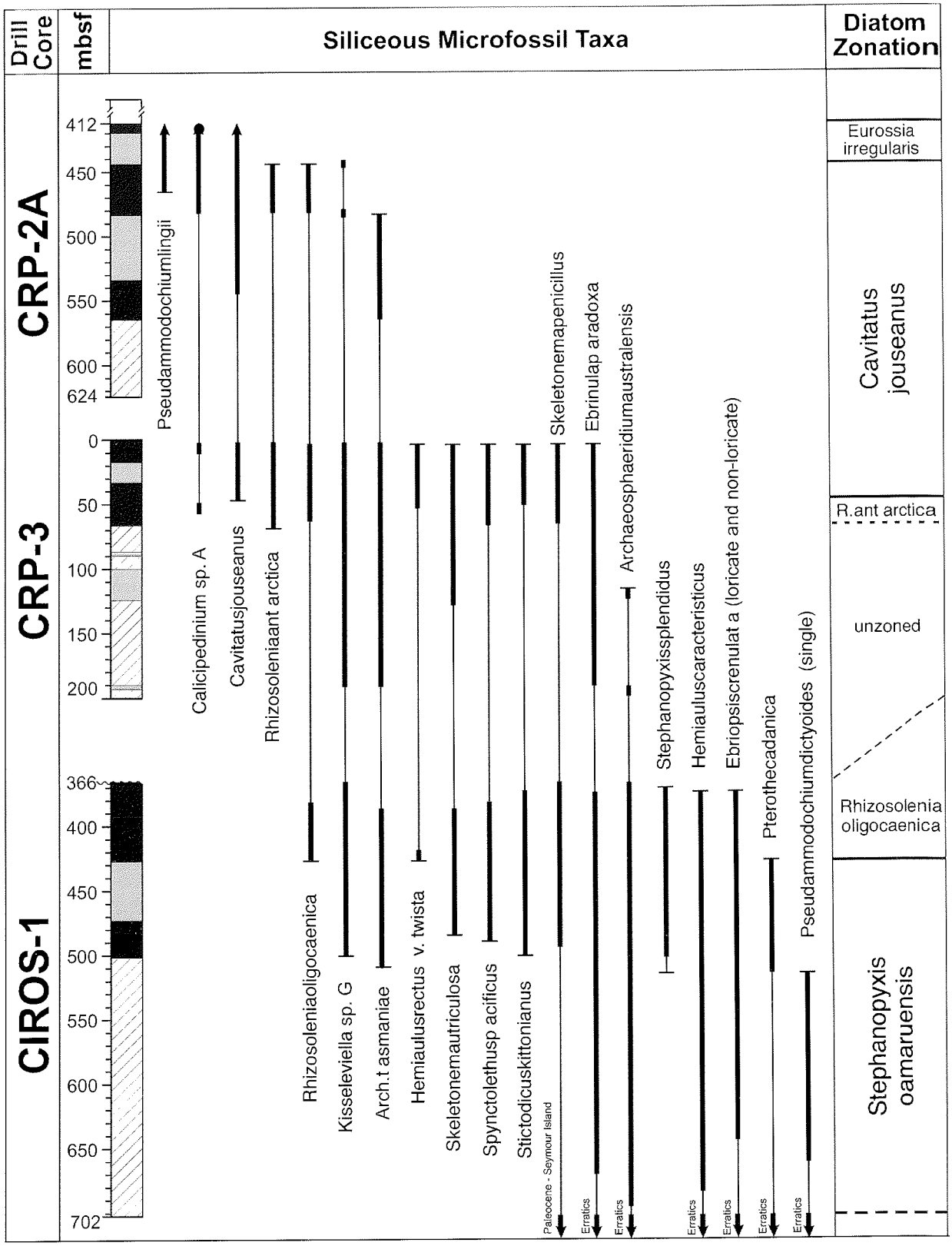

Fig. 5.3 – Comparison and correlation of the CRP-3 drillcore to higher stratigraphical intervals represented in the CRP-2/2A drillcore (Scherer et al., in press), and lower intervals recovered in the CIROS-1 drillcore (Harwood, 1989) based on the biostratigraphical ranges of siliceous microfossil taxa. Number scale on left side of the figure represents metres below sea floor (mbsf) in the three drillcores. Intervals with diagonal lines represent barren intervals or intervals of extremely poor preservation of siliceous microfossils. Dark-grey boxes represent intervals containing abundant and well-preserved assemblages, and those shaded with light grey represent poorly-preserved assemblages. Thick vertical lines reflect the occurrence data for siliceous microfossil taxa in each of the drillholes. The thinner vertical lines reflect an interpretation of the composite range of these taxa between the drillcores.

(see Chronology Chapter, Correlation between CRP-2 and CRP-3).

In addition to CIROS-1, a lowermost Oligocene diatom assemblage is reported from ODP Hole 739C in Prydz Bay, Antarctica (Barron & Mahood, 1993; Mahood et al., 1993). This assemblage is interpreted to be equivalent to a portion of the *Rhizosolenia oligocaenica* Zone of Harwood et al. (1989a) from CIROS-1 and calibrated within Chrons C13n and C12r, within the calcareous nannofossil *Blackites spinosus* Zone (Barron & Mahood, 1993). Similar neritic diatom assemblages were recovered in CRP-3, but are slightly younger than those in the Prydz Bay section. This interpretation is based on the absence in CRP-3 of several taxa that characterize the Prydz Bay assemblage. These taxa include *Hemiaulus caracteristicus, Pseudotriceratium adleri,* and *Stephanopyxis splendidus*.

SUMMARY

The upper *c.* 70 m of CRP-3 contains abundant and well-preserved siliceous microfossil assemblages. Siliceous microfossils are present below this interval down to *c.* 200 mbsf, but they are poorly preserved. All samples examined below 200 mbsf are barren. Well-preserved assemblages in the upper section of CRP-3 are assigned a stratigraphical position of middle lower Oligocene, based on the presence of *Cavitatus jouseanus* (FO at 48.43 mbsf), *Rhizosolenia oligocaenica* (present from 3.05 to 63.64 mbsf), and *Rhizosolenia antarctica* (present from 3.05 to 68.59 mbsf). The FO of *Cavitatus jouseanus* is calibrated at *c.* 31 Ma from Southern Ocean cores, although it is rare and sporadic near its base. Additionally, the absence of *Hemiaulus caracteristicus* in the upper 200 m of CRP-3 indicates an age younger than *c.* 33 Ma, based on its calibrated LO from ODP Hole 744A.

Siliceous microfossil assemblages recovered in the CRP drillcores provide important new data toward the development of an Antarctic shelf biostratigraphy for the lower Miocene to middle lower Oligocene (CRP-2/2A) and the lower lower Oligocene (CRP-3). CRP drillcores span the interval from *c.* 17 to 33 Ma, and provide a composite section to build a biostratigraphical framework based on siliceous microfossil datums. Calibration of zones and siliceous microfossil datums in CRP drillcores to the magnetic polarity time scale will considerably advance future age determinations of the Oligocene and lower Miocene on the Antarctic shelf.

New information on the stratigraphical distribution of siliceous microfossil assemblages from the Oligocene drillcores fills a stratigraphical gap that is present within the disconformity at *c.* 366 mbsf in the CIROS-1 drillcore. Collectively, the CIROS-1 (Harwood, 1989), CRP-1 (Harwood et al., 1998), CRP-2/2A (Scherer et al., in press) and CRP-3 (this report) drillcores document the history of Antarctic neritic diatom evolution and southern high-latitude paleobiogeography for the early Miocene to latest Eocene (*c.* 17 to 34 Ma).

FORAMINIFERA

INTRODUCTION

A total of 151 samples including 30 "fast-track", 101 routine and 20 macrofossil matrix samples, covering the interval from 3.12 to 903.45 mbsf, were selected, processed and examined at Crary Science and Engineering Center. Fifty-six samples, of which 54 were from above 340 mbsf, were found to contain foraminifers, and yielded a fauna of *c.* 34 genera and *c.* 54 species. The following discussion concerns mainly the upper, more consistently fossiliferous, part of the drillhole section. Samples are referred to the lithostratigraphical sub-units (LSU) adopted for classification of the CRP-3 rock succession (see Lithostratigraphy and Sedimentology Chapter).

Lower Oligocene, and possibly older Palaeogene, strata in CRP-3 comprise a *c.* 820-m-thick sequence of diamictite, sandstone and muddy sandstone, sandy or silty mudstone and conglomerate/breccia, encompassing the interval from 2.80 to 823.11 mbsf. These Cenozoic strata rest unconformably on red-brown quartzose sandstones of the Beacon Supergroup (Arena Sandstone), which were drilled to a total depth of 939.42 mbsf (Bottom of Hole). Age determinations rest primarily on diatom and nannofossil evidence. Pre-Oligocene Cenozoic rocks, although possibly present, were not definitely identified, due to lack of diagnostic fossils.

MATERIAL AND METHODS

Our sample selection emphasised fine-grained sediments, mostly sandy or silty mudstones, which are the most likely to contain foraminifers, and we made no attempt to sample all the lithologies present. Samples, most weighing 50-110 g (undried) and representing *c.* 5 cm of quarter-core, were processed using standard techniques, and the resulting residues wet-sieved into >500 μm, >125 μm , and >63 μm fractions. These were dried, weighed and examined for microfossils, and absolute abundances (specimens *per* gram of original sediment) determined for selected samples. We also retained the <63 μm fraction from fast track samples, but not from routine samples, for study by other investigators. We recorded all observed fossil material, including sponge spicules, diatoms, and shell fragments, but here refer to samples lacking foraminifers as "non-fossiliferous (NF)".

Most foraminifers occur in the >125 μm residue, and a systematic search focussed on this fraction. The volume of residue, and the amount examined, varied considerably from sample to sample. Some residues were picked entirely, while others were subdivided with a microsplitter, and a fraction (usually 1/8 to 1/16 of the available >125 μm material) was examined. In all cases, however, at least two well-covered picking trays (9 x 5 cm) were searched for specimens, and this defines the

minimum criterion for determining a sample to be non-fossiliferous. In addition, the >500 μm and >63 μm residues were scanned for large or minute specimens and macrofossil debris.

FAUNAL CHARACTERISTICS AND DISTRIBUTION

As noted above, foraminifers occur consistently only in the upper *c.* 340 m of the CRP-3 stratigraphical section, with 54 of 104 samples (51.9%) proving fossiliferous. Calcareous benthic forms are strongly dominant, with agglutinated taxa occurring only as rare specimens in a few samples. No planktics were recovered from the upper part of the drillhole. Specimen preservation ranges from very good to poor, with most samples (72%) judged as fair to good. Poor preservation results mainly from recrystallisation to coarse calcite, and/or decortication due to leaching. The overall state of preservation suggests that most assemblages have suffered little, if any, leaching or diagenesis, and therefore accurately represent the original *in situ* fauna. In some cases, preservation varies within a single assemblage, perhaps indicating partial reworking, or short range preservation differences over the *c.* 5 cm sample interval.

Only two of the 47 samples collected from the thick sandstone and conglomerate sequence below 340 mbsf (LSU 9.1-13.2) proved fossiliferous. A sample from 705.97 mbsf yielded a single *Globigerina* sp. indet., whereas one from 763.40 mbsf contained a possible specimen of *Cibicides?* sp. These occurrences support the inferred marine origin for these sediments, as interpreted from sedimentological data, but provide little evidence about their age.

The foraminiferal fauna in CRP-3 from *c.* 3-340 mbsf is relatively homogeneous, and displays no major changes in composition over this stratigraphical interval. It is characterised by the consistent occurrence of dominant *Cassidulinoides chapmani,* other *Cassidulinoides/ Globocassidulina* species and *Stainforthia* sp. Many assemblages also contain *Cibicides lobatulus, Epistominella exigua, Nonionella* spp., *Oolina* spp. and *Fissurina* spp. Other microfossils include relatively common molluscan fragments, and less common ostracods and echinoderm spines and plates. Siliceous fossils are notably rare, with only single records of both diatoms and sponge spicules. In CRP-2/2A, we assigned a virtually identical fauna to Foraminiferal Unit III (Cape Roberts Science Team, 1999; Strong & Webb, in press).

Foraminiferal abundance ranges from low to very low as compared with typical marine sediments. The largest assemblage comprised 367 specimens. Thirty-one of the 54 fossiliferous samples yielded but a single foraminifer, with abundances of *c.* 0.02 to 0.5 specimens *per* gram of sediment. Most samples contain <1 specimen *per* gram of sediment, only 8 contain more than 1 specimen *per* gram, and the maximum recorded abundance is 6.2 specimens *per* gram. There appears to be little relationship between quality of preservation and abundance, indicating that dilution by high sedimentation rates, rather than loss of foraminifers through diagenesis or dissolution, is the primary cause of low specimen abundance.

The maximum abundance "peak" observed in CRP-3, of 4-6 specimens *per* gram, spans the interval from *c.* 106 to 115 mbsf, in the lower part of LSU 2.2. Lesser abundance peaks of *c.* 2-3 specimens *per* gram occur at 10.65 mbsf (LSU 1.1), 44.12 mbsf (LSU 1.2), 45.72 mbsf (LSU 1.2) and 162.16 mbsf (LSU 5.1). Lithology in all cases consists of muddy sandstone or siltstone with dispersed clasts.

Species richness is generally low, with 6 or 7 taxa being typical for assemblages of *c.* 20-50 specimens. We observed that, beyond this number of specimens, in most cases diversity tended to increase only slowly, if at all, with additional picking, suggesting environmental limitations. An exception is the maximum diversity of 27 species (367 specimens), which coincides with the foraminiferal abundance maximum at *c.* 106-115 mbsf. Similar abundance peaks also have been observed within this interval for calcareous nannoplankton, dinoflagellates, and non-marine palynomorphs (see sections on Calcareous Nannofossils, and Palynology), suggesting that the interval may be condensed, and possibly represents the most optimal marine environment attained at the CRP-3 site.

Major barren intervals, with consistently non-fossiliferous samples, occur at *c.* 65-82 mbsf (LSU 1.4), *c.* 210-250 mbsf (LSU 7.1 and 7.2) and *c.* 268-310 mbsf (lower LSU 7.3 – upper LSU 8.1). These intervals consist mainly of sandstones to muddy sandstones, with associated conglomerates.

PALAEOENVIRONMENT

All foraminiferal assemblages observed consist mainly of perforate calcareous, benthic foraminifers of moderate to very low abundance and diversity. In overall aspect, they closely resemble some elements of the present-day Ross Sea fauna (*e.g.* Bernhard, 1987). A few large (up to 5 mm in diameter), biloculine miliolids are sprinkled throughout the section, while agglutinated taxa, including *Haplophragmoides, Cyclammina*, and *Textularia* are rare. Planktics are absent except for a single specimen from 705.97 mbsf. It is most likely that the assemblages reflect various mid- to outer- shelf (50-200 m) benthic environments, which were isolated from oceanic circulation and affected by high sedimentation rates. Various other glacially influenced events and processes, such as reduced or variable salinity, may have been important in limiting the assemblage.

AGE AND CORRELATION

All foraminifers recovered from CRP-3 have either long or poorly known ranges, and no age-diagnostic species were encountered to permit external correlation.

However, both calcareous nannofossil and diatom data indicate an early Oligocene age for the entire fossiliferous section in CRP-3 (see sections on Diatoms and Calcareous Nannofossils).

Correlation of the CRP-3 section with that of the nearby CRP-2/2A drillhole is problematical, and poorly constrained by foraminiferal data, particularly the absence of distinctive foraminiferal bioevents. At one extreme, available data are consistent with overlap of up to some 500 m between the drillholes, and at the other, virtually no overlap at all. Diatom and calcareous nannofossil results show that the latter is the more likely.

The CRP-3 foraminiferal fauna down to *c.* 340 mbsf is characterised by persistent occurrences of *Cassidulinoides chapmani*, *C.* spp., and *Stainforthia* sp., and is virtually identical in faunal composition to Foraminiferal Unit III, defined in CRP-2/2A (Cape Roberts Science Team, 1999; Strong & Webb, in press). In CRP-2/2A, Unit III is *c.* 145 m thick, and occupies the interval from *c.* 342 to 486 mbsf. A major faunal change marks its upper boundary with Unit II, the latter being characterised by common *Eponides bradyi* and *Cassidulinoides aequilatera.* This boundary is the only know foraminiferal bioevent with potential for correlating between the two drillholes.

In CRP-2/2A, Unit III overlies the faunally impoverished Foraminiferal Unit IV, at least 138 m thick, which extends from 486 to 624.15 mbsf (Bottom of Hole). The only fossils identified from Unit IV during drilling were scattered, *in situ* large miliolids, and a single specimen of *Stainforthia* sp from a residue. A post-drilling study (Galeotti et al., in press), with more intensive sample processing, increased to 11 the number of species recovered from Unit IV. The unit remains faunally poor, however, since most samples (*c.* 75%) were non-fossiliferous, and the balance yielded sparse to very modest foraminiferal assemblages. Because Unit IV lacks a distinctive, persistently occurring fauna, the Unit III – Unit IV boundary cannot be reliably identified in CRP-3, and is of little value for correlation.

The abrupt faunal change marking the Unit II – Unit III boundary should be locally synchronous and, as noted above, appears to be the only foraminiferal bioevent with potential for correlating between the two drillholes The foraminiferal units themselves are essentially biofacies, and could easily vary in persistence and stratigraphic thickness between the two drillholes. However, the Unit II - III boundary is not present in CRP-3, which commences somewhere within Unit III. This renders any attempted correlations merely speculative.

The Unit III – Unit IV contact, if present at all, is unrecognisable in CRP-3, but could occupy at least 3 possible locations, where there are consistently non-fossiliferous intervals, between 208 and 342 mbsf. All would imply unreasonably large overlaps, of the order of 300-500 m. Further drilling at CRP-2/2A could have even re-entered strata containing the Unit III fauna.

In summary, there is no unambiguous foraminiferal correlation possible between CRP-3 and CRP-2/2A, but foraminiferal results are consistent with the other stratigraphic indicators that suggest little or no overlap between the two drill holes (see Chronology of CRP-3 section).

CRP-3 faunas, while less diverse and lacking planktic species, bear a general resemblance to Oligocene and Miocene faunas reported from lithostratigraphical Unit 2 (especially 2B to 2I) at DSDP Site 270 (Leckie & Webb, 1985). CRP-3 foraminiferal assemblages compare most closely with the *Globocassidulina-Cassidulinoides-Trochoelphidiella* Assemblage Zone from the lower part of DSDP 270. CRP-3 faunas also seem closely related to faunas in Units 8, 9 and 15 (Webb, 1989, p. 105) and Assemblage C (Coccioni & Galeotti, 1997) in CIROS-1. Significantly, however, no fauna equivalent to the lowermost CIROS-1 fauna, (Unit 21) was encountered in CRP-3.

CALCAREOUS NANNOFOSSILS

INTRODUCTION

Calcareous nannofossils are known from Palaeogene hemipelagic and pelagic sediments throughout the Southern Ocean wherever the sediment-water interface was above the Carbonate Compensation Depth (CCD). These assemblages differ significantly from coeval ones from the temperate and tropical regions of the world. Assemblages from warm-water areas are characterized by higher species richness than their Southern Ocean counterparts, indicating significant ecological exclusion of tropical forms (*e.g.* discoasters, sphenoliths) from the high-southern latitudes. In addition, there was some degree of Southern Ocean endemism throughout the later part of the Palaeogene. These palaeobiogeographical dissimilarities necessitate the use of distinctly different biostratigraphical zonations for the Palaeogene.

The Southern Ocean biostratigraphical zonation of Wei & Wise (1990) has been adopted to subdivide the Oligocene of the Cape Roberts cores. This zonation has the advantage of using both prominent Southern Ocean endemic taxa and those cosmopolitan taxa that penetrated into the high southern latitudes. The ranges of these taxa are well calibrated to the palaeomagnetic time scale and, indirectly, to the geochronological time scale. However, experience from the 1998 drilling season (Watkins & Villa, in press) indicates that several key taxa used in the Wei & Wise (1990) zonation are routinely absent in Oligocene samples from this part of the Victoria Land Basin. As a result, it has been necessary to use other taxa as additional biostratigraphical indicators for the Cape Roberts cores.

Samples were examined for calcareous nannofossils throughout the interval lying above the contact with the sandstones of the Beacon Supergroup. Samples were

chosen preferentially from fine-grained lithologies, or at least from sedimentary rocks with fine-grained matrix material. Two types of sample preparations were used for initial examination and characterization. Many of the samples were examined initially by using smear slides of raw sediment. In addition, several samples were examined that had been processed by a gravitational settling technique in which approximately 1 cm^3 of sediment was disaggregated and suspended in sufficient purified water to constitute a column of approximately 2-cm height in a small closed vial. This suspension was allowed to settle undisturbed for 30-60 seconds, at which point an aliquot of the supernatant was withdrawn and mounted on a cover slip. Many of these slides were prepared originally to concentrate siliceous microphytoplankton fossils, and use of these existing preparations greatly expedited our work.

RESULTS

A total of 248 samples were examined for initial characterization of nannofossil occurrence and biostratigraphy in the CRP-3 sequence above 782 mbsf (Fig. 5.4). Fast-track samples and prepared (non-acidified) diatom settled slides were used to locate promising horizons for further examination. Additional smear slides were then prepared and examined to further define the nannofossil-bearing intervals. Calcareous nannofossils were found only in samples above 200 mbsf in CRP-3. In general, nannofossils were restricted to fine-grained sedimentary rocks, with only isolated, poorly preserved specimens in the coarse-grained lithologies within this interval. Calcareous nannofossils are generally sparse even in the finest grain mudstone in the upper 200 m of the core, and only in four cases comprise more than 0.1% of the total rock volume.

Calcareous nannofossil assemblages occur sporadically within fine-grained intervals in the upper 47 m of CRP-3. These assemblages are generally very sparse and contain only a few specimens of *Dictyococcites daviesii*. A sample from 5.0 mbsf also contains *Dictyococcites productus* and *Dictyococcites hampdenensis*, an assemblage very similar to those in the bottom part of CRP-2A. A sample from 44.5 mbsf contains fragments of *Thoracosphaera heimii* and *Thoracosphaera saxae*. These calcareous dinoflagellates are often common in areas of substandard surface-water quality, and are reminiscent of the Quaternary assemblage in CRP-1 documented by Villa & Wise (1998).

In general, these sparse assemblages are not strongly age diagnostic, although they suggest a lower to mid-Oligocene placement based on the lack of other taxa known to occur in the sedimentary sequence of the Victoria Land Basin (*i.e.* CIROS-1 and CRP-2A). The smaller reticulofenetrids (*e.g. R. minuta* and *R. minutula*), which are absent in CRP-3, first occur at *c.* 340 mbsf in CRP-2A, which is no older than early late Oligocene (Wilson et al., in press). In the same way, the lack of

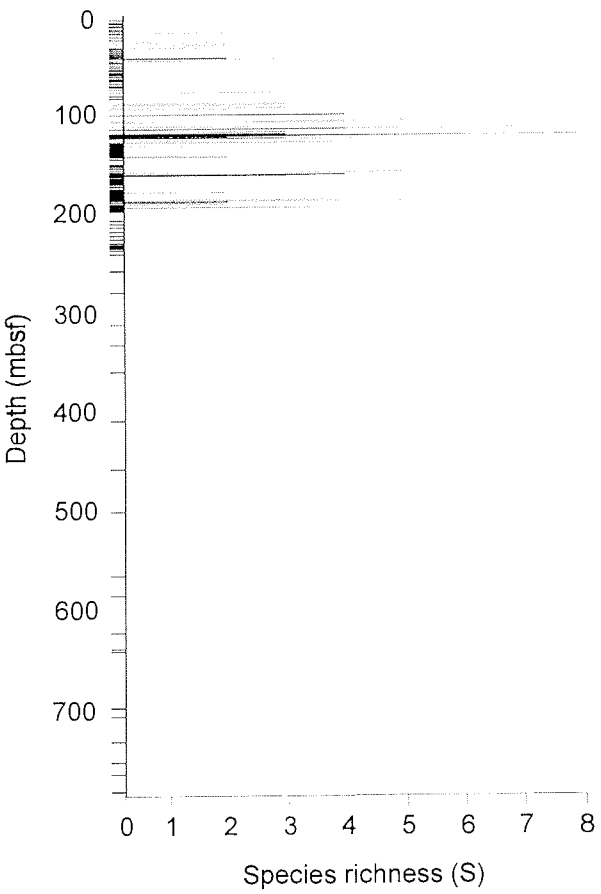

Fig. 5.4 - Distribution of samples and species richness of calcareous nannofossils in CRP-3. Marks to the left of the vertical axis denote positions of samples examined for this report. Species richness values extend to the right of the vertical axis.

Reticulofenestra oamaruensis indicates that this assemblage is not latest Eocene in age. This age determination is corroborated by diatom biostratigraphy and by its stratigraphical position above more diagnostic nannofossil assemblages. These sparse assemblages are underlain by approximately 30 m of sedimentary rock that are barren of calcareous nannofossils.

The interval from 77 to 131 mbsf in CRP-3 contains the richest and most abundant *in situ* nannofossil assemblages in the entire sedimentary section recovered by Cape Roberts drilling (Fig. 5.5). Indeed, these assemblages are the most abundant of any thus far recovered by drilling in the Victoria Land Basin. Few to common *D. daviesii*, accompanied by nearly ubiquitous *D. hampdenensis* and *D. productus*, dominate these relatively rich assemblages. *Dictyococcites bisectus* and *Dictyococcites scrippsae* are common accessory species. Rare specimens of *Chiasmolithus altus* occur in the richest samples in the sequence (114.89 mbsf; Fig. 5.5). In addition, several samples contain *Transveropontis pulcheroides*, a taxon not seen in any higher levels in CIROS-1 or Cape Roberts drilling. The last appearance

datum (LAD) of this species, in Sample 114.3 mbsf, is an important biostratigraphical indicator. This taxon has its highest stratigraphical occurrence near the midpoint of the lowest Oligocene *Blackites spinosus* Zone on the Falkland Plateau (Wise, 1983). This last occurrence datum is best expressed in the relatively shallow Deep Sea Drilling Project (DSDP) Site 511, although it is evident even in the deeper water DSDP Site 513.

The nannofossil-rich interval from 77 to 131 mbsf is underlain by about 10 m of largely barren sedimentary rock comprised of coarse-grained clastics. Samples at 141.32 and 142.93 mbsf contain isolated specimens of *D. daviesii* and *D. hampdenensis*, respectively. The interval from 157.7 to 161.9 mbsf records another episode of relatively high nannofossil abundance accompanied by good preservation. These assemblages reflect the same basic population structure as those from 77 to 131 mbsf, with *D. daviesii* being the dominant species and other *Dictyococcites* sp. comprising the secondary taxa. *Transveropontis pulcheroides* is also present in at least one of the samples in this interval, indicating the persistent nature of this taxon below its LAD in Sample 114.89 mbsf.

An interval barren of calcareous nannofossils extends from 162 to 185 mbsf, interrupted only by a single occurrence of *D. daviesii* in Sample 178.01 mbsf. The

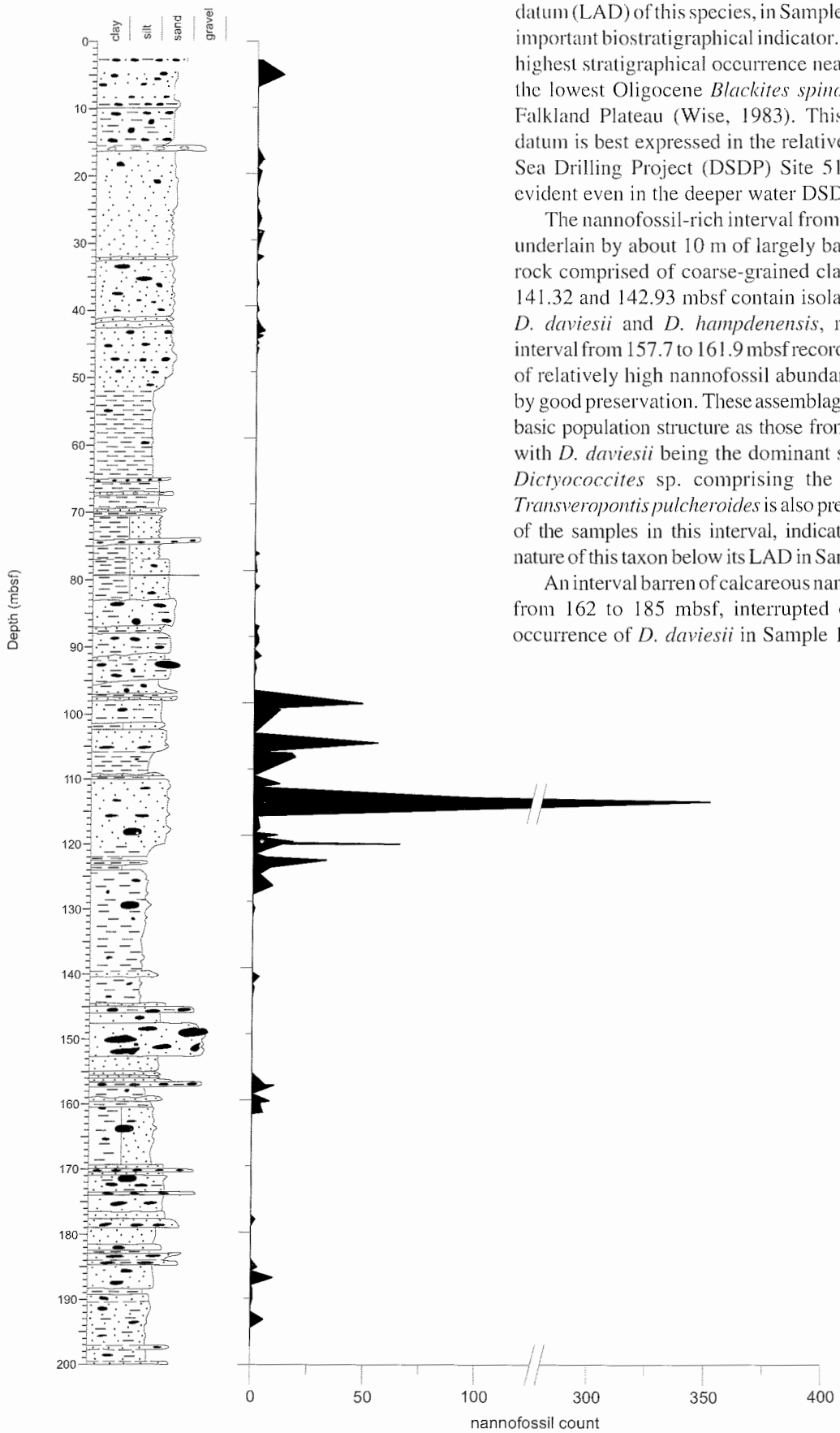

Fig. 5.5 – Specimen counts of nannofossils for the upper 200 m in CRP-3. Counts are totals derived from two traverses of slide using a 40x objective lens.

lowest interval of nannofossil presence occurs between 185 and 193.2 mbsf. Although not as abundant and rich as the best assemblages, these lowest assemblages are comparable to most of the lower Oligocene in CRP-2A and CRP-3. These are largely *Dictyococcites*-dominated assemblages, indicating the restricted nature of the nannoplankton populations that inhabited the surface waters during the early Oligocene. An important occurrence in these assemblages is the presence of *Chiasmolithus oamaruensis* in a sample from 182.25 mbsf. This relatively large nannofossil is characteristic of upper Eocene and lowest Oligocene sediments throughout the oceanic system, but is more common in higher latitudes. Its LAD is within the *Blackites spinosus* Zone of earliest Oligocene age at Site 511 on the Falkland Plateau (Wise, 1983).

A single specimen of *D. daviesii* was found in a sample from 266.27 mbsf. Initial examination of fast-track and other selected samples in the interval from 195 to 781.4 mbsf has failed, thus far, to reveal any nannofossils. This is not unexpected, given the coarse-grained nature of sediment that dominates this interval and the suspected depositional environment and high sedimentation rate for this material. In addition, some of the gravitationally-concentrated fast-track samples between 600 and 780 mbsf yielded what appears to be clay-sized authigenic minerals precipitated interstitially within the sandstone host rock. These may indicate fluid movements and diagentic processes that may be have affected nannofossil preservation in the lower part of the Cenozoic section. Nevertheless, considerable effort is anticipated during the post-drilling phase to locate any additional assemblages below 200 mbsf.

PALYNOLOGY

INTRODUCTION

We collected 208 palynological samples from CRP-3 for processing (Tab. 5.3) at CSEC during the 1999 CRP drilling season. These included 33 "fast-track" and 175 regular samples selected at an interval of approximately 4 m from rocks ranging in grain size between fine sandstone and claystone. A total of 484 slides were prepared for examination.

Palynological sample preparation followed the techniques described by the Cape Roberts Science Team (1998a) and in more detail by Simes & Wrenn (1998). Between 5 and 15 g of rock were processed for each sample. One *Lycopodium* tablet (Lund University batch # 124961) containing approximately 15 500 spores was added to each sample at the beginning of processing. This provided a check on loss of organic matter during processing. Specifically the fewer the *Lycopodium* spores in the final preparation, the more likely they and associated palynomorphs were being poured off during decanting, settled out during heavy liquid separation, or destroyed by excessive oxidation of the residue. In addition, the known quantity of spores provided a means of determining palynomorph concentration per weight of sediment.

Sample digestion in hydrochloric and hydrofluoric acid using a ProLabo M401 microwave was followed by seven minutes oxidation with concentrated nitric acid, and decanting using a swirling method. Most samples were sieved through a 212 mm mesh sieve to remove coarse mineral grains and other debris. Those containing significant coal fragments were passed through a 125 mm sieve. Coal fragments from a few selected samples were macerated in Schulze's reagent (nitric acid and potassium chlorate) heated for 5 minutes in a boiling water bath. This was followed by alkali treatment in a solution of ammonium hydroxide.

Sieved residues were further cleaned of unwanted mineral matter by heavy liquid separation with sodium polytungstate (2.3 specific gravity). The final step for most organic residues was sieving on a 6 mm mesh cloth using a Vidal Filter apparatus (Raine & Tremain, 1992) to remove fine particles. Slides were made with glycerin jelly mounting medium.

Very rare modern contaminant pollen grains (*e.g.* Asteraceae, *Pinus*, and *Betula*) were encountered during microscopic examination of the slides. These appeared in a few preparations shortly after the initial arrival of project members or visitors from New Zealand, Europe, or North America. Their color, the presence of cell contents, and/or their exotic nature easily identified these contaminants.

MARINE PALYNOMORPHS

Assemblage Details

Study of marine palynomorphs from 82 samples yielded well-preserved specimens of 61 species of dinoflagellate cysts (dinocysts), acritarchs, and prasinophycean algal phycoma (Tabs. 5.4 & 5.5). These are present in low to moderate numbers in most samples above 332 mbsf, but only in the occasional sample below that depth down to 788.69 mbsf (Tab. 5.4).

As is the case with marine microplankton from CRP-1 and CRP-2A, many of the taxa recorded from CRP-3 are new and, consequently, are referred to here in open nomenclature. Several new species of *Cymatiosphaera*, dinocysts, and acritarchs were noted, some of which are illustrated in figures 5.6 and 5.7. Several new species first recovered and illustrated from lower Miocene sediments in CRP-1 (Cape Roberts Science Team, 1998 b, c, 1999; Hannah et al., 1998; Wrenn et al., 1998) and new Oligocene taxa described from CRP-2/2A (Hannah et al., 1998) also occur in CRP-3. Currently unnamed new taxa from all three cores will be described and published in a separate paper. A more comprehensive study of the entire flora is planned for the CRP-3 Scientific Report.

Tab. 5.3 - Palynology samples collected and processed from CRP-3. FT denotes "fast-track" samples.

Unit	Depth (m)	FT	Lab.#	Wt.(g)	Lithology
1.1	7.72-7.74		190	10	muddy f. sandstone
1.1	11.13-11.15		191	10	muddy f. sandstone
1.2	16.79-16.81		192	10	muddy f. sandstone
1.2	20.69-20.71		193	10	lam.muddy f.sandstone
1.2	22.27-22.29	X	184	10	lam.muddy f.sandstone
1.2	25.96-25.98		194	10	mudstone
1.2	33.22-33.25		195	10	lam.muddy f.sandstone
1.2	38.46-38.48		196	10	muddy f. sandstone
1.2	41.75-41.77		197	10	lam. mudstone
1.2	44.12-44.18		354	6	calc. mudstone
1.2	44.18-44.27	X	185	10	calc. mudstone
1.2	49.22-49.24		198	10	muddy f. sandstone
1.3	52.20-52.22		203	10	mudstone
1.3	57.52-57.54		205	10	mudstone
1.3	60.54-60.56		225	10	mudstone
1.3	62.96-62.98	X	182	10	mudstone
1.3	64.94-64.96		206	10	mudstone/carb.nodule
1.3	68.73-68.75		226	10	mudstone
1.4	71.52-71.54		207	10	lam.mudstone
1.4	73.73-73.75		231	10	lam.mudstone
1.4	78.56-78.58		208	10	mudstone
1.4	82.36-82.38	X	186	10	mudstone
1.4	83.02-83.04		209	10	lam.mudstone
2.1	87.47-87.49		232	10	sandy mudstone
2.1	88.16-88.18		210	6	clast:bryoz.carb.nodule
2.1	92.28-92.30		233	10	muddy f.sandsone
2.1	98.87-98.89		211	10	mudstone (diamictite)
2.2	101.59-101.61		213	10	mudstone
2.2	106.22-106.24		214	10	sandy mudstone
2.2	107.38-107.40	X	183	10	sandy mudstone
2.2	108.26-108.28		215	10	sandy mudstone
2.2	114.90-114.92		216	10	sandy mudstone
3.1	120.98-121.00		212	10	sandy mudstone
3.1	122.80-122.82		218	10	sandy mudstone
3.1	123.65-123.73	X	187	10	sandy mudstone
3.1	127.88-127.90		219	10	sandy mudstone
3.1	131.17-131.19		220	10	sandy mudstone
3.1	135.54-135.56		221	10	sandy mudstone
3.1	140.67-140.69		222	10	sandy mudstone
3.1	142.37-142.39	X	188	10	sandy mudstone
3.1	144.63-144.65		223	10	sandy mudstone
4.1	155.59-155.61		227	10	mudstone
5.1	158.82-158.84		228	10	sandy mudstone
5.1	162.11-162.13	X	189	10	sandy mudstone
5.1	166.10-166.12		229	10	mudstone
5.1	167.45-167.47		230	10	mudstone
5.3	177.76-177.78		234	10	shelly mudstone
5.3	180.23-180.25		235	10	lam.mudstone
5.3	182.64-182.66		236	10	mudstone
6.1	186.36-186.38		237	10	mudstone
6.1	189.20-189.22		238	10	mudstone
6.1	190.77-190.79	X	199	10	mudstone
6.1	195.62-195.64		239	10	mudstone
6.1	196.19-196.22		389	10	mudstone
6.1	201.00-201.02		240	10	mudstone
7.1	204.82.204.84		241	10	lam. mudstone
7.1	206.58-206.60		242	10	mudstone. coal frags.
7.1	209.98-210.00	X	200	10	muddy f.sandstone
7.2	210.71-210.73		243	10	mudstone
7.2	214.00-214.02		244	10	mudstone
7.2	221.18-221.20		245	10	mudstone
7.2	225.11-225.13		246	10	lam. mudstone
7.2	229.45-229.47		247	10	mudstone
7.2	232.47-232.49	X	201	10	mudstone
7.2	234.15-234.17		248	10	muddy sandst. coal frags.
7.2	234.71-234.73		249	10	coaly v.f.sandstone
7.2	240.24-240.26		250	10	mudstone
7.2	246.93-246.96		251	10	lam. mudstone
7.2	251.00-251.02		252	10	v.f. sandstone
7.2	256.06-256.09		253	10	mudstone
7.2	257.10-257.25	X	202	10	mudstone
7.2	259.94-259.96		254	10	mudstone
7.2	264.42-264.44		255	10	mudstone
7.3	265.41-265.43		256	10	lam. mudstone
7.3	270.13-270.15		258	10	mudstone
7.4	273.70-273.72		259	10	mudstone
7.4	275.32-275.35		260	10	mudstone
7.4	276.17-276.19		261	10	mudstone
7.4	276.72-276.74		262	10	mudstone
7.4	278.50-278.52	X	204	10	muddy f.sandstone
7.4	280.84-280.86		264	10	muddy v.f.sandstone
7.4	285.71-285.73		263	10	muddy f.sandstone
7.4	289.22-289.24		265	10	muddy f.sandstone
7.4	291.43-291.45		266	10	muddy f.sandstone
7.5	300.41-300.43		267	10	f.sandstone
7.5	303.72-303.74		268	10	f.sandstone
7.5	305.62-305.64		269	10	muddy f.sandstone
8.1	311.14-311.16	X	217	10	muddy f.sandstone
8.1	312.12-312.14		270	10	muddy f.sandstone
8.1	316.13-316.15		271	10	mudstone
8.1	319.55-319.57		272	10	mudstone
8.1	320.70-320.72		273	10	muddy f.sandstone
8.1	320.79-320.81		274	10	?clast: mudstone
8.1	321.14-321.16		275	10	clast: f.sandstone
8.1	324.39-324.41		276	10	mudstone
9.1	330.17-330.19		277	10	muddy f.sandstone
9.1	332.00-332.02	X	224	10	muddy f.sandstone
9.1	333.84-333.86		278	10	f.sandstone. coal frags.
9.1	338.23-338.25		279	10	muddy v.f.sandstone
9.1	343.45-343.47		280	10	muddy f.sandstone
9.1	353.59-353.61		283	10	mudstone & f.sandstone
9.1	359.16-359.18	X	257	10	mudstone
9.1	360.03-360.05		284	10	mudstone
9.1	363.77-363.79		285	11	mudstone
9.1	366.53-366.55		286	10	muddy f.sandstone
9.1	370.55-370.57		287	10	f.sandstone
9.1	373.52-373.54		289	10	sandy mudstone
9.1	387.11-387.13		290	10	clast: mudstone
9.1	388.35-388.37		291	17	f.sandstone
9.1	399.81-399.83		292	14	f.sandstone
10.1	406.05-406.07		293	10	mudstone
10.1	408.59-408.61	X	281	10	mudstone
10.1	410.36-410.38		294	10	mudstone
10.1	413.11-413.13		295	10	muddy f.sandstone
11.1	424.52-424.54		296	10	f.sandstone
11.1	429.91-429.93		299	17	f.sandstone
11.1	433.97-433.99		300	15	f.sandstone
11.1	437.07-437.09		301	15	f.sandstone
11.1	439.34-439.36		302	15	f.sandstone
12.1	445.01-445.03		303	15	f.sandstone
12.1	451.81-451.83		304	15	f.sandstone
12.1	457.37-457.39	X	282	10	f.sandstone
12.2	461.01-461.03		305	15	v.f. sandstone
12.2	461.80-461.82		306	10	v.f. sandstone
12.3	466.73-466.75		307	15	f.sandstone
12.3	473.75-473.77		308	15	f.sandstone
12.3	474.73-474.75		314	20	f.sandstone
12.3	489.13-489.15		315	15	f.sandstone
12.3	493.60-493.62		316	14	f.sandstone
12.3	500.23-500.25	X	288	18.4	f.sandstone

Antarctic Dinocyst Record

The assemblages from these cores bridge much of the gap in the Antarctic marine palynomorph record between Palaeogene and recently described Holocene Antarctic dinocyst assemblages (Marret & de Vernal, 1997 and Harland et al., 1998). Attention was first drawn to Antarctic Palaeogene dinocysts by Cranwell (1964) in her study of palynomorphs recovered from erratics collected at Minna Bluff in the southern McMurdo Sound area. Wilson (1967) described many new dinocyst species from other erratics recovered from Black Island

Tab. 5.3 - continued

Unit	Depth (m)	FT	Lab.#	Wt.(g)	Lithology	Unit	Depth (m)	FT	Lab.#	Wt.(g)	Lithology
12.3	509.38-509.40		317	15	f.sandstone	13.1	743.92-743.94		356	15	f.sandstone
12.3	516.48-516.50		319	15	f.sandstone	13.1	749.06-749.08		357	15	lam. muddy f.sandstone
12.3	521.76-521.78		320	15	muddy v.f.sandstone	13.1	751.33-751.35	X	325	16	lam. muddy f.sandstone
12.3	534.14-534.16		322	15	f.sandstone	13.1	756.81-756.83		358	15	lam. muddy f.sandstone
12.3	534.69-534.70		321	15	coal clast in f.sandstone	13.1	764.65-764.67		359	15	gritty & muddy f.sandstone
12.4	542.15-542.17		324	15	f.sandstone	13.1	766.67-766.69		361	15	lam. muddy f.sandstone
12.4	546.26-546.28		326	12	f.sandstone	13.2	770.06-770.10		362	15	f.sandstone
12.4	555.04-555.06		327	12	f.sandstone	13.2	772.50-772.52		363	15	muddy f.sandstone
12.4	558.39-558.41		328	15	f.sandstone	13.2	776.64-776.66		364	15	f.sandstone
12.5	564.40-564.42	X	297	13	f.sandstone	13.2	777.70-777.72		365	15	muddy f.sandstone
12.5	568.82-568.84		329	15	f.sandstone	13.2	781.10-781.12		366	12	mudstone
12.6	577.08-577.10		330	10	f.sandstone	13.2	781.24-781.26	X	341	15	muddy f.sandstone
12.6	581.35-581.37		331	13	f.sandstone	13.2	781.36-781.38	X	342	21	muddy f.sandstone
12.6	584.44-584.46	X	298	17	f.sandstone	13.2	781.50-781.52		367	15	muddy f.sandstone
12.6	591.91-591.93		332	13	f.sandstone	13.2	788.02-788.04		368	15	muddy f.sandstone
12.6	602.07-602.09		333	12	f.sandstone	13.2	788.69-788.71		369	15	muddy f.sandstone
12.7	606.23-606.25		334	10	f.sandstone	14.1	792.51-792.53		370	5	claystone
13.1	617.60-617.62		335	15	f.sandstone	14.1	793.93-793.95		371	5	claystone
13.1	621.75-621.77	X	310	15	f.sandstone	14.1	797.88-797.90		372	5	claystone
13.1	629.28-629.30		336	15	f.sandstone	14.1	798.03-798.04	X	355	6	claystone
13.1	633.20-633.22		337	15	f.sandstone	14.1	799.22-799.23		373	5	claystone
13.1	636.61-636.63		338	15	lam. f.sandstone	14.1	800.35-800.37		374	5	claystone
13.1	?638.30?	X	309	10	mud (in core catcher)	14.1	801.56-801.58		375	6	claystone
13.1	640.69-640.71	X	311	15	f.sandstone	14.1	804.53-804.55		376	5	claystone
13.1	643.60-643.62		339	10	muddy f.sandstone	15.1	811.10-811.12		377	10	f.sandstone
13.1	648.23-648.25		340	15	f.sandstone	15.2	814.21-814.23		378	10	f.sandstone
13.1	656.54-656.56	X	312	15	f.sandstone	15.2	815.84-815.86		379	10	f.sandstone
13.1	662.20-662.22		343	15	muddy f.sandstone	15.2	818.23-818.26		380	10	clast: f.sandstone
13.1	679.81-679.83		344	15	f.sandstone	15.2	822.33-822.35		381	10	f.sandstone
13.1	688.96-688.98		345	15	f.sandstone	15.2	822.70-822.72		382	10	f.-m.sandstone
13.1	690.60-690.62		346	15	lam. mudst.& f.sandstone	15.2	822.85-822.87		383	15	f.-m.sandstone
13.1	697.33-697.35	X	313	15	f.sandstone	16.1	823.16-823.17		384	10	lam. f.-m.sandstone
13.1	703.93-703.95		347	15	f.sandstone	16.1	833.34-833.41		385	10	lam. f.-m.sandstone
13.1	707.55-707.57		348	10	muddy f.sandstone	16.1	835.28-835.30	X	350	15	lam. f.-m.sandstone
13.1	720.10-720.20		351	15	f.sandstone	16.1	855.92-855.94		386	10	lam. f.-m.sandstone
13.1	722.56-722.58		352	15	f.sandstone	16.1	897.25-897.26		387	10	f.-m.sandstone
13.1	731.28-731.30	X	318	20	f.sandstone	16.1	898.83-898.85		388	10	f.-m.sandstone
13.1	739.76-739.78		353	15	f.sandstone	17.1	903.30-903.32	X	360	15	clay

as well as Minna Bluff. The assemblage was subsequently named the Transantarctic Assemblage after its distribution became evident (Wrenn & Hart, 1988). Specimens of constituent species, either *in situ* or reworked, have been reported from throughout the southern high latitudes by Archangelsky (1969; southern Argentina); Kemp (1975; Deep Sea Drilling Project [DSDP] Sites 270 and 274 in the Ross Sea), Hall (1977; Seymour Island, Antarctica), Griggs (1981; the Santos Basin, Brazil); Wrenn (1981; the Ross Ice Shelf Project [RISP] Site J-9); Wrenn & Beckman (1981; [RISP] Site J-9), Wrenn (1982; Seymour Island, Antarctica) Goodman & Ford (1983; DSDP Sites 511, 512, 513A on the Falkland Plateau), and Wrenn & Hart (1988; Seymour Island). Most recently, reworked specimens have been recovered from CRP-1 (Cape Roberts Science Team, 1998a; Hannah et al., 1998) and CRP-2A (Cape Roberts Science Team, 1999).

Reports of modern dinocysts from Antarctica are few in number (Balech, 1975; Marret & de Vernal, 1997; and Harland et al., 1998), and none report any of the dinocysts found in any of the CRP cores. The new taxa recovered from all three CRP cores should permit the establishment of an Antarctic Cenozoic dinocyst zonation. Such a zonation should be useful within the Ross Sea region and, perhaps, generally in Antarctic waters.

The *in situ* dinocyst assemblages in CRP-3 include gonyaulacoid and protoperidinioid taxa, though the latter are the most diverse and usually the most abundant as well. Most of the protoperidinioid cysts belong to the genus *Lejeunecysta*, including three new species from CRP-3 and several new species first reported from CRP-2A.

A variety of acanthomorph acritarchs as well as several species of *Leiosphaeridia* are common in the upper 280 m of the core. Below that depth, occurrences are sporadic and specimens rare. The acritarch *Leiofusa* sp. is one of the most abundant in the core and reaches a peak of 215 specimens at 11.13 mbsf. This species also occurs in considerable numbers in the lower part of CRP-2A. In both cores, it exhibits an antipathy for dinocysts in that it is most numerous where dinocysts are rare or absent, and least numerous where dinocysts are abundant. This relationship may be environmentally significant.

Phycoma of prasinophyte green algae are present throughout the core but most numerous and consistent in occurrence above 330 mbsf. At least three species of *Pterospermella* and several species of *Cymatiosphaera*, some not previously encountered in the Cape Roberts

Tab. 5.4 - Stratigraphical distribution of the marine palynomorphs recovered from CRP-3.

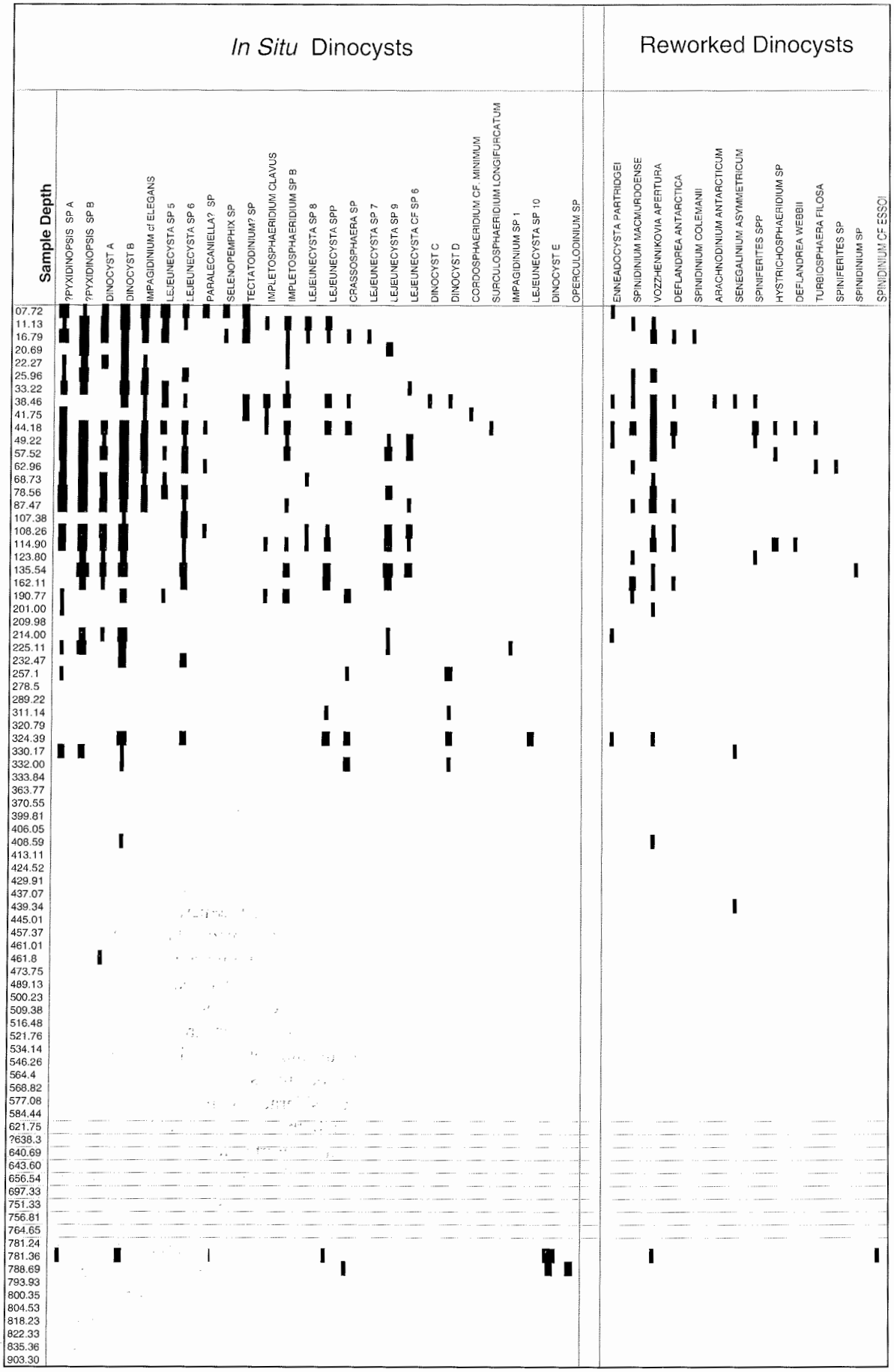

Tab. 5.4 - continued.

	Acritarchs															Prasinophyte Algae										Others	
Sample Depth	MICRHYSTRIDIUM SP 6	MICRYSTRIDIUM SP 3	MICRHYSTRIDIUM SP 6	MICRHYSTRIDIUM SP 8	MICRHYSTRIDIUM SP 2	LEIOFUSA SP	LEIOSPHAERIDIA SPP	SIGMOPOLLIS SP	LEIOSPHAERIDIA SPA	LEIOSPHAERIDIA SPB	ACRITARCH SP 2	ACRITARCH SP1	CYMATIOSPHAERA CF INVAGINATA	PTEROSPERMELLA SP 1	PTEROSPERMELLA SP 2	CYMATIOSPHAERA SP 5	CYMATIOSPHAERA SP6	PEDIASTRUM SP	PTEROSPERMELLA SP 3	CYMATIOSPHAERA SP 7	LEIOSPHAERIDIA SP C	TASMANITES SPP	FORAMINIFERAL LININGS	ARTHROPOD/ANNELID PARTS
07.72																								
11.13																								
16.79																								
20.69																								
22.27																								
25.96																								
33.22																								
38.46																								
41.75																								
44.18																								
49.22																								
57.52																								
62.96																								
68.73																								
78.56																								
87.47																								
107.38																								
108.26																								
114.90																								
123.80																								
135.54																								
162.11																								
190.77																								
201.00																								
209.98																								
214.00																								
225.11																								
232.47																								
257.1																								
278.5																								
289.22																								
311.14																								
320.79																								
324.39																								
330.17																								
332.00																								
333.84																								
363.77																								
370.55																								
399.81																								
406.05																								
408.59																								
413.11																								
424.52																								
429.91																								
437.07																								
439.34																								
445.01																								
457.37																								
461.01																								
461.8																								
473.75																								
489.13																								
500.23																								
509.38																								
516.48																								
521.76																								
534.14																								
546.26																								
564.4																								
568.82																								
577.08																								
584.44																								
621.75																								
?638.3																								
640.69																								
643.60																								
656.54																								
697.33																								
751.33																								
756.81																								
764.65																								
781.24																								
781.36																								
788.69																								
793.93																								
800.35																								
804.53																								
818.23																								
822.33																								
835.36																								
903.30																								

Tab. 5.5 - Full listing of all marine palynomorph taxa recovered from CRP-3. Most are listed in open nomenclature. Species numbering follows on from Hannah et al. (1998) and Cape Roberts Science Team (1999).

?Pyxidinopsis sp A	*Lejeunecysta* sp 5 Cape Roberts Science Team, 1999
?Pyxidinopsis sp B	*Lejeunecysta* sp 6 Cape Roberts Science Team, 1999
Acritarch sp 1	*Lejeunecysta* sp 7 Cape Roberts Science Team, 1999
Acritarch sp 2	*Lejeunecysta* sp 8
Arachnodinium antarcticum Wilson & Clowes, 1982	*Lejeunecysta* sp 9
Cordosphaeridium cf. *minimum* (Morgenroth, 1966), Benedek, 1972	*Lejeunecysta* spp
Crassosphaera sp	*Micrhystridium* sp 2 Hannah et al, 1998
Cymatiosphaera cf *invaginata*	*Micrhystridium* sp 8
Cymatiosphaera sp 5	*Micrhystridium* sp 6
Cymatiosphaera sp 6	*Micrhystridium* sp 7
Cymatiosphaera sp 7	*Micrystridium* sp 3 Hannah et al, 1998
Cymatiosphaera sp	*Operculodinium* sp
Deflandrea antarctica Wilson, 1967	*Paralecaniella?* sp
Deflandrea webbii Wrenn & Hart, 1988	*Pediastrum* sp
Dinocyst A	*Pterospermella* sp 1
Dinocyst B	*Pterospermella* sp 2
Dinocyst C	*Pterospermella* sp 3
Dinocyst D	*Selenopemphix* sp
Dinocyst E	*Senegalinium asymmetricum* (Wilson, 1967), Stover & Evitt, 1978
Enneadocysta partridgei Stover & Williams, 1995	*Sigmopollis* sp
Hystrichosphaeridium sp	*Spinidinium cf essoi* Cookson & Eisenack, 1967
Impagidinium cf *elegans*	*Spinidinium colemanii* Wrenn & Hart, 1988
Impagidinium sp 1	*Spinidinium macmurdoense* Wilson, 1967
Impletosphaeridium clavus Morgenroth, 1966	*Spinidinium* sp
Impletosphaeridium sp B Wrenn & Hart, 1988	*Spiniferites* sp
Leiofusa sp	*Spiniferites* spp
Leiosphaeridia sp A	*Surculosphaeridium longifurcatum* (Firtion, 1952), Davey et al, 1966
Leiosphaeridia sp B	*Tasmanites* spp.
Leiosphaeridia sp C	*Tectatodinium?* sp
Leiospheridia spp	*Turbiosphaera filosa* (Wilson 1967), Archangelsky, 1969
Lejeunecysta cf sp 6 Cape Roberts Science Team, 1999	*Vozzhennikovia apertura* Wilson, 196
Lejeunecysta sp 10	

cores, comprise an important component of many assemblages.

Specimens of several species from the Transantarctic Flora occur in CRP-3 samples (Tab. 5.4). As in CRP-2A, *Vozzhennikovia apertura* is present in the greatest numbers and occurs most consistently, followed by *Spinidinium macnurdoense* and *Deflandrea antarctica*. Rare specimens of *Arachnodinium antarcticum, Deflandrea webbii, Enneadocysta partridgei, Spinidinium colemanni,* and *Turbiosphaera filosa* are present. All specimens are reworked. Most occur above 202 mbsf, with rare occurrences below that depth.

In situ marine palynomorph assemblages from CRP-3 can be subdivided into three informal units based on the distribution of distinctive dinocysts:

Marine Palynomorph Unit I: 7.72 to 87.47 mbsf

The samples comprising Unit I contain some of the richest marine palynomorph floras in the core, including the distinctive and key species *Impagidinium* cf. *elegans*. The assemblage is easily identified by the presence of this species, whose base at 87.47 mbsf in the core marks the base of Unit 1. One or more species of *Lejeunecysta* (*e.g. L.* sp. 5, *L.* sp. 6, *L.* sp. 7, *L.* spp.) and one or more species of ?*Pyxidinopsis* sp. are typically present.

Species of the acritarch *Leiosphaeridia* are accompanied by rare acanthomorph acritarchs in many samples. A fusiform acritarch, *Leiofusa* sp., is the most abundant acritarch within this interval, though it ranges downcore to the 324.39 mbsf level. The number and diversity of spinose acritarchs is very low, and the assemblage is similar to those reported from Unit I of CRP 2A and below 99.01 mbsf in CRP-1.

Prasinophycean algae are represented in Unit 1 by several species of *Cymatiosphaera,* informally referred to as *C. sp. 5, C. sp. 6* (possibly several species lumped together), *C.* cf. *invaginata,* and *C. sp. 7*. Although not restricted to Unit 1, they are particularly evident in it. Three species of *Pterospermella (P. sp. 3, P. sp. 1 and P. sp. 2)* are present and constitute a minor component of the prasinophycean assemblages in Unit 1.

Marine Palynomorph Unit II: 107.38 to 324.19 mbsf

This interval is bounded above by the first appearance datum (FAD) of *Impagidinium* cf. *elegans,* a large and distinctive dinocyst. Its base is placed at the FAD of the dinocyst *Lejeunecysta* sp. 6 and the FAD of *Leiofusa* sp. In addition, below Unit 2, there is a significant decrease in marine palynomorph abundance and diversity. Assemblages from Unit II generally contain one or more species of *Lejeunecysta* and *Pyxidinopsis* sp., and low numbers of acritarchs and prasinophytes.

Marine Palynomorph Unit III: 330.17 m to the bottom of hole

The top of this interval is placed at the FAD of *Lejeunecysta* sp. 6 and of the fusiform acritarch *Leiofusa*. The interval is characteristically barren or yields very few marine palynomorphs, *in situ* or reworked. It extends to the top of the massive light buff sandstone (?Beacon Supergroup) at the bottom of the hole (820 mbsf).

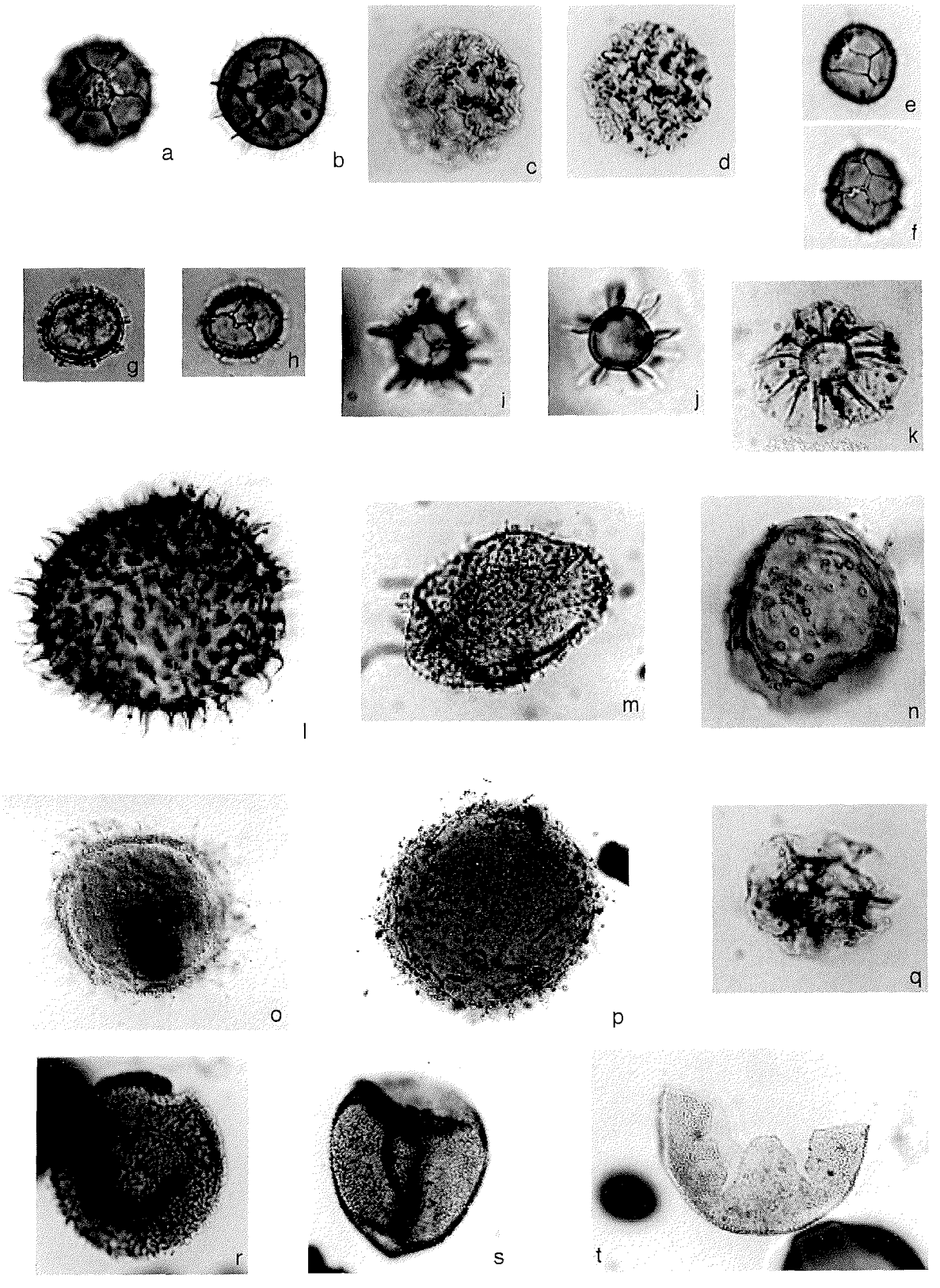

Fig. 5.6 - Selected marine palynomorphs from CRP-3. Data listed includes, in this order: depth, slide number, England finder co-ordinates, and diameter or length x width. a & b) *Cymatiosphaera* sp. 5, 16.79 mbsf, P192-2, X44, 35.4 µm; c & d) *Cymatiosphaera* cf. *invaginata*; 16.79 mbsf, P192-2, K51, 35.7 µm; e & f) *Cymatiosphaera* sp. 6, 16.79 mbsf, P192-2, J52, 19.0 µm; g & h) *Cymatiosphaera* sp. 8, 408.59 mbsf, P281-2, M49, 22.1 x 25.5 µm; i & j) *Cymatiosphaera* sp.7, 793.3 mbsf, P369-1, W37, 18.7 µm; k) *Pterospermella* sp. 2, 7.72 mbsf, P190-2, G50/1, 50.1 x 35.7 µm; l) *Micrhystridium* sp. 2, 162.11 mbsf, P189/3, V30/1, 37 mm; m) *Micrhystridium* sp. 3, 162.11 mbsf, P189/3, F44/3, 26 mm; n) *Micrhystridium* sp. 8, 68.75 mbsf, P266/2, H51, 33 mm; o) Acritarch sp. 2, (Nomarski interference contrast illumination), 123.73 mbsf, P182/1, M28/129 mm; p) Acritarch sp. 2, 38.46 mbsf, P196-1, E47, 81.6 x 85 mm; q) Dinocyst D, 324.39 mbsf, P276/1, X52/1, 28.9 x 35.7 mm; r) ?*Pyxidinopsis* sp. A, 16.79 mbsf, P192-2, F40, 42.5 x 47.6 mm; s) ?*Pyxidinopsis* sp. B, 7.72 mbsf, P190-2, J40/1, 37 mm; t) ?*Pyxidinopsis* sp. B. Note: This specimen was recovered from CRP-2A. 264.42 mbsf, P154-2, V33-2, 57.8 x 90.1 mm.

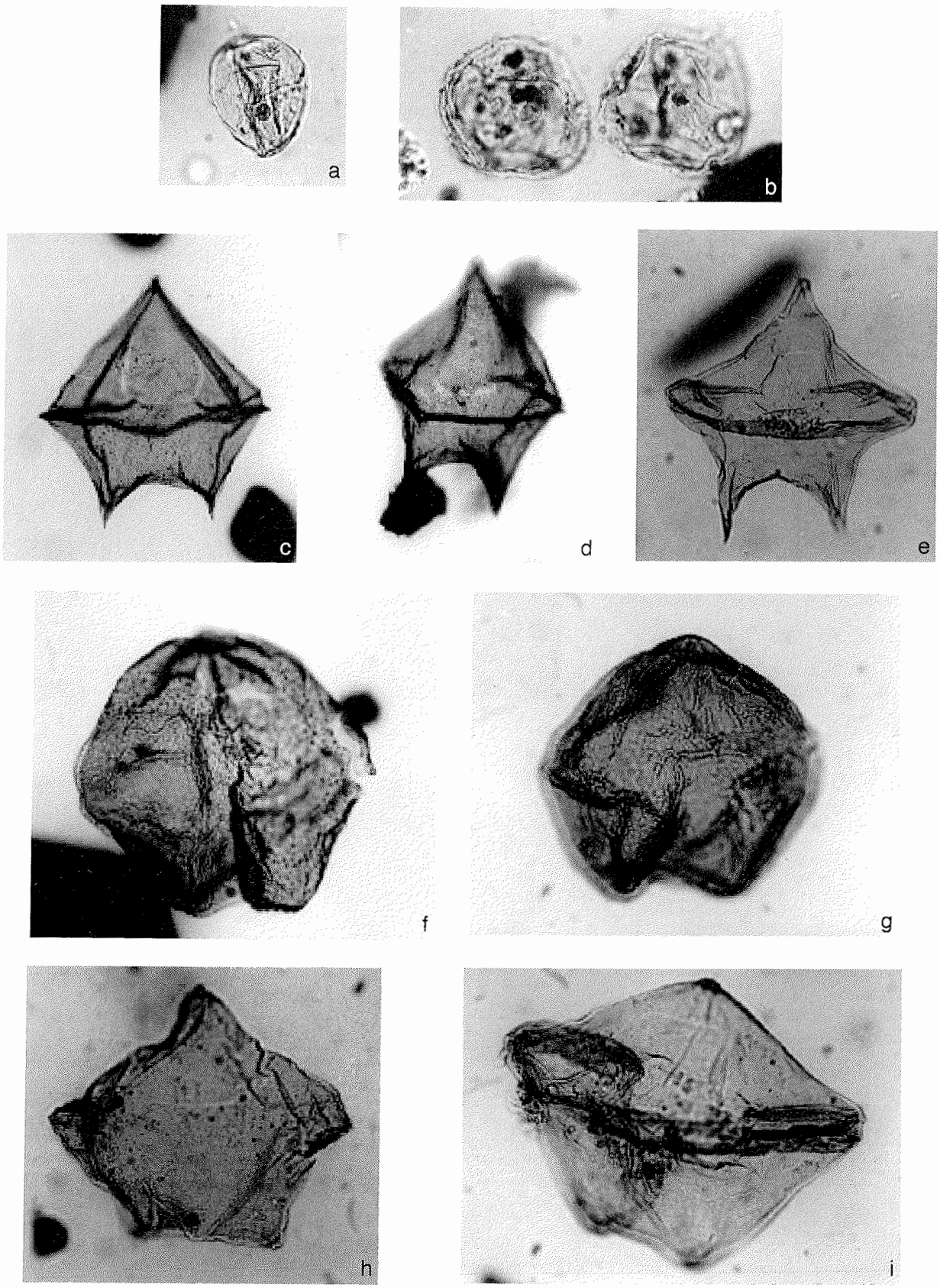

Fig. 5.7 - Selected marine palynomorphs from CRP-3. Data listed includes, in this order: depth, slide number, England finder co-ordinates, and diameter or length x width. a) Dinocyst E; 688.96 mbsf, P342/5, L45/2, 27.2 x 34.0 mm; b) Dinocyst E; 688.96 mbsf, P342-5, L42/1, 27.2 x 25.0 mm; c) *Lejeunecysta* sp. 6, 33.22 mbsf, P195/1, C50/4, length = 101 mm; d) *Lejeunecysta* cf. sp. 6, 33.22 mbsf, P195/1, C50/4, length = 101 mm; e) *Lejeunecysta* sp., 52.22 mbsf, 57.9 x 90.1 mm; f) *Lejeunecysta* sp. 5, 38.46 mbsf, P196-1, D47/1, 81.6 x 79.9 mm; g) *Lejeunecysta* sp. 5, 38.46 mbsf, P196-2, P50, 79.9 x 74.8 mm; h) *Lejeunecysta* sp. 10, 38.46 mbsf, P196-2, K51, 35.7 mm; *i*) *Lejeunecysta* sp. 9. 38.46 mbsf, P196-2, Q57, 85 x 73.1 mm.

Unit III contains stratigraphically dispersed and sparse marine assemblages at only a few levels. *In situ* dinocysts recovered in this unit are usually rare and include *Lejeunecysta* sp. 5 (788.69 mbsf), *Lejeunecysta* sp. (718.36 mbsf), and *Pyxidinopsis* sp. (781.36 mbsf). The sole exception is the dinocyst assemblage occurring in samples at 781.36 and 788.69 mbsf. It consists of a new species, informally referred to as "dinocyst 781." Rare *Lejeunecysta* cysts and a variety of acritarchs and prasinophytes accompany it. We believe it indicates that a marine environment existed at the time of deposition.

Systematic Comments

The following are comments on some of the more prominent undescribed taxa recovered from CRP-3. Those previously noted in CRP-2A are so indicated below, and references to illustrations in the CRP 2A Initial Report are given.

Dinocyst E - Subspherical, cysts consisting of two thin wall layers (<1.0 µm). The endophragm is the more substantial and prominent. The periphragm is often absent, or seems to be. When present it may be kalyptra-like. A very short and blunt apical horn (2-8.5 µm) and asymmetric antapical horn composed of the periphragm are occasionally evident. The apical horn is often folded over on the central body and all but invisible. The cysts are always hyaline but the wall appears very light yellow in optical section. Almost always one or more gold accumulation bodies are present within the cyst. These may be individual bodies or joined together in a short chain. Their shape, wall color, and the yellow accumulation bodies are distinctive of the species. Apparently they have a combination archeopyle, though SEM study will be needed to determine the details. Dinocyst E ranges in width from 22-38 µm in diameter and 25-36 µm in length. (see Fig. 5.7a & b).

Impagidinium cf. *Elegans* - Subspherical to elongate, central body bearing parasutural membranes marking paraplate areas. Membranes appear to be ribbed perpendicular to their length, granulate, occasionally perforate, and their distal margin is irregular. The central body is typically yellow-orange to brown in color, whereas the parasutural membranes are clear and hyaline. An orange accumulation body is often present within the cyst. Paracingulum delineated by a series of transversely elongate paraplates. Type $P_{3''}$ precingular archeopyle; operculum free. Cysts range from 34 to 71 µm long and 34 to 60 µm wide. (See Fig. 5.9a of Cape Roberts Science Team, 1999).

Lejeunecysta sp. 5 - This species of *Lejeunecysta* was first reported from CRP-2A (Cape Roberts Science Team, 1999) and is characterized by its rounded pentagonal-to-elliptical shape and distinct scabrate to verrucate ornamentation. The thin (<1 µm) autophragm may bear sculptural elements up to 2 µm in diameter. Aligned verrucae commonly delineate the paracingulum, and on some specimens a low ridge and/or a fold reinforce this. The parasulcus is indicated by the invagination of the antapical margin and by a loop-shaped flagellar scar located approximately midway between the antapex and the paracingulum. Cysts ranging from 61 to 82 µm long and 52 to 72 µm wide have been measured. (See Fig. 5.8c of Cape Roberts Science Team, 1999).

Lejeunecysta sp. 6 - Cysts of *L.* sp. 6 are symmetrically divided in an anterior/posterior direction by the paracingulum, which is marked by well-defined transverse folds. The large intercalary 2a paraplate extends nearly to the paracingulum, but is separated from it by a very short precingular paraplate. The archeopyle is well marked by the slight separation of the partially dislodged operculum. It is uncertain whether the operculum is adnate or simply adherent along its posterior margin. Sculpturing consists of a very prominent granulation on the entire cyst surface. The horn terminations are solid. The apical horn is blunt, and the antapical horns are sharply pointed. Specimens range from 52-85 µm long and 64-78 µm wide. This cyst species was recovered first from CRP-2A (see Fig. 5.8b of Cape Roberts Science Team, 1999).

Lejeunecysta sp. 7 - This species, originally found in CRP-2A, is characterized by a very narrow cyst overall and an antapical area in particular. The antapical horns are very closely placed to each other (see Fig. 5.8g of Cape Roberts Science Team, 1999, for a clear illustration of this species).

Lejeunecysta sp. 9 - A species of *Lejeunecysta* characterized by its large pentagonal autocyst with a very wide smooth autophragm. The small antapical horn tips are solid. Parallel ridges and folds consistently mark the paracingulum. The 2aI archeopyle is very broad. Cysts have been measured that range in length from 85 to 107 µm, and in width from 100 to 125 µm (see Fig. 5.7i).

?*Pyxidinopsis* sp. A - This moderate-to-large dinocyst ?*Pyxidinopsis* sp. was first encountered in CRP-2A at 316.50 mbsf and was consistently present to the base of the core at 624.15 mbsf (Cape Roberts Science Team, 1999). We concur with observations regarding its variable sculpturing and archeopyle formation (Cape Roberts Science Team, 1998). We refer to the coarsely ornamented form as ?*Pyxidinopsis* sp. A (Figs. 5.6 r & t) and to the finely ornamented form as ?*Pyxidinopsis* sp. B (Fig. 5.6 s). Examination of a hundred or more specimens of ?*Pyxidinopsis* sp. A. from CRP-3 leads us to conclude that it has a combination archeopyle. The archeopyle may involve the loss of only the third precingular paraplate (Type $P_{3''}$ archeopyle), or the additional separation (loss?) of one or more apical paraplates and the partial separation of adnate precingular paraplates. Consequently, we do not believe this new species is assignable to the genus *Pyxidinopsis* as currently defined. Detailed study, including scanning electron microscopy, will be needed to determine its generic assignment. The potential that more than one species is involved certainly exists, as pointed out previously by the Cape Roberts Science Team (1999).

?*Pyxidinopsis* sp. B - The comments above regarding ?*Pyxidinopsis* sp. A, except for ornamentation, pertain to this form as well. ?*Pyxidinopsis* sp. B differs from ?*P.* sp. A by being finely ornamented (Fig. 5.6s). Because their stratigraphic ranges are nearly identical in both CRP-2A, these forms may be end members of one species.

Acritarch - 2 - This acritarch has a dense, poorly delimited central body (70-85 µm in diameter) bearing indistinct, hyaline processes that characterize it. The latter are very short (approximately 8-10 µm long) and look like tiny spheres stacked one upon the other to form straight processes that may bifurcate distally. Central body may be composed of two wall layers, although this is uncertain. Overall, the central body may attain a thickness of 7 µm (see Fig. 5.6 o & p).

Age and Environmental Significance

Age

The marine palynomorph assemblages consist predominantly of undescribed or reworked palynomorphs and can add no firm insights at present to the age interpretation of CRP-3. Diatom and nannofossil data indicate that the age of the upper 114 m of the core is early Oligocene (C12r, 31-32 Ma). Below that interval, no direct age determinations are possible at this time, due to a general scarcity of fossils and the absence of time significant micro- and macrofossils.

However, the same general types of palynological assemblages occur sporadically almost to the bottom of CRP-3 (Fig. 5.7). That is, acanthomorph and psilate acritarchs, *Cymatiosphaera* spp., and protoperidinioid dinocysts (*e.g. Lejeunecysta* sp.) constitute these sparse assemblages, suggesting continuity with overlying assemblages and that they are probably the same age.

Strata containing the distinctive Palaeogene dinoflagellate assemblages correlative to those recovered from the McMurdo erratics (Wilson, 1967; McIntyre & Wilson, 1966), CIROS (Hannah, 1997), and Seymour Island (Hall, 1977; Wrenn, 1982; Wrenn & Hart, 1988), were not cored by CRP-3. The extremely rare, low diversity elements of the Transantarctic Flora present in Unit III are reworked. This interpretation assumes that the upper Eocene marine palynomorph assemblages in East Antarctica should be the same as those documented on Seymour Island.

There is at this time no firm evidence that the Eocene was penetrated by any of the CRP cores. Hypothetical age determinations based solely on anticipated evidence of late Eocene cooling, regardless of where chronostratigraphical boundaries are drawn, cannot be supported until firm evidence, fossil or radiometric data, are found in the cores to support such interpretations.

Nevertheless, recognition of the Eocene dinocyst assemblages in East Antarctica remains a concern because it is conceivable that this area has a somewhat different history from West Antarctica. For instance, if East Antarctica became colder before West Antarctica, the relatively warm Seymour Island dinocyst assemblages may not be representative of age correlative beds in East Antarctica. Slightly earlier East Antarctic cooling resulting from a hypothetical circum-East Antarctic current is possible. Such a current might have existed after Australia moved away from Antarctica, but prior to the initiation of the deep water circulation between South America and the Antarctic Peninsula, and before a large ice sheet joined East and West Antarctica.

In this case, the change from the diverse and abundant Eocene assemblages found on Seymour Island to the sparse, low diversity Oligocene to Quaternary assemblage recovered from the CRP cores would have occurred earlier in East Antarctica. The McMurdo erratics assemblages may be an Eocene dinocyst assemblage that is slightly older in East Antarctica than on Seymour Island. There may exist a unique, transitional assemblage in East Antarctic sediments that has yet to be found. But this, based on current knowledge, is speculation.

Palaeoenvironment

The distribution of *in situ* terrestrial and marine palynomorphs are most consistent, most abundant, and most diverse in the upper 250 m of CRP-3 (Tab. 5.6). They decrease below that level and all but disappear below 350 mbsf. A good dinocyst assemblage appears near the bottom of the core at 781-782 mbsf. This distribution may be a function of the samples studied, the result of climate change, or, more likely, due to depositional processes. Coincidentally, the sediments above 350 mbsf and between 750 and 800 mbsf are the muddiest in the core. Most palynomorphs are hydrodynamic equivalents to silt and fine sand-sized particles, and it is in sediments of those sizes that they are found most abundantly. The general lack of mud in the core may account for the scarcity of palynomorphs in most of the core.

Most of the *in situ* dinocyst assemblages recovered from CRP-3 seem to indicate deposition under shallow marine, inner shelf conditions. However, the presence of *Impagidinium* cf. *elegans* in the upper 100 m of CRP-3 (Fig. 5.7) is interesting in this regard. The present geographical distribution of the nine modern species of this genus indicates that they are all outer shelf to open ocean taxa (Harland, 1983; Wrenn & Kokinos, 1986; Marret & De Vernal, 1997). *Impagidinium pallidum* has been reported from inshore sediments off Wilkes Land, Antarctica. However, the sites vary in depth from 615 to 4 350 mbsf (Marret & De Vernal, 1997). The presence of *I.* cf. *elegans* suggests that deeper water conditions prevailed during deposition of Marine Palynomorph Unit 1 in CRP-3, and the lower part of Marine Palynomorph Unit 3 in CRP-2A. This interpretation assumes that the ancestral species in the genus *Impagidinium* preferred environmental conditions similar to those of the extant species.

In addition, the dinocyst assemblages from the lower

Tab. 5.6 - Summary diagram showing the distribution of terrestrial and marine palynomorphs in CRP-3. The curve for each category shows the total number of specimens counted.

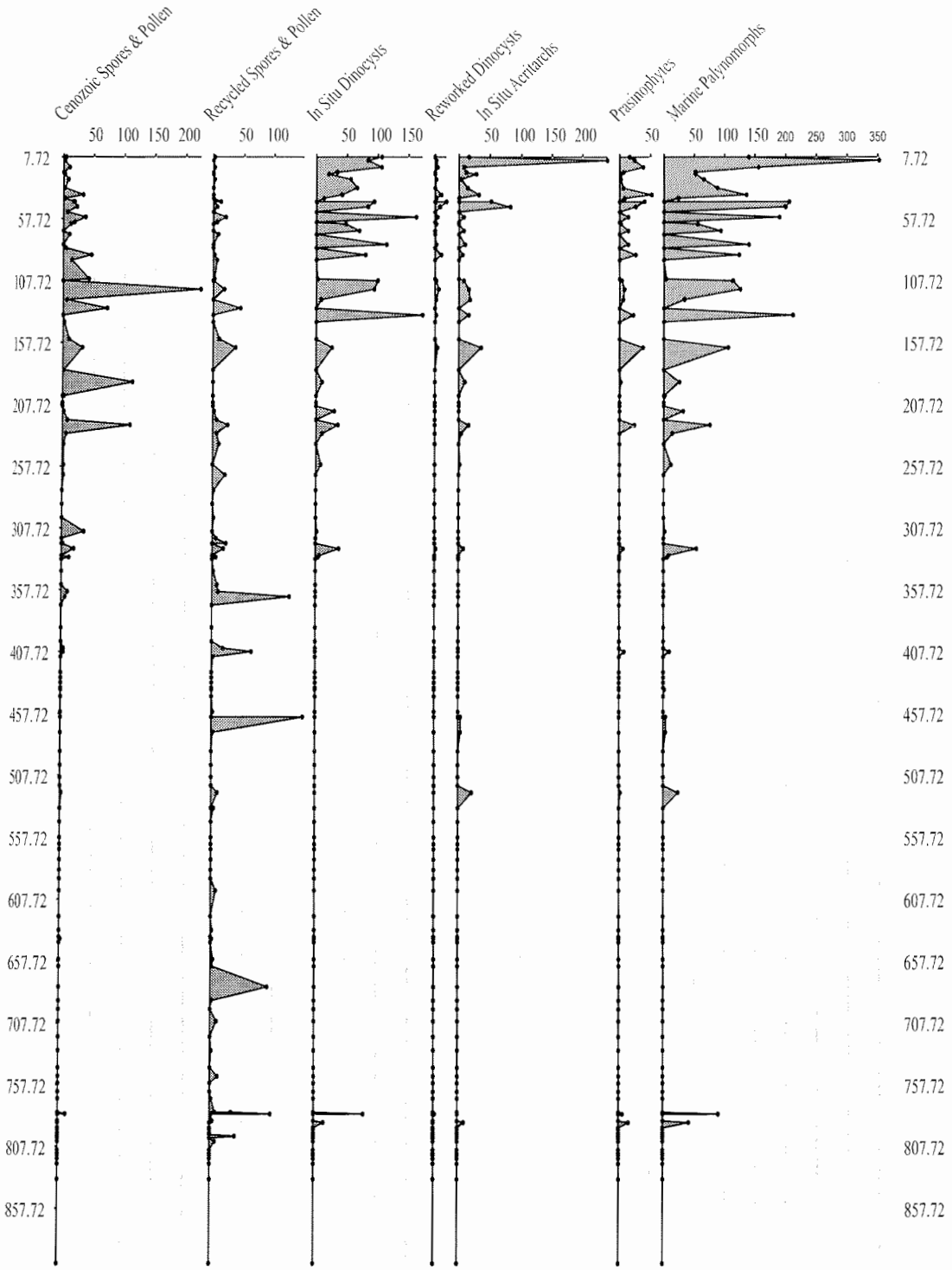

part of CRP-2A and the upper part of CRP-3 are of interest because of the appearance in considerable numbers, for Antarctic Neogene assemblages at least, of the gonyaulacoid dinocysts ?*Pyxidinopsis* spp. (in CRP-2A from 96.77 to 624.15 mbsf; in CRP-3 from 7.72 to 781.36 mbsf), *Impagidinium* cf. *elegans* (in CRP-2A from 444.76 to 624.15 mbsf; from 7.72 to 87.47 mbsf in CRP-3) and the acritarch *Leiofusa* sp. (in CRP-2A from 444.76 to 624.15 mbsf; from 7.72 to 87.47 mbsf in CRP-3). ?*Pyxidinopsis* spp. and *I.* cf. *elegans* are probably the cysts of autotrophic, or rather mixotrophic dinoflagellates, and not those of heterotrophic dinocysts that characterize most of the assemblages in CRP-1 and the uppermost part of CRP-2A. These may represent a transitional

assemblage (though not the transitional assemblage hypothesized above) between the warm autotrophic-rich dinocyst assemblages of the Eocene and the late Oligocene–Pleistocene assemblages dominated by heterotrophic dinocysts.

Acanthomorph acritarchs are relatively uncommon in CRP-2/2A and CRP-3. They rarely, if ever, reach the frequency and abundance recorded in CRP-1. If the tentative linkage made by Wrenn et al. (1998) were to be substantiated, this would suggest that seasonal sea-ice was not common or did not exist during the deposition of most of the Oligo-Miocene interval of CRP-2/2A and most of CRP-3. Alternately, the absence of acanthomorphs may be a result of other, perhaps evolutionary, reasons. Additional studies are needed to evaluate the potential of acritarchs as sea-ice indicators.

TERRESTRIAL PALYNOMORPHS

During the CRP-3 core-characterization phase, we examined a total of 120 samples for spores and pollen (miospores), including all "fast-track" samples and additional samples to secure a sample spacing of *c.* 10 m or less through the Cenozoic section. In the basal part of the Cenozoic section, 781.1 mbsf and below, we examined all of the palynological samples collected. Specimen counts presented in tables 5.7 and 5.8 result from study of the entire organic residue from palynological processing. Since the weight of sample processed was fairly uniform, usually 10 g in the section above *c.* 380 mbsf, and 10 to 20 g below that level, total counts are a reasonable guide to sample-to-sample variation in miospore abundance. This varied from "moderate" (>100 specimens/10 g), through "low" (10 to 100 specimens/10 g), to "sparse" (<10 specimens/10 g) or nil. We also examined 6 samples from the putative Beacon Supergroup section below 823.11 mbsf. Consistent with the coarse-grain size and oxidising paleoenvironment represented, these proved to be barren of palynomorphs or other organic material. A clay sample from 903.30 mbsf (later determined to be from altered volcanic rock) is also barren.

Within the Cenozoic section, both presumed contemporaneous and recycled components can be recognized on the basis of preservational state and known stratigraphical range. The recycled component includes a few Cenozoic forms but mainly comprises Permian to Mesozoic miospores. Distribution and significance of the Cenozoic and older components are discussed separately below.

Cenozoic Palynomorphs

Preservation of the Cenozoic palynomorphs, including presumed contemporaneous and recycled specimens, is generally good to very good. There are some poorly preserved specimens, however, that are broken and torn, or have mineral scarring from pyritization. The Cenozoic specimens are mostly light yellow to yellow in colour, although some have a darker (yellow-orange) hue.

Distribution (Tab. 5.7)

Abundance of Cenozoic miospores is generally sparse to moderate down to *c.* 360 mbsf, but with intervals of barren to sparse recovery from *c.* 200 to 221 mbsf and 232 to 300 mbsf. Below *c.* 370 mbsf (lower LSU 9.1 and below), most samples are barren, with only a few having sparse miospores. Highest abundances in the productive upper section occur in mudstones and sandy mudstones at 114.90 mbsf (count of 224, LSU 2.2), 131.17 mbsf (count 72, LSU 3.1), 190.77 mbsf (count 416, LSU 6.1), and 225.11 mbsf (count 250, LSU 7.2). These abundances exceed those seen in CRP-1 and CRP-2/2A, the most similar being a count of 64 miospores, at 575.36 mbsf in mudstone of LSU 15.3 in the lower part of CRP-2A. The general rarity of miospores in the lower part of the CRP-3 core is believed to result from, in part, removal of the fine fraction of the sediment by winnowing and, in part, dilution by rapid influx of sediment. Sparseness of vegetation in the surrounding landscape may also have contributed to the low abundance of miospores.

Diversity is higher in the samples with greater abundance of miospores, but in general is low. Relatively high total counts are mostly due to high levels of *Nothofagidites* spp., particularly of *N. lachlaniae* and undifferentiated *fusca* group species. Other relatively abundant taxa include *N. flemingii*, *N.* cf. *flemingii* (a smaller form), and various species of *Podocarpidites*. Aggregates of *Nothofagidites lachlaniae* and *Nothofagidites fusca* group pollen grains occur at 114.90, 131.17 and 225.11 mbsf, in association with high counts of individual specimens. Mildenhall (1989) observed similar aggregates of *Nothofagidites* pollen in CIROS-1. As suggested by Mildenhall, such aggregates are very likely to be due to incorporation of anthers in the sediment. Their fragility suggests that they are not recycled but transported, with very little disruption, from contemporaneous vegetation.

The taxonomic composition of the flora is very similar to that encountered in the lower part of CRP-2A (Terrestrial palynomorph Unit II of Cape Roberts Science Team, 1999), with a similar number of species and few different species being encountered. Bryophytic spores of *Coptospora* spp. occur consistently through the sequence; most of these are probably referable to *Coptospora* sp. c of Raine (1998, Fig. 1e & f), and the *Coptospora* sp. from CIROS-1 illustrated by Mildenhall (1989, Pl. 2, Fig. 14). The only other certain bryophytic spore encountered was a single broken specimen of *Ricciaesporites* sp. similar to that seen in CRP-2A, which occurs at 781.36 mbsf. Lycopod spores are noted for the first time in the sequence of CRP wells, as *Lycopodiumsporites* sp. These occur consistently through the upper part of CRP-3. Ferns are represented by rare occurrences of *Cyathidites minor*, *Laevigatosporites*

Tab. 5.7 - Stratigraphical distribution of Cenozoic spores and pollen, CRP-3. Samples barren of all miospores are shaded dark grey, those barren of Cenozoic palynomorphs, but with recycled Permian and lower Mesozoic palynomorphs are shaded light grey. '*' = possible modern contaminant (see text). Total count of Cenozoic spores and pollen is given in the rightmost column.

	CONTEMPORANEOUS AND RECYCLED CENOZOIC TERRESTRIAL PALYNOMORPHS																																									
	Spores and pollen																																						Fungi			
Depth	Asteraceae (Tubuliflorae)*	?Bryophyta	?Campanulaceae	Caryophyllaceae: *Stellaria* type	?Caryophyllaceae	*Chenopodipollis* sp.	*Coptospora* spp.	*Cyathidites minor*	?*Cyperaceaepollis* sp.	*Dilwynites granulatus*	*Laevigatosporites* spp.	*Lycopodiumsporites* sp.	*Microcachryidites antarcticus*	*Myricipites harrisii*	*Nothofagidites asperus*	*Nothofagidites flemingii*	*Nothofagidites* cf. *flemingii*	*Nothofagidites lachlaniae*	*Nothofagidites* spp. (*fusca* group)	*Nothofagidites* aggregates (a)	*Podocarpidites* cf. *exiguus*	*Podocarpidites* sp.a	*Podocarpidites* sp.b	*Podocarpidites* sp.c	*Podocarpidites* sp.d	*Podocarpidites* sp.e	*Podocarpidites* spp.	*Proteacidites* sp.	Ranunculaceae	*Ruscaesporites* sp.	*Rugulatisporites* sp.	*Trichotomosulcites subgranulatus*	cf. *Trichotomosulcites* sp.	*Tricolpites* sp.b	*Tricolpites* sp.d	*Tricolpites* sp.e	*Tricolpites* spp.	*Triporopollenites* sp.	angiosperm pollen (indeterminate)	Fungal mycelia (Microthyriaceae)	Fungal spores	TOTAL CENOZOIC
7.72-7.74																	1	1									3															5
11.13-11.15																			1								1															2
16.79-16.81																2	1	3	4																							10
20.69-20.71																											1															1
22.27-22.29																		1	1																							2
25.96-25.98							1											1	7																							9
33.22-33.25																											2															2
38.46-38.48							1		1			1					7		20																		2					32
41.75-41.77																		1	2																							3
44.12-44.18																1	1	1	8							3	3															17
44.18-44.27																1	3	2	8								3										1					18
49.22-49.24																1	1	6	11							1	2															22
52.20-52.22							1					1					2		1								1															6
57.52-57.54								1									2	1	25		2						4										1					36
60.54-60.56											1							4	4		1	1				1	2		1									2		1		18
62.96-62.98															1	3	1		2								3										2					12
71.52-71.54																3	1	1	2				1			3																11
82.36-82.38															1		1		2							1																5
87.47-87.49			1				2		1							1	4	9	9		1		1			10	3					1							3	1		47
92.28-92.30													1			1	1	3	6			1				1						1										15
107.38-107.40							1					1				6		1	29				1		1		1								1							42
114.90-114.92							3				2	5				15	4	164	12	a	2	1	4			10														1	1	224
123.65-123.73							1									1	1		1								2															6
131.17-131.19							2					2				6	4	42	5	a		1	1			5	3														1	72
142.37-142.39																1			2								2															5
155.59-155.61							1									4		2	1								2														1	11
162.11-162.13							2										7	3	14			3					4															33
167.45-167.47												1						3	3							1	1															9
180.23-180.25																		2	1																							3
190.77-190.79							1					1			1	15	31	128	224		1		1				10							2			1					416
201.00-201.02																											2															2
206.58-206.60																																										0
209.98-210.00																																										0
214.00-214.02							1												1								1															3
221.18-221.20																1		6									1															8
225.11-225.13		1					6				1	8				1	21	60	139	a	1					1	5				2		1	3								250
232.47-232.49							1											1	3								1															6
240.24-240.26																		1									1															2
257.10-257.25																		2																								2
265.41-265.43						1		1																																		2
278.50-278.52																																										0
289.22-289.24																																										0
300.41-300.43																																										0
311.14-311.16																	1	3	31								1										1					37
316.13-316.15																																								1		1
320.70-320.72																		1	1																	1						3
320.79-320.81																																										0
324.39-324.41																		4	16								1															21
332.00-332.02							1					2							4								3	1			2											13
343.45-343.47																																										0
353.59-353.61																			1																							1
359.16-359.18							1					1						2						2			3						1									10
363.77-363.79							1											2	3																							6
370.55-370.57																																										0
388.35-388.37																																										0
399.81-399.83																																										0
406.05-406.07							1												2								1															4
408.59-408.61																			3								2															5
413.11-413.13																																										0
424.52-424.54																																										0
429.91-429.93																																										0
433.97-433.99																																										0
439.34-439.36																																										0
445.01-445.03																																										0
457.37-457.39																																										0
461.80-461.82										1																																1
473.75-473.77																			1																							1
489.13-489.15																																										0
500.23-500.25																																										0
509.38-509.40																																										0
521.76-521.78																			2																							2
534.69-534.70																																										0
546.26-546.28																																										0
558.39-558.41																																										0
564.40-564.42																																										0
577.08-577.10																																										0
584.44-584.46																																										0
591.91-591.93																																										0
602.07-602.09																																										0
621.75-621.77																																										0
633.20-633.22																																										0
640.69-640.71					1																						1															2
643.60-643.62																																										0
656.54-656.56																																										0
662.20-662.22																		1																								1
679.81-679.83																																										0
690.60-690.62																																										0
697.33-697.35																																										0
707.55-707.57																																										0
720.10-720.20																																										0
731.28-731.30																																										0
743.92-743.94																																										0
751.33-751.35																																										0
756.81-756.83																																										0
770.06-770.10																																										0
781.10-781.12																																										0
781.24-781.26																																										0
781.36-781.38	1			1				1			1			2			1	1								2				1							1					12
781.50-781.52																																							1			1
788.02-788.04																																										0
788.69-788.71																			1																							1
792.51-792.53																																										0
793.93-793.95																																										0
797.88-797.90	1																																									1
798.03-798.04																											1															1
799.22-799.23																																										0
800.35-800.37																																										0
801.56-801.58																																										0
804.53-804.55																																										0
811.10-811.12																																										0
814.21-814.23																																										0
815.84-815.86																																										0
818.23-818.26																																										0
822.33-822.35																																										0

spp., and *Rugulatisporites* sp. It is possible that some of these fern spores are recycled from Eocene or older strata. Gymnosperms are mainly represented by *Podocarpidites* species. *Podocarpidites* sp. a, which had a reported LAD at 316.50 mbsf in CRP-2A (Cape Roberts Science Team, 1999, p. 136), occurs in a few samples. A notable occurrence is that of *Podocarpidites* sp. e, a small form with clearly reticulate saccus mesexine, which appears to have a peak in abundance between *c.* 71 and 131 mbsf.

Angiosperm pollen other than *Nothofagidites* is rare. Two occurrences of possible Cyperaceae pollen (?*Cyperaceaepollis* sp.) complement a single occurrence in CRP-2A (Cape Roberts Science Team, 1999). Several species of dicotyledonous angiosperm pollen are recorded as *Tricolpites* spp., including an oblate form with granulate exine, *Tricolpites* sp. b, seen previously in CRP-2A at 453.26 mbsf. Other taxa occur as single specimens. A microechinate tricolpate pollen at 60.54 mbsf is referred to Ranunculaceae; a similarly sculptured but apparently alete pollen grain recorded from CRP-2A (Askin & Raine, in press) was also ascribed to this family. Four triporate pollen taxa are recorded, *Myricipites harrisii* (see below), *Proteacidites* sp. (a small form with granulate exine), *Triporopollenites* sp. (a psilate form), and a distinctive type recorded as ?Campanulaceae. The last has scattered spines and pore annuli, and may be conspecific with the species from CIROS-1 recorded as ?*Proteacidites spiniferus* by Mildenhall (1989, Pl. 2, Figs. 8-9). Three periporate pollen species, all possibly referable to Caryophyllaceae, are recorded as: Caryophyllaceae, *Stellaria* type; ?Caryophyllaceae; and *Chenopodipollis* sp. The latter two are similar to species occurring in CRP-1 (Cape Roberts Science Team, 1998c; Raine, 1998, Figs. 2m & 2k-l respectively).

Recycled and Contaminant Cenozoic Palynomorphs

It is likely that some of the Cenozoic spores and pollen are recycled from older Cenozoic rocks, although the extent of this reworking appears to be less than in the upper part of CRP-2/2A. Rare occurrences of the gymnosperms, *Dilwynites granulatus*, *Microcachryidites antarcticus*, and *Trichotomosulcites subgranulatus*, which occur in samples that lack abundant and presumed contemporaneous *Nothofagidites*, are similar to sporadic occurrences in CRP-1 and CRP-2/2A, and are likely to be of recycled specimens. In New Zealand and Australia these taxa range through the Upper Cretaceous and Palaeogene. Some of the fern spore specimens may also be recycled, as these occur in only a few samples.

Specimens of Asteraceae (Tubuliflorae) pollen were encountered at 781.36 and 797.88 mbsf. These lack protoplasm and may be fossil. Mildenhall (1989) recorded several similar specimens in the lower part of the CIROS-1 sequence, tentatively regarding these as contamination. Pollen of the Asteraceae (= Compositae) family, which are common weeds and thus potential laboratory contaminants, first appeared in Australasia during the late Oligocene (Pocknall & Mildenhall, 1984), but possibly earlier at DSDP Site 254 in the Indian Ocean (Kemp & Harris, 1977). Recovery of further specimens and study of autofluorescence characteristics are required to confirm the fossil nature of the CRP-3 and CIROS-1 specimens.

Age

Marchantiaceae and *Tricolpites* sp. a, two characteristic taxa of the uppermost Oligocene to lower Miocene section of CRP-2/2A and the lower Miocene section of CRP-1, are not recorded in CRP-3. As noted above, the composition and relative abundances of taxa in the upper part of the CRP-3 sequence, down to *c.* 360 mbsf, resemble those of the lowermost Oligocene part of the CRP-2A section. Other than noting this consistency, the lack of established datums at present precludes closer correlation. The apparent absence of the acme of *Podocarpidites* sp. e in CRP-2, however, may suggest that the sequence between *c.* 71 and 131 mbsf in CRP-3 has no equivalent in CRP-2.

The diversity of Cenozoic taxa present in the upper part of the CRP-3 sequence is slightly less than that reported from CIROS-1 by Mildenhall (1989), and considerably less than that of the Eocene McMurdo erratics (McIntyre & Wilson, 1966; Askin, in press). A notable absence from CRP-3 is pollen of the *brassii* group of *Nothofagidites*, which were present in the lower section of CIROS-1 and in the McMurdo erratics. If the CIROS-1 occurrences can be regarded as contemporaneous with deposition, absence of the *N. brassii* group from CRP-3 points to a younger age for the CRP-3 sequence above *c.* 360 mbsf. Below that level in CRP-3, paucity of the assemblages and uncertainty about recycling and contamination prevent any conclusion being drawn with confidence. We note the possiblity, however, that although rich "warm-climate" preglacial Eocene assemblages were not encountered in CRP-3, a latest Eocene age for the lower strata is not precluded. Although only a small number of miospores was recovered, species diversity is apparently high in the 781.36 mbsf sample. This may suggest more diverse parent vegetation, and therefore that a warmer climate prevailed.

Two specimens of *Myricipites harrisii* occur at 781.36 mbsf, the first record for the CRP sequence of holes. This taxon, which represents pollen of the angiosperm family Casuarinaceae, is characteristic and abundant in the Eocene of New Zealand and Australia, and also occurs in the McMurdo erratics (McIntyre & Wilson, 1966; Askin, in press) and MSSTS-1 drill core (Truswell, 1986). In the MSSTS-1 sequence specimens are common through the upper Oligocene, lower Miocene, and Quaternary sections (Truswell, 1986, recorded as *Triorites harrisii*), and were interpreted as

recycled from older sediments. Rare specimens were recorded only in the lowermost part of the CIROS-1 sequence by Mildenhall (1989, as *Haloragacidites harrisii*). In New Zealand, the main vegetational response to cooling occurred some time before the end of the Eocene (*e.g.* Raine, 1984; Pocknall, 1989), near the Kaiatan/Runangan Stage boundary (35.5 Ma, Morgans et al., 1996), and was reflected in the palynoflora by a transition from *Myricipites harrisii*-dominated palynofloras to those dominated by *Nothofagidites* of the *brassii* group. It is likely that a corresponding vegetational change occurred at a similar time, or even earlier, in Antarctica. That such a severe change occurred is attested to by the absence of a large proportion of the rich Eocene flora, as noted above, in the upper CRP-3 record. Whether the specimens of *M. harrisii* in CRP-3 (and those in CIROS-1) are recycled is unclear. Recycling of *M. harrisii* would be unique within the known CRP sequence. If the specimens are not recycled, then their presence may point to a Kaiatan-equivalent or older age, *i.e.* greater than 35.5 Ma, for these strata.

Palaeoenvironmental Significance

As noted above, assemblages in the upper part of CRP-3 never reach the species richness and abundance seen in the Eocene McMurdo Sound erratics (Wilson, 1967; Askin, in press) or in the Eocene (lower) part of CIROS-1 (Mildenhall, 1989). Instead, the CRP-3 assemblages suggest low diversity woody vegetation that included several species of *Nothofagus* and podocarpaceous conifers, a few other angiosperm families, and few cryptogams except for bryophytes (mosses and liverworts). Many of the important components of the prior Eocene flora are missing (*e.g.* several species of Proteaceae, various other angiosperms, gymnosperms and cryptogams). In favourable sites the vegetation may have comprised a low scrub or closed forest intermediate in stature and floristic richness between that of the Eocene and the limited vegetation of the late Oligocene to early Miocene. More stunted vegetation would have existed in exposed and upland sites. Wetland vegetation, which would be indicated by the presence of monocotyledonous angiosperms such as Cyperaceae and *Phormium* (CRP-2; Cape Roberts Science Team, 1999), appears to have been minor, although *Coptospora* may in part represent a mire community.

Further deterioration of conditions in this part of Antarctica resulted in additional loss of various components from the land flora. Unglaciated parts of the late Oligocene to Miocene landscape supported a much reduced flora, probably a low-growing sparse tundra vegetation, as discussed by Raine (1998) for CRP-1. This vegetation included at least one (though possibly more) species of *Nothofagus,* at least one species of podocarpaceous conifer, and a few other angiosperms and cryptogams including mosses.

Palynomorphs in the "Shear Zone", 789.77-805.60 mbsf

Eight samples were examined from LSU 14.1, referred to as "Dolerite (cataclastic) breccia" in the core logs, at 789.77-805.60 mbsf (Tabs. 5.3, 5.7 & 5.8). All samples were collected from the dark-grey claystone matrix of the breccia, which in some cases was laminated. Organic matter is sparse in all samples and consists of coaly material with some brown woody material and tissue. This recycled Beacon organic matter, and the recycled Beacon spores and pollen (Tab. 5.8), which are common in the sample at 800.35-800.37 mbsf, together with the single ?Cenozoic podocarp pollen specimen at 798.03-798.04 mbsf, are all consistent with a sedimentary origin for this breccia.

Recycled Palaeozoic-Mesozoic Palynomorphs

Recycled spores and pollen occur throughout much of CRP-3. These can be distinguished by their distinctive morphology, and usually darker exinal colour (yellow-orange through brown to black) relative to the light yellow contemporaneous miospores. Recycled miospores with restricted stratigraphic ranges are shown in separate Jurassic, Triassic and Permian columns in table 5.8; long-ranging and indeterminate forms are listed in the "undifferentiated" column. In the upper part of CRP-3 (above approximately 410 mbsf), peaks in recycled miospore occurrences correspond in a general way with many of the peaks in occurrences of contemporaneous specimens, implying lithological control on palynomorph preservation (more mud, for example). Below 410 mbsf, where contemporaneous palynomorphs are extremely rare, peaks in abundance may be due to recycled clasts of palynologically-rich sediment, although this middle to lower part of the core is dominated by coaly material recycled from the Beacon Supergroup coal-measures (see below) as well as high dominance of Beacon-derived sands (see Petrology chapter).

Recycled Jurassic Palynomorphs

Corollina spp., which occur as single specimens (listed as monads), and in tetrads and aggregates, are common in two broad intervals, between approximately 220 and 365 mbsf, and between 750 and 782 mbsf. Single specimens occur at 71.52-71.54 and 131.17-131.19 mbsf (Tab. 5.8). They indicate the erosion and redeposition of Jurassic sediments in these intervals. The aggregates must have been recycled within clasts to remain clumped together.

Corollina spp. are typically from the Jurassic to Lower Cretaceous in Southern Hemisphere localities, although some forms such as *C. meyeriana* range from the uppermost Triassic. In New Zealand *Corollina* are particularly abundant in the lowermost Jurassic. The provenance of these specimens is believed to be the

Tab. 5.8 - Stratigraphical distribution of recycled Permian and lower Mesozoic spores and pollen, CRP-3. Samples barren of all miospores are shaded dark grey, those barren of Permian and lower Mesozoic palynomorphs, but with recycled Cenozoic palynomorphs are shaded light grey. Total count of Permian and lower Mesozoic spores and pollen is given in the rightmost column.

	RECYCLED BEACON/FERRAR SPORES & POLLEN																																														
	Jurassic		Triassic								Permian										Undifferentiated																										
Depth	*Corollina* spp. (monads)	*Corollina* spp. (tetrads & clumps)	*Acanthotriletes tereteangulatus*	?*Annulispora microannulata*	*Aratrisporites* spp.	*Cadargasporites senectus*	*Chordasporites australiensis*	*Craterisporites rotundus*	*Lunatisporites* cf. *dettmannii*	*Neoraistrickia taylorii*	*Apiculatisporis cornutus*	*Cannanoropollis mehtae*	*Chordecystia chalasta*	?*Crucisaccites* sp.	*Granulatisporites micronodosus*	*Granulatisporites trisinus*	*Microbaculispora villosa*	?*Pretricolpipollenites* sp.	*Plicatipollenites gondwanensis*	*Fraalispora* sp.	*Alisporites australis*	*Alisporites* spp.	*Anapiculatisporites* sp.	*Baculatisporites* spp.	*Cingutriletes* sp.	*Converrucosisporites* sp.	*Cyathidites minor*	*Cycadopites* sp.	*Deltoidospora/Leiotriletes* spp.	*Dictyophyllidites mortonii*	*Granulatisporites* sp.	*Kraeuselisporites* sp.	*Lunatisporites* spp.	*Neoraistrickia* [illegible]	*Osmundacidites wellmanii*	*Platysaccus* spp.	*Playfordiaspora crenulata*	*Protohaploxypinus* spp.	*Punctatisporites* spp.	?*Retusotriletes* sp.	*Rogalskaisporites cicatricosus*	*Stereisporites antiquasporites*	bisaccate pollen (indeterminate)	taeniate bisaccate pollen (indet.)	monosaccate pollen (indet.)	spores (indet.)	TOTAL BEACON/FERRAR
7.72-7.74																						1														1							1				3
11.13-11.15																																															0
16.79-16.81																																											3				3
20.69-20.71																																															0
22.27-22.29																																															0
25.96-25.98																																											2			1	3
33.22-33.25																					1																										1
38.46-38.48																																											1				1
41.75-41.77																																											1				1
44.12-44.18																					2	6																					4			1	13
44.18-44.27																																											3				3
49.22-49.24																					1	2				1																	1			1	6
52.20-52.22																																															0
57.52-57.54																					5	7																1					8				21
60.54-60.56																												1												1			5				7
62.96-62.98																																											1				1
71.52-71.54	1								1							1																	1										4			1	9
82.36-82.38																																											3				3
87.47-87.49																																											2				2
92.28-92.30																					1						1																4			1	7
107.38-107.40																					1	1																									2
114.90-114.92																				1	3	1																				1	11			2	19
123.65-123.73																																															0
131.17-131.19	1								1												6	11		1				1	1														21	1			44
142.37-142.39																																											1			1	2
155.59-155.61																						2																			1		7			1	11
162.11-162.13					1		1														5	9															4	12					14			2	36
167.45-167.47																						2																					1			1	4
180.23-180.25																																											1				1
190.77-190.79																					1																						7				8
201.00-201.02																																															0
206.58-206.60																																									1		1				2
209.98-210.00																																															0
214.00-214.02																						1																					1				2
221.18-221.20	1																				1	1																					1			2	6
225.11-225.13											1				1						2	6								1	1							1					10			2	25
232.47-232.49																						1																					6				7
240.24-240.26																						3																					6			1	10
257.10-257.25																																															0
265.41-265.43	9	2																				2																					6	1			20
278.50-278.52																						1														1							1				3
289.22-289.24																																															0
300.41-300.43																			1																								1	1			3
311.14-311.16																						1																									1
316.13-316.15																					4	2																					1				7
320.70-320.72					1							1			1	1					3	3									1												9			3	23
320.79-320.81																																															0
324.39-324.41		1																			2	8													1								6			1	19
332.00-332.02		1					1																								1												2			2	7
343.45-343.47																	1																										1				2
353.59-353.61										1											1																						4		1	2	9
359.16-359.18		2																			2	1																					5				10
363.77-363.79	59	6			2																17	16						1			1					1							21	1	1		126
370.55-370.57																																															0
388.35-388.37																																															0
399.81-399.83																																															0
406.05-406.07								1													3	3																					9			2	18
408.59-408.61				1	1		2														11	22						1		1						2							24				65
413.11-413.13																																											3				3
424.52-424.54																																															0
429.91-429.93																																															0
433.97-433.99																																															0
439.34-439.36																																														1	1
445.01-445.03																																															0
457.37-457.39																					1																						1				2
461.80-461.82			1		1		1														20	77						1	1		1			1	1	1							37	1		4	148
473.75-473.77																						2																								1	3
489.13-489.15																																															0
500.23-500.25																																															0
509.38-509.40																																															0
521.76-521.78					1																5	2																					2				10
534.69-534.70																						2																					1			2	5
546.26-546.28																																															0
558.39-558.41																																															0
564.40-564.42																																															0
577.08-577.10																																															0
584.44-584.46																																															0
591.91-591.93																																															0
602.07-602.09																																											6		1	1	8
621.75-621.77																					1																						3				4
633.20-633.22																																											2	1			3
640.69-640.71																																											2				2
643.60-643.62																																															0
656.54-656.56																						3																					1				4
662.20-662.22																						1																					1				2
679.81-679.83					17								1																								1						22	2		50	93
690.60-690.62																						1																	1								2
697.33-697.35																																														2	2
707.55-707.57																					2					1																	5			2	10
720.10-720.20																																															0
731.28-731.30																																											1			1	2
743.92-743.94																													1																		1
751.33-751.35		1			21																									1						1							10				13
756.81-756.83																																															0
770.06-770.10	1																												1																		2
781.10-781.12	2				1																	2																					4				9
781.24-781.26																					6	15																					8			5	34
781.36-781.38	5	4					1												2		11	24			1	1		1	1							1						1	35	1		9	98
781.50-781.52																																	1										1				2
788.02-788.04													1															1															1			2	5
788.69-788.71	1	1							1						1						1	2										1											9			3	20
792.51-792.53																																															0
793.93-793.95																																															0
797.88-797.90																																															0
798.03-798.04																																															0
799.22-799.23																																											2				2
800.35-800.37						1								1				1			1							2															34		1		41
801.56-801.58																		1																													1
804.53-804.55																							1																				6		1		8
811.10-811.12																																															0
814.21-814.23																																															0
815.84-815.86																																															0
818.23-818.26																																															0
822.33-822.35																																															0

Lower-Middle Jurassic Ferrar Group. Outcrops of Ferrar sedimentary rocks occur at Carapace Nunatak, in the northern upstream area of the Mackay Glacier, where palynomorph-bearing (Tasch & Lammons, 1978) lacustrinal sediments are interbedded with basalts. It is likely that some of the *Alisporites* specimens may also have a Ferrar Group provenance, along with some of the long-ranging "undifferentiated" group. Almost all of the *Corollina* specimens have a similar orange exinal colour, as do many of the *Alisporites* and undifferentiated specimens, indicating a similar degree of thermal alteration for the source rocks. No other age-restricted Jurassic taxa were observed in the CRP-3 samples scanned thus far.

Recycled Permian-Triassic Palynomorphs

Well-preserved yellow-orange specimens to barely recognizable black corroded remnants of recycled spores and pollen, many diagnostic of the Permian and Triassic, are common to abundant throughout most of CRP-3 (Tab. 5.8). The provenance of these specimens is the Permian-Triassic Victoria Group (upper Beacon Supergroup). Coal derived from the Victoria Group is noticeably abundant throughout much of the core, concentrated in laminae or as fragments dispersed throughout sandstone beds. Coaly material, including coarse fragments to finely disseminated material, is common in almost all of the CRP-3 palynological preparations, forming the bulk of the preserved organic material.

In outcrops of the Victoria Group in the Transantarctic Mountains of the Mackay Glacier area, coal is most abundant in the Permian Weller Coal Measures. Coal beds also occur in the Triassic Lashly Formation, but they are much less common and occur in thinner, less continuous lenses. Most of the coal occurring in CRP-3 is probably derived from the Weller Coal Measures. Curiously, a large proportion of the identifiable recycled specimens throughout CRP-3 have a Triassic provenance, especially if most of the *Alisporites* specimens are included in this category. *Alisporites* spp., including *A. australis*, are the dominant palynomorphs in the Lashly Formation (Kyle, 1977; Kyle & Schopf, 1982). However, most of the redeposited coal in CRP-3 appears to be of high rank. As with coal from the lower part of CRP-2/2A, attempts at extracting miospores from coal fragments were unsuccessful, quite likely a result of the high rank which renders it impossible to chemically and physically extract recognisable palynomorphs. Palynomorphs associated with coals of low-volatile bituminous to semi-anthracite or higher rank are fragile, corroded and dark brownish black to black in colour, or thermally destroyed, as are palynomorphs from outcrops of the Weller Coal Measures (Kyle, 1976, 1977). Probably very few recognisable miospores were preserved in the Permian coal measures that have been eroded and redeposited in CRP-3.

Organic material preserved in Beacon Supergroup and Ferrar Group sediments of the Transantarctic Mountains owes its high rank and dark coloration to thermal alteration during Jurassic emplacement of Ferrar Group dolerite sills and basalt. Most of the diagnostic Permian specimens from CRP-3 are orange to reddish brown in colour, having suffered relatively little thermal alteration compared with specimens occurring in outcrops of the dolerite-intruded Transantarctic Mountains. Light-coloured Triassic specimens recycled into Neogene glacial beds on Mount Feather, and unusually light-coloured Permian specimens recycled into CRP-2/2A sediments, were interpreted (Askin, 1998; Askin & Raine, in press) as being derived from Beacon sediments that had not been intruded by dolerite sills, well inland (cratonwards) of the Transantarctic Mountains. This is probably also the provenance for the well-preserved CRP-3 recycled Permian assemblages, notably most common between 300 and 350 mbsf, and also between 780 and 802 mbsf.

MACROPALAEONTOLOGY

INTRODUCTION

As many as 239 body macrofossil-bearing horizons have been identified in CRP-3 (Tab. 5.9, Fig. 5.8). We recorded all macrofossils visible in the sampling and archive halves as well as a few identified within micropalaeontological residues. Potential macrofossil-bearing intervals were, in some cases, specifically searched for less obvious body fossils. Macrofossils are most commonly associated with mudstones and muddy sandstones throughout the section from the core top to *c.* 325 mbsf. Only scattered and sometimes dubius macrofossils were noted between 325-782 mbsf, and none below this depth.

We also observed some remarkable trace fossils, *e.g.* a large $CaCO_3$-lined burrow at 62.63 mbsf, but these are not discussed in the present section. In most cases, macrofossils are seen in cross-sections cut by the bit during the drilling or later when the core was split during processing (see section on Core Management).

TAPHONOMY

Preservation of shell material is highly variable. Pristine or well preserved calcareous skeletal parts are quite rare in the CRP-3 drill core and generally belong to calcitic organisms such as pectinid bivalves, serpulid polychaetes, brachiopods and echinoids. Calcareous shells most often show advanced degrees of dissolution. Unlikely the pre-Quaternary sediments in CRP-1 and CRP-2/2A (Claps & Aghib, 1998; Cape Roberts Science Team, 1999), concretions around fossils are a comparatively rare phenomenon in CRP-3. The best examples include semi-lithified concretions entrapping

Tab. 5.9 - Inventory of CRP-3 macrofossils.

LSU 1.1

6.80-6.88	mbsf: modiolid? mussel, echinoid debris
10.80-10.85	mbsf: modiolid mussel mould, articulated
10.88-10.99	mbsf: modiolid mussels, articulated, decalcified
11.00-11.01	mbsf: unidentified plant remain
17.31-17.32	mbsf: unidentified bivalve fragment

LSU 1.2

23.34-23.42	mbsf: unidentified mollusc fragments
27.88-27.96	mbsf: unidentified mollusc fragments
29.94-29.96	mbsf: pectinid bivalve (?*Adamussium* n.sp.), broken fragment, fresh
38.34-38.35	mbsf: unidentified macrofossil (serpulid?)
38.53-38.66	mbsf: serpulid tube (?*Serpula* sp.), aggregates, many large tubes, very fresh
38.81-38.82	mbsf: pectinid bivalve (?*Adamussium* n.sp.), broken fragment, fresh
39.00-39.01	mbsf: serpulid tube (?*Serpula* sp), fresh
39.55-39.56	mbsf: unidentified macrofossil fragments
41.01-41.02	mbsf: unidentified mollusc fragments
41.61-41.63	mbsf: pectinid bivalve (?A*damussium* n.sp.), two fresh broken valves
41.84-41.85	mbsf: serpulid tube, fresh
43.70-43.72	msbf: serpulid tube, slightly concretioned
43.84-43.85	mbsf: ?serpulid tube, chalky
44.12-44.18	mbsf: unidentified mollusc fragments; echinoid debris
45.72-45.80	mbsf: sponge spicules
46.12-46.18	mbsf: platy fragments (unidentified bivalve?); leaf (*cf. Nothofagus*)
47.55-47.57	mbsf: pectinid bivalve (*cf.* ?A*damussium* n.sp)., fragment
50.42-50.43	mbsf: ?scaphopod shell, relatively fresh but broken
50.46-50.48	mbsf: unidentified tiny bivalve fragments
51.20-51.23	mbsf: terebratulid? brachiopod, articulated, incomplete
51.27-51.28	mbsf: small ?serpulid tube

LSU 1.3

59.59-59.60	mbsf: unidentified thin bivalve
60.19-60.20	mbsf: unidentified relatively large bivalve, chalky
62.62-62.69	mbsf: 3 unidentified bivalves, chalky; terebratulid brachiopod;associated with a large burrow lined by $CaCO_3$
64.42-64.43	mbsf: unidentified articulated bivalve mould (pyritized)
66.91-66.92	mbsf: unidentified thin bivalve
68.52-68.53	mbsf: unidentified macrofossil fragments
68.69-68.70	mbsf: unidentified macrofossil fragments
69.54-69.55	mbsf: unidentified macrofossil fragments

LSU 1.4

75.53-75.54	mbsf: unidentified articulated small bivalve, chalky
76.03-76.04	mbsf: six small articulated bivalves, chalky

LSU 2.1

83.95-83.97	mbsf: unidentified thick-shelled pectinid bivalve (?*Adamussium* n.sp.?)
85.39-85.40	mbsf: unidentified small bivalve fragments
86.37-86.39	mbsf: unidentified bivalve fragment
88.19-88.20	mbsf: bryozoan colony, encrusting pebble
89.02-89.03	mbsf: unidentified bivalve fragment, fresh
94.18-94.19	mbsf: unidentified thin bivalve fragment
94.37-94.38	mbsf: unidentified bivalve fragment, fresh; thin tube (scaphopod? serpulid?)

LSU 2.2

96.27-96.29	mbsf: unidentified fragments of thick-shelled costate? bivalve
96.52-96.53	mbsf: unidentified small bivalve fragment
96.27-96.29	mbsf: unidentified bivalve fragments
96.52-96.53	mbsf: unidentified bivalve fragment
97.99-98.01	mbsf: unidentified bivalve, ?brachiopod
98.09-98.11	mbsf: 3 brachiopod valves, fresh; one or two unidentified bivalve fragments, chalky
98.12-98.14	mbsf: unidentified bivalve fragment
98.31-98.33	mbsf: unidentified bivalve fragments, chalky (smooth, only concentric growth lines)
99.59-99.6	mbsf: articulated carditid bivalve
102.80-102.8	mbsf: unidentified thin ?bivalve, fragment
103.99-104.01	mbsf: small unidentified bivalve fragment
105.04-105.05	mbsf: small, thick bivalve fragment
111.78-111.81	mbsf: unidentified bivalve fragment, chalky
114.19-114.22	mbsf: pectinid bivalve (?*Adamussium* n.sp)
114.23-114.31	mbsf: unidentified mollusc fragments;echinoid fragments
114.39-114.41	mbsf: unidentified tiny bivalve
115.09-115.10	mbsf: unidentified bivalve
115.73-115.75	mbsf: unidentified bivalve fragment
116.95-116.96	mbsf: unidentified thick bivalve small fragment
119.08-119.10	mbsf: unidentified bivalve (smooth)
119.13-119.15	mbsf: ?serpulid tube fragment
119.45-119.47	mbsf: unidentified articulated small bivalve
119.61-119.70	mbsf: unidentified mollusc fragments

LSU 3.1

120.34-120.37	mbsf: rounded carditid bivalve
120.43-120.47	mbsf: carditid bivalve(s), chalky
120.55-120.56	mbsf: carditid? bivalve, unidentified articulated bivalve
120.58-120.60	mbsf: carditid bivalve, chalky, articulated bivalve (concentric ornamentation), chalky
120.60-120.62	mbsf: large rounded carditid bivalve; serpulid? tube
120.75-120.79	mbsf: small articulated bivalves (~ 5 shells), chalky
121.06-121.07	mbsf: elongated shell (?scaphopod), fragment
121.19-121.22	mbsf: carditid bivalve; terebratulid brachiopod
121.23-121.27	mbsf: elongate carditid bivalve; rounded carditid bivalve
121.29-31	mbsf: rounded carditid bivalve, unidentified bivalve
121.41-121.43	mbsf: unidentified bivalve, small fragment; echinoid debris
121.49-121.51	mbsf: large carditid bivalve, articulated, chalky, sliced
122.22-122.24	mbsf: small articulated bivalves
124.93-124.96	mbsf: small articulated bivalves
124.96-125.01	mbsf: echinoid test; small brachiopod; small bivalves
125.18-125.20	mbsf: carditid bivalve, ?scaphopod (aligned)
125.27-125.29	mbsf: unidentified ?bivalve fragment
125.57-125.60	mbsf: small articulated bivalve, chalky
125.68-125.70	mbsf: unidentified ?bivalve fragment
126.32-126.35	mbsf: unidentified small bivalves (~3), chalky
126.40-126.42	mbsf: unidentified small articulated bivalve, chalky and fragments
126.45-126.47	mbsf: small articulated bivalve, sliced
126.48-126.51	mbsf: carditid bivalve
126.66-126.69	mbsf: carditid bivalve; gastropod
126.94-126.96	mbsf: unidentified bivalve, small fragment
127.09-127.11	mbsf: small articulated bivalve
127.17-127.20	mbsf: two articulated carditid bivalves and fragments
127.26-127.28	mbsf: small articulated bivalve, chalky
127.34-127.36	mbsf: unidentified articulated, bivalve
127.49-127.50	mbsf: unidentified bivalve, small fragment
127.75-127.76	mbsf: unidentified bivalve, small fragment
127.84-127.87	mbsf: elongate carditid bivalve; ?lucinacean bivalve; unidentified bivalve
127.94-127.97	mbsf: unidentified bivalve, chalky, unidentified bivalve fragments
128.37-128.39	mbsf: unidentified bivalve fragment
128.58-128.60	mbsf: unidentified bivalve fragment

Tab. 5.9 - Continued.

128.64-128.66 mbsf: unidentified small articulated ?bivalve, chalky
129.79-129.81 mbsf: unidentified small articulated bivalve, chalky
130.23-130.31 mbsf: echinoid debris
130.55-130.57 mbsf: small paired bivalve (?nuculanid),chalky
136.35-136.38 mbsf: articulated rounded carditid bivalve
137.21-137.25 mbsf: solitary scleractinian coral, sugar-like texture; serpulid? tube
137.33-137.35 mbsf: articulated carditid bivalve, flattened and chalky
138.80-138.84 mbsf: rounded carditid bivalve
139.46-139.47 mbsf: unidentified articulated bivalve (?*Corbula*-like)
140.03-140.04 mbsf: unidentified bivalve, fragment
140.12-140.13 mbsf: unidentified bivalve, small fragment
140.69-140.74 mbsf: solitary scleractinian coral; elongate carditid bivalve; serpulid tube
140.79-140.81 mbsf: rounded carditid bivalve
141.20-141.23 mbsf: thin shelled, ?articulated, crenulate bivalve; large unidentified bivalve
141.62-141.70 mbsf: unidentified mollusc fragments
141.92-141.95 mbsf: unidentified mollusc fragments

LSU 5.1
157.37-157.38 mbsf: unidentified bivalve, small fragment
157.71-157.75 mbsf: large, unidentified bivalve
157.76-157.83 mbsf: unidentified gastropod (pyritized); echinoid debris
157.83-157.86 mbsf: scaphopod?, unidentified bivalve
158.20-158.21 mbsf: unidentified bivalve, highly fragmented
160.37-160.43 mbsf: unidentified mollusc fragments
162.16-162.24 mbsf: unidentified gastropod (?silicified)
162.25-162.26 mbsf: thin bivalves fragment
162.26-162.28 mbsf: unidentified bivalve fragments, small
162.39-162.41 mbsf: unidentified bivalve fragments, chalky
162.72-162.74 mbsf: unidentified bivalve fragments, aligned, chalky
163.65-163.68 mbsf: unidentified costate bivalve (carditid?), chalky
165.30-165.31 mbsf: unidentified bivalve, small fragment
165.35-165.36 mbsf: unidentified bivalve, small fragment
165.66-165.68 mbsf: unidentified costate bivalve (carditid?), chalky
166.00-166.02 mbsf: unidentified bivalve fragment, chalky
166.16-166.17 mbsf: unidentified bivalve, small fragments
166.64-166.66 mbsf: unidentified bivalve fragment, fresh
168.39-168.41 mbsf: small crenulate shell fragment
171.54-171.55 mbsf: unidentified bivalve, small fragment
174.17-174.18 mbsf: unidentified bivalve, small fragment

LSU 5.3
176.97-176.98 mbsf: unidentified bivalve, small fragment
177.23-177.26 mbsf: small unidentified bivalve fragment

LSU 6.1
186.14-186.16 mbsf: indet bivalve fragment (concentric growths)
186.28-186.29 mbsf: unidentified bivalve, small fragment
186.62-186.64 mbsf: unidentified bivalve fragment, fresh
186.78-186.81 mbsf: unidentified macrofossil fragment, fresh
187.12-187.15 mbsf: unidentified small bivalve fragment,fresh
187.40-187.41 mbsf: unidentified bivalve, small fragment
187.77-187.78 mbsf: unidentified thin bivalve small fragment
188.82-188.83 mbsf: unidentified thin bivalve small fragment
188.87-188.88 mbsf: unidentified thin bivalve small fragment
190.22-190.24 mbsf: unidentified bivalve, chalky
190.29-190.31 mbsf: pectinid bivalve (?*Adamussium* n.sp.),fragments: unidentified bivalve, chalky
190.50-190.52 mbsf: unidentified small articulated bivalve, chalky
190.72-190.75 mbsf: unidentified bivalves, chalky
190.77-190.87 mbsf: unidentified mollusc fragments
192.62-192.63 mbsf: unidentified thin bivalve small fragment
192.72-192.73 mbsf: unidentified small bivalve fragment
193.13-193.14 mbsf: unidentified thin bivalve small fragment
193.40-193.41 mbsf: unidentified thin bivalve small fragment
194.39-194.40 mbsf: unidentified thin bivalve small fragment
196.82-196.83 mbsf: unidentified thin ?bivalve small fragment
196.96-196.97 mbsf: bryozoan?
196.99-197.02 mbsf: small unidentified bivalve
197.29-197.32 mbsf: gastropod (early whorls, chalky)
197.32-197.33 mbsf: unidentified mollusc fragments
197.61-197.64 mbsf: unidentified bivalve, fragmented
197.76-197.79 mbsf: small, incomplete but articulated unidentified bivalve
197.85-197.86 mbsf: unidentified bivalve fragment
198.50-198.53 mbsf: naticid gastropod, chalky but complete
198.79-198.81 mbsf: small unidentified bivalve fragment
198.88-198.89 mbsf: incomplete fresh (some nacreous layer left) small bivalve ('*Nucula*')
199.06-199.07 mbsf: unidentified bivalve (smooth)
199.16-199.17 mbsf: unidentified thin ?bivalve small fragment
200.12-200.14 mbsf: veneroidan bivalve (concentric ridges)
200.93-200.94 mbsf: unidentified bivalve fragment
201.50-201.51 mbsf: unidentified thin bivalve fragment
211.75-211.76 mbsf: unidentified thin bivalve small fragment
216.00-216.01 mbsf: unidentified thin ?bivalve small fragment
217.30-217.31 mbsf: unidentified macrofossil
223.79-223.80 mbsf: unidentified thin ?bivalve small fragment
224.28-224.29 mbsf: unidentified ?bivalve fragment (partially rextal)
225.74-225.75 mbsf: unidentified thin bivalve small fragment
228.70-228.72 mbsf: unidentified ?bivalves (pseudomorphs?)

LSU 7.3
257.10-257.25 mbsf: unidentified mollusc fragments
264.34-264.42 mbsf: unidentified mollusc fragments
266.13-266.14 mbsf: unidentified articulated thin ?bivalve
266.73-266.81 mbsf: unidentified mollusc fragments
269.37-269.41 mbsf: unidentified semicircular thin macrofossil

LSU 7.4
274.25-274.27 mbsf: unidentified bivalve fragment, chalky
274.27-274.31 mbsf: unidentified bivalve (?*Adamussium* n.sp., ?doubtful fragment)
275.42-275.50 mbsf: unidentified mollusc fragments
275.72-275.74 mbsf: unidentified bivalve chalky fragments
278.02-278.03 mbsf: unidentified semicircular thin macrofossil
286.89-286.90 mbsf: unidentified macrofossil

LSU 8.1
308.20-308.25 mbsf: one articulated shell and fragments of pectinid bivalve (?*Adamussium* n.sp).
308.68-308.71 mbsf: many small fragments of unidentified bivalves
309.29-309.33 mbsf: pectinid bivalve (?*Adamussium* n.sp)., two broken, well preserved valves
310.63-310.71 mbsf: unidentified mollusc fragments
311.25-311.27 mbsf: turritellid gastropod, only cast showing concentric ornamentation
311.40-311.41 mbsf: tiny unidentified bivalve fragment
311.59-311.60 mbsf: tiny unidentified bivalve fragment
312.10-312.12 mbsf: unidentified bivalve fragment, chalky
314.59-314.67 mbsf: unidentified mollusc fragments
315.04-315.05 mbsf: tiny unidentified bivalve fragment
315.06-315.09 mbsf: unidentified bivalve fragment
315.57-315.61 mbsf: unidentified macrofossil fragment, chalky
315.66-315.69 mbsf: unidentified taxodont bivalve hinge, chalky
315.96-315.97 mbsf: tiny unidentified bivalve fragment
316.08-316.09 mbsf: unidentified bivalve fragment

Tab. 5.9 - Continued.

316.74-316.75	mbsf: unidentified macrofossil fragment, chalky
316.85-316.86	mbsf: tiny unidentified bivalve fragment
317.52-317.53	mbsf: tiny unidentified bivalve fragment
317.59-317.60	mbsf: tiny unidentified bivalve fragment
317.88-317.92	mbsf: unidentified inflated gastropod, mould
318.37-318.38	mbsf: tiny unidentified bivalve fragment
318.38-318.40	mbsf: small unidentified macrofossil fragment
318.88-318.90	mbsf: tiny unidentified bivalve fragments
318.90-318.92	mbsf: tiny unidentified bivalve fragments
319.09-319.10	mbsf: ?gastropod mould, chalky
319.19-319.21	mbsf: unidentified macrofossil fragment
319.28-319.31	mbsf: unidentified bivalve fragment, chalky
319.44-319.52	mbsf: small unidentified bivalve fragments, chalky
319.88-319.91	mbsf: unidentified bivalve fragment, chalky
319.97-319.99	mbsf: articulated crenulate bivalve (carditid?), chalky
320.3-320.04	mbsf: unidentified bivalve fragment (crenulate)
320.36-320.38	mbsf: unidentified bivalve fragment, chalky
320.40-320.43	mbsf: large unidentified bivalve fragment (*cf.* ?*Adamussium* n.sp)
320.68-320.70	mbsf: unidentified macrofossil fragments
321.60-321.62	mbsf: small unidentified macrofossil fragment
323.53-323.54	mbsf: tiny unidentified bivalve fragment and mould
323.56-323.57	mbsf: tiny unidentified bivalve fragment
324.35-324.39	mbsf: unidentified gastropod
324.72-324.74	mbsf: gastropod mould (?naticid)
LSU 9.1	
359.07-359.11	mbsf: gastropod, mould within concretion, some shell material
LSU 12.3	
406.36-406.44	mbsf: unidentified fish bone fragment
410.38-410.46	mbsf: unidentified fish tooth fragment
465.77-465.79	mbsf: unidentified ?bivalve fragment (uncertain nature)
509.16-509.17	mbsf: unidentified ?macrofossil fragment, sugar-like texture (uncertain nature)
533.47-533.48	mbsf: unidentified ?macrofossil fragment with chambers (silicified?) (uncertain nature; perhaps a clast)
LSU 13.2	
730.48-730.56	mbsf: unidentified plant impression (stem)
781.34-781.36	mbsf: one modiolid mussel, articulated, very chalky.

an articulated bivalve at 141.20 mbsf and a gastropod shell at 359.07 mbsf, and the cemented sediment infilling serpulid tubes at 43.70 mbsf. Pyritization associated with macrofossils has been only rarely observed (*e.g.* 64.42 and 157.76 mbsf), notwithstanding the occurrence of potentially suitable dark, fine-grained lithologies.

The high frequency of broken shell material observed in some lithostratigraphical units (*e.g.* mollusc remains in LSU 5.1) is interpreted as due to the advanced dissolution of most fossils. Breakage and fragmentation may also result as a consequence of reworking processes. However, the substantial lack of fresh shell material considerably diminishes the possibilities of inspecting shell surfaces for wear patterns.

TAXONOMY

Only a very small percentage of the total macrofossil record from CRP-3 proved suitable for on-ice taxonomic identification. This fact is largely a consequence of (1) the poor to extremely poor preservational state of most fossil remains, (2) the damage caused by drilling and core-processing operations, and (3) the decision to apply minimal palaeontological preparation for exceedingly friable and delicate fossils processed at CS&EC at McMurdo Station. Therefore, most taxonomic nomenclature is left open and suitable for revision.

CRP-3 yielded fossil remains belonging to various phyla of marine invertebrates that are, in order of abundance: Mollusca, Brachiopoda, Annelida, Cnidaria, Bryozoa, Echindodermata and Porifera. Vertebrata are represented by the occurrences of microscopic chips at 406.36 and 410.38 mbsf belonging to an undeterminable osteichthyes fish. Plant remains are documented by the occurrences of an impression at 11.00 mbsf, a leaf (probably *Nothofagus* sp.) at 46.12 mbsf (Fig. 5.9d), and a stem at 730.48 mbsf (Fig. 5.9m).

Mollusca

Fossilized shells of bivalves outnumber quantitatively and qualitatively the other taxonomic groups identified in CRP-3. A similar situation has been documented for the other drill holes obtained in the Ross Sea region during the Deep Sea Drilling Project (Dell & Fleming, 1975), CIROS-1 (Beu & Dell, 1989), CRP-1 (Jonkers & Taviani, 1998), and CRP-2 (Cape Roberts Science Team, 1999; Taviani et al., in press).

Class Bivalvia. Fragmented or whole marine bivalves occur in LSU 1.1, 1.2, 1.3, 1.4, 2.1, 2.2, 3.1, 5.1, 5.3, 6.1, 7.3 (not confirmed), 7.4, 8.1, 12.3 (not confirmed) and 13.2. The exact number of species cannot be assessed with any certainty but exceeds 11.

1 - Protobranchs are rare and positively recognized in LSU 6.1 ("*Nucula*" s.l.) and 8.1 (a taxodont hinge); small bivalves having a general "nuculanid" shape have been observed in LSU 3.1, but the impossibility of examining the diagnostic hinge prevents any positive identification.

2 - Mussels have been positively identified in LSU 1.1 and 13.2 and are apparently represented by two different species of modiolids. The modiolid from the top of the core (Fig. 5.9a) is conspecific with the undescribed mussel recorded from CRP-2A (Cape Roberts Science Team, 1999; Taviani et al., in press). The single specimen identified at 781 mbsf apparently belongs to a distinctive, probably still undescribed species (Fig. 5.9n).

3 - Pectinids occur in LSU 1.2, 2.1(?), 2.2, 6.1, 8.1. The scallops all belong to the non-costate ?*Adamussium* n.sp. of Beu & Dell (1989); this lower Miocene-Oligocene taxon (Fig. 5.9i, l) is under formal description (H.A.Jonkers, in prep.).

4 - Carditids; shells belonging to two different, probably undescribed species of Carditidae are the most common bivalves in CRP-3, although they are not

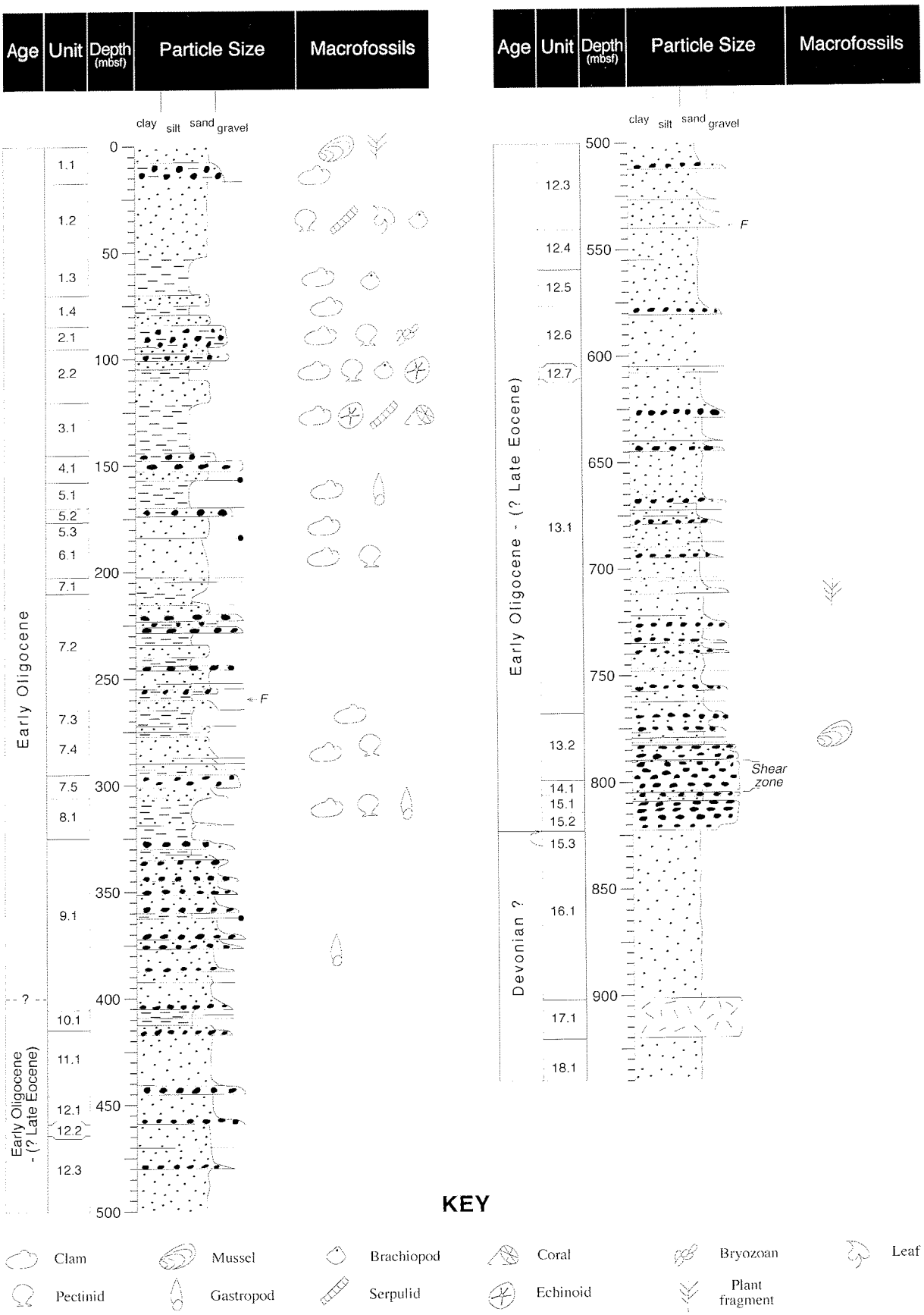

Fig. 5.8 - Lithostratigraphical summary of CRP-3 drill hole showing position and composition of the major macrofossil assemblages and their palaeoenvironmental significance.

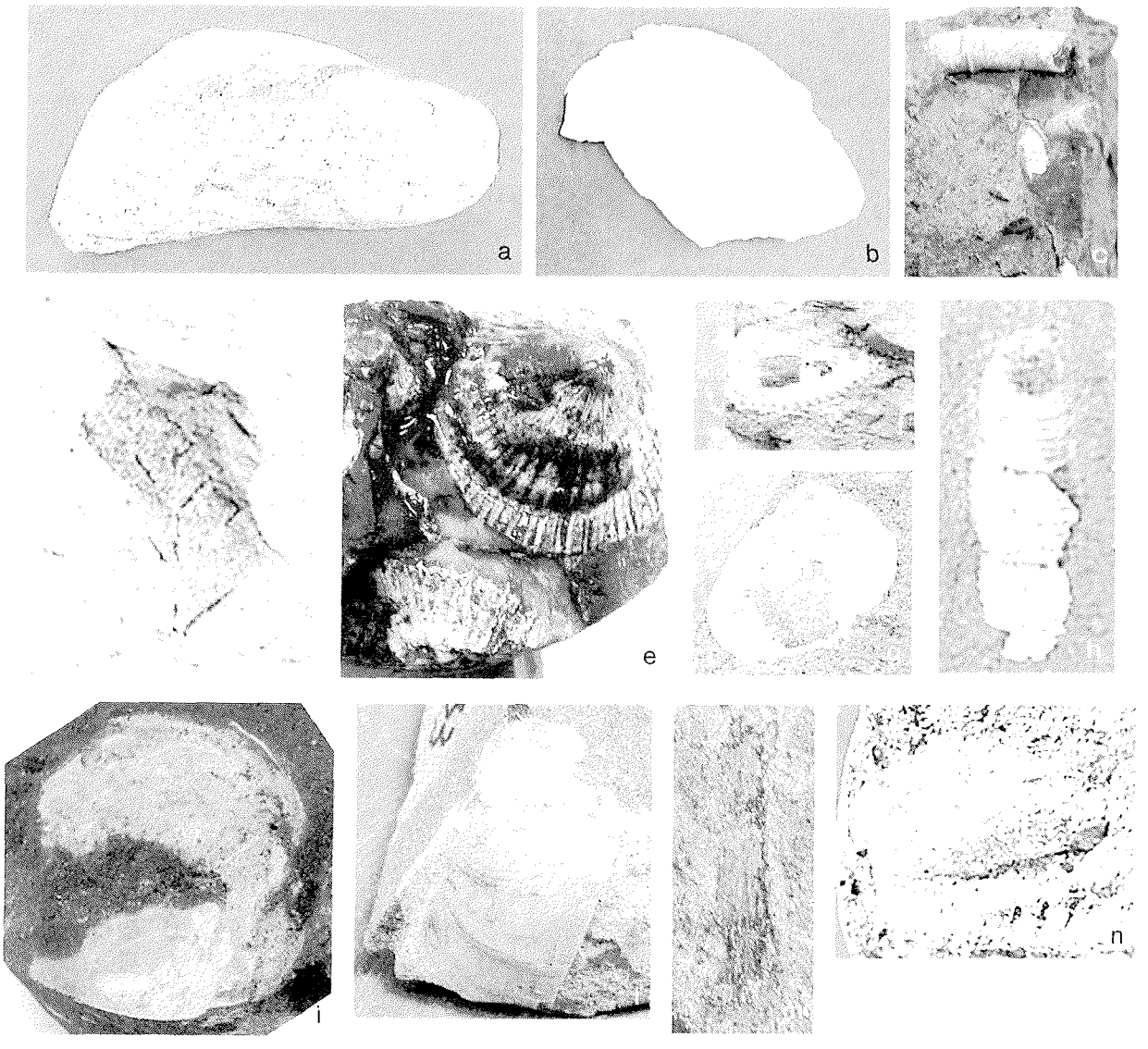

Fig. 5.9 - a) Articulate modiolid mussel from LSU 1.1 at 10.88 showing advanced decalcification. b) Very fresh valve of ?*Adamussium* n.sp, broken by core cutter (LSU 1.2, 29.94 mbsf). c) Serpulid polychaete tubes (?*Serpula* sp.) from LSU 1.2 at 38.53 mbsf. d) Impression of a leaf attributed to *Nothofagus*, found associated with marine fossils in LSU 1.2 at 42.16 mbsf. e) Solitary scleractinian corals from LSU 3.1 at 140.69 mbsf. f) Carditid bivalve (elongate species, from LSU 3.1, at 140.69 mbsf). g) Naticid gastropod, chalky, from LSU 6.1 at 198.50 mbsf. h) Turritellid gastropod, cast showing ornamentation from LSU 8.1 at 311.25 mbsf. i) ?*Adamussium* n.sp, almost complete articulated shell, exposed on the internal surface of the core (LSU 1.2, 308.20 mbsf). l) ?*Adamussium* n.sp, broken by core-cutting (LSU 1.2, 309.29 mbsf). m) Plant stem from LSU 13.2, at 730.48 mbsf (Fig. 5Gm). n) Articulate modiolid mussel with chalky shell from LSU 13.2 at 781.34 mbsf.

ubiquitously distributed. One species shows an elongate shell (Fig. 5.9f), while the other taxon has a more rounded outline. They occur in LSU 2.2, 3.1, and 5.1(?). Carditid-dominated assemblages are particularly evident in LSU 3.1.

5 - Shells belonging to ?veneroidean, ?lucinacean, *Corbula*-like, and other unidentified bivalves have been noted in LSU 2.1, 3.1 and 6.1.

Class Gastropoda. Gastropods are very rare in CRP-3. Poorly preserved moulds have been observed in LSU 3.1, 5.1,6.1,8.1,9.1. Gastropods are represented by at least 4 taxa, including a turritellid (311.25 mbsf, Fig. 5.9h) and a naticid (198.50 mbsf; Fig. 5.9g). An unidentified gastropod, sliced by the core splitter and retaining only a minimal amount of shell material, is the only macrofossil recovered from LSU 9.1.

Class Scaphopoda. Broken tubes tentatively attributed to scaphopods have been identified in LSU 3.1 and, possibly, 2.1. The poor preservation and the incompleteness of the shells prevent any further taxonomic remarks on the little material available to study at present.

Brachiopoda

Terebratulid brachiopods have been positively recorded in LSU 1.2, 2.2, and 3.1, where they are

reasonably common. Most specimens retain at least part of their calcitic shell. It is difficult to assess whether more than one species occurs in CRP-3; the best preserved specimens are all medium-sized, punctate shells with concentric growth lines. At least one specimen is articulated with both brachial and pedicle valves preserved and the foramen partially visible.

Annelida

Serpulid polychaete tubes are one of the most conspicuous elements of the macrofaunal assemblages in LSU 1.2. Serpulid tubes do not occur elsewhere in the core, with possible exceptions in LSU 2.1, 2.2 and 3.1. Spectacular worm-tube aggregates are present at 38.53 mbsf (LSU 1.2; Fig. 5.9c). These tubes are relatively large and one of the best preserved tubes displays raised rings, such as the extant Antarctic species *Serpula narconensis* Baird, 1865. The CRP-3 Oligocene taxon may belong to this genus and appears to be an undescribed species, apparently different from serpulids recovered in CRP-1 and CRP-2/2A (Jonkers & Taviani, 1998; Taviani et al., in press). The activity of soft-bodied worms is documented by the extensive occurrence of bioturbated sediments and burrowing galleries in some facies of the CRP-3 core.

Cnidaria

Solitary scleractinian hexacorals occur at 137.21 and 140.69 mbsf (LSU 3.1). Although most of the original aragonitic shell has been leached away, details of the sculpture of this trochoid corallum (*Flabellum*-like) are still discernible (Fig. 5.9e). Solitary corals have been reported from Oligocene sediments in CRP-2A (Taviani et al., in press) and King George Island (Gazdzicki & Stolarski, 1992). They also occur in Paleogene-Cretaceous rocks of the James Ross Basin (Filkorn, 1994).

Bryozoa

Unidentified bryozoans occur at two levels in CRP-3, consisting of a colony encrusting a pebble at 88.19 mbsf (LSU 2.1) and of a doubtful record at 196.96 mbsf (LSU 6.1).

Echinodermata

Fragments of spines and tests belonging to some undeterminable echinoids have been detected rarely within micropalaeontological residues in LSU 1.1, 1.2, 3.1 and 5.1. A partially complete test has been found in LSU 3.1 at 124.96 mbsf.

Porifera

Fragmented spicules from an unknown sponge have been observed at 45.72 mbsf (LSU 1.2). Minute spicule fragments have also been detected in diatom preparations from the upper 195 m of CRP-3. The virtual absence of sponge skeletal remains below this depth is relevant and perhaps reflects the lack of suitable environments to settle and/or selective diagenesis of biosiliceous material.

PALAEOENVIRONMENTS

All lithostratigraphical units containing macrofossils are interpreted to have been deposited under fully marine conditions and in normal salinity. Reconstructed environments based on macrofaunal criteria solely are proposed below. Palaeobathymetric figures must be taken as speculative. Pending more accurate taxonomic investigations and stable isotope analyses of shell material, the CRP-3 assemblages seem consistent with warmer-than-present sea temperatures, although still indicative of a generically "cold" setting (*cf.* Taviani et al., in press).

LSU 1.1 - A very distinct, almost monospecific mussel-assemblage dominated by semi-infaunal modiolids characterizes this lithostratigraphical unit. The mussels are in life position, with the shell still articulated. It is hypothesized that these organisms may have settled in a relatively deep (100-300 m?) shelf/upper slope environment. The absolute dominance of these smooth mussels is interpreted as the signature of peculiar bottom conditions, perhaps characterized by significant H_2S production possibly linked to organic matter reduction (Taviani et al., in press).

LSU 1.2 - The macrofaunal assemblages show the predominance of epifaunal organisms such as the swimming scallop ?*Adamussium* n.sp. and serpulid polychaete aggregates. The presence of spicules may indicate the occurrence of sponges as well. The hypothesized environment is a relatively shallow (20-100 m) shelf setting.

LSU 1.3 - Marine. No specific environment.

LSU 1.4 - Marine. No specific environment.

LSU 2.1 - Macrofaunal assemblages consist of both epifaunal (?*Adamussium* n.sp.) and infaunal (*e.g.* carditids) bivalves; brachiopods are present. The hypothesized environment is a relatively shallow shelf (30-120 m ?)

LSU 2.2 - Macrofaunal assemblages consist of epifaunal organisms including encrusting bryozoans and ?*Adamussium* n.sp; the hypothesized environment is a relatively shallow shelf (30-120 m ?)

LSU 3.1 - Macrofaunal assemblages show the predominace of infaunal bivalves (mostly carditids), together with ?scaphopod and brachiopods. The hypothesized environment is a relatively shallow shelf (40-120 m?).

LSU 5.1 - Most macrofossils are badly preserved. The environment is possibly similar to the previous one.

LSU 5.3 - Marine. No specific environment.

LSU 6.1 - Macrofaunal assemblages consist of both epifaunal (?*Adamussium* n.sp.) and infaunal (*e.g.* carditids) bivalves and gastropods; the hypothesized environment is a relatively shallow shelf (30-120 m?)

LSU 7.3 - Marine. No specific environment.

LSU 7.4 - Macrofaunal assemblages consist of both epifaunal (?*Adamussium* n.sp.) and infaunal bivalves. The hypothesized environment is a relatively shallow shelf (30-120 m?)

LSU 8.1 - Macrofaunal assemblages consist of both epifaunal (?*Adamussium* n.sp.) and infaunal (*e.g.* carditids) bivalves and gastropods; The hypothesized environment is a relatively shallow shelf (30-120 m?).

LSU 9.1 - Marine. No specific environment.

LSU 12.3 - Doubtful fossil record. No indication of environment.

LSU 13.2 - Modiolid mussel assemblage. It is hypothesized that these assemblages may have settled in a relatively deep (100-300 m?) shelf/upper slope environment, perhaps characterized by a significant H_2S production.

BIOSTRATIGRAPHIC REMARKS

Based on the bivalve distribution, the entire section of CRP-3 between 0-324 mbsf is Oligocene in age. Mussel beds have been identified in both CRP-2/2A and CRP-3. We believe these modiolid assemblages mark relatively short-lived peculiar bottom conditions and assume they are correlatable between the two holes. Modiolid assemblages occur in the lower Oligocene in CRP-2/2A from 440 mbsf to the bottom of the hole. Such an assemblage occurs in the top 11 mbsf in CRP-3, and, therefore, may well correlate with any of the mussel beds in CRP-2/2A or, perhaps, even with a potential missing part of the record below 624 mbsf in CRP-2/2A.

The occurrence of the non-costate scallop ?*Adamussium* n.sp, whose known distribution ranges between the lower Miocene and the lower Oligocene (Taviani et al., in press), confirms an Oligocene age between 23 and 324 mbsf in CRP-3.

The interval between 359 and 781 mbsf generally lacks macrofossils, with only two confirmed occurrences of marine molluscs, including a mussel (modiolid) in the deepest horizon. Nothing can be said *a-priori* about the age of such macrofossils, which may well be early Oligocene or late Eocene.

6 - Palaeomagnetism

INTRODUCTION

Palaeomagnetic investigations of CRP-3 were aimed at developing a magnetic polarity zonation for the core. We only expected to encounter Cenozoic sediments in CRP-3, therefore, the main focus of this chapter is on the Cenozoic rocks encountered in the upper *c.* 790 mbsf of the CRP-3 record. Sedimentary rocks that are inferred to represent the Beacon Supergroup (823.11-939.42 mbsf) will be the subject of future studies. CRP-3 consists mainly of sandstones with minor diamictites, conglomerates and mudstones (see Lithostratigraphy and Sedimentology chapter). Coarse-grained sediments are usually not suitable for palaeomagnetic analysis. However, in previous palaeomagnetic studies of sedimentary units from the Victoria Land Basin, strong and stable magnetizations have been recorded and even coarse-grained units have proved suitable for palaeomagnetic analysis (Wilson et al., 1998, in press a; Roberts et al., 1998). We attribute the stability of the magnetizations to the presence of fine magnetic particles within the fine-grained sediment matrix in these otherwise coarse-grained units (*cf.* Sagnotti et al., 1998a, b; Wilson et al., 1998, in press a; Roberts et al., 1998; Verosub et al., in press).

The goal of developing a magnetic polarity zonation is to enable correlation to the magnetic polarity time scale (MPTS) of Cande & Kent (1995) and Berggren et al. (1995) to help constrain an age model for CRP-3. Polarity is a binary signal that is difficult to interpret uniquely in glaciomarine environments where the lithostratigraphical record is incomplete and where sedimentation rates are variable. Additional chronostratigraphical constraints are required from biostratigraphy or numerical dating techniques.

METHODS

We sampled unconsolidated sediments (from 3.08 to 35.73 mbsf) with plastic cubes (6.25 cm^3) and consolidated sediments (below 35.73 mbsf) by drilling conventional cylindrical palaeomagnetic samples with a modified drill press. The palaeomagnetic sampling techniques, laboratory facilities and equipment installed at the Crary Science and Engineering Center, McMurdo Station, Antarctica, were described by the Cape Roberts Science Team (1998a). We used a modified sample measurement scheme this season, in contrast to previous CRP drilling seasons. In previous seasons, the majority of samples were measured at McMurdo Station. However, 1011 samples were collected from CRP-2/2A, and time constraints precluded measurement of many of these samples during the drilling season. We expected a similar number of samples would be obtained from CRP-3. Palaeomagnetic measurements for CRP-3 at McMurdo Station were, therefore, restricted to the measurement of the natural remanent magnetization (NRM) and low-field magnetic susceptibility of all samples, along with a pilot demagnetization study of paired samples from *c.* 10-m intervals. The remaining samples were analysed in the palaeomagnetic laboratories at the *Istituto Nazionale di Geofisica*, Rome, and at the University of California, Davis. At both laboratories, the samples were measured on an automated, pass-through cryogenic magnetometer and were subjected to in-line, stepwise, alternating field (AF) demagnetization up to peak fields of either 60 or 70 mT.

Information was collected at the drill site to enable azimuthal orientation of the core. However, these constraints were not available at the time of data analysis and no effort has been made to re-orient the core. Lack of azimuthal orientation does not pose a problem for magnetostratigraphical studies because the geomagnetic field has a steep inclination at the latitude of the CRP-3 site (77°S). As a consequence, the palaeomagnetic inclinations, which were determined from principal component analysis (Kirschvink, 1980) of characteristic remanence components on vector demagnetization plots, are sufficient to uniquely determine polarity (*i.e.* negative (upward) magnetizations correspond to normal polarity; positive (downward) magnetizations correspond to reversed polarity).

Where possible, CRP-3 was sampled at 0.5-m intervals. This strategy was adopted to avoid missing any short polarity intervals due to inadequate sampling. Lower sampling resolution was achieved in intervals where the lithology was unsuitable for sampling. Sediment-accumulation rates in the CRP-1 and CRP-2/2A cores were consistently high (about 20 m/m.y. in CRP-1 (Roberts et al., 1998) and between 25 and 1000 m/m.y. in CRP-2/2A (Wilson et al., in press a). If sedimentation rates in CRP-3 were similar to those of CRP-1 and CRP-2/2A, it is unlikely that short polarity intervals were missed due to inadequate sampling resolution.

Most of the CRP-3 succession consists of sandstones (*c.* 80%) and diamictites and conglomerates (*c.* 10%) (see Lithostratigraphy and Sedimentology chapter). Whenever possible, samples were selected from fine-grained horizons. However, most samples were taken from sandstone-dominated lithofacies. Above *c.* 380 mbsf, the sandstones are muddy and are therefore potentially useful for palaeomagnetic study. However, between *c.* 380 and 580 mbsf, the sandstones are well sorted and clean (*i.e.* they have little or no fine-grained matrix).

Below *c.* 580 mbsf, sandstone is still the major lithofacies but with a possible authigenic mud matrix. Primary mud increases down to the top of a shear zone at *c.* 790 mbsf (see Depositional History section). However, coarse sand grains, granules and pebbles are dispersed throughout the CRP-3 succession. Samples from coarse-grained intervals pose a problem because the deposition of such large particles would be controlled by gravitational rather than magnetic forces. Thus, their orientation could not be expected to represent the geomagnetic field at or near the time of deposition. This problem would be most severe for strongly magnetic basic igneous material, which is a common clast constituent in CRP-3 (see Petrology chapter). The presence of such grains means that care should be taken in interpreting palaeomagnetic data from coarse-grained intervals. The possible presence of clasts was taken into account by adopting a conservative interpretive approach within coarse-grained lithologies. After magnetic measurements were completed, such samples were examined to determine the presence of clasts. Results from such samples are considered reliable only if no clasts were visible, if the palaeomagnetic inclinations are consistently steep throughout coarse-grained intervals, and if the results from these intervals are consistent with results from surrounding finer-grained intervals.

Eleven hundred seventeen samples were collected from CRP-3 (105 of these are from the inferred Beacon Supergroup strata in the lower part of the core; pilot results from these samples are discussed at the end of this chapter). For the pilot studies, 92 pairs of samples, each separated stratigraphically by a few cm, were collected at *c.* 10-m intervals from varying lithofacies throughout the Cenozoic succession. The pilot study was aimed at determining the most suitable demagnetization technique for routine treatment of the samples. The pilot study was conducted by subjecting one sample from each pair to stepwise AF demagnetization, while the corresponding sample was subjected to thermal demagnetization. After measurement of the NRM, AF demagnetization was conducted at successive peak fields of 5, 10, 15, 20, 25, 30, 40 and 50 mT. Thermal demagnetization was conducted on the paired samples at temperatures of 120, 180, 240, 300, 350, 400, 450, 500, 550, 600 and 650°C. Magnetic susceptibility was measured after each step to monitor for thermal alteration.

A total of 617 samples were subjected to detailed stepwise demagnetization (including the 92 pairs of samples from the pilot study). Time constraints limited the number of samples that could be measured, but all samples have been measured to 376.48 mbsf. In this report, we present detailed palaeomagnetic results down to *c.* 350 mbsf. Below this level, we only present results of the pilot studies.

Attempts have been made to study magnetic mineralogy by continuous monitoring of low-field magnetic susceptibility of selected samples during heating. The temperature dependence of susceptibility, up to a maximum temperature of 700°C, was measured with a CS-2 furnace attached to a Kappabridge KLY-2 (AGICO) magnetic susceptibility meter (Hrouda, 1994). The KLY-2 meter has an operating frequency of 920 Hz and a magnetic induction of 0.4 mT. These analyses were conducted at the *Istituto Nazionale di Geofisica*, Rome.

RESULTS

DOWN-CORE MAGNETIC PROPERTIES

Prior to demagnetization, we measured the low-field magnetic susceptibility and the NRM intensity for all samples. These parameters generally vary in phase with each other and significant down-core variations are evident (Fig. 6.1). It is possible to subdivide the CRP-3 record into four intervals on the basis of these magnetic properties. In the upper part of the record (magnetic-intensity interval I down to *c.* 243 mbsf), susceptibility and NRM are variable but generally have higher values than in the underlying magnetic-intensity interval II (between *c.* 243 and 440 mbsf). The range of susceptibility and NRM values is larger in magnetic-intensity interval II than in magnetic-intensity interval I. Magnetic-intensity interval III (*c.* 440-628 mbsf) coincides with part of the core that is dominated by clean sands and susceptibility, and NRM values are consistently low (with the exception of a marked peak from *c.* 539 to 560 mbsf). In magnetic-intensity interval IV (*c.* 628-790 mbsf), the values and range of variability of susceptibility and NRM are more similar to those observed in magnetic-intensity interval I. This subdivision on the basis of magnetic susceptibility and NRM intensity is consistent with low-resolution petrological results that indicate a higher relative input of detritus from the Ferrar Dolerite in magnetic-intensity intervals I and IV. As will be seen below, these intervals also generally correspond to different types of palaeomagnetic behaviour.

Magnetic susceptibility was measured after each heating step for pilot samples treated with thermal demagnetization (Fig. 6.2). These results indicate that thermal alteration was limited. For samples with high magnetic susceptibility (magnetic-intensity intervals I, IV and parts of magnetic-intensity intervals II and III), there is no evidence for the formation of new magnetic minerals as a result of heating. At temperatures above 500°C, the existing magnetic minerals generally lose susceptibility, possibly as a result of oxidation to hematite. The lack of evidence for thermal alteration suggests that thermal demagnetization is an appropriate method for treating such samples. Different behaviour is evident in the low susceptibility samples in magnetic-intensity intervals II and III. For these samples, susceptibility generally increases above 400°C, which indicates thermogenic production of new magnetic minerals. This

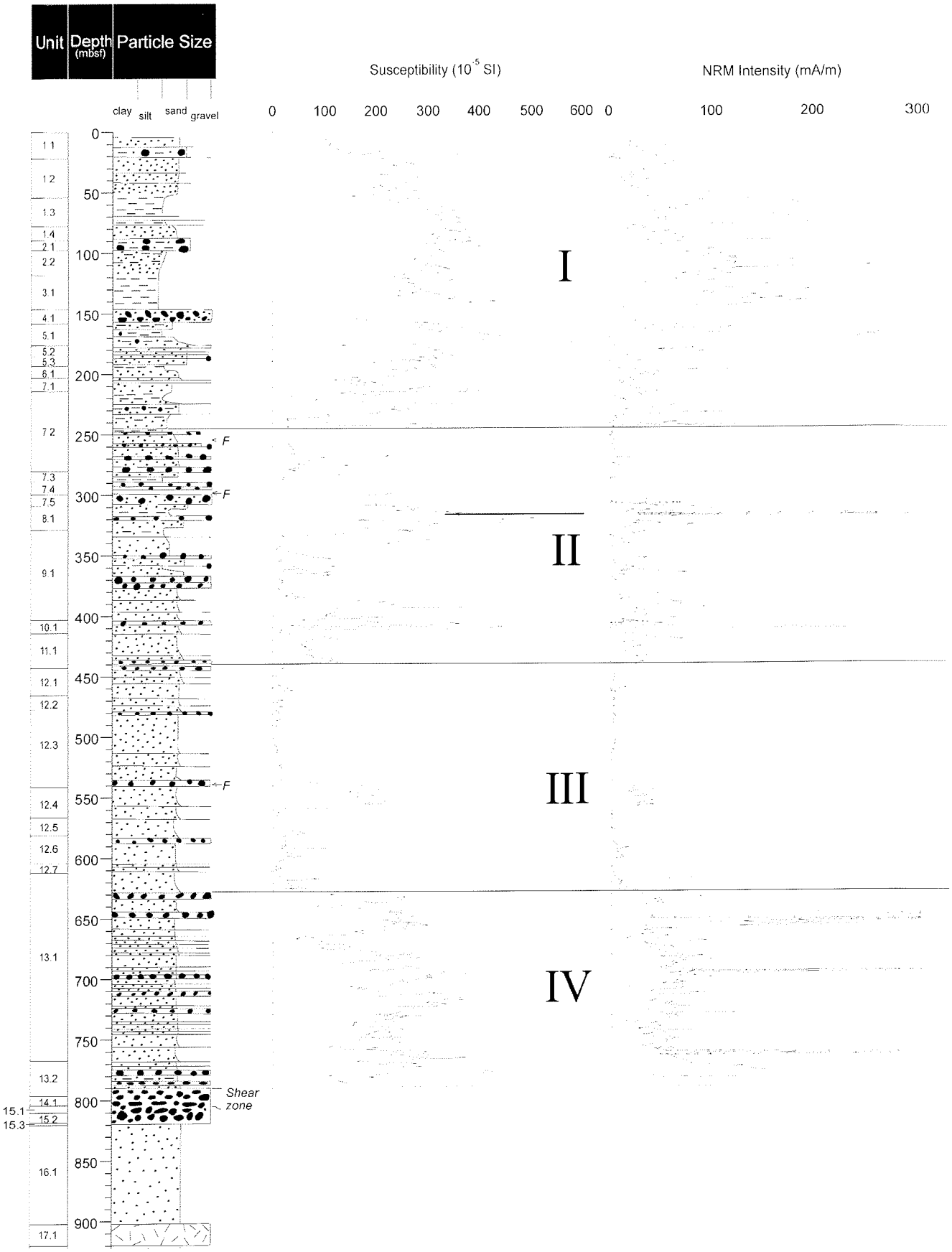

Fig. 6.1 - Plot of down-core variations in low-field magnetic susceptibility and NRM intensity. On the basis of these data, the CRP-3 record can be subdivided into four intervals with different magnetic intensities (see text for description).

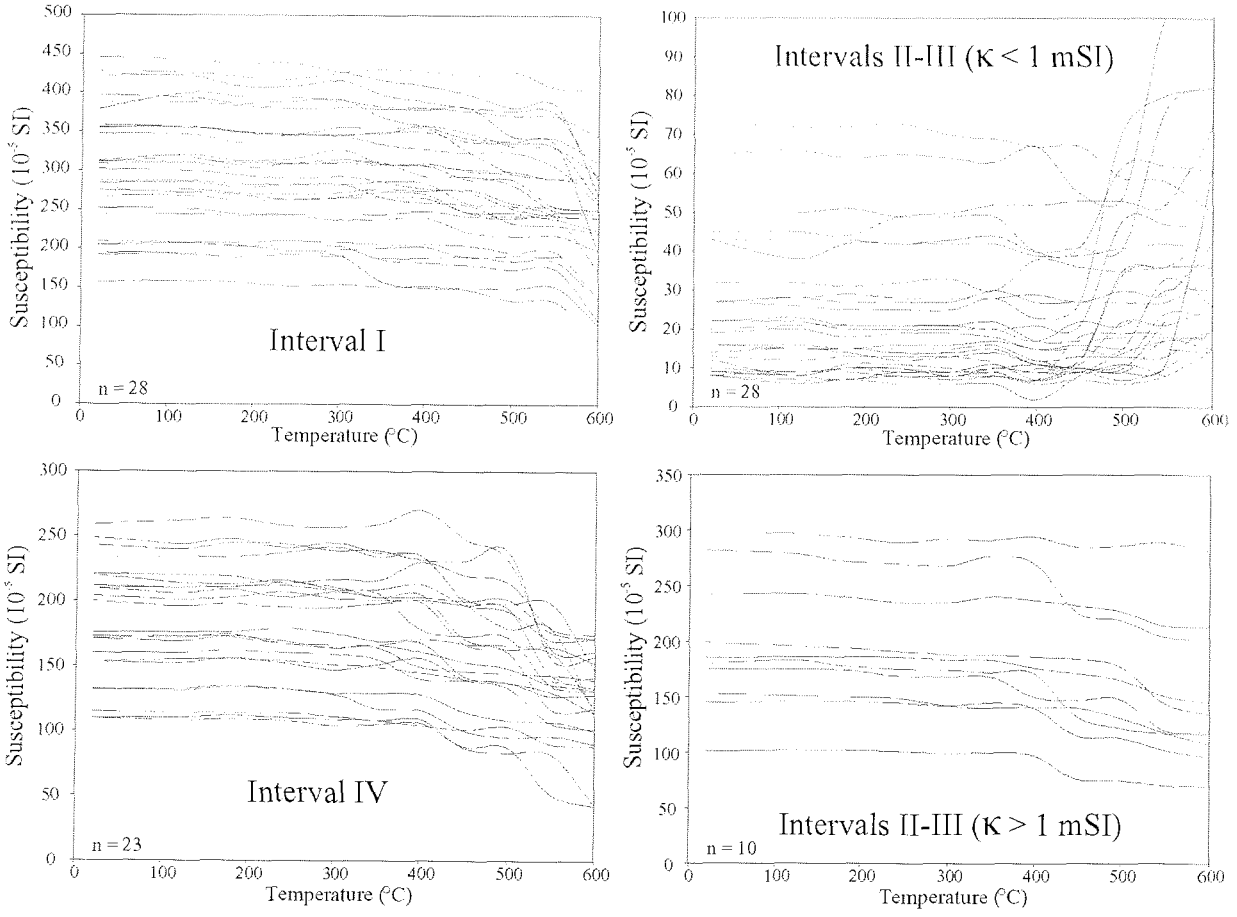

Fig. 6.2 - Magnetic susceptibility (κ), as measured after each thermal demagnetization step, for pilot samples from different intervals in CRP-3. The intervals are based on magnetic susceptibility and NRM intensity variations, as shown in figure 6.1.

probably indicates a difference in matrix mineralogy between high and low susceptibility samples. It also suggests that thermal demagnetization will be less useful in low susceptibility intervals than in high susceptibility intervals.

PILOT STUDY

Results of the pilot study indicate that thermal and AF demagnetization have variable efficiency in removing secondary remanence components and in isolating characteristic remanent magnetization (ChRM) components. For many samples, particularly those from the intervals with high magnetic susceptibility, the two techniques were comparable and identical ChRM components were identified for both normal and reversed polarity samples (Fig. 6.3 c-h, o & p). However, in many cases, AF demagnetization was clearly more efficient in removing secondary remanence components (Fig. 6.3 a, b, k-n). In some of these cases, thermal demagnetization at higher temperatures reveals a ChRM component that is similar to that revealed by AF demagnetization (Fig. 6.3 a & b, m & n). However, in such cases it is clear that the ChRM component is more clearly revealed at lower demagnetization levels using AF demagnetization. In the interval dominated by clean sands (magnetic-intensity interval III), AF demagnetization indicates that the samples have extremely low coercivity, which is consistent with a dominance by multi-domain magnetic particles (Fig. 6.3i). The thermal demagnetization behaviour of samples from these intervals is in marked contrast to the AF demagnetization behaviour (Fig. 6.3 i & j). With thermal demagnetization, a steep normal polarity component is gradually removed up to between 400 and 500°C. The fact that samples from this interval have low coercivity suggests that the steep and apparently stable remanence component revealed by thermal demagnetization is a viscous remanent magnetization (VRM) that has completely remagnetized the samples. Also, these samples are more prone to thermal alteration during heating (Fig. 6.2). For such samples, it is apparent that neither AF nor thermal demagnetization enables identification of a stable ChRM component: thermal demagnetization reveals a spurious VRM component, and AF demagnetization produces data from which no meaningful polarity interpretation can be made. This suggests that it will be difficult to extract useful polarity information for much of the interval containing clean

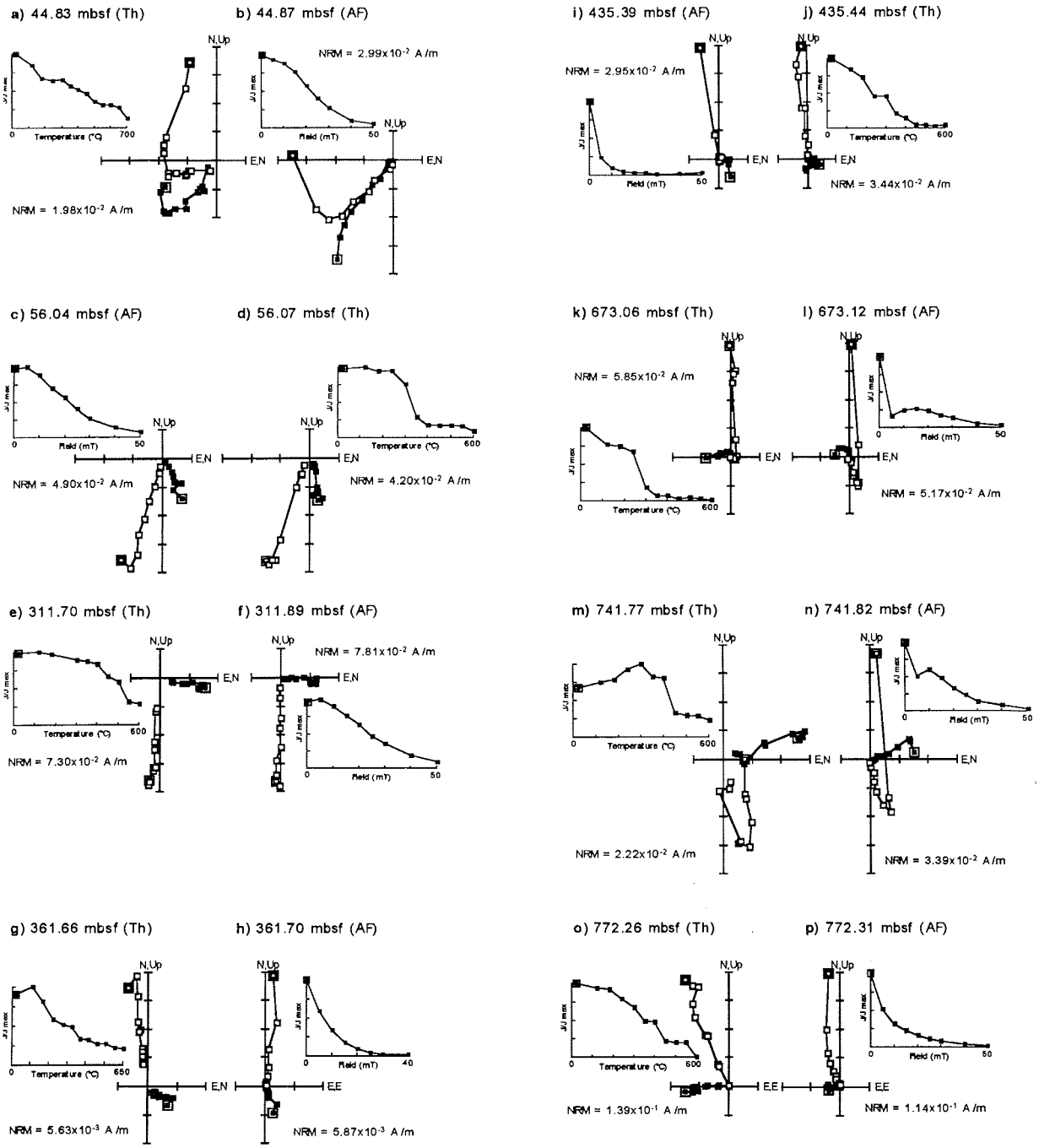

Fig. 6.3 - Vector component diagrams for selected pairs of pilot samples from CRP-3 that were subjected to AF and thermal demagnetization, respectively. Projections onto the vertical (horizontal) plane are represented by open (solid) symbols, respectively. Samples are not azimuthally oriented and declination projections are given in the laboratory component system, samples are oriented with respect to vertical. a) and b) comparison of thermal and AF demagnetization from samples at 44.83 and 44.87 mbsf, respectively. These data indicate that AF demagnetization is more efficient in isolating the reversed polarity ChRM direction. AF and thermal demagnetization seem to be equally efficient for samples from: c) 56.04 mbsf, d) 56.07 mbsf (both reversed polarity), e) 311.70 mbsf, f) 311.89 mbsf (both reversed polarity), g) 361.66 mbsf, and h) 361.70 mbsf (both normal polarity). For samples from i) 435.39 mbsf and j) 435.44 mbsf, AF demagnetization indicates low-coercivity behaviour while thermal demagnetization isolates a steep normal polarity component. The thermal demagnetization data from such intervals are interpreted to be dominated by a VRM. The thermal demagnetization data from k) 673.06 mbsf are also interpreted to represent a VRM, while the AF demagnetization data from the paired sample from l) 673.12 mbsf indicate a reversed polarity ChRM after removal of a VRM component. Reversed polarity directions are isolated by both demagnetization methods at m) 741.77 mbsf and n) 741.82 mbsf, although AF demagnetization data are less noisy. Consistent normal polarity data were obtained by both techniques at o) 772.26 mbsf and p) 772.31 mbsf.

sands. Finally, for some samples, a steep, normal polarity remanence component is indicated by thermal demagnetization, and a clear reversed polarity ChRM is indicated by AF demagnetization (Fig. 6.3 k, l). In such cases, we interpret the thermal demagnetization data to be dominated by a VRM, and AF demagnetization is apparently more successful in removing this secondary component.

For all of the above cases, AF demagnetization appears to be the preferable technique for routine sample treatment. In cases where the results from both techniques are identical, AF demagnetization is preferable because it is less time-consuming than thermal demagnetization and because it avoids thermal alteration, which means that the samples can be used for subsequent environmental magnetic studies. In other cases, AF demagnetization is preferable because it is more efficient in isolating ChRM components than thermal demagnetization. In cases where thermal demagnetization data are dominated by a VRM component, AF demagnetization is preferable because it is better not to interpret polarity due to the dominance of low coercivities than to be misled by thermal demagnetization data that are dominated by an apparently stable VRM.

Except for intervals where thermal demagnetization was less efficient in removing secondary magnetic overprints and intervals where the magnetization was unstable, the results from pairs of pilot samples are in excellent agreement. A summary of polarity results from paired pilot samples is shown for the Cenozoic interval of CRP-3 in figure 6.4. Several features are immediately evident in this figure. First, for the upper *c.* 243 mbsf (magnetic-intensity interval I), the pilot samples are stably magnetized, with a dominance of reversed polarity. Second, the frequency of stably magnetized samples is lower for magnetic-intensity interval II (*c.* 243 to 440 mbsf), although significant parts of the interval contain stable magnetizations. Third, in magnetic-intensity interval III (*c.* 440 to 628 mbsf), many thermally-demagnetized samples are dominated by a VRM, and many AF-demagnetized samples have such low coercivity that no stable ChRM can be identified. It is, therefore, impossible to define palaeomagnetic polarity for large parts of magnetic-intensity interval III with the current data. Fourth, magnetic-intensity interval IV has a high proportion of stably magnetized samples. Reversed polarity is dominant between *c.* 660 and 760 mbsf, and normal polarity is dominant from *c.* 760 to 790 mbsf. The potential for obtaining useful magnetostratigraphical results from magnetic-intensity interval IV is therefore good.

On the basis of the pilot studies, all remaining samples from magnetic-intensity intervals I and II were sent to the palaeomagnetic laboratories in Rome and Davis for detailed stepwise AF demagnetization analysis. These results are presented and discussed below. Magnetic-intensity interval III is palaeomagnetically problematical, and the remaining samples from this interval will be analysed after the drilling season. Magnetic polarity data from magnetic-intensity interval IV are difficult to interpret in terms of chronology because of the lack of data from the overlying magnetic-intensity interval III. As a result, most of the samples from magnetic-intensity interval IV were also reserved for analysis after the drilling season.

PALAEOMAGNETIC BEHAVIOUR

Many of the analysed samples display a low-coercivity (or low-temperature), near-vertical, normal-polarity remanence component that is interpreted to represent a drilling-induced overprint (Fig. 6.3). This type of overprint has been observed in all other cores that we have studied from the McMurdo Sound area (Wilson et al., 1998, in press a; Roberts et al., 1998) and is generally removed without difficulty at peak AFs of less than 20 mT. In cases where the drilling-induced overprint and the ChRM had completely overlapping coercivity spectra, it was not possible to isolate the two components, and such samples were excluded from subsequent magnetostratigraphical interpretations. In some cases, particularly in dominantly sandy lithologies, another overprint is present. This overprint has a nearly horizontal inclination and a southward-directed declination, as described by Wilson et al. (in press a). We attribute this overprint to contamination introduced by cutting the samples (after drilling) because the overprint is always perpendicular to the cut face of the sample (*i.e.* in sample coordinates, the overprint is entirely in the x-z plane, with y = 0). Rotation of the saw blade produces a measurable magnetic induction perpendicular to the blade (Wilson et al., in press a). In most cases, the overprint produced by this field was easily removed by application of peak AFs of 10 mT. Where present, this overprint is usually stronger than the drilling-induced overprint. The saw-overprint is only sporadically present in CRP-3.

Many of the samples are from intervals where clasts may dominate the magnetic properties of the sample and produce a magnetization that does not represent the geomagnetic field orientation at or near the time of deposition. Samples that contain such clasts usually display abnormal palaeomagnetic behaviour and are readily detected (*e.g.* Roberts et al., 1998; Wilson et al., in press a). Such samples were rare in CRP-3 and were excluded from subsequent magnetostratigraphical interpretations.

Stable palaeomagnetic behaviour was evident from the vector component plots of 518 of the 617 demagnetized samples (84%). In most cases, the ChRM direction was determined using a best-fit line that was constrained, using principal component analysis, through the origin of the vector component diagram (*e.g.* Fig. 6.3). In some cases, the best-fit lines were not constrained through the origin of the plots. In other cases, the polarity of the ChRM component was clear, but because of a low signal/noise

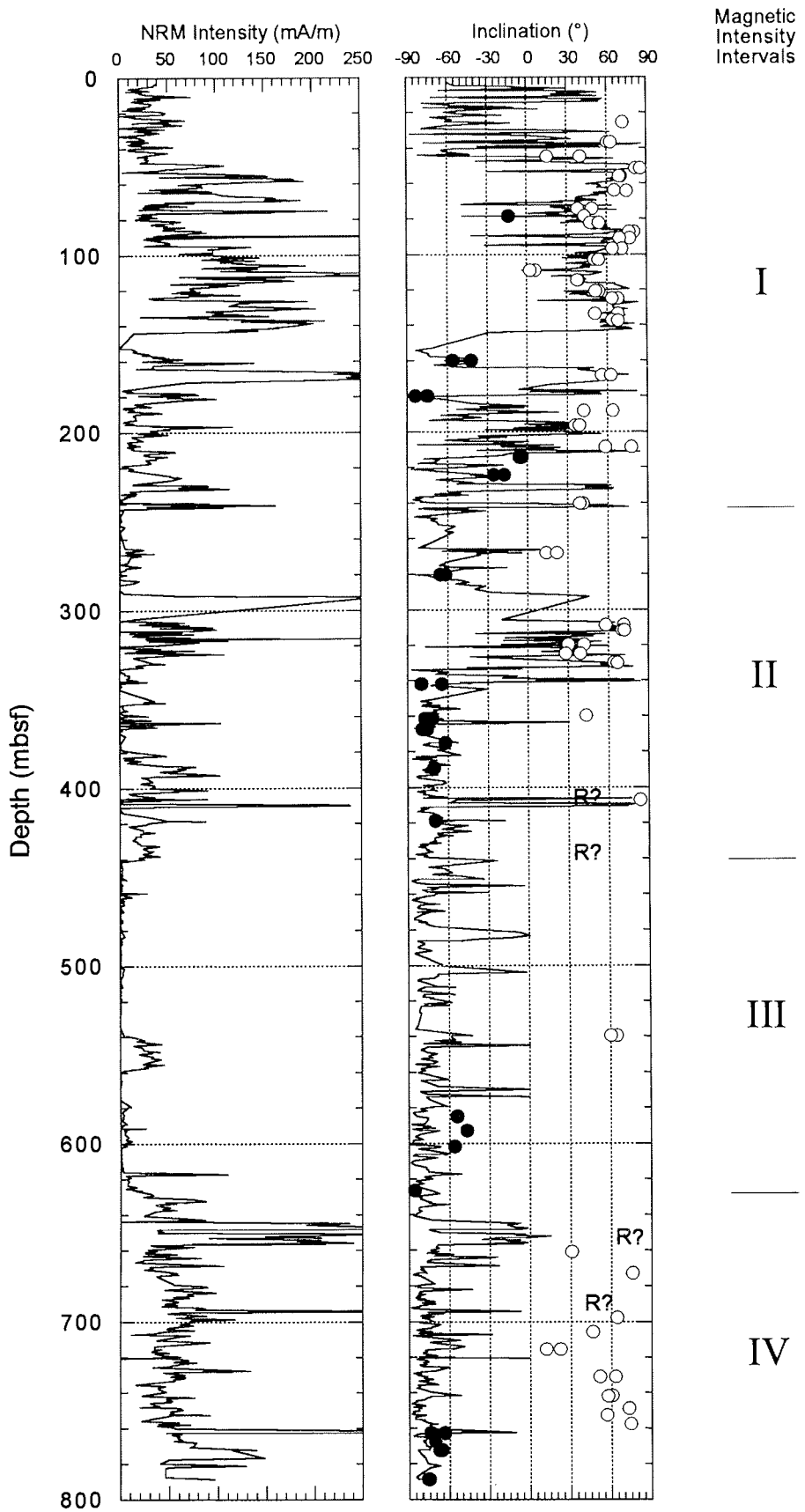

Fig. 6.4 - Summary of NRM intensity (left-hand side), palaeomagnetic inclination before demagnetization (solid line) and inclinations from pilot samples after demagnetization (right-hand side) for CRP-3. For the pilot samples, solid symbols indicate normal polarity and open symbols indicate reversed polarity. Pilot samples from the upper 350 mbsf and between *c.* 650 and 790 mbsf generally have stable magnetizations. The data are of poorer quality between *c.* 350 and 650 mbsf, and few pilot samples from Interval III (*cf.* Fig. 6.1) yielded useful palaeomagnetic data.

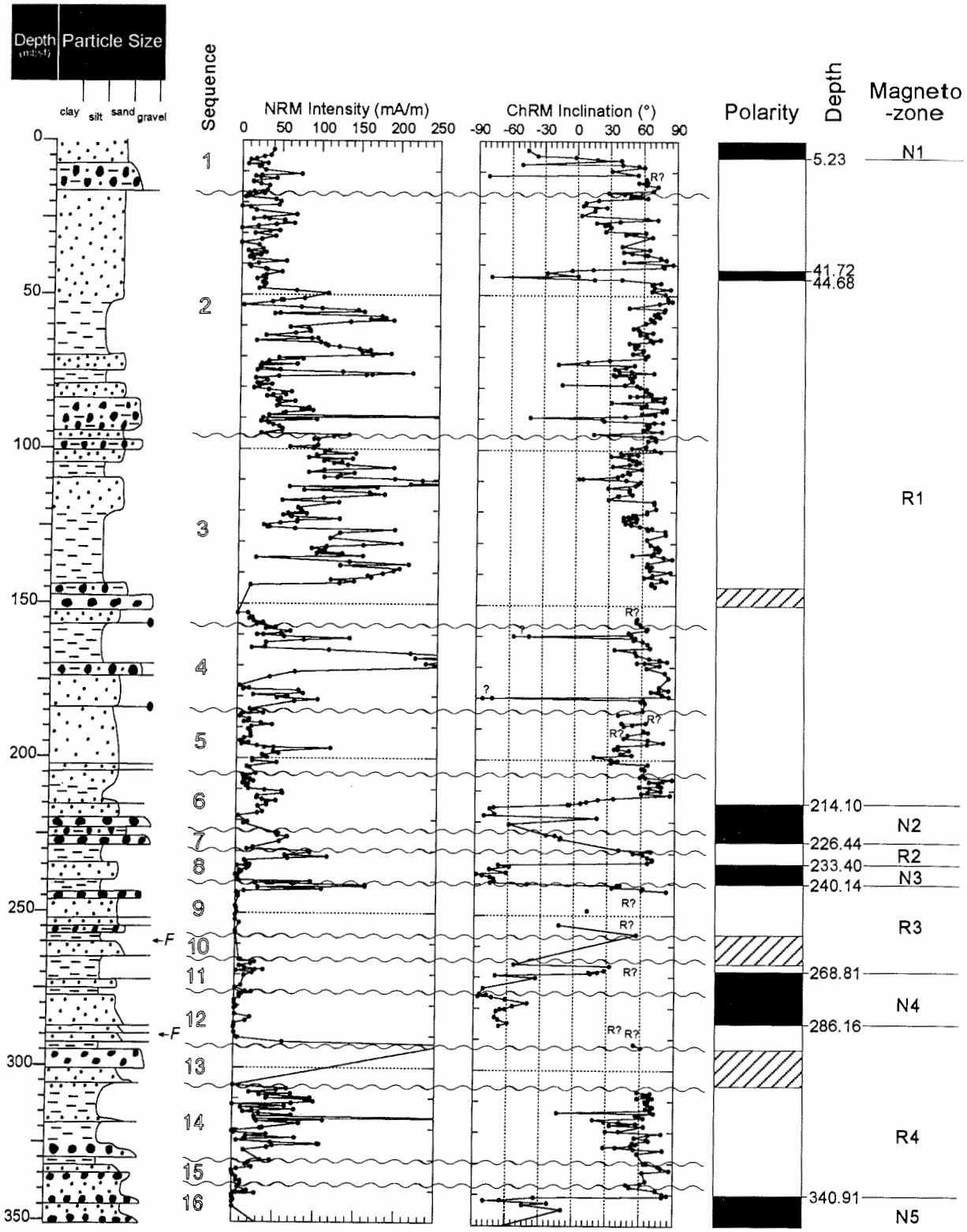

Fig. 6.5 - Interpretation of the polarity zonation for CRP-3. Characteristic remanent magnetizations (ChRMs) were determined by principal component analysis of data from multiple demagnetization steps. Polarity intervals are interpreted from the stratigraphical variations in ChRM inclination (black = normal polarity; white = reversed polarity). The polarity zonation for the upper 350 mbsf of CRP-3 is subdivided into 9 magnetozones (N1 to N5). The boundaries of the magnetozones do not correspond to sequence stratigraphical boundaries.

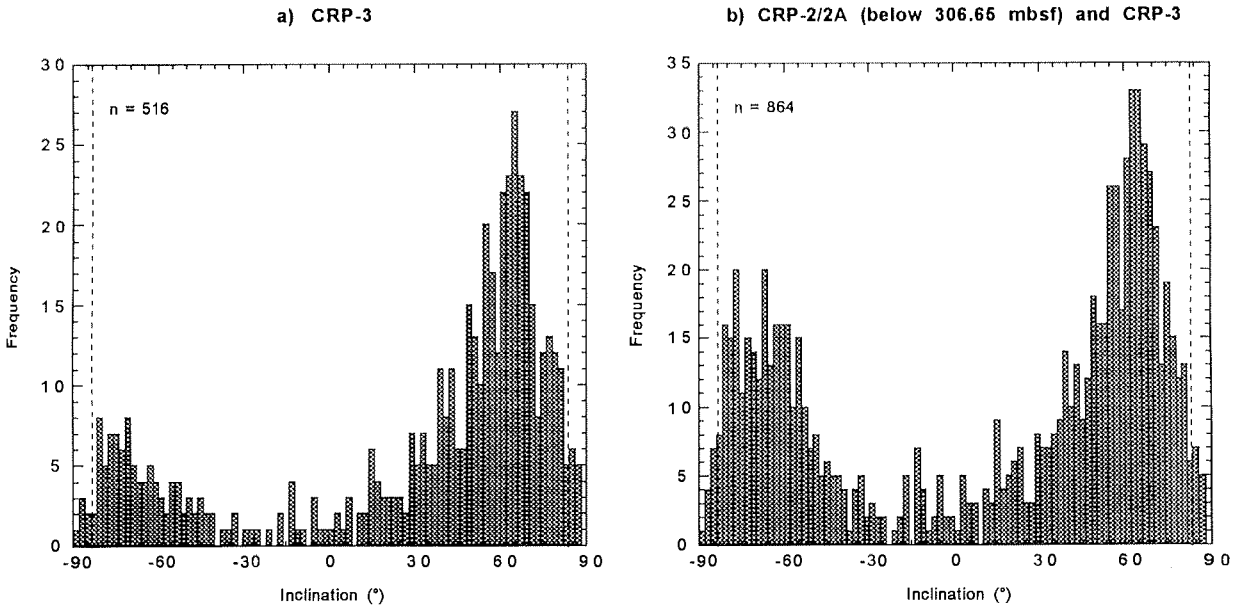

Fig. 6.6 - Frequency histogram of ChRM inclinations from stepwise-demagnetized samples from a) CRP-3 and b) CRP-2/2A (below the prominent unconformity at 306.65 mbsf) and CRP-3. There is a clear bimodal distribution of polarities, with a bias to reversed polarity that results from the rapid sedimentation rates during a long period of reversed polarity in CRP-3 (see discussion in text). The expected inclinations are shown as dashed lines at ±83.4°. The palaeomagnetic inclinations are shallower than expected (see text).

ratio or incomplete removal of secondary remanence components, the final direction of magnetization could not be precisely determined. In these cases, which were most evident for reversed polarity samples, the sample is represented on figure 6.5 by an "R?".

The inclinations of the ChRM directions have a clear bimodal distribution that demonstrates the dominance of the two stable polarity states (Fig. 6.6a). Steep normal and reversed polarity directions, as would be expected at high latitudes, are clearly dominant. In conjunction with evidence from vector component diagrams (*e.g.* Fig. 6.3), this indicates that secondary remanence components have been successfully removed. The distribution of inclinations is strongly biased toward reversed polarity (in contrast to CRP-2/2A, which was dominated by normal polarity; Wilson et al., in press a). The dominance of a single polarity results from a combination of factors, including relatively high sedimentation rates, high measurement density and the predominance of reversed polarity in this part of the polarity time scale (see magnetostratigraphical interpretation below).

There are insufficient normal polarity data to test whether there is a statistically significant difference between the modes of the two polarity states. For similar reasons given above for the dominance of reversed polarity in CRP-3, there was a dominance of normal polarity in CRP-2/2A. By combining the data sets from CRP-2/2A (below the angular unconformity at 306.65 mbsf) and CRP-3, it is possible to test whether there is a significant difference between the modes of the two polarity states (Fig. 6.6b). The normal polarity distribution is not as tightly peaked as the reversed polarity distribution, although the modes for the two polarity states appear to be *c.* –66° and 64° for normal and reversed polarity, respectively. On the basis of these data, it appears that the normal and reversed polarity data are antipodal as would be expected for reliable ChRM directions.

The palaeomagnetic inclinations in figure 6.6 are up to 18° shallower than expected (±83.4°) for the site latitude (77°S). The sedimentary succession dips at an angle of *c.* 21±5° to the east (see Core Properties and Downhole Geophysics chapter). Because the magnetization of the sediment lies in the N-S plane, an eastward stratal tilt is likely to have a limited effect in producing the discrepant palaeomagnetic inclinations. The 18° maximum discrepancy between the expected and observed palaeomagnetic inclinations may partially result from inclination error. This phenomenon is commonly observed in sedimentary environments where bioturbation is not widespread, such as seems to be the case for some lithostratigraphical units in CRP-3. In environments where bioturbation is widespread, magnetic particles have freedom to rotate and to follow the geomagnetic field in water-saturated shallow sediments. Thus, when the remanence is locked in during shallow burial, the magnetization of bioturbated sediments can provide an accurate record of the geomagnetic field. On the other hand, in sediments where bioturbation is absent, magnetic grains can roll as they settle onto the substrate and the resultant inclination can be retained in the absence of bioturbation (Verosub, 1977). Sediment compaction has also been interpreted

to be responsible for inclination errors (*e.g.* Anson & Kodama, 1987; Arason & Levi, 1990).

In addition to the dominantly steep normal and reversed polarity directions, a significant number of samples display a ChRM that is transitional between normal and reversed polarity (*e.g.* Figs. 6.5 & 6.6). Most of these samples display stable palaeomagnetic behaviour and are not obviously affected by the presence of clasts. It is not surprising that transitional directions are recorded because there is a higher probability of recording deposition during geomagnetic polarity transitions in rapidly deposited sediments such as those recovered in the CRP drill holes.

MAGNETIC MINERALOGY

Different magnetic minerals display different behaviour during heating. The temperatures at which the susceptibility falls to zero on heating (Curie or Néel temperatures) are diagnostic of mineralogy. Two temperature-dependent susceptibility curves (from 80.77 and 193.52 mbsf) are shown in figure 6.7. Both samples are from magnetic-intensity interval I, but they display different behaviour. The sample from 80.77 mbsf has a clear Curie temperature at *c.* 580°C (Fig. 6.7a), which indicates that magnetite (Hunt et al., 1995) is the dominant magnetic mineral. The sample from 193.52 mbsf also shows a clear Curie temperature at *c.* 580°C, but it does not completely lose its susceptibility at this temperature (Fig. 6.7b). The susceptibility continues to decrease to *c.* 700°C. The Néel temperature of hematite is *c.* 680°C (Hunt et al., 1995), and the high-temperature behaviour is indicative of the presence of hematite. The fact that the cooling curve is reversible might indicate that the hematite is primary. Thermal demagnetization data can provide additional information concerning magnetic mineralogy. For many of the thermally-demagnetized samples, the magnetization drops to near-zero values between 550 and 600°C, which is consistent with the presence of magnetite (Fig. 6.3 d, e, j, k, o). However, in many samples, the magnetization persists to between 650 and 700°C (Fig. 6.3 a, g), which indicates that hematite is also present. These results are consistent with the thermomagnetic data shown in figure 6.7.

In addition to the presence of magnetite and hematite, some of the thermal demagnetization data indicate a significant unblocking at *c.* 300°C (Fig. 6.3 d, k). Several magnetic minerals undergo thermal unblocking at these temperatures, including iron sulphide minerals such as greigite (Roberts, 1995) and pyrrhotite (Dekkers, 1989), and iron oxide minerals such as maghemite and titanomagnetite (Hunt et al., 1995). At present, we have insufficient evidence to distinguish between these possibilities. However, it should be noted that if magnetic iron sulphides are present, they would almost certainly be authigenic in origin. This could cause complications in polarity interpretation if the authigenic phases formed a long time after deposition. In many cases, however,

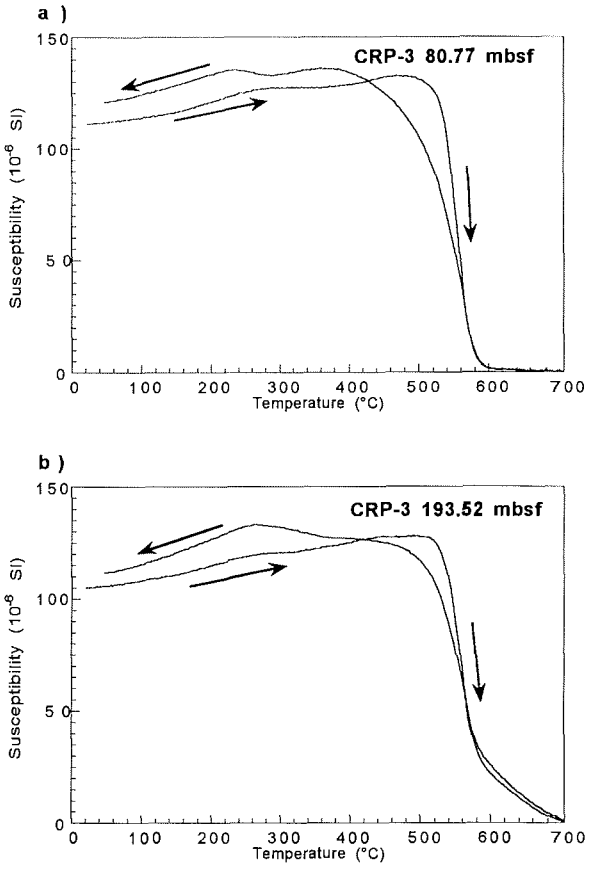

Fig. 6.7 - Temperature-dependence of magnetic susceptibility for samples from a) 80.77 mbsf and b) 193.52 mbsf. Both samples are dominated by magnetite (Curie temperature at *c.* 580°C), although the sample from 193.52 mbsf probably also contains significant hematite (Néel temperature at *c.* 680°C).

such iron sulphide minerals form during early burial, and there is little time-lag in acquisition of magnetization between detrital and authigenic magnetic phases, particularly in rapidly-deposited sediments (*e.g.* Roberts & Turner, 1993). This interpretation is preferred in the case of the CRP-3 samples because the component that unblocks at *c.* 300°C (possible magnetic iron sulphide) carries the same palaeomagnetic direction as the component that unblocks between 550 and 600°C (probable magnetite) (Fig. 6.3 d, k). We, therefore, conclude that the magnetizations recorded by the CRP-3 sediments can be interpreted to have been acquired at, or close to, the time of deposition.

MAGNETIC POLARITY STRATIGRAPHY

In the following treatment, we describe only the magnetic polarity stratigraphy for the upper 350 mbsf of the CRP-3 record. There are three intervals from which no palaeomagnetic samples were taken, because the lithologies were too coarse-grained to allow sampling (144.67-152.84, 259.0-264.33 and 293.43-306.26 mbsf, respectively). The magnetic polarity zonation described

below is preliminary and awaits refinement after measurement of further samples from the lower part of the record.

The magnetic polarity stratigraphy shown in figure 6.5 is tentatively divided into 9 magnetozones: 5 of dominantly normal polarity and 4 of dominantly reversed polarity. In many of the magnetozones, there are samples with opposite polarities to those of the surrounding rocks. In each case, the palaeomagnetic behaviour is stable, and the presence of a steep, normal polarity drill-string overprint suggests that the samples have not been inadvertently inverted. In the following discussion, no interpretations are based on results from single samples. In two cases (at *c.* 160 and 180 mbsf, respectively), pairs of pilot samples display clear normal polarity behaviour that stands out from the surrounding stratigraphical intervals (that are dominated by reversed polarity). In both of these cases, the pilot samples were taken from thin carbonate-cemented intervals because they are harder than the surrounding lithology, and it was therefore possible to measure the samples on the high-speed spinner magnetometer at McMurdo Station. Samples from the surrounding intervals were sandy and would have disintegrated during measurement on the high-speed spinner magnetometer. The contrast in polarity between the carbonate concretions and the surrounding lithology raises questions about whether this material was remagnetized during the diagenetic event that gave rise to the carbonate-cemented intervals. Thus, despite the fact that these two intervals represent polarity zones that are defined by two samples, we refrain from treating them as separate polarity zones in our interpretation. This approach is supported by the likelihood that sedimentation rates are high in this interval and that true polarity zones would normally be recorded across a wide stratigraphical interval rather than only in carbonate concretions that have been more strongly affected by diagenesis than the surrounding sediments.

Reversed polarity dominates the interval from 5.25 to 340.91 mbsf. In the upper part of magnetozone R1, there is a short interval from 41.72 to 44.68 mbsf where samples have transitional and shallow normal polarity inclinations. This interval is indicated as having normal polarity (Fig. 6.5), but it is not treated as a separate magnetozone because there is only one sample with fully normal polarity behaviour (*i.e.* inclination is steeper than -50°). Other thin normal polarity intervals are treated as distinct magnetozones because they contain at least three samples with full normal polarity behaviour.

The transitions from magnetozones R2 to N2 and from magnetozones N2 to R1 are gradual, and transitional palaeomagnetic directions are recorded over a stratigraphical interval of several metres (Fig. 6.5). It is well known that the process of polarity reversal occurs over periods of about 5-10 k.y. (Jacobs, 1994). If sedimentation rates were roughly uniform through these polarity transitions and through the intervening polarity interval, it can be inferred that magnetozone N2 represents a short-period polarity interval on the order of tens of thousands of years in duration.

Between *c.* 245 and 306 mbsf, magnetizations are weak, and there are two gaps in sampling (Fig. 6.5). The palaeomagnetic behaviour from this interval is not ideal, and it is difficult to construct a clear magnetic polarity stratigraphy. However, this interval appears to contain three magnetozones (R3, N4 and R4). Between 306 and 350 mbsf, the magnetization intensities are higher, palaeomagnetic behaviour is more stable, and magnetozones R4 and N5 are well defined (Fig. 6.5).

Unlike the CRP-2/2A record, it appears that there are no sequence stratigraphical boundaries that coincide with polarity boundaries in the CRP-3 record (Fig. 6.5). The only magnetozone boundary that lies close to a sequence stratigraphical boundary is the one between magnetozones R3 and N3. The first normal polarity sample that defines magnetozone N3 lies at 239.93 mbsf, which is immediately below the sequence boundary at 239.89 mbsf. However, without additional chronological constraints, it is impossible to determine whether significant amounts of time are missing in sequence stratigraphical boundaries in CRP-3.

DISCUSSION

"TINY WIGGLES" AND THEIR SIGNIFICANCE IN EOCENE - OLIGOCENE MAGNETOSTRATIGRAPHY

Before presenting possible interpretations of the CRP-3 magnetic polarity zonation, it is necessary to discuss a chronostratigraphical issue that is particularly important in sediments of Eocene - Oligocene age. The standard MPTS was constructed by identifying the positions of magnetic reversals on marine magnetic anomaly records. In order to make this process robust, numerous records from different ocean basins were stacked, and the resultant anomaly pattern was superimposed on an age/distance template from the South Atlantic Ocean (Cande & Kent, 1992a). In many marine magnetic anomaly profiles from fast-spreading oceanic crust, additional short-period, low-amplitude anomalies are evident (with durations <30 k.y.). These anomalies have been named "tiny wiggles". It is difficult to resolve magnetic anomalies when their spatial wavelength represents less than 0.5 km of seafloor and, as a result, the origin of "tiny wiggles" has been debated for the last 30 years. Two possibilities have been suggested: "tiny wiggles" represent either short-period polarity intervals (Blakely & Cox, 1972; Blakely, 1974) or large-scale fluctuations in the ancient field intensity (Cande & LaBrecque, 1974; Cande & Kent, 1992b). The dominant view has been that "tiny wiggles" represent fluctuations in intensity of the geomagnetic field (Cande & Kent, 1992b). However, the possibility that they may represent short polarity intervals is implicitly recognised in the designation of the term "cryptochron", which is

used in cases where magnetostratigraphical evidence exists for short polarity intervals. "Tiny wiggles" are particularly common in Eocene - Oligocene marine magnetic anomaly records. The uncertainty concerning the origin of "tiny wiggles" led Cande & Kent (1992a) to label the positions of cryptochrons as dashes on the side of the polarity log on their MPTS (Fig. 6.8).

Several tests of the origin of Eocene - Oligocene cryptochrons have been made. Lowrie & Lanci (1994) and Lanci & Lowrie (1997) analysed Italian pelagic limestone successions of Eocene - Oligocene age and did not observe short polarity zones that coincided with the positions of expected "tiny wiggles". Hartl et al. (1993) and Tauxe & Hartl (1997) also reported nearly continuous sedimentary palaeomagnetic records for an 11 m.y. period in the Oligocene, in which a number of "tiny wiggles" have been reported. They concluded that "tiny wiggles" resulted from periods of low palaeointensity that were sometimes accompanied by directional excursions. In all of these examples, however, the sedimentation rates were low (~1 cm/k.y.), and it is possible that such short polarity events were smoothed out of the records as a result of sediment remanence acquisition processes (*i.e.* bioturbation and delays in remanence lock-in).

Although the origin of "tiny wiggles" is not yet settled, cryptochrons should be clearly evident in rapidly deposited sedimentary successions, such as those recovered in the Cape Roberts Project, if they represent short polarity intervals. This possibility should, therefore, be taken into account when interpreting magnetostratigraphical records from CRP holes.

INTERPRETATION OF THE CRP-3 MAGNETIC POLARITY ZONATION

A preliminary correlation of the CRP-3 polarity zonation to the MPTS is plotted in figure 6.9, and includes constraints from available biostratigraphical data (see Palaeontology chapter). Diatom preservation above 67 mbsf is excellent, and the first occurrence (FO) of *Cavitatus jouseanus* (which represents the base of the *C. jouseanus* Zone of Scherer et al., in press) is recorded at 48.44-49.69 mbsf. This datum occurs within the lower part of the *Chiasmolithus altus* Zone, which is expected to lie in Chron 12n, although it spans the boundary between C12n and C12r in ODP hole 744B (Baldauf & Barron, 1991; Barron et al., 1991; Harwood et al., 1992; Wei & Wise, 1992). The FO of the diatom *Rhizosolenia antarctica*, which occurs within the *Blackites spinosus* (calcareous nannofossil) Zone (Chron 12r in DSDP hole 511; Wise, 1983), is recorded at 68.60-70.61 mbsf. The last occurrence (LO) of the calcareous nannofossil *Transveropontis pulcheroides*, which occurs in the midpoint of the lowest Oligocene *Blackites spinosus* Zone (Wise, 1983), lies at 114.3 mbsf. This suggests an age of *c.* 32 Ma at 114 mbsf (see Calcareous Nannofossil section). Furthermore, diatom taxa that are documented below the prominent unconformity in the CIROS-1 hole (at

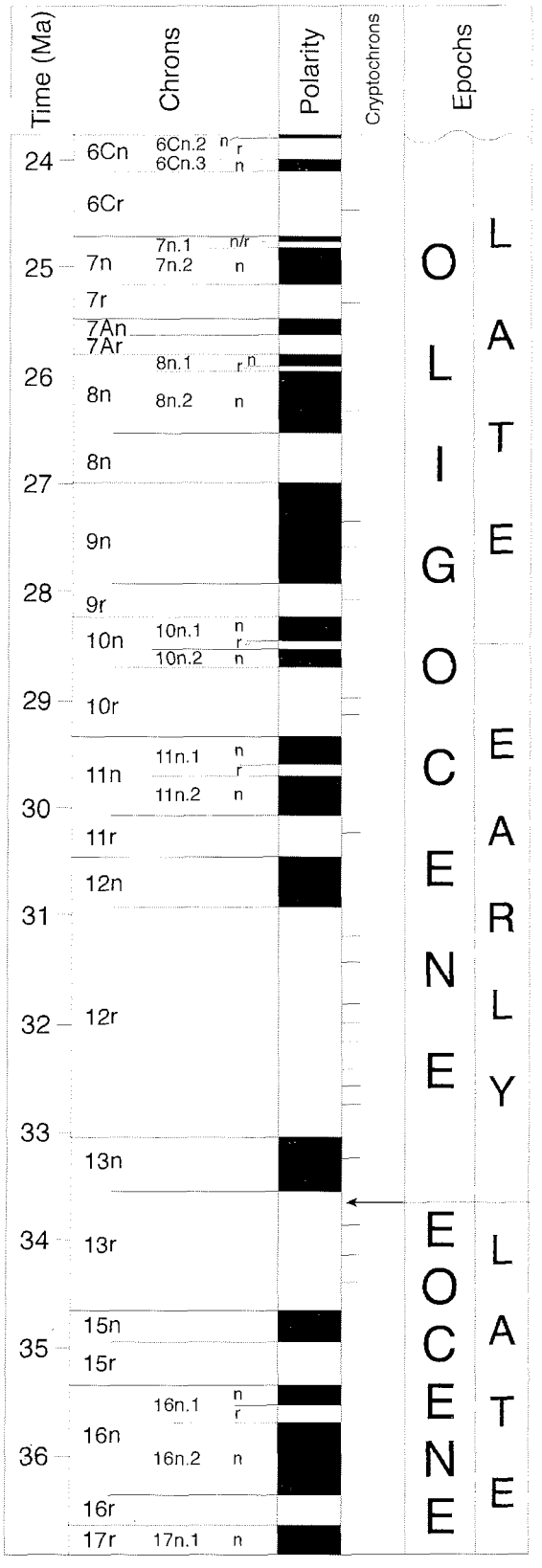

Fig. 6.8 - Magnetic polarity time scale (MPTS) for the late Eocene and for much of the Oligocene, from Cande & Kent (1992a). Beside the standard succession of polarity zones observed from marine magnetic anomalies, Cande & Kent (1992a) indicate the possibility of short-period polarity intervals, called cryptochrons, as dashes on the side of the polarity log. When dealing with rapidly-deposited sediments of this age, as is the case with the Cape Roberts Project, the possibility of encountering cryptochrons must be considered.

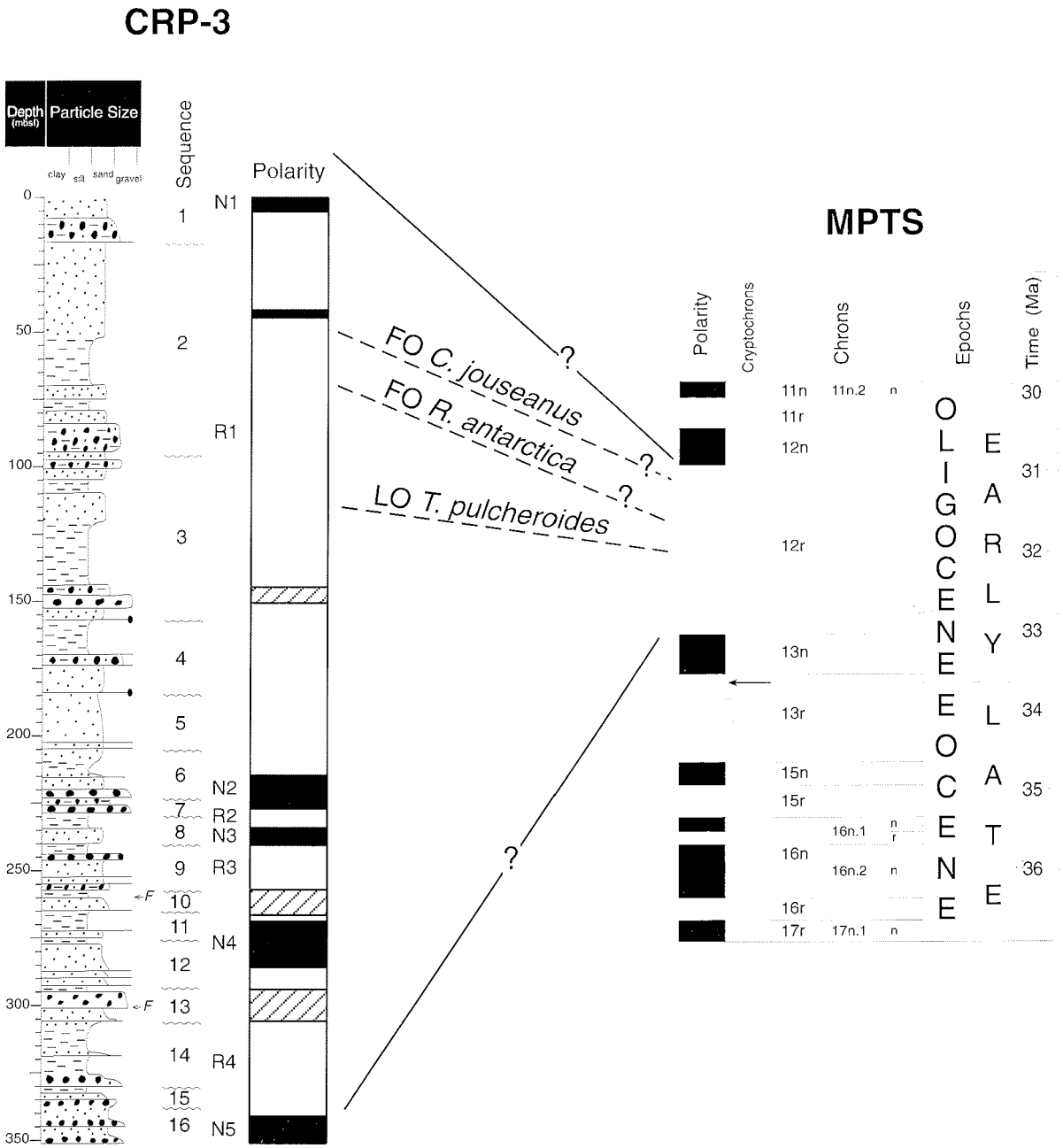

Fig. 6.9 - Tentative correlation of the polarity zonation for the upper 350 mbsf of CRP-3 with the MPTS of Cande & Kent (1992a, 1995). The dominance of reversed polarity in CRP-3 is consistent with biostratigraphical datums (the FO of the diatom *Cavitatus jouseanus* and the LO of the calcareous nannofossil *Transveropontis pulcheroides*) which are expected to lie in Chron 12r. It is likely that most of the normal polarity magnetozones in CRP-3 correspond to cryptochrons rather than to normal polarity subchrons. However, age constraints are insufficiently precise to allow correlation of individual cryptochrons to those on the MPTS.

c. 366 mbsf) are absent in the upper 200 mbsf of CRP-3. This suggests that the upper 200 mbsf of CRP-3 is younger than late Eocene to earliest Oligocene in age.

Below 200 mbsf, CRP-3 is barren of diatoms and calcareous nannofossils. Marine palynology provides the primary biostratigraphical age constraint for the lower part of CRP-3. Dinoflagellate cysts are present to the base of the Cenozoic succession (*c.* 812 mbsf). These assemblages are similar to those found in CRP-2/2A. The Transantarctic assemblage seen in sediments from the base of CIROS-1 (Hannah, 1997) and in Eocene glacial erratics from the southern McMurdo Sound area (Levy & Harwood, in press), is not seen in CRP-3 (see Palynology section). This suggests that the base of CRP-3 is younger than mid-late Eocene in age (Hannah et al., 1997; Wilson et al., 1998).

In summary, the biostratigraphical constraints suggest that the top of CRP-3 should lie in Chron 12r. This is

consistent with the dominance of reversed polarity in the upper 350 mbsf in CRP-3. If it is assumed that the top of CRP-3 corresponds to C12r and that each of the magnetozones documented in CRP-3 has a correlative in the MPTS, this would suggest that magnetozones N2 to N5 represent normal polarity zones in the Eocene. Based on the biostratigraphical constraints, this interpretation is highly unlikely. Furthermore, this interpretation would imply average sediment accumulation rates on the order of 50 m/m.y. Average sediment accumulation rates in CRP-2/2A were considerably higher than this (up to 1 000 m/m.y.; Wilson et al., in press a, b), and the lithofacies indicate similarly high sedimentation rates in CRP-3 (see Lithostratigraphy and Sedimentology chapter). Also, the upper and lower boundaries of magnetozone N2 are defined by transitional palaeomagnetic directions which suggest that this magnetozone is brief (< 30 k.y. in duration) and that sediment accumulation rates are closer to ~600 m/m.y. in this part of CRP-3. It is, therefore, more likely that the short normal polarity interval at 41.72-44.68 mbsf and magnetozones N2, N3 and N4 represent cryptochrons in the lower part of C12r. The biostratigraphical age constraints are not sufficiently precise to enable correlation of the polarity zonation to specific cryptochrons within C12r. The correlation lines on figure 6.9 are therefore shown with question marks. It is possible that magnetozone N5 correlates with Chron 13n, however, it could also represent a cryptochron within Chron 12r. Regardless, the magnetic polarity zonation and the biostratigraphical constraints indicate that the entire upper *c.* 350 mbsf of CRP-3 is early Oligocene in age.

CORRELATION OF CRP-3 WITH CRP-2/2A

Wilson et al. (in press a) presented three possible correlations with the MPTS for the lower 200 m of CRP-2/2A. Correlation C predicts that strata at the base of CRP-2/2A are latest Eocene in age. Correlations A and B suggest that strata at the base of CRP-2/2A are early Oligocene in age (C11r and C12r, respectively). Interpretations of seismic reflection data that were used to choose the CRP-3 drill site predicted that it would have a small amount of overlap (*c.* 50 m) with the base of CRP-2/2A. The C12r age assignment for the uppermost strata from CRP-3 confirm that correlations A or B are more likely to be correct, which implies that strata from the base of CRP-2/2A are early Oligocene in age (C12). Furthermore, initial biostratigraphical examination of CRP-3 (see Palaeontology chapter) suggests that the uppermost strata from CRP-3 were deposited during the middle of Chron 12r and that as much as 1 m.y. could be missing between the base of CRP-2/2A and the top of CRP-3.

Short polarity intervals were also recognised in the Oligocene strata of CRP-2/2A (Wilson et al., in press a). These had no correlative in the MPTS and probably also represent cryptochrons in chrons C9 - C11.

PALAEOMAGNETIC RESULTS FROM BELOW 790 MBSF IN CRP-3

A breccia with dolerite clasts was encountered between 789.77 and 822.87 mbsf. This interval was unsuitable for palaeomagnetic sampling. Beneath a major unconformity, from 823.11 mbsf to the bottom of the CRP-3 hole, a lithified medium-grained light red/brown quartz sandstone was recovered. This unit may represent the Arena Sandstone of the Beacon Supergroup (Devonian). Most outcrops of Beacon Supergroup strata were thermally overprinted by intrusion of the Jurassic Ferrar Dolerite, and the apparent polar wander path for Antarctica has no palaeomagnetic constraints from the Devonian to the Triassic (Grunow, 1999). Because the strata appear fresh and unaltered, it was decided to sample this interval for palaeomagnetic study. Because of previous problems with magnetic overprinting and poor palaeomagnetic behaviour of Beacon Supergroup strata, a pilot study was conducted at McMurdo Station before routine sampling was undertaken. Four closely-spaced samples were collected from three horizons. One sample from each horizon was subjected to AF demagnetization, and the remaining 3 samples were subjected to thermal demagnetization. Results of the pilot study indicate that thermal demagnetization is more efficient than AF demagnetization. The thermal demagnetization data indicate the presence of a reversed polarity overprint with a consistent normal polarity ChRM. Future thermal demagnetization studies will be conducted to determine the nature of this magnetization and whether it can be used to identify a reliable palaeomagnetic pole for this unit.

ADDITIONAL WORK

The above-reported initial characterization studies indicate several areas that warrant additional work. The magnetostratigraphy of CRP-3 clearly needs to be refined, particularly in the lower part of the record. This could have significant implications for the chronostratigraphical interpretation. The present interpretation is preliminary and should be used with caution. Although high-quality palaeomagnetic results have been obtained from the majority of the CRP-3 samples, it is still important to characterize the mineral magnetic properties of different parts of the core. The mineral magnetic measurements will provide the basis for studies of the environmental magnetic record of CRP-3. A suite of samples will also be analysed from the inferred Beacon Supergroup strata (below 823.11 mbsf) in an attempt to determine a palaeomagnetic pole.

Terra Antartica
Initial Report on CRP-3
2000, **7** (1/2)

7 - Summary of Results

INTRODUCTION

When drilling began at CRP-3 there was still the expectation that this final hole of the project would pass down from the sub-polar marine glacial sediments cored in CRP-2A into temperate or even warm-climate marine or terrestrial sediments beneath. This was not to be. The 939 m of strata cored by CRP-3 yielded but a mere 3 m.y. of Cenozoic time (31-34 Ma), an unconformity representing around 300 m.y., and over 100 m of Devonian strata beneath. The last section of this report presents the current state of the chronostratigraphy for these strata. It also provides a summary of both the depositional record of the Victoria Land Basin margin during this short but dynamic period of its development, and the tectonic history of this part of the West Antarctic Rift System.

The dating of core from the upper part of CRP-3 is found to be well constrained by diatom and calcareous nannofossil datums to within the early Oligocene epoch (31 to 33 Ma) for the upper 200 m. Potential for improving the dating extends to around 360 mbsf and possibly further with magnetostratigraphy, more biostratigraphical sampling and from Sr-isotope analysis of macrofossil shell material. The age of the oldest Cenozoic strata, resting on the Devonian Beacon Supergroup sandstone at 823 mbsf, is judged to be "earliest Oligocene and possibly latest Eocene" and *c.* 34 Ma. This judgement is based on the prospect that strata down to 350 mbsf or even deeper lie within Chron 12R (see Chapter 6), and hence within the 31 to 33 Ma age bracket, and the increasing coarseness of sediment to the basin floor, which implies initial very rapid sedimentation.

Depositional styles and trends in CRP-3 core are reviewed from the initial deposition of sandstone breccia as sub-aerial talus on a hillside near sea level to the sandy glacial sediment deposited in outer shelf depths at the top of the core. The sediment becomes finer upcore from coarse dolerite gravel and Beacon-sourced sand on the margins of first an alluvial fan and then a shallow marine delta front. Marine conditions persisted with intervals of finer grained sediment increasing above *c.* 360 m. Although it seems that there were glaciers on land during the deposition of the oldest sediment, there is no indication that they influenced sedimentation at the drill site directly until around the 300 m level when indications of grounding line oscillation appear. The pattern of sequences so well developed in CRP-2A can still be seen above this level, but is simplified and obscured below it.

Evidence of climate on land, although not reviewed in this section, is described earlier from clay mineralogy in Chapter 4 and from terrestrial palynology in Chapter 5. Climatic evidence is mentioned in brief here because it confirms the persistence of a cold climate from earliest Oligocene times. In particular the terrestrial palynomorphs, though present in low numbers on account of the relatively coarse sediment, also show the low diversity characteristic of cold climates, even in the few samples where they are common. The assemblages from CRP-3 record a woody vegetation with *Nothofagus* and podocarps occurring as a low scrub or closed forest intermediate between that of Eocene erratics from McMurdo Sound and the sparse tundra found in lower Miocene core from CRP-1 and upper CRP-2A. In addition, the clay mineral assemblages from 410 mbsf and above are characterised by chlorite and illite , which dominate modern high-latitude sediment, but are largely smectite-bearing below 650 mbsf, indicating the erosion of products of a warmer climate. The inference from these observations is that climate on land was most likely warmer just prior to the initiation of deposition in the Victoria Land Basin, but cold for the period represented by CRP-3.

The surprising achievement of CRP-3 was to core through the oldest Cenozoic strata in the Victoria Land Basin, and into a basement that had stratigraphical significance. Tectonic implications of these and other observations form the third main part of this summary section, with comment on basin subsidence history, age of initial rifting (probably not much older than the oldest sediment cored) and the total post-Jurassic displacement across this margin of the West Antarctic Rift System. Post-early Oligocene faulting is classic dip slip, but a shear zone below 790 mbsf and fractures beneath indicate oblique shear that is not readily explained. This section also reviews data on erosion history from clasts and sand composition, concluding that most of the sediment below 200 mbsf in CRP-3 came from the 2000-m-thick Beacon sandstone (first upper coal-bearing feldspathic beds and then lower quartzose beds). The base of these strata now lies at around 1500 m above basement granitoids in the foothills of the mountains west of Cape Roberts, but most basin subsidence and probably mountain uplift also had been completed by 17 Ma. Indeed clasts of granitoid can be found in the core to depths of 780 mbsf (see Chapter 4), indicating that erosion of the mountains had cut through to the basement by earliest Oligocene times (like granitoid clasts in CIROS-1 core 70 km south and of similar age, Barrett, 1989). Most mountain uplift was plainly an early Cenozoic event.

The section ends with some conclusions and comments on further related work.

CHRONOLOGY

The biostratigraphical framework for CRP-3 is provided primarily by diatoms with additional data from calcareous nannofossils. There is considerable variation in the abundance and preservational quality of the microfossils throughout the core (see chapter 5), and this variation affects the degree of biostratigraphical resolution. In addition, these pelagic diatom and calcareous nannofossil assemblages differ significantly from those of coeval open oceanic sites in the Southern Ocean, so that only some of the calibrated biohorizons are present in CRP-3. Nevertheless, there is concordance between the age determinations provided by the diatom and calcareous nannofossil data, suggesting that the age determinations are robust. Biostratigraphical age control by pelagic microphytoplankton fossils is restricted to the upper 200 mbsf of the CRP-3 sequence.

Diatom assemblages above 48.4 mbsf contain both *Cavitatus jouseanus* and *Rhizosolenia antarctica*, indicating the *C. jouseanus* Zone of early Oligocene age. The FAD of *C. jouseanus* has been calibrated from several Southern Ocean deep-sea sites, both directly and indirectly, to the palaeomagnetical time scale. This datum occurs within the lower part of Chron C12n at ODP Site 748 on the central Kerguelen Plateau (Harwood & Maruyama, 1992). Based on the time scale of Berggren et al. (1995), the inferred age of this datum is approximately 30.9 Ma. Further to the south, at Kerguelen Plateau ODP Site 744, this datum lies close to the C12n/C12r boundary in the lower *Chiasmolithus altus* nannofossil Zone (Baldauf & Barron, 1991; Barron et al., 1991), corresponding to a similar age of approximately 31 Ma. *Cavitatus jouseanus* tends to be rare and sporadic in occurrence near its first appearance at oceanic sites, as noted by Fenner (1984) for DSDP Site 274 and Harwood & Matuyama (1991) for ODP Site 748. This suggests that the FAD of *C. jouseanus* may be slightly older than reported from Southern Ocean deep-sea sites. As a result, a conservative placement of this datum near the top of Chron C12r is adopted herein (chapter 5).

The interval from 49.68 to 68.60 mbsf contains *Rhizosolenia antarctica* without *C. jouseanus*, indicating the *R. antarctica* Zone of early Oligocene age. The base of this zone, defined by the FAD of *R. antarctica*, corresponds with a significant degradation in the preservation and abundance of siliceous microfossils downcore. The actual absence of *R. antarctica* in the underlying rock cannot be reliably ascertained at this time. It is likely, therefore, that the FAD is not the evolutionary first appearance but a diagenetically mediated one. Thus, the lower boundary of this zone must remain tentatively placed for the present. The FAD of *R. antarctica* at Falkland Plateau DSDP Site 511 occurs within the *Blackites spinosus* nannofossil Zone (in Chron C12r) of early Oligocene age (Fenner, 1984). Further to the south at ODP Site 744 on the Kerguelen Plateau, this FAD occurs in the lower *Blackites spinosus* nannofossil Zone (Chron C13; Baldauf & Barron, 1991; Barron et al., 1991). These occurrences suggest an age of approximately 33 Ma for this datum. Given the tentative placement of this biohorizon in CRP-3 (discussed above), this age must be considered a maximum age estimation for this part of the core.

The calcareous nannofossil *Transversopontis pulcheroides* has its LAD at 114 mbsf in an interval of relatively high microfossil abundance. This species has its LAD near the centre of the *Blackites spinosus* Zone on the Falkland Plateau (Wise, 1983) at both Sites 511 and 513. Assuming that the entirety of the zone is present at Site 511, which has the more complete record, this FAD correlates to the mid-point of the zone. This extrapolates to an age of approximately 32.4 ± 0.5 Ma.

Siliceous microfossils occur as poorly preserved, sparse assemblages from *c.* 70 to 195 mbsf. Despite this, the species composition indicates the age of these assemblages. In general, the composition of the assemblages indicates that they are dissolved counterparts of those from above 70 mbsf. The absence of the highly dissolution-resistant *Hemiaulus caracteristicus* in these assemblages indicates that they are younger than the LAD of that species. The LAD of *H. caracteristicus* is well-dated within Chron C13n on the southern Kerguelen Plateau (Site 744; Baldauf & Barron, 1991), indicating an age of *c.* 33 Ma. The absence of this species in the upper 200 mbsf of CRP-3 indicates that this interval is younger than this age.

Initial characterization of the palaeomagnetical sequence is complete through the upper 350 mbsf. This interval is dominated by reversed polarity with relatively thin intervals of normal polarity (chapter 6). These thin intervals of normal polarity are interpreted to represent cryptochrons (short polarity intervals with durations <30 ky). All of the biostratigraphical information indicates that the upper 200 mbsf of CRP-3 was deposited between 31 and 33 Ma. Since this 200 m is part of the continuous sequence of reversed polarity, it follows that the entire sequence is probably part of a single polarity chron. Given that this is part of a single continuous interval, the age and the dominantly reversed polarity indicate that it must represent part of Chron 12r of early Oligocene age.

The sediment accumulation rate for this interval can be calculated following these assumptions. As discussed below, it is not possible at present to estimate the thickness of any sedimentary rock above the top of CRP-3 that may be part of this reversed polarity interval. In addition, palaeomagnetical results are currently not available for the interval below 350 mbsf (chapter 6). Thus, any estimation of sediment accumulation rate must be regarded as a minimum. Berggren et al. (1995) assigned a duration of 2.12 Ma for Chron 12r. Thus, a minimum sediment accumulation rate for the upper 350 m of CRP-3 is approximately 165 m/m.y. This rate is entirely reasonable given the type of sediment (coarse grain clastics) and the sedimentary environment (glaciomarine). This rate is also

close to the average sediment accumulation rate calculated for the upper *c.* 300 m of CRP-2.

Chronological characterization of the interval below 350 mbsf is difficult at this time. Many palaeontological and palaeomagnetical samples remain to be examined. Initial inspections suggest that some portions of the core material may not yield any conclusive age information (chapters 5 and 6). There are data that imply that the base of the section above the sandstones identified as Beacon Supergroup may be as young as early Oligocene (marine palynomorphs) or as old as late Eocene (terrestrial palynomorphs) in age, but neither of these estimates can be considered in any way conclusive. In addition, none of the material identified as Beacon Supergroup has yielded fossil material. The material intruding this Beacon Supergroup probably will be dateable by one or more methods, and this may help restrict the age of some of the associated sedimentary material.

CORRELATION BETWEEN CRP-2A AND CRP-3

The location of CRP-3 was selected to provide core that had a stratigraphical overlap (<100 m) with the lowest core from CRP-2A (see Introduction chapter). However, a revision of the seismic data suggests that the lower strata cored by CRP-2A truncate against reflector "l" and that the uppermost strata cored by CRP-3 truncate through downlap against reflector "o" (Fig. 7.1). Thus, there may not be a stratigraphical overlap between these drill holes.

A composite of palaeontological, magnetic polarity, and lithological information provides data to examine possible overlap or underlap (gap) between these two drill holes (Fig. 7.2). Six siliceous microfossil taxa range to the top of CRP-3 but are not present in the lower diatom-bearing intervals of CRP-2A (above *c.* 565 mbsf), suggesting a stratigraphical gap or underlap between the two holes. However, a 60-m interval at the base of CRP-2A that is barren of diatoms complicates this interpretation of overlap or gap. Several species of palynomorphs are in common between the two drill holes, but are long-ranging. *Lejeunocysta* sp. #7 has the shortest range in both drill cores. Foraminiferal assemblages are facies-controlled and offer no basis for correlation. A broad mussel-bearing zone in CRP-2A (from 442 mbsf to the bottom of the hole) may continue with the uppermost 11 mbsf of CRP-3. Magnetostratigraphical data for the lower part of CRP-2A are mixed, but most of the lower 35 m is of normal polarity. In contrast, the upper 200 m of CRP-3 is almost entirely of reversed polarity, with normal polarity in the uppermost metres of the recovered core.

The upper ranges of the six diatom taxa in question may have terminated within the interval of poor preservation in CPR-2A (Fig. 7.2), but this record is lost due to dissolution of the diatoms. Alternatively, given the rapid rates of sediment accumulation and assuming the absence of a significant unconformity within the barren zone, the truncation of the diatom ranges may indicate a stratigraphical gap between these two drill cores. If an overlap exists, magnetostratigraphical data indicate that it must be less than 5 m. Lithological and sequence stratigraphic data suggest that there is no overlap (Fig. 7.3).

DEPOSITIONAL HISTORY

INTRODUCTION

The depositional history derived from the CRP-2/2A core was intimately concerned with the history of growth and decay of the Antarctic ice sheet. However, in the case of CRP-3, although it is clear that glacial advance and retreat played a significant part in the depositional history of the upper third of the core, the lower portion was less directly influenced by glacial processes. Base-level fluctuations, evident in the CRP-2/2A core and sometimes associated with glacial advance and retreat, are not clearly distinguishable in the lower two-thirds of the CRP-3 core. This may be because of a rapid sedimentation rate, coupled with rapid and continuous subsidence of the basin and uplift of the source area.

Lithological and facies relationships are summarised in columns presented in figure 7.4.

The Victoria Land Basin succession represented in the CRP-3 drillcore can be divided into six main lithofacies associations, in upward succession:

1. monomictic conglomerate and breccia, derived from the Beacon Supergroup (823.11-822.88 mbsf);
2. clast-supported conglomerate and minor sandstones (822.88-789.77 mbsf);
3. muddy sandstones with subordinate conglomerates (798.77-~580 mbsf);
4. clean sandstones with subordinate conglomerates (~580-378.36 mbsf);
5. muddy sandstones and mudstones, with subordinate conglomerates and diamictites (378.36-0.00 mbsf).

LITHOFACIES ASSOCIATION 1: MONOMICTIC CONGLOMERATE AND BRECCIA

This lithofacies association is limited to the lowest 23 cm of Victoria Land Basin section, immediately above the basal unconformity at 823.11 mbsf (Fig. 7.5). Clast-supported breccia, consisting of unsorted angular clasts (up to 6 cm) of Beacon Supergroup quartzitic sandstone, in a matrix of quartzose sandstone, rests directly on the basal unconformity surface, and extends up to 822.94 mbsf, 17 cm above the unconformity.

The breccia is separated by an irregular wavy surface from an overlying matrix-supported conglomerate. Clasts in the conglomerate are up to 2 cm across and are of Beacon Supergroup quartzitic sandstone; they are within a matrix of quartzose sandstone. This conglomeratic facies extends up to 822.88 mbsf, giving a thickness of 6 cm.

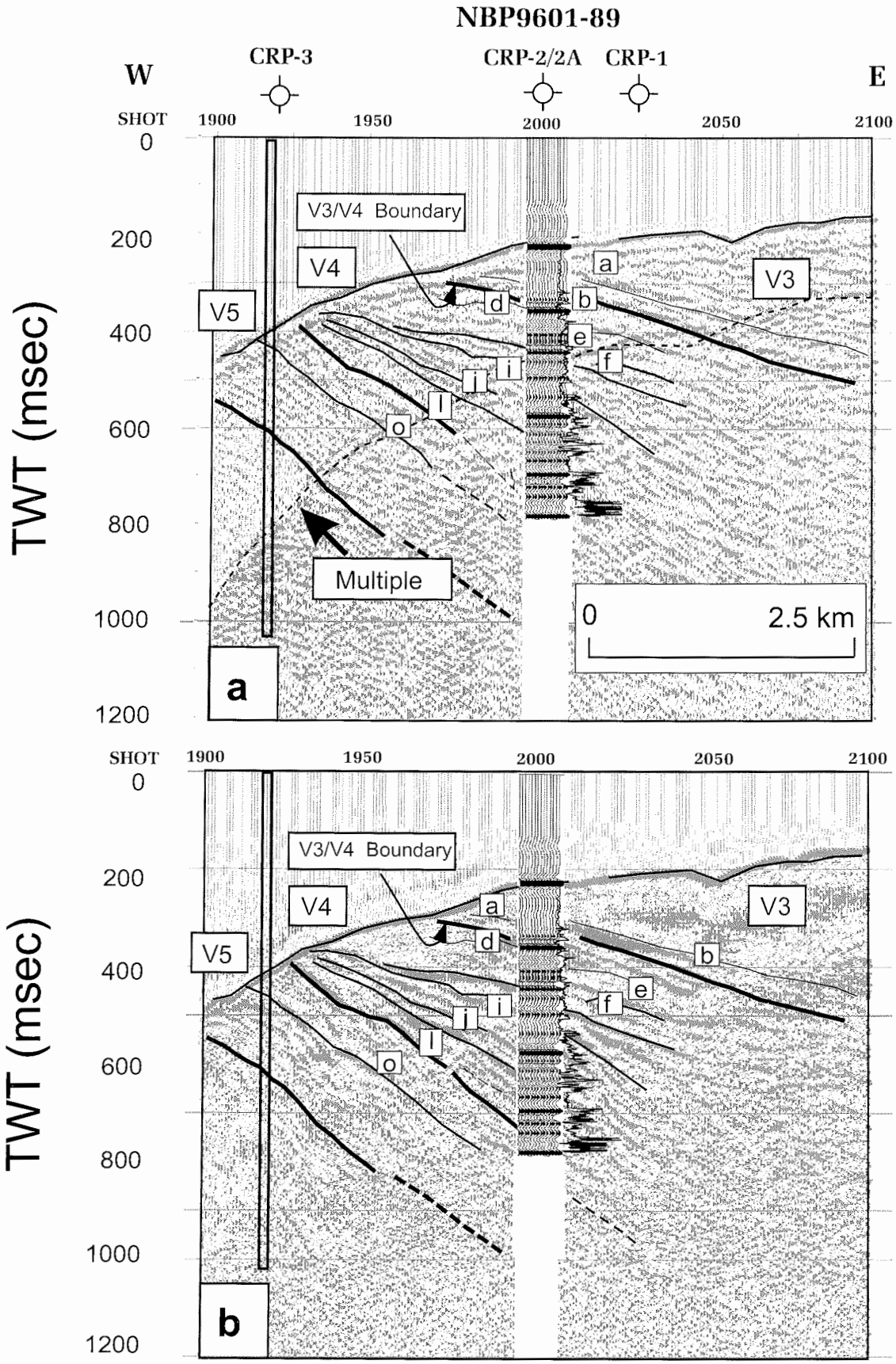

Fig. 7.1 - Section of seismic profile NBP9601-89 showing detail of the overlap of CRP-2/2A and CRP3 with synthetic seismic data and measured velocity log from CRP-2. Note the truncation of reflectors by reflector "l" in the re-processed multichannel data (b), which is not evident in the single channel data (a).

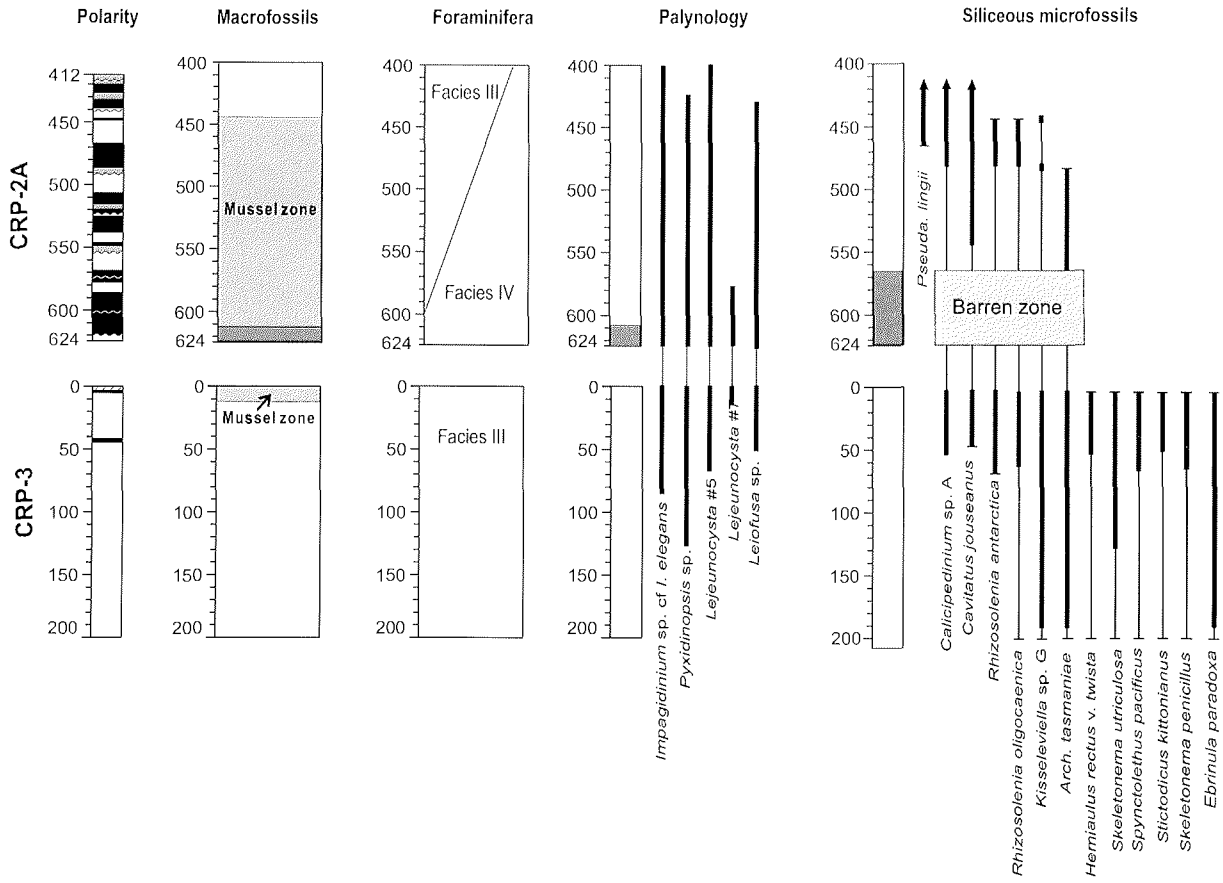

Fig. 7.2 - A compilation of palaeontological and magnetostratigraphical data from the upper 200 m of CRP-3 and the lower 224 m of CRP-2A. The data indicate a varying degree of possible overlap (dark grey boxes) with each set of data. Magnetostratigraphy provides the strongest indication that little to no overlap is possible.

Depositional Processes and Environment

The angular and unsorted nature of the monomictic breccia suggests that it is unlikely to have been transported by water. It is inferred to be talus, deposited adjacent to steep topography. The erosionally overlying monomictic conglomerate has undergone some degree of aqueous transport, resulting in the rounding of clasts, but has a poorly-sorted matrix, suggesting that there has been minimal sorting and transport has been only for a short distance. Deposition from a debris flow or sheet flow on an alluvial fan, adjacent to steep topography, is inferred.

LITHOFACIES ASSOCIATION 2: CLAST-SUPPORTED CONGLOMERATE, WITH MINOR THIN SANDSTONES

This lithofacies association extends from 822.88 to 789.77 mbsf, a thickness of 33.11 m. The conglomerate (mainly Facies 9), is dominated by well-rounded boulders and cobbles of dolerite, some over 1 m in diameter. However, smaller clasts of Beacon Supergroup quartzose sandstone are included, particularly towards the base. The base of the unit rests on an erosion surface of irregular relief cut into the underlying quartzose conglomerate of Association 1. The basal conglomerate is clast-supported, and exhibits coarse-tail coarsening-upward over about 85 cm. At the base, clasts are less than 1 cm across and are an admixture of rounded dolerite and quartzite which coarsen upward into angular blocks of quartzitic sandstone and larger rounded dolerite boulders now supported by matrix. Dolerite clasts in the lower few centimetres appear altered, and may have been subjected to weathering processes.

The bulk of the association, however, consists of rounded and subordinate subrounded and subangular, clast-supported boulders and cobbles. These are dominated by dolerite but with subordinate sandstone clasts. Sandstones are quartzose, angular to subangular and up to 70 cm across. They decrease in proportion upward until they are absent in the upper half of the unit. Interspersed with the conglomerate beds in the lower half of the assemblage are thin (up to 50-cm thick), medium to coarse-grained sandstone beds of Facies 5, many showing reverse grading.

A change in the succession occurs from approximately 804 mbsf, the upper portion of the association, where quartzitic sandstone clasts are lacking and where the conglomerates include more matrix, in some instances becoming matrix-supported. Interbedded thin sandstones

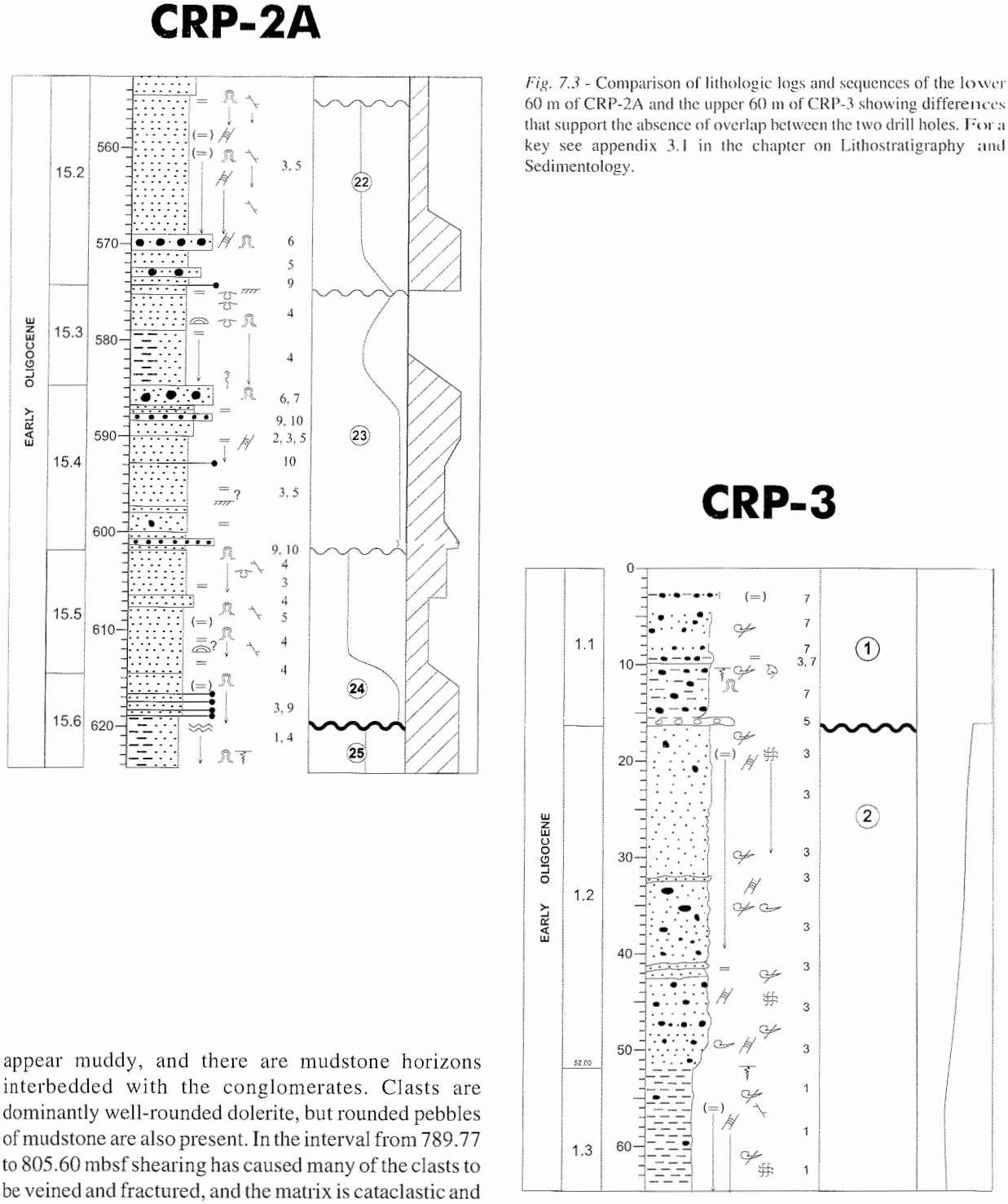

Fig. 7.3 - Comparison of lithologic logs and sequences of the lower 60 m of CRP-2A and the upper 60 m of CRP-3 showing differences that support the absence of overlap between the two drill holes. For a key see appendix 3.1 in the chapter on Lithostratigraphy and Sedimentology.

appear muddy, and there are mudstone horizons interbedded with the conglomerates. Clasts are dominantly well-rounded dolerite, but rounded pebbles of mudstone are also present. In the interval from 789.77 to 805.60 mbsf shearing has caused many of the clasts to be veined and fractured, and the matrix is cataclastic and slickensided.

This interval, described as a dolerite (cataclastic) breccia on the 1:20 scale core logs, displays evidence of intense shearing and fracturing. We initially considered the possibility that the clasts could be the result of fracturing and shearing of a dolerite body. However, studies of clast roundness characteristics (see section on Clast Features) indicate that the body is primarily a sedimentary deposit that has been subsequently modified by shearing. The presence in it of sedimentary clasts, and the occurrence of spores and pollen together with woody material and tissue (see section on Palynology) further support this.

Depositional Processes and Environment

Clasts in the association are well-rounded, suggesting that water transport has played a major part in depositional processes. However, the continued but declining presence

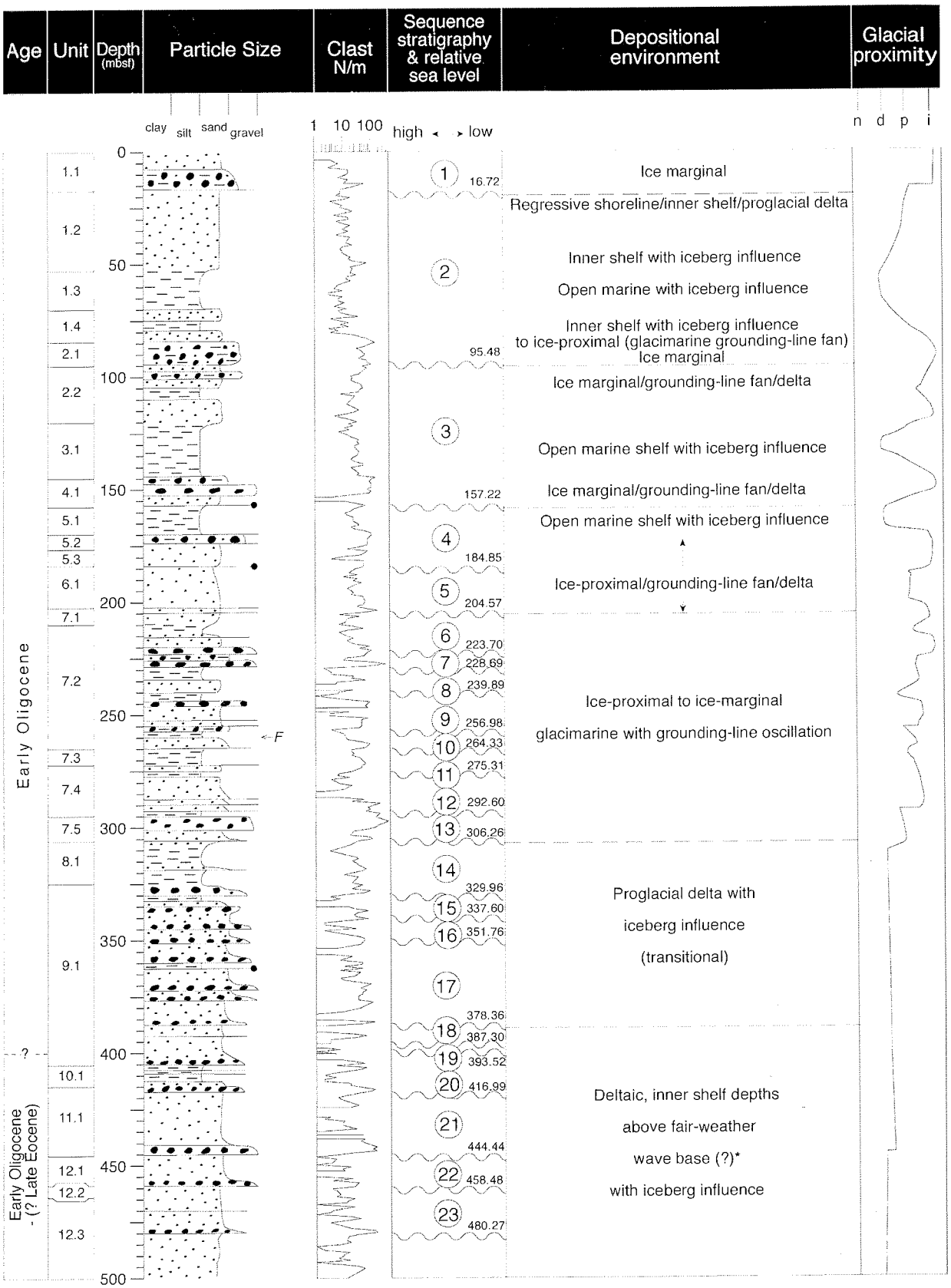

Fig. 7.4 - Stratigraphical summary and interpretation of the CRP-3 core. For *, see text for alternative minority opinion.

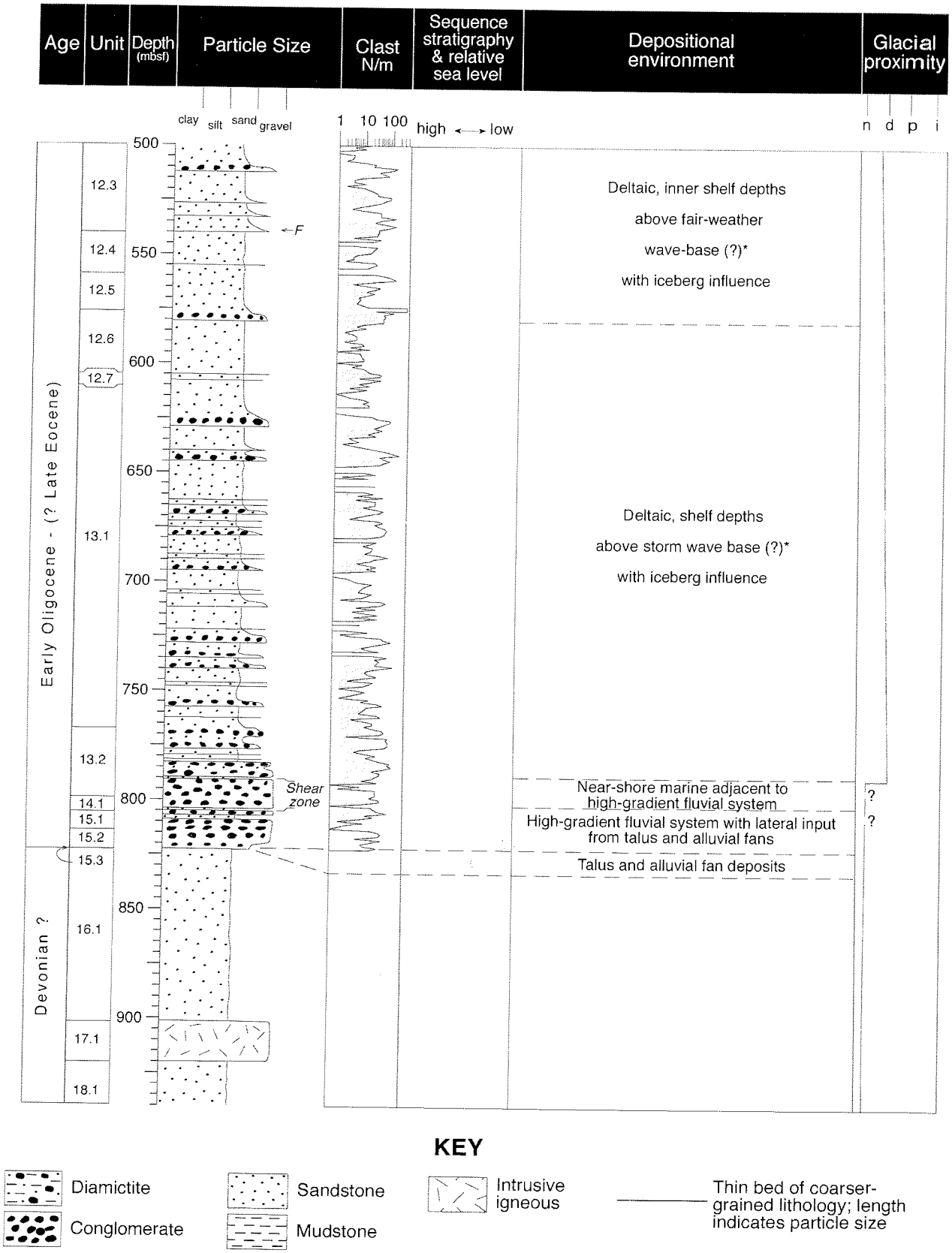

Fig. 7.4 - continued.

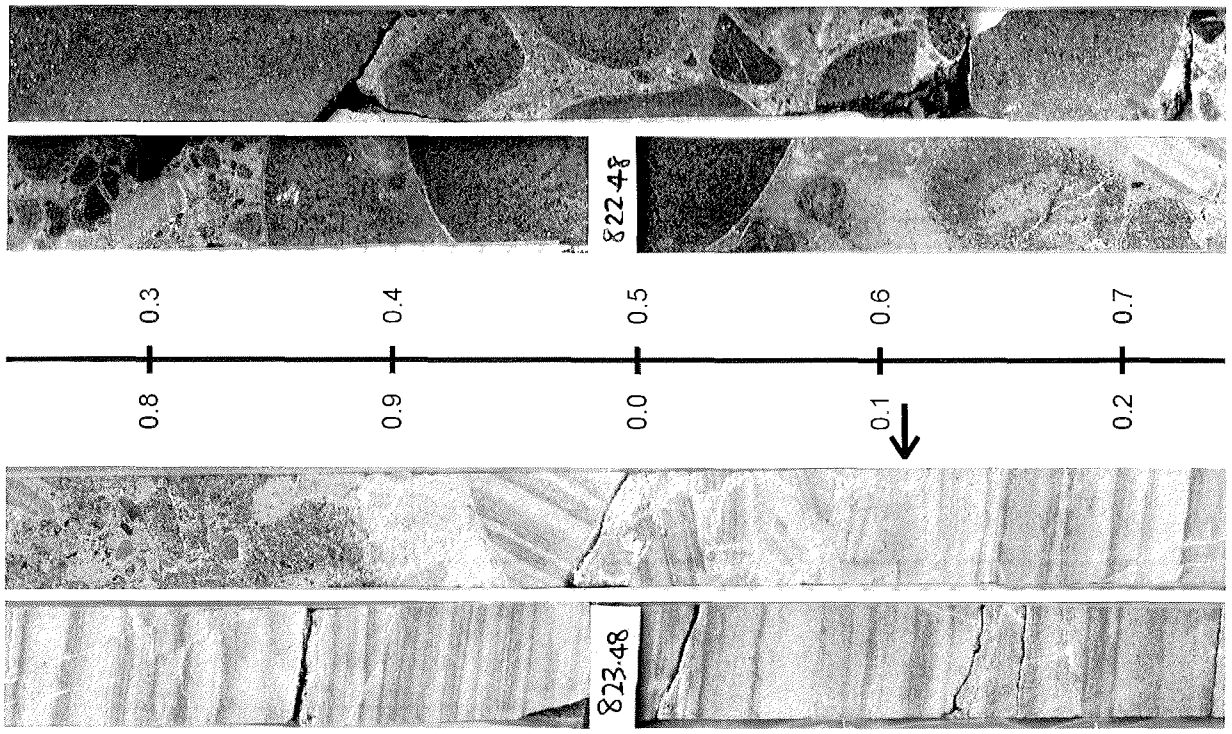

Fig. 7.5 - Core image of the basal unconformity (arrowed) of the Victoria Land Basin at 823.11 mbsf in CRP-3. Strata beneath the unconformity are laminated quartzose sandstone of the Beacon Supergroup. The unconformity is overlain by thin (17 cm) clast-supported sandstone breccia followed by 6 cm of matrix-supported fine conglomerate. This is overlain by, and in sharp contact with, a much thicker sequence of rounded and clast-supported cobbles and boulders, mainly of dolerite. The scale is in metres and keyed to the depth tags, which are in mbsf.

up the core of angular clasts of quartzitic sandstone, many in discrete layers, throughout the lower half of the succession, indicates that local debris showing little sign of transport (talus?) was still being shed into the environment. Similarly, thin reverse graded beds of monomictic quartzose sandstone are inferred to be local debris flow deposits on alluvial fans. However, the dominant lithofacies of large, well-rounded, clast-supported dolerite boulder conglomerate, suggests a fluvial environment with sufficient energy to remove fine grains and to transport boulders in excess of one metre. The environment of deposition for the lower part of the succession is inferred to be a high-gradient fluvial system accessing a dolerite source area, with lateral input from more local alluvial fans and talus slopes fed by cliffs of quartzitic sandstones of the Beacon Supergroup.

Upcore from approximately 804 mbsf quartzose sandstone clasts are absent and the quartzose sandstone component is limited to thin, stratified units and conglomeratic matrix. Concomitantly, mud becomes a major matrix component. Although large quantities of gravel and boulders were transported and deposited, the environment was quiet enough to allow mud and fine sand to accumulate occasionally. A fan-delta consisting of a steep-gradient fluvial system debouching into the sea is a possible environment for these deposits.

LITHOFACIES ASSOCIATION 3: MUDDY SANDSTONES WITH SUBORDINATE CONGLOMERATES

The massive, clast-supported conglomerates end at 798.77 mbsf, above which are pebble to cobble conglomerates and pebbly sandstones up to approximately 767.70 mbsf. Upcore from that sandstones become slightly muddy (Facies 3), with subordinate, mainly matrix-supported conglomerates (Facies 10) up to about 580 mbsf. Conglomerates become a minor constituent in the upper portion of this association between approximately 660 and 580 mbsf. The association also includes rare intervals of moderately to well-sorted sandstones of Facies 4 and 5, as far as 580 mbsf, incorporating LSU 13.1 and 13.2. The lithofacies association forms a generally fining upward succession, with conglomerates and pebbly sandstones dominating in the lower third, grading up to a sandstone-dominated succession. Soft-sediment deformation occurs sporadically throughout the association, most commonly throughout the lower half, associated with a higher mud content.

The slightly muddy sandstones range from vaguely stratified to well-stratified, dominated by parallel lamination, but also with intervals of ripple cross-lamination and cross-stratification. Convex-upward and low-angle divergent laminae, particularly between 767

and 744 mbsf, may represent hummocky cross-stratification. Soft-sediment deformation is present locally within the muddy fine-grained sandstones. Sandstone beds commonly show a generally fining-upward trend from a thin layer of fine gravel or granules at the base, often with rapid transition upwards through increasingly finer sandstone, in many cases with good cross lamination. Thickness of individual sandstone beds ranges up to 2 m.

Although the sandstones appear muddy macroscopically, microscopical examination of some samples suggests that the clay cement filling the interstices between grains is diagenetic and derived from post-depositional fluids (see section on Diagenesis), rather than it being modified primary matrix. Thus, at the time of deposition many of the sands were probably clean.

Many conglomerates, particularly in the lower portion of the association, show grading to sandstone in their uppermost few centimetres. A few are symmetrically graded or ungraded. In the upper portion of the association, many conglomerates have gradational contacts, although sharp-based conglomerates also occur. Individual conglomerate beds range up to 4 m thick.

Marine palynomorphs and a macrofossil occur in the lowest part of the association at 781 mbsf, showing that this part of the section at least is marine. Striated clasts occur at several locations throughout the association (see section on Clast Features). Outsized clasts, some of which are angular, occur in every lithofacies (see section on Clast Features), and angular gravel forms a constituent in most conglomerates. It also occurs as isolated clasts on bedding planes of well-sorted sandstones. Soft-sediment deformation is relatively common, particularly in the lower half of the succession.

Depositional Processes and Environment

The depositional environment is clearly marine, at least at 781 mbsf, because of the presence of marine fossils.

The common occurrence of thick, poorly-sorted matrix-supported conglomerate units, many showing crude grading in their upper portions, and the absence within the conglomerate units of traction features, suggests deposition by sediment-gravity flows. A number of conglomerate units are graded throughout and were probably deposited by debris flows or high-density turbidity currents.

Likewise, the fining-upwards trend evident in many of the sandstone beds may also indicate deposition from sediment-gravity flows. Alternatively, they may represent deposition in offshore bars, or deposition by periodic floodwaters from a feeder fluvial system. The slightly muddy nature of sandstones and the presence of soft-sediment deformation suggest rapid sedimentation and entrainment of water and fines.

Of alternative depositional environments, the most probable is relatively shallow water. The site was probably not very distant from a debouching high-gradient fluvial system, whence periodic floodwaters brought both coarse and fine sediments. This system may have been a glacifluvial outwash plain fed by glaciers up-valley to enhance episodic discharge. In this scenario sediment was entrained as high-density turbidity currents or debris flows either by the flood waters themselves, or by retrogressive failure and slumping from a delta edge down a delta front (*e.g.* Carlson et al., 1989, 1992). Both finer-grained delta-top sandstones and sandy delta front deposits were likely to have been above storm wave base, as indicated by both hummocky cross-stratification, which is generally inferred to be representative of storm deposits and therefore formed above storm wave base (Harms et al., 1975), and common cross stratification. These structures suggest that wave action, including storm-wave action, sorted and redeposited the finer-grained deposits.

A minority of us considered that both the conglomerates and the thick fining-upward sandstone units constituted turbidites, which frequently show an array of sedimentary structures formed during a declining flow regime arranged as Bouma sequences, although all intervals are not always present. The volume of sediment transported to form each unit and the cobble size of the coarsest debris was thought to require a gravity-driven mechanism of deposition, probably episodic, high-volume, high-density turbulent flows. A laterally extensive slope was thought be required to provide acceleration for the flowing suspension, and a base of slope setting in relatively deep water was suggested.

Whatever the primary environment, it was under some glacial influence in the form of iceberg rafting. Outsized and angular clasts are incongruous in the primary depositional environments envisioned for this association and indicate that glaciation in Antarctica at this time was sufficiently strong to support glaciers to sea level somewhere in the region.

LITHOFACIES ASSOCIATION 4: CLEAN SANDSTONES WITH SUBORDINATE CONGLOMERATES

The muddy sandstones of Association 3 die out gradationally upwards, and are replaced increasingly by beds of clean fine- to medium-grained sandstone of Facies 5. The first thick units of clean sandstones appear at approximately 580 mbsf and persist until about 340 mbsf. However, from about 364 mbsf upwards, intercalations of mudstone and slightly muddy sandstone begin to appear and become more common upwards; the first diamictites also appear.

The dominant lithofacies is light-coloured, clean, fine- to medium-grained sandstone, with minor pebbly sandstone to pebble conglomerate. The sandstones are clean, without a muddy matrix, and are dominantly well-sorted with equigranular well-rounded quartz grains. A minor component consists of clean but poorly-sorted subangular to subrounded quartz grains, some with a coating consisting of a clay mineral which gives a

greenish-grey hue to the sediment. Most beds exhibit vague to well-developed parallel stratification. Cross-bedding is common, and low-angle divergent laminae, coupled with apparent convex-upwards lamination at 520 and 558 mbsf, may indicate hummocky cross-stratification. Mottling, possibly representing burrowing, is present at scattered horizons. Other evidence of life is limited to extremely rare and questionable macrofossil fragments. However, thin-section study of the clean sandstone reveals that it is strongly cemented with calcite (see section on Diagenesis), some of which may have been derived from detrital shelly material.

As in Association 3, sandstone beds commonly show a generally fining-upward trend from a thin layer of fine gravel or granules at the base. The fining often occurs as a rapid transition upwards through increasingly finer sandstone with moderate to well-developed planar lamination.

The subordinate conglomerates are poorly-sorted, matrix- to clast-supported, with a matrix of fine-grained sandstone, and contain angular to well-rounded clasts consisting almost entirely of dolerite. Conglomerate beds commonly have sharp bases and frequently show crude normal grading, consisting either of coarse-tail grading, or of massive conglomerate passing with rapid transition upwards into laminated sandstone.

As for Association 3, outsized clasts occur in association with angular clasts isolated on bedding planes of the well-sorted sandstone, and within conglomerates. Striated clasts also occur rarely (see section on Clast Features).

Depositional Processes and Environment

Shelly material is rare, and possible bioturbation is limited to two stratigraphical intervals. However, the widespread occurrence of carbonate cement suggests that more shelly material may have originally been present, although it does not account for the quantity of cementation. A marine environment is inferred for the association.

The architecture of the sandstone and conglomerate facies are very similar to those in Association 3. The main differences are that many of the sandstones are well-sorted and are carbonate cemented rather than clay cemented, and that conglomerates form a much lower proportion of the sediments. The low mud content of Association 4 compared with Association 3 is emphasised by the relative scarcity of soft-sediment deformation.

The sediments of Association 4 were most likely to have been deposited in a shallow-water marine setting. This was probably shallower than Association 3 because the apparent cleanness and better sorting of the sandstones and the much more common large-scale cross-bedding suggest a greater influence of wave or current activity. Again, the possible occurrence of hummocky cross stratification suggests that the succession was deposited above storm wave base. Deposition as delta-front deposits seems probable. The graded conglomerates may have been deposited, as for Association 3, as high-density turbidity currents or debris flows forming delta-front deposits.

A minority view considers that, as for Association 3, both the conglomerates and the thick fining-upward sandstone units were likely to have been deposited as sediment gravity flows in deeper waters considerably below wave base.

Association 4 is under iceberg influence as described for Association 3, with glaciers probably supplying much of the sediment for the association from further inland.

LITHOFACIES ASSOCIATION 5: MUDDY SANDSTONES AND MUDSTONES, WITH SUBORDINATE CONGLOMERATES AND DIAMICTITES

Above *c.* 378 mbsf, the nature of the sediments changes significantly. They become notably more muddy, with thick units of mudstone (Facies 1) and poorly-sorted, muddy, very fine to coarse-grained sandstone of Facies 3. Moderately sorted, stratified or massive, medium- to coarse-grained sandstones of Facies 5, and matrix-supported conglomerates of Facies 10 form subordinate but important units. The new and significant facies is massive diamictite of Facies 7, which occurs with increasing frequency and unit thickness towards the top of the drillcore.

Association 5 is also notable for the common occurrence of trace fossils and shelly fossils, including unbroken shells. Soft-sediment deformation structures are also common throughout; cross stratification is rare.

Units of mudstone, often with shelly fossils and burrow mottling, are up to 24-m thick. The mudstone is commonly sandy, stratified at a decimetre scale, and contains dispersed clasts. Soft-sediment deformation and water-escape structures are common. Lonestones locally appear to penetrate underlying laminae.

Fine-grained muddy sandstone with dispersed clasts is also common, grading locally into clast-poor, sandy diamictite. The dispersed clasts are dominated by dolerite, with granule-sized coal fragments and small clasts of granitoids appearing intermittently. Various forms of soft-sediment deformation are common to pervasive, including load casts, load balls and deformed bedding, sedimentary dykes and water-escape structures. Some sandstone beds show loading into underlying mudstones, and slumping is evident at some horizons.

Conglomerate units are commonly matrix-supported, and moderately to poorly-sorted with angular to rounded clasts. Crude upward-fining, with coarse-tail grading in conglomerate beds which may be in excess of 1-m thick, is relatively common. Diamictites, some in excess of 6-m thick, occur sporadically throughout the facies association, but are most common in the upper part. They vary from clast-poor sandy to muddy diamictite, which is commonly weakly stratified to locally massive, and muddy sandstone with dispersed clasts.

Depositional Processes and Environment

The depositional environment is clearly fully marine, as shown by the common presence of macro- and microfossils, trace fossils and frequent bioturbation. Foraminiferal studies in the section of core from 0 - ~200 mbsf suggest that deposition occurred in mid- to outer-shelf depths (50-200 m: see section on Foraminifera); and study of macrofossils in the section of core from 16.72-300 mbsf indicates deposition within much the same range (30-120 m: see section on Macrofossils). Macrofossils from the uppermost part of the core (0-16.72 mbsf) suggest slightly increased depth ranges between 100-300 m.

Probably the most critical lithofacies from the point of view of environment is diamictite, which in previous Cape Roberts drillcores has been interpreted mainly as having a direct or indirect glacial origin. The diamictitic character may originate from debris-flow deposition primarily originating from ice-contact deposits, or some units, especially those that grade into and out of massive diamictites, may be from direct rain-out of ice-borne debris that is then acted on by currents. Alternatively, subglacial tills can exhibit these types of structures. Massive diamictite is the facies most likely to be of subglacial origin, although it too may originate from debris-flow processes associated with ice contact, or rain-out processes. Based on the association of other lithofacies with diamictites, the subglacial origin for diamicts thus far appears unlikely.

Conglomerate units which show coarse-tail grading are inferred to be debris-flow deposits, either directly associated with ice-marginal processes, or deposited at the base of locally developed slopes. Slump structures and other evidence of downhill creep within muddy sandstone and mudstone facies also suggest the presence of a slope or glacial pushing or overriding. The combination of Lithofacies 2 and 8 is common in ice-proximal glacimarine settings associated with grounding-line fans and subglacial stream discharges (Powell, 1990).

Many sandstone beds that are ungraded and show poor lamination are inferred to be the results of deposition by traction currents. Others, which show some grading and which are loaded into underlying mudstones, show indications of rapid deposition and entrainment of water, causing soft-sediment deformation and suggesting emplacement by sediment gravity flow.

These facies are interpreted in terms of deposition in glacimarine and open coastal/shelf environments by a combination of traction currents, fall-out from suspension, sediment-gravity flows and rain-out from icebergs. Proximity to a glacial terminus is inferred to account for deposition of diamictites, conglomerates and associated Lithofacies 2 and 8. Better-sorted sandstones are likely to have been deposited in a relatively shallow marine environment, possibly as delta top or delta front deposits. The periodic occurrence of diamictites suggests a cyclic history of glacial advance and retreat for the period of time covered by Association 1. Based on the inferred degree of meltwater influence on the succession, a cool-temperate to sub-polar climate is inferred, similar to that at the base of CRP-2/2A.

BASIN HISTORY

The genesis of the western margin of the Victoria Land Basin is encapsulated in the first few centimetres above a sharp, nearly planar contact with basement Beacon Supergroup quartzose sandstone at 823.11 mbsf. This contact, which is an unconformity, is overlain by a thin sequence of breccia and conglomerate composed of Beacon Supergroup sandstone, and inferred to represent debris deposited on talus and alluvial fans (Lithofacies Association 1). These deposits imply a steep topography in a subaerial environment, probably caused by vertical movement on boundary faults during the initial phase of Victoria Land Basin rifting.

These earliest deposits are followed by a sedimentary system dominated by conglomerate deposited initially in a high-gradient fluvial system, and then in close-inshore marine conditions. This association (Lithofacies Association 2) suggests sedimentation on a subaerial to marine fan-delta system as an adjacent fault scarp(s) erodes and continued basin subsidence occurs.

The overlying deposits are dominated initially by conglomerates and granular sands and then by a mixture of conglomerates and muddy sandstones (Lithofacies Association 3). This association records a phase of rapid subsidence and basin infilling indicating high sedimentation rates. Some sedimentary structures in the sands may suggest that the basin floor was mainly within shelf depths, and at times probably shallower than storm wave-base. The basin appears to be shallower from about 580 m upwards, containing an abundance of clean, well-sorted sand with common traction current features, and only a minor conglomerate component (Lithofacies Association 4). We infer that the nature of these sediments reflects a decline in the pace of subsidence, allowing the basin to fill to a higher level. The pace of uplift also declined slightly, resulting in lower gradients and dominant deposition of sand, in a shallow-marine environment with active current and wave activity possibly above fair-weather wave-base.

The common rounded pebbles in pebbly sandstones and conglomerates in both lithofacies associations suggest derivation from a nearby fluvial system, and deposition was probably on the marine portion of a delta. Sediment gravity-flows were triggered either by floods in the fluvial system, or by seismic activity along the active adjacent fault system, and deposited as delta front sands and conglomerates: the well-sorted sands were deposited largely on the delta top where they were exposed to winnowing wave and current action. The primary environment was under some glacial influence

in the form of iceberg rafting, indicating that glaciation at this time was sufficiently strong to support glaciers to sea level somewhere in the region.

From about 380 mbsf upwards, the nature of the sedimentary record changes. Well-sorted clean sands become rare and are replaced by muddy sands, and mud, diamictites and conglomerates become more prominent upcore (Lithofacies Association 5). Soft-sediment deformation and fluid-escape structures become common, and rare slumps occur. Water depths indicated by the fossil record are mainly in the mid to outer shelf range, although the top 16 m of core may be deeper, suggesting that the basin is generally deepening. The facies association indicates a glacimarine and open shelf environment, subject to cyclical glacial advances and retreats. Proximity to a glacier terminus is inferred to account for deposition of diamictites and conglomerates, associated with morainal banks and grounding-line fans. Although rapid sedimentation is suggested by the high water content of the finer-grained sediments, the apparent continued deepening of the basin indicates that subsidence was outpacing sediment.

TECTONIC HISTORY

BASIN HISTORY

CRP-3 cored the oldest part of the Cenozoic sequence off Cape Roberts, with biostratigraphical work showing that all of the core is of early Oligocene age, possibly extending into the latest Eocene at the base of the section at 823 mbsf. If we include the lower Oligocene strata in CRP-2A below the unconformity at 443 mbsf in CRP-2A, and accept a small stratigraphical gap between the two holes (see section on Chronology), we find that *c.* 1 000 m of lower Oligocene strata are present at the western edge of the Victoria Land Basin. Assuming the age at the base of the Cenozoic strata is *c.* 34 Ma, this represents at an average rate of net sediment accumulation *c.* 200 m/m.y.

The consensus view of the depositional setting for the CRP-3 strata is that all but the lowermost section is shallow marine. The consistency of the depositional setting, never far from the shoreline, suggests steady, rapid subsidence and an abundant sediment supply to fill the basin continuously. Although more chronological data and more complete palaeobathymetrical data are being gathered for a more rigorous and complete analysis (Wilson et al., in preparation), a diagram has been prepared to show the history of basin subsidence (Fig. 7.6). The diagram is presented as if for a stratigraphical column located at CRP-1, but is based on ages and thicknesses from all three CRP drill holes. The trend indicates rapid subsidence from *c.* 34 to 31 Ma, much slower subsidence from 31 to 16 Ma, and from that time no net basin subsidence to the present.

A subaerial erosion surface marks the basal contact between the lower Oligocene (or possibly uppermost Eocene) strata and underlying quartz sandstone interpreted to be part of the Devonian Taylor Group, the lower part of the Beacon Supergroup. The sandstone is considered most likely to be part of the Arena Sandstone, a formation that typically lies 400 to 600 m above the Kukri Erosion Surface (Barrett & Webb, 1973; Woolfe et al., 1989). This surface is a major regional unconformity separating Beacon strata from underlying upper Precambrian-Ordovician igneous and metamorphic basement rocks.

The presence of rift-basin fill resting directly on Devonian Beacon Supergroup strata has several important tectonic implications:

1) the major part of the Beacon section, the sills of Ferrar Dolerite within it and the overlying Kirkpatrick Basalt, must have been eroded prior to or coeval with the early phases of down-faulting that displaced the Beacon to form the rift-basin floor;
2) the age of the Cenozoic strata just above the unconformity on the Beacon most likely represents the age of the rifting event that formed this section of the Victoria Land Basin. USGS seismic line 403/404 shows that almost most of the floor of the basin off Cape Roberts is younger than the oldest Cenozoic strata cored in CRP-3 (Fig. 7.7), and
3) the Beacon strata cored in CRP-3 provide a marker horizon that can be matched with reasonable confidence to the middle part of the Devonian Beacon strata in the adjacent Transantarctic Mountains. This suggests *c.* 3 000 m of down-to-the-east displacement across the Transantarctic Mountain Front (Fig. 7.8).

A key result of CRP drilling has been the demonstration that most of the regional seismic sequences originally correlated through the Victoria Land Basin by

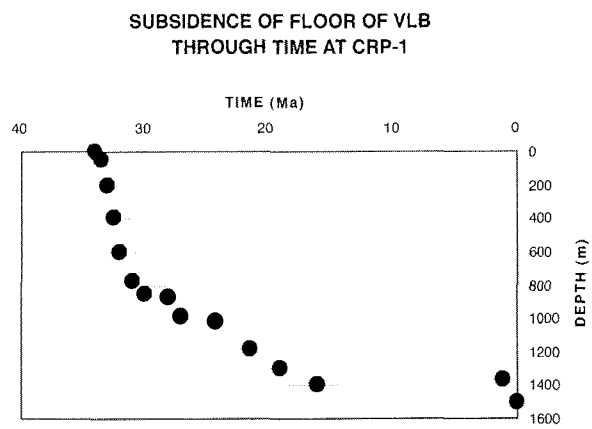

Fig. 7.6 - Diagram showing the subsidence of the floor of the Victoria Land Basin at CRP-1 through time, projecting data from CRP-2 and CRP-3 to the CRP-1 site. No account has been taken of compaction, or of the many unconformities. The diagram shows a short period of rapid subsidence from 34 to 31 Ma, followed by a longer period of slower subsidence to 16 Ma with virtually no net subsidence from that time to the present day.

Tab. 7.1 - Comparison of ages for seismic sequences inferred from regional geological data in 1987 compared with the ages established from Cape Roberts core. Ages from the core are found to be much younger than expected.

Sequence	Cooper et al., 1987	Cape Roberts Science Team
V1	E.-M. Miocene to Present	Quaternary
V2	Late Oligocene to E.-M. Miocene	?
V3	Paleogene to late Oligocene	E. Miocene at base
V4	Paleogene and/or older	Late Oligocene
V5	Cretaceous to early Paleogene	Early Oligocene (possibly latest Eocene)
V6	Paleogene to Holocene, & Jurassic to Paleogene	Late Oligocene-Holocene (McMurdo Volcs), & Jurassic (Ferrar Supergroup)
*V7	Precambrian to E. Paleozoic	Precambrian to E. Paleozoic

Cooper et al. (1987) are much younger than was inferred from the regional geology (Tab. 7.1). The V4/V5 sequence boundary was transected in CRP-2A at *c.* 443 mbsf, coincident with a upper/lower Oligocene unconformity (Henrys et al., in press). A series of seismic events, informally labeled o-v, have been identified from preliminary analysis of the vertical seismic profiling in CRP-3 and seismic reflection interpretation (see section on Correlation of Seismic Reflectors). These reflectors must all mark lower Oligocene horizons, and all occur within the V5 seismic sequence, which extends to the floor of the basin a few kilometres east of CRP-1 on Roberts ridge (Fig. 7.7).

Seismic sequence V6 comprises the discontinuous to chaotic reflections that occur at shallow depths in some places and at large depths in the middle of the basin. It

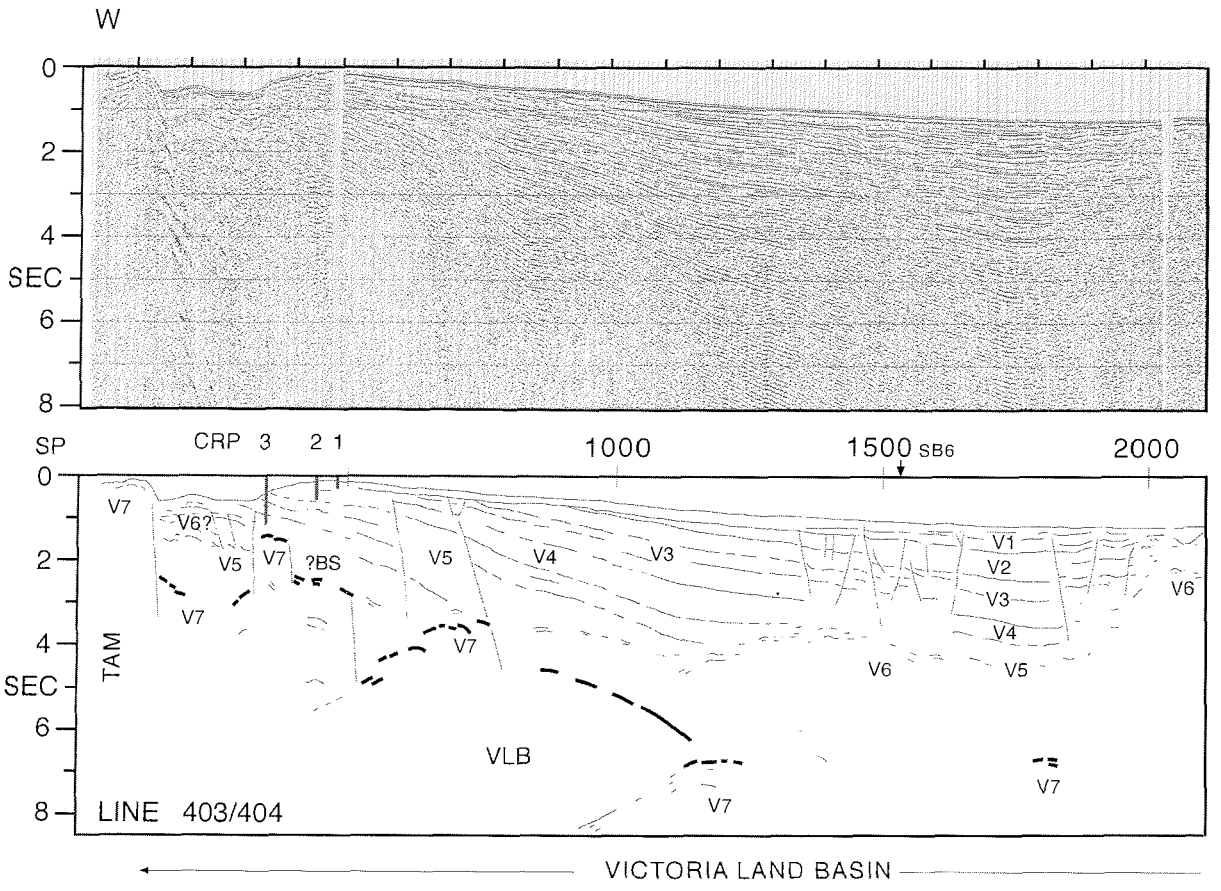

Fig. 7.7 - Seismic section showing the western margin of the Victoria Land Basin off Cape Roberts (from Cooper et al., 1987, plate 2). The 3 CRP holes are projected onto the section, which runs less than 2 km to the north. The section shows that the Cenozoic strata to be onlapping to the east, and indicates that CRP-3 cored into the oldest body of Cenozoic strata in the basin. As CRP-3 cored into lower Beacon Supergroup strata at 823 mbsf, we show the Beacon to underlie the Cenozoic sequence for several km eastward into the basin.

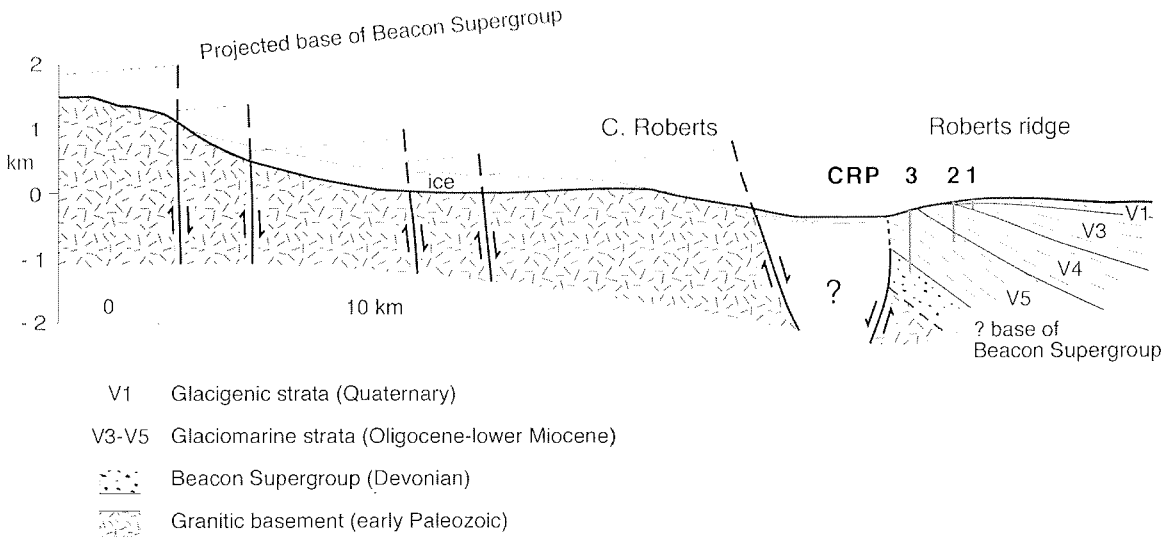

Fig. 7.8 - Schematic cross-section across the Transantarctic Mountain Front, showing our current view of the geometric relationship between the Cenozoic strata at the western margin of the Victoria Land Basin, the Beacon Supergroup strata beneath, and the granitic basement of the Transantarctic Mountains. The faults to the west of Cape Roberts, and their displacements, have been taken from Fitzgerald (1992, Fig. 21).

lies just beneath the sea floor off volcanic Beaufort Island, and hence is in part McMurdo Volcanic Group, but it was considered also to include Paleogene (as yet unsampled early rift volcanic rocks) or possibly Mesozoic (Ferrar Supergroup) at depth in the middle of the basin. It was not mapped west under Roberts ridge, where seismic sequence V5 rests directly on V7, but was tentatively inferred in the small graben with magnetic anomaly between Roberts ridge and the coast (Cooper et al., 1987, plate 2). Perhaps the intrusive body in CRP-3 is a sample of this unit.

Seismic sequence V7 is acoustic basement for the region, and comprises rocks that pre-dated the Victoria Land Basin. This unit was interpreted to include igneous and metamorphic rocks of Ordovician and older age, and probably the sedimentary Beacon Supergroup and the igneous Ferrar Group. V7 was inferred by Cooper et al. (1987) to lie at approximately 1.0 seconds TWT beneath the western margin of Roberts ridge, but CRP-3 cored into Beacon Supergroup strata, a unit previously considered part of the 'acoustic basement', at 823.11 mbsf, considerably shallower than the 1.0 second reflector (shown below CRP-3 in Fig. 7.7). We think, therefore, that the reflector identified by Cooper et al. (1987) instead marks the top of an igneous or metamorphic (or both) basement underlying the Beacon strata. On the seismic profiles in proximity to CRP-3, the region beneath *c.* 770 mbsf is obscured by a strong multiple, making it impossible at present to identify or trace reflectors that may correspond to the Oligocene/Beacon unconformity surface.

The dip pattern documented in CRP-2/2A, with gradually steepening dip with depth (Jarrard et al., in press), continues in CRP-3, where dips steepen from *c.* 10° up to *c.* 22° above the unconformity truncating the Beacon strata. The dip direction appears to be toward the east-northeast, based on preliminary interpretation of dipmeter and BHTV data. In addition, these log data, as well as analysis of bedding dip on whole-core scan images, indicate that there is little angular discordance between the Oligocene strata and the Devonian Beacon strata across the unconformity (the downhole logging data indicate that the dips are similar but the Beacon has a more northerly dip direction). This is surprising because in similar settings down-faulted strata typically dip toward the uplifted block.

East-west seismic reflection profiles also show a fanning array of stratal wedges that thicken to the east. The greater subsidence to the east indicates either growth faulting on a west-dipping, west-side-down normal fault zone, or greater thermal subsidence along the basin axis, or both. Regional seismic lines (Cooper & Davey, 1987; Brancolini et al., 1995) show that this east-dipping, eastward-thickening pattern continues at least to the eastern margin of the Terror Rift. Tracing the Oligocene seismic reflectors cored in CRP eastward, they disappear beneath the base of the seismic lines and indicate that over 8 km of Oligocene strata are present within the Victoria Land Basin.

IGNEOUS INTRUSION

An igneous body *c.* 16 m in vertical thickness intrudes the Beacon strata between 901 and 918 mbsf. The igneous rock is pervasively altered such that no original

mineralogy is preserved. All four chemical analyses carried out are highly altered, but trace element ratios suggest a sub-alkaline chemical affinity, which excludes the McMurdo Volcanic Group (see section in Petrology).

Possible origins for the body are a previously undiscovered phase of the Jurassic Ferrar Dolerite, which forms extensive sills, and in places dykes, within Beacon strata cropping out within the Transantarctic Mountains, or a heretofore unrecognised episode of early rift-related magmatism (older than 34 Ma). An aeromagnetic survey over the Cape Roberts region documented a strong anomaly to the west and northwest of the CRP drill sites, modelled as a sheet-like igneous body (Bozzo et al., 1997). It is possible that the igneous body cored in CRP-3 is related to this body.

DEFORMATION

Naturally-formed microfaults are particularly abundant in the Oligocene strata cored in CRP-3. Most of the microfaults cutting the Oligocene strata are dip-slip normal. The density of small faults in CRP-3 records significant strain, suggesting proximity to one or more major faults. Three larger-scale faults of unknown displacement were cored in CRP-3. Faults at 260 and 540 mbsf are brittle faults characterized by veining and high-fracture permeabilities, whereas a third is inferred from a zone of shear between 790 and 806 mbsf that includes cataclastic features.

Striae on fault surfaces record a kinematic change down-core from consistent dip-slip motion to more complex oblique shearing within the shear zone below 790 mbsf. The oblique shear pattern is continuous into and is characteristic of the entire lower section of the core, including the Devonian Beacon sandstone. All observed faults above 823 mbsf cut strata of earliest Oligocene age, and must therefore be Oligocene or younger. It is not yet possible to say whether the two kinematic types mark discrete deformation episodes or, alternatively, whether all the deformation is the same age, but there is a partitioning of strain between different faults or with depth in the section.

The attitude of the larger-scale fault planes is hard to estimate. None close to CRP-3 can be seen in the seismic data. If the large faults are parallel to small faults imaged by the BHTV, it is possible that the fault at 260 mbsf dips eastward, and the fault at 790 mbsf dips westward. However, further analysis of seismic, log, and core-based data will be required to provide adequate constraints on orientation. VSP data provide 3 depths to the top of a strong reflector at 790 mbsf, indicating a plane dipping *c.* 10° to the east. This plane has the same depth and strike as the top of the sheared layer of coarse conglomerate found in the core at this level, though a shallower dip than estimated from well logs. The VSP data do not indicate any offset of strata by a fault through the drill hole at this level.

Both the Beacon strata and the intrusive igneous body are characterized by extensive faulting. Brecciation of the Beacon sandstone is also very common, associated with injections of clastic material. These deformation features are atypical of Beacon strata that crop out in the Transantarctic Mountains. The deformation is therefore likely to be due to rift-related down-faulting along the Transantarctic Mountains Front. This brecciation and mobilisation may also have been associated with intrusion-related hydrothermal activity.

PROVENANCE AND TRANSANTARCTIC MOUNTAINS UPLIFT

Petrological investigations in CRP-3 have revealed a continuation of compositional trends observed in CRP-1 and CRP-2/2A (Cape Roberts Science Team, 1998, 1999). The absence of fresh alkaline volcanic detritus below *c.* 300 mbsf (*c.* 25 Ma) in CRP-2A continues down to the oldest Cenozoic strata in CRP-3. However, this observation is tempered by the presence in CRP-3 of rare grains of fresh brown, green and colourless glass of unknown composition. If that glass is alkaline in composition, its scarcity and the very fine size of the fragments suggest that it represents products of eruptions from a volcanic source distant from the McMurdo Sound region. Possible sources include the alkaline volcanic centres in northern Victoria Land.

The uppermost 200 m of CRP-3 is dominated by clasts of Ferrar Supergroup (dolerite and basalt). The sand grains also show peak values for clinopyroxene, which has its sole source in the Ferrar Supergroup in CRP-3. In the bulk mineralogy XRD study, feldspar/quartz (F/Q) ratios are high and alkali feldspar/quartz (K/Q) ratios are low, indicating enhanced Ferrar-derived plagioclase above *c.* 200 mbsf. Below 200 mbsf, Ferrar clasts diminish in abundance, and there is a notable increase in the proportion of sedimentary rock types that were probably derived mainly from the Beacon Supergroup. This is also evident from sand grain modes, which are dominated by quartz grains (mean value for total quartz grains *c.* 82%), and reflected in diminished F/Q ratios from XRD study. The proportions of rounded grains (Qr/Qa>0.3) between 200 and 500 mbsf also has significance because this ratio offers a proxy for the relative proportion of rounded quartz grains contributed by the lower Beacon Supergroup (Devonian Taylor Group). These relationships suggest that the change at *c.* 200 mbsf represents a down-core shift from basement-dominated detritus to more detritus derived from the Beacon-Ferrar 'cover' sequence. Such a down-core shift was also recognised at the 307 mbsf unconformity in CRP-2A (Smellie, in press; Talarico et al., in press). The significance of its recurrence in CRP-3 is still unclear.

The sand-grain modes and XRD bulk mineralogy investigations also highlight a second possible petrological transition, although it is not supported by any evidence

from the clast studies. At *c.* 550 mbsf, the sand mode and bulk mineralogy studies show a series of coincident compositional changes affecting samples below that depth. These include a diminished proportion of quartz and increased feldspar grains, much lower Qr/Qa ratios, higher F/Q ratios, and much lower K/Q ratios. These petrological changes suggest that the provenance has undergone a compositional shift to detritus dominated by material derived from the *upper* Beacon Supergroup (Permian–Triassic Victoria Group), which the sandstone resembles to a remarkable degree. Work is in progress to assess this view.

Coal fragments of sand and granule size have been observed in CRP-3 from 150 mbsf to a depth of 780 mbsf (see the Petrology chapter and the core logs in the Supplement to this volume). These extend up-section to the unconformity at 307 mbsf in CRP-2A. The coal is of high rank and almost certainly from the Weller Coal Measures, a 180- to 250-m-thick formation with coal beds totalling 10 to 35 m in thickness that today crop out *c.* 100 km to the west in the Transantarctic Mountains (see section descriptions in Barrett & Webb, 1973). Terrestrial palynomorphs of Permian, Triassic and Jurassic age also record a Beacon provenance (see section on Palynology). Some of these forms are much less thermally altered than palynomorphs from outcrops in the mountains, and they are, therefore, presumed to have been eroded from Beacon strata with a smaller proportion of intrusive dolerite, perhaps further inland. The provenance implications of the distribution of coal fragments and palynomorphs as compared with petrological provenance indicators are not clear, and plainly deserve further study.

IMPLICATIONS FOR REGIONAL RIFT HISTORY

The Cape Roberts site is only the second place along the Transantarctic Mountains rift shoulder where offset of Beacon strata along the frontal fault system can be directly demonstrated. At Cape Surprise, in the central Transantarctic Mountains near Shackleton Glacier, Barrett (1965) documented down-faulted Beacon at the coast, estimating 5 000 m displacement. At Cape Roberts, assuming a marker horizon at the level of the Devonian Arena Sandstone, the offset is estimated at *c.* 3 000 m.

Fission-track data from the Transantarctic Mountains in southern Victoria Land indicate that large-scale uplift commenced at *c.* 55 Ma (Fitzgerald, 1992). Although no lower Eocene strata are present at the Cape Roberts site, the unconformity documented in CRP-3 shows that a thick section of Beacon Supergroup and Ferrar Supergroup must have been eroded prior to the earliest Oligocene, and this erosion could have occurred during Eocene mountain uplift.

The great thickness of Oligocene strata that can now be demonstrated in the Victoria Land Basin shows that rapid basin subsidence began no later than the earliest Oligocene and possibly somewhat earlier, slowing significantly in late Oligocene and Miocene times. The Oligocene and younger faulting of the strata implies syn-depositional rifting, although the geometry of faulting remains to be determined. This major rifting event in the western Ross Sea is contemporaneous with, and very likely related to, newly documented sea-floor spreading in the Adare Trough, immediately north of the northern Victoria Land continental margin (Cande et al., 2000).

CONCLUSIONS AND FUTURE PLANS

Drilling of CRP-3 completes the coring planned for the Cape Roberts Project. With a depth of 939.46 m, it exceeded the target depth of 700 m by around 30% and created a new record for bedrock drilling in Antarctica. Core recovery was 97%, with losses mostly in the upper 10 m and occasional loose sand between 400 and 600 mbsf.

If CRP-2/2A fed largely the climatic goals of the project, with its fine record of early Miocene glacial cyclicity and the means of dating it, CRP-3 has provided a treat for the tectonic objectives, revealing

i) the total post-Jurassic offset across the margin of the West Antarctic Rift System off Cape Roberts (*c.*3000 m),
ii) the age and nature of the oldest sediment in this section of the Victoria Land Basin (34 Ma, conglomerate), and
iii) subsidence history for the life of the basin (rapid from 34 to 31 Ma, then slower to 17 Ma and with none at all after then).

Further work on analysis of fractures, along with core oriented from bore hole televiewer data, will contribute directions of movements from which changes in regional stress regime through time can be deduced.

The recovery of 116 m of Beacon sandstone and intrusive was significant not only in providing a reference plane for calculating offset across the margin of the West Antarctic Rift System, but also in showing that with CRP-3 the entire Cenozoic section off Cape Roberts had been cored. The seismic section figured by Cooper et al. (1987) had previously shown that these were the oldest strata in the basin (7.7). We can therefore conclude that there is no further point in coring off Cape Roberts to find the transition into strata representing warm Eocene times. The Eocene McMurdo erratics show that such strata do exist, but we must now presume that they occur only to the south of their current position (Minna Bluff, 150 km south of Cape Roberts), and must have been eroded from beneath the Ross Ice Shelf (Levy and Harwood, 1999).

Despite the discovery from CRP-3 that deposition began in the Victoria Land Basin just after the late Eocene cooling, there was some success in extracting a climate record from the core. The cyclic patterns recognised in the strata of CRP-2A continue down into the upper part of CRP-3. Below *c.* 300 m the motif

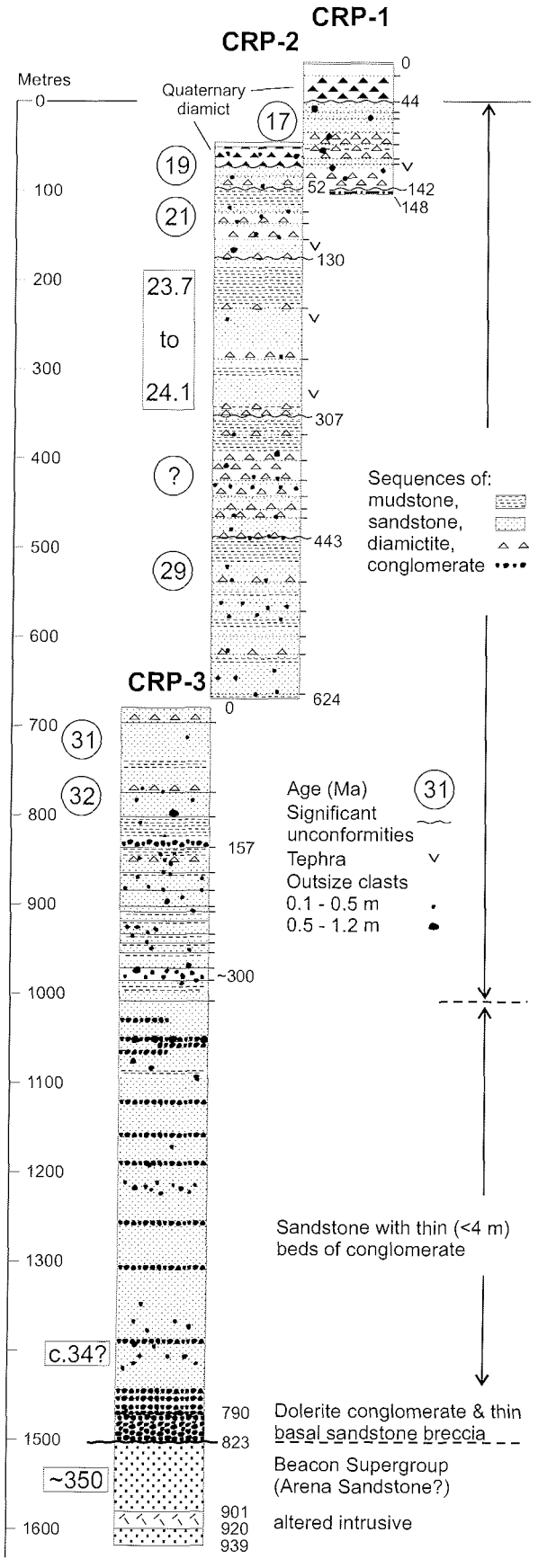

Fig. 7.9 - Composite stratigraphic section from CRP-1, 2A and 3 for the western margin of the victoria Land Basin. Lithologic data and stratigraphic data are from CRST (1998) and CRST (1999) and this volume. Chronology for CRP-2A from Wilson et al. (in press).

changes as sediment becomes coarser downhole to comprise largely sandstone with significant conglomerate beds. Much of the obvious glacial character of this lower section of core has been lost, but reminders persist in the occasional survival of small striated clasts, and the occurrence of isolated and out-sized clasts (>0.1 m) to within a few tens of m of the base of the Cenozoic section. Analysis of a range of biotic and lithological datasets will be important in reaching an understanding of the causes of the cyclicity but possibly none so important as the range of high quality downhole logs and core properties measurements that were recovered from almost the entire drillhole.

Biostratigraphical datums indicate that the upper 200 m of CRP-3 lies in the range 31 to 33 Ma, though deeper strata could also fall within this range. Virtually no siliceous or calcareous microfossils were found below this level in the initial survey, because of either dissolution or higher sedimentation rates or most likely both, though further searches are planned. Preliminary magnetostratigraphic data suggest that the upper 350 m represents C12R – further work on this, and on Sr isotopes from shell material, which occur down to 350 mbsf, will help strengthen the chronostratigraphy in at least the upper part of CRP-3.

Despite the sparse biotic record, marine palynomorphs were extracted as far down as 781 mbsf, revealing further species (eventually to be part of a robust new biostratigraphical scheme for Antarctic margin sediments), but plainly not old enough to have included the warm Eocene Transantarctic Flora of Wilson (1967). Terrestrial palynomorphs, though sparse, also represent an important record of climate back to 34 Ma in the adjacent mountains, which at that time supported, near sea level at least, a relatively cold-climate, low diversity woody vegetation of low scrub or closed forest.

Work on tectonic, depositional, climatic, and chronostratigraphical aspects of the CRP-3 core will continue over the next few months, with results presented at a workshop in Columbus, Ohio, in September, 2000. These results will be published as contributions to the third and final volume of Scientific Results from the Cape Roberts Project in early 2001.

The 3 Cape Roberts drill holes have now cored a total of 72 m of Quaternary (and some Pliocene) strata, and a sequence around 1500 m thick (cored a total of 1523 m but with 31 m overlap between CRP-1 and CRP-2, and a gap of the order of no more than a few tens of m between CRP-2A and CRP-3) (Fig. 7.9; Tab. 7.2). In addition, CRP-3 cored 116 m into the bedrock floor of the basin. Recovery for the entire cored interval has averaged just over 95%.

As work continues on CRP-3, ODP Leg 188 is coring on the continental shelf and slope in Prydz Bay (Fig. 7.10), seeking an early glacial, and if possible a pre-glacial, record of climate from the other side of the continent. The search for more detailed paleoclimatic data is also the main justification for two further ODP legs proposed for

Tab. 7.2 - Data on cored strata at the three Cape Roberts drill sites.

	CRP-1 (1997)	*CRP-2/2A (1998)*	*CRP-3 (1999)*
WATER DEPTH	153 m	178 m	295 m
Depth to top of first core	15 mbsf	5 mbsf	2 mbsf
Quaternary (-Pliocene)	28 m	22 m	0
Older Cenozoic strata	105 m	597 m	821 m
Stratigraphical overlap between holes	31 m overlap between CRP-1 and CRP-2		Gap of m to 10s of m between CRP-2A and CRP-3
Basement			116 m
Recovery (avr – 95%)	86%	94%	97%
TOTAL DEPTH BSF	148 mbsf	624 mbsf	939 mbsf
Downhole logging	Nil	340/540/620 m	910-920 m

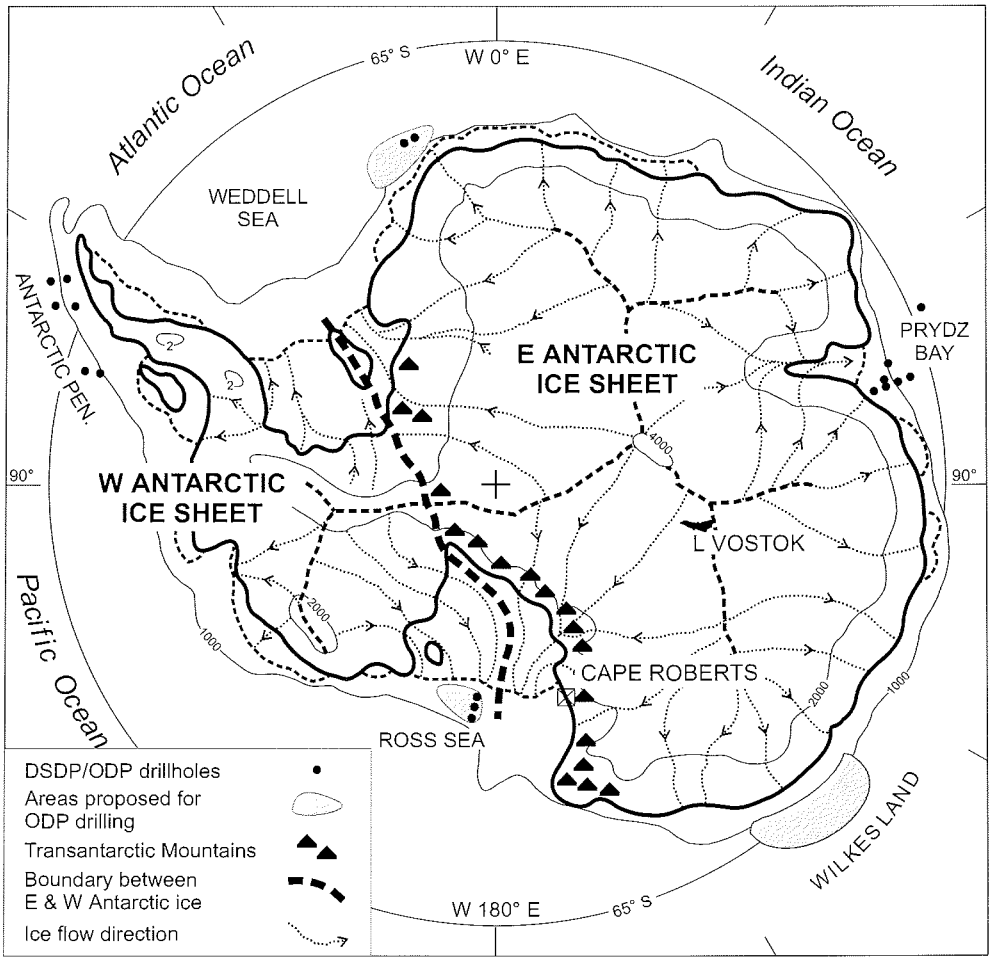

Fig. 7.10 - Map of Antarctica, showing regions where future deep earth sampling is being planned.

the eastern Ross Sea and Wilkes Land. These studies will provide complementary data to those from the Cape Roberts Project for testing ice-sheet and climate models being developed to improve our understanding of the global climate system (Webb & Cooper, 1999). In addition, principals from Cape Roberts countries are examining means by which equipment and experience can be maintained for further work with the Cape Roberts drilling system at a number of places around the Antarctic margin where deep earth sampling may be required for climatic or tectonic objectives. In the longer term this might include sub-glacial Lake Vostok.

References

Aghib F.S., Claps M. & Sarti M., in press. Preliminary report on the Main Carbonate Diagenetic Features of the Oligocene Strata from CRP-2/2A, Victoria Land Basin, Antarctica. *Terra Antartica.*

Allibone A.H., 1992. Low pressure/high temperature metamorphism of Koettlitz Group schists in the Taylor Valley and Ferrar Glacier regions. *New Zealand Journal of Geology and Geophysics*, **35**, 115-127.

Allibone A.H., Cox S.C., Graham I.J., Smillie R.W., Johnstone R.D., Ellery S.G. & Palmer K., 1993a. Granitoids of the Dry Valleys area, southern Victoria Land, Antarctica: field relationships, and isotopic dating. *New Zealand Journal of Geology and Geophysics*, **36**, 281-291.

Allibone A.H., Cox S.C. & Smillie R.W., 1993b. Granitoids of the Dry Valleys area, southern Victoria Land: geochemistry and evolution along the early Paleozoic Antarctic Craton margin. *New Zealand Journal of Geology and Geophysics*, **36**, 299-316.

Anson G.L. & Kodama K.P., 1987. Compaction-induced shallowing of the post-depositional remanent magnetization in a synthetic sediment. *Geophysical Journal of the Royal Astronomical Society*, **88**, 673-692.

Arason P. & Levi S., 1990. Compaction and inclination shallowing in deep sea sediments from the Pacific Ocean. *Journal of Geophysical Research*, **95**, 4501-4510.

Archangelsky S., 1969. Estudio del paleomicroplancton de la Formacíon Río Turbio (Eoceno), Provincia de Santa Cruz. *Ameghiniana*, **6**, 181-218.

Armienti P., Pompilio M. & Rocchi S., 1994. Cenozoic magmatism between Campbell and Icebreaker Glaciers, northern Victoria Land, Antarctica. *Field data reports, Italian Antarctic Research Programme, Earth Sciences, IX ItaliAntartide Expedition*, 39-41.

Askin R.A., 1998. Palynological investigations of Mount Feather Sirius Group samples: recycled Triassic assemblages. In: Wilson G.S. & Barron J. (eds.), *Mount Feather Sirius Group Core Workshop and Collaborative Sample Analysis, Byrd Polar Research Center Report*, **14**, 59-65.

Askin R.A., in press. Spores and pollen from the McMurdo Sound erratics, Antarctica. In: Stilwell J.D. & Feldmann R.M. (eds.), *Paleobiology and Paleoenvironments of Eocene Fossiliferous Erratics, McMurdo Sound, East Antarctica*, Antarctic Research Series, American Geophysical Union.

Askin R.A. & Raine J.I., in press. Oligocene and Miocene Terrestrial Palynology of CRP-2/2A, Victoria Land Basin, Antarctica. *Terra Antartica.*

Baker J.C. & Fielding C.R., 1998. Diagenesis of Glacimarine Miocene Strata in CRP-1, Antarctica. *Terra Antartica*, **5**(3), 647-653.

Baldauf J.G. & Barron J.A., 1991. Diatom biostratigraphy: Kerguelen Plateau and Prydz Bay regions of the Southern Ocean. In: Barron J.A., Larsen B. et al. (eds.), *Proceedings of the Ocean Drilling Program, Scientific Results*, College Station, TX (Ocean Drilling Program), **119**, 547-598.

Balech E., 1975. *Clave ilustrada de dinoflagelados Antarticos.* Publicación del Instituto Antartico Argentino No. **11**, Buenos Aires, 99 p.

Barrett P.J., 1965. Geology of the area between the Axel Heiberg and Shackleton Glaciers, Queen Maud Range, Antarctica – Part 2, Beacon Group. *N Z Journal of Geology & Geophysics*, **3**, 344-370.

Barrett P.J. (ed.),1989. Antarctic Cenozoic history from CIROS-1 drill hole, McMurdo Sound. *DSIR Bulletin*, **245**, Science Information Publishing Centre, Wellington, 254 p.

Barrett P.J. & Webb P.N., 1973. Stratigraphic sections of the Beacon Supergroup (Devonian and older (?) to Jurassic) in south Victoria Land. Victoria University of Wellington, *Antarctic Data Series*, **3**, 165 p.

Barron J.A. & Mahood A.D., 1993. Exceptionally well-preserved early Oligocene diatoms from glacial sediments of Prydz Bay, East Antarctica. *Micropaleontology*, **39**(1), 29-45.

Barrett P.J., McKelvey B.C. & Walker B.C., 1986. Sand provenance. *DSIR Bulletin*, **237**, 137-144.

Barrett P.J., Henrys S.A., Bartek L.R., Brancolini G., Busetti M., Davey F.J., Hannah M.J. & Pyne A.R., 1995. Geology of the margin of the Victoria Land basin off Cape Roberts, southwest Ross Sea. In: A.K. Cooper, P.F. Barker & G. Brancolini (eds.), *Geology and Seismic Stratigraphy of the Antarctic Margin, Antarctic Research Series*, **68**, AGU, Washington, 183-208.

Barron J.A., Baldauf J.G., Barrera E., Caulet J.-P., Huber B.T., Keating B.H., Lazarus D., Sakai H., Thierstein H.R. & Wei W., 1991. Biochronologic and magnetochronologic synthesis of Leg 119 sediments from the Kerguelen Plateau and Prydz Bay, Antarctica. In: Barron J.A., Larsen B. et al (eds.), *Proceedings of the Ocean Drilling Program, Scientific Results*, College Station, TX (Ocean Drilling Program), **119**, 813-847.

Bellanca A., Neri R. & Sprovieri M., in press. Bulk Geochemistry of the Sand Fraction from CRP-2/2A, Victoria Land Basin, Antarctica. *Terra Antartica.*

Berger A., 1984. Accuracy and frequency stability of the earth's orbital elements during the Quaternary. In: Berger A.L., Imbrie J., Hays J., Kukla G. & Saltzman B. (eds.), *Milankovitch and Climate, Part 1*, Reidel Publ. Co., Dordrecht, 3-39.

Berger A. & Loutre M.F., 1994. Astronomical forcing through geological time. In: de Boer P.L. & Smith D.G. (eds.), *Orbital forcing and cyclic sequences*, IAS Special Publication, **19**, 15-24.

Berggren W.A., Kent D.V., Swisher III C.C. & Aubrey M.P., 1995. A revised Cenozoic geochronology and biostratigraphy. In: Berggren W.A., Kent D.V., Aubrey M.P. & Hardenbol J. (eds.), *Geochronology, Time Scales, and Stratigraphic Correlation, Society of Economic Paleontologists and Mineralogists, Special Publication*, **54**, 129-212.

Berner R.A., 1984. Sedimentary pyrite formation: An update. *Geochimica et Cosmochimica Acta*, **48**, 605-615.

Bernhard J.M., 1987. Foraminiferal biotopes in Explorers Cove, McMurdo Sound, Antarctica. *Journal of Foraminiferal Research*, **17**, 286-297.

Beu A.G. & Dell R.K., 1989. Mollusca. In: Barrett P.J. (ed.), *Antarctic Cenozoic history from the CIROS-1 drillhole, McMurdo Sound, DSIR Bulletin*, **245**, 135-141.

Blackman R.B. & Tukey J.W., 1958. *The measurement of power spectra from the point of view of communication engineering.* Dover Publications, New York, 190 p.

Blakely R.J., 1974. Geomagnetic reversals and crustal spreading rates during the Miocene. *Journal of Geophysical Research*, **79**, 2979-2985.

Blakely R.J. & Cox A., 1972. Evidence for short geomagnetic polarity intervals in the early Cenozoic. *Journal of Geophysical Research*, **77**, 7065-7072.

Blatt H., 1992. *Sedimentary Petrology.* 2nd ed., W.H. Freeman (ed.), New York.

Bohaty S.M. & Harwood D.M., in press. Ebridian and silicoflagellate biostratigraphy from Eocene McMurdo erratics and the Southern Ocean. In: Stilwell J.D. & Feldmann R.M. (eds.), *Paleobiology and Paleoenvironments of Eocene Fossiliferous Erratics, McMurdo Sound, Antarctica*, Antarctic Research Series, American Geophysical Union.

Bozzo E., Damaske D., Caneva G., Chiappini M., Ferraccioli F., Gambetta M. & Meloni A., 1997. A High Resolution Aeromagnetic Survey over Proposed Drill Sites Off Shore of Cape Roberts in the Southwestern Ross Sea (Antarctica). In: Ricci C.A. (ed.), *The Antarctic Region: Geological Evolution and Processes*, Terra Antartica Publication, Siena, 1129-1134.

Brancolini G., Busetti M., Marchetti ,A., De Santis L., Zonolla C., Cooper A.K., Cochrane G.R., Zayatz I., Belyaev V., Knyazev M., Vinnikovskaya O., Davey F.J. & Hinz K., 1995. Descriptive text for the seismic stratigraphic atlas of the Ross Sea, Antarctica. In: *Geology and Seismic Stratigraphy of the Antarctic Margin, Antarctic Research Series*, **68**, Am. Geophys. Union, Washington, D.C., 209-233.

Breitzke M., Grobe H., Kuhn G. & Müller P., 1998. Full waveform ultrasonic transmission seismograms: A fast new method for determination of physical and sedimentological parameters of

marine sediment cores. *Journal Geophysical Research*, **101**(B10), 22,123-22,141.

Bridle I. M. & Robinson P. A., 1990. Diagenesis. In: Barrett P. J. (ed.), *Antarctic Cenozoic history from the CIROS-1 drillhole McMurdo Sound. DSIR Bulletin*, **245**, 201-207.

Brink J.D. & Jarrard R.D., in press. Petrophysics of Core Plugs from CRP-2, Victoria Land Basin, Antarctica. *Terra Antartica*.

Brink J.D., Jarrard R.D., Bücker C. & Wonik T., in press. Sedimentological Interpretation of Well Logs from CRP-2/2A, Victoria Land Basin, Antarctica: Glacial and Sea-Level Significance. *Terra Antartica*.

Bucher G. & E.R. Decker, 1976. Down hole temperature measurements in DVDP 15, McMurdo Sound. *Dry Valley Drilling Project Bulletin*, **7**, 111-112.

Bücker C., Jarrard R.D., Brink J.D. & Wonik T., in press a. Analysis of Downhole Logging Data from CRP-2/2A, Victoria Land Basin, Antarctica: a Multivariate Statistical Approach. *Terra Antartica*.

Bücker C., Wonik T. & Jarrard R.D., in press b. Temperature and Salinity Profile in CRP-2/2A, Victoria Land Basin, Antarctica. *Terra Antartica*.

Cande S.C. & Kent D.V., 1992a. A new geomagnetic polarity time scale for the late Cretaceous and Cenozoic. *Journal of Geophysical Research*, **97**, 13917-13951.

Cande S.C. & Kent D.V., 1992b. Ultrahigh resolution marine magnetic anomaly profiles: A record of continuous paleointensity variations? *Journal of Geophysical Research*, **97**, 15075-15083.

Cande S.C. & Kent D.V., 1995. Revised calibration of the geomagnetic polarity time scale for the Late Cretaceous and Cenozoic. *Journal of Geophysical Research*, 100, 6093-6095.

Cande S.C. & LaBrecque J.L., 1974. Behaviour of the Earth's palaeomagnetic field from small scale marine magnetic anomalies. *Nature*, **247**, 26-28.

Cande S.C., Stock J.M., Mueller D. & Ishihara T., 2000. Cenozoic Motion between East and West Antarctica. *Nature*, **404**, 146-150.

Cape Roberts Science Team, 1998. Initial Report on CRP-1, Cape Roberts Project, Antarctica. *Terra Antartica*, **5**(1), 1-187.

Cape Roberts Science Team, 1998a. Background to CRP-1, Cape Roberts Project, Antarctica. *Terra Antartica*, **5**, 1-30.

Cape Roberts Science Team, 1998b. Quaternary Strata in CRP-1, Cape Roberts Project, Antarctica. *Terra Antartica*, **5**(1), 31-61.

Cape Roberts Science Team, 1998c. Miocene Strata in CRP-1, Cape Roberts Project, Antarctica. *Terra Antartica*, **5**(1), 63-124.

Cape Roberts Science Team, 1998d. Summary Results from CRP-1, Cape Roberts Project, Antarctica. *Terra Antartica*, **5**(1), 125-138.

Cape Roberts Science Team, 1999. Studies from the Cape Roberts Project, Ross Sea, Antarctica. Initial Report on CRP-2/2A. *Terra Antartica*, **6**(1/2), 1-173. With Supplement, 245 p.

Carlson P.R., Powell R.D. & Phillips A.C., 1992. Submarine sedimentary features on a fjord delta front, Queen Inlet, Glacier Bay, Alaska. *Canadian Journal of Earth Sciences*, 29, 565-573.

Carlson P.R., Powell R.D. & Rearic D.M., 1989. Turbidity-current channels in Queen Inlet, Glacier Bay, Alaska. *Canadian Journal of Earth Sciences*, 26, 807-820.

Chamley H., 1989. *Clay Sedimentology*. Springer, Berlin, 623 p.

Chen P.Y., 1977. *Table of key lines in x-ray powder diffraction patterns of minerals in clays and associated rocks*. Indiana Department of Natural Resources, Geological Survey Occasional Paper 21, Bloomington, Indiana.

Claps M. & Aghib F.S., 1998. Carbonate Diagenesis in Miocene Sediments from CRP-1, Victoria Land Basin, Antarctica. *Terra Antartica*, **5**(3), 655-660.

Claps M. & Masetti D., 1994. Milankovitch periodicities recorded in Cretaceous deep-sea sequences from Southern Alps (Northern Italy). In: de Boer P.L. & Smith D.G. (eds.), *Orbital forcing and cyclic sequences*, IAS Special Publication, **19**, 99-107.

Claps M., Niessen F. & Florindo F., in press. High-Frequency Analysis of Physical Properties from CRP-2/2A, Victoria Land Basin, Antarctica, and Implication for Sedimentation Rate. *Terra Antartica*.

Coccioni R. & Galeotti S., 1997. Foraminiferal Biostratigraphy and Paleoecology of the CIROS-1 Core from McMurdo Sound (Ross Sea, Antarctica). *Terra Antartica*, **4**(2), 103-117.

Cooper A.K. & Davey F.J. (eds.), 1987. *The Antarctic Continental Margin: Geology & Geophysics of the Western Ross Sea, Earth Sci.Ser.* Circum-Pacific Council for Energy & Mineral Resources. Earth Sciences Series, **5B**, Houston, Texas, 253 p.

Cooper A.K., Davey F.J. & Behrendt J.C., 1987. Seismic stratigraphy and structure of the Victoria Land Basin, western Ross Sea, Antarctica. In: A.K. Cooper & F.J. Davey (eds.), *The Antarctic continental Margin: Geology and Geophysics of the Western Ross Sea, Circum-Pacific Council Energy and Mineral Resources, Earth Sci. Ser.*, **5B**, Houston, TX, 93-118.

Cranwell L.M., 1964. Hystrichospheres as an aid to Antarctic dating with special reference to the recovery of *Cordosphaeridium* in erratics at McMurdo Sound. *Grana Palynologica*, **5**(3), 397-405.

de Boer P.L & Smith D.G., 1994. Orbital forcing and cyclic sequences. In: de Boer P.L. & Smith D.G. (eds.), *Orbital forcing and cyclic sequences*, IAS Special Publication, **19**, 1-14.

Dekkers M.J., 1989. Magnetic properties of natural pyrrhotite. II. High- and low-temperature behaviour of J_{rs} and TRM as function of grain size. *Physics of the Earth and Planetary Interiors*, **57**, 266-283.

Dell R.K. & Fleming C.A., 1975. Oligocene-Miocene bivalve Mollusca and other macrofossils from Sites 270 and 272 (Ross Sea), DSDP Leg 28. *Initial Reports of the Deep-Sea Drilling Project*, **28**, 693-703.

Diggle P.J., 1990. *Time series. A Biostatistical Introduction*. Oxford University Press, London, 257 p.

Dowdle W.L. & Cobb W.M., 1975. Static formation temperature from well logs – an empirical method. *J. Petroleum Tech.*, **27**, 1326-1330.

Ehrmann W.U., 1997. Smectite Concentrations and Crystallinities: Indications for Eocene Age of Glaciomarine Sediments in the CIROS-1 Drill Hole, McMurdo Sound, Antarctica. In: Ricci C.A. (ed.), *The Antarctic Region: Geological Evolution and Processes*, Terra Antartica Publications, Siena, 771-780.

Ehrmann W.U., 1998a. Implications of late Eocene to early Miocene clay mineral assemblages in McMurdo Sound (Ross Sea, Antarctica) on paleoclimate and ice dynamics. *Palaeogeography, Palaeoclimatology, Palaeoecology*, **139**, 213-231.

Ehrmann W.U., 1998b. Lower Miocene and Quaternary Clay Mineral Assemblages from CRP-1. *Terra Antartica*, **5**(3), 613-619.

Ehrmann W.U. & Mackensen A., 1992. Sedimentological evidence for the formation of an East Antarctic ice sheet in Eocene/Oligocene time. *Palaeogeography, Palaeoclimatology, Palaeoecology*, **93**, 85-112.

Ehrmann W.U., Melles M., Kuhn G. & Grobe H., 1992. Significance of clay mineral assemblages in the Antarctic Ocean. *Marine Geology*, **107**, 249-273.

Elliot D.H., Fleming T.H., Haban M.A. & Siders M.A., 1995. Petrology and Mineralogy of the Kirkpatrick basalt and Ferrar Dolerite, Mesa Range region, North Victoria Land, Antarctica. *Contribution to Antarctic Research IV*, Antarctic Research Series, **67**, 103-141.

Elliot D.H., Haban M.A. & Siders M.A., 1986. The Exposure Hill formations, Mesa Range. In: Stump E. (ed.), *Geological Investigations in Northern Victoria Land, Antarctic Research Series*, **46**, 267-278.

Erickson S.N. & Jarrard R.D., 1998. Porosity/formation-factor relationships for high-porosity siliciclastic sediments from Amazon Fan. *Geophysical Research Letters*, **25**, 2309-2312.

Fenner J., 1984. Eocene-Oligocene planktic diatom stratigraphy in the low latitudes and the high southern latitudes. *Micropaleontology*, **30**(4), 319-342.

Fielding C.F., Naish T.R., Woolfe K.J. & Lavelle M., in press, Facies Analysis and Sequence Stratigraphy fromCRP-2/2A, Victoria Land Basin, Antarctica *Terra Antartica*.

Fielding C.R., Woolfe K.J., Howe J.A. & Lavelle M., 1998. Sequence Stratigraphic Analysis of CRP-1, Cape Roberts Project, McMurdo Sound, Antarctica. *Terra Antartica*, **5**(3), 353-361.

Filkorn H.F., 1994. Fossil Scleractinian corals from James Ross Basin, Antarctica. *AGU, Antarctic Research Series*, **65**, 96 p.

Findlay R.H., Skinner D.N.B. & Craw D., 1984. Lithostratigraphy and structure of the Koettlitz Group, McMurdo Sound, Antarctica. *New Zealand Journal of Geology and Geophysics*, **27**, 513-536.

Fischer A.G., 1986. Climatic rhythms recorded in strata. *Ann. Rev.*

Earth and Planetary Sciences, **14**, 351-376.

Fischer A.G. & Bottjer D.J., 1991. Orbital forcing and sedimentary sequences. *Journal of Sedimentary Petrology*, **61**, 1063-1069.

Fischer A.G., de Boer P.L. & Premoli Silva I., 1990. Cyclostratigraphy. In: Ginsburg R.N. & Beaudoin B. (eds.), *Cretaceous Resources, Events and Rhythms - Background and Plans for Research*, Kluwer Academic Publ., Dordrecht, 139-172.

Fischer A.G., Herbert T.D., Napoleone G., Premoli Silva I. & Ripepe M., 1991. Albian Pelagic Rhythms (Piobbico Core). *Journal of Sedimentary Petrology*, **61**, 1164-1172.

Fitzgerald P.G., 1992. The Transantarctic Mountains of southern Victoria Land: The application of apatite-fission track analysis to a rift shoulder uplift. *Tectonics*, **11**, 634-662.

Floyd P.A. & Whinchester J.A., 1978. Identification and discrimination of altered and metamorphosed volcanic rocks using immobile elements. *Chem.Geol.*, **21**, 291-306

Foscolos A.E., 1990. Catagenesis of argillaceous sedimentary rocks. In: McIlreath I.A. & Morrow D.W. (eds.), *Diagenesis*, Runge Press, Ltd., Ottawa, Ontario, 177-187.

Galeotti S., Cita M.B. & Coccioni R., in press. Correlation of Foraminifera from CRP2/2A, Victoria Land Basin, Antarctica, with European Epochs. *Terra Antartica*.

Gazdzicki A. & Stolarski J., 1992. An Oligocene record of the coral *Flabellum* from Antarctica. *Polish Polar Research*, **13**(3-4), 265-272.

George A., 1989. Sand provenance. *DSIR Bulletin*, **245**, 145-167.

Gladenkov A.Y., 1998. Oligocene and lower Miocene diatom zonation in the North Pacific. *Stratigraphy and Geological Correlation (Stratigrafiya, Geologicheskaya Korrelyatsiya)*, **6**(2), 150-164.

Gladenkov A.Y. & Barron J.A., 1995. Oligocene and early middle Miocene diatom biostratigraphy of Hole 884B. In: Rea D.K., Basov I.A., Scholl D.W. & Allan J.F. (eds.), *Proceedings of the Ocean Drilling Program, Scientific Results*, College Station, TX (Ocean Drilling Program), **145**, 21-41.

Gombos A.M. Jr., 1977. Paleogene and Neogene diatoms from the Falkland Plateau and Malvinas Outer Basin. In: Barker P.F., Dalziel I.W.D. et al. (eds.), *Initial Reports of the Deep Sea Drilling Project*, Washington, U.S. Government Printing Office, **36**, 575-687.

Gombos A.M. Jr. & Ciesielski P.F., 1983. Late Eocene to early Miocene diatoms from the southwest Atlantic. In: Ludwig W.J., Krasheninikov V.A. et al. (eds.), *Initial Reports of the Deep Sea Drilling Project*, Washington (U.S. Government Printing Office), **71**, 583-634.

Goodman D.K. & Ford Jr. L.N., 1983. Preliminary dinoflagellate biostratigraphy for the middle Eocene to lower Oligocene from the southwest Atlantic Ocean. *Initial Reports of the Deep Sea Drilling Project*, Government Printing Office, Washington, D.C., **71**, 859-877.

Griffin J.J., Windom H. & Goldberg E.D., 1968. The distribution of clay minerals in the World Ocean. *Deep-Sea Res.*, **15**, 433-459.

Griggs P., 1981. Tertiary dinoflagellate morphologies, Santos Basin, Brazil. *"Hexrose" Conference on Modern and fossil dinoflagellates*. Tubingen, West Germany, August 31-September 4, 1981. Poster session handout, unpaged.

Grindley G.W. & Warren G., 1964. Stratigraphic nomenclature and correlation in the western part of the Ross Sea. In: Adie R.J. (ed.), *Antarctic geology*, Amsterdam, North Holland Publishing Co., 314-333.

Grunow A.M., 1999. Gondwana events and palaeogeography: A palaeomagnetic review. *Journal of African Earth Science*, **28**, 53-69.

Gunn B.M. & Warren G., 1962. Geology of Victoria Land between the Mawson and Mulock Glaciers, Antarctica. *New Zealand Geological Survey Bulletin*, **71**, 157p.

Hajós M., 1976. Upper Eocene and lower Oligocene diatomaceae, archaeomonadaceae, and silicoflagellatae in southwestern Pacific sediments, DSDP Leg 29. In: Hollister C.D., Craddock C. et al. (eds.), *Initial Reports of the Deep Sea Drilling Project*, Washington, U.S. Government Printing Office, **35**, 817-884.

Hall S.A., 1977. Cretaceous and Tertiary dinoflagellates from Seymour Island, Antarctica. *Nature*, **267**, 239-241.

Hambrey M.J., Barrett P.J. & Robinson P.H., 1989. Stratigraphy. In: Barrett P.J. (ed.), Antarctic Cenozoic history from the CIROS-1 drillhole, McMurdo Sound. *DSIR Bulletin*, **245**, 23-48.

Hamilton E.L., 1971. Elastic properties of marine sediments. *Journal of Geophysical Research*, **76**, 579-604.

Hamilton E.L., 1976. Variations of density and porosity with depth in deep-sea sediments. *Journal of Sedimentary Petrology*, **46**, 280-300.

Hamilton R.J., Sorlien C.C., Luyendyk B.P., Bartek L.R. & Henrys S.A., 1998. Tectonic Regimes and Structural Trends off Cape Roberts, Antarctica. *Terra Antartica*, **5**(3), 261-272.

Hannah M.J., 1997. Climate Controlled Dinoflagellate Distribution in Late Eocene-Earliest Oligocene Strata from CIROS-1 Drillhole, McMurdo Sound, Antarctica. *Terra Antartica*, **4**(2), 73-78.

Hannah M.J., Wrenn J.H. & Wilson G.J., 1998. Early Miocene and Quaternary Marine Palynomorphs from Cape Roberts Project CRP-1, McMurdo Sound, Antarctica. *Terra Antartica*, **5**(3), 527-538.

Hannah M.J., Cita M.B., Coccioni R. & Monechi S., 1997. The Eocene/Oligocene Boundary at 70° South, McMurdo Sound, Antarctica. *Terra Antartica*, **4**(2), 79-87.

Harland R., 1983. Distribution maps of Recent dinoflagellate cysts in bottom sediments from the North Atlantic Ocean and adjacent seas. *Paleontology*, **26**, 321-387.

Harland R., Pudsey C.J., Howe J.A. & Fitzpatrick M.E.J., 1998. Recent dinoflagellate cysts in a transect from the Falkland Trough to the Weddell Sea, Antarctica. *Paleontology*, **41**(6), 1093-1131.

Harms J.C., Southard J.B., Spearing D.R. & Walker R.G., 1975. Depositional environments as interpreted from primary sedimentary structures and stratification sequences. *Society of Economic Paleontologists and Mineralogists, Short Course* 2, 161 p.

Harris F.J., 1978. On the use of windows for harmonic analysis with the discrete Fourier transform. *Proceedings of the IEEE*, **66**, 51-83.

Hartl P., Tauxe L. & Constable C.G., 1993. Early Oligocene geomagnetic field behaviour from Deep Sea Drilling Project Site 522. *Journal of Geophysical Research*, **98**, 19649-19665.

Harwood D.M., 1986. Diatoms. In: Barrett P.J. (ed.), *Antarctic Cenozoic History from the MSSTS-1 Drillhole, McMurdo Sound, DSIR Bulletin*, **237**, 69-107.

Harwood D.M., 1989. Siliceous microfossils. In: Barrett P.J. (ed.), *Antarctic Cenozoic History from the CIROS-1 Drillhole, McMurdo Sound, DSIR Bulletin*, **245**, 67-97.

Harwood D.M. & Bohaty S.M., in press. Marine diatom assemblages from Eocene and younger erratics, McMurdo Sound, Antarctica. In: Stilwell J.D. & Feldmann R.M. (eds.), *Paleobiology and Paleoenvironments of Eocene Fossiliferous Erratics, McMurdo Sound, Antarctica*, Antarctic Research Series, American Geophysical Union.

Harwood D.M. & Maruyama T., 1992. Middle Eocene to Pleistocene diatom biostratigraphy of Southern Ocean sediments from the Kerguelen Plateau, Leg 120. In: Wise S.W. Jr., Schlich R. et al. (eds.), *Proceedings of the Ocean Drilling Program, Scientific Results*, College Station, TX, Ocean Drilling Program, **120**(2), 683-733.

Harwood D.M., Bohaty S.M. & Scherer R.P., 1998. Lower Miocene Diatom Biostratigraphy of the CRP-1 Drillcore, McMurdo Sound, Antarctica. *Terra Antartica*, **5**(3), 499-514.

Harwood D.M., Barrett P.J., Edwards A.R., Rieck H.J. & Webb P.-N., 1989a. Biostratigraphy and chronology. In: Barrett P.J. (ed.), *Antarctic Cenozoic History from the CIROS-1 Drillhole, McMurdo Sound, DSIR Bulletin*, **245**, 231-239.

Harwood D.M., Scherer R.P. & Webb P.-N., 1989b. Multiple Miocene productivity events in West Antarctica as recorded in upper Miocene sediments beneath the Ross Ice Shelf (Site J-9). *Marine Micropaleontology*, **15**, 91-115.

Harwood D.M., Lazarus D., Abelmann A., Aubry M.P., Berggren W.A., Heider F., Inokuchi H., Maruyama T., McCartney K., Wei W. & Wise S.W. Jr., 1992. Neogene integrated magneto-biostratigraphy of the Southern Kerguelen Plateau, ODP Leg 120. *Proceedings of the Ocean Drilling Program, Scientific Results*, **120**, College Station, TX, 1031-1052.

Hayes J.B., 1979. Sandstone diagenesis — the hole truth. In: Scholle P.A. & Schluger P.R. (eds.), *Aspects of Diagenesis, SEPM Special Publication*, **26**, 127-139.

Hedberg H.D., 1936. Gravitational compaction of clays and shales.

American Journal of Science, Series 5, **31**, 241-287.

Henrys S.A., Bartek L.R., Brancolini G., Luyendyk B., Hamilton R.J., Sorlien C.C. & Davey F.J., 1998. Seismic Stratigraphy of the Pre-Quaternary Strata off Cape Roberts, and their Correlation with Strata Cored in the CIROS-1 Drill Hole, McMurdo Sound. *Terra Antartica*, **5**(3), 273-279.

Hinnov L.A. & Goldhammer R.K., 1991. Spectral analysis of the Middle Triassic Latemar Limestone. *Journal of Sedimentary Petrology*, **61**, 1173-1193.

Hornig I., 1993. High –Ti and Low-Ti Tholeites in Jurassic Ferrar Group, Antarctica. *Geologisches Jahrbuch*, **E47**, 335-369

House M.R., 1995. Orbital forcing timescales. In: House M.R. & Gale A.S. (eds.), *Orbital Forcing Timescales and Cyclostratigraphy*, The Geological Society of London, London, 1-18.

Hrouda F., 1994. A technique for the measurement of thermal changes of magnetic susceptibility of weakly magnetic rocks by the CS-2 apparatus and KLY-2 Kappabridge. *Geophysical Journal International*, **118**, 604-612.

Hunt C.P., Moskowitz B.M. & Banerjee S.K. 1995. Magnetic properties of rocks and minerals. *Rock Physics and Phase Relations, AGU Reference Shelf*, **3**, 189-204.

Hutcheon I., 1990. Aspects of the diagenesis of coarse-grained siliciclastic rocks. In: McIlreath I.A. & Morrow D.W. (eds.), *Diagenesis*, Runge Press, Ltd., Ottawa, Ontario, 165-176.

Jacobs J.A., 1994. *Reversals of the Earth's Magnetic Field*. 2nd ed., Cambridge University Press, 346 p.

Jarrard R.D., Brink J.D., Bücker C., Wonik T., Wilson T. & Paulsen T., in press. Bedding Dips from CRP-2A, Victoria Land Basin, Antarctica. *Terra Antartica*.

Jonkers H.A. & Taviani M., 1998. Lower Miocene Macrofossils from CRP-1 Drillhole, Cape Roberts (Victoria Land Basin, Antarctica). *Terra Antartica*, **5**(3), 493-498.

Kemp E.M., 1975. Palynology of Leg 28 Drill Sites, Deep Sea Drilling Project. *Initial Reports of The Deep Sea Drilling Project*, Government Printing Office, Washington, D.C., **28**, 599-623.

Kemp E.M. & Harris W.K., 1977. The palynology of early Tertiary sediments, Ninetyeast Ridge, Indian Ocean. *Special papers in palaeontology*, **19**, 70 p.

Kirschvink J.L., 1980. The least-squares line and plane and the analysis of palaeomagnetic data. *Geophysical Journal of the Royal Astronomical Society*, **62**, 699-718.

Kretz R., 1983. Symbols for rock forming minerals. *American Mineralogist*, **68**, 277-279.

Krissek L. & Kyle P.R., in press. Geochemical Indicators of Weathering Cenozoic Palaeoclimate and Provenance from Fine-Grained Sediments in CRP-2/2A, Victoria Land Basin, Antarctica. *Terra Antartica*.

Krumbein W.C., 1941. Measurement and geological significance of shape and roundness of sedimentary particles. *Journal of Sedimentary Petrology*, **11**, 64-72.

Kyle R.A., 1976. Palaeobotanical studies of the Permian and Triassic Victoria Group (Beacon Supergroup) of south Victoria Land, Antarctica. *Unpublished Ph.D dissertation*, Victoria University of Wellington, New Zealand, 306 p.

Kyle R.A., 1977. Palynostratigraphy of the Victoria Group of South Victoria Land, Antarctica. *New Zealand Journal of Geology and Geophysics*, **20**, 1081-1102.

Kyle P.R., 1999. Ferrar Dolerite Clasts from CRP-1 Drillcore. *Terra Antartica*, **5**(3), 611-612.

Kyle R.A. & Schopf J.M., 1982. Permian and Triassic palynostratigraphy of the Victoria Group, Transantarctic Mountains. In: Craddock J.C. (ed.), *Antarctic Geoscience*, University of Wisconsin Press, Madison, p. 649-659.

Lamothe M., Hillaire-Marcel C. & Page P., 1983. Decouverte de concretions calcaires dans le till de Gentilly, basses-terres du Saint-Laurent, Quebec. *Canadian Journal of Earth Sciences*, **20**, 500-505.

Lanci L. & Lowrie W., 1997. Magnetostratigraphic evidence that 'tiny wiggles' in the oceanic magnetic anomaly record represent geomagnetic paleointensity variations. *Earth and Planetary Science Letters*, **148**, 581-592.

Leckie M.A. & Webb P.N., 1985. Late Paleogene and early Neogene foraminifers of Deep Sea Drilling Project Site 270, Ross Sea, Antarctica. In: Kennett J.P., Von der Broch C.C. et al. (eds.), *Initial Reports of the Deep Sea Drilling Project* XC, 1093-1142.

Levy R.H. & Harwood D.M., in press. Marine palynomorph biostratigraphy and age(s) of the McMurdo Sound erratics. In: Stillwell J.D. & Feldmann R.M. (eds.), *Paleobiology and paleoenvironments of Eocene fossiliferous erratics, McMurdo Sound, East Antarctica, AGU Antarctic Research Series*.

Li Y. & Schmitt D.R., 1997. Well-bore bottom stress concentration and induced core fractures. *American Association of Petroleum Geologists Bulletin*, **81**, 1909-1925.

Li Y. & Scmitt D.R., 1998. Drilling-induced core fractures and in situ stress. *Journal of Geophysical Research*, **103**, 5225-5239.

Lorenz J.C., Finley S.J. & Warpinski N.R., 1990. Significance of coring-induced fractures in Mesaverde core, northwestern Colorado. *American Association of Petroleum Geologists Bulletin*, **74**, 1017-1029.

Lowrie W. & Lanci L., 1994. Magnetostratigraphy of Eocene-Oligocene boundary sections in Umbria, Italy: No evidence for short subchrons within chron 13r. *Earth and Planetary Science Letters*, **126**, 247-258.

Magara K., 1980. Comparison of porosity-depth relationships of shale and sandstone. *Journal of Petroleum Geology*, **3**, 175-185.

Mahood A.D., Barron J.A. & Sims P.A., 1993. A study of some unusual, well-preserved Oligocene diatoms from Antarctica. *Nova Hedwigia, Beiheft*, **106**, 243-267.

Marret F. & De Vernal A., 1997. Dinoflagellate cyst distribution in surface sediments of the southern Indian Ocean. *Marine Micropaleontology*, **29**, 367-392.

McCollum D.W., 1975. Diatom stratigraphy of the Southern Ocean. In: Hayes D.E., Frakes L.A. et. al. (eds.), *Initial Reports of the Deep Sea Drilling Project*, Washington, U.S. Govt. Printing Office, **28**, 515-571.

McIntosh W.C., in press. $^{40}Ar/^{39}Ar$ Geochronology of Volcanic Tephra and Clasts in CRP-2A, Victoria Land Basin, Antarctica. *Terra Antartica* (in press).

McIntyre D.J. & Wilson G.J., 1966. Preliminary palynology of some Antarctic Tertiary erratics. *New Zealand Journal of Botany*, **4**, 315-321.

Mildenhall D.C., 1989. Terrestrial palynology. In: Barrett P.J. (ed.), Antarctic Cenozoic history from the CIROS-1 drillhole, McMurdo Sound, *DSIR Bulletin*, **245**, 119-127.

Moos D., Jarrard R.D., Paulsen T., Scholz E. & Wilson T., in press. Acoustic Borehole Televiewer Results from CRP-2A, Victoria Land Basin, Antarctica. *Terra Antartica*.

Morgans H.E.G., Scott G.H., Beu A.G., Graham I.J., Mumme T.C., St George W. & Strong C.P., 1996. New Zealand Cenozoic time scale (1996). *Institute of Geological and Nuclear Sciences, Science Report*, **96/38**.

Naish T.R. & Kamp P.J.J., 1997. Sequence Stratigraphy of 6th order (41 k.y.) Pliocene-Pleistocene Cyclothems, Wanganui Basin, New Zealand: A Case for the Regressive Systems Tract. *Geological Society of America Bulletin*, **109**, 979-999.

Naish T.R., Browne G.H., Carter R.M., Kamp P.J.J. & Wehland F., in press a. Forced Regressions During a Period of Glacio-eustatic Sea-level Cyclicity: Sytematics and Definition of the Regressive Systems Tract. *Bulletin of the Geological Society of America*.

Naish T.R., Woolfe K.J., Dunn A.G., Claps M., Stewart L. & Fielding C.F., in press b. The Periods of Depositional Cyclicity in CRP2/2A, Victoria Land Basin, Antarctica: Frequency Analysis of Grain Size Data and some Palaeoclimatic Implications. *Terra Antartica*.

Niessen F. & Jarrard R.D., 1998. Velocity and Porosity of Sediments from CRP-1 Drillhole, Core, Ross Sea, Antarctica. *Terra Antartica*, **5**(3), 311-318.

Niessen F., Jarrad R.D. & Bücker C., 1998. Log-Based Physical Properties of the CRP-1 Core, Ross Sea, Antarctica. *Terra Antartica*, **5**(3), 299-310.

Niessen F., Kopsch K. & Polozek K., in press. Velocity and Porosity from CRP-2/2A, Victoria Land Basin, Antarctica. *Terra Antartica*.

Paillard D., Labeyrie L. & Yiou P., 1996. Macintosh program performs time-series analysis. *Eos Trans. AGU*, **77**, 379 p.

Paulsen T., Wilson T.J., Moos D., Jarrard R.D. & Wilson G.S., in press. Orientation of CRP-2A Core, Victoria Land Basin. *Terra*

Antartica.

Pestiaux P. & Berger A., 1984. An optimal approach to the spectral characteristics of deep-sea climatic records. In: Berger A.L., Imbrie J., Hays J., Kukla G. & Saltzman B. (eds.), *Milankovitch and Climate, Part 1*, Reidel Publ. Co., Dordrecht, 417-445.

Plint A.G., 1988. Sharp-Based Shoreface Sequences and "Offshore Bars" in the Cardium Formation of Alberta: Their Relationship to Relative Changes in Sea-level. In: Wilgus C.K. et al. (eds), *Sea-level changes: an integrated approach, Society of Economic Paleontologsts and Mineralogists*, **42**, 357-370.

Pocknall D.T., 1989. Late Eocene to Early Miocene vegetation and climate history of New Zealand. *Journal of the Royal Society of New Zealand*, **19**(1), 1-18.

Pocknall D.T. & Mildenhall D.C., 1984. Late Oligocene-early Miocene spores and pollen from Southland, New Zealand. *New Zealand Geological Survey Paleontological Bulletin*, **51**, 66 p.

Posamentier H.W., Jervey M.T. & Vail P.R., 1988. Eustatic Controls on Clastic Deposition I - Conceptual Framework. In: Wilgus C.K. et al. (eds), *Sea-level changes: an inegrated approach, Society of Economic Paleontologsts and Mineralogists*, **42**, 109-124.

Powell R.D., 1990. Grounding-line fans and their growth to ice-contact deltas. In: Dowdswell J.D. & Scourge J.D. (eds.), *Glacimarine environments:processes and sediments*, Geological Society of London Special Publication No. **53**, 53-73.

Powell R.D., Hambrey M.J. & Krissek L.A., 1998. Quaternary and Miocene Glacial and Climatic History of the Cape Roberts Drillsite Region, Antarctica. *Terra Antartica*, **5**(3), 341-352.

Powell R.D., Krisseck L.A. & van der Meer J.J.M., in press. Preliminary Depositional Environmental Analysis of CRP-2/2A, Victoria Land Basin, Antarctica: Palaeoglaciological and Palaeoclimatic Inferences. *Terra Antartica.*

Powers M.C., 1953. A new roundness scale for sedimentary particles. *Journal of Sedimentary Petrology*, **23**, 117-119.

Press W.H., Flannery B.P., Teukolsky S.A. & Vetterling W.T., 1989. *Numerical recipes in Pascal: the art of scientific computing.* Cambridge University Press, Cambridge, 759 p.

Pyne A.R., 1986. Sea-ice operations: McMurdo Sound-Granite Harbour. *NZ Antarctic Record*, **7**, 5-13.

Pyne A.R, 1999. Ross Fast Ice History, *Victoria University of Wellington FTP site.*

Raine J.I., 1984. Outline of a palynological zonation of Cretaceous to Palaeogne terrestrial sediments in West Coast Region, South Island, New Zealand. *New Zealand Geological Survey Report NZGS*, **109**, 82 p.

Raine J.I., 1998. Terrestrial palynomorphs from Cape Roberts Project drillhole CRP-1, Ross Sea, Antarctica. *Terra Antartica*, **5**(3), 539-548.

Ramsay A.T.S. & Baldauf J.G., 1999. *A Reassessment of the Southern Ocean Biochronology.* Geological Society, London, Memoir **18**, 122 p.

Reijmer J.J.G., Sprenger A., Ten Kate W.G.H.Z., Schlager W. & Krystyn L., 1994. Periodicities in the composition of Late Triassic calciturbitides (Eastern Alps, Austria). In: de Boer P.L. & Smith D.G. (eds.), *Orbital forcing and cyclic sequences*, IAS Special Publication, **19**, 323-343.

Roberts A.P., 1995. Magnetic properties of sedimentary greigite (Fe_3S_4). *Earth and Planetary Science Letters*, **134**, 227-236.

Roberts A.P. & Turner G.M., 1993. Diagenetic formation of ferrimagnetic iron sulphide minerals in rapidly deposited marine sediments, New Zealand. *Earth and Planetary Science Letters*, **115**, 257-273.

Roberts A.P., Wilson G.S., Florindo F., Sagnotti L., Verosub K.L. & Harwood D.M., 1998. Magnetostratigraphy of Lower Miocene Strata from the CRP-1 Core, McMurdo Sound, Ross Sea, Antarctica. *Terra Antartica*, **5**(3), 703-713.

Roland N.W. & Worner G., 1996. Kirkpatrick flows and associated pyroclastics: new occurrences, definition, and aspect of a Jurassic Transantarctic rift. *Geologisches Jahrbuch*, **B89**, 97-121.

Sagnotti L., Florindo F., Verosub K.L., Wilson G.S. & Roberts A.P., 1998a. Environmental magnetic record of Antarctic palaeoclimate from Eocene-Oligocene glaciomarine sediments, Victoria Land Margin. *Geophysical Journal International*, **134**, 653-662.

Sagnotti L., Florindo F., Wilson G.S., Roberts A.P. & Verosub K.L., 1998b. Environmental Magnetism of Lower Miocene Strata from the CRP-1 Core, McMurdo Sound, Antarctica, *Terra Antartica*, **5**(3), 661-667.

Savage M.L. & Ciesielski P.F., 1983. A revised history of glacial sedimentation in the Ross Sea region. In: Oliver R.L., James P.R. & Jago J.B. (eds.), *Antarctic Earth Science, Australian Academy of Science*, Canberra, 555-559.

Scherer R.P. & Koç N., 1996. Late Paleogene diatom biostratigraphy and paleoenvironments of the northern Norwegian-Greenland Sea. In: Thiede J., Myhre A.M., Firth J.V., Johnson G.L. & Ruddiman W.F. (eds.), *Proceedings of the Ocean Drilling Program, Scientific Results*, College Station, TX, Ocean Drilling Program, **151**, 75-99.

Scherer R.P., Bohaty S.M. & Harwood D.M., in press. Oligocene and Lower Miocene Siliceous Microfossil Biostratigraphy of CRP-2/2A, Victoria Land Basin, Antarctica. *Terra Antartica.*

Schrader H.-J., 1976. Cenozoic planktonic diatom biostratigraphy of the Southern Pacific Ocean. In: Hollister C.D., Craddock C. et al. (eds.), *Initial Reports of the Deep Sea Drilling Project*, Washington, U.S. Govt. Printing Office, 35, 605-672.

Schrader H.-J. & Fenner J., 1976. Norwegian Sea Cenozoic diatom biostratigraphy and taxonomy. In: Talwani M., Udintsev G. et al. (eds.), *Initial Reports of the Deep Sea Drilling Project*, Washington, U.S. Government Printing Office, **38**, 921-1099.

Shumway G., 1960a. Sound speed and absorption studies of marine sediments by a resonance method, Part 1. *Geophysics*, **25**, 451-467.

Shumway G., 1960b. Sound speed and absorption studies of marine sediments by a resonance method, Part 2. *Geophysics*, **25**, 659-682.

Simes J. & Wrenn J.H., 1998. Palynologic Processing in Antarctica. *Terra Antartica*, **5**(3), 549-552.

Sissons B.A., 1980. Down hole temperatures. In: Pyne A. & Waghorn D.B. (eds.), *Immediate Report of VUWAE 24 and McMurdo Sound Sediment and Tectonic Studies (MSSTS)*, Victoria Univ., Wellington.

Smellie J.L., 1998. Sand Grain Detrital Modes in CRP-1: Provenance Variations and Influence of Miocene Eruptions on the Marine Record in the McMurdo Sound Region. *Terra Antartica*, **5**(3), 579-587.

Smellie J.L., in press. Erosional History from the Transantarctic Mountains Deduced from Sand Grain Detrital Modes from CRP-2/2A, Victoria Land Basin, Antarctica. *Terra Antartica.*

Steinhauff D.M., Renz M.E., Harwood D.M. & Webb P.N., 1987. Miocene diatom biostratigraphy of DSDP Hole 272: stratigraphic relationship to the underlying Miocene of DSDP Hole 270, Ross Sea, Antarctica. *Antarctic Journal of the U.S.*, **22**(5), 123-125.

Strong C.P. & Webb P.N., in press. Oligocene and Miocene Foraminifera from CRP-2/2A, Victoria Land Basin, Antarctica. *Terra Antartica.*

Talarico F. & Sandroni S., 1998. Petrography, Mineral Chemistry and Provenance of Basement Clasts in the CRP-1 Drillcore (Victoria Land Basin, Antarctica). *Terra Antartica*, **5**(3), 601-610.

Talarico F., Sandroni S., Fielding C. & Atkins C., in press. Variability, Petrography and Provenance of Basement Clasts in Core from CRP-2/2A, Victoria Land Basin, Antarctica. *Terra Antartica.*

Tasch P. & Lammons J.M., 1978. Palynology of some lacustrine interbeds of the Antarctic Jurassic. *Palinologia*, **1**, 455-462.

Tauxe L. & Hartl P., 1997. 11 million years of Oligocene geomagnetic field behaviour. *Geophysical Journal International*, **128**, 217-229.

Taviani M., Beu A. & Lombardo C., 1998. Pleistocene Macrofossils from CRP-1 Drillhole, Victoria Land Basin, Antarctica. *Terra Antartica*, **5**(3), 485-491.

Taviani M., Beu A.G. & Jonkers H.A., in press. Macrofossils from CRP-2/2A Drillhole, McMurdo Sound (Victoria Land Basin, Antarctica). *Terra Antartica.*

Taylor J.M., 1950. Pore space reduction in sandstones. *AAPG Bull.*, **23**, 701-717.

Tonarini S., Rocchi S., Armienti P. & Innocenti F., 1997. Constraints on Timing of Ross Sea Rifting inferred from Cainozoic Intrusions from Northern Victoria Land, Antarctica. In: Ricci C.A. (ed.), *The Antarctic Region: Geological Evolution and Processes*, Terra Antartica Publication, Siena, 511-522.

Truswell E.M., 1986. Palynology. In: Barrett P.J. (ed.), Antarctic Cenozoic history from the MSSTS-1 drillhole, McMurdo Sound,

DSIR Bulletin, **237**, 131-134.

Turnbull I.M., Allibone A.H., Forsyth P.J. & Heron D.W., 1994. Geology of the Bull Pass - St Johns Range area, southern Victoria Land, Antarctica. Scale 1:50000. *Institute of Geological & Nuclear Sciences geological map 14*. 1 sheet + 52 p. Institute of Geological & Nuclear Sciences Ltd, Lower Hutt, New Zealand.

Vail P., 1987. Seismic Stratigraphy Interpretation Using Sequence Stratigraphy, part 1: Seismic Stratigraphy Interpretation Procedure. In: Bally A.W. (ed.), *Atlas of Seismic Stratigraphy, AAPG*, Tulsa, Oklahoma, **27**, 1-10.

van Wagoner J.C., Mitchum R.M., Campion K.M. & Rahmanian V.D., 1990. Siliciclastic Sequence Stratigraphy in Well Logs, Cores, and Outcrops. *Concepts for High-Resolution Correlation of Time and Facies, AAPG Methods in Exploration*, **7**, 55 p.

van Wagoner J.C., Posamentier H.W., Mitchum R.M., Vail P.R., Sarg, J.F., Loutit T.S. & Hardenbol J., 1988. An Overview of Sequence Stratigraphy and Key Definitions. In: Wilgus C.K. et al. (eds). *Sea-Level Changes: An Integrated Approach, Society of Economic Paleontologists and Mineralogists*, Special Publication, **42**, 39-40.

Verosub K.L., 1977. Depositional and postdepositional processes in the magnetization of sediments. *Reviews of Geophysics and Space Physics*, **15**, 129-143.

Verosub K.L., Florindo F., Sagnotti L., Roberts A.P. & Wilson G.S., in press. Environmental Magnetism of Oligocene - Miocene Glaciomarine Strata from CRP-2/2A, Victoria Land Basin, Antarctica. *Terra Antartica*.

Villa G. & Wise S.W. Jr., 1998. Quaternary Calcareous Nannofossils from the Antarctic Region. *Terra Antartica*, **5**(3), 479-484.

Watkins D.K. & Villa G., in press. Palaeogene Calcareous Nannofossils from CRP-2/2A, Victoria Land Basin, Antarctica. *Terra Antartica*.

Waxman M.H. & Smits L.J.M., 1968. Electrical conductivities in oil-bearing shaly sands. *Trans. Amer. Inst. Mech. Eng.*, **243**, 107-122.

Webb P.N., 1989. Benthic foraminifera. In: Barrett P.J. (ed.), Antarctic Cenozoic history from the CIROS-1 drillhole, McMurdo Sound, *DSIR Bulletin*, **245**, 99-118.

Weber M.E., Niessen F., Kuhn G. & Wiedicke M., 1997. Calibration and application of marine sedimentary physical properties using a mult-sensor core logger. *Marine Geology*, **136**, 151-172.

Wei W. & Wise S.W. Jr., 1990. Middle Eocene to Pleistocene calcareous nannofossils recovered by Ocean Drilling Program Leg 133 in the Weddell Sea. *Proc. Ocean Drilling Program Sci. Results*, **113**, 639-666.

Wei W. & Wise S.W. Jr., 1992. Oligocene-Pleistocene calcareous nannofossils from Southern Ocean sites 747, 748, and 751. *Proceedings of the Ocean Drilling Program, Scientific Results*, **120**, College Station, TX, 509-522.

White P., 1989. Downhole logging. In: Barrett P.J. (ed.), Antarctic Cenozoic history from the CIROS-1 drillhole, *DSIR Bulletin*, **245**, 7-14.

Williams P.F., Hobbs B.E., Vernon R.H. & Anderson D.E., 1971. The structural and metamorphic geology of basement rocks in the McMurdo Sound area, Antarctica. *Journal of the Geological Society of Australia*, **18**, 127-142.

Wilson G.J., 1967. Some new species of lower Tertiary dinoflagellates from McMurdo Sound, Antarctica. *New Zealand Journal of Botany*, **5**, 57-83.

Wilson G.S., Roberts A.P., Verosub K.L., Florindo F. & Sagnotti L., 1998. Magnetobiostratigraphic chronology of the Eocene-Oligocene transition in the CIROS-1 core, Victoria Land Margin, Antarctica: Implications for Antarctic glacial history, *Geological Society of America Bulletin*, **110**, 35-47.

Wilson G.S., Florindo F., Sagnotti L., Verosub K.L. & Roberts A.P., in press a. Magnetostratigraphy of Oligocene - Miocene Glaciomarine Strata from CRP-2/2A Core, Victoria Land Basin, Antarctica. *Terra Antartica*.

Wilson G.S., Bohaty S.M., Fielding C.R., Florindo F., Hannah M.J., Harwood D.M., McIntosh W.C., Naish T.R., Roberts A.P., Sagnotti L., Scherer R.P., Verosub K.L., Villa G., Watkins D.K. & Woolfe K.J., in press b. Chronostratigraphy of CRP-2/2A, Victoria Land Basin, Antarctica. *Terra Antartica*.

Wilson T.J., 1995. Cenozoic transtension along the Transantarctic Mountains-West Antarctica rift boundary, southern Victoria Land, Antarctica. *Tectonics*, **14**, 531-545.

Wilson T.J. & Paulsen T., in press. Brittle Deformation Patterns of CRP-2A Core, Victoria Land Basin, Antarctica. *Terra Antartica*.

Wise S.W. Jr., 1983. Mesozoic and Cenozoic calcareous nannofossils. *Initial Reports of the Deep-Sea Drilling Project*, **71**, 481-550.

Woolfe K.J., Kirk P.A. & Sherwood A.M., 1989. Geology of the Knobhead area, southern Victoria Land, Antarctica. *New Zealand Geological Survey, DSIR, Miscellaneous map series*, **19**.

Wrenn J.H., 1981. Preliminary palynology of the RISP Site J-9, Ross Sea, Antarctica. *Antarctic Journal of the United States*, **16**(5), 72-74.

Wrenn J.H., 1982. Dinocyst biostratigraphy of Seymour Island, Palmer Peninsula, Antarctica. *Unpublished Ph.D. dissertation*, Louisiana State University, Baton Rouge, LA, 467 p.

Wrenn J.H. & Beckman S.W., 1981. Maceral and total organic carbon analyses of RISP Site J-9 Cores. *Antarctic Journal of the United States*, **16**(5), 69-71.

Wrenn J.H. & Hart G.F., 1988. Paleogene dinoflagellate cyst biostratigraphy of Seymour Island, Antarctica. In: Feldmann R.M. & Woodburne M.O. (eds.), *Geology and Palaeontology of Seymour Island, Antarctic Peninsula*, Geological Society of America Memoir, **169**, 321-447.

Wrenn J.H. & Kokinos J.J., 1986. Preliminary comments on Miocene through Pleistocene dinoflagellate cysts from DeSoto Canyon, Gulf of Mexico. *American Association of Stratigraphic Palynologists*, Inc., AASP Contributions Series No. **17**, 169-225.

Wrenn J.H., Hannah M.J. & Raine J.I., 1998. Diversity and Palaeoenvironmental Significance of late Cainozoic Marine Palynomorphs from the CRP-1 Core, Ross Sea, Antarctica. *Terra Antartica*, **5**(3),553-570.

Zachos J.C., Quinn T.M. & Salamy K.A., 1996. High-resolution Deep-Sea Foraminiferal Stable Isotope Records of the Eocene-Oligocene Climate Transition. *Paleoceanography*, **11**, 256-266.

TERRA ANTARTICA

Università di Siena
Museo Nazionale dell'Antartide
Sezione Scienze della Terra

Direttore Responsabile:
Maurizio Boldrini

Direttore Scientifico:
Carlo Alberto Ricci

Autorizzazione del Tribunale di Siena
n. 633 del 18 Luglio 1996

Tipografia Senese

Via Sallustio Bandini, 51 - Siena Italy
Tel. 0577 280719 - Fax 0577 271126
E-mail: tipsenese@tin.it